PROGRESS IN SUSTAINABILITY WITHIN THE REALM OF DESIGNING NEW THERMOSETTING MATERIALS

Adrià Roig Gibert

UNIVERSITAT ROVIRA i VIRGILI

Progress in sustainability within the realm of designing new thermosetting materials

Adrià Roig Gibert

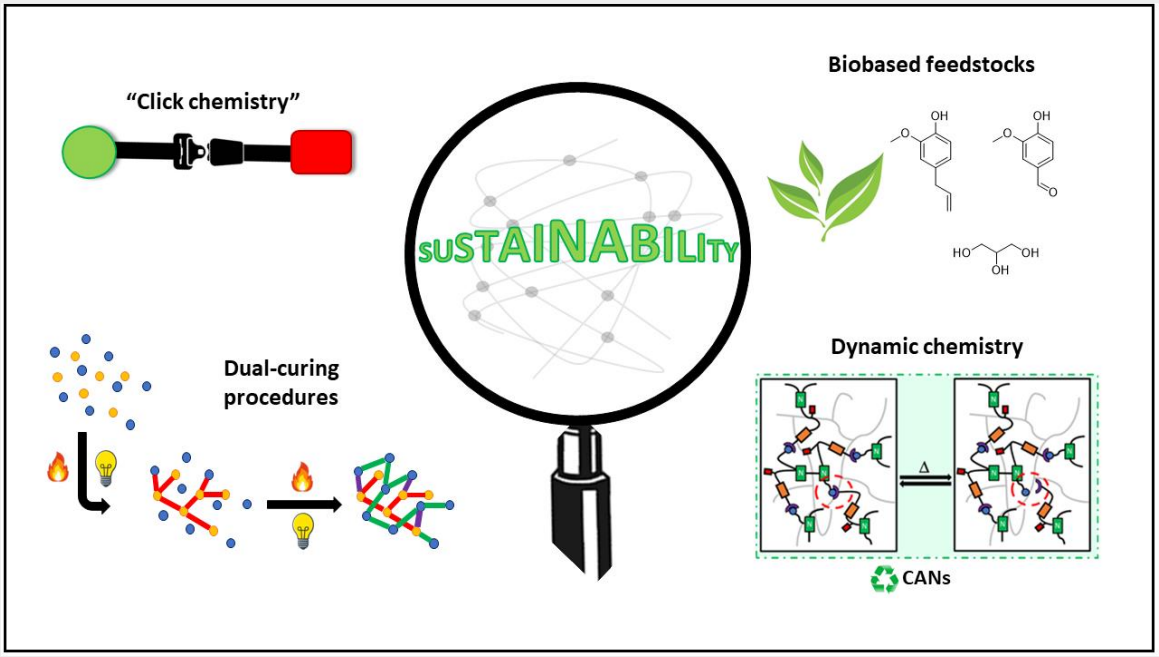

DOCTORAL THESIS

2023

UNIVERSITAT ROVIRA I VIRGILI
PROGRESS IN SUSTAINABILITY WITHIN THE REALM OF DESIGNING NEW THERMOSETTING MATERIALS
Adrià Roig Gibert

Progress in sustainability within the realm of designing new thermosetting materials

by

Adrià Roig Gibert

Doctoral Thesis

Supervisors:

Àngels Serra i Albet

Silvia De la Flor López

Department of Analytical Chemistry and Organic Chemistry

UNIVERSITAT
ROVIRA i VIRGILI

Tarragona

2023

UNIVERSITAT ROVIRA I VIRGILI
PROGRESS IN SUSTAINABILITY WITHIN THE REALM OF DESIGNING NEW THERMOSETTING MATERIALS
Adrià Roig Gibert

UNIVERSITAT ROVIRA i VIRGILI

Departament de Química Analítica I Química Orgànica

Campus Sescelades, Edifci N4

Carrer Marcel·lí Domingo s/n

43007 Tarragona

Professor Àngels Serra i Albet of the Department of Analytical and Organic Chemistry at the Universitat Rovira i Virgili, and Doctor Silvia De la Flor López of the Department of Mechanical Engineering at the Universitat Rovira i Virgili,

Certify:

that the Doctoral Thesis, entitled "Progress in sustainability within the realm of designing new thermosetting materials" presented by Adrià Roig Gibert to obtain the title of Doctor, has been carried out under our direction and that it fulfils all the requirements to be eligible for the Doctor International Mention.

Tarragona, 1st of September 2023

Doctoral Thesis Supervisors

Prof. Àngels Serra i Albet

Dr. Silvia De la Flor López

UNIVERSITAT ROVIRA I VIRGILI
PROGRESS IN SUSTAINABILITY WITHIN THE REALM OF DESIGNING NEW THERMOSETTING MATERIALS
Adrià Roig Gibert

Agraïments

Diuen que fer el doctorat és un camí dur ple d'alts i baixos. Hi ha dies de felicitat i satisfacció perquè s'ha aconseguit un rendiment alt en una reacció i dies de molta frustració perquè el resultat que esperaves no ha sortit i et toca tornar-ho a fer. Després de passar 4 anys, puc dir que en certa manera és veritat, però no només és pot resumir en això. Les reaccions van i venen i els resultats poden sortir o no, però sens dubte, el més important són les persones que t'acompanyen, t'ajuden i et donen el seu suport durant el dia a dia dels transcurs d'aquest camí.

Per sort, he pogut conviure i conèixer moltes persones que, durant aquest etapa, han aportat el seu granet de sorra per aguantar-me o simplement treure'm un somriure en algun dels molts dies complicats. Per aquest motiu, volia donar-vos les gràcies i dir que no em puc sentir-me més afortunat d'haver viscut aquesta aventura amb tots vosaltres al costat.

Primer de tot, i com no podia ser d'una altra manera, volia donar-te les GRÀCIES (sí, en majúscula i ben gros) a tu, Àngels. La veritat és que no tinc paraules per expressar la meva enorme gratitud cap a tu. No sé si te'n recordes, però el primer somriure ja me'l vas treure al laboratori de 3r quan em deies que m'assemblava algun polític català o quan em confonies amb l'Oriol. Passats 6 anys, he canviat personalment i professional i tu hi tens molt a veure. M'has transmès la teva passió per la química i m'has ensenyat que, amb treball, constància i dedicació no hi ha meta impossible i que el límit el poses tu. També he vist que l'edat només és un número i que el que realment conta són les ganes que hi posis a les coses. Químicament, ets una referent per mi, però personalment, ets molt més que això. M'he sentit acollit, respectat i valorat en tot moment i m'has tractat de 100, cosa que m'ha fet créixer i aprendre moltíssim. Sempre has estat disposada a ajudar-me i a escoltar-me (amb el cafetó al despatx, això si), m'has deixat aportar idees (a vegades masses i tot), i dur-les a terme i m'has dirigit sempre cap al bon camí. Mai hagués pogut imaginar una directora com tu i sempre donaré gràcies per haver pogut fer el doctorat amb tu. T'estaré eternament agraït.

En segundo lugar, que en realidad también es primer lugar, quería darte las GRACIAS a ti, Silvia. No voy a negar que cuando empecé, tenía un poco de miedo a la mecánica y todo lo que comporta y no estaba seguro de si me gustaría, pero fue hablar contigo y la cosa dio un giro de 180 grados. Me has enseñado que la mecánica es una ciencia fascinante y te doy las gracias por mostrármela como tú lo has hecho. Tu forma de explicar y tu pasión han hecho que me interese cada día más y ahora no entiendo nuestra química sin la mecánica. Tu trabajo y dedicación es impresionante y admirable, pero, aun así, lo que más me fascina eres tú como persona. Siempre me has atendido y has estado dispuesta a explicarme (más de una vez) las ecuaciones,

fórmulas y conceptos que hay detrás de cada ensayo con una sonrisa y de la mejor manera posible. Me has dado mucha confianza y tranquilidad desde el primer minuto, me has escuchado y me has guiado hasta este punto y por eso, no puedo estar más agradecido. Sin ti (y sin tu iPad), este camino hubiera sido mucho más complicado. Ahora no puedo estar más ansioso por todo lo que está por venir. De verdad, muchas gracias.

Xavi Ramis, a tu també et vull expressar el meu agraïment. Gràcies pels consells i l'ajuda que m'has brindat i per obrir-me les portes del teu laboratori sempre que ha calgut, però sobretot per la teva simpatia i amabilitat. Als companys de Barcelona, Xavi Fernández, Osman i Sasán, moltes gràcies pels moments i xerrades compartits en els dinars de grup.

He de continuar donant les gràcies a totes les persones que han passat pel laboratori 330 siguin del grup o no i els primers noms que em venen al cap són el Francesco i el Claudio.

Al principio, os tenía un poco de rencor por el horario del turno que me pusisteis en el congreso de Baekeland, pero después me acogisteis como uno más desde esa "Gala Dinner" y me habéis enseñado mucho. Francesco, eres uno de mis mentores. Tú pusiste los primeros cimientos de la "ROIG S.L." y sin ti, esa empresa no habría podido existir. Grazzie mille. Claudio, hacías que los días en el laboratorio pasaran mucho más rápido y verte trabajar era un espectáculo, siempre recordaré el hecho de conseguir verte comer pasta con mayonesa.

Gracias por todos los momentos dentro y fuera del laboratorio. È stato un piacere conoscervi e sono molto grato di potervi chiamare amici!!

Gracias a ti también Federico, has dejado huella en el grupo y aunque a veces tus tioles se han notado de más en el laboratorio, tu amabilidad y tranquilidad se echaran en falta. ¡Mucha suerte en tu nueva aventura! Tommaso (Dio Ca**), compañero de cafés y fiestas del último año, me has hecho reír un montón en el laboratorio. Eres un tio muy listo y no tengo ninguna duda de que vas a ser un grandísimo doctor, Grazzie da vero! Jesús, el meu primer TFG (ara ja Màster), gràcies per aquest "pique" Barça-Madrid. Aquest any has vist que amb constància, temps i unes quantes gotes de suor, la feina acaba sortint. Ànims que això ja ho tens! Anna, gràcies per ser la "cabra-loca" del lab. Encara que hem passat algun momentet difícil (molt aïllat), les teves ganes d'aprendre i la teva dedicació només em demostren que tens un gran futur per endavant. Molts d'ànims!

Dailyn, gracias por todos tus consejos y ayuda. ¡Mi antecesora del eugenol! Me pusiste firme desde el primer día y aunque en ese momento me molestaba, ahora te lo agradezco. David, moltes gràcies per la teva ajuda amb el DMA i el reòmetre. Sempre has tret temps de la teva agenda per ajudar-me, aconsellar-me i donar-me suport.

Estic molt content per haver-te conegut i espero poder anar a molts més congressos junts i poder fer les "cervesetes" de després. Pere, a tu ja et vaig conèixer durant l'època a Suspol. Has entrat al grup com un coet. Gràcies per ajudar-me amb la teva química. Espero que algun cop ens trobem a Tomorrowland je je.

I would also like to thank you Marco, I laughed a lot with you in the lab. We did not spend as much time as I would have liked together, but I will never forget your curly hair, your happiness and your hangovers. Valeria, despite that you always arrived at 11 in the lab, your eager to learn, your motivation, but more importantly you, fascinated me. We miss you and you will always have a little piece of my heart. Thank you both for listening me when I needed it and for those great beers near Piazza del Plebiscito in Napoli! Pere Hidalgo, el tio més tot terreny i més manetes que ha passat pel laboratori. Gràcies per estar sempre disposat a ajudar en el que faci falta, sense ni una mala paraula ni cap retret. Ets un tio increïble. Laura, gràcies per la feina feta. Em va faltar temps per acabar-te de conèixer bé, però sé que hi poses moltes ganes i mentre vas estar al laboratori vaig gaudir molt treballant amb tu. I would also like to thank you Aina Petrauskaitė, my first Master student. We did a great a job together. I will always remember how you tried to teach me how to say the name of your lituanian professor. Emilija and Ieva, thank you for those 3 months here, you brought a lot of joy and happiness during your stage! Armando, ánimos en el doctorado, eres una gran persona y te mereces todo lo bueno que te pueda pasar, pero no me aprietes tan fuerte la mano que un día me la vas a romper. Sara (esearre), pasaste por el lab como un torbellino, dejaste una huella única. Eres una persona espectacular y doy gracias por haberte podido conocer y poder mantener nuestra amistad.

Jordi, company de carrera i company de laboratori. És un goig veure't treballar. Ara ja ets el següent en presentar i el doctorand més vell al lab. Molts d'ànims pels mesos que et venen, que seran durets, però no tinc cap dubte que ho tiraràs endavant i seràs un gran doctor. Yasmin, thank you for being as you are. My predecessor in the purchase of reagents. You are a hard-worker, and your dedication and time only confirms me your great future. Alireza, thank you for all the moments in the lab. I will always remember that photo in the computer. Man, we are getting older!!! Isaac, no vaig arribar a veure't treballar al laboratori, però m'encanta compartir moments amb tu. Cada moment amb tu és únic, tu ets únic. Gràcies per fer-me riure sempre. Xavi, què puc dir de tu? Una de les millors persones que conec i que m'ha donat el doctorat. Sempre proactiu amb ganes de menjar-te el món i un bon "cachopo". Gràcies per escoltar-me i tranquil·litzar-me durant els descansets. Gràcies per tots els moments dins, però sobretot fora del laboratori, i tots els dinars, soparets, congressos per Paris, birretes i festes. Espero fer-ne molts més.

També m'agradaria agrair a la gent d'altres laboratoris del departament. Gràcies als companys de Sucres, Albert, Miguel, Pablo, Isabel, Javier, Jordi i Paula per sempre tenir

un somriure pel passadís i sempre estar disposats a deixar qualsevol reactiu. Esperem que algun dia l'AC funcioni com ha de funcionar. Gràcies als companys que han passat pel grup de Suspol, Aaron, Nabil, Marc i especialment a tu Adri. Tu ets la persona que em vas iniciar en un laboratori i és el que vas posar la primera pedra perquè jo pugui arribar fins aquí. Gràcies pel teu suport, ajuda i predisposició. Ets un exemple a seguir per mi. #teambatabruta. Gràcies també als companys del departament de baix, per mi sempre sereu el grup d'OMICHis. Sara, Pol, Lola Joris, Paula, Maria, Daniel, Angie i Anna. Gràcies per acollir-me amb els braços oberts en algun sopar i alguna festa. Sou unes persones excepcionals i estic molt agraït d'haver-vos conegut.

També volia dedicar unes paraules a tots els professors del departament i d'altres facultats, per sempre estar disposats a ajudar-me. Toni, gràcies per donar-me consell quan l'he necessitat, Juan Carles, gràcies per resoldre'm algun dubte sobre alguna reacció i gràcies per l'ajuda i predisposició en les pràctiques del lab. Albert, gràcies per la teva amabilitat, simpatia i consells, sempre has tingut bones paraules cap a mi. Marta, gracias por los momentos vividos y por compartir esa boda en Nápoles con nosotros. També vull agrair als tècnics que fan que els equips funcionin correctament i que per tant, son peça clau per la nostra recerca. Ramon, gràcies per sempre tenir a punt els equips de ressonància, Àlex, gràcies per la teva infinita ajuda amb el DSC i TGA. Sempre estàs disponible i ens has solucionat més d'algun problema. Josep, gràcies per la teva responsabilitat, per solucionar algun tema de la premsa i per sempre tenir les màquines del 04 com si fossin noves.

I would also like to express my sincere gratitude to my supervisor in Delft. Gràcies Santiago per la càlida acollida al teu grup. Vaig gaudir molt de l'experiència i en gran part és gràcies a tu. Tens un grup molt gran però amb persones molt vàlides i molt bones i això només demostra com ets. Thank you Prof. Sybrand for giving me advice when needed and always having your office door opened. Hugo, the one and only beer-lover dutch in the group. Thank you for being how you are. You were the first person who helped me there. Serena, my italian pillar there. You listened and helped me more than you can imagine. You make me feel like home. Miisa, thank very much. You're a hard-worker and an incredibly good person. Thank you for opening the doors of your home and show me your little, scary but adorable snakes. Tinashe, thank you, I laughed a lot with you. You deserve the best. Gawel, JingJing, Anton, Marlon, Jaylan, Bernadine, Riccardo, Elif and Alessandro thank you all for the moments, trips and beers we shared. I will always remember you! Once a NovAMer, always a NovAMer!!

Finalment, hi ha altres persones que, encara que no he compartit laboratori o tema de recerca amb elles, són igual o més importants i m'han acompanyat durant aquest viatge. Mireia, ets una gran persona, companya i amiga. En un tres i no res has entrat a formar part de la meva vida quotidiana i estic molt agraït per això. Pel que sé, també ets una gran química i la passió que tens farà que arribis fins allà on vulguis, no en tinc

cap dubte. Gràcies per aguantar-me (algun "enfadito" hi ha hagut) i escoltar-me. Jordi, tet, més que company, un bon amic. Des de la carrera que ja hem fet molt bones migues, hem viscut junts i hem tirat endavant junts, recolzant-los l'un amb altre. Que content estic de poder haver viscut gran part de la meva vida amb tu. Et queda ben poquet per acabar i et dono tots els ànims possibles. No tinc cap dubte que seràs un dels millors doctors que conegui. Glòria, una altra bona millor amiga que ha anat acompanyant-me des de la carrera. Una persona de 10 que vull que formi part de la meva vida per sempre. Tot i ser del costat "enemic" del departament, t'admiro molt com a química però més com a persona. Gràcies per suportar els meus mal genis, aguantar-me i animar-me en moments difícils d'aquest camí. Ets incondicional. Una altra doctora excepcional que ens deixarà aquesta universitat. Javi, otro de mis mejores amigos que me ha dejado la universidad y que será un pedazo de doctor. Gracias por todos los momentos, (sí, también los de fiesta), charlas y viajes. Cada momento contigo es un regalo. Sigue adelante que los frutos de las semillas siempre acaban saliendo y recuerda que, a mayor esfuerzo, mayor será la satisfacción.

Uri, sempre comencem igual, però és la veritat, més que un amic, un germà. M'has aguantat cada dia d'aquest viatge. M'has animat en els dies dolents i has celebrat amb mi els dies bons i no només de la tesi, sinó de tota la vida universitària. Et vaig veure ser químic, treure't un màster i finalment ser doctor. Quin orgull! No m'imagino un millor company de viatge que tu i no puc estar més agraït per tot el que has arribat a fer per mi. La complicitat i connexió que tenim no es pot descriure amb paraules i això ha fet aquesta aventura única. Gràcies company, amic i germà. Sense tu al costat res hagués sigut el mateix.

Per últim, per no menys important, vull donar les MOLTES GRÀCIES a la meva família; mama, papa, Marta, iaia, avi i àvia. Vosaltres sou els que m'heu criat i jo no seria com soc si no es gràcies a vosaltres. També heu patit alguna conseqüència de la tesi com per exemple no veure'm tant, però tot i això, no heu deixat de recolzar-me i animar-me en cap moment, us heu interessat sempre en tot el què faig (encara que costi explicar-ho i entendre-ho), us heu preocupat pel meu estat d'ànim i celebrat amb mi cada passet que he anat donant. Sou el meu motor de vida i els autèntics artífexs de tot això. Mai hi haurà paraules suficients per donar-vos les gràcies per tot, però el que sigui puc dir és: US ESTIMO MOLT!

UNIVERSITAT ROVIRA I VIRGILI
PROGRESS IN SUSTAINABILITY WITHIN THE REALM OF DESIGNING NEW THERMOSETTING MATERIALS
Adrià Roig Gibert

"Come on up for the rising,
Come on up for the rising tonight"
(Bruce Springsteen)

UNIVERSITAT ROVIRA I VIRGILI
PROGRESS IN SUSTAINABILITY WITHIN THE REALM OF DESIGNING NEW THERMOSETTING MATERIALS
Adrià Roig Gibert

Abstract

Thermosetting materials are a class of polymers used in day-to-day applications or fields where superior mechanical properties are needed, such as automobiles, coatings or construction areas. Notwithstanding their remarkable thermomechanical performance and chemical resistance, their irreversible crosslinked structure prevents them from being recycled or reprocessed once cured. Consequently, a significant volume of waste is generated after the completion of its useful lifespan, which mostly ends up in landfills or is incinerated, causing a severe problem from the sustainability point of view. This pressing issue underscores the substantial and urgent challenge faced by academic and industrial spheres to develop strategies to prevent waste buildup and ensure the preservation of the planet's environment. There are several strategies at hand to craft environmentally conscious and sustainable thermosets. These options encompass click chemistry and dual-curing approaches, the exploitation of monomers sourced from biomass or synthesizing covalent adaptable networks (CANs).

In this work, all these approaches have been used to design different types of thermosetting materials with different characteristics and properties, always highlighting the sustainable point of view.

Chapter 3 establishes a novel dual-curing system based on a first thermal epoxy-amine and a second thermal or photoinitiated homopolymerization of methacrylates. The curing procedure is studied and characterized using non-isothermal isoconversional and rheological analysis. Depending on the curing conditions and careful selection of the monomers, gelled or viscous intermediate materials and final highly crosslinked thermosets can be obtained.

Subsequently, in Chapter 4, commercially available monomers are used to design a first homopolymerization of (meth)acrylates and a further thiol-epoxy reaction dual-curing system. During the first stage, the occurrence of different reactions leads to an imbalance in the stoichiometry that affects the second thermal step. Nevertheless, by adequately selecting the feed ratio of the initial formulation, the thermal and mechanical properties of the final materials can be tailored to specific requirements.

Then, a fully renewable dual-curing procedure based on eugenol, glycerol and pentaerythritol derivatives is described in Chapter 5. By using click thio-Michael and thiol-epoxy reactions, thermosets with high homogeneity and T_g values around room temperature are prepared. Moreover, it is found that a ratio between two of the initial monomers determines the thermal and mechanical performance of the intermediate and final materials.

A different sustainable perspective is explained in Chapter 6. Glutaric, suberic and dodecanedioic dihydrazides, are synthesized. Combined with an epoxy derivative of

vanillin, they are used to prepare biobased poly(acylhydrazone) CANs. The associative dynamic nature of imine metathesis between acylhydrazone bonds enables the materials to be mechanically recycled and reprocessed. Furthermore, this exchange reaction allows to self-heal small damages in the samples.

In Chapter 7, a biobased diimine-diglycidyl derivative of vanillin is synthesized and cured with several Jeffamines with different chain lengths. The thermal, mechanical and dynamic behavior is studied, revealing good thermal stability, T_gs above room temperature and rapid stress relaxation. The mechanical recycling is achieved, and the chemical degradation of imine bonds is tested.

In Chapters 8 and 9, aliphatic disulfide dynamic materials from renewable resources and commercially available monomers, respectively, are prepared. First, the catalytic effect of the covalently bonded tertiary amines on the disulfide metathesis is investigated. By varying proportions of two amines, different viscoelastic behaviors are obtained and characterized. Chapter 9 focuses on developing materials with extremely fast relaxation rates while maintaining a certain creep resistance. Extensive creep studies on all the materials are performed to understand the behavior of the materials in a wide range of temperatures. Finally, the self-healing and self-welding abilities are evaluated.

Chapter 10 is devoted to developing two reversible vitrimeric adhesives based on epoxy and thiol commercially available monomers. The mechanical characterization is performed to understand the range of possible applications. Thanks to the dynamic transesterification, the dismantling and debonding are easily accomplished at high temperatures. Moreover, the re-bonding ability is confirmed by comparing the adhesion strength to the original adhesive.

In the last chapter, a fully bio-based dual-curing system using an epoxy acrylate derivative of eugenol, the triacrylate derivative of glycerol and cystamine, has been established. Click low-temperature-triggered aza-Michael addition and high-temperature epoxy-amine reactions are combined to achieve sequentiality in the curing system. Viscous or gelled intermediates and highly crosslinked final materials with multiple dynamic bonds are obtained. The dynamicity of the network is demonstrated, and the associative or dissociative behavior is proved through rheology. In addition, the mechanical properties are evaluated, and the possibility of mechanical recycling is brought out by comparing the chemical and thermal properties of the virgin and recycled samples.

Table of contents

UNIVERSITAT ROVIRA I VIRGILI
PROGRESS IN SUSTAINABILITY WITHIN THE REALM OF DESIGNING NEW THERMOSETTING MATERIALS
Adrià Roig Gibert

List of Abbreviations

A	Area/Pre-exponential factor
Abs	Absorbance
AcEU	Acetyl eugenol
AEEU	Acrylate epoxy eugenol
AEU	Acrylate eugenol
4AFD	4-Aminophenyl disulfide
AIBN	2,2'-Azobisisobutyronitrile
ATR	Attenuated total reflection
B	Benzaldehyde
BG	Base generator
BPA	Bisphenol A
BTMA	Benzyl trimethylammounium chloride
CALB	*Candida antarctica* lipase B
CAN	Covalent adaptable network
CFRP	Carbon fibre reinforced plastics
Cys	Cystamine
d	Doblet
DA	Diels-Alder/Dodecanedioic acid
DBN	1,5-diazabicyclo[4.3.0]non-5-ene
DBTDL	Dibutyltin dilaurate
DBU	1,8-diazabicyclo[5.4.0]undec-7-ene
DCB	Dichlorobenzene
DCC	Dicyclohexyl carbodiimide
DCM	Dichloromethane
DETA	Diethylenetriamine
DEPOEU	Diepoxy eugenol
DGEBA	Diglycidyl ether of bisphenol A

Dh	Dihydrazide
dh/dt	Heat release rate
DIDG	Diimine-diglycidyl monomer
DIDP	Diimine-diphenol monomer
dx/dt	Curing rate
DMA	Dynamical mechanical analysis
DMF	N,N-Dimethyl formamide
DMPA	2,2-Dimethoxy-2-phenylacetophenone
DMSO	Dimethyl sulfoxide
DSC	Differential scanning calorimetry
DTG	Derivative of thermogravimetric curve
E	Elastic modulus/ Young modulus/ Tensile modulus
E_a	Activation energy
E'	Storage modulus/ Relaxed modulus
E''	Loss modulus
E'_{glassy}	Storage modulus at glassy region
$E'_{rubbery}$	Storage modulus at rubbery region
ECH	±-Epichlorohydrin
EHP	Electrically heated plate
EpAcEU	Epoxy acetyl eugenol
EPO-Van	Glycidyl derivative of vanillin
ESR	Electron spin resonance
EU	Eugenol
F	Force
F_{max}	Maximum force
f	Functionality
FTIR	Fourier transform infrared spectroscopy
FWHM	Full width at half maximum

G	Shear modulus
G'	Storage shear modulus
G''	Loss shear modulus
GA	Glutaric acid
GC	Gas chromatography
GC-MS	Gas chromatography coupled mass spectrometry
GMA	Glycidyl methacrylate
Gly	Glycerol
GTA	Glycerol triacrylate
HDGE	1,6-Hexanediol diglycidyl ether
HP	Hewlett Packard
Hz	Hertz
HzH	Hydrazine hydrate
IPDA	Isophorone diamine
J	Heat flux per unit area/Joule
JEFFA	Jeffamine D400
K	Kelvin degree
L	Length
m	Meters/Multiplet
MA	Methyl acrylate
MCPBA	*m*-Chloroperbenzoic acid
MCT	Mercury-Cadmium-Telluride
min	Minutes
Mt	Million metric tons
M_w	Molecular weight
N	Newton
n	Fragility index
NOE	Nuclear Overhauser effect

NGP	Neighboring group participation
NMR	Nuclear magnetic resonance
OA	Octanoic acid
ODA	4,4'-Oxidianiline
PTU	Poly(thiourethane)
PHU	Poly(hydroxy urethane)
ppm	Part per million
PU	Poly(urethane)
q	Quadruplet
R	Gas constant
r	Ratio
s	Seconds/Singlet
S3	Trimethylolpropane tris(3-mercaptopropionate)
S4	Pentaerythritol tetrakis(3-mercapto propionate)
S6	Di-pentaerythritol hexakis (3-mercapto propionate)
SA	Suberic acid
SIM	Selected ion monitoring
SM	Shape-memory
SMP	Shape-memory polymer
t	Time/thickness/triplet
T	Temperature
TAA	Thioacetic acid
Tan δ	Tangent of the phase angle
TBP	Di-*tert*-butyl peroxide
TEA	Triethylamine
TEBAC	Triethyl benzyl ammonium chloride
TGAP	Triglycidyl-*p*-aminophenol
THF	Tetrahydrofuran

$T_{1\%}$	Temperature of decomposition for a 1% weight loss
$T_{2\%}$	Temperature of decomposition for a 2% weight loss
$T_{5\%}$	Temperature of decomposition for a 5% weight loss
T_b	Boiling temperature
T_g	Glass transition temperature
$T_g^{E''}$	Onset temperature
T_m	Melting temperature
T_{max}	Maximum temperature
$T_{tan\delta}$	Temperature of maximum of the tan δ peak
T_v	Topology freezing temperature
TEA	Triethylamine
TGA	Thermogravimetric analysis
TMPTA	Trimethylolpropane triacrylate
TMPTE	Trimethylolpropane triglycidylether
TMPTM	Trimethylolpropane trimethacrylate
TMS	Tetramethylsilane
TREN	Tris(2-aminoethyl)amine
V	Vanillin
VOC	Volatile organic compound
VU	Vinylogous urethane
w	Width
WLF	William-Landel-Ferry
x	Conversion
°C	Celsius degree
1MI	1-Methyl imidazole
2MI	2-Methyl imidazole
3D	Three dimensional
α_{gel}	Conversion at the gel point

ε	Absorptivity coefficient/Strain
$\dot{\varepsilon}$	Strain rate
ε_{break}	Strain at break
δ	Chemical shift/Phase angle
σ	Stress
σ_0	Initial stress
σ_{break}	Stress at break
η	Viscosity
τ	Relaxation time
τ^*	Characteristic relaxation time
$\tau_{0.37}$	Time to reach a value of $\sigma/\sigma_0 = 0.37$
$\tau_{100\%}$	Time to reach a total relaxation
ΔH	Enthalpy of the curing process
Δh_{tot}	Total heat involved normalized to sample size

Chapter 1

Introduction and objectives

UNIVERSITAT ROVIRA I VIRGILI
PROGRESS IN SUSTAINABILITY WITHIN THE REALM OF DESIGNING NEW THERMOSETTING MATERIALS
Adrià Roig Gibert

1.1 Green chemistry and sustainable development

The exponential growth of the human population and their diverse needs inevitably lead to increased resource utilization and environmental degradation. Pollution, global warming, ozone depletion, deforestation, and loss of biodiversity are among the most urgent environmental challenges faced by humanity. These issues emerged in the late 19th century due to urbanization, industrial development, and the expansion of chemical research and industrial production [1].

In response to these pressing concerns, radical solutions involving industry, academia, and governments became necessary, giving rise to the emergence of green and sustainable chemistry. The concept of green chemistry revolves around twelve principles aimed at making future chemistry safer and more environmentally friendly. This approach includes waste prevention, using renewable feedstock, designing safer chemicals, and, ideally, creating degradable substances once the their purpose is fulfilled [2].

One significant environmental challenge concerns the need for the degradability and persistence of plastics in the environment. Mass-produced plastic products, like plastic bags, are often intended for short-term single use but accumulate in the land and oceans for hundreds of years [3]. Despite their adverse environmental impact, plastics are indispensable in modern life due to their unique properties, including versatility, low cost, strength, light weight, flexibility, and durability. They find use in various sectors, such as packaging, construction, textiles, transportation, and electronics, and hold potential for future technological and medical advances [4]. Global production of plastics has exponentially increased from 2 million metric tons (Mt) in 1950 to almost 350 Mt in 2017 [5].

Nevertheless, this great demand produces several amounts of plastic pollution and waste. According to Geyer *et al*. about 6,000 Mt of plastic waste has been generated from 1950 to the present [6]. Of this amount, approximately 5,000 Mt ended up or discarded in landfills, 800 Mt have been incinerated, and only 600 Mt have been recycled. If current practices regarding plastic waste management are perpetuated, it is projected that an alarming 12,000 Mt will be accumulated in the environment. Thus, many efforts still need to be made to change this perspective.

For this reason, balancing the demand for plastics in society with the need to reduce their environmental footprint is crucial. Sustainable approaches can be adopted to achieve this balance. For example, substituting plastics derived from fossil fuels with bio-renewable alternatives, recycling end-of-life polymeric materials, or designing them to be biodegradable at the end of their useful life are essential steps in mitigating the impact of plastics on the environment [7]. Finding this golden mean is of utmost relevance to ensure a sustainable future for society and the planet.

1.2 Thermoplastics and thermosets

In general, plastic is the term commonly used to describe polymeric materials or polymers, which are large molecules (macromolecules) composed of repeating units called monomers that are chemically bonded into a chain or network. Different factors, such as the arrangement, chain length, branching, crosslinking, or the type of constituent monomers, determine their wide range of applications. These materials can be classified according to different criteria. If the classification of polymers is based on the source of availability, they can be classified as natural, synthetic, or semi-synthetic. If they are classified according to their structure, they can be divided into linear, branched, or crosslinked polymers. They can even be divided by their types of polymerization mechanism, like polyaddition, polycondensation, or ring-opening [8].

Finally, they can also be classified according to their behavior in front of temperature which relies on the existence of different transition temperatures depending on their molecular structure and will be the classification used in this thesis. Polymers can be divided into two main groups depending on their thermal behavior: thermoplastics or thermosets.

Thermoplastics are high-molar-mass macromolecular chains that are not covalently linked but rather entangled. These entanglements lead to topological constraints that limit the molecular motion due to interactions with neighboring chains (Figure 1.1a).

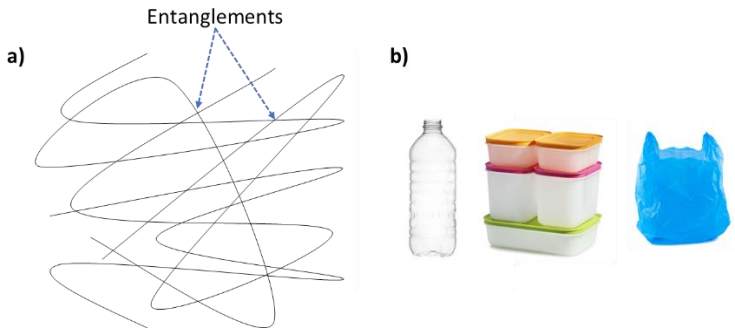

Figure 1.1. a) Molecular structure of thermoplastics. b) Some examples of daily-life applications of thermoplastics.

Thermoplastics are linear or branched polymer chains that can be either amorphous or semi-crystalline in a solid state, and they can flow when heated above a characteristic temperature. Amorphous polymers can flow when heated well above the glass transition temperature (T_g), experiencing first a transition from glass to rubber and then to a viscous melt. Differently, semi-crystalline thermoplastics will

behave as glassy materials until they are heated above their melting temperature (T_m), in which the chains are free to move and, therefore, able to flow.

Thanks to this ability to flow, thermoplastics can deal with several heating and cooling cycles without significantly altering their molecular structure or properties, which makes them able to be recycled or reshaped at high temperatures (above T_g or T_m) as well as to be processed via industrial techniques such as extrusion or injection molding [9]. However, thermoplastics are usually weak, which results in poor chemical and solvent resistance, easy degradability by heat, and poor mechanical properties when increasing the temperature. Despite this, the family of thermoplastics represents almost 80% of the plastic demand nowadays since they are widely used in many daily-life applications (Figure 1.1b) [10]. The most common examples of thermoplastics used in manufacturing are polyethylene, polypropylene, polyvinyl chloride, polystyrene, polyethylene terephthalate, and polycarbonate [11].

Contrarily, thermosets are crosslinked structures with strong covalent bonds forming a three-dimensional network that has become hardened permanently through a polymerization process called curing (Figure 2.1a). This procedure is irreversible and can be generally achieved by treating the initial mixture of polyfunctional organic molecules with heat, pressure, suitable irradiation, or curing agents and occurs in a mold designed with the final desired shape. The resulting rigid, infusible, and densely crosslinked network architecture of thermosets is the critical driver for their strength, superior mechanical and thermal properties, dimensional stability, and high solvent resistance.

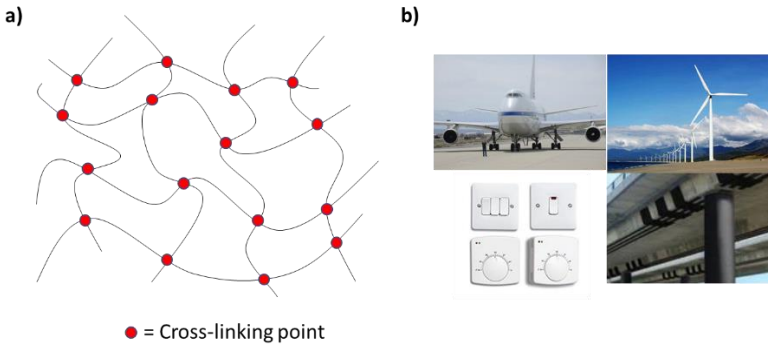

Figure 1.2. a) Molecular structure of thermosets. b) Some examples of daily-life applications of thermosets.

Unlike thermoplastics, thermosetting polymers are usually amorphous due to the impossibility of order in the network structure because of the restrictions imposed by the presence of crosslinks. Some exceptions exist when rigid monomers exhibiting nematic-isotropic transitions are used [12].

Due to crosslinking points, thermosets do not flow when heated above the T_g, but they adopt a rubber-like behavior when this temperature is overpassed. Generally, these materials show T_g values above room temperature, and high T_g is usually related to high mechanical and thermal performance, robustness, and rigidity. These outstanding properties make them very interesting for day-to-day usage and applications where superior mechanical properties at elevated temperatures are required, such as adhesives, coatings, building and construction industry, or aviation applications (Figure 1.2b) [13]. This is why thermosets production accounts for roughly 20% of the worldwide annual polymeric production. Among the most commonly used thermosetting resins are epoxies, phenolics, polyesters, vinyl esters, polyimides or bismaleimides [14].

As previously mentioned, the irreversible covalent linkages hamper their solubility in any organic solvent; thus, a suitable solvent will only swell the polymer, but it will never dissolve them unless the action of temperature or reactive solvents compromises the network integrity. Moreover, their impossibility to flow at elevated temperatures makes them unable to be recycled, reprocessed, or reshaped leading to serious environmental issues. For these reasons, careful strategies involving the use of sustainable synthesis and renewable feedstocks, the employment of curing methodologies that minimize the generation of waste and the energetical-cost production, or a deeper investigation into the recyclability or reprocessability of these materials must be selected to design thermosetting polymers in a greener, eco-friendly and energy-efficient way.

1.3 Strategies for a sustainable design of thermosets

Despite the excellent mechanical properties and chemical resistance of thermosets, they cannot be recycled or reprocessed once cured due to their permanently cross-linked structure, which leads to several amounts of waste accumulating in landfills after the end of their service life that possibly may need hundreds of years to be degraded. This problem evidences the big current challenge that the academic and industrial worlds have to face to prevent the accumulation of litter and protect the planet's environment.

The European Union has adopted its first movements towards waste management by publishing a directive encouraging the prevention, reuse, careful treatment, and recycling of polymer waste [15].

In any case, different strategies can be used to design thermosets in a green and sustainable way. These can be the use of click chemistry, adopting dual-curing methodologies or taking advantage of monomers derived from biomass to prepare

thermosetting polymers. The following sections will be addressed in explaining these methods.

1.3.1 Dual curing

One methodology to obtain high-added-value thermosetting polymers with tailorable properties is the dual-curing methodology. This procedure combines two different polymerization processes, sequential or simultaneous, that can be triggered by an external stimulus such as heat or UV light [13]. Simultaneous dual-curing is not as interesting since both reactions take place at the same time, so it is only focused on the properties of the final material. Conversely, sequential dual curing allows obtaining a first intermediate material with specific properties and a final material with totally different characteristics after a second curing reaction, making this procedure highly interesting in the scientific community (Figure 1.3) [16–19].

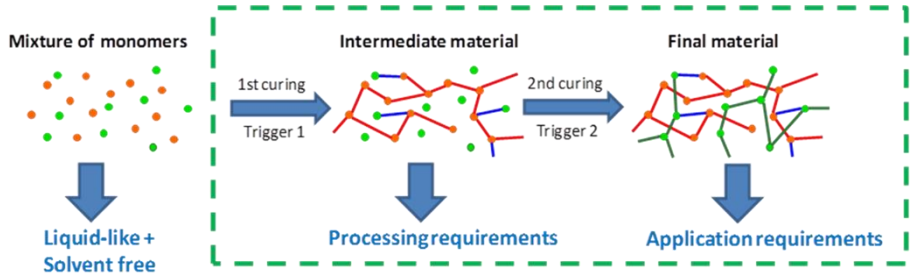

Figure 1.3. Schematic representation of a dual curing procedure extracted from [13].

The network structure and the properties of the intermediate and final materials can be designed by controlling the monomer's functionality, chemical structure, and feed ratio in the initial formulation. Depending on the previous parameters, after the first curing stage, it is possible to obtain a viscous intermediate material in which the chains are not totally bonded in the structure, which is useful, for example, in the adhesion field [20] or a gelled intermediate material in which a network has been formed. However, some more functional groups still have to react, which can be a good advantage in programming a desired final shape [21]. Moreover, off-stoichiometric mixtures can also enhance the thermal and thermomechanical properties of the prepared thermosets [22,23].

For these reasons, sequential dual curing can be considered an evolution of other thermoset synthetic methodologies, such as prepolymer crosslinking or B-stage processes. B-stage processing is a multistage fabrication technology that is used for dry bond adhesives or complex composite parts [24,25]. Nevertheless, this procedure is subjected to tight time-temperature specifications to control the extent of polymerization, which maximizes the possibility of over-curing compared to dual

curing, in which the intermediate material will not react unless the corresponding stimulus is triggered. Compared to prepolymer synthesis, processing can be made much easier in dual-curing systems since the prepolymer is obtained in the first curing stage with low-molecular-weight monomers rather than mixing large amounts of polymeric components. However, dual-curing extends well beyond these concepts, allowing the creation of bespoke materials with adaptable processing capabilities, making them extremely valuable for various advanced applications. An additional advantage of dual-curing systems is the potential for solvent-free processing, utilizing liquid monomers and mild conditions to prepare the materials. This fact significantly minimizes volatile organic compound (VOC) emissions into the atmosphere and reduces processing energy costs. This aspect evidences the importance of using dual-curing procedures from a sustainability point of view, thus indicating that this methodology may be a good strategy for the environmentally friendly and energetically efficient design of thermosetting materials.

However, achieving a successful sequential dual-curing procedure is not that easy, and three crucial requirements must be met: i) both reactions must be selective and compatible to avoid undesired inhibition or side products; ii) different stimuli can trigger both reactions or alternatively, they exhibit significantly distinct reaction rates, enabling their control from a kinetic perspective. By using this procedure, the properties of the intermediate and final materials can be custom-tailored. Photo latent and thermally latent catalysts [26,27] or the use of blocked species [28] are usually exploited for reaching sequentiality in the design of dual-curing systems. Nonetheless, click-type reactions are the most used for developing network buildup processes due to their easiness, orthogonality and great compatibility [29].

1.3.2 Click chemistry

The concept of click chemistry was introduced by Sharpless and co-workers in 2001 in response to the continuous and rigorous research efforts dedicated to developing methods for synthesizing increasingly complex natural products [29]. This chemistry involves the formation of heteroatom linkages (C-X-C) and has a high thermodynamic driving force (> 20 kcal mol^{-1}), but they have to meet some stringent criteria to be used in this context. Click reactions must be modular, wide in scope, give very high yields (or even be quantitative), regio and stereospecific (not necessarily enantioselective), insensitive to oxygen or water, and orthogonal [30,31]. Moreover, they must be performed with readily available starting materials in solventless or aqueous media and very simple conditions. Thus, these reactions can be assessed as environmentally friendly regarding the low generation of residues, atom economy, and high energy saving, which makes them very interesting from the sustainability point of view for

the preparation of thermosetting materials. Figure 1.4 shows a visual representation of the click chemistry.

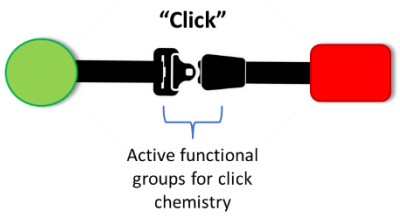

Figure 1.4. Conceptual representation of click chemistry.

In the field of thermosets, click reactions mark the difference with their allowance in obtaining well-defined macromolecular structures. Combined with their high tolerance to various functional groups, they are suitable for implementing dual-curing systems [21,32–34]. Although meeting the requirements of a "click" reaction is a tall order, multiple processes have been identified that step up to the mark in the design of polymers:

- Nucleophilic ring opening of epoxides or aziridines [35]:

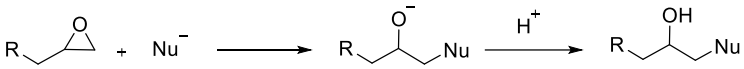

Scheme 1.1. Scheme of a nucleophilic ring opening reaction.

- Michael addition reactions [36,37]:

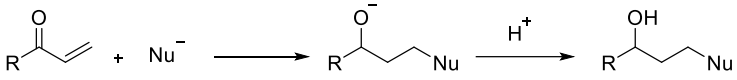

Scheme 1.2. Scheme of a Michael addition reaction.

- Photochemical addition of thiols to alkenes and alkynes [38,39]:

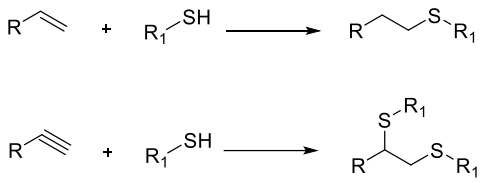

Scheme 1.3. Scheme of thiol-ene and thiol-yne reactions.

- Diels-Alder cycloadditions [40]:

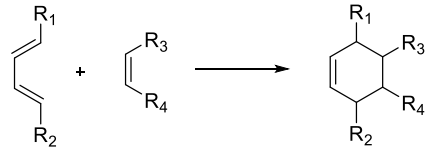

Scheme 1.4. Scheme of Diels- Alder cycloaddition.

- Carbonyl additions of thiol to isocyanate [41]:

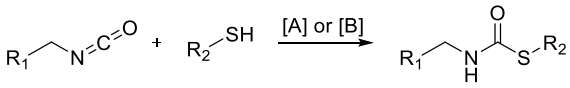

Scheme 1.5. Scheme of thiol additions to isocyanates.

- Imine or acylhydrazone formation [42]:

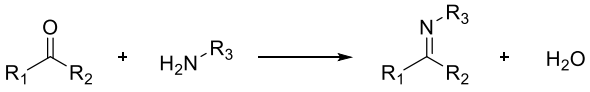

Scheme 1.6. Scheme of imine formation.

Many examples of these reactions have been used to prepare thermosetting polymers with multiple different chemical structures for a wide range of applications.

To tune the properties of the final materials, monomers with different structures containing aromatic rings or aliphatic chains need to react with the proper hardeners. Unfortunately, in the polymer field, many reagents are still derived from petrol-based

feedstocks, which can result in fossil resource depletion. For this reason, the academic world has to challenge substituting petrol-derived monomers for materials derived from biomass such as terpenes, terpenoids, vegetable oils, carbohydrates, or lignin [43].

1.3.3 Use of renewable feedstocks

Thermosetting materials on an industrial scale are typically prepared from non-renewable resources [44]. However, reducing the use and dependence on fossil fuels is not only necessary due to environmental concerns but also economically crucial. Nowadays, biobased feedstocks are gaining traction as an alternative to petrol-derived products [45]. Typical examples of thermosets used in the industry are phenolic and urea-formaldehyde resins, unsaturated polyesters, and epoxy resins, which account for approximately 70% of the market of thermosetting polymers (polyurethanes not included). Above all the monomers to formulate epoxy networks, the most used is the diglycidyl ether of bisphenol A (DGEBA), which can be obtained by the reaction of bisphenol A (BPA) and epichlorohydrin in the presence of sodium hydroxide. Nevertheless, this product is reported to be hazardous and toxic. Thus, there has been an increasing interest in looking for alternatives for DGEBA-based polymers [46]. Figure 1.5 shows the most abundant biomass structures for bio-based polymers.

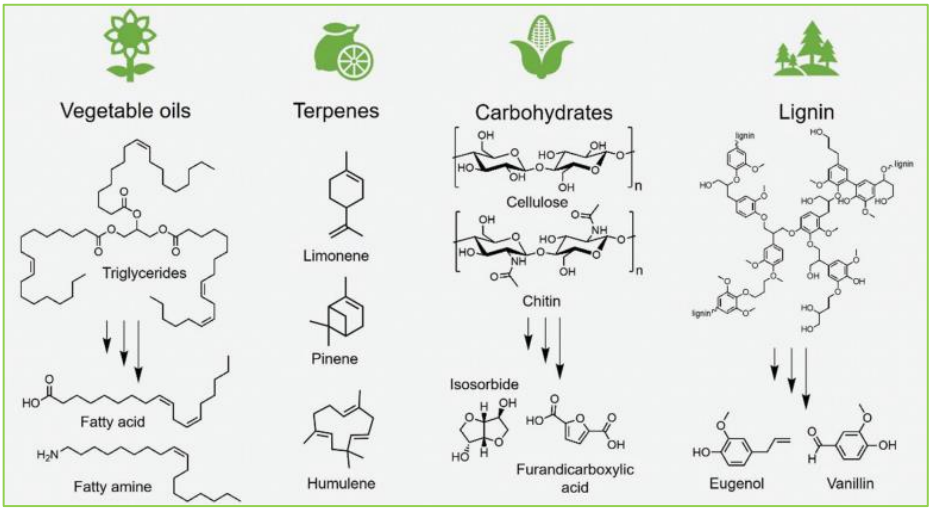

Figure 1.5. Most abundant biomass and structures of common biobased building blocks in polymer science extracted from [47].

Vegetable oils are widely used as renewable alternatives to epoxy monomers since they are cheap and abundant. They comprise 90-95% triglycerides with many double bonds, which can be easily functionalized with epoxy groups. The most used vegetable

oils in thermosetting materials are soybean and linseed oils. Nevertheless, the long aliphatic chain in their structure leads to thermosets with low thermomechanical performance, which limits their usage to non-structural applications [48]. For this reason, they are mostly used as matrices for bio-composites or as toughening in blends with petroleum-derived epoxy resins [49,50]. The presence of glycerol ester bonds makes them potentially biodegradable [51].

Another possibility of bio-based compounds to substitute fossil resources that are gaining increasing interest is terpenes [52]. This is due to their structural diversity and the presence of double bonds with different reactivities that convert them into promising building blocks with great potential in biopolymers' production. The most commonly employed terpenes are pinene and limonene. The last, limonene, which can be obtained from the isomerization of pinene and the residues of the juice industry, is a potential monomer for thermosetting materials. The two double bonds in its chemical structure allow the epoxidation to limonene dioxide to be further reacted with different hardeners, such as amines or anhydrides, to obtain high-T_g materials [53,54].

Polysaccharides such as cellulose or glucose are also exciting bio-based raw materials for the obtention of pivotal building monomers such as isosorbide or furan derivatives. Isosorbide production begins with the hydrogenation of glucose to sorbitol and its further dehydration in acidic conditions [55]. Due to its rigid structure provided by the two *cis*-fused tetrahydrofuran (THF) rings, its use is basically focused on synthesizing high-performance materials. The diglycidyl derivative can be easily obtained and cured with amines or anhydrides to yield crosslinked thermosets with high T_g values and good mechanical properties [56]. Even more interesting are the furan derivatives, produced through dehydration processes from hexoses [57]. These reactions mainly yield 5-hydroxymethyl-2-furfural and 2-furfural that can be functionalized to a vast range of molecules such as amines, acids, aldehydes, ketones, epoxides that are highly potential starting monomers in the thermosetting field [58]. For example, Palmese *et al.* prepared a fully bio-based furan crosslinked polymer through an epoxy-amine reaction, obtaining thermosets with high glass transition temperatures and high thermal stability suitable for coating, adhesives and composite materials [59].

Lignin, one of the most abundant renewable resources, is a large and complex natural polymer that can also be used to synthesize thermosets. It contains many hydroxyl and phenolic groups that can be converted to suitable functional groups that commonly lead to crosslinked materials, e.g., epoxy [60], phenolic [61], and polyester materials [62]. However, lignin is also well-known for its heterogeneous structure, relatively low reactivity, and poor compatibility, limiting its use as a resin component.

Consequently, lignin derivatives such as vanillin, eugenol, or catechol can be utilized as precursors for synthesizing different polymeric materials. Indeed, the first two will be discussed since they are used in a significant part of this thesis.

1.3.3.1 Vanillin

The history of vanillin traces back to the famous Spanish conqueror Cortés, who, in around 1520, is believed to have been served a chocolate drink flavored with vanilla by the Aztecs. He introduced chocolate and vanilla to Spain and Europe, where they gained rapid popularity [63]. In 1858, Gobley was the first to isolate and identify the vanillin compound in the vanilla bean and confirm its role as the primary flavor component. Nowadays, around 20,000 tons of vanillin are produced annually, being the most available pure monoaromatic phenol currently produced at an industrial scale from lignin [64].

Vanillin (4-hydroxy-3-methoxybenzaldehyde) is used as a flavoring and fragrance ingredient in the food or cosmetic industries. Vanillin is a key compound in chocolate and ice cream manufacture, making large producers such as Unilever, Nestle, or Suchard important players in its market [64]. However, the aromatic ring, the phenol, and the aldehyde groups make vanillin very interesting as a crucial bio-based starting material for synthesizing thermosetting materials [65]. Indeed, vanillin offers a promising solution to the persistent challenge of discovering bio-based aromatic monomers capable of replacing conventional petrol-based alternatives, and its potential has been proved in epoxy polymers, where it results as an excellent substitute for BPA [66–68].

1.3.3.2 Eugenol

Eugenol is the main constituent of clove oil, derived from the species *Eugenia caryophyllata*. Clove has served as a spice and fragrance in ancient China for over two millennia. Its well-known application as a traditional toothache remedy was first documented in France's "Practice of Physic" in 1640 [69]. The annual eugenol production was estimated at 2,000 tons, representing a significant annual market value.

Eugenol is an extraordinarily versatile molecule and has been included as an ingredient in cosmetics and several perfumes such as Opium® or Yves Saint Laurent, as a spicy flavoring in whisky and ice creams, and as a surgical dressing in dentistry. Moreover, its anti-inflammatory and chemo-preventive effects and its superior anti-oxidant activity have attracted the attention of many researchers [70]. Its rigid structure provided by the aromatic ring and the phenol and allylic groups converts eugenol into a great platform for designing polymeric materials. Some researchers

have focused their attention on the epoxy derivatives of eugenol. For example, Faye *et al.* described the synthesis of a tri-epoxy eugenol compound by reacting eugenol with phosphorous oxychloride and its curing with different amines [71]. They obtained high-performance thermosets with flame-retardant properties due to the presence of phosphorous atoms in the polymer structure. Nevertheless, due to its great versatility, other reports direct their efforts on its allyl derivatives to achieve thiol-ene-made thermosets [35,38] or even to synthesize hardeners from eugenol to cure epoxy resins [72].

As can be seen, a wide variety of natural products are used in industrial applications to replace partially or even entirely petroleum-based polymers. Materials designed under this strategy can compete with or surpass existing thermosets with superior environmental qualities. For this reason, using renewable and bio-based feedstocks arises as an efficient and promising pathway for the design of thermosetting materials. However, bio-based does not mean biodegradable or recyclable, which is one of the main current issues to be solved.

1.3.4 Recyclability and reprocessability of thermosets

Unlike thermoplastics that, at high temperatures, can flow until they melt, facilitating reprocessability or solubility in a determined solvent, thermoset recycling technologies are much more difficult for the permanent covalent bonds forming a 3D network [73]. Despite this, some approaches have been made to process and recycle thermosets. These techniques can be divided into mechanical, thermal and chemical processing [74]. Figure 1.6 shows a representative scheme of possible treatments of thermosetting materials.

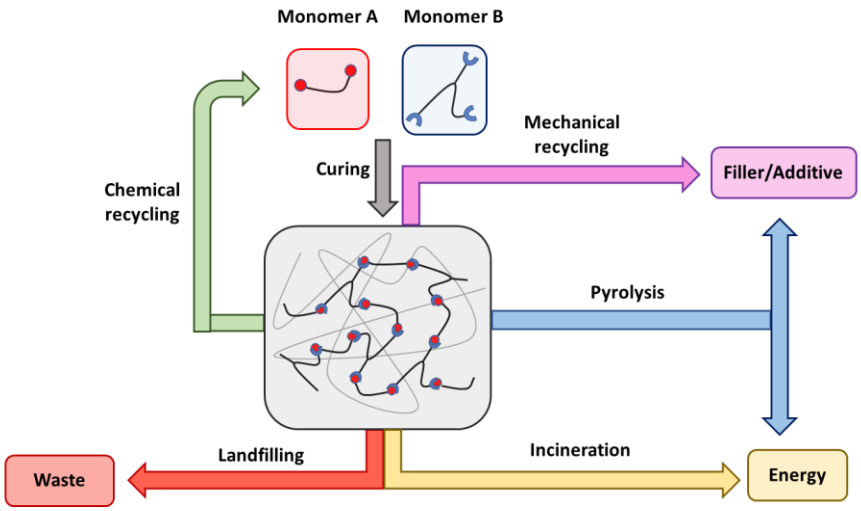

Figure 1.6. Representative scheme of treatment of thermosetting residues.

Mechanical recycling involves cutting and grinding steps and transforming scrap products into uniformly sized flakes using speed cutting. Unfortunately, these technique does not work properly in thermosets. It has some disadvantages in carbon fiber reinforced composites (CFRP) since the matrix and the fiber cannot treated separately, resulting in a loss of mechanical properties and value of the product. However, suppose the thermoset is mechanically ground into powder. In that case, they can be used as fillers in new thermoset and thermoplastic materials, but they cannot compete economically with conventional filler materials [75].

Thermal recycling can be classified into incineration and pyrolysis. However, in the first case, no material can be recovered. Therefore, this cannot be categorized as a strategy of thermoset recycling. On the other hand, pyrolysis is a powerful strategy to obtain low-molecular-weight organic compounds from the polymer matrix, which can be applied for further chemical processing [76]. Nevertheless, the high temperatures needed and the required process energy, as well as the pollutant emission, make its feasibility questionable.

Chemical recycling is ascribed to the solvolysis procedure. This methodology uses a liquid medium to degrade and dissolve the polymer. Usually, this liquid medium is a reactive solvent that can attack determined bonds of the polymer, thus degrading the polymer into organic compounds that can further be re-used as molecular building blocks and, in some cases, recover the fibers in CFRP, breaking down the polymer [13]. Nevertheless, the highly crosslinked structure of thermosets complicates this procedure, so, recently, supercritical fluids have been used due to their high diffusivities and low viscosities. Another drawback is the frequent use of hazardous solvents, which makes the environmental impact of chemical recycling debatable.

Due to the problematic recycling of thermosets, most of them end up in landfills, leading to serious amounts of polymer waste, generating severe environmental problems that gravely affect the planet. For this reason, reprocessing and re-using thermosetting materials remains a big challenge for the academic and industrial worlds.

Recently, stimuli-triggered degradable thermosets have been developed, which consist of introducing cleavable linkages in the polymer network, such as esters, carbonates, acetals or hemiacetals, or DA addition bonds. By adding these bonds in the polymer structure and depending on the amount, type and location, mechanisms that break down the polymer matrix result into either (i) non-reusable components or (ii) reusable monomer/oligomer systems that can be re-polymerized again [77].

This is directly linked to the latest discovery for closed-loop thermosets: dynamic chemistry. This methodology allows the obtention of covalent adaptable networks (CANs) capable of self-repair on a micro and macro scale [78].

1.4 Covalent adaptable networks (CANs)

As we have seen, the recyclability of thermosets often requires high energetical costs, hazardous solvents or reagents, and harsh conditions. Even with that, the successful recycling of the thermosets is usually not guaranteed since most of the techniques affect the polymer irreversibly, leading to high pollution emissions and a large amount of polymer waste in landfills, which is a severe problem from the environmental and sustainability point of view. Previously mentioned strategies like using dual-curing procedures and click chemistry, substituting petrol-based resources for biomass-derived feedstocks, or, sometimes, recycling change future perspectives and offer a pathway to be followed to solve this problem.

More recently, covalent adaptable networks (CANs) have attracted great interest in both the academic and industrial worlds since they are the most promising solution for closed-loop recyclable thermosets, creating a boundary line between thermoplastics and thermosets (Figure 1.7).

Figure 1.7. Representation of the boundary line between thermoplastics and thermosets thanks to CANs.

The idea is to incorporate dynamic chemical bonds in the structure of the polymer network that, upon applying a specific stimulus (usually heat or light), produce macroscopic responses from a change in the material's molecular architecture (rearrangement or reorganization of the polymer components) [79]. These dynamic bonds can reversibly be broken and then reform under certain conditions, providing the final polymer with malleability, adaptability, and self-healing properties, which, at the same time, enable the recyclability and re-use of thermosetting material without losing the network integrity [80]. These networks behave as thermosetting materials before applying the stimulus, and they can flow like thermoplastics after the stimulus is applied.

This concept has been exploited since Leibler and co-workers, in 2011, described the preparation of malleable epoxy polymers from DGEBA and tri- and dicarboxylic acids that could be recycled or reshaped at high temperatures [81]. Nevertheless, Tobolsky *et al.,* in 1946, demonstrated how crosslinked polysulfide rubbers can relax the stress at elevated temperatures due to the interchange of disulfide linkages [82]. Unfortunately, no further investigation has been done on that topic until 2011. Since then, many studies have been published on CANs regarding different chemistries and reactions that will be later discussed [83–85].

1.4.1 Types of CANs

Currently, CANs are being explored by many researchers, and, as we have said, they are based on the chemical exchange reactions of their dynamic covalent bonds present in their structure. Based on the mechanism of the exchange reactions, CANs can be divided into two main groups: dissociative and associative [86].

1.4.1.1 Dissociative CANs

In the dissociative CANs, the dynamic linkages are first broken (dissociate) and then reformed in the same or another place (Figure 1.8).

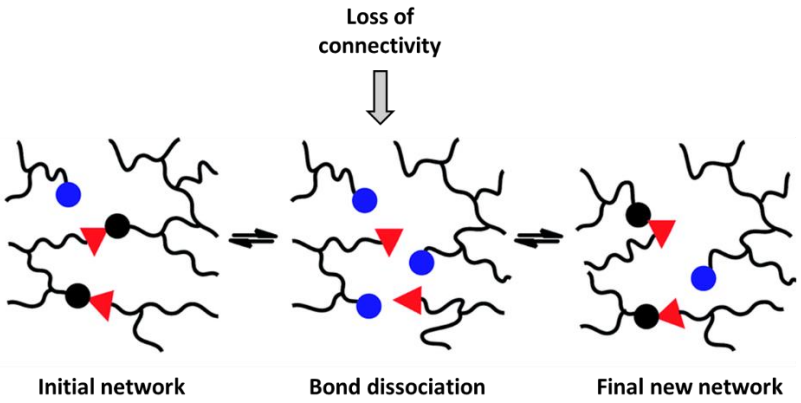

Figure 1.8. Visual representation of the dissociative-type mechanism, adapted from Denissen *et al*. [86].

Upon heating, the bond breaking and reforming rate increases, causing a net bond dissociation as the chemical equilibrium shifts towards the endothermic side. As a result, these materials experience rapid topology rearrangements, such as stress relaxation and flow, due to the decreased connectivity. This temporary loss of cross-linking density often results in a sudden drop in viscosity, similar to what is typically observed in thermoplastic materials. However, upon cooling, the crosslinks are

reformed (equilibrium shifted to the formation of linkages), usually to the same extent as in the starting material, thus preserving or re-establishing the desirable thermosetting properties such as stiffness, insolubility, and infusibility. Consequently, these dynamic crosslinks allow these polymeric networks' thermal reprocessing.

Many types of reactions can be categorized as dissociative, such as Michael additions [87] or disulfide exchange [88]. However, the most known dissociative-type exchange mechanism used in the design of CANs is the Diels-Alder (DA) reaction, discovered in 1928 by Otto Diels and Kurt Alder [89]. These reactions will be explained later in this introduction.

Although the drop in viscosity can provide beneficial properties in the easiness of polymer reshaping and self-healing properties, the complexity of designing a system that could combine enough mechanical strength and the required drop in viscosity is still a challenge that needs further investigation [77].

1.4.1.2 Associative CANs

In the case of associative CANs, the bond rupture and the bond formation occur concertedly, which maintains the crosslinking density and the network integrity always constant (Figure 1.9).

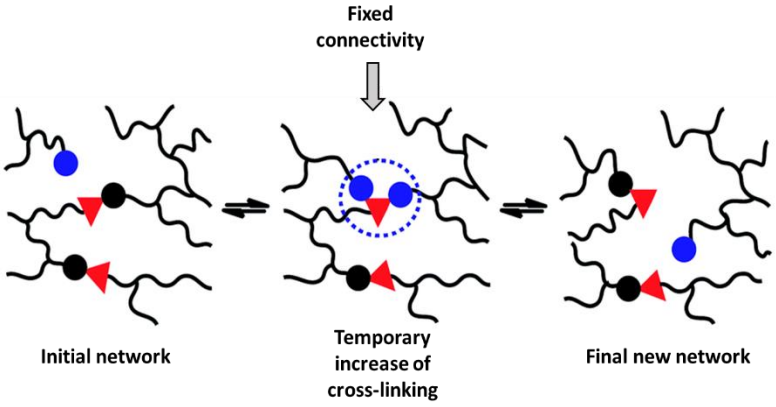

Figure 1.9. Visual representation of the associative-type mechanism, adapted from Denissen *et al*. [86].

Compared to thermoplastics, there is no sudden drop in viscosity; thus, after the exchange reaction, the chemical functionality is the same but has different connectivity. In associative CANs, the viscosity gradually decreases with temperature, enabling a flow similar to the one adopted by vitreous inorganic silica. For this reason, these types of covalent adaptable networks were named vitrimers by Leibler in 2011 [81].

Due to their dynamic nature, vitrimers exhibit unique properties that combine the merits of thermosets and thermoplastics. On the one hand, they behave like permanently crosslinked thermosetting materials, preserving a constant crosslinking density such that the network does not depolymerize and remains mechanically robust and insoluble. On the other hand, at high temperatures, they alter their behavior from a viscoelastic solid to a material with a fluid-like plastic flow, which endows malleability, recyclability, and thermal healing [90].

In stark contrast to most dissociative CANs and thermoplastic materials, vitrimers defy the conventional norms with their unique viscosity control dictated by the kinetics of exchange reactions. While classical polymers undergo a sudden drop in viscosity near their T_g, adhering to the Williams-Landel-Ferry (WLF) model, vitrimers showcase an intriguingly gradual shift in their viscosity patterns following the Arrhenius law, akin to the behavior observed in typical inorganic silica materials and other glass formers [86]. This allows their processing without precise control over the temperature. It offers remarkable advantages by enabling the materials to be welded and reshaped only by applying heat without requiring complex molds. This distinctive feature opens new avenues for industrial application and positions them as reprocessable thermosets.

To realize the full potential of vitrimers and promote their recycling, special consideration must be paid to two crucial transition temperatures during material design. The first is the widely recognized glass transition temperature (T_g), common in conventional polymers, which marks the change from a glassy to a rubbery state due to long-range molecular motion. On the other hand, the second temperature, known as topology freezing temperature (T_v), holds particular importance for vitrimers, as it is linked to crosslink exchange reactions. This is the temperature at which reversible chemical reactions start to occur, causing the network to undergo flow and granting vitrimers the ability to be reshaped and reprocessed, but, at the same time, physically, it also corresponds to the temperature at which the polymer reaches a viscosity of 10^{12} Pa·s.

This means that, below T_v, the network's topology freezes, rendering vitrimers similar in behavior to traditional thermosets. On the other hand, the rate of exchange reactions intensifies, causing the characteristic flow of covalent adaptable networks. As such, T_v is a critical parameter for determining the upper-temperature limit for vitrimer service and the lower temperature for recycling.

1.4.1.3 Vitrimer-like CANs

A third type of CANs is currently of interest to many researchers since their viscoelastic behavior needs to be further studied. Vitrimer-like polymers have the particularity to

chemically behave as a dissociative covalent adaptable network, meaning that its exchange mechanism occurs in a two-step mechanism (rupture and reforming of the bonds) but physically behave like associative CANs or vitrimers since they exhibit an Arrhenius dependence of the viscosity with the temperature [91].

The enigma behind the vitrimer-like properties in dissociative CANs lies in the intricate interplay of thermodynamics and kinetics governing the exchanges. If the equilibrium constant of dissociative bonds is shifted towards the associative state, the overall number of bonds and the crosslinking density are barely reduced. This is attributed to the rapid rate of the association reaction, surpassing that of dissociation. Consequently, the dissociated state assumes a transient nature, scarcely affecting the overall bond count, thereby preserving the network's integrity with minimal alterations [92,93].

One way to distinguish these materials from vitrimers would be the possible dissolution in an appropriate solvent. Nonetheless, as the dissociation step is so transient, a proper selection of the solvent and the conditions would be required since the crosslinking density and the polymer integrity are maintained in the whole exchange process.

Anilinium salts and disulfide bonds in the presence of an excess of amines or amine catalysts are reported as vitrimer-like materials [94–96].

Such borderline materials indicate that the definition of a vitrimer still remains questionable, depending on the viewpoint adopted.

1.4.2 Dynamic exchangeable reactions in CANs

Since Leibler and coworkers coined the term these malleable and repairable materials "vitrimers", several studies have been focused on the development and preparation of not only associative CANs (vitrimers) but also dissociative CANs to mitigate the detrimental effect of thermosetting-waste accumulation that concerns the world. The network's dynamic bonds, enabling the recyclability, reprocessability, and reshapability, puts CANs on stand as a potentially sustainable and environmentally-friendly strategy for synthesizing crosslinked materials.

Many chemistries based on well-known organic reactions have been explored for the synthesis of covalent adaptable networks. This section will intend to encompass some examples of these chemistries.

1.4.2.1 Transesterification

The first reported covalent adaptable network, specifically a vitrimer, was based on a transesterification exchange reaction (Scheme 1.7) [81]. They prepared epoxy cross-

linked materials by reacting diglycidyl ether of bisphenol A (DGEBA) with di- and tricarboxylic fatty acids in the presence of zinc acetate ($Zn(Ac)_2$) as the transesterification catalyst.

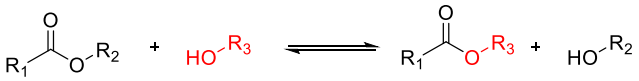

Scheme 1.7. Transesterification reaction between esters and hydroxy groups.

β-Hydroxy esters allow the network's topological rearrangement to obtain malleable and recyclable thermosets.

Later on, Altuna *et al.* described the synthesis of β-hydroxy ester networks employing covalently attached tertiary amines able to catalyze the exchange reactions, demonstrating similar stress relaxation rates compared with other external catalysts. [97]. Moreover, Zhang and coworkers prepared a biobased epoxy vitrimer derived from eugenol that was cured with succinic anhydride at various epoxy/anhydride rates [98]. Apart from demonstrating that stoichiometry affects relaxation rates, materials revealed excellent shape memory and crack-healing properties.

However, not only β-hydroxy esters can undergo transesterification reactions. This exchange reaction can also occur if esters and hydroxyl groups are present in the network. Hayashi *et al.* synthesized materials with ester-containing thiols [99]. They prepared colorless and transparent samples with shape memory properties using this click-type reaction. Finally, UV-cured thiol-acrylate vitrimers were prepared for digital light processing 3D printing [100]. They not only reported the use of a photocatalyst able to promote the transesterification reaction but also the 3D printing of complex structures with high resolution.

It is worth saying that transesterification reaction is the most studied exchangeable reaction for its monomer availability, excellent thermosetting properties, and wide range of applicability [101].

It is also important to mention that in the sulfur analogs, the transthioesterification, or thiol-thioester exchange, has also been reported for dynamic covalent networks by Bowman and coworkers for the obtention of hydrogel materials showing dynamic and frequency-dependent flow behavior [102,103].

1.4.2.2 Diels-Alder reaction

The Diels-Alder reaction is a dissociative-type reaction described in 1928 [89]. Unlike other cycloadditions, this reaction is a [4+2] cycloaddition between a diene and a

dienophile thermally reversibly driven. In this case, the electronic effects of the substituents on dienes and dienophiles drastically affect the reaction.

In the preparation of covalent adaptable networks, the furan/maleimide system has been widely studied due to its excellent thermal and mechanical properties and recycling and self-healing capabilities (Scheme 1.8) [104].

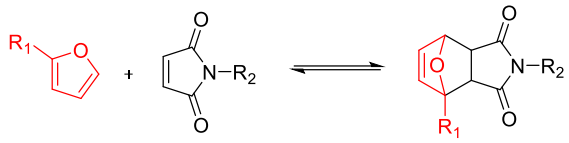

Scheme 1.8. Reversible Diels-Alder reaction involving furans and maleimides.

In 2002, the first furan/maleimide-based polymers were reported by Chen *et al.*[105]. They synthesize extremely transparent materials with the ability to restore a fractured part of the polymer multiple times with high recoveries without using catalysts, additional monomers, or special surface treatment. From that moment, many researchers explored this type of reaction in CANs using different starting monomers, highlighting the polymers' outstanding self-healing abilities and its uses in polymer composites [106,107].

[4+4] cycloadditions of anthracene have also been explored for preparing thermosetting materials [108]. These types of photochemical reactions allow temperature control for the desired application.

1.4.2.3 Imine-amine exchange

A reversible condensation reaction between aldehydes or ketones with primary amines can quickly form imine bonds. Their dynamic behavior is widely known since they undergo two different types of associative mechanisms depending on the stoichiometric conditions between aldehydes or ketones and amines (Scheme 1.9) [86].

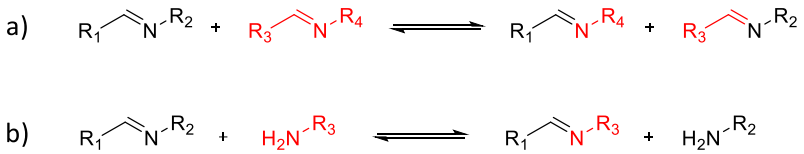

Scheme 1.9. Reversibility of imines via a) imine metathesis and b) transamination.

If the conditions are stoichiometric, the dynamic behavior comes from the imine metathesis (Scheme 1.9a). Alternatively, the leading exchange reaction is transamination if an excess of primary amines is present in the network (Scheme

1.9b). In any case, when preparing imines, the complete removal of water is crucial since these bonds can undergo hydrolysis in the presence of water, shifting the equilibrium of the reaction towards the formation of the starting monomers. In 2014, Taynton *et al.* reported the synthesis of different polyimine networks that exhibited Arrhenius-like malleability in response to heat, leading to 100% recycling efficiency through multiple generations [109]. Moreover, they showed that using water, the malleability of the polymer changes, and the material could be reshaped even at room temperature thanks to a reversible imine condensation/hydrolysis reaction. Later, they also demonstrated their applicability for repairable carbon fiber composites with full recyclability [110]. In addition, imines offer intriguing chemistry prospects, as they allow the synthesis of polyimine materials from bio-based compounds such as vanillin or different furans, among many others [111–113]. Imine materials also show exciting properties, such as self-healing, self-welding or 3D-printing [114,115].

Nevertheless, not only imine groups can undergo transamination exchange reactions. Lehn and co-workers reported the preparation of "dynamers", which were poly(acylhydrazone) materials synthesized by the reaction of dialdehydes and dihydrazides [116]. They demonstrated that these groups behave dynamically in the presence of additional aldehydes or hydrazides promoted by acid catalysis thanks to the imine group in the acylhydrazone moiety [117].

1.4.2.4 Transcarbamoylation

The high importance of polyurethanes (PUs) in the polymer industry and their great applicability makes that deep studies on their possible reshapability and recyclability have been performed. The transcarbamoylation reaction involves two urethane units. Nevertheless, it has been demonstrated that this reaction can proceed *via* associative or dissociative pathways depending on the chemical environment of the urethane units (Scheme 1.10).

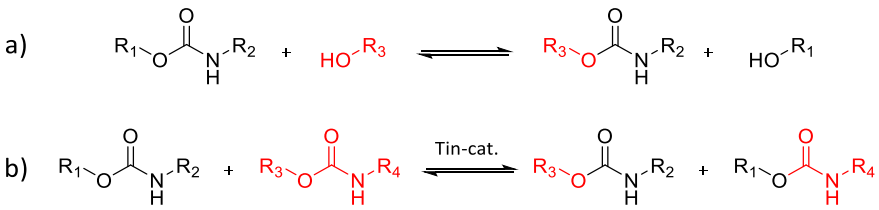

Scheme 1.10. a) Hydroxyl-mediated transcarbamoylation (associative) and b) Tin-mediated transcarbamoylation (dissociative).

In the presence of hydroxyl groups in the network, transcarbamoylation proceeds *via* an associative pathway without needing a catalyst, similar to a transesterification reaction [118]. On the other hand, when no hydroxyl groups are present in the

network, the exchange reaction undergoes a dissociative mechanism towards forming isocyanate and hydroxy groups that will further react to reform the PU network [119]. This is promoted by Lewis-acid catalysts such as dibutyltin dilaurate (DBTDL). Even though the hydroxy-mediated transcarbamoylation is not as efficient as the dissociative counterpart, polyhydroxy urethanes (PHUs) can be afforded by a greener and more sustainable approach since their synthesis starts from carbonates and amines instead of from isocyanates [120].

More recently, thiols, the sulfur analogous to alcohols, have been used to prepare polythiourethanes through a thiol-isocyanate click reaction [121–124]. In these materials, the exchange reaction, in this case, transthiocarbamoylation, can proceed in the same ways as PUs. These materials are gaining particular interest not only for their homogeneity or excellent mechanical properties but also for their high refractive indexes, which enable the preparation of optical materials [125].

1.4.2.5 Olefin metathesis

Guan and coworkers first reported this reaction in adaptive materials in 2012 by incorporating a Grubbs 2nd generation Ru catalyst in polybutadiene [126]. They obtained lightly crosslinked samples with high malleability at room temperature enabled by the olefin metathesis (Scheme 1.11).

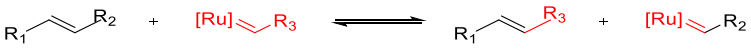

Scheme 1.11. Olefin metathesis promoted by Ru Grubbs catalyst.

They demonstrated that the use of catalysts is crucial in the obtention of dynamic networks since samples without Grubbs catalysts did not show stress relaxation behavior and malleability. Moreover, as expected, the higher the loads of catalysts, the higher the dynamic performance. Finally, when the catalyst was added, these materials revealed good self-healing abilities at sub-ambient temperatures. Catalyst-free materials did not show self-healing capabilities *a priori*, but when small amounts of Ru catalyst were applied to the fracture surface, this was completely healed [127].

Nevertheless, due to the extremely malleability and adaptability of the materials at room temperature, they revealed creep phenomena, compromising their possible applications at service temperatures. For this reason, the same group proposed incorporating secondary amide side chains to generate hydrogen bonds in the polymer structure that could enhance the mechanical performance of the materials [128].

1.4.2.6 Transamination of vinylogous urethanes

It was Pomposo and coworkers who, for the first time, prepared dynamic vinylogous urethane polymers for pH-responsive nanoparticles as a proof of concept [129]. Nevertheless, Du Prez's group explored their potential use for crosslinked dynamic thermosetting materials [130]. These materials can be prepared by the reaction of polyfunctional acetoacetate esters with primary amines. The transamination of vinylogous urethanes (VUs) always requires an excess of amines and occurs *via* an associative mechanism. However, depending on the environment of the vinylogous urethane, aprotic or protic, the reaction undergoes through a Michael-type addition or the formation of an iminium intermediate [131]. The general transamination reaction is shown in Scheme 1.12.

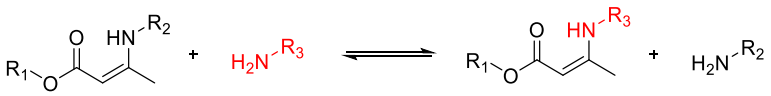

Scheme 1.12. Reversible transamination reaction of vinylogous urethanes.

Recently, Engelen *et al.* showed how the preparation of vinylogous urethanes can be performed from a sustainable point of view by synthesizing a diamine-derivative of vanillin and acetyl acetoacetate-derivative from a terpene [132]. They demonstrated that these polymers, with a high renewable carbon content (86%), had extremely fast exchange rates enhanced by β-hydroxy-amine groups. Later on, Lijsebetten *et al*. proposed the incorporation of masked amines in the network that, at high temperatures, are released, enabling rapid stress relaxation, but at low temperatures, they cannot react, thus improving the creep resistance at service temperatures [133]. Finally, Weder and coworkers could achieve complete depolymerization of vinylogous urethane, quantitively recovering the initial acetoacetate monomer, which was able to be re-polymerized [134]. This puts on stand the characteristics of VUs for enhanced closed-loop recyclability.

1.4.2.7 Transalkylation of triazolium salts

Drockenmuller and coworkers first described the use of transalkylation exchange reactions in covalent adaptable networks inspired by their ion-conducting polymer materials [135]. They reported the catalyst-free and solvent-free synthesis of poly(1,2,3-triazolium) networks from the stoichiometric amounts of azide, alkyne, and quaternizing groups. Moreover, an extensive study with model compounds showed that transalkylation reactions may proceed *via* an associative mechanism. Materials also confirmed this behavior with an Arrhenius-type dependence of the viscosity with the temperature and their insolubility at high temperatures in different solvents. The reaction is shown in Scheme 1.13.

Scheme 1.13. Transalkylation of 1,2,3 triazolium networks.

However, further studies demonstrated that the trans-*N*-alkylation occurs through a dissociative mechanism, even displaying rheological behavior almost indiscernible from vitrimers [95,136]. This was the first study that published a possible vitrimer-like behavior of the networked material, demonstrating that even having groups that can be transformed by a chemical dissociative mechanism, materials could follow Arrhenius-dependence and could maintain the polymer connectivity constant.

These materials also revealed self-healing properties and are known to be very useful for applications in solid electrolytes [137].

1.4.2.8 Boronic esters and dioxaborolanes

Guan and coworkers first reported the use of boronic esters in dynamic chemistry in 2015 [138]. They synthesized crosslinked polymers that contained free diols and boronic esters, which enabled the associative-type exchange reaction, resulting in highly malleable, reprocessable, and self-healable vitrimers (see Scheme 1.14a).

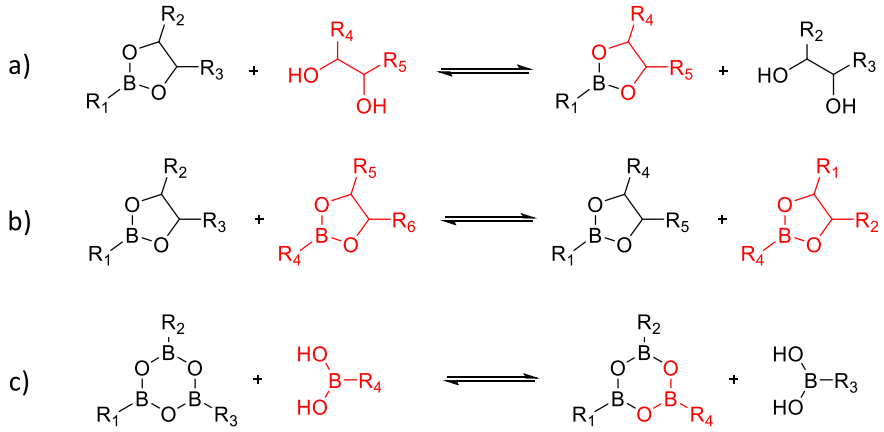

Scheme 1.14. a) Exchange reaction between boronic esters and diols, b) metathesis of dioxaborolane and c) boroxine exchange.

A few years later, Leibler and coworkers demonstrated by model compounds that in a hydroxyl-free network, dioxaborolane metathesis can also occur (Scheme 1.14b) [139]. Moreover, they could prepare a thermoplastic that was crosslinked through dioxaborolane metathesis, converting a thermoplastic into a vitrimer for the first time,

which could also be extruded [140]. Finally, they show a higher resistance to hydrolysis of dioxaborolane networks than hydroxyl-containing boronic ester networks.

Guan's group also prepared crosslinked networks with boroxine moieties [141]. This 6-membered heterocyclic of alternating oxygen and boron atoms could undergo a rapid boroxine exchange at 55 °C, displaying an Arrhenius-type dependence which demonstrated their vitrimeric behavior (Scheme 1.14c). In addition, these materials could be recycled, and the starting monomer could be recovered after water treatment.

1.4.2.9 Silyl ether exchange

The dynamic equilibrium of silyl ether was reported in 2017 by Nishimura *et al.* in which they crosslinked a styrene-based copolymer with bis-alkoxysilanes through pendant hydroxyl groups functionalized on the styrene monomer units [142]. The materials exhibited high thermal stability and full reprocessability after hot-pressing them, thanks to the addition/elimination reaction (Scheme 1.15a).

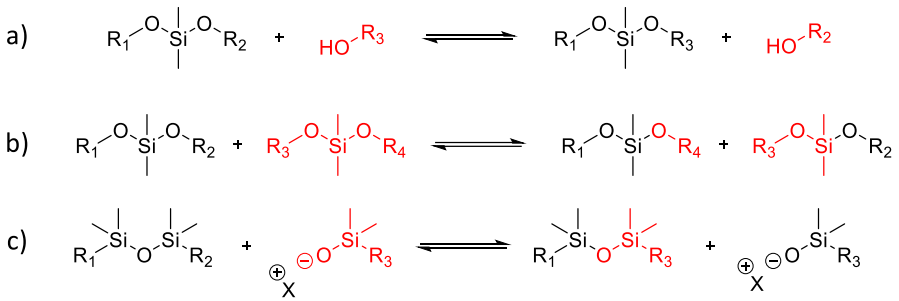

Scheme 1.15. a) Exchange of silyl ether and hydroxyl groups and b) silyl ether metathesis and c) siloxane exchange.

Later, the same group unveiled that silyl ether groups can undergo direct exchange without free alcohols via acid-catalyzed metathesis of silyl ether groups (Scheme 1.15b) [143]. The outcome was malleable thermosets exhibiting remarkable thermal and oxidative stability attributed to the lack of free alcohol groups.

Another type of vitrimers based on Si chemistry are the siloxanes, which undergo a similar exchange mechanism as silyl ether and alcohols but, in this case, are usually base-catalyzed, thus generating the corresponding alkoxide (Scheme 1.15c) [144]. Since then, this chemistry has been implemented involving different types of monomers and for different types of applications such as self-healing or composites [145,146].

1.4.2.10 Disulfide interchange and thiol exchange

Since Stern and Tobolsky published stress-time-temperature relations in polysulfide rubbers in the 1940s [82], many researchers have put their efforts into the preparation of polymers containing disulfide links in their structure thanks to its great malleability, recyclability, and excellent self-healable properties. For example, Tesoro *et al*., reported the synthesis of epoxy resins with dihydrazides and diamines that contained disulfide bonds in their monomer structure [147]. They were able to reversibly break and reform these bonds by reducing and oxidizing the disulfide.

Nevertheless, Klumperman and coworkers described for the first time the dynamic disulfide metathesis mechanism and a thiol-disulfide exchange both for self-healing processes (Scheme 1.16) [88,148].

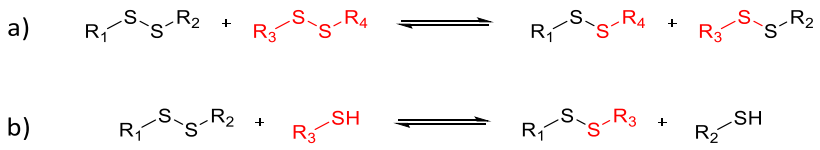

Scheme 1.16. a) Disulfide metathesis and b) Thiol-disulfide exchange.

More recently, Ruiz de Luzuriaga *et al.* put on the stand the disulfide metathesis on aromatic disulfide bonds in epoxy resins with excellent reprocessability and recyclability while maintaining excellent thermomechanical properties that could be implemented in the transportation of energy and construction industries [149].

Nonetheless, while the thiol-disulfide exchange mechanism seems to occur through an associative mechanism, *via* addition/elimination substitution with free thiols, in the disulfide metathesis, the mechanism is still unclear. The presence of carbon radicals, nucleophiles, or free thiols influences the kinetics of disulfide exchange, prompting the mechanism to adopt either a dissociative or associative mechanism [150]. For this reason, usually, these materials are classified as vitrimer-like polymers.

Moreover, the nucleophiles play a role in increasing the relaxation rates. Rekondo and coworkers reported the synthesis of multiple disulfide materials with excess primary amines and tertiary-amine catalysts, demonstrating faster relaxation in the last case [96]. Also, phosphines are great catalysts for this exchange reaction, as Ramström and coworkers reported [151].

Michal *et al.* exhibited an alternative facet of disulfide metathesis wherein photoactivation plays a pivotal role [152]. This was exemplified through the preparation of photo-healable polydisulfide networks in which the application of UV irradiation rapidly mended cracks, demonstrating a great self-healing ability.

The great interest in this type of covalent adaptable network also relies on the possibility of easily synthesizing monomers containing disulfide bonds or derived from renewable resources such as vanillin or eugenol or using hardeners incorporating this dynamic bond in their structure [153].

In light of this, disulfide materials are widely used in many industrial applications such as self-healing, self-welding, shape-memory, composites, or adhesion [154,155].

1.4.2.11 Reversible Michael-type additions

While the Michael addition has been employed for more than 130 years to synthesize a vast diversity of compounds, the reversibility of this reaction when heteronucleophiles are involved, has been generally less considered. The reaction involves the addition of a nucleophile, such as thiols or amines, over a Michael acceptor.

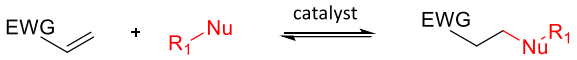

Scheme 1.17. Reversible Michael-addition reaction.

Konkolewicz and coworkers demonstrated the reversible behavior of thio-Michael addition using model compounds [156]. Additionally, they prepared polymers of 2-hydroxyethyl acrylate crosslinked with a thiol-acrylate-based crosslinker, displaying properties such as rehealing and malleability, and dynamic behavior at elevated temperatures. Later, the same group reported that this type of materials could also be malleable upon exposure to pH-stimuli [157].

More recently, the group of Du Prez synthesized β-amino esters from commercially available di and tri acrylates and amines that showed excellent reprocessability and good thermal stability [158]. Moreover, using model compounds, they could prove the reversibility of the aza-Michael reaction, later confirmed by the excellent relaxation rates of these materials. One year later, they synthesize fully biobased β- amino esters with different crosslinking densities that show high creep resistance up to 120 °C and good reprocessability at 180 °C [159].

However, the development of these materials is still in the early stages. Further investigations will indeed be done, thanks to the great properties which can lead to new avenues for industrial fields [87].

1.4.2.12 Neighboring group participation (NGP)

It has to be mentioned that this process is not an exchange bond mechanism itself. However, the effect of neighboring groups in a network can drastically affect the

dynamic behavior of an exchange mechanism. For this reason, it is considered to mention this effect briefly.

Du Prez and coworkers reported for the first time a dissociative-type transesterification reaction [160]. This could be due to the neighboring group participation of free-carboxylic acids in phthalate monoesters. The reaction *via* the addition of the carboxylic acid to the ester forms phthalic anhydride and alcohol that reversibly undergo again the formation of phthalate monoesters (Scheme 1.18).

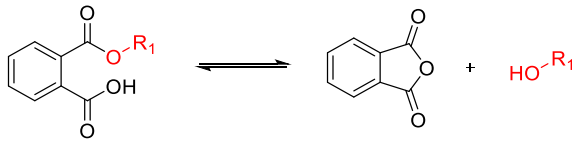

Scheme 1.18. Transesterification reaction in phthalate monoesters.

Later, a similar effect was reported when mono-esterified cyclic maleic and succinic anhydrides were cured with epoxy resins in off-stoichiometric conditions [161]. The stress relaxation and reprocessability could be achieved thanks to dynamic transfer catalysis.

In 2021, Lijsebetten *et al.* reported the introduction of internally catalyzed amide bonds based on the dissociation equilibrium between dicarboxamides and imides [162]. Since the dynamic behavior involved the formation of an imide, the proper selection of the corresponding esters is essential for the dynamic properties due to the ring-size effect of the imide. However, polyamides could be easily reprocessed and displayed higher creep resistance at service temperatures.

1.5 Applications of CANs

As it has been seen, many chemistries have been used in synthesizing covalent adaptable networks since they can be recycled or reprocessed, offering an outstanding solution from the sustainability point of view. Their recyclability, which is more successful and far less energetically demanding in comparison to thermosets, enables the reuse of the polymer material reducing the possible amount of polymer waste in landfills or preventing them from incinerating. Additionally, their unique properties and characteristics makes them extremely interesting for many different fields.

1.5.1 Self-healing and self-welding capabilities

Manufacturing defects, improper usage, or prolonged stress can lead to minor damages in the material, often incongruent with its intended application. Without

mechanical intervention, materials with self-healing capabilities can mend such minor damages, significantly extending their lifespan.

However, the terms self-healing and self-welding need to be differentiated. The distinction lies in their purpose: while self-healing targets the rectification of minor imperfections arising from manufacturing or usage, self-welding aims to join larger surface areas (Figure 1.10). In both cases, the main objective is to maintain the thermomechanical properties of the original material.

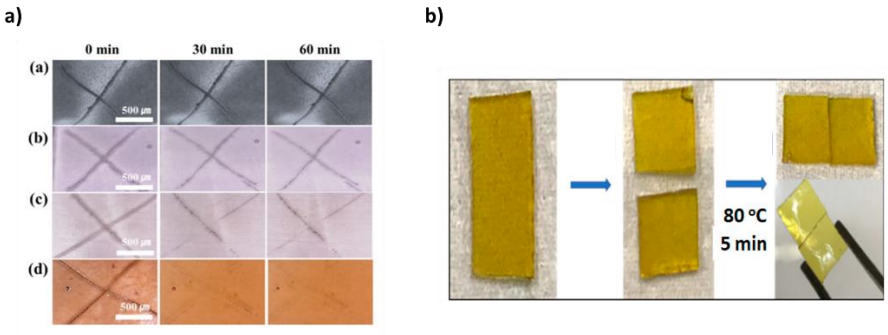

Figure 1.10. a) Photographs of self-healing examples by [163] and b) example of self-welding capabilities extracted from [164].

This is one of the most critical applications in CANs due to their dynamic behavior at high temperatures. It enables a certain flow that can self-healed or self-weld damage or fracture. Diels-Alder, imine metathesis, or disulfide exchange covalent adaptable networks are the main ones used for self-healing and self-welding [107,152,163].

1.5.2 Adhesion

Adhesives are materials with applications in several fields, even in daily-life usage. The more commercial adhesives are epoxy or acrylic resins, polyurethanes, or phenolic resins. In this field, CANs have a significant impact. Their ability to flow at high temperatures leads to a maximum contact surface, guaranteeing better adhesion. Moreover, the exchange reactions at elevated temperatures can enable the debonding or dismantling of the adhesive substrates and the subsequent rebounding. The concentration of dynamic bonds, activation energy and kinetics directly correlate with the adhesive strength.

In our group, Santiago and coworkers recently developed epoxy-based vitrimeric reversible adhesives from combinations of DGEBA, glutaric anhydride, and glycerol [165]. Apart from demonstrating the recyclability, dynamic behavior, and reprocessability of the materials, the debonding and dismantling of these adhesives were tested, obtaining high values of adhesive strength, which were slightly lower than the original material.

Later, Van Lijsebetten *et al.* prepared epoxy adhesives by hardening epoxy monomers and two synthesized polyamidoamines [166]. The dynamic behavior is based on the amide-imide exchange described in the previous section. They could demonstrate that as the debonding/rebonding process is more thermally demanding and, more thermally robust than previously reported CANs, the resulting materials can be triggered at high temperatures and, at the same time, remain bonded over a wide range of temperatures.

1.5.3 3D-Printing

3D-printing is a powerful tool for manufacturing small-scale components with high precision and resolution. There are stereolithographic 3D printers, where the laser moves along the material surface, and injection 3D printers, where the material is poured and cured over a substrate. Recently, 3D printers based on extrusion, where a viscous resin is applied in an injector, and then photo or thermal cured have appeared. Due to their mechanical and thermal performance, thermosetting materials are preferred over thermoplastics for some applications. However, these materials cannot be recycled and reprocessed; thus, vitrimers are gaining a great interest in this technique.

Acrylate polymers are extensively used in this technique since they could be photo or thermal-cured and are widely available in the market. Schlögl and coworkers developed a thiol-acrylate system that could be photocured and 3D-printed [100]. They covalently introduced a new transesterification catalyst in the network that enabled the stress relaxation of the network. They could print precise 3D objects with triple shape memory and thermal mendability, demonstrating the incredible versatility of these materials for functional devices in soft robotics or biomedicine.

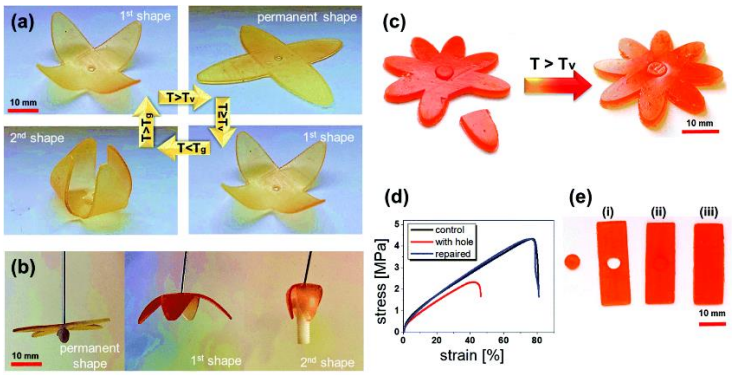

Figure 1.10. Examples of 3D-printed structures and triple shape memory capabilities [100].

Stouten *et al.* recently prepared a biobased photopolymer acrylate derived from renewable vanillin and Priamine 1075 [167]. To achieve a crosslinked polymer, tris(2-

aminoethyl) amine (TREN) was also added. Materials containing imine dynamic groups could be 3D-printed, obtaining high-resolution objects. Moreover, they demonstrated that materials could be recycled up to 3 times without losing mechanical and dynamic behavior.

1.5.4 Shape memory

Polymers possessing shape memory (SMPs) can retain a temporary shape until they are subjected to an external stimulus, such as temperature, light, pressure or pH. At this point, they recover the original shape. These polymers fall within the realm of smart polymers, which display responsiveness beyond mere mechanical reactions. The shape memory attribute is not inherently ingrained in the material but rather emerges from a combination of three different factors: structure, morphology and thermal treatment.

In these polymers, when the temperature is above the T_g, the mobility of the chains increases. If, at this point, a force is imposed, these changes will rearrange along the force's orientation, causing a reduction in their entropy. Upon cooling ($T<T_g$) and sustaining the applied force, the mobility of the chains is reduced, thus disabling them to return to their initial maximum entropy. This results in the storage of tension as potential energy in which the stimulus supplies the energy necessary to release this stored tension, thereby inducing material movement.

Nevertheless, SMPs can only retain two shapes, the fixed and the programmed one, so introducing vitrimers in this field may overcome this problem since the possibility to generate a permanent shape can allow multiple shape memory effect. This can happen by increasing the temperature above the T_v and then applying a force during a determined time. Then, by cooling down, the shape will be fixed, enabling the possibility of programming a new form if the material is heated only above the T_g.

Epoxy vitrimers, polyurethanes and polythiourethanes are the most used thermosetting vitrimeric materials in this technique, enabling the creation of complex shapes in the materials [122,168,169].

1.5.5 Composites

Composite materials are formulations of two or more incompatible materials that exhibit properties surpassing those of their individual components. The phases involved can be organic, mineral, or metallic, which results in endless possibilities combined with various fillers, morphologies and preparation methods. The main disadvantage of these materials relies on their heterogeneity and challenges related to phase dispersion [170].

As the demand for composite materials increases, the challenge of their recycling becomes a severe problem due to the disentangling of the filler from the matrix. Composites can be recycled through mechanical, thermal or chemical methods [171]. Additionally, recycling becomes even more complex if the polymeric matrix does not achieve a fluid state upon heating and instead degrades. This predicament becomes exceptionally intricate for composite endowed with thermosetting matrices, which have excellent mechanical and thermal properties but, at the same time, are not recyclable. Replacing these thermosetting matrices with vitrimers makes recycling of such materials more feasible. Among the commonly employed matrices are epoxy resins based on different dynamic linkages [172]. As an example, Zhao *et al.*, reported the preparation of a novel biobased guaiacol epoxy resin that was cured with 4-aminophenyl disulfide [173]. The vitrimer had appreciable thermal stability, good mechanical properties, and considerable stress relaxation. Moreover, they prepared carbon fiber composites that could be completely recovered by dissolving the polymer matrix in a mixture of dimethyl formamide (DMF) and 2-mercaptoethanol that promotes the thiol-disulfide exchange. Carbon allotropes, such as carbon fibers, nanotubes, and graphene, have been explored as fillers [174].

1.6 Objectives

1.6.1 Goals of the thesis

The main objective of this doctoral thesis is the design, exploration and development of emerging methodologies to prepare thermosetting materials employing sustainability-driven techniques like dual curing, click chemistry, the use of renewable resources, and the utilization of dynamic chemistry.

The work of this thesis has been divided into several chapters were the objectives and goals can be resumed in four different sections:

1) Development of novel dual-curing methodologies for preparing thermosetting materials from commercially available monomers and renewable feedstocks. Detailly, the following objectives where identified:

    a. Study of the viability of the epoxy-amine and methacrylate homopolymerization reactions in a dual-curing system and its characterization through isoconversional, rheological and dynamic mechanical analysis.
    b. Investigation of a photo-thermal dual curing using (meth)acrylates, epoxides and thiols, understanding their reactivity and optimization of the initial formulation for adequate properties of the materials.

c. Design and characterization of a novel dual-curing system entirely derived from renewable resources like eugenol, glycerol and pentaerythritol.

2) Preparation of new vitrimeric materials based on different dynamic bonds by click methodologies and starting from renewable feedstocks. The specific objectives of this section were the following:

   a. Development of recyclable thermosetting materials derived from biobased vanillin and glutaric, sebacic and dodecanedioic acids, and comprehending their dynamic exchange through model compounds and thermomechanical analysis.
   b. Synthesis of an imine-containing epoxy monomer, further preparation of crosslinked vitrimeric materials through epoxy-amine reaction and study of their recyclability and degradability.
   c. Design of dynamic materials from natural eugenol and cystamine, study their thermomechanical properties, and investigation of the catalytic effect of covalently linked tertiary amines win the disulfide exchange.

3) Study the thermomechanical behavior of vitrimeric materials and evaluation of their potential applications in self-healing, self-welding and adhesion fields. More in detail, the objectives are identified as the following:

   a. Characterization of the mechanical properties of disulfide materials from commercially available monomers, understanding their viscoelastic properties and demonstration of their self-healing abilities.

   b. Design of reversible adhesives based on dynamic transesterification reaction and study of their properties at service temperatures.

4) Development of new reprocessable materials from renewable feedstocks using dual-curing methodologies and click chemistry.

All these objectives and goals aim to learn and acquire knowledge about all the different techniques used, the design of new structures and novel materials and the evaluation of their characteristics and properties.

1.6.2 Observations for the reader

This thesis work is presented as a compilation of scientific papers published or submitted during the PhD period.

We have studied and characterized four different dual-curing systems; i) Epoxy-amine and methacrylate homopolymerization using glycidyl methacrylate, ii) photo-thermal dual-curing of (meth)acrylate-epoxy thiol formulations, iii) dual-cured thermosets based on eugenol derivatives and biobased thiols, and iv) eugenol-based dual-curing systems with dynamic exchangeable bonds using amines as hardeners. Moreover, five different exchangeable bonds: i) acylhydrazones, ii) imines, iii) disulfide, iv) esters, and v) β-amino esters were characterized and analyzed through thermomechanical, stress-relaxation, creep and rheological analyses as well as possible applications such as self-healing, self-welding, adhesion or shape-memory.

References

[1] Dunlap, R. E.; Jorgenson, A. K. Environmental Problems. In The Wiley-Blackwell Encyclopedia of Globalization; John Wiley & Sons, Ltd, **2012**.

[2] Anastas, P. T.; Warner, J. C. Green Chemistry: Theory and Practice; Oxford University Press, **1998**.

[3] Barnes, D. K. A.; Galgani, F.; Thompson, R. C.; Barlaz, M. *Philos. Trans. R. Soc. B Biol. Sci.* **2009**, *364*, 1985–1998.

[4] Rhodes, C. J. Plastic Pollution and Potential Solutions. *Sci. Prog.* **2018**, *101*, 207–260.

[5] The New Plastics Economy: Rethinking the future of plastics. https://ellenmacarthurfoundation.org/the-new-plastics-economy-rethinking-the-future-of-plastics (accessed 2023-08-03).

[6] Geyer, R.; Jambeck, J. R.; Law, K. L. *Sci. Adv.* **2017**, *3*, e1700782.

[7] Sheldon, R. A.; Norton, M. *Green Chem.* **2020**, *22*, 6310–6322.

[8] Ebewele, R. O. Polymer Science and Technology; CRC Press: Boca Raton, Florida, **2000**.

[9] Grigore, M. E. Methods of Recycling, Properties and Applications of Recycled Thermoplastic Polymers. *Recycling* **2017**, *2*, 24.

[10] Harrison, R. M.; Hester, R. E. Plastics and the Environment; Royal Society of Chemistry: United Kingdom, **2018**.

[11] Brazel, C. S.; Rosen, S. L. Fundamental Principles of Polymeric Materials; John Wiley & Sons, **2012**.

[12] Pascault, J. P.; Sautereau, H.; Verdu, J.; Williams, R. J. J. Thermosetting Polymers; CRC Press: New York, USA, **2002**.

[13] Guo, Q. Thermosets: Structure, Properties, and Applications, 2nd edition.; Elsevier: Amsterdam, Netherlands, **2017**.

[14] Nguyen, H.; Zatar, W.; Mutsuyoshi, H. 4 - Mechanical Properties of Hybrid Polymer Composite. In Hybrid Polymer Composite Materials; Thakur, V. K., Thakur, M. K., Pappu, A., Eds.; Woodhead Publishing, **2017**, 83–113.

[15] Directive 2008/98/EC of the European Parliament and of the Council of 19 November 2008 on Waste and Repealing Certain Directives (Text with EEA Relevance); 2008; Vol. 312. http://data.europa.eu/eli/dir/2008/98/oj/eng (accessed 2023-08-04).

[16] Konuray, A. O.; Fernández-Francos, X.; Serra, À.; Ramis, X. *Eur. Polym. J.* **2016**, *84*, 256–267.

[17] Lian, Q.; Li, Y.; Yang, T.; Li, K.; Xu, Y.; Liu, L.; Zhao, J.; Zhang, J.; Cheng, J. *J. Mater. Sci.* **2016**, *51*, 7887–7898.

[18] Kim, H.; Han, S.; Seo, Y. *Langmuir* **2020**, *36*, 9250–9258.

[19] Russo, C.; Fernandez-Francos, X.; De La Flor, S. *Express Polym. Lett*. **2021**, *15*, 58–71.

[20] Russo, C.; Bustamante, F.; Fernández-Francos, X.; De la Flor, S. *Int. J. Adhes. Adhes.* **2022**, *112*, 102959.

[21] Gamardella, F.; Sabatini, V.; Ramis, X.; Serra, À. *Polymer* **2019**, *174*, 200–209.

[22] Sherman, C. L.; Zeigler, R. C.; Verghese, N. E.; Marks, M. J. *Polymer* **2008**, *49*, 1164–1172.

[23] Fernández-Francos, X.; Santiago, D.; Ferrando, F.; Ramis, X.; Salla, J. M.; Serra, À.; Sangermano, M. J. *Polym. Sci. Part B Polym. Phys.* **2012**, *50*, 1489–1503.

[24] Studer, J.; Dransfeld, C.; Masania, K. *Compos. Part Appl. Sci. Manuf.* **2016**, *87*, 282–289.

[25] White, S. R.; Kim, Y. K. *Compos. Part Appl. Sci. Manuf.* **1996**, *27*, 219–227.

[26] Konuray, O.; Areny, N.; Morancho, J. M.; Fernández-Francos, X.; Serra, À.; Ramis, X. *Polymer* **2018**, *146*, 42–52.

[27] Guzmán, D.; Ramis, X.; Fernández-Francos, X.; Serra, A. *Eur. Polym. J.* **2014**, *59*, 377–386.

[28] Decker, C.; Masson, F.; Schwalm, R. *Macromol. Mater. Eng.* **2003**, *288*, 17–28.

[29] Kolb, H. C.; Finn, M. G.; Sharpless, K. B. *Angew. Chem. Int. Ed.* **2001**, *40*, 2004–2021.

[30] Moses, J. E.; Moorhouse, A. D. *Chem. Soc. Rev.* **2007**, *36*, 1249–1262.

[31] Xi, W.; Scott, T. F.; Kloxin, C. J.; Bowman, C. N. *Adv. Funct. Mater.* **2014**, *24*, 2572–2590.

[32] Carlborg, C. F.; Vastesson, A.; Liu, Y.; van der Wijngaart, W.; Johansson, M.; Haraldsson, T. *J. Polym. Sci. Part Polym. Chem.* **2014**, *52*, 2604–2615.

[33] Konuray, A. O.; Liendo, F.; Fernández-Francos, X.; Serra, À.; Sangermano, M.; Ramis, X. *Polymer* **2017**, *113*, 193–199.

[34] Guzmán, D.; Ramis, X.; Fernández-Francos, X.; Serra, A. *RSC Adv.* **2015**, *5*, 101623–101633.

[35] Guzmán, D.; Serra, A.; Ramis, X.; Fernández-Francos, X.; De la Flor, S. *React. Funct. Polym.* **2019**, *136*, 153–166.

[36] Retailleau, M.; Ibrahim, A.; Croutxé-Barghorn, C.; Allonas, X. *Prog. Org. Coat.* **2016**, *100*, 51–55.

[37] Berne, D.; Lemouzy, S.; Guiffrey, P.; Caillol, S.; Ladmiral, V.; Manoury, E.; Poli, R.; Leclerc, E. *Chem. – Eur. J.* **2023**, *29*, e202203712.

[38] Tian, Y.; Wang, Q.; Cheng, J.; Zhang, J. *Green Chem.* **2020**, *22*, 921–932.

[39] Lowe, A. B. *Polymer* **2014**, *55*, 5517–5549.

[40] Yang, K.; Grant, J. C.; Lamey, P.; Joshi-Imre, A.; Lund, B. R.; Smaldone, R. A.; Voit, W. *Adv. Funct. Mater.* **2017**, *27*, 1700318.

[41] Yan, J.; Ariyasivam, S.; Weerasinghe, D.; He, J.; Chisholm, B.; Chen, Z.; Webster, D. *Polym. Int.* **2012**, *61*, 602–608.

[42] Dai, Y.; Zhang, X.; Xia, F. *Macromol. Rapid Commun.* **2017**, *38*, 1700357.

[43] Schneiderman, D. K.; Hillmyer, M. A. *Macromolecules* **2017**, *50*, 3733–3749.

[44] Janik, H.; Sienkiewicz, M.; Kucinska-Lipka, J. Handbook of Thermoset Plastics; Elsevier Inc. San Diego USA, **2004**.

[45] Baroncini, E. A.; Kumar Yadav, S.; Palmese, G. R.; Stanzione III, J. F. *J. Appl. Polym. Sci.* **2016**, *133*, 44103.

[46] Ma, S.; Li, T.; Liu, X.; Zhu, J. *Polym. Int.* **2016**, *65*, 164–173.

[47] Vidil, T.; Llevot, A. *Macromol. Chem. Phys.* **2022**, *223*, 2100494.

[48] Supanchaiyamat, N.; Shuttleworth, P. S.; Hunt, A. J.; Clark, J. H.; Matharu, A. S. *Green Chem.* **2012**, *14*, 1759–1765.

[49] Takahashi, T.; Hirayama, K.; Teramoto, N.; Shibata, M. *J. Appl. Polym. Sci.* **2008**, *108*, 1596–1602.

[50] Jin, F.-L.; Park, S.-J. *Polym. Int.* **2008**, *57*, 577–583.

[51] Uyama, H.; Kuwabara, M.; Tsujimoto, T.; Kobayashi, S. *Biomacromolecules* **2003**, *4*, 211–215.

[52] Monica, F. D.; W. Kleij, A. *Polym. Chem.* **2020**, *11*, 5109–5127.

[53] Schutz, L.; Kazemi, F.; Mackenzie, E.; Bergeron, J.-Y.; Gagnon, E.; Claverie, J. P. *J. Polym. Sci.* **2021**, *59*, 321–328.

[54] Mija, A.; Louisy, E.; Lachegur, S.; Khodyrieva, V.; Martinaux, P.; Olivero, S.; Michelet, V. *Green Chem.* **2021**, *23*, 9855–9859.

[55] Dussenne, C.; Delaunay, T.; Wiatz, V.; Wyart, H.; Suisse, I.; Sauthier, M. *Green Chem.* **2017**, *19*, 5332–5344.

[56] Feng, X.; East, A. J.; Hammond, W. B.; Zhang, Y.; Jaffe, M. *Polym. Adv. Technol.* **2011**, *22*, 139–150.

[57] Tong, X.; Ma, Y.; Li, Y. *Appl. Catal. Gen.* **2010**, *385*, 1–13.

[58] Eid, N.; Ameduri, B.; Boutevin, B. *ACS Sustain. Chem. Eng.* **2021**, *9*, 8018–8031.

[59] Hu, F.; Yadav, S. K.; La Scala, J. J.; Sadler, J. M.; Palmese, G. R. *Macromol. Chem. Phys.* **2015**, *216*, 1441–1446.

[60] Jung, J. Y.; Park, C.-H.; Lee, E. Y. *J. Wood Chem. Technol.* **2017**, *37*, 433–442.

[61] Zhao, S.; Abu-Omar, M. M. *ACS Sustain. Chem. Eng.* **2017**, *5*, 5059–5066.

[62] Scarica, C.; Suriano, R.; Levi, M.; Turri, S.; Griffini, G. *ACS Sustain. Chem. Eng.* **2018**, *6*, 3392–3401.

[63] Hocking, M. B. *J. Chem. Educ.* **1997**, 74, 1055.

[64] Fache, M.; Boutevin, B.; Caillol, S. *ACS Sustain. Chem. Eng.* **2016**, *4*, 35–46.

[65] Fache, M.; Boutevin, B.; Caillol, S. *Eur. Polym. J.* **2015**, *68*, 488–502.

[66] Fache, M.; Auvergne, R.; Boutevin, B.; Caillol, S. *Eur. Polym. J.* **2015**, *67*, 527–538.

[67] Fache, M.; Viola, A.; Auvergne, R.; Boutevin, B.; Caillol, S. *Eur. Polym. J.* **2015**, *68*, 526–535.

[68] Zhi, M.; Yang, X.; Fan, R.; Yue, S.; Zheng, L.; Liu, Q.; He, Y. *ACS Appl. Polym. Mater.* **2023**, *5*, 1312–1324.

[69] Hartnoll, G.; Moore, D.; Douek, D. *Arch. Dis. Child.* **1993**, *69*, 392–393.

[70] Kamatou, G. P.; Vermaak, I.; Viljoen, A. M. *Molecules* **2012**, *17*, 6953–6981.

[71] Faye, I.; Decostanzi, M.; Ecochard, Y.; Caillol, S. *Green Chem.* **2017**, *19*, 5236–5242.

[72] Guzmán, D.; Ramis, X.; Fernández-Francos, X.; De la Flor, S.; Serra, A. *Eur. Polym. J.* **2017**, *93*, 530–544.

[73] Gutiérrez, T. J. Reactive and Functional Polymers Volume Four: Surface, Interface, Biodegradability, Compostability and Recycling; Springer Nature, **2020**.

[74] Oliveux, G.; Dandy, L. O.; Leeke, G. A. *Prog. Mater. Sci.* **2015**, *72*, 61–99.

[75] Bernardeau, F.; Perrin, D.; Caro-Bretelle, A.-S.; Benezet, J.-C.; Ienny, P. *J. Mater. Cycles Waste Manag.* **2018**, *20*, 1320–1336.

[76] Al-Salem, S. M.; Antelava, A.; Constantinou, A.; Manos, G.; Dutta, A. *J. Environ. Manage.* **2017**, *197*, 177–198.

[77] Post, W.; Susa, A.; Blaauw, R.; Molenveld, K.; Knoop, R. J. I. *Polym. Rev.* **2020**, *60*, 359–388.

[78] Garcia, S. J. *Eur. Polym. J.* **2014**, *53*, 118–125.

[79] Wojtecki, R. J.; Meador, M. A.; Rowan, S. J. *Nat. Mater.* **2011**, *10*, 14–27.

[80] Khan, A.; Ahmed, N.; Rabnawaz, M. *Polymers* **2020**, *12*, 2027.

[81] Montarnal, D.; Capelot, M.; Tournilhac, F.; Leibler, L. *Science* **2011**, *334*, 965–968.

[82] Stern, M. D.; Tobolsky, A. V. *Rubber Chem. Technol.* **1946**, *19*, 1178–1192.

[83] J. Kloxin, C.; N. Bowman, C. *Chem. Soc. Rev.* **2013**, *42*, 7161–7173.

[84] M. Winne, J.; Leibler, L.; Prez, F. E. D. *Polym. Chem.* **2019**, *10*, 6091–6108.

[85] Podgórski, M.; Fairbanks, B. D.; Kirkpatrick, B. E.; McBride, M.; Martinez, A.; Dobson, A.; Bongiardina, N. J.; Bowman, C. N. *Adv. Mater.* **2020**, *32*, 1906876.

[86] Denissen, W.; M. Winne, J.; Prez, F. E. D. *Chem. Sci.* **2016**, *7*, 30–38.

[87] Berne, D.; Ladmiral, V.; Leclerc, E.; Caillol, S. *Polymers* **2022**, *14*, 4457.

[88] Canadell, J.; Goossens, H.; Klumperman, B. *Macromolecules* **2011**, *44*, 2536–2541.

[89] Diels, O.; Alder, K. *Justus Liebigs Ann. Chem.* **1928**, *460*, 98–122.

[90] Lei, Q.-L.; Xia, X.; Yang, J.; Pica Ciamarra, M.; Ni, R. *Proc. Natl. Acad. Sci.* **2020**, *117*, 27111–27115.

[91] Elling, B. R.; Dichtel, W. R. *ACS Cent. Sci.* **2020**, *6*, 1488–1496.

[92] Cuminet, F.; Caillol, S.; Dantras, É.; Leclerc, É.; Ladmiral, V. *Macromolecules* **2021**, *54*, 3927–3961.

[93] Hayashi, M. *Polymers* **2020**, *12*, 1322.

[94] Chakma, P.; Morley, C. N.; Sparks, J. L.; Konkolewicz, D. *Macromolecules* **2020**, *53*, 1233–1244.

[95] Jourdain, A.; Asbai, R.; Anaya, O.; Chehimi, M. M.; Drockenmuller, E.; Montarnal, D. *Macromolecules* **2020**, *53*, 1884–1900.

[96] Ruiz de Luzuriaga, A.; Solera, G.; Azcarate-Ascasua, I.; Boucher, V.; Grande, H.-J.; Rekondo, A. *Polymer* **2022**, *239*, 124457.

[97] Altuna, F. I.; Hoppe, C. E.; Williams, R. J. J. *Eur. Polym. J.* **2019**, *113*, 297–304.

[98] Liu, T.; Hao, C.; Wang, L.; Li, Y.; Liu, W.; Xin, J.; Zhang, J. *Macromolecules* **2017**, *50*, 8588–8597.

[99] Hayashi, M.; Katayama, A. *ACS Appl. Polym. Mater.* **2020**, *2*, 2452–2457.

[100] Rossegger, E.; Höller, R.; Reisinger, D.; Strasser, J.; Fleisch, M.; Griesser, T.; Schlögl, S. *Polym. Chem.* **2021**, *12*, 639–644.

[101] Liu, T.; Zhao, B.; Zhang, J. *Polymer* **2020**, *194*, 122392.

[102] Wang, C.; Mavila, S.; Worrell, B. T.; Xi, W.; Goldman, T. M.; Bowman, C. N. *ACS Macro Lett.* **2018**, *7*, 1312–1316.

[103] Worrell, B. T.; Mavila, S.; Wang, C.; Kontour, T. M.; Lim, C.-H.; McBride, M. K.; Musgrave, C. B.; Shoemaker, R.; Bowman, C. N. *Polym. Chem.* **2018**, *9*, 4523–4534.

[104] Pratama, P. A.; Sharifi, M.; Peterson, A. M.; Palmese, G. R. *ACS Appl. Mater. Interfaces* **2013**, *5*, 12425–12431.

[105] Chen, X.; Dam, M. A.; Ono, K.; Mal, A.; Shen, H.; Nutt, S. R.; Sheran, K.; Wudl, F. *Science* **2002**, *295*, 1698–1702.

[106] Khan, N. I.; Halder, S.; Gunjan, S. B.; Prasad, T. *IOP Conf. Ser. Mater. Sci. Eng.* **2018**, *377*, 012007.

[107] Ratwani, C. R.; Kamali, A. R.; Abdelkader, A. M. *Prog. Mater. Sci.* **2023**, *131*, 101001.

[108] Xu, J.-F.; Chen, Y.-Z.; Wu, L.-Z.; Tung, C.-H.; Yang, Q.-Z. *Org. Lett.* **2013**, *15*, 6148–6151.

[109] Taynton, P.; Yu, K.; Shoemaker, R. K.; Jin, Y.; Qi, H. J.; Zhang, W. *Adv. Mater.* **2014**, *26*, 3938–3942.

[110] Taynton, P.; Ni, H.; Zhu, C.; Yu, K.; Loob, S.; Jin, Y.; Qi, H. J.; Zhang, W. *Adv. Mater.* **2016**, *28*, 2904–2909.

[111] Geng, H.; Wang, Y.; Yu, Q.; Gu, S.; Zhou, Y.; Xu, W.; Zhang, X.; Ye, D. *ACS Sustain. Chem. Eng.* **2018**, *6*, 15463–15470.

[112] Yu, Q.; Peng, X.; Wang, Y.; Geng, H.; Xu, A.; Zhang, X.; Xu, W.; Ye, D. *Eur. Polym. J.* **2019**, *117*, 55–63.

[113] Dhers, S.; Vantomme, G.; Avérous, L. *Green Chem.* **2019**, *21*, 1596–1601.

[114] Wu, J.; Yu, X.; Zhang, H.; Guo, J.; Hu, J.; Li, M.-H. *ACS Sustain. Chem. Eng.* **2020**, *8*, 6479–6487.

[115] Xu, Y.; Odelius, K.; Hakkarainen, M. *ACS Sustain. Chem. Eng.* **2020**, *8*, 17272–17279.

[116] Skene, W. G.; Lehn, J.-M. P. Proc. Natl. Acad. Sci. **2004**, *101*, 8270–8275.

[117] Lehn, J.-M. Dynamers: Dynamic Molecular and Supramolecular Polymers. *Prog. Polym. Sci.* **2005**, *30*, 814–831.

[118] Fortman, D. J.; Brutman, J. P.; Cramer, C. J.; Hillmyer, M. A.; Dichtel, W. R. *J. Am. Chem. Soc.* **2015**, *137*, 14019–14022.

[119] Yan, P.; Zhao, W.; Fu, X.; Liu, Z.; Kong, W.; Zhou, C.; Lei, J. *RSC Adv.* **2017**, *7*, 26858–26866.

[120] Carré, C.; Ecochard, Y.; Caillol, S.; Avérous, L. *ChemSusChem* **2019**, *12*, 3410–3430.

[121] Li, L.; Chen, X.; Torkelson, J. M. *Macromolecules* **2019**, *52*, 8207–8216.

[122] Gamardella, F.; Guerrero, F.; De la Flor, S.; Ramis, X.; Serra, A. *Eur. Polym. J.* **2020**, *122*, 109361.

[123] Huang, S.; Podgórski, M.; Han, X.; Bowman, C. N. *Polym. Chem.* **2020**, *11*, 6879–6883.

[124] Guerrero, F.; Ramis, X.; De la Flor, S.; Serra, À. *Polymers* **2023**, *15*, 1583.

[125] Lü, C.; Cui, Z.; Li, Z.; Yang, B.; Shen, J. *J. Mater. Chem.* **2003**, *13*, 526–530.

[126] Lu, Y.-X.; Tournilhac, F.; Leibler, L.; Guan, Z. *J. Am. Chem. Soc.* **2012**, *134*, 8424–8427.

[127] Lu, Y.-X.; Guan, Z. *J. Am. Chem. Soc.* **2012**, *134*, 14226–14231.

[128] Neal, J. A.; Mozhdehi, D.; Guan, Z. *J. Am. Chem. Soc.* **2015**, *137*, 4846–4850.

[129] Sanchez-Sanchez, A.; Fulton, D. A.; Pomposo, J. A. *Chem. Commun.* **2014**, *50*, 1871–1874.

[130] Denissen, W.; Rivero, G.; Nicolaÿ, R.; Leibler, L.; Winne, J. M.; Du Prez, F. E. *Adv. Funct. Mater.* **2015**, *25*, 2451–2457.

[131] Guerre, M.; Taplan, C.; Nicolaÿ, R.; Winne, J. M.; Du Prez, F. E. *J. Am. Chem. Soc.* **2018**, *140*, 13272–13284.

[132] Engelen, S.; Wróblewska, A. A.; Bruycker, K. D.; Aksakal, R.; Ladmiral, V.; Caillol, S.; Prez, F. E. D. *Polym. Chem.* **2022**, *13*, 2665–2673.

[133] Van Lijsebetten, F.; De Bruycker, K.; Winne, J. M.; Du Prez, F. E. *ACS Macro Lett.* **2022**, *11*, 919–924.

[134] Ma, Y.; Jiang, X.; Shi, Z.; Berrocal, J. A.; Weder, C. *Angew. Chem. Int. Ed*. **2023**, e202306188.

[135] Obadia, M. M.; Mudraboyina, B. P.; Serghei, A.; Montarnal, D.; Drockenmuller, E. *J. Am. Chem. Soc.* **2015**, *137*, 6078–6083.

[136] Obadia, M. M.; Jourdain, A.; Cassagnau, P.; Montarnal, D.; Drockenmuller, E. *Adv. Funct. Mater.* **2017**, *27*, 1703258.

[137] Mudraboyina, B. P.; Obadia, M. M.; Allaoua, I.; Sood, R.; Serghei, A.; Drockenmuller, E. *Chem. Mater.* **2014**, *26*, 1720–1726.

[138] Cromwell, O. R.; Chung, J.; Guan, Z. *J. Am. Chem. Soc.* **2015**, *137*, 6492–6495.

[139] Röttger, M.; Domenech, T.; van der Weegen, R.; Breuillac, A.; Nicolaÿ, R.; Leibler, L. *Science* **2017**, *356*, 62–65.

[140] Ricarte, R. G.; Tournilhac, F.; Cloître, M.; Leibler, L. *Macromolecules* **2020**, *53*, 1852–1866.

[141] Ogden, W. A.; Guan, Z. *J. Am. Chem. Soc.* **2018**, *140*, 6217–6220.

[142] Nishimura, Y.; Chung, J.; Muradyan, H.; Guan, Z. *J. Am. Chem. Soc.* **2017**, *139*, 14881–14884.

[143] Tretbar, C. A.; Neal, J. A.; Guan, Z. *J. Am. Chem. Soc.* **2019**, *141*, 16595–16599.

[144] Zheng, P.; McCarthy, T. J. *J. Am. Chem. Soc.* **2012**, *134*, 2024–2027.

[145] Li, X.; Yu, R.; Zhao, T.; Zhang, Y.; Yang, X.; Zhao, X.; Huang, W. *Eur. Polym. J.* **2018**, *108*, 399–405.

[146] Debsharma, T.; Amfilochiou, V.; Wróblewska, A. A.; De Baere, I.; Van Paepegem, W.; Du Prez, F. E. *J. Am. Chem. Soc.* **2022**, *144*, 12280–12289.

[147] Tesoro, G. C.; Sastri, V. *J. Appl. Polym. Sci.* **1990**, *39*, 1425–1437.

[148] Pepels, M.; Filot, I.; Klumperman, B.; Goossens, H. *Polym. Chem.* **2013**, *4*, 4955–4965.

[149] Luzuriaga, A. R. de; Martin, R.; Markaide, N.; Rekondo, A.; Cabañero, G.; Rodríguez, J.; Odriozola, I. *Mater. Horiz.* **2016**, *3*, 241–247.

[150] Orrillo, A. G.; Furlan, R. L. E. *Angew. Chem. Int. Ed.* **2022**, 61, e202201168.

[151] Caraballo, R.; Rahm, M.; Vongvilai, P.; Brinck, T.; Ramström, O. *Chem. Commun.* **2008**, *48*, 6603–6605.

[152] Michal, B. T.; Jaye, C. A.; Spencer, E. J.; Rowan, S. J. *ACS Macro Lett.* **2013**, *2*, 694–699.

[153] Guggari, S.; Magliozzi, F.; Malburet, S.; Graillot, A.; Destarac, M.; Guerre, M. *ACS Sustain. Chem. Eng.* **2023**, *11*, 6021–6031.

[154] Ji, F.; Liu, X.; Sheng, D.; Yang, Y. *Polymer* **2020**, *197*, 122514.

[155] Zhou, F.; Guo, Z.; Wang, W.; Lei, X.; Zhang, B.; Zhang, H.; Zhang, Q. *Compos. Sci. Technol.* **2018**, *167*, 79–85.

[156] Zhang, B.; Digby, Z. A.; Flum, J. A.; Chakma, P.; Saul, J. M.; Sparks, J. L.; Konkolewicz, D. *Macromolecules* **2016**, *49*, 6871–6878.

[157] Chakma, P.; Possarle, L. H. R.; Digby, Z. A.; Zhang, B.; Sparks, J. L.; Konkolewicz, D. *Polym. Chem.* **2017**, *8*, 6534–6543.

[158] Taplan, C.; Guerre, M.; Du Prez, F. E. *J. Am. Chem. Soc.* **2021**, *143*, 9140–9150.

[159] Stricker, L.; Taplan, C.; Du Prez, F. E. *ACS Sustain. Chem. Eng.* **2022**, *10*, 14045–14052.

[160] Delahaye, M.; Winne, J. M.; Du Prez, F. E. *J. Am. Chem. Soc.* **2019**, *141*, 15277–15287.

[161] Liu, Y.; Ma, S.; Li, Q.; Wang, S.; Huang, K.; Xu, X.; Wang, B.; Zhu, J. *Eur. Polym. J.* **2020**, *135*, 109881.

[162] Van Lijsebetten, F.; Spiesschaert, Y.; Winne, J. M.; Du Prez, F. E. *J. Am. Chem. Soc.* **2021**, *143*, 15834–15844.

[163] Lee, S.-H.; Shin, S.-R.; Lee, D.-S. *Mater. Des.* **2019**, *172*, 107774.

[164] Rana, S.; Solanki, M.; Sahoo, N. G.; Krishnakumar, B. *Polymers* **2022**, *14*, 4338.

[165] Santiago, D.; Guzmán, D.; Padilla, J.; Verdugo, P.; De la Flor, S.; Serra, À. *ACS Appl. Polym. Mater.* **2023**, *5*, 2006–2015.

[166] Van Lijsebetten, F.; Maiheu, T.; Winne, J. M.; Du Prez, F. E. *Adv. Mater.* **2023**, *35*, 2300802.

[167] Stouten, J.; Schnelting, G. H. M.; Hul, J.; Sijstermans, N.; Janssen, K.; Darikwa, T.; Ye, C.; Loos, K.; Voet, V. S. D.; Bernaerts, K. V. *ACS Appl. Mater. Interfaces* **2023**, *15*, 27110–27119.

[168] I. Altuna, F.; E. Hoppe, C.; J. Williams, R. J. *RSC Adv.* **2016**, *6*, 88647–88655.

[169] Wen, Z.; McBride, M. K.; Zhang, X.; Han, X.; Martinez, A. M.; Shao, R.; Zhu, C.; Visvanathan, R.; Clark, N. A.; Wang, Y.; Yang, K.; Bowman, C. N. *Macromolecules* **2018**, *51*, 5812–5819.

[170] Hsissou, R.; Seghiri, R.; Benzekri, Z.; Hilali, M.; Rafik, M.; Elharfi, A. *Compos. Struct.* **2021**, *262*, 113640.

[171] Qureshi, J. *Sustainability* **2022**, *14*, 16855.

[172] Yang, Y.; Xu, Y.; Ji, Y.; Wei, Y. *Prog. Mater. Sci.* **2021**, *120*, 100710.

[173] Tang, S.; Lin, H.; Dong, K.; Zhang, J.; Zhao, C. *Polym. Degrad. Stab.* **2023**, *210*, 110298.

[174] Schenk, V.; Labastie, K.; Destarac, M.; Olivier, P.; Guerre, M. *Mater. Adv.* **2022**, *3*, 8012–8029.

UNIVERSITAT ROVIRA I VIRGILI
PROGRESS IN SUSTAINABILITY WITHIN THE REALM OF DESIGNING NEW THERMOSETTING MATERIALS
Adrià Roig Gibert

Chapter 2

Experimental methods

UNIVERSITAT ROVIRA I VIRGILI
PROGRESS IN SUSTAINABILITY WITHIN THE REALM OF DESIGNING NEW THERMOSETTING MATERIALS
Adrià Roig Gibert

2.1 Nuclear magnetic resonance (NMR)

Nuclear magnetic resonance spectroscopy serves as an analytical method to deduce the molecular arrangement of a chemical compound and to validate the purity of a given sample. The foundation of NMR lies in the notion that the nuclei being studied possess intrinsic spins, and those active nuclei within the molecular structure exhibit unique electronic surroundings. By applying an external magnetic field, energy is transferred between the lower energy state and a higher one. This energy exchange occurs within the radiofrequency wavelength range. As the spin reverts to its original state, energy is emitted within the same radiofrequency spectrum. The emitted signal is captured and processed to generate an NMR spectrum [1].

The different chemical environments of each of the analyzed types of atoms cause disruptions in the surrounding electron cloud, known as deshielding. To facilitate the spectra interpretation, the concept of chemical shift (δ) is defined with Eq. 2.1:

$$\delta = \frac{V_{sample} - V_{reference}}{V_{reference}} \cdot 10^6 \qquad \text{(Eq. 2.1)}$$

where the reference is usually tetramethylsilane (TMS).

In this thesis, nuclear magnetic resonance of two types of nuclei has been used: ^{1}H and ^{13}C. Deuterated solvents are used to dissolve the samples. Herein, deuterated chloroform ($CDCl_3$) and deuterated dimethyl sulfoxide (DMSO-d_6) were used to perform NMR spectra.

Proton nuclear magnetic resonance is characterized by the high isotopic abundance of ^{1}H (99.985%) and the sensitivity of the nucleus. It exhibits a chemical shift range mainly spanning from 0 to 12. The substantial abundance and sensitivity of ^{1}H require smaller sample amounts, and the area under the curve (integral) provides information about the relative number of protons in each signal. Moreover, it enables the determination of neighboring protons, as these can lead to signal splitting.

On the other hand, the lower abundance of ^{13}C (1.1%) and their reduced sensitivity limit the information provided. Typically, the proton absorption region is irradiated, which renders the ^{13}C spectrum non-quantitative due to the NOE effect, causing the signals corresponding to each carbon to appear as individual signals.

In this thesis, the proton and carbon spectra were recorded with a Varian VNMR-S400, as shown in Figure 2.1.

Figure 2.1. Varian VNMR-S400 instrument utilized to record NMR spectra.

2.2 Differential scanning calorimetry (DSC)

Differential scanning calorimetry involves studying the heat flow experienced by a sample and a reference when subjected to a controlled temperature gradient [2]. Quantitative and qualitative information is obtained about processes involving exothermic and endothermic reactions and changes in heat capacity.

During the crosslinking process, also known as curing, the formation of new bonds releases energy, leading to the observation of an exothermic peak (Figure 2.2a). The presence of multiple exothermic peaks, whether well-defined or overlapped, may indicate a two-step curing process or heterogeneity in the formulation preparation.

In the DSC kinetic analysis, the heat released during the reaction is presumed to be proportional to the degree of conversion. Moreover, the curing rate (*dx/dt)* is directly proportional to the heat released (*dh/dt)*. Once the reaction is complete, the integral associated with the obtained signal yields the total evolved heat Δh_{tot}. The reaction rate and the degree of conversion can be calculated as follows:

$$\frac{dx}{dt} = \frac{dh/dt}{\Delta h_t} \qquad \text{(Eq. 2.2)}$$

$$X = \frac{\Delta h_t}{\Delta h_{tot}} \qquad \text{(Eq. 2.3)}$$

where *dh/dt* and Δh_{tot} represent the heat release rate and the total evolved heat normalized to the sample size, Δh_t is the heat released normalized concerning the sample size, and X stands for the degree of curing.

In a degradation process, breaking bonds in the material requires energy. At elevated temperatures, one typically observes endothermic peaks that are generally abrupt and poorly defined. This is due to thermal degradation being a complex process involving several steps (Figure 2.2b). Other endothermic processes like melting (T_m) or boiling (T_b) points can be accurately determined using this technique (Figure 2.2c).

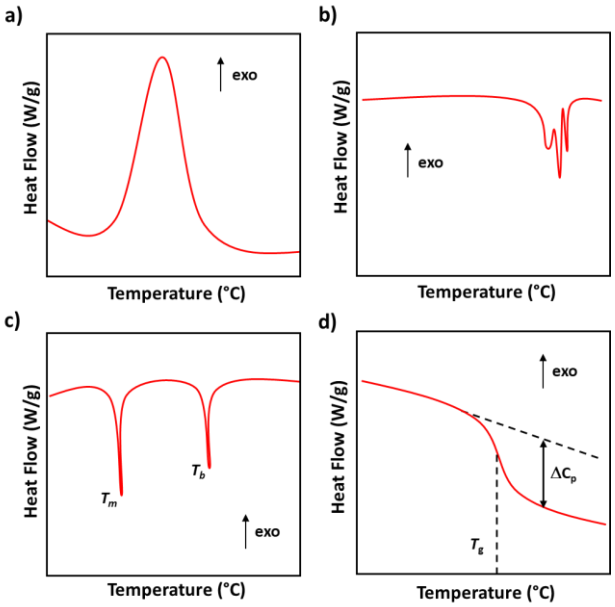

Figure 2.2. DSC analysis of polymeric materials: a) Heat released as a function of temperature during the curing process, b) Heat absorbed as a function of temperature during a degradation process, c) Heat absorbed during a melting point and a boiling point and d) Variation in heat capacity as a function of temperature during a glass transition.

Moreover, second-order transitions, like the glass transition (T_g), are assessed by tracking the abrupt change in heat capacity linked to the structural rearrangement of the network (Figure 2.2d).

In this thesis, DSC experiments were carried out using a Mettler DSC 3+ (Figure 2.3a). Samples of 5-10 mg weight were placed in covered aluminum pans with pierced lids and analyzed in a nitrogen atmosphere with a gas flow of 50 $cm^3 \cdot min^{-1}$. The equipment was calibrated using indium (heat flow calibration) and zinc (temperature calibration) standards.

Figure 2.3. DSC 3+ device from Mettler Toledo (left) and zoom of its furnace (right).

2.3. Fourier-transformed infrared spectroscopy (FTIR)

When infrared radiation interacts with the sample, it engages with the molecules present, absorbing some energy to trigger changes in the molecular vibrational states. This results in either an absorption spectrum (absorbance) or a transmission spectrum (transmittance), depending on whether the energy absorbed by the sample or the energy not absorbed is measured (Figure 2.4). To work with the obtained data, the spectrum needs to undergo Fourier transformation to obtain the spectra commonly employed for analysis [3].

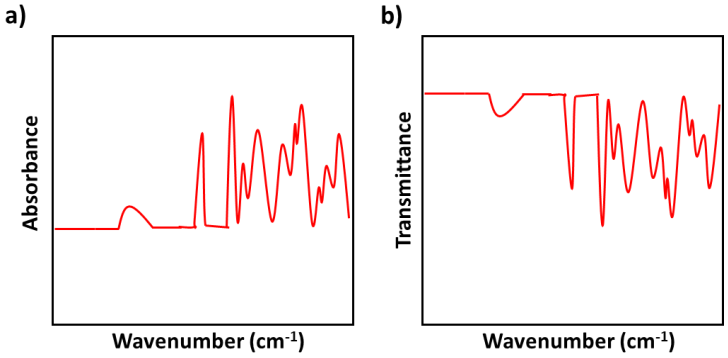

Figure 2.4. FTIR spectra in a) absorbance and b) transmittance.

Every covalent bond absorbs radiation at a distinct wavelength, offering qualitative insights into their structural characteristics. Additionally, quantitative information can be extracted by employing Lambert Beer's law, which directly correlates the area of the peak with the concentration of that particular bond type (Eq. 2.4)

$$Abs = \varepsilon \cdot C \cdot L \qquad \text{(Eq. 2.4)}$$

where *Abs* is the absorbance of a species at a specific frequency, ε is the absorptivity coefficient, *C* is the concentration, and *L* is the optical pathway.

The resulting absorbance band directly correlates with the concentration of the different functional groups. As a result, it becomes possible to track the curing process by observing the signals from the involved groups prior to, during and following the curing sequence. Given that absorbance is proportionate to the optical path length (L), it is necessary to normalize the analyzed band to a reference band that remains constant throughout the curing process. Consequently, the conversion factor X can be ascertained through FTIR experiments and expressed as follows:

$$x = 1 - \frac{A_t'}{A_0'} \qquad \text{(Eq. 2.5)}$$

where A_t' is the normalized absorbance at a certain time and A_0' is the initial.

In this thesis, kinetic studies and evaluation of possible changes in the spectra of the initial formulations and final materials, as well as after a recycling process, have been performed in a Jasco FT/IR-680 Plus spectrometer (Figure 2.5) equipped with an attenuated total reflection accessory (ATR) (Golden Gate, Specac Ltd, Teknokroma) with controlled temperatures. Real-time spectra were recorded in the wavenumber range between 4000 and 600 cm^{-1} with a resolution of 4 cm^{-1} and averaged over 20 scans.

Figure 2.5. Jasco FT/IR-680 Plus spectrometer (left) and Specac Golden Gate ATR Teknokroma accessory in detail (right).

2.4. Thermogravimetric analysis (TGA)

This technique is based on exploring changes in sample mass while subjected to controlled heating with a specific temperature gradient or at constant temperature under carefully chosen conditions such as inert (nitrogen or argon), oxidative (oxygen or synthetic air) or reducing (hydrogen or methane) [4]. It has a highly precise thermobalance, on which the sample is placed within a tared capsule. This capsule is located inside an oven through which the chosen gas flows. This technique provides a wide range of information, including the amount of moisture in the material, degradation studies (number of stages, degradation kinetics, and temperatures), the time the sample withstands at a fixed temperature, and the determination of the organic and inorganic content of the sample (residues). The mass loss curve concerning temperature is often complemented by its first derivative, which more easily reveals the sample's mass loss processes (Figure 2.6).

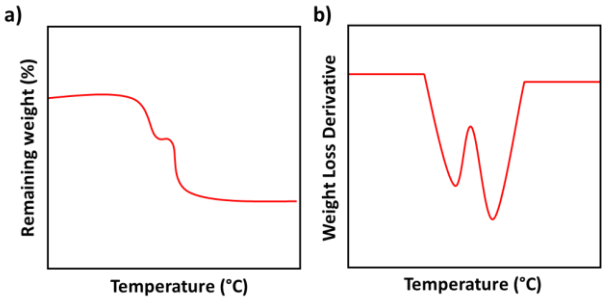

Figure 2.6. TGA analysis of polymeric materials: a) Mass loss as a function of temperature during the degradation process and b) first derivative of this function.

In this thesis, the TGA studies were performed in a Mettler Toledo TGA 2 (Figure 2.7). Samples weighing around 10 mg in uncovered alumina capsules were degraded between 30 and 600 °C at a heating rate of 10 °C·min^{-1} in an N_2 atmosphere with a flow of 50 cm^3·min^{-1}.

Figure 2.7. Mettler Toledo TGA 2 equipment (left) and detail of the furnace with the thermobalance (right).

2.5. Rheological analysis

Rheology encompasses the study of material deformation and flow. Every material can flow if provided with sufficient time. Polymers can exhibit solid-like properties within very short processing intervals, while during overextended processing periods, the material can adopt fluid-like qualities. This interplay of characteristics, blending fluidic and solid behaviors, is called viscoelastic behavior.

For small strain amplitudes and time-independent polymers, the mechanical response of the material can be written in terms of the storage shear modulus (G') and the loss shear modulus (G''). The storage modulus G' corresponds to the in-phase component and signifies the material's elastic reaction or capacity to accumulate energy during deformation. Conversely, the loss modulus G'' corresponds to the out-of-phase component and signifies the material's viscous reaction or ability to dissipate energy. The interplay between these moduli defines the damping capabilities of the polymer:

$$\tan\delta = \frac{G''}{G'} \qquad \text{(Eq. 2.6)}$$

The tangent of the phase angle (tan δ) or damping factor provides a measure of how much energy is lost due to the viscous nature of the material.

Monitoring these three parameters, it is possible to obtain valuable information about the curing process (conversion at the gel point, evolution of viscosity) or even the behavior of G' at high temperatures in multifrequency mode once they are cured, which is especially interesting for covalent adaptable networks and the study of their associative or dissociative nature.

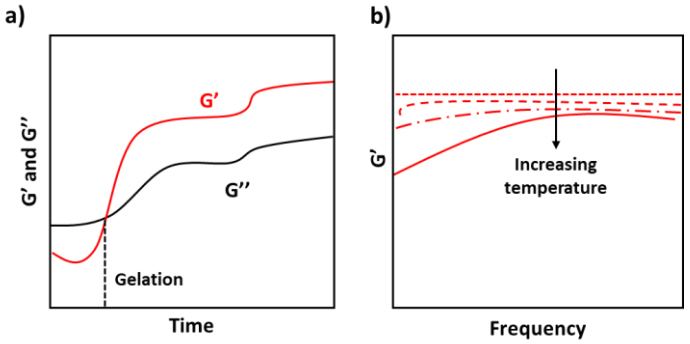

Figure 2.8. Schematical representation of a) evolution of G' and G'' during a curing process and b) possible multifrequency test at high temperatures of a cured material (dissociative CAN).

In this thesis, the study of the curing processes and the multifrequency at high temperatures tests were performed in an ARES G2 rheometer (TA Instruments, New Castle, DE) equipped with an electrically heated plate (EHP) and parallel plate geometry (Figure 2.9). The curing process was analyzed by dynamic mechanical tests at three different frequencies, 0.5, 1.75 and 3 Hz. They were performed maximizing the points per decade in a discrete sweep, and the evolution of the storage and loss moduli (G' and G'', respectively), and tan δ were measured during the curing process. The gelation point was considered as the crossover between G' and G'' at each frequency or the crossover of the tan δ curves at each frequency.

Relaxation tests were conducted in the same instrument. Strain sweep experiments were carried out at a specific temperature to determine the linear viscoelastic regime of the materials. Then, frequency sweep experiments were carried out in a specific temperature interval applying the previous determined strain for each material. The frequency was changed from 100 to 0.1 rad s^{-1} with a 10 N normal force.

Figure 2.9. a) ARES G2 rheometer instrument and b) detail of the parallel plate geometry and the electrical heated plate.

2.6. Gas chromatography-mass spectrometry (GC-MS)

GC-MS finds utility across liquid, gaseous and solid samples alike. The analysis starts with the gas chromatograph, where the sample transforms into a gas phase and segregates into its constituents via a capillary column coated with a stationary phase. Inert carrier gas like helium, hydrogen or nitrogen propels the compounds. As the mix separates, each component emerges from the column at distinct intervals based on boiling point and polarity, termed retention time (Figure 2.10a). Complex mixtures or extracts containing numerous compounds can be resolved using GC.

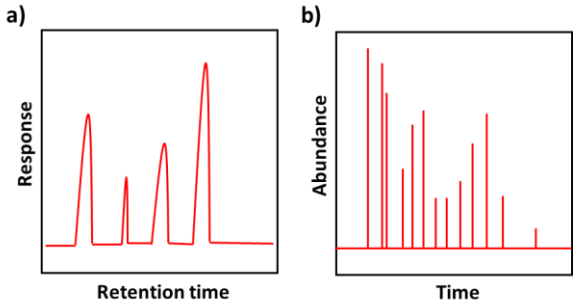

Figure 2.10. a) Example of GC chromatogram and b) Example of mass spectrum.

Components undergo ionization and fragmentation via mass spectrometry using electron or chemical ionization sources following the GC column. The ionized molecules and fragments advance through the mass analyzer, typically a quadrupole or ion trap, which separates ions by varying mass-to-charge (m/z) ratios. Data acquisition in GC-MS can occur in full scan mode, covering a broad m/z range, or selected ion monitoring (SIM) mode, gathering data for specific masses of interest.

The final stages entail ion detection and analysis, wherein fragmented ions appear based on their m/z ratios. Peak areas correlate with compound quantities. GC-MS separation of intricate samples produces numerous peaks in the chromatogram, each corresponding to a unique mass spectrum for compound identification.

In this thesis, gas chromatography tests were performed in a gas chromatograph 6890 Series with an automatic liquid sampler HP7683 Series and mass spectrometer 5973 (Hewlett Packard) (Figure 2.11). The analytical column used was HP-5MS (30 m x 0.25 mm x 0.25 μm) (Agilent Technologies).

Figure 2.11. HP 6890 gas chromatograph instrument.

2.7. Dynamic-thermal-mechanical analysis (DMA)

Polymers showcase a blend of elastic and viscous responses when subjected to a deformation. Dynamic-thermal-mechanical analysis (DMA or DMTA) is a powerful and commonly used technique to study the viscoelastic behavior of polymers.

This kind of test is used to analyze the viscoelastic response of the material with time or/and temperature. In this type of test, an oscillating stress (σ) is applied to the material, which induces a deformation or strain (ε). The applied oscillating stress over time, $\sigma(t)$, follows a sinusoidal pattern, similar to the generated $\varepsilon(t)$ response which depends on the viscoelastic characteristics of the polymer and can be in phase or out of phase to the applied stress [5]:

a) In totally elastic materials, both functions are in phase, with a phase shift angle (δ) of 0 radians (Figure 2.12a).
b) In viscoelastic materials, both functions diverge with a phase shift angle ranging from 0 to $\pi/2$ radians (Figure 2.12b).
c) In totally viscous materials, both functions diverge, showing a phase shift angle of $\pi/2$ radians (Figure 2.12c).

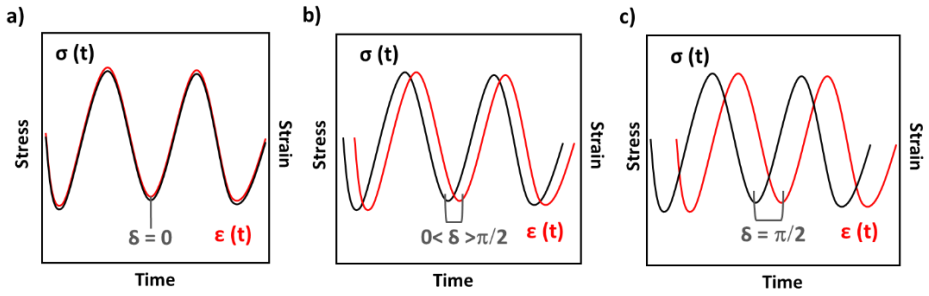

Figure 2.12. Stress (σ) and strain (ε) over time for a) elastic materials, b) viscoelastic materials and c) viscous materials.

The underlying principles of oscillatory DMA analysis are identical to those of oscillatory rheology. Consequently, we can establish storage modulus E', loss modulus E'', and loss factor tan δ, similarly carrying the same significance. The only difference is the stress state induced in the sample: in DMA, this stress state can be tensile, bending or shear and, in the rheometer, the stress state used is torsion (shear). Depending on this stress state, the complex modulus measured will be G* (in shear) or E* (in tensile or bending), resulting in a significant change [2].

Moreover, DMA analysis is typically conducted on solid samples, but it can also be used in curing processes with certain limitations.

When investigating cured materials, DMA analysis is generally performed at a fixed frequency, typically 1 Hz, and with a constant heating rate ranging between 2 and 5 °C min^{-1}. This methodology aims to uncover the essential thermomechanical and structural attributes of the polymer. An illustrative DMA plot of a crosslinked polymer is depicted in Figure 2.13.

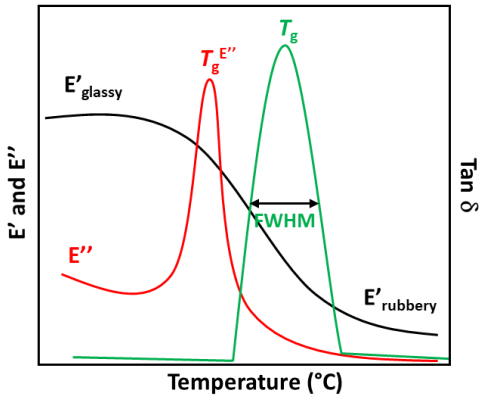

Figure 2.13. Evolution of tan δ, storage modulus (E') and loss modulus (E'') as a function of time, at a fixed frequency in an oscillatory stress test.

The network structure of the material experiences mechanical relaxation linked to its devitrification as it is heated beyond its glass transition temperature. This network relaxation is evident through a notable decrease in the storage modulus (E') and the appearance of a peak in the tan δ curve and the loss modulus (E").

At lower temperatures, the material is in a vitreous state, which restricts the molecular mobility and hence renders a mechanical response akin to that of a rigid elastic solid (high E') with a low tan δ value. Segmental mobility increases when temperature increases, which induces a network relaxation in the material manifested with a response like a softer elastic solid (low E') with tan δ approaching zero. Between these two solid-like phases lie the mechanical relaxation process, characterized by a

gradual easing of segmental mobility, resulting in friction between polymer chains and dissipation of mechanical energy, thus giving rise to the presence of tan δ peak.

The shape of the relaxation curve serves as an indicator of material homogeneity, where a narrower tan δ peak corresponds to a more homogenous network. The parameter quantifying this homogeneity is the full width at half maximum (FWHM). The peak of the tan δ curve typically aids in evaluating the glass transition temperature (T_g). Another method used to ascertain T_g is the peak of the loss modulus, referred to as $T_g^{E''}$. It is important to note that T_g occurs within a temperature range, and the DMA analysis results rely on the temperature-dependent relaxation time of the structure of the material (and, consequently, on the temperature ramp used) and the frequency employed in the analysis.

In this thesis, T_g is considered as the temperature of the maximum of tan δ curve. The storage modulus at lower temperatures corresponds to the glassy state (E'_{glassy}) of the polymer. The storage modulus at high temperatures, above T_g, is ascribed to the rubbery state ($E'_{rubbery}$) and is linked with the crosslinking density of the network. These tests have been performed in a DMA Q800 and a DMA Q850 (TA Instruments) in a tensile or bending clamp at 1 Hz, with a strain of 0.1%, and at a heating rate of 2 °C min^{-1}.

2.8. Creep tests

Creep tests involve subjecting the material to a constant (non-oscillating) stress within its viscoelastic regime, leading to a deformation recorded over time. Typically, these tests are complemented by observing how the strain of the material evolves after the stress has been removed, corresponding to the recovery process without load or viscoelastic recovery [6]. Stress relaxation tests, that are explained in next section, are based on the inverse concept: a fixed strain is applied to the material, while the necessary stress to maintain it is recorded over time. This stress can decrease over time depending on the behavior of the material. Both tests are conducted at different constant temperatures.

Thermosetting polymer materials are unable to flow, or their flow is severely limited due to the covalent bonds between their chains. In a creep test, under constant stress over time, these bonds begin to deform until the deformation reaches a maximum at extended testing times. This phenomenon does not occur in thermoplastic materials, which can flow due to weak intermolecular forces between chains, allowing them to continue deforming until fracture.

The behavior after the stress ceases, in the recovery process, is also distinct. In thermosetting materials, the deformation returns to zero after an extended testing

time, whereas in thermoplastics, there always remains residual deformation (Figure 2.14a-b).

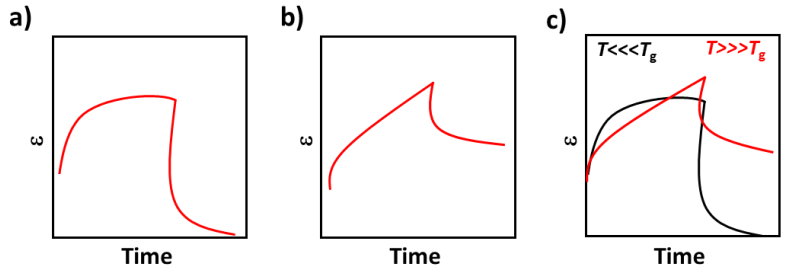

Figure 2.14. Behavior of a) a thermoset, b) a thermoplastic and c) a covalent adaptable network in a creep and recovery test.

In the case of covalent adaptable networks, the behavior during creep tests depends on the temperature. At low temperatures, their behavior is similar to thermosetting materials due to the existing covalent bonds that do not experience enough stimulation to exchange. At high temperatures, their behavior resembles that of thermoplastics (Figure 2.14c).

In this thesis, creep tests have been performed to evaluate the materials' resistance to creep at different temperatures.

Creep and recovery properties were studied by the same DMA Q800 apparatus equipped with a film tension clamp at different temperatures, maintaining the stress (always ensuring that the stress is in the viscoelastic regime) for 30 min and, after this time, immediately released, and the sample was left to recover for 30 min.

2.8.1. Angell fragility plot

When conducting creep tests at different increasing temperatures, it is possible to establish the relationship between viscosity and temperature. This can be done with the obtained plot strain-time at each temperature, and by calculating the slope of the linear segment of strain with time, and then determining the viscosity (η) using Eq. 2.7. By plotting the logarithm of viscosity against the relative temperature (T_g/T), the Angell fragility plot can be obtained (Figure 2.15).

$$\sigma = \eta \cdot \frac{d\varepsilon}{dt} \qquad \text{(Eq. 2.7)}$$

The concept of fragility was introduced by Angell in supercooled liquids [7,8]. By giving insights into glass transition and structural relaxation phenomena, two types of glass

formers could be determined: i) strong glass formers, showing an Arrhenius behavior and ii) fragile glass formers, in which the temperature dependence of viscosity is non-Arrhenius. Later in 1994, this concept was applied to metallic glass formers [9]. Finally, the Angell plot was also extrapolated in vitrimers, discovering their similar viscosity-temperature dependence compared to strong glass formers.

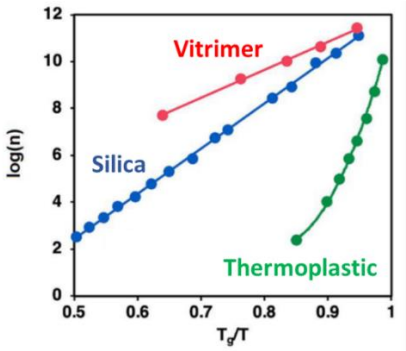

Figure 2.15. Angell fragility plot of a vitrimer (red), vitreous silica (blue) and a thermoplastic (green).

Considering the relationship between viscosity and relative glass temperature in silica as a reference, we observe distinct behavior between associative covalent adaptable networks (vitrimers) in which the viscosity gradually decreases with temperature following a linear tendency (Arrhenius relationship), and dissociative networks or thermoplastics, in which a drastic drop in viscosity is produced when the temperature is increased.

In this thesis, Angell plots were obtained by performing a series of creep tests on the materials studied at several temperatures, increasing 10 °C in each scan. The selected temperature was equilibrated for 3 min, and then a stress level of 0.1 MPa was applied for 30 min. The viscosity at each temperature was obtained as explained above.

2.9. Stress-relaxation tests

Concerning the stress relaxation tests, the differences in behavior between thermoplastics, thermosets and CANs can also be observed. In thermosetting materials, when plotting the stress evolution with time at a specific temperature, the curve decreases to a finite value, where the stress necessary to sustain that constant deformation becomes steady (Figure 2.16a) [10]. Conversely, in thermoplastic materials, the stress curve gradually diminishes to zero at an extended test duration: the material requires decreasing the applied stress to uphold the constant deformation imposed (Figure 2.16b). For CANs, the behavior in a stress relaxation test hinges on temperature: at low temperatures, it is similar to thermosetting materials,

while, at elevated temperatures, it resembles that of thermoplastic due to their ability to flow (Figure 2.16c).

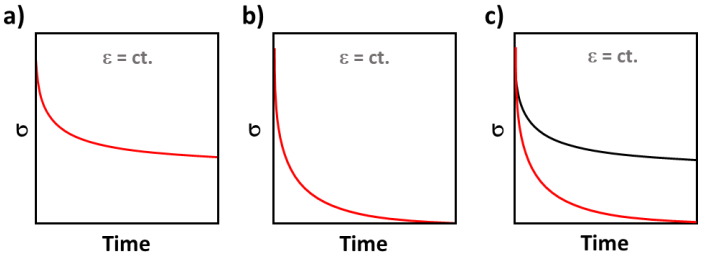

Figure 2.16. Behavior of a) thermoset, b) thermoplastic and c) CAN in a stress relaxation test.

The relaxation time (τ*), defined as the time required for the stress to reach 37% (1/e) of the initial stress (σ_0) at a specific temperature, is commonly employed for comparing the vitrimeric behavior properties of different materials. The relaxation time can be linked to viscosity through the Maxwell equation, where η represents viscosity, $E'_{rubbery}$ the storage modulus in the rubbery state and τ the relaxation time:

$$\eta = E'_{rubbery} \cdot \tau^* \quad \text{(Eq. 2.8)}$$

When conducting several stress relaxation tests on vitrimeric materials at different increasing temperatures (above T_g) and plotting the obtained relaxation times against the temperature, it becomes evident that both variables exhibit an Arrhenius relationship (Figure 2.17). This relationship can be defined using Eq. 2.9 and linearized with Eq. 2.10. In these equations, τ represents the relaxation time, τ_0 is the relaxation time at infinite temperature, E_a stands for the activation energy of the bond exchange process, R denotes the universal gas constant, and T corresponds to the temperature.

$$\tau = \tau_0 \cdot e^{Ea/RT} \quad \text{(Eq. 2.9)}$$

$$ln\tau = ln\tau_0 + \frac{E_a}{RT} \quad \text{(Eq. 2.10)}$$

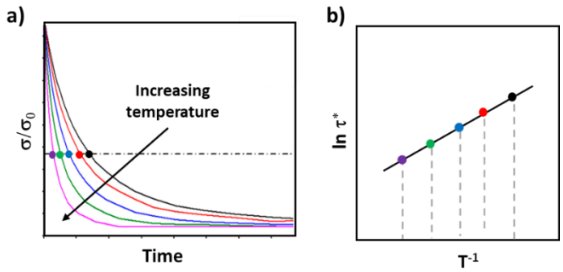

Figure 2.17. a) Schematic representation of stress relaxation tests at different temperatures for a vitrimeric material and b) Representation of logarithm of the relaxation time in front of temperature and its linear relationship.

The activation energy (E_a) of the exchange process can be calculated from the slope of the linear relationship in Figure 2.17(b).

Another critical parameter in the characterization of vitrimeric materials is the topology freezing temperature (T_v). Chemically, it is defined as the temperature below which the exchange processes are negligible but physically is defined as the temperature at which the material reaches a viscosity (η) of 10^{12} Pa·s. By substituting this viscosity value into Eq. 2.8 yields the characteristic relaxation time (τ^*), and T_v can be obtained using the linear equation (Eq. 2.10). This temperature can also be determined by creep tests since the viscosity can be directly obtained and, therefore, a direct extrapolation can be done to get a viscosity of 10^{12} Pa·s.

Tensile or bending stress-relaxation tests were conducted in DMA Q800 and DMAQ850 (TA Instruments) in a film or bending clamp. The samples were firstly equilibrated at the relaxation temperature for 5 min, and a constant strain of 1% was applied, measuring the consequent stress level as a function of time.

2.10. Dilatometry tests

Dilatometry experiments rely on tracking the expansion and contraction of a material as it is subjected to a controlled heating temperature gradient without (or with an extremely small) stress to measure only the deformation produced by temperature and not by any stress. The transformations that unfold within the material upon heating play a decisive role in shaping the trajectory of this unique volume variation. Particularly, in covalent adaptable networks, it usually becomes feasible to ascertain both the glass transition temperature (T_g) and the topological freezing temperature (T_v) through the intricate interplay of volume changes (Figure 2.18).

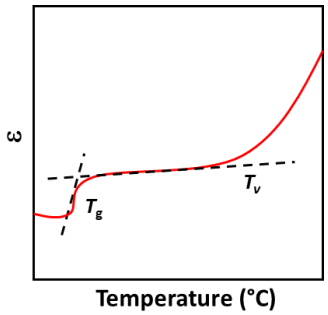

Figure 2.18. Dilatometry test of a covalent adaptable network.

Dilatometry experiments were performed in a DMA Q800 using a film tension clamp. The sample length was continuously measured while increasing the temperature at a

heating rate of 1 °C min^{-1} from -30 to 200 °C, applying a slight stress of 0.01 MPa to avoid buckling.

Dynamic-mechanic-thermal analysis tests, creep tests, stress relaxation tests and dilatometry experiments were carried out in a DMA Q800 and a DMA Q850 instruments (Figure 2.19)

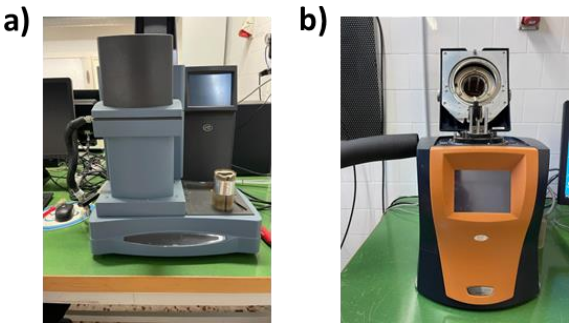

Figure 2.19. a) DMA Q800 instrument and b) DMA Q850 instrument (right).

2.11. Tensile tests

Tensile experiments involve inducing a uniaxial controlled displacement on a sample until it reaches its failure. Throughout this evaluation, the necessary exerted force (F) to induce the displacement of the specimen is meticulously tracked by a controlling unit. Through the collected dataset of force versus displacement, the engineering stress (σ) and strain (ε) can be determined using the subsequent equations:

$$\sigma = \frac{F}{A} = \frac{F}{t \cdot w} \quad \text{(Eq. 2.11)}$$

Where A is the transverse section of the sample, t, is the specimen thickness and w, is the specimen width.

$$\varepsilon = \frac{L - L_0}{L_0} \quad \text{(Eq. 2.12)}$$

where L_0 is the initial gauge length and L is the increasing gauge length.

The tensile properties of a material are influenced by several experimental factors like temperature, humidity and testing speed. An illustrative simple stress/strain plot of a thermoset at room temperature is displayed in Figure 2.20a. The stress at break (σ_{break}) and the strain at break (ε_{break}) are determined from the failure point. The tensile elastic modulus (E) is computed from the slope of the initial linear segment of the curve.

In this thesis, the tensile tests were performed on dog bone samples adapted from ASTM D638 requirements (Type V) at room temperature in an electromechanical

universal testing machine Shimadzu AGS-X with a load cell of 10 kN at 5 mm·min^{-1} (Figure 2.20b).

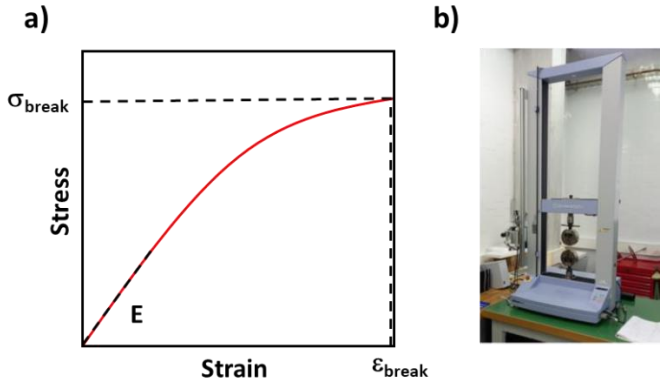

Figure 2.20. a) Typical stress-strain curve of a thermoset at room temperature and b) Shimadzu AGS-X instrument.

2.12. Mechanical recycling tests

Mechanical recycling is one of the most important characteristics of covalent adaptable networks. Thanks to the dynamic bonds in their structure, their ability to flow at high temperatures makes them very interesting for reprocessing.

To prove the recyclability of the materials studied in this thesis, cured materials were ground into powder and poured into a 90 cm diameter aluminum mold. Then, this mold was put in a Specac Atlas manual 15 T hydraulic press (Figure 2.21) with a temperature unit under determined temperature and pressure conditions during a specific time depending on the material studied

After that, the obtained recycled materials were die-cut for further investigation.

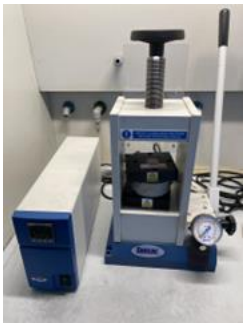

Figure 2.21. Specac Atlas hot-press.

2.13. Self-healing tests

As mentioned in the Introduction section, self-healing is the ability to self-repair minor damages in the material. It is one of the most studied properties in covalent adaptable networks since upon applying an external stimulus such as heat or light and the exchange reaction takes place, the material is able to self-heal the damage and extend the lifespan of the polymer.

To evaluate the self-healing abilities of the covalent adaptable networks, we used hydraulic manual press with a round steel indenter of 2.5 mm diameter to make plastic indentations on the surface of the sample by applying increasing loads from 300 MPa to 360 MPa. Later on, the samples were heated in an oven, exploring the evolution of the indentation in the healing process from time to time by taking pictures with a Digital Stereo microscope Leica s9i (Figure 2.22).

Figure 2.22. Stereo microscope Leica s9i.

References

[1] Balci, M. Basic 1H and 13C-NMR Spectroscopy, Elsevier B. V, Ankara, Turkey, **2005**.

[2] Turi, E. A. Thermal Characterization of Polymeric Materials, 2nd Edition, Academic Press, San Diego, California, **1997**.

[3] Griffiths, P. R. Fourier Transform Infrared Spectrometry, John Wiley & Sons, Hoboken, New Jersey, **2006**.

[4] Menczel, J. D.; Prime, R. B. Thermal Analysis of Polymers: Fundamentals and Applications, John Wiley & Sons, Hoboken, New Jersey, **2009**.

[5] Menard, K. P.; Menard, N. R. Dynamic Mechanical Analysis, 3rd edition, CRC Press, Boca Raton, Florida, **2020**.

[6] Strong, A. B. Plastics: Materials and Processing, Prentice Hall, Saddle River, New Jersey, **2000**.

[7] Angell, C. A. *J. Non-Cryst. Solids*, **1985**, *73*, 1.

[8] Angell, C. A. *J. Phys. Chem. Solids*, **1988**, *49*, 863.

[9] Komatsu, T. *J. Non-Cryst. Solids*, **1995**, *185*, 199-202.

[10] Turner, S. The Physics of Glassy Polymers, Springer, Dordrecht, Netherlands, **1973**.

UNIVERSITAT ROVIRA I VIRGILI
PROGRESS IN SUSTAINABILITY WITHIN THE REALM OF DESIGNING NEW THERMOSETTING MATERIALS
Adrià Roig Gibert

Chapter 3

Dual-cured thermosets from glycidyl methacrylate obtained by epoxy-amine reaction and methacrylate homopolymerization

(*React. Funct. Polym.* **2021**, *159*, 104822)

UNIVERSITAT ROVIRA I VIRGILI
PROGRESS IN SUSTAINABILITY WITHIN THE REALM OF DESIGNING NEW THERMOSETTING MATERIALS
Adrià Roig Gibert

React. Funct. Polym. **2021**, *159*, 104822

Dual-cured thermosets from glycidyl methacrylate obtained by epoxy-amine reaction and methacrylate homopolymerization

Adrià Roig,[1] Xavier Ramis,[2] Silvia De la Flor,[3] Àngels Serra[1]

[1] Universitat Rovira i Virgili, Department of Analytical and Organic Chemistry, C/ Marcel·lí Domingo 1, Edif. N4, 43007 Tarragona, Spain

[2] Universitat Politècnica de Catalunya, Thermodynamics Laboratory, ETSEIB, Av. Diagonal, 08028 Barcelona, Spain

[3] Universitat Rovira i Virgili, Department of Mechanical Engineering, Av. Països Catalans 26, 43007 Tarragona, Spain

ABSTRACT

Dual-curing is a processing technology based in the combination of two polymerization processes and the proper selection of the formulation. This methodology allows the preparation of intermediate materials with tailored characteristics, which can be viscous-liquids or rubbery solids according to their application. Once applied, the second stage is performed leading to a high crosslinked network. Usually, different monomers are involved, and unreacted monomer are still present in the intermediate material. This monomer experiments polymerization during the second step, but it can drip or be exuded during storage. In the present work, a commercial monomer, glycidyl methacrylate has been selected, because of the presence in the same molecule of an epoxide group, which can react with amines in the first stage of the dual-curing, and a methacrylate group that can be thermally or photochemically homopolymerized to complete the curing process. Diglycidylether of bisphenol A has been added to obtain a gelled intermediate material. The evolution of both curing steps has been studied by DSC and FTIR. The stability of the intermediate material has been confirmed and the characteristics of intermediate and final material have been evaluated by TGA and DMTA.

KEYWORDS

Dual-curing, thermosets, click chemistry, epoxy-amine, radical homopolymerization

Chapter 3

1. Introduction

Nowadays thermosets are an important type of industrial materials due to their wide range of applications in several sectors such as coatings, [1] automobile [2] or optoelectronic industry [3]. The preparation of these crosslinked materials involves irreversible curing processes that must be very well-controlled to produce components with the required characteristics and shapes. In this field, dual-curing has arisen as a promising synthetic methodology to obtain thermosets in a well-controlled manner. This procedure consists in two different polymerization processes that can take place sequentially or simultaneously and can be triggered by different stimuli *i.e.* temperature or UV-light [4]. Sequential dual curing allows to obtain partially cured materials in a first stage that can be easily stored or just sent for further processing to obtain a fully cured polymer with higher performance once the second polymerization is completed. The characteristics of the intermediate materials can be modulated and depend on the formulation composition which in turn, defines the extension of the first and second curing stages. The intermediate materials can be viscous liquids, with adhesive properties, or conformable solid materials, which after performing the second step will be converted into hard thermosets.

The sequentiality and the control of the intermediate characteristics are based on the selection of the curing reactions, the composition of the formulation and the tuning of the curing parameters like time or temperature of the process and in some cases the use of an adequate catalyst [5]. Dual-curing processing presents several advanced applications in shape memory polymers [6-9], adhesive coatings [10,11], lithography [9,12], holography [13,14], photopatterning [15] or dental materials [16] among many others.

To achieve sequential dual curing processes, “click chemistry” is a great tool because it provides selectivity, great kinetic control, high yields in mild reaction conditions, and can be performed in air atmosphere [17-20]. Among all the possible reactions that are included in this type of chemistry, one of the most used in the synthesis of thermosets is the epoxy-amine reaction as it can be carried out at low temperatures in case of using aliphatic amines as curing agents. Many researchers used this reaction as a first step in dual curing schemes. Konuray *et al.* employed a two-stage curing process in which the diglycidyl ether of bisphenol A (DGEBA) and an aliphatic amine are involved in the first curing step to synthesize a wide range of intermediate materials, with different properties depending on the composition of the formulation, whereas a homopolymerization of the remaining epoxy groups initiated by a latent imidazole catalyst constituted the second stage [21]. Similarly, Morancho *et al.* described the dual-curing of off-stoichiometric diethylenetriamine-diglycidyl ether of bisphenol A using tertiary amine as initiator for high temperature homopolymerization of the epoxy excess [22]. After the first curing stage, intermediate materials showed a high

latency and could be safely stored for long time, since in addition of the kinetic control in the initiation of the second stage, vitrification of the intermediate material helps to improve their storability if storage temperatures are lower than the T_g. Furthermore, the same group also reported a new family of dual-cured thermosets based on commercial amine-epoxy formulations with two amines of different reactivity and rigidity reaching promising materials for applications such as adhesives or smart materials [23].

As said, the second curing stage is also a very important step to produce the fully cured material because it will generate the final network in the thermoset and subsequently, determine the final characteristics. This reaction can be activated by UV-light or thermally, depending on the type of reactive groups and the chemistry involved, having both processes their advantages and drawbacks. From the point of view of energy saving and technical easiness, photoirradiation is very advantageous, but its application is reduced to thin layers and flat shapes that can be fully illuminated without shadowy parts [24]. Thermal activation is better for thick and complex shaped samples because of its uniformity, but high temperatures in ovens and long curing times are needed. In addition, vitrification of the final material must be avoided and from this point of view, thermal activation is more convenient.

Taking all of this into account, in the present article, we report the preparation and characterization of a new dual-curing system based on the epoxy and methacrylate groups of a commercially available compound, glycidyl methacrylate (GMA). A stoichiometric epoxy-amine reaction will be used as the first curing stage and a radical homopolymerization of the methacrylate groups in both thermal and UV-curing conditions as the second curing stage. The addition of DGEBA to the formulation has also been explored to achieve gelation during the first step. As far as we know, this dual curing system has not been previously described in the literature, and the combination of both polymerization mechanism can open broad industrial applications. However, Mustata et al. reported the curing of GMA/DGEBA mixtures with adducts of Diels-Alder reaction of rosin acids derivatives and maleic anhydride, being the first step the thermal curing of methacrylates and the second, the reaction of epoxides with acids and anhydrides [25]. The most valuable advancement of the present study relies on the fact that no unreacted monomers will be present after the first step avoiding their possible dripping or exudation in the conformation or processing of the intermediate material, which is a great advantage in its final application. In addition, this novel curing system has great versatility as different excesses of diepoxide can be added to modify not only the characteristics of the intermediate material, but also of the final material. Of course, mono or multifunctional methacrylates could also be added to the formulation to adapt the properties of the materials, although in the latter case there will be unreacted

monomer in the intermediate material. Thermal and photoinitiated homopolymerization of the methacrylate moieties have been studied in order to compare the characteristics of the final materials.

The evolution of both curing stages, the conversion achieved and the latency after the first stage have been evaluated by calorimetry and FTIR spectroscopy and the gelation time during epoxy-amine condensation by rheology. The materials obtained have been characterized by calorimetric, thermomechanical, and thermogravimetric analyses.

2. Experimental methods

2.1 Materials

Glycidyl methacrylate (GMA) was supplied by Miwon. Diethylenetriamine (DETA, 20.63 g/eq), isophorone diamine (IPDA, 42.58 g/eq), tris(2-aminoethyl) amine (TREN, 24.37 g/eq) and 2,2-dimethoxy-2-phenylacetophenone (DMPA) were supplied by Sigma Aldrich and used without further purification. Jeffamine D400 (JEFFA, 115 g/eq) was provided by Huntsman Corporation. Diglycidyl ether of bisphenol A (DGEBA, 172 g/eq) was supplied by Hexion Specialty Chemicals and dried in vacuum for 2 hours at 80°C before use and the peroxidic radical initiator 1,1-di(t-amylperoxy)-cyclohexane (Luperox 531M60) was kindly supplied by ARKEMA.

2.2 Sample preparation

Formulations of GMA were prepared in 5 mL vials in approximately 1 g batches were 1% w/w of Luperox (to GMA) for thermal acrylate homopolymerization or 5% w/w of DMPA (to GMA) for photoinitiated systems were weighted. Then, GMA and the stoichiometric amount of amine (IPDA, JEFFA, TREN, DETA) was added. The mixtures were vigorously and manually stirred at room temperature and then immediately analyzed.

Formulations of GMA with DGEBA were prepared in 5 mL vials in 1-2 gr batches were 1% w/w of Luperox (to GMA) and 5% w/w of DMPA (to GMA) were weighted for thermal and photoinitiated methacrylate homopolymerization, respectively. Then, DGEBA and the corresponding amount of GMA were added using the calculated molar ratio between DGEBA and GMA (nDGEBA/mGMA = 0.4). Finally, the stoichiometric amount of amine (IPDA, JEFFA, TREN or DETA) was added. The reactive mixtures were homogenized at room temperature by manual stirring and then immediately analyzed.

The formulations prepared with only GMA were coded as G_X_Y and the formulations containing DGEBA as GDG_X_Y, where, in both cases, X indicates the amine used and Y the initiator selected for the second stage of the dual process. As an example,

React. Funct. Polym. **2021**, *159*, 104822

GDG_DETA_Lup is a formulation in which GMA and DGEBA are in the mixture, DETA is the amine used and the second stage was initiated by 1% w/w of Luperox. Table 3.1 shows the composition of the different formulations studied.

Table 3.1. Composition of the dual formulations prepared.

Sample	GMA (wt. %)	DGEBA (wt. %)	IPDA (wt. %)	JEFFA (wt. %)	TREN (wt. %)	DETA (wt. %)	Lup. (wt. %)	DMPA (wt. %)
G_IPDA_Lup	76.3	-	22.9	-	-	-	0.8	-
G_JEFFA_Lup	56.6	-	-	42.8	-	-	0.6	-
G_TREN_Lup	84.6	-	-	-	14.6	-	0.8	-
GDG_DETA_Lup	43.0	45.3	-	-	-	11.2	0.5	-
GDG_DETA_DMPA	42.3	44.5	-	-	-	11.1	-	2.1
G_DETA_Lup	86.5	-	-	-	-	12.6	0.9	-
G_DETA_DMPA	83.6	-	-	-	-	12.2	-	4.2

Fully cured samples for dynamomechanical (DMA) and thermogravimetric (TGA) analyses were prepared in an open mold, with dimensions of 1.5 x 5 x 15 mm^3, made of metal and covered with PTFE to avoid the formation of bubbles and to facilitate the samples release. The liquid formulations were poured into the mold and kept in an oven at 45 °C for 4.5 h (stage 1) and cured at 120 °C during 1.5 h and post-cured at 150 °C and 200 °C during 1 h and 1.5 h, respectively in the case of Luperox-based compositions, and 1.5 min under UV-light on both sides for DMPA formulations (stage 2). These curing times were optimized according to Fourier transform infrared spectroscopy (FTIR) and differential scanning calorimetry (DSC). The samples were polished with sandpaper to obtain uniform final dimensions.

2.3 Characterization techniques

DSC analyses were carried out on a Mettler DSC-821 instruments calibrated using indium (heat flow calibration) and zinc (temperature calibration) standards. Samples of approximately 8-10 mg were placed in aluminum pans with pierced lids and analyzed in nitrogen atmosphere with a gas flow of 50 cm^3/min. Dynamic studies between 30 and 250 °C with heating rate of 10 °C/min were performed to characterize the curing process and to measure the final glass transition temperature (T_g). Dynamic curing tests were also performed with heating rates of 2, 5, 10 and 20 °C/min to

determine the kinetic parameters. The reaction enthalpy (Δh) was integrated from the calorimetric heat flow signal (dh/dt) using a straight baseline with help of the STARe software. The T_gs of the intermediate materials were determined with the following procedure: i) isothermal curing at 45 °C until the first reaction comes to end (270 min); ii) dynamic heating from -30 to 250 °C at 10 °C/min.

To monitor the dual-curing process and to quantitatively determine the degree of curing, a FTIR spectrometer Bruker Vertex 70 with an attenuated total reflection accessory with thermal control and a diamond crystal (Golden Gate Heated Single Reflection Diamond ATR Specac-Teknokroma) and equipped with a mid-band liquid nitrogen-cooled mercury-cadmium-telluride (MCT) detector was used. Real-time spectra were collected in absorbance mode with a resolution of 4 cm^{-1} in the wavelength range 4000 to 600 cm^{-1} averaging 20 scans for each spectrum. The first step of the dual-curing process was conducted at 45 °C. Real-time spectra of the UV photoinitiated 2nd stage were recorded at the same conditions previously detailed. The characteristic absorbance peak of the epoxy at 915 cm^{-1} (epoxy bending) was used to monitor the conversion of the epoxy group during the epoxy-amine reaction [26]. The disappearance of the absorbance peak at 1636 cm^{-1} corresponding to stretching of the C=C bond of the methacrylate was used to monitor the homopolymerization of this group (2nd stage) [27]. Absorbance of each scanned sample were normalized with that of the DGEBA's aromatic protons at 1600 cm^{-1}. In the case of formulations without DGEBA the peak corresponding to the carbonyl group of the methacrylate at 1718 cm^{-1} was taken as the reference. Epoxy groups conversion (X_{epoxy}) and methacrylate group conversion (X_{meth}) were calculated by Eq. 3.1 and Eq. 3.2, respectively:

$$\chi_{epoxy} = 1 - \frac{A_{915}}{A_{915,0}} \qquad \text{(Eq. 3.1)}$$

$$\chi_{meth} = 1 - \frac{A_{1636}}{A_{1636,0}} \qquad \text{(Eq. 3.2)}$$

where A_{915} *and* $A_{915,0}$ are the normalized absorbances of the epoxy peak at 915 cm^{-1} at a given reaction time at the beginning of the curing process, respectively and A_{1636} and $A_{1636,0}$ the normalized absorbances of the methacrylate peak at 1636 cm^{-1} at the same given reaction time.

The gelation time was determined using a rheometer AR-G2 (TA Instruments) equipped with an electrical heated plate device (EHP) and 20 mm parallel plate geometry. The oscillation amplitude was set at 0.2% and the frequencies at 0.5, 1.75 and 3 Hz. Gel point was determined as the tan δ crossover at the three different frequencies. The evolution of the tan δ was monitored through dynamo-mechanical experiment at 45 °C during 4.5 h.

React. Funct. Polym. **2021**, *159*, 104822

The thermomechanical properties were evaluated using DMA Q800 (TA Instruments) equipped with a three-point bending clamp. Prismatic rectangular samples of 1.5 x 5 x 15 mm^3 were analyzed from 25 to 150 °C at 1 Hz, 0.1 % strain and with a heating rate of 3 °C/min.

TGA analyses were carried out with a Mettler Toledo TGA2 thermo-balance. Cured samples, weighting around 10 mg, were degraded between 30 and 600 °C at a heating rate of 10 °C/min in N_2 atmosphere with a flow of 50 cm^3/min.

3. Theoretical part

In non-isothermal kinetics of heterogeneous condensed phase reactions, it is usually accepted that the reaction rate is given by Eq. 3.3 [28,29].

$$\frac{d\alpha}{dt} = \beta\frac{d\alpha}{dT} = Aexp\left(-\frac{E}{RT}\right)f(\alpha) \qquad \text{(Eq. 3.3)}$$

where α is the degree of conversion, T temperature, t time, $f(\alpha)$ the differential conversion function, R the gas constant, β the linear constant heating rate $\beta = dT/dt$ and A and E the pre-exponential factor and the activation energy given by the Arrhenius equation.

By integrating Eq. 3.3, in non-isothermal conditions, the integral rate equation, so-called temperature integral, may be expressed as Eq. 3.4.

$$g(\alpha) = \int_0^\alpha \frac{d\alpha}{f(\alpha)} = \frac{A}{\beta}\int_0^T e^{-(E/RT)}dT \qquad \text{(Eq. 3.4)}$$

where $g(\alpha)$ is the integral conversion function.

By using the Coats-Redfern approximation to solve Eq. 3.4 and considering that $2RT/E$ is much lower than 1, the Kissinger-Akahira-Sunose (KAS) equation (Eq. 3.5) may be written [30-32]:

$$ln\left(\frac{\beta}{T^2}\right) = ln\left[\frac{AR}{g(\alpha)E}\right] - \frac{E}{RT} \qquad \text{(Eq. 3.5)}$$

For each conversion degree, the linear plot of $ln\ (\beta/T^2)$ versus T^{-1} enables E and $ln\ [AR/(g(\alpha)\ E)]$ to be determined from the slope and the intercept. Iso-conversional kinetic parameters were obtained in this work by using Eq. 3.5. If the reaction model, $g(\alpha)$, is known, the corresponding pre-exponential factor can be calculated for each conversion. Rearranging Eq. 3.5, the Coats-Redfern equation can be written as Eq. 3.6. [30,33].

$$ln\left(\frac{g(\alpha)}{T^2}\right) = ln\left[\frac{AR}{\beta E}\right] - \frac{E}{RT} \qquad \text{(Eq. 3.6)}$$

For a given model and heating rate, the linear plot of the left-hand side of Eq. 3.6 versus T^{-1} allowed us to obtain the average activation energy and average pre-exponential factor from the slope and the intercept. In this study, we chose the kinetic

model with an activation energy similar to that obtained iso-conversionally (Eq. 3.5) and with a good correlation coefficient in Eq. 3.6 (Model Fitting method). The rate constant *k* and the reaction rate *dα/dt* were calculated for each conversion from non-isothermal *E*, and *A* data using the Arrhenius equation and Eq. 3.3 and the kinetic model, respectively. Integrating Eq. 3.3 for isothermal experiments, we can obtain Eq. 3.7:

$$ln(t) = ln\left[\frac{g(\alpha)}{A}\right] + \frac{E}{RT} \qquad \text{(Eq. 3.7)}$$

This equation relates, for each conversion, the temperature and the time of curing. The constant *ln [g(α)/A]* is directly related to the value *ln [AR/(g(α) E)]* by *E/R*, which can be deduced from the non-isothermal adjustment (Eq. 3.5), if isothermal and non-isothermal curing take place in the same conditions. In this work we used *ln [AR/(g(α) E)]* and *E/R* obtained by dynamic experiments and (Eq. 3.5) to estimate the time of curing for both curing stages by using Eq. 3.7.

4. Results and discussion

4.1 Study of the curing process by calorimetry

With the aim to know the most adequate composition for the dual-curing process, we firstly studied the epoxy-amine reaction (1st stage) using GMA with structurally different amines (IPDA, TREN, JEFFA, and DETA) by means of DSC dynamic studies. Figure 3.1 shows the curing exotherms obtained.

We can observe that the reactions with IPDA and JEFFA start at higher temperatures than with TREN and DETA. As it has been said, the thermal dual-curing includes a second stage which consists in a radical homopolymerization of the GMA methacrylate, which is initiated when Luperox decompose forming radical species close to 120 °C. Accordingly, the lower the starting temperature for the epoxy-amine reaction, the better to get sequentiality in the curing process. Moreover, the curing exotherms of TREN and DETA formulations are monomodal which may indicate that side reactions do not take place. Figure 3.1 also shows, for TREN and DETA formulations, that the whole reaction has been completed between 30 °C and 170 °C and the reaction is fast once initiated.

Table 3.2 collects the most characteristic calorimetric data of the reactions studied in terms of reaction enthalpy (ΔH) and temperature of the maximum of exothermic peak (T_{max}). As we can see, all reaction heats are relatively close to 90-100 kJ/eq, which is the standard value for an epoxy-amine reaction [34]. We can observe that IPDA releases a higher enthalpy than the other amines, but the peak appears at high temperature with a shoulder, which could indicate the presence of a homopolymerization of epoxides, According to these results, both TREN and DETA

could be selected as curing agents for the epoxy-amine reaction in these formulations. Nevertheless, TREN contains a tertiary amine that can act as a catalyst for aza-Michael addition between the methacrylate and the amine itself, hypothesis that we could confirm by FTIR analysis (Figure 3.S1). The absorbance band corresponding to the double bond of the methacrylate at 1636 cm^{-1} decreased at the same time as the peak at 915 cm^{-1} of the epoxide at 45 °C, suggesting that the aza-Michael addition was taking place simultaneously with the epoxy-amine condensation. With these results, we selected DETA as the amine to continue our study.

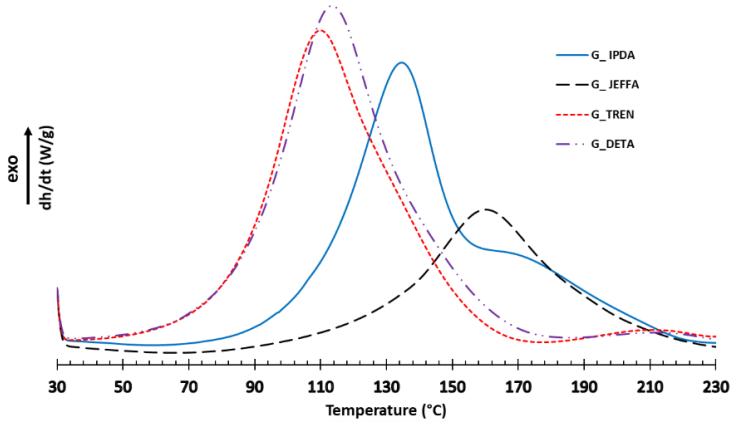

Figure 3.1. DSC thermograms corresponding to the dynamic curing at 10 °C/min of formulations with GMA and the different amines.

Table 3.2. Calorimetric data of the epoxy-amine reaction using different amines.

Sample	$\Delta H_{epoxy\text{-}amine}$[a] (J/g)	$\Delta H_{epoxy\text{-}amine}$[a] (kJ/eq)	T_{max}[b] (°C)
G_JEFFA	292.2	73.1	160.2
G_DETA	496.7	81.0	113.5
G_TREN	504.5	84.0	110.0
G_IPDA	497.5	92.2	134.5
GDG_DETA	478.9	87.5	106.7

[a] Enthalpy released in the epoxy-amine process by gram of mixture and by equivalent of epoxy.
[b] Temperature of the maximum of the exotherm of the epoxy-amine reaction.

Once the amine is chosen, the initiator required to perform the second step must also be selected. According to Figure 3.1 the epoxy-amine reaction embraces a big range of temperatures so it will be difficult to obtain a great sequentiality because many thermal radical initiators generate their radicals between 50 and 120 °C. Therefore, an initiator that releases its radicals at high temperature is needed to produce the

epoxy-amine condensation and the homopolymerization of the methacrylate as the first and second curing stage, respectively. Among many thermal radical initiators like di-*tert*-butyl peroxide (TBP), 2,2'-azobisisobutyronitrile (AIBN), benzoyl peroxide etc. we selected 1,1-di(t-amylperoxy)-cyclohexane (Luperox 531M60, Luperox or Lup hereafter) as the thermal radical initiator for the homopolymerization of the methacrylate moiety of the GMA because it generates radicals at 120 °C [35]. To test this initiator, a dynamic DSC scan was carried out for the formulation G_DETA_Lup which is shown in Figure 3.2.

As it can be seen, the green curve presents a small shoulder at 110 °C corresponding to the maximum peak of the epoxy-amine condensation and then a high peak at 120 °C attributable to the homopolymerization of the methacrylate groups. Moreover, the global reaction heat was 128.1 kJ/eq., but taking into account that the epoxy-amine reaction releases 87.5 kJ/eq. the second step has 40.6 kJ/eq. which is a little bit lower than the standards for the methacrylate homopolymerization.

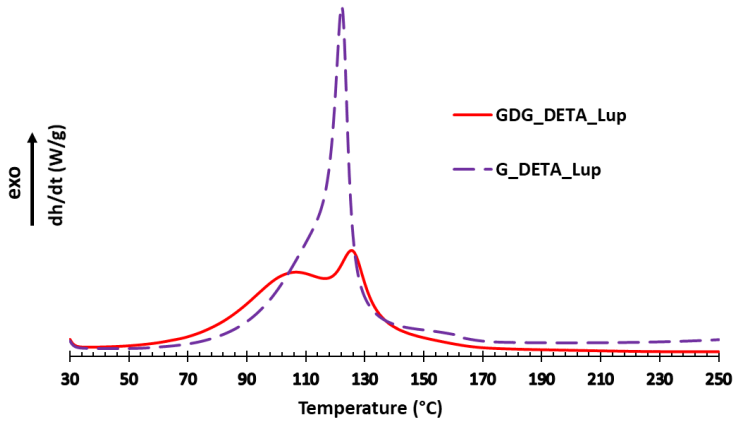

Figure 3.2. DSC thermograms corresponding to the dynamic curing at 10 °C/min for GDG_DETA_Lup (red) and G_DETA_Lup (dotted purple) formulations.

It is worth saying that GMA-amine formulations cannot gel during the first stage of the dual-curing, due to the monofunctionality of GMA in the epoxy-amine reaction, so that they produce a viscous liquid intermediate. Thus, to get a gelled intermediate material the addition of DGEBA, with a functionality of two, is necessary to get crosslinking points when amines have reacted. To investigate the amount of DGEBA needed to get gelation, the theoretical conversion of the epoxy groups at the gel point, *αgel*, during the epoxy-amine condensation had to be calculated assuming the ideal random step-wise reaction, using the well-known Flory-Stockmayer equation (Eq. 3.8) [36,37]:

$$\alpha_{gel}^{theor} = \sqrt{\frac{r}{(f_1-1)\cdot(f_2-1)}} \qquad \text{(Eq. 3.8)}$$

where r is the hydrogen amine/epoxy equivalent ratio, f_1 the epoxy monomer functionality and f_2 the amine functionality.

With this equation, a ratio of nDGEBA/mGMA = 0.166 was calculated as the lowest to achieve the gelation at 100% of conversion. Two different possibilities were studied herein: a) a ratio nDGEBA/mGMA = 0.4, in which gelation will be achieved before full conversion to obtain a conformable solid-intermediate material and b) a ratio nDGEBA/mGMA = 0, where gelation will not occur, and a viscous liquid will be obtained.

Figure 3.2 shows that the addition of DGEBA to the formulation accelerates the epoxy-amine reaction and a better splitting of both stages is observed although they are partially overlapped. In this formulation, the maximum of the epoxy-amine exotherm appears at about 105 °C, whereas the methacrylate homopolymerization reaches its maximum at about 120 °C, because of the formation of radicals at this temperature. As it can be observed in Table 3.2, in formulations with or without DGEBA, $\Delta H_{\text{epoxy-amine}}$ and T_{max} are very similar, but with a slightly higher enthalpy and a slightly lower temperature of the maximum for GDG_DETA, facilitating the separation of the first and the second stages.

Although sequentiality cannot be reached in dynamic scans, it must be considered that in a technological process, each step of curing requires a different temperature to be completed without overlapping them. To find out these appropriate temperatures we perform kinetic studies of both stages separately.

To obtain the kinetic parameters of the epoxy-amine reaction, dynamic DSC experiments were performed. Figures 3.3a and 3b show the DSC thermograms and the plot of the conversion against temperature, respectively for the epoxy-amine reaction of GDG_DETA formulation at different heating rates (2.5, 5, 10 and 20 °C). These formulations did not contain the radical initiator to suppress acrylate homopolymerization. In Supporting Information, Figure 3.S2a and 3.S2b report the same study for G_DETA formulation.

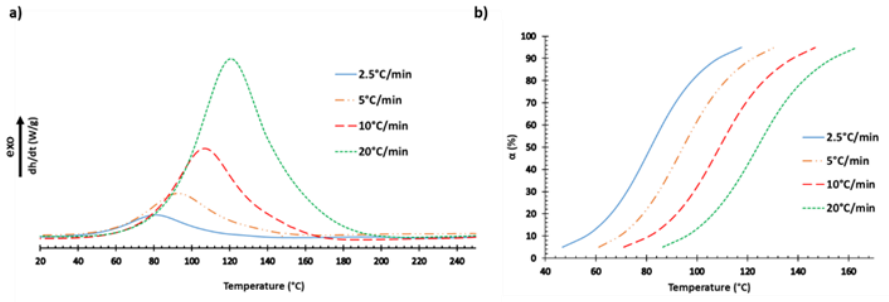

Figure 3.3. a) DSC thermograms for the GDG_DETA formulation at different heating rates and b) degree of conversion versus temperature for the same formulation.

As it can be observed, the temperature of the maximum of the exotherm is lower when the heating rate is slower, but in all cases the reaction heat remains constant with values between 87-87.9 kJ/eq, reaching almost 100% of conversion. The kinetic parameters of non-isothermal curing for GDG_DETA formulation obtained by DSC experiments are collected in Table 3.3 and for G_DETA in Table 3.S1. If we look in Table 3.3, it is possible to observe that the activation energy remains relatively constant in the process which indicates that the same mechanism is maintained in the whole reaction.

Table 3.3. Kinetic parameters from dynamic DSC studies of GDG_DETA formulation.

α[a]	E[b] (kJ/mol)	$ln[AR/g(\alpha)E]$ ($K^{-1}\cdot min^{-1}$)	r[c]	lnA[d] (min^{-1})	k[e] (min^{-1})	$d\alpha/dt$[f] (min^{-1})	Isothermal time[g] (min)
0.05	45.5	6.44	0.991	13.77	0.032	0.009	8.52
0.1	47.51	6.66	0.998	14.47	0.031	0.010	14.12
0.15	48.53	6.71	0.999	14.82	0.029	0.014	19.42
0.2	49.20	6.71	0.999	15.05	0.029	0.012	24.63
0.3	50.06	6.66	0.999	15.34	0.028	0.009	35.20
0.4	50.71	6.61	0.999	15.58	0.028	0.008	46.68
0.5	51.40	6.60	0.999	15.83	0.027	0.007	60.44
0.6	52.19	6.62	0.999	16.11	0.027	0.005	78.78
0.7	53.08	6.64	0.999	16.41	0.026	0.003	106.51
0.8	53.91	6.56	0.999	16.68	0.025	0.002	155.46
0.9	55.31	6.48	0.999	17.11	0.022	0.001	279.31

[a] Conversion degree. [b] Activation energy. [c] Correlation coefficient. [d] Pre-exponential factor calculated using kinetic the autocatalytic model. [e] Rate constant calculated by Arrhenius equation. [f] Reaction rate calculated by Eq. 3.3. [g] Simulated isothermal time using non-isothermal isoconversional data.

Moreover, it suggests that a single kinetic model is needed to describe the curing. Furthermore, the reaction rate increases at low conversions but after reaching a maximum, decreases, confirming the autocatalytic behavior of the epoxy-amine reaction. The hydroxyl groups formed during the epoxy-amine condensation catalyze the ring opening of the epoxides by forming hydrogen bonds between hydroxylic protons and the epoxides [38]. Moreover, the theoretical isothermal curing time for the first stage at 45 °C needed to achieve a 90% of conversion is 279 min, which is very close to the reaction time in the oven that we obtained experimentally which was 270 min.

React. Funct. Polym. **2021**, *159*, 104822

Once the first curing stage has been studied by DSC the characterization of the second stage is needed to optimize the global system. The standard reaction heat for a methacrylate homopolymerization is around 60 kJ/eq [39,40], and therefore it is important to verify the heat that the second curing stage releases after the epoxy-amine condensation.

A dynamic DSC of the intermediate material prepared from GDG_DETA_Lup formulation, cured in the oven, gave us the T_g reached, and the heat evolved by the homopolymerization while confirming that the first stage has been completed in the curing conditions determined by kinetic studies. Figure 3.4a shows that the first stage has been completed giving a flexible solid material with a T_g= 14 °C without the possibility to suffer dripping or exudation because no free unreacted molecules are present in the material. Moreover, we could check that the reaction heat released by the methacrylate homopolymerization was 41 kJ/eq. This value is lower than that reported, since not all methacrylate groups in the mixture will react due to topological restrictions, produced by the short distance between reactive groups in the GMA molecule.

In the same way than for the 1st stage we determined the kinetic parameters by performing DSC experiments at the same heating rates to fully optimize the curing conditions.

The reaction heat in all the experiments remained relatively constant with values in the range 42.5-40.7 kJ/eq. Moreover, it can be seen in Figure 3.4c that the conversion at the beginning increases slowly but rapidly gets higher values in a short range of temperatures, which can be attributed to the fast propagation once radicals are generated.

If we look at the plot of the activation energy (Figure 3.4d) we can see higher values at low conversions (initiation step) but a decrease when the conversion increases, due to the fact that termination, with a very low activation energy, begins to occur. The kinetic parameters of non-isothermal curing for the second stage obtained by DSC dynamic experiments are reported in Table 3.S2. The higher activation energy of methacrylate homopolymerization in comparison to the epoxy-amine condensation puts in evidence the dual nature of the curing process.

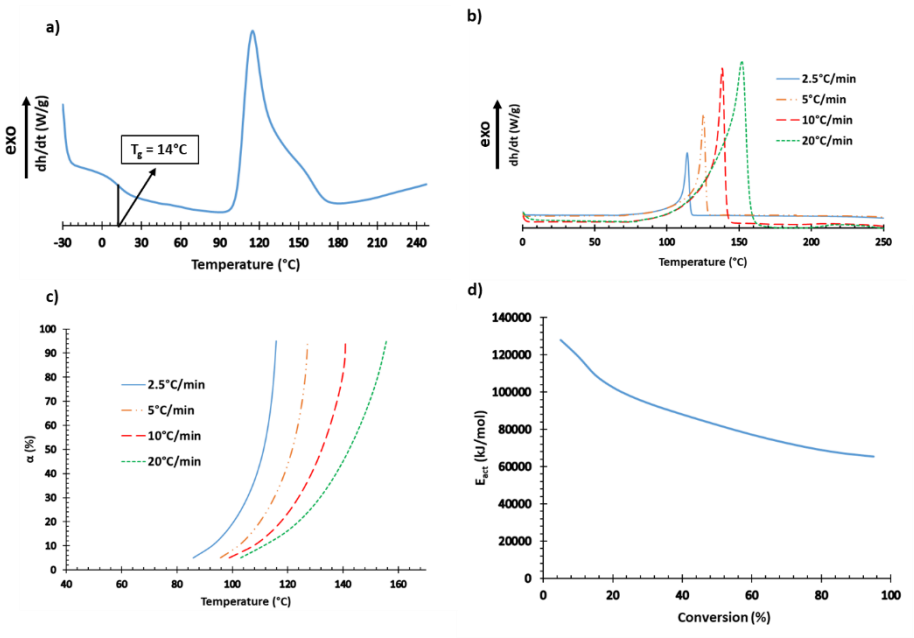

Figure 3.4. a) DSC thermogram corresponding to the dynamic curing at 10°C/min of the intermediate material for the formulation GDG_DETA_Lup, b) DSC thermograms for the 2nd curing of a G_Lup formulation at different heating rates, c) degree of conversion *vs.* temperature for the same sample and d) plot of activation energy *vs* conversion of the 2nd stage.

The intermediate materials obtained after performing the 1st stage in the oven were stable at least for 4 days, since the T_g of this material remained unchanged, such as expected from the stability of the radical initiator at temperatures lower than 120 °C.

The thermomechanical characterization of this intermediate material was done and the obtained DMTA curves are represented in Figure 3.S3, where a maximum of tan δ of 23.5 °C and a storage modulus around 50 MPa at room temperature was determined. As expected, the modulus increases when the second curing stage initiates.

4.2 Study of the curing process by FTIR spectroscopy

DSC provides information of the whole process but not about the evolution of the chemical reactions that occurs during curing. To get structural information, FTIR spectroscopy was applied to the isothermal curing of the reaction mixture. This methodology allows to determine the progress of the conversion at different reaction times for the functional groups involved in the reaction, taking as reference an invariable absorption band. In addition, it gives information of the chemical structure

of the network formed. Figure 3.5 shows the evolution of the epoxy bands during the reaction for the GDG_DETA mixture, which corresponds to the first stage of curing.

As it can be clearly seen, at 3400 cm^{-1} an increase of the peak corresponding to the OH groups formed by the ring opening of the epoxide by the amine is taking place during the whole reaction time, while the band corresponding to the epoxy groups at 910 cm^{-1} is declining, until complete disappearance, leading to the conclusion that the reaction has been completed during the curing process. Moreover, the band of the double bond of the methacrylate group at 1636 cm^{-1} does not suffer any change, confirming that the methacrylate does not react in these conditions. The small band at 1636 cm^{-1} attributed to the aromatic signals of DGEBA is maintained during the curing process and has been used as internal reference for kinetic studies.

Figure 3.S4 shows the FTIR conversion plot during isothermal curing at 45 °C (epoxy-amine reaction) for the GDG_DETA sample (blue curve). We can see that the process starts relatively slowly at this temperature, which is in accordance with the calorimetric studies (red curve). The aforementioned autocatalytic character leads to an increased curing rate. Although the conversion reaches 90% in about 150 min, it takes a few more minutes to complete the reaction.

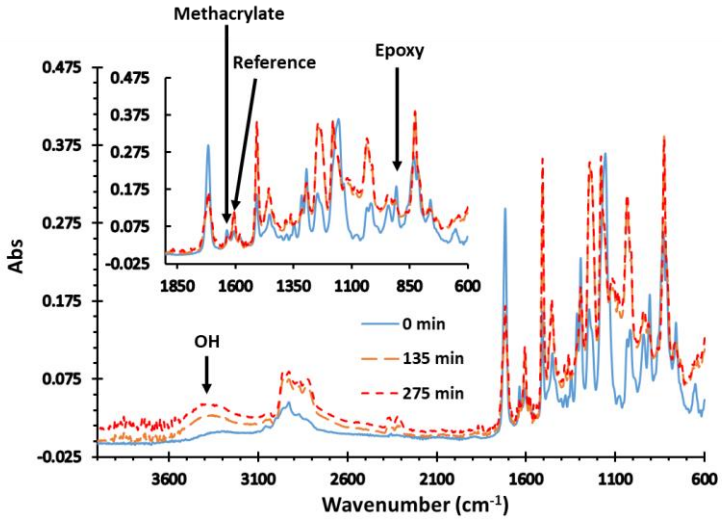

Figure 3.5. Evolution of FTIR spectra at 45 °C for GDG_DETA monitored during 270 min.

FTIR analysis was also applied to evaluate the conversion achieved in the second step of the curing process in both thermal and photochemical conditions. Figure 3.6 present the FTIR spectra of the cured materials, when the homopolymerization of acrylates was initiated by Luperox (thermal) and DMPA (photochemical). The spectrum of the intermediate material has been added to visualize the changes produced.

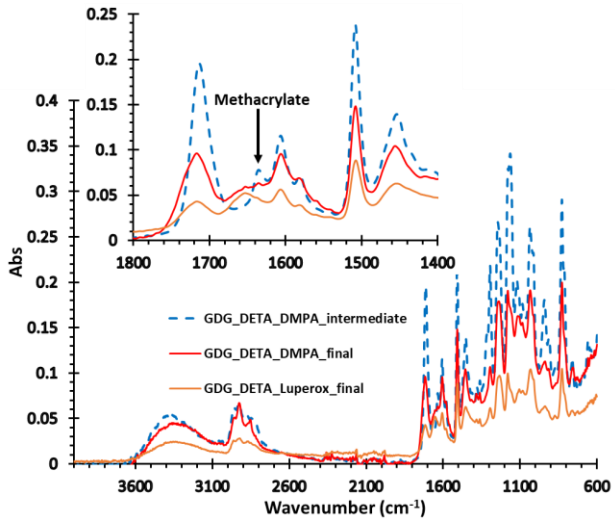

Figure 3.6. FTIR spectra of the intermediate material (blue line) and of the final thermosets obtained in thermal (orange line) or in photochemical conditions (red line)

After homopolymerization the absorption at 1636 cm^{-1}, corresponding to the C=C st. of the methacrylate groups, has completely disappeared in case of GDG_DETA_Luperox formulation after heating at 120 °C, 150 °C and 200 °C during 90 min, 60 min and 90 min respectively indicating a full conversion of these groups and a complete curing. On the contrary for GDG_DETA_DMPA formulation there is still a small peak after long irradiation times (1.5 min at room temperature), which indicates that some methacrylic groups remain unreacted after long irradiation times. This observation leads us to conclude that vitrification has occurred when irradiating, hindering the achievement of a complete reaction at these temperature conditions, which will affect the final performance of this thermoset.

4.3 Study of the gelation process by rheology

As mentioned before, the addition of DGEBA to the GMA formulation enables the system to achieve the gelation during the 1st stage. At the gelation point there is a change of liquid to solid behavior and the gelled material can be processed by different manufacturing processes like, for example, compression molding.

To determine the gel time, rheology is the best methodology among those used. Rheometric measurements were carried out for G_DETA and GDG_DETA formulations to compare the behavior of both compositions and to find out the gelation time of the latter. Figure 3.7 shows the plot of tan δ *vs.* time for GDG_DETA formulation at three different frequencies. The point at which the three tan δ intersect corresponds to the gelation time, which was 88 min at 45 °C. Figure 3.S5 shows the same graph for the G_DETA formulation in which we can see that the tan δ curves do not intersect at any

point in the whole process indicating that no gelation occurs and, consequently, a viscous liquid will be obtained as the intermediate material, which can be applied on surfaces as adhesive or coating. Both intermediate materials will improve their mechanical performance once the 2nd stage has been completed.

Rheological experiments by themselves do not allow to determine the conversion at the gelation for the GDG_DETA formulation, but this value can be calculated from the conversion evolution obtained by isothermal DSC or FTIR at 45 °C for 4.5 h (Figure 3.S4). In this figure it is possible to see that at 88 min the epoxy group has reached a conversion of about 70%, which fits quite well with the $\left(\alpha_{gel}^{theor}\right)$ calculated by Eq. 3.8, 75%.

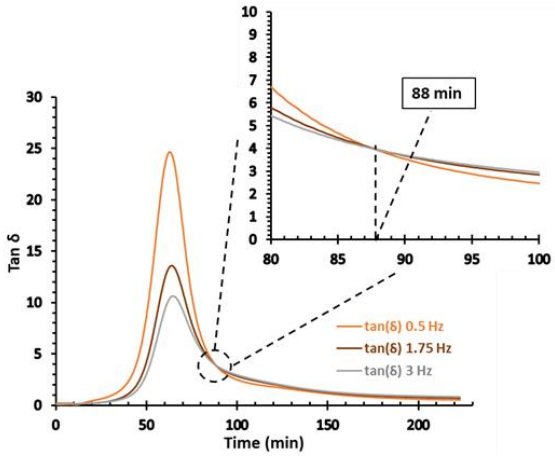

Figure 3.7. Evolution at 45 °C of tan δ *vs*. time at three different frequencies for GDG_DETA formulation.

4.4 Thermogravimetric and dynamo mechanical analysis of thermosets

The thermal stability of the cured materials was studied by thermogravimetry (TGA). Figure 3.8 shows the TGA curves and their derivatives for all the thermosets prepared. Table 3.4 collects the most significant data extracted.

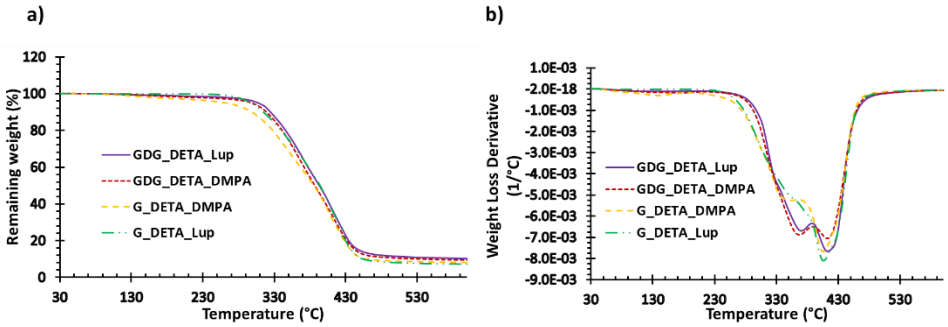

Figure 3.8. TGA and DTG curves for all the thermosets prepared in thermal and photochemical conditions in N_2 atmosphere.

Table 3.4. Thermogravimetric and thermomechanical data of the thermosets prepared.

Sample	$T_{5\%}$[a] (°C)	T_{max}[b] (°C)	Char Yield[c] (%)	$T_{tan\ \delta}$[d] (°C)	E'_{glassy}[e] (MPa)	$E'_{rubbery}$[f] (MPa)
GDG_DETA_Lup	307.3	368.5/412.8	10.3	168.4	3209	199.6
G_DETA_Lup	295.0	362.1/406.7	9.0	127.7	-	-
GDG_DETA_DMPA	297.9	366.7/411.5	9.7	100.7	3541	78.3
G_DETA_DMPA	261.2	354.6/405.9	9.1	97.8	-	-

[a] Temperature of 5% of weight loss. [b] Temperature of the maximum rate of degradation of the two main steps. [c] Char residue at 600 °C. [d] Temperature at the maximum of tan δ peak at 1 Hz. [e] Glassy storage modulus determined by DMTA. [f] Rubbery storage modulus determined by DMTA.

It can be observed that the shape of the degradation curves is similar for all the materials and takes place in two main steps. The presence of DGEBA slightly increases the temperature of initial degradation (taken as $T_{5\%}$) and the thermosets obtained thermally show a higher stability, because of their higher crosslinked character. The first stage at the temperature range of 270-370 °C can be assigned to the degradation of the poly(hydroxy-amine) network because of the high content of labile C-N bonds. The second step between 390-430 °C can be related to the poly(methacrylate) breakage [41]. The presence of aromatic moieties in the DGEBA containing thermosets leads to a slightly higher char yield.

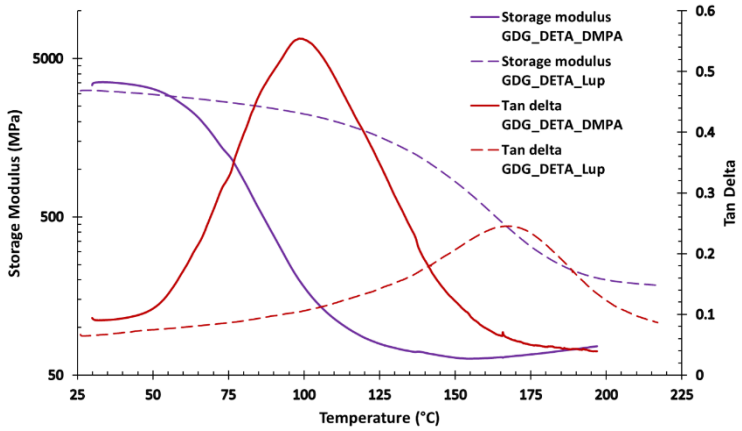

Figure 3.9. Evolution of tan δ and storage modulus against temperature of GDG_DETA_Lup and GDG_DETA_DMPA thermosets.

The thermomechanical behavior of both materials prepared was evaluated by DMTA analyses. Figure 3.9 presents the tan δ curves as well as the storage modulus obtained for GDG_DETA_Lup and GDG_DETA_DMPA cured materials and the most representative data are collected in Table 3.4. The cured materials without DGEBA

React. Funct. Polym. **2021**, *159*, 104822

result in brittle and defective samples and the moduli could not be determined accurately enough (because the non-uniform dimensions) so they are not shown.

As we can see, the glassy moduli are similar and high for thermally and photochemically cured thermosets indicating the high rigidity of these materials at room temperature. The temperature at the tan δ peak is related to the glass transition temperature of the materials, and if we compare both values, we can observe a big difference of about 70 °C between them. This difference can be attributed to the vitrification of GDG_DETA_DMPA that takes place during UV-curing, since the temperature of curing is lower than its T_g. Due to vitrification, the photo-cured formulation is only partially cured, as we saw by FTIR, with lower crosslinking density, which is also reflected by its lower modulus in the rubbery state.

5. Conclusions

In this work, a new dual-cure system has been developed based on the joint presence of epoxy and methacrylate groups in a commercially available compound, glycidyl methacrylate. The first curing stage is a stoichiometric epoxy-amine condensation with the addition or not of DGEBA and the second, a free radical polymerization of methacrylate groups, thermally or UV-initiated.

The curing kinetics of both thermally induced stages have been studied by non-isothermal isoconversional analysis using DSC and monitored by real time FTIR analysis. Although dynamic DSC studies on complete formulations show that epoxy-amine and methacrylate homopolymerization processes occur overlapped, an adequate temperature has been found to perform a sequential curing with two well-differentiated steps, with the formation of a stable intermediate material. Depending on the radical initiator selected for the formulation, the second stage can be carried out in thermal or photochemical conditions.

The intermediate materials can be a deformable rubbery solid or a viscous liquid, depending on the addition or not of diglycidylether of bisphenol A to the reactive formulation. They have high stability, and no dripping or exudation will take place as no unreacted monomers are present. The appropriate selection of the formulation composition allows to tailor the characteristics of the intermediate and final materials.

The final thermosets have a high glassy storage modulus which indicates their high rigidity at room temperature. Thermally cured materials have a higher glass transition temperature and crosslink density than the photo-cured ones, due to the vitrification of the latter. Despite this, the glass transition temperature exhibited by UV-cured material is high enough for most applications of interest. All these above-mentioned features together with the great thermal stability of the prepared materials open the possibility of working with them in applications that require high temperatures.

Acknowledgments

The authors would like to thank MINECO (Ministerio de Economia, Industria y Competitividad, MAT2017-82849-C2-1-R and 2-R) and Generalitat de Catalunya (2017-SGR-77 and BASE3D) for their financial support. Miwon Spain S.L. is thanked for donating glycidyl methacrylate.

References

[1] X. Luo, P.T. Mather, Shape memory assisted self-healing coating, ACS Macro Lett. 2 (2013) 152-156.

[2] J. Verrey, M.D. Wakeman, V. Michaud, J.A.E. Månson, Manufacturing cost comparison of thermoplastic and thermoset RTM for an automotive floor pan, Compos. Part A 37 (2006) 9-22.

[3] M. Giordano, A. Laudati, M. Russo, J. Nasser, G.V. Persiano, A. Cusano, Advanced cure monitoring by optoelectronic multifunction sensing system, Thin Solid Films 450 (2004) 191-194.

[4] X. Ramis, X. Fernández-Francos, S. De La Flor, F. Ferrando, À. Serra, Click-based dual-curing thermosets and their application in: Q. Guo (Ed.), Thermosets 2nd ed. Structure, Properties and Application, Ch.16, pp. 511-541, Elsevier, 2018.

[5] F. Gamardella, V. Sabatini, X. Ramis, À. Serra, Tailor-made thermosets obtained by sequential dual-curing combining isocyanate-thiol and epoxy-thiol click reactions, Polymer 174 (2019) 200-209.

[6] S. Chatani, C. Wang, M. Podgórski, C.N. Bowman, Triple shape memory materials incorporating two distinct polymer networks formed by selective Thiol-Michael addition reactions, Macromolecules 47 (2014) 4949-4954.

[7] K. Chen, X. Kuang, V. Li, G. Kang H.J. Qi, Fabrication of tough epoxy with shape memory effects by UV-assisted direct-ink write printing, Soft Matter 14 (2018) 1879-1886.

[8] A. Belmonte, C. Russo, V. Ambrogi, X. Fernández-Francos, S. De La Flor, Epoxy-based shape-memory actuators obtained via dual-curing of off-stoichiometric “thiol-epoxy” mixtures, Polymers 9 (2017) 113-131.

[9] X. Zhang, L. Cox, Z. Wen, W. Xi, Y. Ding, C.N. Bowman, Implementation of two distinct wavelengths to induce multistage polymerization in shape memory materials and nanoimprint lithography, Polymer 156 (2018) 162-168.

[10] S.H. Cho, S.R. White, P.V. Braun, Self-healing polymer coatings Adv. Mater. 21 (2009) 3308-3313.

[11] C.-H. Park, S.-W. Lee, J.-W. Park, H.-J. Kim, Preparation and characterization of dual curable adhesives containing epoxy and acrylate functionalities, React. Funct. Polym. 73 (2013) 641-646.

[12] V. S. Khire, Y. Yi, N.A. Clark, C. N. Bowman, Formation and surface modification of nanopatterned thiol-ene substrates using step and flash imprint lithography, Adv. Mater. 20 (2008) 3308-3313.

[13] A. M. Prenen, J. C. A. van der Werf, C. W. M. Bastiaansen, D. J. Broer, Monodisperse, polymeric nano- and microsieves produced with interference holography, Adv. Mater. 21 (2009) 1751-1755.

[14] H. Peng, D. P. Nair, B. A. Kowalski, W. Xi, T. Gong, C. Wang, M. Cole, N. B. Cramer, X. Xie, R.R. McLeod, C. N. Bowman, High performance graded rainbow holograms via two-stage sequential orthogonal thiol-click chemistry, Macromolecules 47 (2014) 2306-2315.

[15] W. Xi, H. Peng, A. Aguirre-Soto, C. J. Kloxin, J. W. Stansbury, C. N. Bowman, Spatial and temporal control of thiol-Michael addition via photocaged superbase in photopatterning and two-stage polymer networks formation, Macromolecules 47 (2014) 6159-6165.

[16] N. B. Cramer, C. L. Couch, K. M. Schreck, J. E. Boulden, R. Wydra, J. W. Stansbury, C. N. Bowman, Properties of methacrylate-thiol-ene formulations as dental restorative materials, Dent Mater. 26 (2010) 799-806.

[17] J.E. Moses, A.D. Moorhouse, The growing applications of click chemistry, Chem Soc. Rev. 36 (2007) 1249-1262.

[18] W. H. Binder, R. Sachsenhofer, “Click” chemistry in polymer and materials science, Macromol. Rapid Commun. 28 (2007) 15-54.

[19] H. C. Kolb, M. G. Finn, K. B. Sharpless, Click chemistry: diverse chemical function from a few good reactions, Angew. Chem. Int. Ed. 40 (2001) 2005-2021.

[20] O. Konuray, X. Fernández-Francos, S. De la Flor, X. Ramis, À. Serra, The use of click-type reactions in the preparation of thermosets, Polymers 12 (2020) 1084.

[21] O. Konuray, N. Areny, J. M. Morancho, X. Fernández-Francos, À. Serra, X. Ramis, Preparation and characterization of dual-curable off-stoichiometric amine-epoxy thermosets with latent reactivity, Polymer 146 (2018) 42-52.

[22] J. M. Morancho, X. Ramis, X. Fernández.Francos, J. M. Salla, O. Konuray, À. Serra, Curing of off-stoichiometric amine-epoxy thermosets, J. Therm. Anal. Calorim. 133 (2018) 519-527.

[23] O. Konuray, A. García, J. M. Morancho, X. Fernández-Francos, À. Serra, F. Ferrando, M. García-Alvarez, X. Ramis, Hard epoxy thermosets obtained via two sequential epoxy-amine condensations, Eur. Polym. J. 116 (2019) 222-231.

[24] K. Studer, C. Decker, E. Beck, R. Schwalm, Thermal and photochemical curing of isocyanate and acrylate functionalized oligomers, Eur. Polym J. 41 (2005) 157-167.

[25] F. Mustata, N. Tudorachi, I. Bicu, Thermosetting resins obtained via sequential photo and thermal crosslinking of epoxy resins. Curing kinetics, thermal properties and morphology, Compos. Part B 55 (2013) 470–478.

[26] R. Thomas, C. Sinturel, J. Pionteck, H. Puliyalil, S. Thomas, In-situ cure and cure kinetic analysis of a liquid rubber modified epoxy resin, Ind. Eng. Chem. Res. 51 (2012) 12178-12191.

[27] C. Russo, À. Serra, X. Fernández-Francos, S. De La Flor, Characterization of sequential dual-curing of thiol-acrylate-epoxy systems with controlled thermal properties, Eur. Polym. J. 112 (2019) 376-388.

[28] S. Vyazovkin, Isoconversional Kinetics of Thermally Stimulated Processes, Springer, New York, NY, USA, pp. 166-231, 2015.

[29] S. Vyazovkin, N. Sbirrazzuoli, Kinetic methods to study isothermal and nonisothermal epoxy-anhydride cure, Macromol. Chem. Phys., 200 (1999) 2294-2303.

[30] A. W. Coats, J. P. Redfern, Kinetic parameters from thermogravimetric data, Nature 201 (1964) 68-69.

[31] H. E. Kissinger, Reaction kinetics in differential thermal analysis, Anal. Chem. 29 (1957) 1702-1706.

[32] R. L. Blaine, H. E. Kissinger, Homer Kissinger and the Kissinger equation, Thermochim. Acta, 540 (2012) 1-6.

[33] S. Vyazkovin, D. Dollimore, Linear and nonlinear procedures in isoconversional computations of the activation energy of non-isothermal reactions in solids, J. Chem. Inf. Model. 36 (1996) 42-45.

[34] R. J. Varley, J. H. Hodgkin, D. G. Hawthorne, G. P. Simon, Toughening of a trifunctional epoxy system. II. Thermal characterization of epoxy/amine cure, J. Appl. Polym. Sci. 60 (1996) 2251-2263.

[35] O. Konuray, F. Di Donato, M. Sangermano, J. Bonada, A Tercjak, X. Fernández-Francos, À. Serra, X. Ramis, Dual-curable stereolithography resins for superior thermomechanical properties, EXPRESS Polym. Lett. 14 (2020) 881-894.

[36] J. P. Pascault, H. Sautereau, J. Verdu, R. J. J. Williams, Thermosetting Polymers, Marcel Dekker, New York, 2002.

[37] J. P. Pascault, R. J. J. Williams, Overview of thermosets: present and future, in: Q. Guo (Ed.), Thermosets 2nd Ed. Structure, Properties and Application, Ch.11, pp. 3-34, Elsevier, 2018.

[38] B. A. Rozenberg, Kinetics, thermodynamics and mechanism of reactions of epoxy oligomers with amines, Adv. Polym. Sci. 75 (1986) 113-165.

[39] A. Cadenato, J. M. Morancho, X. Fernández-Francos, J.M. Salla, X. Ramis, Comparative kinetic study of the non-isothermal termal curing of bis-GMA/TEGDMA systems, J. Therm. Anal. Cal. 89 (2007) 233-244.

[40] A. C. Uzcategui, A. Muralidharan, V. L. Ferguson, S. J. Bryant, R.R. McLeod, Understanding and improving mechanical properties in 3D printed parts using a dual-cure acrylate-based resin for stereolithography, Adv. Eng. Mater. 20 (2018), 1800876.

[41] G. González, X. Fernández-Francos, À. Serra, M. Sangermano, X. Ramis, Environmentally-friendly processing of thermosets by two-stage sequential aza-Michael addition and free-radical polymerization of amine-acrylate mixtures, Polym. Chem. 6 (2015) 6987-6997.

Supporting Information

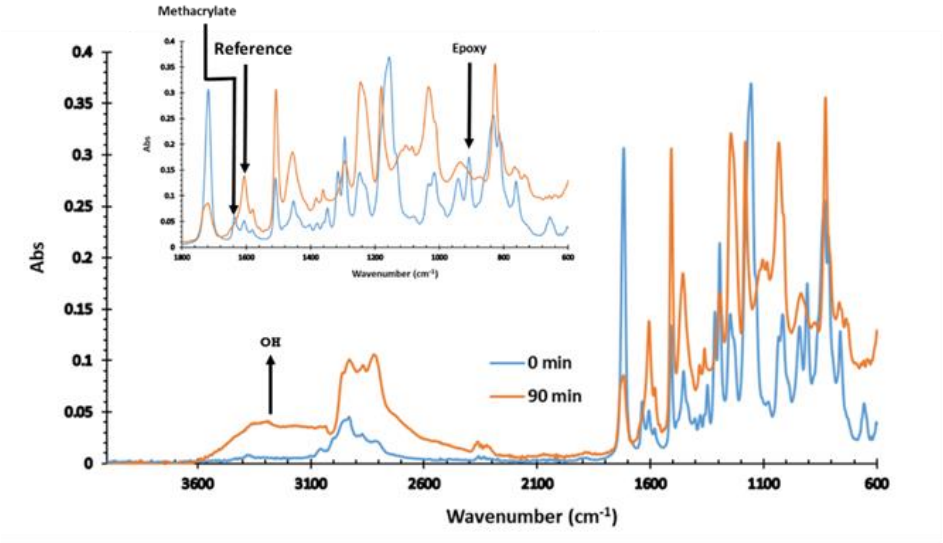

Figure 3.S1. Evolution of FTIR spectra at 45 °C for GDG_TREN monitored during 90 min.

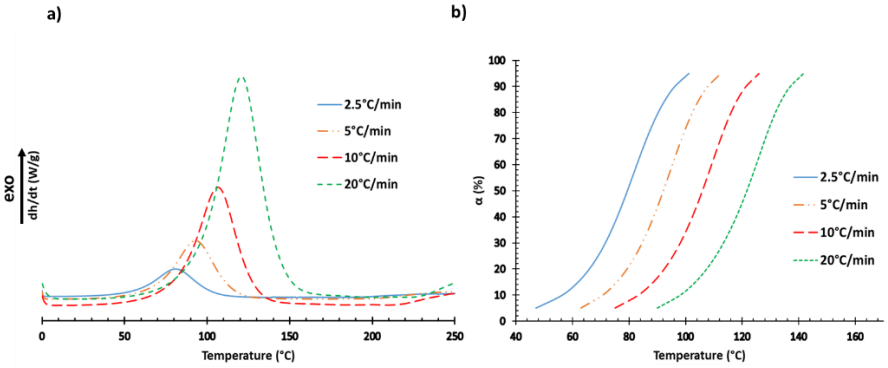

Figure 3.S2. a) DSC thermograms for the G_DETA formulation in different heating rates and b) degree of conversion versus temperature for the same formulation.

Table 3.S1. Kinetic parameters of dynamic curing obtained by DSC of G_DETA formulation.

α[a]	E[b] (kJ/mol)	ln[AR/g(α)E] (K^{-1}·min^{-1})	r[c]	lnA[d] (min^{-1})	k[e]	dα/dt[f] (min^{-1})	Isothermal time[g] (min)
0.05	41.68	4.98	0.993	12.20	0.028	0.008	9.54
0.1	45.24	5.80	0.998	13.56	0.029	0.010	14.87
0.15	46.98	6.13	0.999	14.21	0.029	0.011	19.89
0.2	48.00	6.28	0.999	14.59	0.029	0.013	24.66
0.3	49.23	6.40	0.999	15.07	0.029	0.010	33.76
0.4	50.01	6.45	0.999	15.40	0.030	0.009	42.74
0.5	50.79	6.52	0.999	15.74	0.031	0.008	52.36
0.6	51.77	6.68	0.999	16.16	0.033	0.006	63.84
0.7	53.12	6.95	0.999	16.72	0.035	0.004	79.34
0.8	54.95	7.33	0.999	17.47	0.037	0.003	103.93
0.9	57.57	7.88	0.998	18.55	0.040	0.001	155.50

[a] Conversion degree. [b] Activation energy. [c] Correlation coefficient. [d] Pre-exponential factor calculated using kinetic the autocatalytic model. [e] Rate constant calculated by Arrhenius equation. [f] Reaction rate calculated by Eq. 3.3. [g] Simulated isothermal time using isoconversional data.

Table 3.S2. Kinetic parameters of dynamic curing obtained by DSC of G_Lup formulation.

α[a]	E[b] (kJ/mol)	ln[AR/g(α)E] (K^{-1}·min^{-1})	r[c]	lnA[d] (min^{-1})	k[e] (min^{-1})	dα/dt[f] (min^{-1})
0.05	113.71	27.14	0.954	35.37	0.0005	0.0001
0.1	109.24	24.93	0.977	33.57	0.0005	0.0002
0.15	105.48	23.27	0.982	32.16	0.0005	0.0002
0.2	102.58	22.01	0.985	31.09	0.0005	0.0002
0.3	94.16	18.91	0.994	28.23	0.0006	0.0002
0.4	88.01	16.70	0.997	26.22	0.0009	0.0003
0.5	82.40	14.77	0.998	24.47	0.0013	0.0003
0.6	77.17	13.03	0.999	22.91	0.0019	0.0004
0.7	72.66	11.56	0.999	21.65	0.0030	0.0004
0.8	68.90	10.35	0.999	20.71	0.0048	0.0003
0.9	66.36	9.54	0.999	20.36	0.0090	0.0003

[a] Conversion degree. [b] Activation energy. [c] Correlation coefficient. [d] Pre-exponential factor calculated using kinetic the autocatalytic model. [e] Rate constant calculated by Arrhenius equation. [f] Reaction rate calculated by Eq. 3.3.

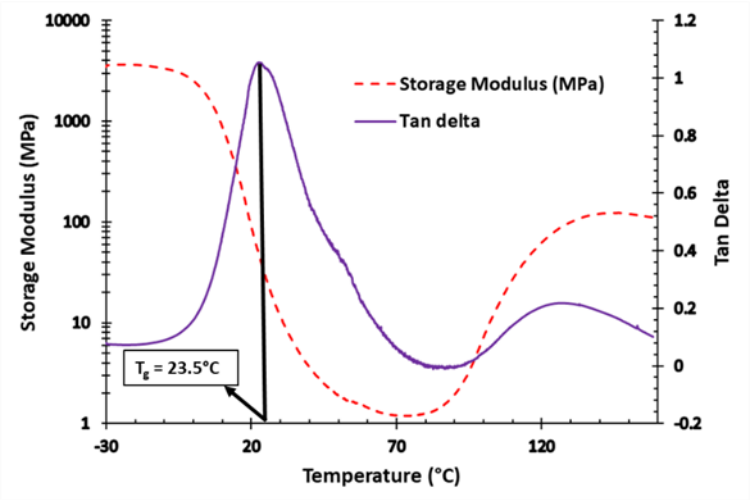

Figure 3.S3. Evolution of the tan δ and storage modulus against temperature of GDG_DETA_Lup during the second curing.

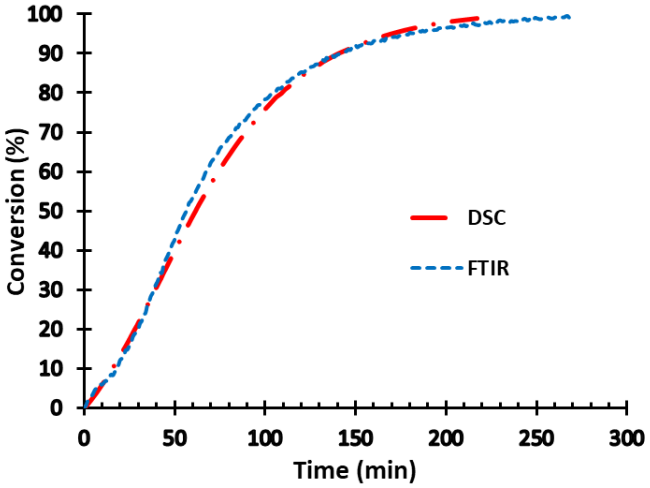

Figure 3.S4. Plot of the conversion versus time of the isothermal curing at 45 °C in DSC (red) and FTIR (blue) for the formulation GDG_DETA.

React. Funct. Polym. **2021**, *159*, 104822

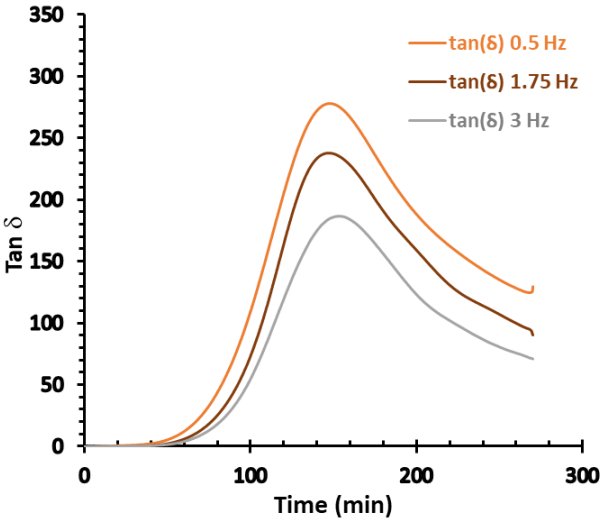

Figure 3.S5. Rheological analysis of G_DETA formulation showing the tan δ evolution with time during the 1st stage of the dual-curing process at three different frequencies.

UNIVERSITAT ROVIRA I VIRGILI
PROGRESS IN SUSTAINABILITY WITHIN THE REALM OF DESIGNING NEW THERMOSETTING MATERIALS
Adrià Roig Gibert

Chapter 4

Sequential photo-thermal curing of (meth)acrylate-epoxy thiol formulations

(*Polymer* **2021**, *230*, 124073)

UNIVERSITAT ROVIRA I VIRGILI
PROGRESS IN SUSTAINABILITY WITHIN THE REALM OF DESIGNING NEW THERMOSETTING MATERIALS
Adrià Roig Gibert

Polymer **2021**, *230*, 124073

Sequential photo-thermal curing of (meth)acrylate-epoxy thiol formulations

Adrià Roig,[1] Xavier Ramis,[2] Silvia De la Flor,[3] Àngels Serra[1]

[1] Universitat Rovira i Virgili, Department of Analytical and Organic Chemistry, C/ Marcel·lí Domingo 1, Edif. N4, 43007 Tarragona, Spain

[2] Universitat Politècnica de Catalunya, Thermodynamics Laboratory, ETSEIB, Av. Diagonal, 08028 Barcelona, Spain

[3] Universitat Rovira i Virgili, Department of Mechanical Engineering, Av. Països Catalans 26, 43007 Tarragona, Spain

ABSTRACT

In this work, a novel dual-curing procedure has been developed. It is a combination of a first radical UV-initiated thiol-(meth)acrylate reaction, followed by a second thermal thiol-epoxy step catalyzed by a base. Since (meth)acrylates can lead to homopolymerization by radical mechanism, the amount of thiol has to be optimized to reach crosslinked materials with T_gs above room temperature and good mechanical performance. It should be considered, that if the amount of thiol in the intermediate materials is too low, epoxy homopolymerization can take place during the second step. The use of glycidyl methacrylate in combination with trifunctional meth(acrylates) allows this system to gel in the 1st stage and avoids possible dripping or exudation of free monomers during the storage of the intermediate materials. Moreover, this compound reacts in both stages acting as a covalent coupling between (meth)acrylates and epoxy networks. We selected trimethylolpropane tris(3-mercaptopropionate) as the thiol, 2,2-dimethoxy-2-phenylacetophenone as UV initiator and 1-methylimidazole as the base catalyst.

The curing evolution was studied by DSC and FTIR. All the materials obtained were characterized by thermogravimetry, thermomechanical analysis and tensile tests.

KEYWORDS

Dual-curing, thiol-ene, thiol-epoxy, glycidyl methacrylate, UV-curing

1. Introduction

Thermosets are very important industrial materials because they cover a wide range of applications in many different fields such as coatings [1,2], adhesives [3], aerospace [4] or automobile industry [5]. Dual-curing is an efficient and versatile synthetic methodology that allows to fabricate thermoset devices or apply them in a controlled way with a broad range of characteristics. This consists in a sequential or simultaneous combination of two different curing reactions that can be initiated by different stimuli like temperature or UV-light [6]. Sequential dual-curing has many advantages but one of them is that it permits the preparation of stable intermediate materials in viscous or solid state with specific mechanical properties that can be directly applied or processed in order to get, once the second stage has been completed, a fully cured polymer with higher mechanical performance. The most traditional dual-curing system relies on a first step performed under UV-light and a second step triggered at high temperature. This is a useful procedure because it avoids the vitrification of the final material during the thermal stage since this is carried out at temperatures above the ultimate glass transition temperature (T_g) of the polymer. This type of sequential dual-curing is now implemented in the field of 3D-printing [7-12]. The most used reactions in the first stage of this type of dual-curing are thiol-ene [13,14], homopolymerization of meth(acrylates) [10,15] and cationic homopolymerization of epoxides [16,17] combined with epoxy-amine [11], epoxy-anhydride [8], homopolymerization of epoxides [18] or thiol-epoxy [19] reactions as the second stages.

Recently, a huge interest has arisen on the thiol-ene photoinitiated polymerizations. Typical monomers are allyl derivatives of bisphenol A or unsaturated fatty acids derivatives [20,21]. This reaction takes place via step-grown radical addition mechanism and implies some advantages like the promptness of the reaction, relatively high oxygen tolerance and low shrinkage, leading to highly transparent materials. Despite this, the flexible thioether bonds formed during the thiol-ene reaction as well as the flexible chain of the commercially available thiols cause some drawbacks in the final cured materials such as low T_g's, poor rigidity and hardness promoted by low modulus values [22,23]. In contrast, the photocuring of thiol-(meth)acrylate mixtures does not provide this kind of problems due to the occurrence of a competitive reaction, which is the radical (meth)acrylate homopolymerization, which follows a chain-growth mechanism [24]. Another advantage of (meth)acrylates is their good commercial availability with different structural characteristics. Whereas (meth)acrylate groups have a functionality of 1 in thiol-ene reactions, they have a functionality of 2 in the homopolymerization mechanism. This fact, increases crosslinking densities of the final networks and helps to diminish the required amount of thiol monomer in the formulation, leading to harder materials with a higher T_g. It is

Polymer **2021**, *230*, 124073

reported that the kinetic constant of the radical homopolymerization of acrylates is 1.5 greater than that of the abstraction of the hydrogen of the thiol and the subsequent reaction between a thiyl radical and an acrylate [25]. This situation can generate difficulties in the calculations of the stoichiometric imbalance to reach an improvement on mechanical properties of the final thermosets.

As far as we know, very few investigations have been made in the radical thiol-(meth)acrylate/thiol-epoxy dual-curing due to the high complexity of the reaction process. Jian *et al*. [19] reported the synthesis of materials using a simultaneous thiol-epoxy/thiol-acrylate system. In the curing, they used 1,5,7-triazabicyclo[4.4.0]dec-5-enyl tetraphenylborate, a photobase generator which when it is irradiated by UV light is able to generate free radicals and a strong base that can trigger both reactions. Moreover, they used isopropylthiolxanthone to extend the wavelength absorption of the catalyst. However, as the photobase generator also releases the base, base-catalyzed Michael addition also took place. They found that thiol-acrylate and acrylate homopolymerization were much faster than thiol-epoxy reactions and that polymerization shrinkage decreased on enhancing the thiol-epoxy mechanism, while storage modulus, glass transition temperature and hardness increased as well.

Taking all of this into account, we report a new sequential photo-thermal curing of (meth)acrylate-thiol-epoxy formulations based on glycidyl methacrylate (GMA) and trimethylolpropane tris(3-mercaptopropionate) (S3), using 2,2-dimethoxy-2-phenyl-acetophenone (DMPA) as UV radical initiator and 1-methylimidazole (1MI) as the catalyst for the thermal step. We also added trimethylolpropane triacrylate (TMPTA) or trimethylolpropane trimethacrylate (TMPTM) to the formulation, which have a higher functionality to obtain gelled intermediate materials during the first UV curing step. It should also be noticed that the selection of GMA as the epoxy monomer makes this reactive system highly advantageous, due to the absence of free unreacted molecules after the first step, avoiding possible dripping or exudation during the application or storage of the intermediate materials. Moreover, GMA capable to react in both curing stages, acts as a coupling agent. The competition of the radical thiol-acrylate and acrylate homopolymerization during the first step affects the T_g of the intermediate and final materials, since it leads to the stoichiometric imbalance and to the presence of unreacted thiol groups in the final material, which reduces T_g values. On the other side, reducing the proportion of thiols in the initial formulation, the homopolymerization of unreacted epoxides, once the thiol groups are exhausted, can occur. This will increase the T_g of the final material as well as the crosslinking density. Thus, because of such a complex curing mechanism, we have optimized the formulation composition to reach the adequate characteristics of the intermediate and final materials.

The evolution of both curing stages was evaluated by calorimetry (DSC) and FTIR spectroscopy and the materials obtained have been characterized by calorimetric, thermomechanical and thermogravimetric analyses and the mechanical properties by tensile test.

2. Experimental Methods

2.1 Materials

Glycidyl methacrylate (GMA) was supplied by Miwon. Trimethylolpropane trimethacrylate (TMPTM), trimethylolpropane triacrylate (TMPTA), trimethylolpropane tris(3-mercapto-propionate) (S3), 1-methylimidazole (1MI) and 2,2-dimethoxy-2-phenylacetophenone (DMPA) were provided by Sigma Aldrich and used without further purification.

2.2 Preparation of the samples

All formulations (with compositions detailed in Table 4.1) were prepared in 5 mL vials in approximately 2 g batches. First of all, 5% w/w of 1MI (to GMA) and 7% w/w of DMPA (to GMA) were weighted in a vial. Then GMA was added, and the mixture was manually stirred. Once dissolved, the corresponding amount (0.2 mol/mol GMA) of TMPTM or TMPTA were added, followed by the thiol, S3. The mixtures were vigorously and manually stirred at room temperature. In this study, different proportions of S3 were added to the formulations. They were coded as G_X_Y% where G indicates the presence of GMA, X indicates TMPTA or TMPTM and Y% the amount of S3 in molar percentage in reference to the stoichiometric amount. The stoichiometry of thiol-acrylate/thiol epoxy reaction is one mol of tri(meth)acrylate per mol of thiol and 1 mol of GMA per 2/3 mol of thiol. As an example, G_TMPTA_46% is a formulation in which GMA and TMPTA are used and a 46% mol of S3 has been added to the mixture.

The formulations prepared, were poured in a pre-silanized glass mold and left under a 36W UV lamp during 6 minutes (stage 1) in time intervals of 2 min to limit the increase of temperature. At the end of this first stage, the mixtures were cured in a conventional oven at 100°C during 2 h and post-cured at 150°C during 1 h. Fully cured samples for dynamomechanical (DMA) and thermogravimetric (TGA) analyses were die-cut and slightly polished with sandpaper to obtain rectangular specimens of 20 x 5 x 0.8 mm^3.

Polymer **2021**, *230*, 124073

Table 4.4. Compositions of the formulations prepared.

Sample	GMA (mol %)	TMPTA (mol %)	TMPTM (mol %)	S3 (mol %)	1MI (mol %)	DMPA (mol %)
G_TMPTA_stoich	45.6	9.1	-	39.6	3.9	1.8
G_TMPTA_62%	53.8	10.8		28.7	4.6	2.1
G_TMPTA_58%	54.8	11.0	-	27.4	4.7	2.1
G_TMPTA_54%	55.8	11.2	-	26.0	4.8	2.2
G_TMPTA_50%	56.9	11.4	-	24.6	4.9	2.2
G_TMPTA_46%	57.9	11.6	-	23.2	5.0	2.3
G_TMPTA_42%	59.1	11.8	-	21.6	5.1	2.4
G_TMPTA_38%	60.2	12.1	-	20.1	5.2	2.4
G_TMPTM_58%	54.8	-	11.0	27.4	4.7	2.1
G_TMPTM_54%	55.8	-	11.2	26.0	4.8	2.2
G_TMPTM_50%	56.9	-	11.4	24.6	4.9	2.2
G_TMPTM_46%	57.9	-	11.6	23.2	5.0	2.3
G_TMPTM_42%	59.1	-	11.8	21.6	5.1	2.4
G_TMPTM_38%	60.2	-	12.1	20.1	5.2	2.4

2.3 Characterization methods

Differential Scanning Calorimetry (DSC) analyses were carried out on a Mettler DSC-3+ instrument calibrated using indium (heat flow calibration) and zinc (temperature calibration) standards. Samples of approximately 8-10 mg were placed in aluminum pans with pierced lids and analyzed in nitrogen atmosphere with gas flow of 50 cm^3/min. Dynamic studies between -80 °C and 250 °C with a heating rate of 10 °C/min were performed in order to characterize the curing process. The T_gs of the intermediate and final materials were determined by performing a scan between -80 °C or -30 °C and 250 °C with a heating rate of 20 °C/min. The reaction enthalpy (Δh) was integrated from the calorimetric heat flow signal (dh/dt) using a straight baseline with help of the STARe software.

To follow the whole curing process, a FTIR spectrometer Bruker Vertex 70 with an attenuated total reflection accessory with thermal control and a diamond crystal (Golden Gate Heated Single Reflection Diamond ATR, Specac-Teknokroma) and equipped with a mid-band liquid nitrogen-cooled mercury-cadmium-telluride (MCT)

detector was used. Real-time spectra were collected in absorbance mode with a resolution of 4 cm^{-1} in the wavelength range 4000 to 600 cm^{-1} averaging 20 scans for each spectrum. The disappearance of the absorbance peak at 1636 cm^{-1} corresponding to the stretching of the C=C bond of (meth)acrylates as well as the decrease of the thiol (S-H) peak at 2570 cm^{-1} were used to confirm that the first step of the curing was complete [26]. The characteristic absorbance peak at 915 cm^{-1} corresponding to the bending of the epoxy group and the appearance of a peak at 3500 cm^{-1} related to the formation of OH groups during the thiol-epoxy reactions were used to characterize the second stage [27].

The thermomechanical properties were evaluated using a DMA Q800 (TA Instruments) with the film tension clamp. All samples were stretched under an amplitude of 10 µm and a frequency of 1 Hz using ramp temperature from -30 °C to 200 °C with a heating rate of 2 °C/min.

TGA analyses were carried out with a Mettler Toledo TGA2 thermobalance. Cured samples, weighting around 10 mg were degraded between 30 and 600 °C at a heating rate of 10 °C/min in N_2 atmosphere with a flow of 50 cm^3/min.

Final materials were tested until break in tensile mode at room temperature using an electromechanical universal testing machine (Shimadzu AGS-X) with a 1 kN load cell at 10 mm/min and using Type V samples with a thickness of 1 mm according to ASTM D638-14 standard. Three samples of each material were analyzed, and the results were averaged.

3. Results and discussion

3.1 Study of the curing process

The dual-curing process that we develop in the present work consists in a first photoinitiated thiol-(meth)acrylate polymerization followed by a thermal thiol-epoxy reaction as a second stage. Acrylates can react with thiols via two different pathways depending on the catalyst and conditions used: (a) Thermal thiol-acrylate Michael addition in the presence of a base [28] or (b) radical mediated thiol-acrylate reaction that can be initiated by UV irradiation in the presence of photoinitiators such as DMPA (Scheme 4.1). Through both reaction pathways, the structure of the final products is identical, formed by attachment of the sulfur to the methylene carbon of the vinyl group. As it is shown in the scheme, in the UV pathway, first of all, a thiyl radical is generated by reaction of the thiol and the radical produced by the photolysis of the UV initiator (reaction a). This thiyl radical can be added to the acrylic monomer in order to form a new acrylic radical (reaction b). The radical formed either abstracts a hydrogen from the thiol forming a new thiol-acrylate product and a new thiyl radical (reaction c) or propagates through another acrylate functional group generating an acrylic radical that leads to the growing of homopolymer chains (reaction d). The

occurrence of this last process leads to a stoichiometric imbalance with high proportion of thiol unreacted in the intermediate and final materials. This fact means that the T_g of the material will be reduced, and the final material could evolve over time due to the presence of unreacted thiol groups.

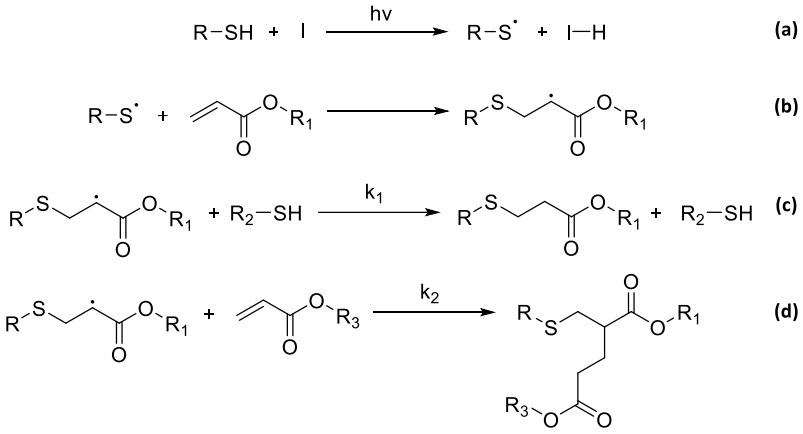

Scheme 4.1. Radical-mediated thiol-acrylate polymerization mechanism.

The presence of the 1MI in the initial formulation can initiate the thiol-Michael addition in concurrence with the radical UV-initiated thiol-ene mechanism. This increases the complexity of this curing process. It is worth to note, that acrylates and methacrylates have different reactivity in front of the thiol-Michael addition, being acrylates more reactive since the presence of a methyl group in methacrylates makes more difficult the nucleophilic attack.

On preparing the formulation, we added to the GMA monomer, 0.2 mol of a tri(meth)acrylate, TMPTA or TMPTM, per mol of GMA to ensure gelation during the first step, and the stoichiometric amount of S3 and the initiators, DMPA and 1MI, for the first and second step, respectively. Figure 4.S1 shows the DSC curves of the stoichiometric formulation prepared with TMPTA after irradiation and after the second thermal step. The most representative data are collected in Table 4.2. We evaluated that the T_g of the intermediate material was about - 45 °C and the T_g of the completely cured material was 4 °C, being both too low for practical applications. The calorimetric curve of the intermediate material presented a well-defined exotherm with an enthalpy released of about 129 kJ per epoxy equivalent, which agrees with the previously reported for thiol-epoxy reaction [29].

To increase the T_g, the proportion of S3 in the reactive mixtures was progressively decreased and subsequently DSC studies of intermediate and final materials containing TMPTA or TMPTM were performed. Figure 4.1 shows the DSC curves corresponding to the second curing step of the photocured intermediate materials, for TMPTA formulations containing different mol % of S3 in reference to the

stoichiometric amount. Figure 4.S2 provides the same information for parallel formulations with TMPTM. The calorimetric data are collected in Table 4.2.

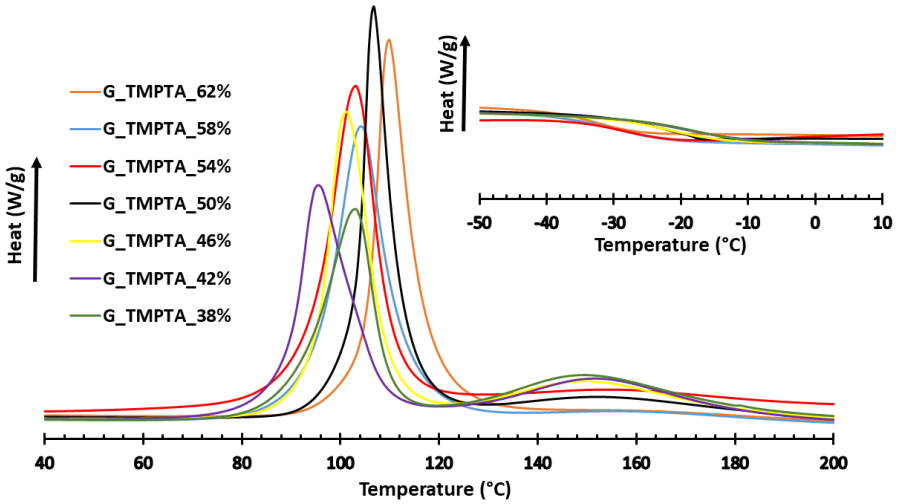

Figure 4.1. DSC curves at 10 °C/min of the thermal step for the formulations containing different % mol of thiol.

In Figure 4.1, it is possible to see an exotherm between 80 °C and 130 °C corresponding to the thermal thiol-epoxy reaction. Moreover, in the formulations containing 58% of thiol or less, a small wide peak appears between 130 °C and 175 °C. This broad exotherm can be attributed to epoxy homopolymerization, because thiols have been run out and unreacted epoxy groups are left. In the presence of 1MI, they can homopolymerize by a ring opening mechanism. We can see in Table 4.2 the values of enthalpies for both reactions, which are influenced by the composition of the formulation. A lower proportion of thiol in the mixture leads to a reduction of the thiol-epoxy enthalpy released and to an increase in the epoxy homopolymerization heat. Accordingly, the T_g of the TMPTA final materials increases on reducing the proportion of thiol in the formulation, due to the epoxy homopolymerization that takes place, which leads to increase the crosslinking density. It should be mentioned that epoxide groups have a functionality of two in homopolymerization and only one in thiol-epoxy reaction, which implies an increase of the crosslinking density, when homopolymerization occurs. Moreover, the structure of S3 is quite flexible and the lower the proportion the higher the rigidity of the network. Formulations containing TMPTM released more enthalpy in the thiol-epoxy reaction, because less thiol reacts during UV-irradiation and consequently less epoxy homopolymerization occurs. The T_g of the TMPTM materials could not be determined by DSC, probably due to the higher inhomogeneity of the network obtained that did not lead to a well-defined

transition. However, as it will be shown later, DMA of TMPTM formulations allows us to see this transition.

Table 4.5. Main calorimetric data of the intermediate and final materials.

Sample	$T_{g\ interm}$ (°C)	$T_{g\ final}$ (°C)	$\Delta H_{thiol\text{-}epoxy}$[a] (J/g)	$\Delta H_{thiol\text{-}epoxy}$[a] (kJ/eq)	$\Delta H_{ep.\ homo.}$[b] (J/g)	$\Delta H_{ep.\ homo.}$[b] (kJ/eq)
G_TMPTA_stoich	-45.5	3.9	243.6	129.3	-	-
G_TMPTA_62%	-33.7	29.8	240.5	119.1	-	-
G_TMPTA_58%	-30.7	35.3	230.9	100.1	6.9	2.1
G_TMPTA_54%	-26.1	39.7	217.7	89.0	15.9	7.0
G_TMPTA_50%	-21.4	44.9	210.8	82.4	20.6	9.1
G_TMPTA_46%	-16.9	49.0	167.6	63.3	52.4	25.6
G_TMPTA_42%	-13.3	56.1	146.9	53.6	59.1	29.9
G_TMPTA_38%	-11.9	59.8	137.9	48.4	73.9	31.2
G_TMPTM_62%	-35.1		250.9	125.7	-	-
G_TMPTM_58%	-32.1		249.1	104.4	2.1	0.9
G_TMPTM_54%	-28.2		240.4	99.2	3.4	1.4
G_TMPTM_50%	-26.8		225.6	90.1	11.2	4.5
G_TMPTM_46%	-22.4		194.4	75.1	18.4	7.1
G_TMPTM_42%	-20.8		175.2	65.3	30.2	11.3
G_TMPTM_38%	-18.5		151.6	54.5	41.8	15.0

[a] Enthalpy released in the thiol-epoxy reaction by gram of mixture and by epoxy equivalent.
[b] Enthalpy released in the epoxy homopolymerization by gram of mixture and by epoxy equivalent.

It should be deduced from Table 4.2, that by decreasing the amount of thiol in the formulation, the T_gs of all the intermediate materials become higher compared to those obtained from the stoichiometric formulation. Moreover, TMPTA intermediate materials have slightly higher T_gs than the TMPTM ones. This indicates that thermal thiol-Michael reaction competes with the thiol-ene during irradiation, because the heat evolved in the thiol-ene can favor this reaction, being easier for acrylate derivatives, as previously commented. Thus, less unreacted thiols are present in the formulation and consequently, T_gs are higher.

The enthalpy of the thiol-epoxy reaction is a bit higher in the case of methacrylates, because more thiol groups are left unreacted in the intermediate materials, which are able to react with epoxides. Consequently, less homopolymerization takes place, as we can see from the heat evolved in the broad exotherm at higher temperatures.

In both types of formulations, the progressive reduction of S3 proportion in the mixture produces a subsequent increase in epoxy homopolymerization, increasing the T_g of the cured materials as a result of the higher crosslinking density and the increase in the rigidity of the network. We can also see, that for higher concentrations of thiol (above 54%) the epoxy homopolymerization is meaningless. Nevertheless, we are able to achieve materials with T_gs above room temperature in all TMPTA formulations. However, the lower T_g of the thiol rich materials (G_TMPTA_stoich and G_TMPTA_62%) led to these proportions being discarded for further studies.

To confirm that the reactions of each step of the dual curing have been completed, we registered the FTIR spectra of the intermediate and final materials, which were compared with the spectrum of the initial formulation. Figure 4.2 shows these spectra for the G_TMPTA_58% formulation.

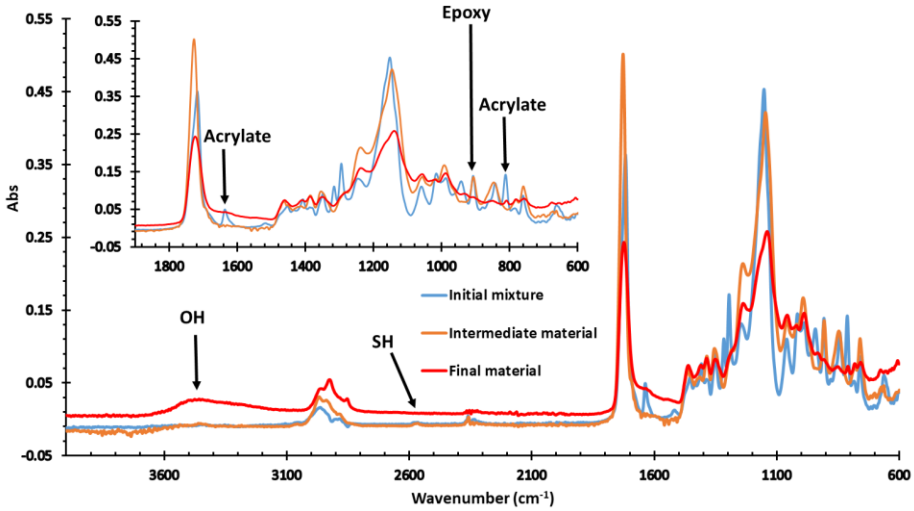

Figure 4.2. FTIR spectra of initial mixture (blue), intermediate material (orange) and final material (red) of the G_TMPTA_58% formulation.

As we can see, the acrylate bands at 1636 cm^{-1} and 810 cm^{-1} have disappeared in the spectrum of the intermediate materials, due to the thiol-ene, thiol-Michael and (meth)acrylate homopolymerization. Therefore, the proportion of the acrylate in the formulation controls the extension of the first stage of the curing. Thiol absorption at 2576 cm^{-1} is still visible in the intermediate material and disappears completely after the thermal process together with epoxy band at 910 cm^{-1}.

3.2 Thermal characterization of the materials

The thermal stability of the fully cured materials was evaluated by thermogravimetry. Figure 4.3 shows the weight loss curves against temperature and their derivatives for

TMTPA formulations. Parallel formulations with TMTPM are shown in Fig. 4.S3 of the SI. Table 4.3 shows the main values extracted from the tests.

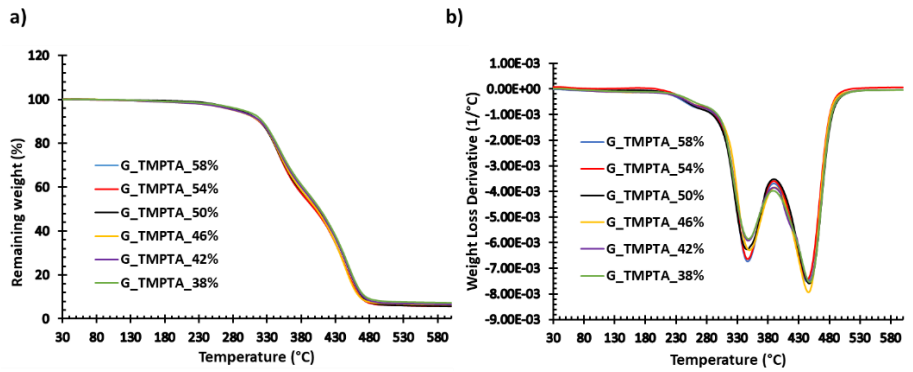

Figure 4.3. TGA (a) and DTG (b) curves for all the thermosets obtained from TMPTA formulations in N_2 atmosphere.

The values of the initial degradation temperature in the table do not show significant differences among all the materials, but the occurrence of epoxy homopolymerization delays the initial degradation to occur and this temperature increases about 20 °C on reducing the proportion of thiol from 58 to 38 % in TMPTA formulations. The effect is less noticeable in TMPTM formulations, because of the lower homopolymerization of epoxides that occurs. There is no difference in the temperature of the maximum degradation rate, but the char yields follow the tendency to increase on decreasing the thiol percentage in the formulation.

The thermomechanical characteristics of the materials were evaluated by DMTA. Figure 4.4 shows the tan δ and storage moduli curves for the TMPTA materials. Figure 4.S4 shows parallel results for TMPTM thermosets. The main data extracted from these experiments are collected in Table 4.3.

The tan δ curves show a monomodal shape indicating that there is only one network structure, in spite of the various reactions taking place during the whole curing process. However, the homogeneity of the material increases as the epoxy homopolymerization decreases and the curves become narrower as it is shown in Table 4.3. In the same sense, the damping capacity increases, due to the higher mobility of the network thanks to the higher proportion of linear aliphatic structures. A similar behavior presents the tan δ curves in Figure 4.S4. In this case, the curves are broader and lower, which indicates a higher inhomogeneity of the network structure due to the higher occurrence of methacrylate homopolymerization that also leads to a lower damping capacity.

Although, the moduli in the glassy state for all the materials prepared are similar without significant differences, the values of the moduli in the rubbery state show a

clear trend. The lower the proportion of thiol, the higher occurrence of epoxy homopolymerization and the higher the modulus in the rubbery state, which reflects the higher crosslinking density achieved. TMPTM materials show higher rubbery moduli than their acrylate counterparts (Figure 4.S5). In these materials, less epoxy homopolymerization has been observed, but the presence of the methyl group on the methacrylate units in the network can help to increase these values.

Table 4.3. Main thermogravimetric and thermomechanical data of the final materials prepared.

Sample	$T_{5\%}$[a] (°C)	T_{max}[b] (°C)	Char Yield[c] (%)	$T_{tan\ \delta}$[d] (°C)	FWHM[e] (°C)	E'_{glassy}[f] (MPa)	$E'_{rubbery}$[g] (MPa)
G_TMPTA_58%	275	346/445	5.5	49.1	21.1	2964	28.6
G_TMPTA_54%	277	346/446	5.6	62.1	30.6	3112	37.6
G_TMPTA_50%	279	346/447	5.8	71.5	33.8	2957	39.1
G_TMPTA_46%	280	347/446	6.4	75.6	36.8	2905	43.3
G_TMPTA_42%	283	348/447	6.6	87.9	44.9	3105	53.6
G_TMPTA_38%	295	348/448	7.3	98.8	50.9	2939	69.3
G_TMPTM_58%	298	345/442	5.3	70.4	40.3	3100	49.2
G_TMPTM_54%	299	345/442	5.9	76.6	42.6	2666	54.4
G_TMPTM_50%	299	345/442	6.0	87.3	43.8	2794	55.4
G_TMPTM_46%	300	346/442	6.4	93.8	45.6	2998	65.1
G_TMPTM_42%	301	346/442	6.7	97.5	58.5	3500	83.1
G_TMPTM_38%	304	346/442	6.8	112.1	61.9	2579	83.9

[a] Temperature of 5% of weight loss. [b] Temperature of the maximum rate of degradation of two main steps. [c] Char residue at 600 °C. [d] Temperature of the maximum of the tan δ peak at 1 Hz. [e] Full width at half maximum of the tan δ peak. [f] Glassy storage modulus determined by DMTA at -10 °C. [g] Rubbery storage modulus determined by DMTA at 125 °C.

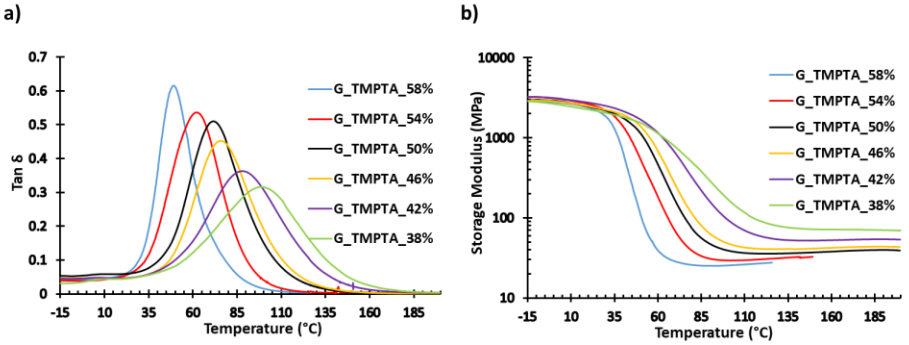

Figure 4.4. Evolution of tan δ (a) and storage modulus (b) against temperature of G_TMPTA thermosets.

3.3 Mechanical characterization

The mechanical characterization of all the materials prepared was performed by stress-strain experiments at room temperature in the universal testing machine. It should be mentioned that we selected only to test those materials with $T_{\tan\delta}$ above enough with respect to room temperature ($T_{r.t.}$) in order to obtain a comparable mechanical behavior in glassy state. In those materials with a $T_{\tan\delta}$ very near to $T_{r.t.}$, network relaxation can occur during the strain-stress experiment and the results will not be comparable between them.

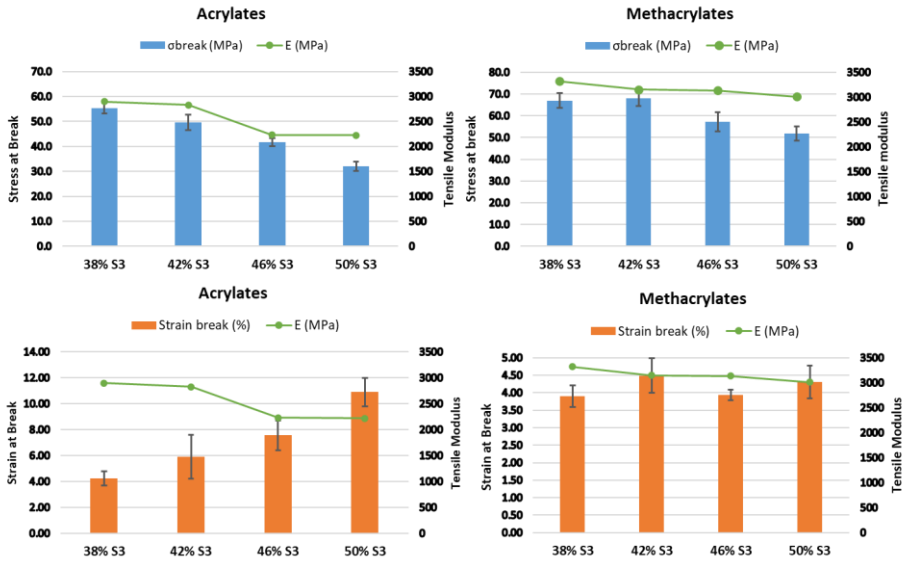

Figure 4.5. Strain and stress at break and tensile modulus for the thermosets obtained from TMPTA and TMPTM materials.

The values of strain at break, stress at break and tensile modulus are presented graphically in Figure 4.5. As it can be seen, the materials containing TMPTM show higher values of tensile modulus as well as stress at break than their TMPTA counterparts. Although in these materials there is not much epoxy homopolymerization, the presence of the methyl group in the structure of methacrylates as well as the homopolymerization of methacrylate during the UV-initiated step may produce an increase in the stiffness and the strength of the materials, which is reflected by an increase in the tensile modulus and stress at break, respectively. Moreover, it is possible to observe that the higher the proportion of S3 in the materials, the lower the values of tensile modulus and stress at break which can be attributed to the lower occurrence of epoxy homopolymerization that provides high crosslinking density and therefore more stiffness and strength to the specimens. With respect to the strain at break results, a similar behavior is observed regardless

the proportion of S3 although the rigidity is slightly higher when reducing the proportion of S3 for the same reason above mentioned. TMPTA materials present higher values in comparison to TMPTM ones because of the higher proportion of thiol-ene/thiol-Michael reaction that occurs during the first step and therefore more flexible chains are present in these materials that provides to the materials more flexibility.

4. Conclusions

A novel dual curing procedure, consisting in a first UV initiated step followed by a thermal process, has been implemented. Thermosets based on meth(acrylate)-epoxy thiol formulations containing 2,2-dimethoxy-2-phenylacetophenone (DMPA) and 1-methylimidazole (1MI) as UV and thermal initiators, have been cured and characterized. Tri(meth)acrylates (TMPTA and TMPTM) used as the limiting monomers that allow the control of the extension of the first curing stage and the characteristics of the intermediate material.

The use of glycidyl methacrylate (GMA) in combination with trifunctional meth(acrylates) allows this system to gel in the first stage and avoids possible dripping or exudation of free monomers during the storage of the intermediate materials.

In the UV stage a thiol-ene reaction occurs (meth)acrylate groups and thiols, although (meth)acrylate homopolymerization competes. In case of formulations of TMPTA, thermal thiol-Michael reaction was detected, because of the presence of 1MI in the initial mixture that catalyzes this reaction.

The concurrence of the (meth)acrylate homopolymerization leads to a stoichiometric imbalance in the second stage, in which thiol-epoxy reaction occurs and consequently lead to materials with T_g below or around room temperature. To increase this parameter, lower proportions of thiol were added to the formulation, but the scarcity of thiol leads to the occurrence of epoxy homopolymerization catalyzed by the base. This homopolymerization increases the crosslinking density, tan δ temperature and modulus in the rubbery state.

TMPTM formulations experiment less epoxy homopolymerization than their corresponding TMPTA formulations since methacrylates homopolymerize in a lesser extent than acrylates and consequently a higher proportion of unreacted thiol is present in the intermediate material, able to react with epoxides.

The higher the proportion of thiol in the formulation the lower the tan δ temperature of the thermoset and the higher the damping characteristics and the homogeneity of the material. TMPTM thermosets show higher rubbery moduli and tan δ temperatures than their acrylate counterparts.

The characterization of the tensile properties at room temperature reveals an increase in stiffness and strength when reducing the proportion of trithiol due to the epoxy homopolymerization in both TMPTM and TMPTA, although higher values are obtained in TMPTM samples due to the presence of the methyl group in the structure and the higher proportion of homopolymerization of methacrylate during the first UV step. The occurrence of thiol-ene/thiol-Michael reaction in TMPTA samples produces higher strain at break than TMPTM material, more evident for higher proportion of trithiol.

To sum up, a wide range of properties can be obtained combining glycidyl methacrylate with trifunctional (meth)acrylates and thiol compounds. The use of off-stoichiometric (meth)acrylates-epoxy thiol formulations is a useful strategy that allows tailoring the properties of the intermediate and final materials when (meth)acrylate homopolymerization competes with radical UV-initiated thiol-(meth)acrylate reaction.

Acknowledgments

The authors would like to thank MINECO (Ministerio de Economia, Industria y Competitividad, MAT2017-82849-C2-1-R and 2-R) and Generalitat de Catalunya (2017-SGR-77 and BASE3D) for their financial support. Miwon Spain S.L. is thanked for donating glycidyl methacrylate.

References

[1] Decostanzi, M.; Lomège, J.; Ecochard, Y.; Mora, A. S.; Negrell, C.; Caillol, S. Fatty acid-base cross-linkable polymethacrylate coatings. Prog. Org. Coat. 2018, 124, 147-157.

[2] Guzmán, D.; Ramis, X.; Fernández-Francos, X.; De la Flor, S.; Serra, À. Preparation of new biobased coatings from triglycidyl eugenol derivative through thiol-epoxy click reaction. Prog. Org. Coat. 2018, 114, 259-267.

[3] Panchireddy, S.; Thomassin, J.-M.; Grignard, B.; Damblon, C.; Tatton, A.; Jerome, C.; Detrembleur, C. Reinforced poly(hydroxyurethane) thermosets as high performance adhesives for aluminium substrates. Polym. Chem. 2017, 8, 5897-5909.

[4] Hamerton, I.; Kratz, J. The use of thermosets in modern aerospace applications. In Thermosets Structure, Properties and Applications, 2nd ed.; Qipeng Guo, Ed.; Elsevier: Amsterdam, Netherlands 2018; Chapter 9.

[5] Verrey, J.; Wakeman, M.D.; Michaud, V.; Månson, J.A.E. Manufacturing cost comparison of thermoplastic and thermoset RTM for an automotive floor pan. Composites Part A 2006, 37, 9-22.

[6] Ramis, X. Fernández-Francos, X.; De la Flor, S.; Ferrando, F.; Serra, À. Click-based dual-curing thermosets and their application. In Thermosets Structure, Properties and Applications, 2nd ed.; Guo, Q., Ed.; Elsevier: Amsterdam, Netherlands, 2018; Chapter 16.

[7] Poelma, B.J.; Rolland, J. Rethinking digital manufacturing with polymers. Science 2017, 9, 1820-1829.

[8] Kuang, X.; Zhao, Z.; Chen, K.; Fand, D.; Kang, G.; Qi, H.J.; Qi Hang, J. High-Speed 3D Printing of High-Performance Thermosetting Polymers via Two-Stage Curing. Macromol. Rapid Commun. 2018, 39, 1700809.

[9] Griffini, G.; Invernizzi, M.; Levi, M.; Natale, G.; Postiglione, G.; Turri, S. 3D-printable CFR polymer composites with dual-cure sequential IPNs. Polymer 2016, 91, 174-179.

[10] Chen, K.; Kuang, X.; Li, V.; Kang, G.; Qi, H.J. Fabrication of tough epoxy with shape memory effects by UV-assisted direct-ink write printing. Soft Matter 2018, 14, 1879-1886.

[11] Konuray, O.; Di Donato, F.; Sangermano, M.; Bonada, J.; Tercjak, A.; Fernández-Francos, X.; Serra, À.; Ramis, X. Dual-curable stereolithography resins for superior thermomechanical properties. Express Polym. Lett. 2020, 14, 881-894.

[12] Fernández-Francos, X.; Konuray, O.; Ramis, X.; Serra, À.; De la Flor, S. Enhancement of 3D-Printable Materials by Dual-Curing Procedures. Materials 2021, 14, 107-129.

[13] Chen, L.; Quingyang, W.; Guo, W.; Ren, L.; Zhiquan, L. Highly stable thiol-ene systems: from their structure-property relationship to DLP 3D printing. J. Mater. Chem C 2018, 6, 11561-11568.

[14] Cook, C.C.; Fong, E.J. Schwartz, J.J.; Porcincula, D.H.; Kaczmarek, A.C.; Oakdale, J.S.; Moran, B.D.; Champley, K.M.; Rackson, C.M.; Muralidharan, A. McLeod, R.R. Shusteff, M. Highly tunable thiol-ene photoresins for volumetric additive manufacturing. Adv. Mater. 2020, 32, 2003376.

[15] Weigand, J.J.; Miller, C.I.; Janisse, A.P.; Mcnair, O.D.; Kim, K.; Wiggins, J.S. 3D printing of dual-cure benzoxazine networks. Polymer 2020, 189, 122193.

[16] Noè, C.; Malburet, S.; Milani, E.; Bouvet-Marchand, A.; Graillot, A.; Sangermano, M. Cationic UV-curing of epoxidized cardanol derivatives. Polym. Int. 2020, 69, 668-674.

[17] Malik, M.s.; Schlögl, S.; Wolfahrt, M.; Sangermano, M. Review on UV-Induced Cationic Frontal Polymerization of Epoxy Monomers. Polymers 2020, 12, 2146.

[18] Yu, R.; Yang, X.; Zhang, Y.; Zhao, X.; Wu, X.; Zhao, T.; Zhao, Y.; Huang, W. Three dimensional printing of shape memory composites with epoxy-acrylate hybrid photopolymer. ACS Appl. Mater. Interfaces 2017, 9, 1820-1829.

[19] Jian, Y.; He, Y.; Sun, Y.; Yang, H.; Yang, W.; Nie, J. Thiol-epoxy/thiol-acrylate hybrid materials synthesized by photopolymerization. J. Mater. Chem. C. 2013, 1, 4481-4489.

[20] Zhao, Y.H.; Hupin, S.; Lecamp, L.; Vuluga, D.; Alfonso, C.; Burel, F.; Loutelier-Bourhis, C. Thiol-ene chemistry of vegetable oils and their derivatives under UV and air: a model study by using infrared spectroscopy and mass spectrometry. RSC Adv. 2017, 7, 3343.

[21] Zhang, J.; Chunhai, L.; Cheng, J.; Miao, M.; Zhang, D. Simultaneous toughering and strengthening of diglycidyl ether of bisphenol A using epoxy-ended hyperbranched polymers obtained from thiol-ene click reaction. Polym. Eng. Sci. 2017, 58, 1703-1709.

[22] Sangermano, M.; Cerrone, M.; Colucci, G.; Roppolo, I.; Acosta Ortiz, R. Preparation and characterization of hybrid thiol-ene/epoxy UV-thermal dual-cured systems. Polym. Int. 2010, 59, 1046-1051.

[23] Matsushima, H.; Shin, J.; Bowman, C.N.; Hoyle, C.E. Thiol-isocyanate-acrylate ternary networks by selective thiol-click chemistry. J. Polym. Sci., Part A: Polym. Chem. 2010, 48, 3255-3264.

[24] Morgan, C.R.; Magnotta, F.; Ketley, A.D. Thiol/Ene Photocurable Polymers. J. Polym. Sci. Polym. Chem. Ed. 1977, 15, 627-645.

[25] Cramer, N.B.; Bowman, C.N. Kinetics of thiol-ene and thiol-acrylate photopolymerizations with real-time Fourier transform infrared. J. Polym. Sci. Part A Polym. Chem. 2001, 39, 3311-3319.

[26] Russo, C.; Serra, À.; Fernández-Francos, X.; De la Flor, S. Characterization of sequential dural-curing of thiol-acrylate-epoxy systems with controlled thermal properties. Eur. Polym. J. 2019, 112, 376-388.

[27] Thomas, R.; Sinturel, C.; Pionteck, J.; Puliyalil, H.; Thomas, S. In-situ cure and cure kinetic analysis of a liquid rubber modified epoxy resin. Ind. Eng. Chem. Res. 2012, 51, 12178-12191.

[28] Xi, W.; Wang, C.; Kloxin, C.J.; Bowman, C.N. Nitrogen-centered nucleophile catalysed thiol-vinylsulfone addition, another thiol-ene “click” reaction. ACS Macro Lett. 2012, 1, 811-814.

[29] Guzmán, D.; Ramis, X.; Fernández-Francos, X.; Serra, A. New catalysts for diglycidyl ether of bisphenol A curing based on thiol–epoxy click reaction. Eur. Polym. J. 2014, 59, 377–386.

Supporting Information

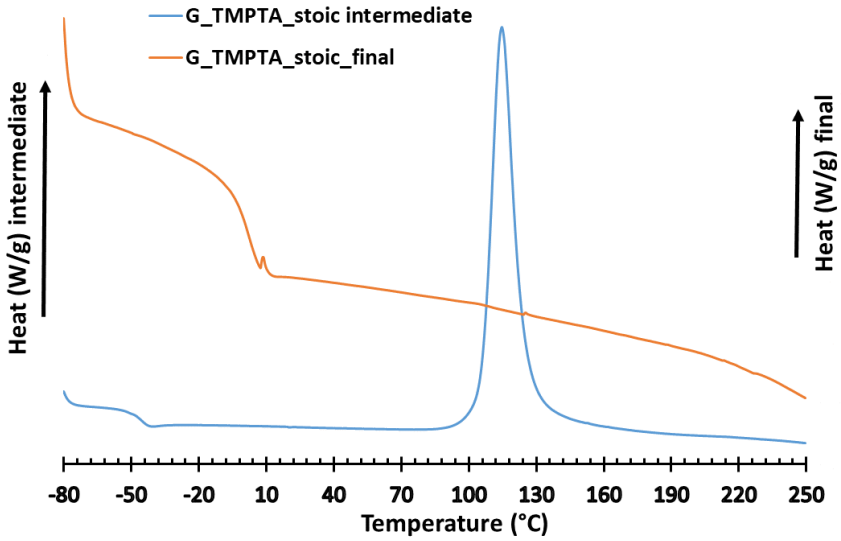

Figure 4.S1. DSC curves at 10 °C/min of the thermal step for the stoichiometric formulation containing TMPTA of the intermediate (blue) and final (orange) material.

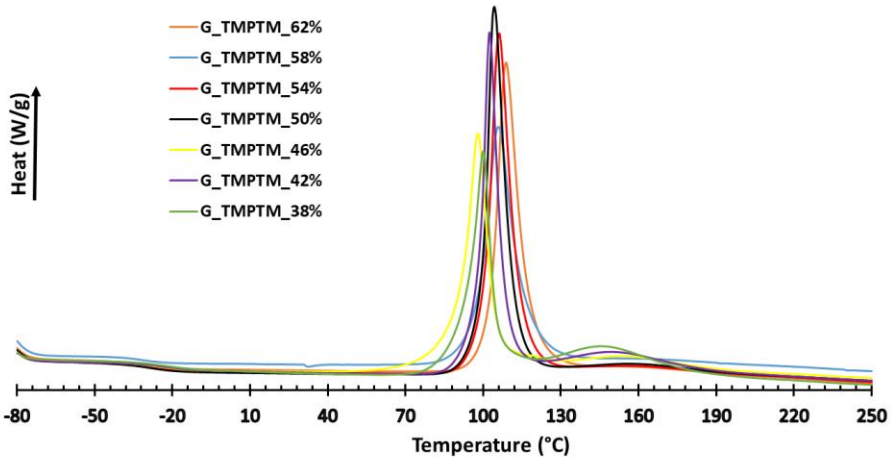

Figure 4.S2. DSC curves at 10 °C/min of the thermal step for the formulations containing different % mol of thiol.

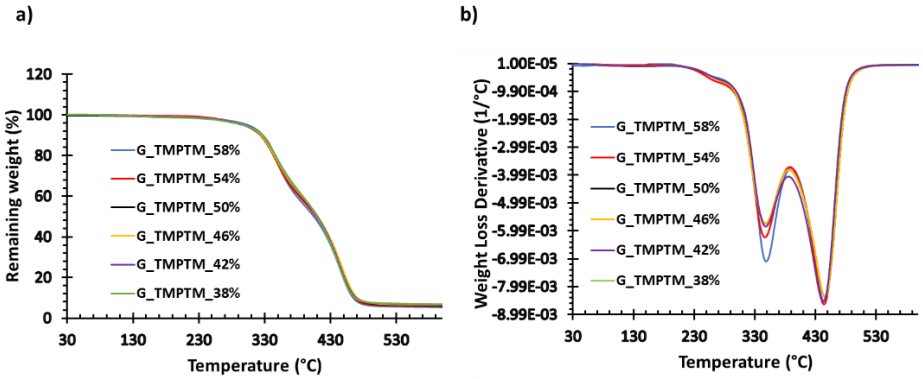

Figure 4.S3. TGA and DTG curves for all thermosets containing TMPTM in N_2 atmosphere .

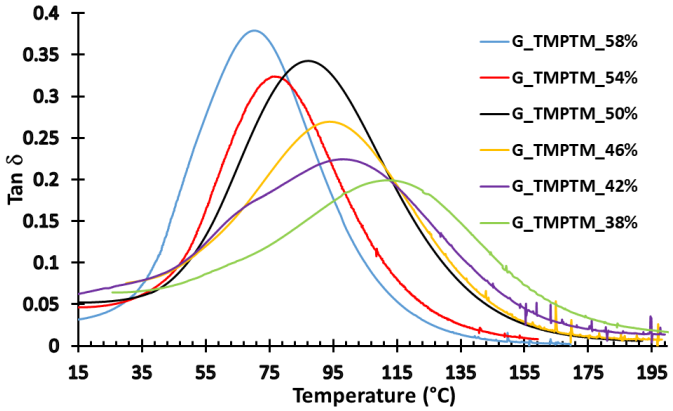

Figure 4.S4. Evolution of tan δ against temperature of all G_TMPTM thermosets.

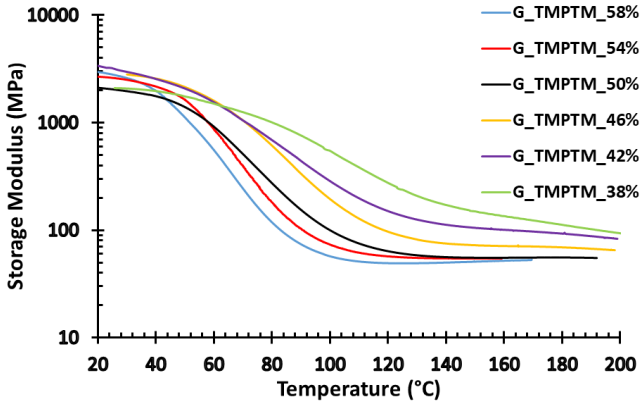

Figure 4.S5. Evolution of storage modulus against temperature of all G_TMPTM thermosets.

UNIVERSITAT ROVIRA I VIRGILI
PROGRESS IN SUSTAINABILITY WITHIN THE REALM OF DESIGNING NEW THERMOSETTING MATERIALS
Adrià Roig Gibert

Chapter 5

Dual-cured thermosets based on eugenol derivatives and thiol chemistry

(submitted)

UNIVERSITAT ROVIRA I VIRGILI
PROGRESS IN SUSTAINABILITY WITHIN THE REALM OF DESIGNING NEW THERMOSETTING MATERIALS
Adrià Roig Gibert

(submitted)

Dual-cured thermosets based on eugenol derivatives and thiol chemistry

Adrià Roig,[1] Xavier Ramis,[2] Silvia De la Flor,[3] Àngels Serra[1]

[1] Universitat Rovira i Virgili, Department of Analytical and Organic Chemistry, C/ Marcel·lí Domingo 1, Edif. N4, 43007 Tarragona, Spain

[2] Universitat Politècnica de Catalunya, Thermodynamics Laboratory, ETSEIB, Av. Diagonal, 08028 Barcelona, Spain

[3] Universitat Rovira i Virgili, Department of Mechanical Engineering, Av. Països Catalans 26, 43007 Tarragona, Spain

ABSTRACT

This paper aims to increase sustainability in thermosetting polymeric fields using bio-based monomers and environmentally friendly processing technologies based on dual-curing. Eugenol has been transformed into acrylate epoxy eugenol (AEEU) that can participate in thio-Michael additions and thiol-epoxy reactions. These reactions constitute the first and second steps of the sequential dual-curing process. A basic catalyst has been added to favor the kinetics of the curing process. We have selected three thiols with functionalities 3, 4, and 6, the first is derived from eugenol, and the others are derived from pentaerythritol, all can be obtained from renewable resources. To tailor and improve the intermediate material characteristics in the dual-curing process, we have added the triacrylate of glycerol. By changing its proportion, a liquid or a rubbery solid can be obtained as an intermediate, which allows a significant number of application technologies. Rheology, DSC, and FTIR were used to follow the evolution of both curing steps and to confirm the sequential character of the dual-curing. The thermal characteristics of intermediate and final materials have been evaluated by TGA and DMTA. Tensile tests at break were performed to evaluate the mechanical properties.

KEYWORDS

Biobased, eugenol, dual-curing, thio-Michael, thermosets.

1. Introduction

Eugenol is a natural antimicrobial and analgesic compound used as a fragrance and flavoring additive in the cosmetics and food industry. Moreover, it has interesting pharmacologic properties such as antioxidant, antispasmodic, antidepressant, and anticarcinogenic, etc [1,2]. The particular structure and commercial availability of eugenol have turned the natural product into an exciting feedstock for building bio-based polymers that can substitute petrol-based ones in a more environmentally friendly manner.

There are many publications on the use of eugenol in the synthesis of thermosets [3-8]. The chemistries implied in their preparation are quite varied because of the functionality of the eugenol molecule with a phenol and an allyl group that can be further modified. Thiol-ene reactions, taking advantage of the allyl group, and the possibility to transform the phenol into the allyl ether, have been proposed in the preparation of adhesives [9]. Moreover, homopolymerization of acrylic derivatives have been explored in the preparation of dental materials [10]. Also, bisbenzoxazines [11] and bismaleimides [12] were prepared and polymerized obtaining high-performance thermosets. However, most of the thermosetting derivatives of eugenol are based on the chemistry of the epoxy groups, introduced in the phenol function as glycidyl ether [13], by epoxidation of the allyl group [5,8,14] or both [15,16].

Dual curing is a practical and versatile methodology to prepare thermosets by combining two different polymerization processes simultaneously or sequentially, which can be activated by different stimuli such as temperature or UV light or by applying different reaction conditions. When the functionality of the monomers is adequate, this process leads to thermosets and can be applied in multi-stage or advanced fabrication technologies [17]. For the sequential dual curing, the control of the polymerization sequence is relevant. It is advantageous in front of the B-stage process since the control of the first and second steps is based on the composition of the formulation and not to tight time-temperature conditions. Thus, in sequential dual curing, the reactions involved in both stages must be well controlled; for this reason, click reactions are preferred. According to the formulation's composition, the intermediate material's characteristics can be tailored as desired. It can be a conformable solid or a viscous liquid, depending on the application of this material in the following fabrication steps. In this way, higher flexibility can be reached during the fabrication of the devices, which usually leads to less waste material and reduces the processing energy costs, making this process more environmentally friendly.

There are a great number of click reactions used in the synthesis of thermosets such as nucleophilic attack to epoxides [18,19], Michael addition [20,21], photoinitiated thiol-ene and thiol-ine additions [22,23], thiol-isocyanate addition [24], Diels-Alder and azide-ine cycloadditions [25,26], as the more extended. The most relevant

characteristic of click reactions in the dual-curing procedure is their orthogonality [27]. This allows both polymerization reactions to occur independently with a temporal control and well-defined and predictable characteristics of the intermediate material. Moreover, the possibility of being performed in an air atmosphere without solvents and soft conditions is also advantageous technologically.

In previous work in our group, we applied a dual-cured methodology for preparing thermosets based on eugenol derivatives [28]. We combined a UV-initiated thiol-ene with a thermal thiol-epoxy starting from diallyl epoxy eugenol and various thiol derivatives. Although the first thiol-ene process was UV-initiated and the second thiol-epoxy was thermal, we could not observe a clean sequential character since the first thiol-ene process did not reach completion, and the photochemical and thermal processes partially overlapped. This was attributed to stabilized allyl-benzylic radicals forming in the eugenol structure with low reactivity.

In the present work, we synthesized epoxy eugenol acrylate (AEEU) to react with multifunctional thiols with different structures and functionalities. The dual-curing process is constituted by a thio-Michael addition occurring at low temperatures followed by a thiol-epoxy reaction in the second step at higher temperatures. It is worth commenting that thermal triggering is more convenient for thick and complex-shaped samples because it is more uniform than photoinitiation, and vitrification of the final material, which can occur in photopolymerized samples, is avoided. Since AEEU is monofunctional in the thio-Michael reaction and the aim is to reach a networked structure during the first step, different proportions of the triacrylate of glycerol have been added. By selecting the proper proportion of this glycerol derivative, the characteristics of the intermediate material, viscous or rubbery, have been tailored. The fact that the multifunctional thiol monomer participates in both polymerization reactions hinders exudation or bleeding. The intermediate and final materials have been characterized by thermal, mechanical and thermomechanical analysis, and the gelation time during the first or second step by rheology.

2. Experimental methods

2.1 Materials

Eugenol (EU, 99%), *m*-chloroperbenzoic acid (MCPBA, 70-75%), sodium bicarbonate ($NaHCO_3$, 99%), glycerol (Gly, 98%), 1-methyl imidazole (1MI, 99%), and sodium chloride (NaCl, 99%) were purchased from Thermo Scientific. Acryloyl chloride (≥97%), *candida antarctica* lipase B (CALB), methyl acrylate (MA, 98%), allyl bromide (97 %), thioacetic acid (TAA), 2,2-dimethoxy-2-phenylacetophenone (DMPA), and oxone were obtained from Sigma Aldrich. Triethylamine (TEA), *tert*-butanol (*t*BuOH), methyl *tert*-butyl ether (M*t*BE) and sodium disulfite ($Na_2S_2O_5$) were purchased from Scharlau, and triethyl benzyl ammonium chloride (TEBAC, 99%) from Alfa Aesar. Pentaerythritol

tetrakis (3-mercapto propionate) (S4, 98%, 122.17 g/eq) and dipentaerythritol hexakis (3-mercapto propionate) (S6, 98%, 130.5 g/eq) were kindly supplied from Bruno Bock Thiochemicals and used as received. All chemicals were used without any purification except CALB that was put in a desiccator under vacuum overnight with anhydrous $MgSO_4$.

2.2 Synthesis of acrylate eugenol (AEU)

EU (10.0 g, 61 mmol) and TEA (13 mL, 71.4 mmol) were dissolved in 30 mL of anhydrous dichloromethane (DCM) under inert conditions. The solution was cooled down to 0-5 °C and stirred for 30 min before adding dropwise acryloyl chloride (5.9 mL, 71.4 mmol) dissolved in 10 mL of dry DCM. The reaction was allowed to proceed for 24 h at room temperature. Then, the reaction was vacuum filtered and washed once with HCl 1M (100 mL), twice with saturated $NaHCO_3$ solution (100 mL), and finally with saturated NaCl solution (100 mL). The organic layer was dried over anhydrous $MgSO_4$, and the solvent was removed in a rotary evaporator to afford AEEU as a yellowish viscous oil (12.6 g, 95%).

^{1}H NMR ($CDCl_3$, δ in ppm): 6.99 (d, 1H); 6.79 (m, 2H); 6.61 (dd, 1H); 6.35 (dd, 1H); 6.00 (dd, 1H); 5.99 (m, 1H); 5.11 (m, 2H); 3.81 (s, 3H); 3.39 (d, 2H) (see Figure 5.S1). ^{13}C NMR ($CDCl_3$, δ in ppm): 164.29, 150.95, 139.09, 137.82, 137.07, 132.42, 127.70, 122.53, 120.71, 116.18, 112.81, 55.88, 40.12 (see Figure 5.S2).

2.3 Synthesis of acrylate epoxy eugenol (AEEU)

The synthesis of AEEU was performed in two different ways. Here, we described the one using oxone as a reagent. The other one can be seen in the SI. AEU (1 g, 4.60 mmol), acetone (47.0 mL, 0.64 mol), H_2O (25 mL), ethyl acetate (50 mL), TEBAC (0.21 g, 0.92 mmol), and $NaHCO_3$ (16.9 g, 0.20 mol) were added in a 500 mL three-necked flask and stirred for 5 minutes and cooled down to 0-5 °C. Then, oxone (22.5 g, 73.3 mmol) in portions of 7.15 g diluted in 50 mL of H_2O was added every day for 2 days. The mixture was allowed to react another day at 0-5 °C. Then, the organic product was extracted with diethyl ether (3 x 100 mL), and the organic layer was washed with H_2O twice, dried over anhydrous $MgSO_4$, and the solvent removed in the rotary evaporator obtaining AEEU as a yellowish solid (0.86 g, 80%). Melting point was 62.2 °C (by DSC).

^{1}H NMR ($CDCl_3$, δ in ppm): 7.01 (d, 1H); 6.85 (m, 2H); 6.60 (dd, 1H); 6.35 (dd, 1H); 6.00 (dd, 1H); 3.82 (s, 3H); 3.16 (m, 1H); 2.85 (d, 2H); 2.81 (dd, 1H); 2.56 (dd, 1H) (Figure 5.1). ^{13}C NMR ($CDCl_3$, δ in ppm): 164.22, 151.04, 138.32, 136.32, 132.53, 127.63, 122.70, 121.12, 113.27, 55.93, 52.34, 46.84, 38.69 (Figure 5.2). FTIR (ATR): 1737 cm^{-1} (C=O acrylate); 1636 cm^{-1} (C=C acrylate); 1600 cm^{-1} (aromatics); 825 cm^{-1} (epoxide) (Figure 5.S3).

2.4 Synthesis of glycerol triacrylate (GTA)

The synthesis of GTA was performed in two different ways. Here, the one using CALB is described while the other route is described in the SI. In a 250 mL two-necked round bottom flask equipped with a magnetic stirrer and a Soxhlet system with glass wool, activated 4 Å molecular sieves, and a condenser, glycerol (1 g, 10.9 mmol) was mixed with 80 mL of M*t*BE/*t*BuOH (1:1 v/v). Then, MA (14.7 mL, 0.2 mol) was added, the mixture heated until reflux, and the Soxhlet drained 4 times. Next, CALB (200 mg, 20% w/w to Gly) was added, and the mixture was kept for 24 h at reflux. Afterward, the mixture was vacuum filtered and washed twice with 1 M NaOH solution. The organic phase was dried with anhydrous $MgSO_4$ and filtered, and the solvent and the excess of MA were removed in a rotary evaporator yielding GTA as a brownish viscous oil (30%).

^{1}H NMR ($CDCl_3$, δ in ppm): 6.45 (dd, 1H); 6.15 (dd, 1H); 5.88 (dd, 1H); 4.27 (m, 4H); 4.18 (m, 1H) (Figure 5.S4). ^{13}C NMR ($CDCl_3$, δ in ppm): 165.55, 165.13, 131.94, 131.74, 127.75, 127.68, 69.16, 62.33 (Figure 5.S5).

2.5 Synthesis of the triallyl derivative eugenol (DAllylEU)

DAllylEU was prepared by a reported procedure [9]. The synthesis went through the allylation of eugenol in a basic medium to obtain O-allyl eugenol (OAllylAEU) (Figure 5.S6-S7). By heating the previous product, a Claisen rearrangement led to 6-allyleugenol (6-AllylAEU) (Figure 5.S8-S9). This product was finally allylated to obtain the 6-allyl O-allyl eugenol (DAllylEU).

^{1}H NMR ($CDCl_3$, δ in ppm): 6.7 s (Ar, 2H), 6.05 m (-CH=,1H), 5.90 m (-CH=, 2H), 5.34 dd (CH_2=, 1H), 5.19 dd (CH_2=, 1H), 5.15-5.0 m (CH_2=, 4H), 4.46 d (-CH_2-O-, 2H), 3.87 s (CH_3-O-, 3H), 3.38 d (-CH_2-Ar, 2H), 3.31 d (-CH_2-Ar, 2H) (Figure 5.S10). ^{13}C NMR ($CDCl_3$, δ in ppm): 152.6, 144.1, 137.5, 137.3, 135.7, 134.5, 133.7, 121.7, 117.0, 115.8, 115.5, 110.5, 73.7, 55.7, 40.1 and 34.3 (Figure 5.S11). FTIR (ATR): 3072, 3018, 2901, 2825, 1637, 1583, 1510, 1451, 1418, 1256, 1230, 1141, 1026, 986, 907, 804 and 752 cm^{-1}.

2.6 Synthesis of the trithiol derivative of eugenol (3SHEU)

2.6.1 Photochemical thiol-ene reaction (SAcEU)

The synthesis followed a reported procedure [28]. A mixture of 5 g (20.5 mmol) of DAllylEU, 22.2 g (291.6 mmol) of TAA and 0.1290 g (0.50 mmol) of DMPA were photoirradiated with a UV lamp at 356 nm for 1 h. The product obtained was dissolved in $CHCl_3$, extracted with a saturated NaOH solution, washed with water, and dried over anhydrous $MgSO_4$. The solvent was eliminated on a rotary evaporator. The product obtained was a viscous liquid with 96 % yield.

^{1}H NMR ($CDCl_3$, δ in ppm): 6.52 s and 6.50 s (Ar, 2H), 3.91 t (-CH_2-O-, 2H), 3.80 s (CH_3-O-, 3H), 3.10 (-CH_2-S-, 2H), 2.85 m (-CH_2-Ar, 4H), 2.56 m (-CH_2-S-, 4H), 2.31 s (CH_3-CO-S-, 9H), 1.99 m (-CH_2-CH_2-CH_2-O-, 2H), 1.8 m (-CH_2-CH_2-CH_2-Ar, 4H) (Figure 5.S12). ^{13}C NMR ($CDCl_3$, δ in ppm): 195.7, 195.6, 195.5, 152.3, 143.9, 136.6, 134.5, 121.4, 110.3, 70.0, 55.5, 34.5, 31.0, 30.5, 30.3, 30.2, 29.1, 28.7, 28.4 and 25.8. (Figure 5.S13). FTIR (ATR): 2930, 2825, 1680, 1587, 1505, 1460, 1424, 1355, 1260, 1232, 1135, 1010, 950, 800 and 607 cm^{-1}.

2.6.2 Hydrolysis of SAcEU (3SHEU)

9.31 g (19.7 mmol) of SAcEU were dispersed in 100 mL of methanol in a flask with magnetic stirring and then 1.70 g (42.5 mmol) of pulverized NaOH were added. The mixture was heated to reflux temperature under inert atmosphere for 5.5 h. The solution was cooled, and the solvent was removed. The product obtained was dissolved in HCl acidic water solution and extracted with $CHCl_3$. Then washed with distilled water and dried over anhydrous $MgSO_4$. The product obtained was a pale-yellow viscous liquid with 84 % yield.

^{1}H NMR ($CDCl_3$, δ in ppm): 6.56 s (Ar, 2H), 3.98 t (-CH_2-O-, 2H), 3.82 s (CH_3-O, 3H), 2.77 q (-CH_2-S-, 2H), 2.61 m (-CH_2-S-, 4H), 2.51 q (-CH_2-Ar, 4H), 2.1 m (-CH_2-CH_2-CH_2-O-, 2H), 1.85 m (-CH_2-CH_2-CH_2-Ar, 4H), 1.5 t (-SH, 1H), 1.35 t (-SH, 1H) and 1.33 t (-SH, 1H) (Figure 5.S14). ^{13}C NMR ($CDCl_3$, δ in ppm): 152.2, 143.9, 136.7, 134.6, 121.5, 110.2, 70.3, 55.5, 35.3, 34.6, 34.3, 34.0, 28.5, 24.1, 23.8 and 21.2 (Figure 5.S15). FTIR (ATR): 2930, 2825, 2580, 1587, 1503, 1460, 1430, 1260, 1230, 1150, 1090, 1010, 950 and 830 cm^{-1}.

2.7 Preparation of the formulations

In a 20 mL vial, a certain amount of AEEU was added and melted at 70 °C for 10 minutes. Then, the corresponding amount of GTA was added and manually mixed with the melted AEEU. Later, the stoichiometric amount (SH:acrylate+epoxy = 1:1) of the corresponding thiol was added, followed by the addition of 5% mol/eq of thiol of 1MI. Finally, the mixture was vigorously stirred in an ice bath, poured into Teflon molds of 30 x 5 x 1.5 mm^3 dimensions and cured in an oven at 35 °C for 1 h (first curing step), 80 °C for 1h, 120 °C for 2 h and 150 °C for 1 h (second curing step). The materials were coded as polyX_Y, where X indicates the thiol used and Y is ascribed to the gelation of the intermediate material. As an example, polyS4_gel is a material in which S4 was used as the crosslinker and the intermediate material of the dual curing was gelled due to the fact that the gelation occurred in the first curing step. Table 5.1 shows the composition of the different formulations studied.

Table 5.1. Molar composition of the formulations prepared and acrylates ratio.

Formulation	AEEU (% mol)	GTA (% mol)	3SHEU (% mol)	S4 (% mol)	S6 (% mol)	1MI (% mol to SH)	nGTA/nAEEU
poly3SHEU_gel	38.6	17.8	43.6	-	-	5	0.461
poly3SHEU_nogel	53.9	5.0	41.1	-	-	5	0.092
polyS4_gel	43.4	20.0	-	36.6	-	5	0.461
polyS4_nogel	60.2	5.6	-	34.2	-	5	0.092
polyS6_gel	49.4	22.7	-	-	27.9	5	0.459
polyS6_nogel	68.9	6.4	-	-	26.2	5	0.093

2.8 Characterization methods

^{1}H NMR and ^{13}C NMR spectra were recorded using a Varian VNMR-S400 NMR spectrometer. $CDCl_3$ was used as a solvent. All chemical shifts are given in δ in part per million (ppm) using the signals of the solvent as internal standard (^{1}H NMR: $CDCl_3$ = 7.26 ppm; ^{13}C NMR: $CDCl_3$ = 77.16 ppm).

A Mettler DSC-3+ differential scanning calorimeter (DSC) was employed to study the curing process. It was calibrated using indium (heat flow calibration) and zinc (temperature calibration) standards. Samples of 8-10 mg were used and analyzed in aluminum pans with pierced lids in N_2 atmosphere with gas flow of 50 cm^3/min. Temperatures between -80 °C and 250 °C were scanned with a heating rate of 10 °C/min to characterize the curing process. The T_gs of the intermediate and final materials were determined with a heating rate of 20 °C/min. The reaction enthalpy (Δh) was obtained by integration of the the calorimetric heat flow signal (dh/dt) using a straight baseline using the STARe software.

FTIR spectra were recorded in a Jasco FT/IR-680 Plus with an attenuated total reflection accessory with thermal control and a diamond crystal (Golden Gate Heated Single Reflection Diamond ATR, Specac-Teknokroma) to confirm that the complete curing of the samples was achieved. Real-time spectra were collected in absorbance mode in the wavelength range 4000 to 600 cm^{-1} with a resolution of 4 cm^{-1}. 20 scans were taken and averaged for each spectrum. The disappearance of the absorbance peak at 1636 cm^{-1} corresponding to the stretching of the C=C bond of acrylates as well as the decrease of the thiol (S-H) peak at 2570 cm^{-1} were used to confirm that the first step of the curing was complete. The peak at 915 cm^{-1} corresponding to the epoxy group and the appearance of a peak at 3500 cm^{-1} related to the formation of OH

groups by the thiol-epoxy reaction were used to confirm the completion of the second stage [29].

Thermomechanical properties were determined with a DMA Q800 (TA Instruments) using a film tension clamp. The samples (with dimensions of 30 x 5 x 1.5 mm^3) were tested with an amplitude of 10 µm and a frequency of 1 Hz in the temperature range from -30 °C to 200 °C with a heating rate of 2 °C min^{-1}.

TGA analyses were performed using a Mettler Toledo TGA2 thermobalance. Cured samples of about 10 mg were heated between 30 and 600 °C at a heating rate of 10 °C min^{-1} in nitrogen atmosphere with a gas flow of 50 $cm^3 \cdot min^{-1}$.

The gelation time was determined using a rheometer ARES-G2 (TA Instruments) equipped with an electrical heated plate device (EHP) and 20 mm parallel plate geometry. The strain was set at 0. 05 % and the frequencies at 0.5, 1.75 and 3 Hz. Gel point was determined as the crossover of storage modulus (G') with the loss modulus (G'') at the three different frequencies. The procedure intends to simulate the curing in the oven: 35 °C for 1 h, temperature ramp from 35 to 80 °C at 3 °C min^{-1}, and 30 min at 80 °C.

The fully cured materials were tested in tensile until break using the DMA in static mode with 3 N/min of force ramp at 20 °C and applying 0.01 N as preload force.

3. Results and discussion

3.1 Synthesis of the starting monomers

The epoxy acrylate of eugenol (AEEU) was synthesized *via* a high-yielding two-step procedure. The first step was the acylation reaction with acryloyl chloride in the presence of TEA, and the second was the epoxidation of the allylic group (Scheme 5.1a). The literature offers the alternative of using acrylic acid and dicyclohexyl carbodiimide (DCC) in the presence of a base. However, it was reported that this procedure yields only 30 % of the product and therefore it was not used [30]. As a more sustainable alternative to preparing eugenol acrylate, we tried the enzymatic esterification with CALB of eugenol with methyl acrylate following a reported procedure [31], but the desired product was not obtained (Scheme 5.1b). The reason for that is the phenolic character of the substrate since it is reported that the enzymatic reaction works only well with primary and secondary alcohols.

The quality of AEU was confirmed by ^{1}H NMR spectroscopy (see Figure 5.S1) by the appearance of the acrylic protons between 6.61 and 6.00 ppm, whereas a carbonyl signal appears in the ^{13}C NMR spectrum at 164.29 ppm (see Figure 5.S2).

The further epoxidation of the allyl group was done with MCPBA at 0 °C for 24 h, with a yield of 96 %. As a greener alternative, we tried to use Oxone to perform the epoxidation of the allyl group [32]. In this case, a biphasic system with TEBAC as a

phase transfer catalyst was used, obtaining good yields of the desired product after 3 days (80%), demonstrating the possibility to synthesize AEEU more sustainably.

The completion of the reaction was confirmed by the vanishment of the allyl signals between 6.00 and 5.11 ppm and the appearance of the epoxydic signals between 3.16 and 2.56 ppm in the ^{1}H NMR spectrum shown in Figure 5.1 and at 52.34 and 46.84 ppm in the ^{13}C NMR shown Figure 5.2. Both spectra confirm the purity of the product obtained. Moreover, FTIR spectroscopy presented the characteristic absorptions of the ester moiety, the stretching of the acrylate C=C bond, and the epoxy group at 1740, 1637, and 825 cm^{-1}, respectively.

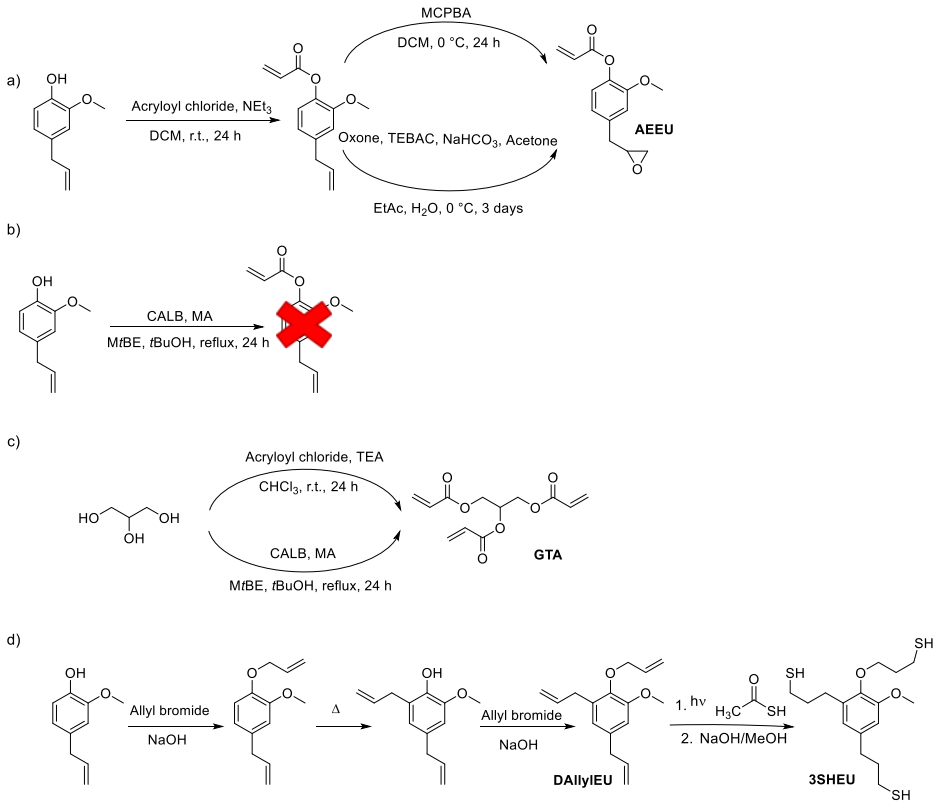

Scheme 5.1. Synthetic routes to AEEU starting from eugenol (a and b), GTA starting from glycerol (c), and d) 3SHEU from eugenol.

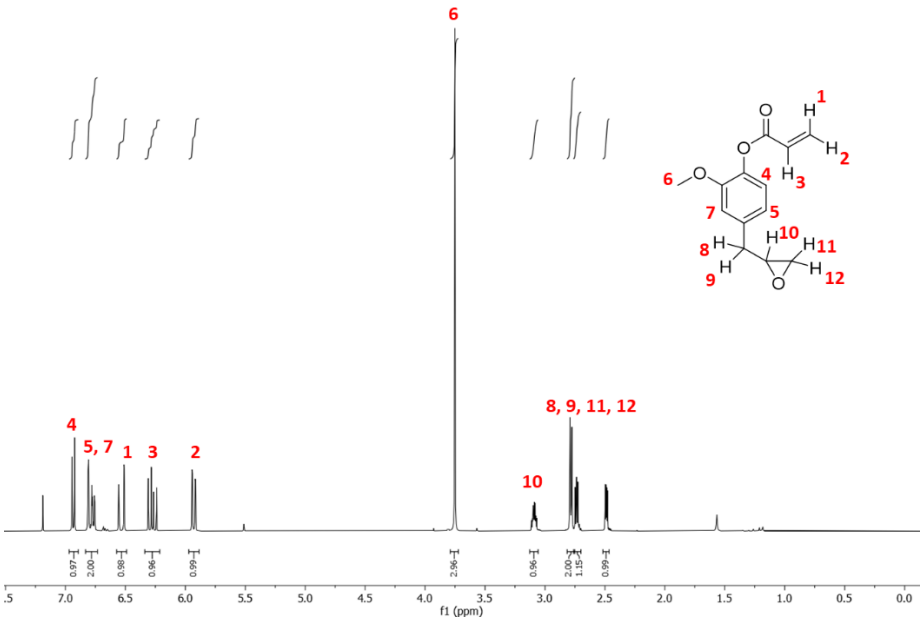

Figure 5.1. ^{1}H NMR spectrum of AEEU in $CDCl_3$.

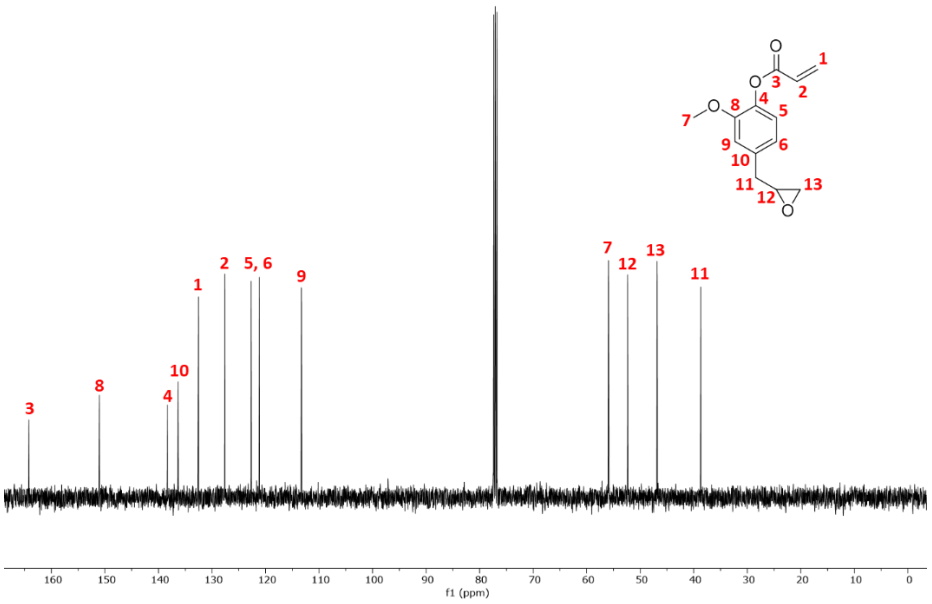

Figure 5.2. ^{13}C NMR spectrum of AEEU in $CDCl_3$.

To synthesize GTA, the first approach tested was using acryloyl chloride and TEA in $CHCl_3$ as a solvent due to its higher polarity than DCM (Scheme 5.1c). The product was obtained in good yields (94 %). The structure and purity were confirmed by ^{1}H NMR by the appearance of the signals of the double bonds between 6.45 and 5.88 ppm (Figure 5.S4) and the four signals between 127 and 133 ppm in its ^{13}C NMR spectrum (Figure 5.S5). Despite this, the enzymatic CALB methodology could be used to acrylate the primary and secondary alcohols after 2 days of reaction in relatively low yields (30%) but proving that GTA can also be obtained in a green way.

The preparation of 3SHEU was performed as described in previous papers [28,33]. As seen in Scheme 5.1d, the process consists of a first allylation followed by a thermal Claisen rearrangement and a second allylation of the formed phenolic group, obtaining the triallyl derivative of eugenol. By a photoinitiated thiol-ene reaction with thioacetic acid and further saponification, 3SHEU was obtained and characterized by NMR spectroscopy. The spectra of intermediates and final materials are collected in the SI (Figures 5.S6-S15). All spectra show the high purity of the corresponding products.

3.2 Study of the dual curing of the formulations

The curing procedure by the dual curing methodology includes, as the first step, the thio-Michael addition and the thiol-epoxy reaction as the second one. All formulations include 1-MI as the base catalyst that favors the nucleophilic character of the thiol by forming thiolate groups. Both reactions are represented in Scheme 5.2. Since in the thio-Michael addition, AEEU acts as a monofunctional monomer, the addition of a multifunctional acrylate is needed to get a network or an oligomeric product, depending if the intermediate material is gelled or not. In our case, we selected triacrylate derived from glycerol because of its bio-based character and its compact structure. As thiols, the trifunctional derivative of eugenol has been selected, and the tetra and hexa functional derivatives of pentaerythritol were also tested. These last thiols were commercially available, but they could be also synthesized from bio-based pentaerythritol [34].

From both reactions, the thio-Michael addition is the most favored from the kinetics point of view, and it begins at room temperature during the first curing step. However, to ensure that this reaction has been completed, the curing mixture was maintained at 35 °C in an oven for 1 h. Once the thio-Michael reaction has been completed, the thiol-epoxy reaction can proceed at higher temperatures. Thus, the curing mixture was then cured in an oven using the following curing schedule: 80 °C for 1h, 120 °C for 2 h, and 150 °C for 1 h.

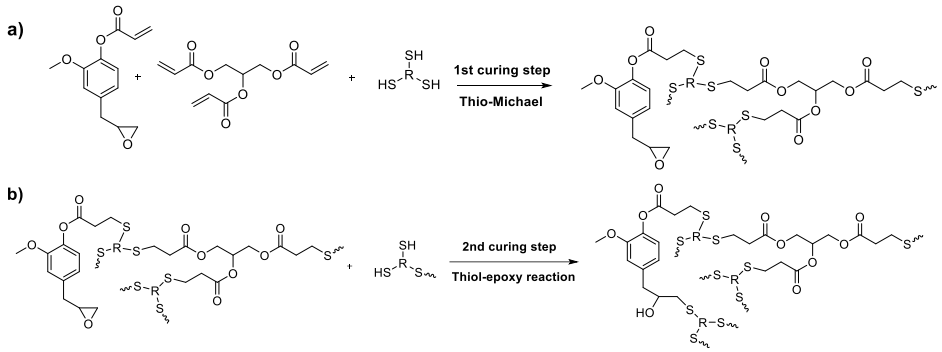

Scheme 5.2. Chemical processes occurring in the first and second steps of the dual curing.

We could prove by FTIR that in these conditions, the first and the second step were completed and well-differentiated. For example, Figure 5.3 shows the FTIR spectra of the intermediate and final material recorded for the polyS6_gel formulation.

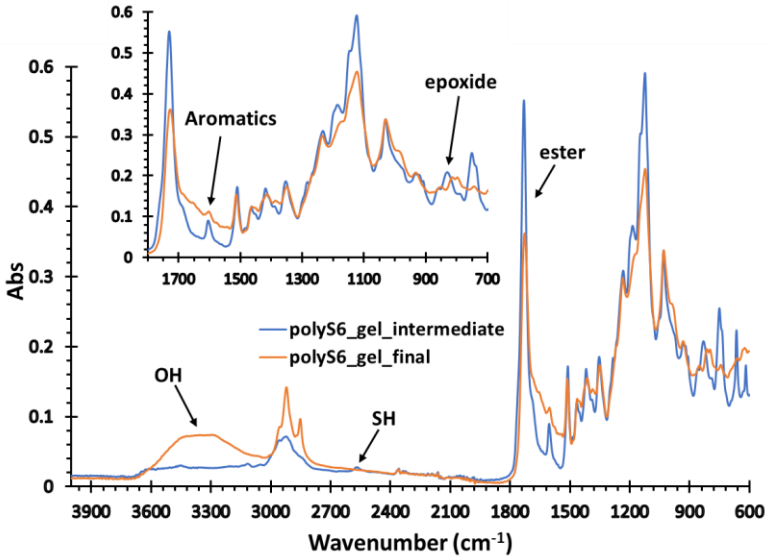

Figure 5.3. FTIR spectra of the intermediate and final materials obtained in the curing of the polyS6_gel formulation.

Dual curing can be applied to advanced manufacturing processes mainly due to the possibility of tailoring the characteristics of the intermediate material. Thus, the intermediate can be a viscous liquid, and in this case, it can be used as a coating or an adhesive, or it can be a moldable solid that can be further processed to lead to complex shapes, as we could demonstrate in previous works in this topic [17,28,29,35]. The tailoring of these characteristics is done by the composition of the formulation, being the proportion of GTA, the one that defines if the formulation gels during the first or the second step. It is worth noting that no free monomers are left

after the first step is completed since AEEU participates in both processes as the thiols do. It means no dripping or exudation of monomers will occur during the storage of the intermediate material.

The use of the Flory-Stockmayer equation (Eq. 5.1) allows the calculation of the amount of GTA necessary to gel [36,37]. The theoretical conversion of the acrylate groups at the gel point α_{gel} during the thio-Michael reaction can be calculated by Eq. 5.1, assuming an ideal random step-wise reaction.

$$\alpha_{gel}^{theor} = \sqrt{\frac{r}{(f_1-1)\cdot(f_2-1)}} \qquad \text{(Eq. 5.1)}$$

where r is the thiol/acrylate equivalent ratio, f_1 the acrylate monomer functionality and f_2 the thiol functionality. Since the functionality of the thiols tested are 3, 4 or 6, we obtained three different values of α_{gel}, each one for each thiol.

By this equation, the critical molar ratio nGTA/nAEEU = 0.287 was obtained as the lowest to achieve gelation at complete conversion of acrylate moieties. Thus, two different possibilities were studied: a) a molar ratio nGTA/nAEEU = 0.46, in which gelation will occur before full conversion to obtain a solid-like intermediate material, and b) a molar ratio nGTA/nAEEU = 0.09, where gelation will not occur in the first step and a viscous-like intermediate material will be obtained.

Rheological measurements confirmed that gelation occurs in the first or second curing step, according to the formulation composition. The formulation is transformed into a solid-like material in the gelation, and the storage modulus (G', solid contribution) becomes higher than the loss modulus (G'', liquid contribution). Figure 5.4 represents the storage and loss moduli evolution with temperature for all the formulations prepared herein.

As we can see in Figure 5.4 when the amount of GTA is low (polyX_no gel samples), the gelation cannot occur in the first step at 35 °C where thio-Michael addition is the only reactive process and G'' is higher than G', as corresponds to a liquid-like behavior. G' overpass G'' when the temperature increases to 80 °C when the gelation occurs as a result of a thiol epoxy process. Contrarily, in formulations with a higher proportion of GTA (polyX_gel samples) already in the first curing stage at 35 °C the gelation can be observed, indicating that the functionality of the acrylate mixture is enough to reach a networked structure during thio-Michael addition. The same trends are observed for polyS4 and polyS6 materials. If we compare the times needed to get the gelation during the first step in (polyX_gel samples), we can see that the time is shorter in the case of polyS6_gel, according to the higher functionality of the thiol, which allows reaching the gel point at a lower conversion of acrylate. When comparing the rheological curves of (polySH3EU_gel samples) with (polyS4_gel samples) we see that is slightly faster in the former. Since the functionality is lower in (polySH3EU_gel

samples), the explanation can be found in a more rapid reaction of SH3EU in the thio-Michael addition. This can be related to the lower viscosity of this formulation.

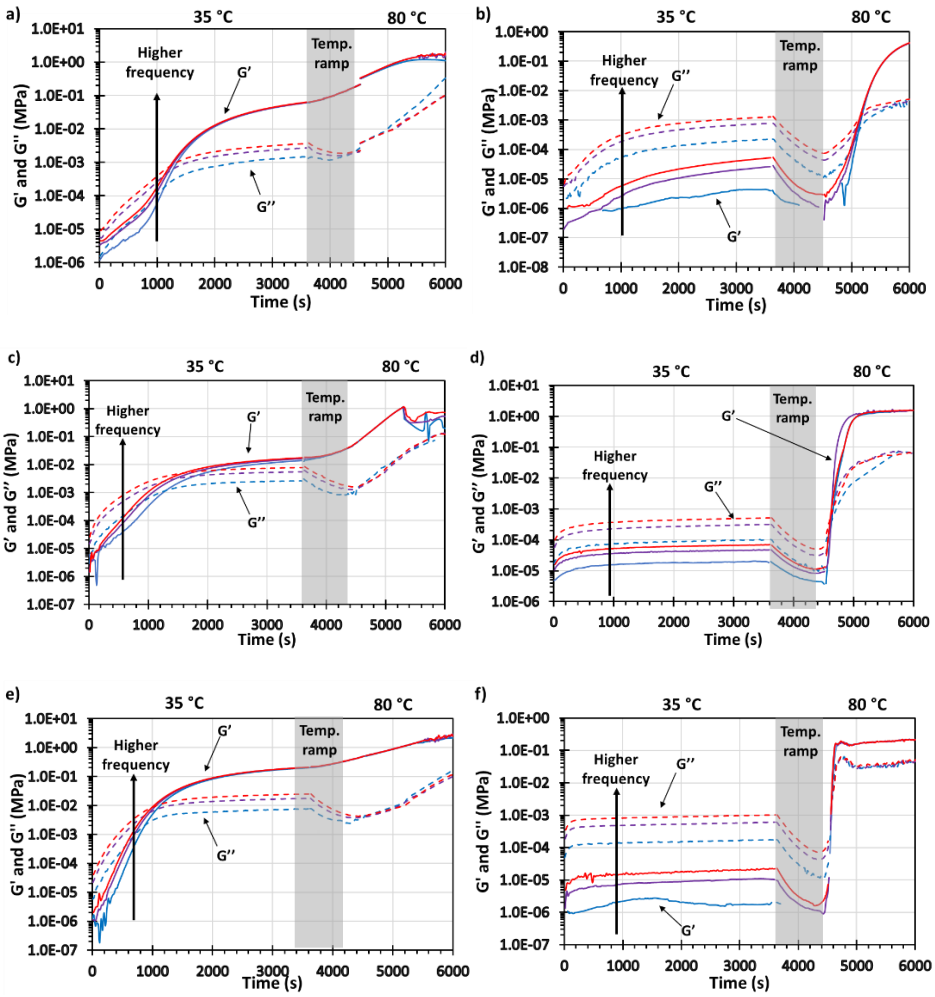

Figure 5.4. Evolution of storage modulus (G') and loss modulus (G'') vs. time at different frequencies (0.5 Hz, 1.75 Hz and 3 Hz) for a) poly3SHEU_gel, b) poly3SHEU_nogel, c) polyS4_gel, d) polyS4_nogel, e) polyS6_gel, and f) polyS6_nogel during 1 h at 35 °C and 30 min at 80 °C.

DSC was used to confirm the sequentiality of the curing process. Since the thio-Michael addition begins at room temperature, we could not measure the enthalpy released during the first curing step. Thus, the DSC curves of all the materials after the first curing step were recorded. Figure 5.5 presents the DSC curves for all the formulations studied. Table 5.2 collects the enthalpy released in the second step and the T_g of the intermediate and final materials. The enthalpy released by the epoxy equivalent is between 120 and 129 kJ, which agrees with previously published data

[38]. Moreover, the curing exotherm begins at a temperature not below 75 °C. This confirms that the dual-curing process is sequential and that both steps occur independently.

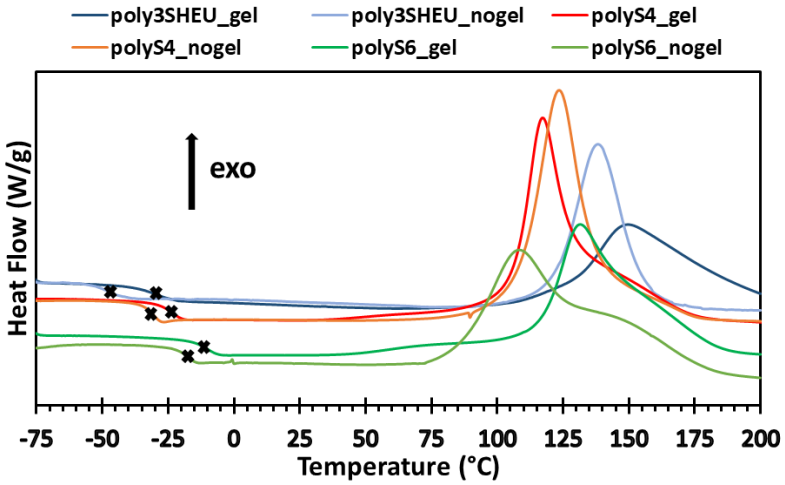

Figure 5.5. DSC curves at 10 °C/min of the curing of all the intermediate materials prepared.

Table 5.2. Main calorimetric and thermogravimetric data obtained for all formulations.

Formulation	ΔH^a (kJ/ee)	$T_g{}^b$ interm (°C)	$T_g{}^b$ final (°C)	$T_{2\%}{}^c$ (°C)	$T_{max}{}^d$ (°C)	Char yield^e (%)
poly3SHEU_gel	120.4	-27.9	33.0	228	360	15.7
poly3SHEU_nogel	122.3	-42.3	37.0	220	363	16.3
polyS4_gel	126.5	-22.7	23.4	240	342	15.0
polyS4_nogel	128.9	-30.9	31.8	247	329	14.9
polyS6_gel	123.8	-9.8	39.3	250	346	14.5
polyS6_nogel	120.3	-17.3	45.1	235	330	15.3

[a] Enthalpy released in the thiol-epoxy reaction by epoxy equivalent. [b] Glass transition temperatures of the intermediate and final materials. [c] Temperature of 2 % of weight loss. [d] Temperature of the maximum rate of degradation. [e] Char residue at 600 °C.

Looking at the T_gs determined for all the intermediate materials, we can see that they are well below room temperature, indicating their rubbery or fluid-like characteristics for gelled and non-gelled materials. As expected, the non-gelled materials have lower T_gs than the gelled ones. However, the contrary behavior is observed for the final materials. The materials with a lower proportion of GTA have higher T_g values. This can be explained by the flexibility introduced in the network by the GTA structure, and the flexible moieties originated through the thio-Michael addition. Moreover, the higher proportion of GTA requires more thiol in the formulation, which imparts a

higher flexibility. A parallel behavior of the evolution of the T_gs on changing the formulation composition was observed in previous studies [29,39].

The highest T_gs of the cured materials were obtained from S6 due to its higher functionality, increasing the crosslinking density. Although the functionality of S4 is higher than that of SH3EU, the rigidity of its aromatic ring in the eugenol derivative reduces the network's flexibility and mobility, leading to higher T_g values.

3.3 Thermal characterization of the materials

Thermogravimetry was used to evaluate the thermal stability of the fully cured materials. Figure 5.6 shows the weight loss evolution with temperature and the derivative curves. The main data extracted can be seen in Table 5.2.

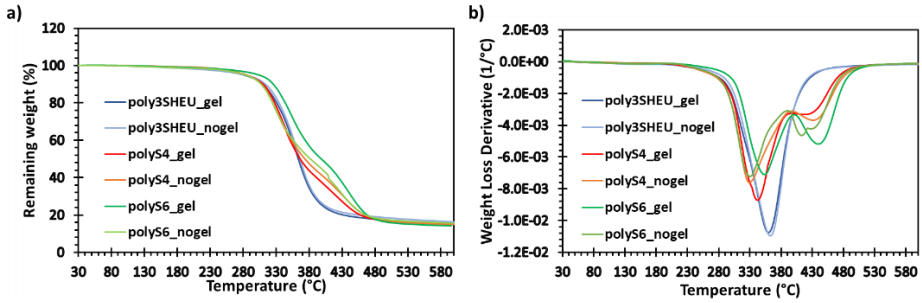

Figure 5.6. TGA (a) and DTG (b) curves for the dual-cured thermosets prepared in N_2 atmosphere.

The DTG curves show that the degradation process occurs in two steps, except for poly3SHEU formulations. Since a significant proportion of ester groups are present in the network structure, the β-elimination process can happen to a great extent. The first degradation step can be attributed to this process, whereas the second can be attributed to the complete network degradation.

From the values collected in Table 5.2, no significant differences in the initial degradation among all the materials can be observed, and all the values are higher than 220 °C. There are also no significant differences in the char residues at 600 °C. However, the temperatures of the faster degradation rates are higher for poly3SHEU materials, showing only one degradation step.

The thermomechanical properties of the fully cured materials were determined by DMA. Figure 5.7 shows the evolution of storage moduli and tan δ against temperature. The main data extracted from these studies are presented in Table 5.3.

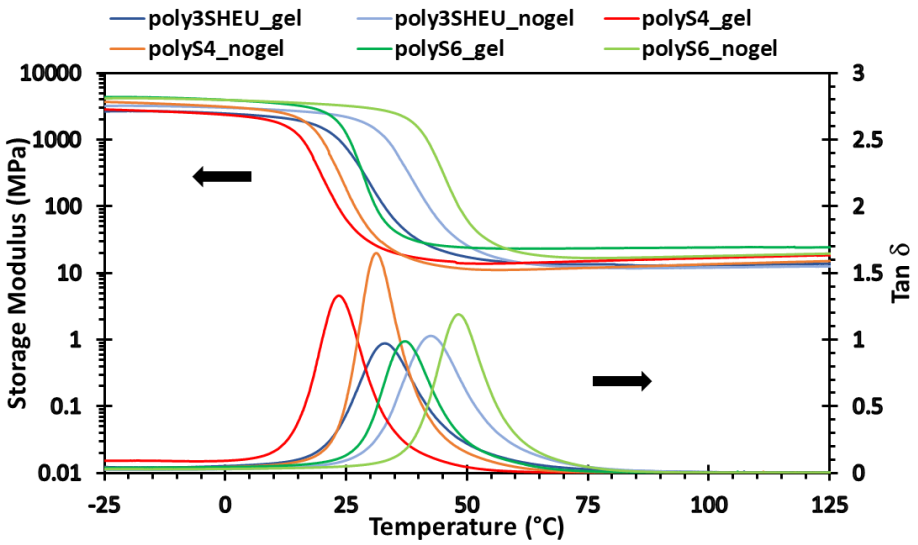

Figure 5.7. Evolution of tan δ and storage modulus against temperature for all the fully cured materials.

Table 5.3. Main thermomechanical and mechanical data obtained for all the fully cured materials

Formulation	$T_{tan\,\delta}$[a] (°C)	E'_{glassy}[b] (MPa)	$E'_{rubbery}$[c] (MPa)	FWHM[d] (°C)	σ_{break} (MPa)	ε_{break} (%)	Tensile modulus (MPa)
poly3SHEU_gel	32.9	2602	14.5	15.5	3.1±0.5	12.1±1.0	150±12
poly3SHEU_nogel	42.4	2977	12.9	16.2	4.5±1.1	2.4±0.4	754±75
polyS4_gel	23.5	3000	18.7	11.8	3.7±0.3	32.3±3.6	32.4±6.3
polyS4_nogel	31.3	3761	15.3	11.7	3.9±1.7	23.0±3.5	78.5±18.6
polyS6_gel	37.2	4000	24.3	12.2	4.2±0.2	6.4±0.4	648±82
polyS6_nogel	48.2	4050	19.6	11.9	4.0±0.5	1.6±0.7	1354±125

[a] Temperature of the maximum of tan δ peak at 1 Hz. [b] Glassy storage modulus at T_g – 50 °C determined by DMA. [c] Rubbery storage modulus at T_g + 50 °C determined by DMA. [d] Full width at half maximum of the tan δ peak.

In Figure 5.7, we can see that the tan δ curves are monomodal and relatively narrow, with similar and low FWHM values, indicating the high homogeneity of the material due to the click character of the thio-Michael and thiol-epoxy reactions. The T_g values (considered as the temperature of the maximum of tan δ peak) agree well with the T_gs measured by DSC following the same trend as explained before. The damping capacities (maximum of the tan δ peak) are higher in those materials that gel in the second step of curing due to their lower crosslinking density. Storage moduli increase

with the functionality of the thiol selected in both glassy and rubbery states. The storage moduli in the glassy state are slightly higher in those materials that gel in the second step of curing, whereas the storage moduli in the rubbery state are somewhat lower. This is due to the GTA added. In polyX_gel, its amount is higher, increasing the crosslinking density (increasing E' in the rubbery state) but introducing more flexibility in the network due to its aliphatic structure and the higher proportion of flexible thiols needed. Contrarily, in polyX_nogel, the ratio of GTA is lower, reducing the crosslinking density and the flexibility of the network structure.

3.4 Mechanical characterization of the materials

The mechanical characterization of the final materials was done in tensile in the DMA (in static mode) using the tension clamp at 20 °C. Figure 5.8 presents the stress-strain curves, and the main parameters extracted are presented in Table 5.3.

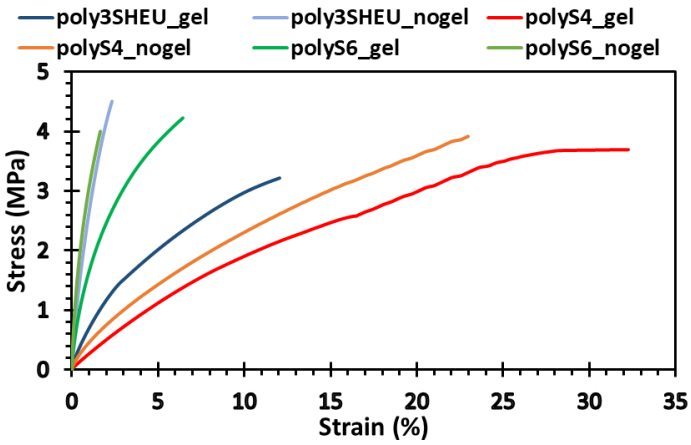

Figure 5.8. Stress-strain curves for the thermosets obtained.

The behavior observed in the tensile tests reflects two different factors. The first one is the network structure at the testing temperature (20 °C), being samples poly3SHEU_nogel and polyS6_nogel in the glassy state but all the other in the transition zone. This fact explains the higher rigidity (higher tensile modulus) and fragility (lower ε_{break}) of poly3SHEU_nogel and polyS6_nogel samples, the high ductility of S4 materials (almost totally relaxed at 20 °C) and the similar stress at break values of around 5 MPa. The second factor to consider is the ratio of GTA. The materials that gel in the first curing step, with a higher ratio of GTA, are more ductile that their counterparts with a lower ratio. This is due to the higher aliphatic character that allows an easier deformation without breaking.

4. Conclusions

A sequential dual-curing procedure using bio-based monomers as starting compounds has been implemented. Eugenol was transformed into acrylate epoxy eugenol, which was reacted with thiols of different functionalities: 3, 4, and 6. The trithiol used was also obtained from eugenol. The curing process consisted of a first step of thio-Michael addition and a second thiol-epoxy reaction catalyzed by 1-methylimidazole.

The addition of different ratios of the triacrylate of glycerol allowed to modify the characteristics of the intermediate materials. Low proportions of this compound led to a viscous intermediate material, whereas higher proportions led to rubbery solids since the gelation occurred during the first steps.

The fully cured materials were thermally stable until temperatures higher than 200 °C and showed T_gs in the 23 to 45 °C range. The materials with a higher proportion of the triacrylate showed lower T_gs and storage moduli in the glassy state but higher in the rubbery state due to their higher crosslinking densities.

The aliphatic moieties of the network structure enhance the flexibility and deformation ability of the prepared thermosets and this fact was confirmed with the thermomechanical and the mechanical characterization of the samples.

Acknowledgments

This work is part of the R&D projects PID2020-115102RB-C21 and PID2020-115102RB-C22 funded by MCNI/AEI/10.13039/501100011033 and European Union "NextGenerationEU"/PRTR. We acknowledge these grants, and we also thank the Generalitat de Catalunya (2021-SGR-00154). Bruno Bock Thiochemicals is acknowledge for kindly giving us thiol monomers.

References

[1] T. S., Kaufman, The Multiple Faces of Eugenol. A Versatile Starting Material and Building Block for Organic and Bio-Organic Synthesis and a Convenient Precursor Toward Bio-Based Fine Chemicals, J. Braz. Chem. Soc. 26 (2015) 1055-1085.

[2] Eugenol. Chemistry Research and Applications. Megan Shelton Ed. Nova Science Publishers, 2019, New York, USA.

[3] J. Qin, H. Liu, P. Zhang, M. Wolcott, J. Zhang, Use of eugenol and rosin as feedstocks for biobased epoxy resins and study of curing and performance properties, Polym. Int. 63 (2014) 760–765.

[4] R. Morales-Cerrada, S. Molina-Gutierrez, P. Lacroix-Desmazes, S. Caillol, Eugenol, a Promising Building Block for Biobased Polymers with Cutting-Edge Properties, Biomacromolecules 22 (2021) 3625−3648.

[5] T. Liu, C. Hao, L. Wang, Y. Li, W. Liu, J. Xin, J. Zhang, Eugenol-Derived Biobased Epoxy: Shape Memory, Repairing, and Recyclability, Macromolecules 50 (2017) 8588-8597.

[6] S. Gazzotti, M. Hakkarainen, K. H. Adolfsson, M. A. Ortenzi, H. Farina, G. Lesma, A. Silvani, One-Pot Synthesis of Sustainable High-Performance Thermoset by Exploiting Eugenol Functionalized 1,3-Dioxolan-4-one, ACS Sustain. Chem. Eng. 6 (2018) 15201−15211.

[7] J. Kerosenewala, P. Vaidya, V. Ozarkar, Y. Shirapure, A. P. More, Eugenol: extraction, properties and its applications on incorporation with polymers and resins-a review, Polym. Bull. 80 (2023) 7047-7099.

[8] I. Faye, M. Decostanzi, Y. Ecochard, S. Caillol, Eugenol bio-based epoxy thermosets: from cloves to applied materials, Green Chem. 19 (2017) 5236-5242.

[9] T. Yoshimura, T. Shimasaki, N. Teramoto, M. Shibata, Bio-based Polymer networks by thiol-ene photopolymerizations of allyl-etherified eugenol derivatives, Eur. Polym J. 67 (2015) 397-408.

[10] L. Rojo, B. Vázquez, J. San Román, S. Deb, Eugenol functionalized poly(acrylic acid) derivatives in the formation of glass-ionomer cements, Dental Mat. 24 (2008) 1709-1716.

[11] L. Dumas, L. Bonnaud, M. Olivier, M. Poorteman, P. Dubois, Eugenol-based benzoxazine: from straight synthesis to taming of the network properties, J. Mater. Chem. A, 3 (2015) 6012-6018.

[12] M. Shibata, N. Tetramoto, A. Imada, M. Neda, S. Sugimoto, Bio-based thermosetting bismaleimide resins using eugenol, bieugenol and eugenol novolac, React. Funct. Polym. 73 (2013) 1086–1095.

[13] H. Hao Jiang, L. Sun, Y. Zhang, Q. Liu, C. Ru, W. Zhang, C. Zhao, Novel biobased epoxy resin thermosets derived from eugenol and vanillin, Polym. Degrad. Stab. 160 (2019) 45-52.

[14] D. J. Kalita, I. Tarnavchyk, B. J. Chisholm, D. C. Webster, Novel bio-based epoxy resins from eugenol as an alternative to BPA epoxy and high throughput screening of the cured coatings, Polymer 233 (2021) 124191.

[15] A. Roig, M. Agizza, À. Serra, S. De la Flor, Disulfide vitrimeric materials based on cystamine and diepoxy eugenol as bio-based monomers, Eur. Polym. J. 194 (2023) 112185.

[16] D. Guzmán, X. Ramis, X. Fernández-Francos, S. De la Flor, A. Serra, Preparation of new biobased coatings from a triglycidyl eugenol derivative through thiol-epoxy click reaction, Prog. Org. Coat. 114 (2018) 259–267.

[17] X. Ramis, X. Fernández-Francos, S. De la Flor, F. Ferrando, A. Serra, Click-based dual-curing thermosets and their applications, in: Thermosets, 2nd ed. Qipeng Guo, Ed. 2018, Elsevier, Amsterdam, Netherlands.

[18] O. Konuray, X. Fernández-Francos, S. De la Flor, X. Ramis, A. Serra, The use of click-type reactions in the preparation of thermosets, Polymers 12 (2020) 1084.

[19] I. T. Smith, The mechanism of the crosslinking of epoxide resins by amines. Polymer 2 (1961) 95–108.

[20] D. P. Nair, M. Podgórski, S. Chantani, T. Gong, W. Xi, C. R. Fenoli, C. N. Bowman, The thiol-Michael addition click reaction: A powerful and widely used tool in materials chemistry, Chem. Mat. 26 (2014) 724–744.

[21] S. Parker, R. Reit, H. Abitz, G. Ellson, K. Yang, B. Lund, W. E. Voit, High-Tg thiol-click thermoset networks via the thiol-maleimide Michael addition, Macromol. Rapid Commun. 37 (2016) 1027–1032.

[22] O. D. McNair, A. P. Janisse, D. E. Krzeminski, D. E. Brent, T. E. Gould, J. W. Rawlins, D. A. Savin, Impact properties of thiol-ene networks, ACS Appl. Mater. Interfaces 5 (2013) 11004–11013.

[23] A. B. Lowe, Thiol-yne 'click'/coupling chemistry and recent applications in polymer and materials synthesis and modification, Polymer 55 (2014) 5517–5549.

[24] F. Gamardella, X. Ramis, S. De la Flor, A. Serra, Preparation of poly(thiourethane) thermosets by controlled thiol-isocyanate click reaction using a latent organocatalyst, React. Funct. Polym. 134 (2019) 174–182.

[25] C. Zeng, H. Seino, J. Ren, K. Hatanaka, N. Yoshie, Self-healing bio-based furan polymers cross-linked with various bis-maleimides, Polymer 54 (2013) 5351–5357.

[26] N. Le Baut, D. D. Díaz, S. Punna, M. G. Finn, H. R. Brown, Study of high glass transition temperature thermosets made from the copper(I)-catalyzed azide-alkyne cycloaddition reaction, Polymer 48 (2007) 239–244.

[27] H. C. Kolb, M. G. Finn, K. B. Sharpless, Click Chemistry: Diverse chemical function from a few good reactions, Angew. Chem. Int. Ed. 40 (2001) 2004–2021.

[28] D. Guzmán, X. Ramis, X. Fernández-Francos, S. De la Flor, A. Serra, New bio-based materials obtained by thiol-ene/thiol-epoxy dual curing click procedures from eugenol derivates, Eur. Polym. J. 93 (2017) 530–544.

[29] C. Russo, À. Serra, X. Fernández-Francos, S. De la Flor, Characterization of sequential dual-curing of thiol-acrylate-epoxy systems with controlled thermal properties, Eur. Polym. J. 112 (2019) 376-388.

[30] F. J. Seixas Xavier, K. A. da Franca Rodrigues, R. Guerra de Oliveira, C. G. Lima Junior, J. da Câmara Rocha, T. S. Lima Keesen, M. R. de Oliveira, F. P. Lins Silva, M. L.

Araújo de Almeida Vasconcellos, Synthesis and In Vitro Anti Leishmania amazonensis Biological Screening of Morita-Baylis-Hillman Adducts Prepared from Eugenol, Thymol and Carvacrol, Molecules 21 (2016) 1483.

[31] D. Popescu, R. Hoogenboom, H. Keul, M. Moeller, Hydroxy Functional Acrylate and Methacrylate Monomers Prepared Via Lipase-Catalyzed Transacylation Reactions, J. Mol. Catal. B Enzym. 62 (2010) 81-90.

[32] R. A. Setien, S. Ghasemi, G. Pourhashem, D. C. Webster, Comparison of Epoxidation Methods for Biobased Oils: Dioxirane Intermediates Generated from Oxone Versus Peracid Derived from Hydrogen Peroxide, Polym. Int. 70 (2021) 594-603.

[33] M. Neda, K. Okinaga, M. Shibata, High-performance bio-based thermosetting resins based on bismaleimide and allyl-etherified eugenol derivatives, Mater. Chem. Phys. 148 (2014) 319-27.

[34] https://www.perstorp.com/en/news_center/news/2011/20110329_discover_voxtar, (accessed 08/08/2023).

[35] X. Fernández-Francos, A-O. Konuray, A. Belmonte, S. De la Flor, A. Serra, X. Ramis, Sequential curing of off-stoichiometric thiol–epoxy thermosets with a custom-tailored structure, Polym. Chem. 7 (2016) 2280-2290.

[36] J. P. Pascault, H. Sautereau, J. Verdu, R. J. J. Williams, Thermosetting Polymers, Marcel Dekker, New York, USA, 2002.

[37] J. P. Pascault, R. J. J. Williams, Overview of Thermosets: Present and Future, in: Q. Guo (Ed.), Structure, Properties and Application, Thermosets 2nd ed. Chapter. 11, pp 3-34, Elsevier, Amsterdam, Netherlands, 2018.

[38] R. Meizoso Loureiro, T. Carballeira Amarelo, S. Paz Abuin, E. R. Soulé, R. J. J. Williams, Kinetics of the epoxy–thiol click reaction initiated by a tertiary amine: Calorimetric study using monofunctional components, Thermochim. Acta 616 (2015) 79-86.

[39] A. Belmonte, X. Fernández-Francos, À. Serra, S. De la Flor, Phenomenological characterization of sequential dual-curing of off-stoichiometric “thiol-epoxy” systems: towards applicability, Mater. Des. 113 (2017) 116-127.

Supporting Information

Synthesis of acrylate epoxy eugenol (AEEU). In a 500 mL three-necked flask equipped with a magnetic stirrer and ice bath, AEU (15.0 g, 68.7 mmol) was dissolved in 25 mL of DCM and then a solution of MCPBA (24.5 g, 0.1 mol) in 250 mL of DCM was added dropwise. The reaction was kept at 0 °C for 24 h until complete disappearance of AEU. The resulting mixture was washed once with a 10% w/w aqueous solution of $NaHSO_3$, twice with concentrated aqueous solution of $NaHCO_3$ and finally brine. The organic layer was dried over anhydrous $MgSO_4$, filtered and concentrated in a rotary evaporator to yield AEEU as a yellowish solid in a 96% of yield.

Synthesis of glycerol triacrylate (GTA). In a 250 mL three-necked flask equipped with a magnetic stirrer and ice bath, Gly (5 g, 54.3 mmol) was dissolved in 25 mL of $CHCl_3$. Then, TEA (37.8 mL, 0.27 mol) was added in the mixture and the system put in inert atmosphere. Later, a solution of acryloyl chloride (24.3 mL, 0.3 mol) in 50 mL of $CHCl_3$ was added dropwise. The mixture was allowed to proceed for 36 h at room temperature. Then, the reaction was vacuum filtered and washed once with HCl 1M (100 mL), twice with saturated $NaHCO_3$ solution (100 mL), twice with 20% w/w Na_2CO_3 solution (100 mL) and finally saturated NaCl solution (100 mL). Finally, the organic layer was dried over anhydrous $MgSO_4$, filtered and the solvent removed in a rotary evaporator to afford GTA as a brownish viscous oil (13.0 g, 94%).

Synthesis of O-allyl eugenol (OAllylEU). To a solution of EU (16.4 g, 0.100 mol) in DMSO (150 mL), pulverized NaOH (4.40 g, 0.110 mol) was added, and the resulting mixture was stirred for 10 min. Allyl bromide (13.3 g, 0.110 mol) was added dropwise over a period of 1 h at 40 °C. After the addition, the mixture was stirred maintaining the temperature for 3 h. The reaction mixture was poured into water and extracted with $CHCl_3$. The organic layer was washed with water twice, dried over Na_2SO_4 and concentrated in vacuo to yield AEU as a yellow liquid (18.0 g, 88 %).

Synthesis of 6-allyl eugenol (6-AllylEU). OAllylEU (12.8 g, 62.7 mmol) was stirred at 200 °C for 3 h using a pressure tube to give rearranged DAEU as a yellow oil in a quantitative yield

Synthesis of 6-allyl O-allyl eugenol (DAllylEU). To a solution of 6-AllylEU (6.13 g, 30.0 mmol) in 100 mL of DMSO, pulverized NaOH (1.39 g, 33.0 mmol) was added, and the resulting mixture was stirred for 10 min. Allyl bromide (3.99 g, 33.0 mmol) was added dropwise over a period of 1 h at 40 °C. After the addition, the mixture was stirred maintaining the temperature for 3 h. The reaction mixture was poured into water and then extracted with $CHCl_3$. The organic layer was washed with water twice, dried over Na_2SO_4 and concentrated in vacuo to yield DAllylEU as a yellow liquid (6.59 g, 90%).

Synthesis of the trithiol derived from eugenol (3SHEU).

Thiol-ene reaction (SAcEU). A mixture of 5 g (20.5 mmol) of DAllylEU, 22.2 g (291.6 mmol) of TAA and 0.1290 g (0.50 mmol) of DMPA was photoirradiated with a UV lamp at 356 nm for 1 h. The product obtained was dissolved in $CHCl_3$, extracted with a saturated NaOH solution, washed with water, and dried over anhydrous MgSO4. The solvent was removed on a rotary evaporator. The product obtained was a viscous liquid with 96% yield.

Saponification (3SHEU). 9.31 g (19.7 mmol) of the previous synthesized product were added to 100 mL of MeOH in a flask equipped with magnetic stirrer. 1.70 g (42.5 mmol) of pulverized NaOH were added and the mixture was heated to reflux temperature under inert atmosphere for 5.5 h. The solution was allowed to cool down and the solvent was removed. The product obtained was dissolved in water and acidified with 0.1 M HCl solution and then extracted with $CHCl_3$. The organic phase was washed with distilled water and then dried over anhydrous $MgSO_4$. The product obtained was a pale-yellow viscous liquid in 84% yield.

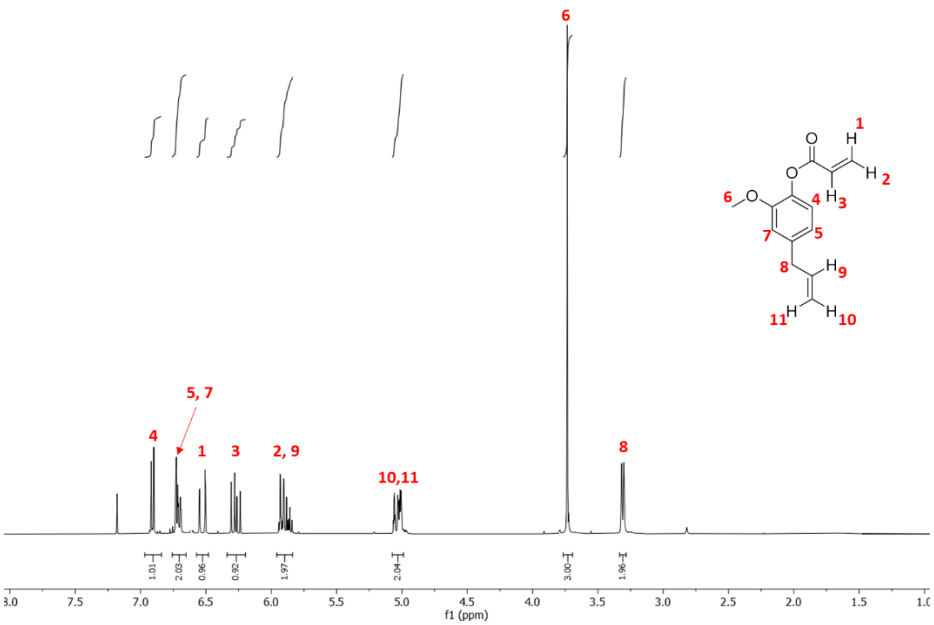

Figure 5.S1. ^1H NMR spectrum of AEU in $CDCl_3$.

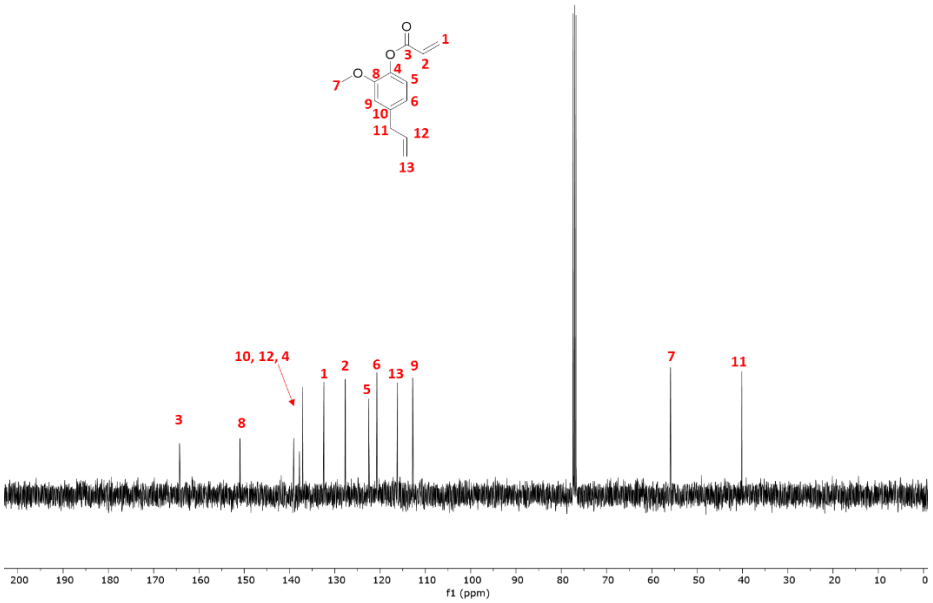

Figure 5.S2. ^{13}C NMR spectrum of AEU in $CDCl_3$.

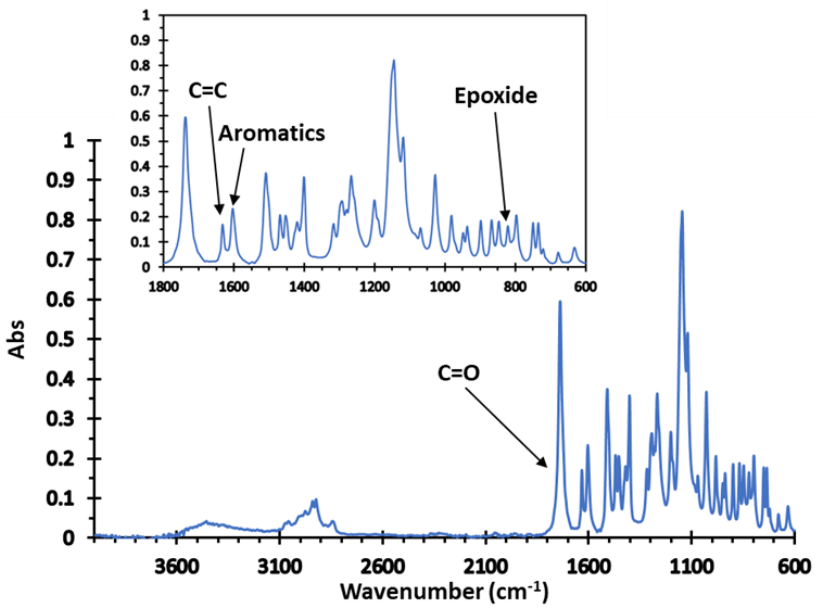

Figure 5.S3. FTIR-ATR spectrum of AEEU.

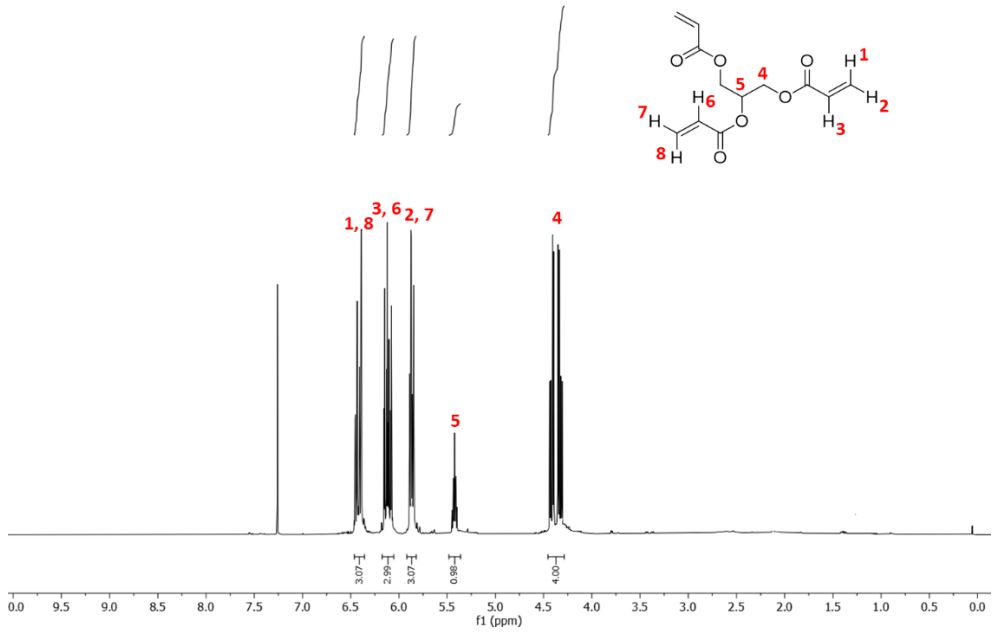

Figure 5.S4. ^{1}H NMR spectrum of GTA in $CDCl_3$.

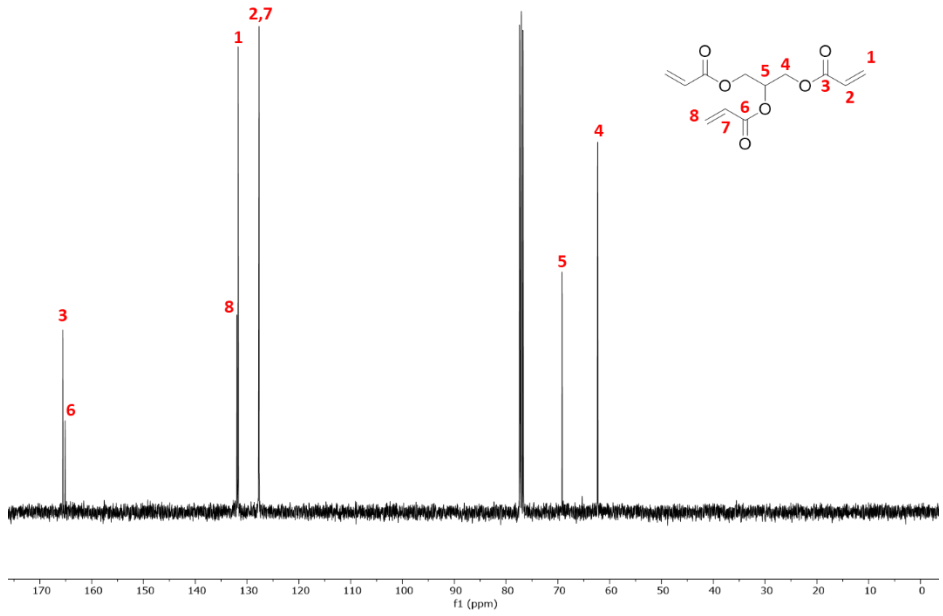

Figure 5.S5. ^{13}C NMR spectrum of GTA in $CDCl_3$.

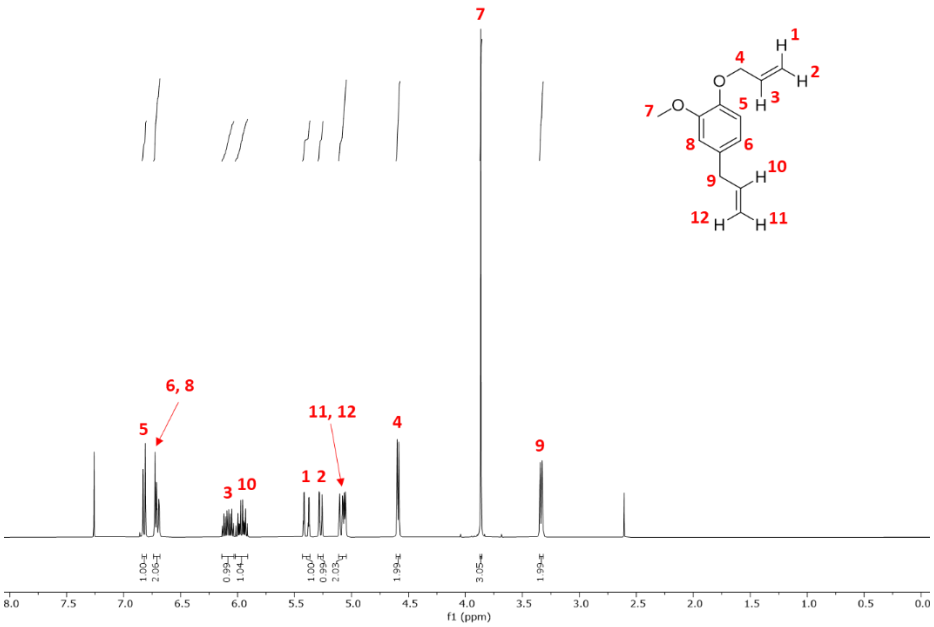

Figure 5.S6. ^{1}H NMR spectrum of O-allyl eugenol (OAllylEU) in $CDCl_3$.

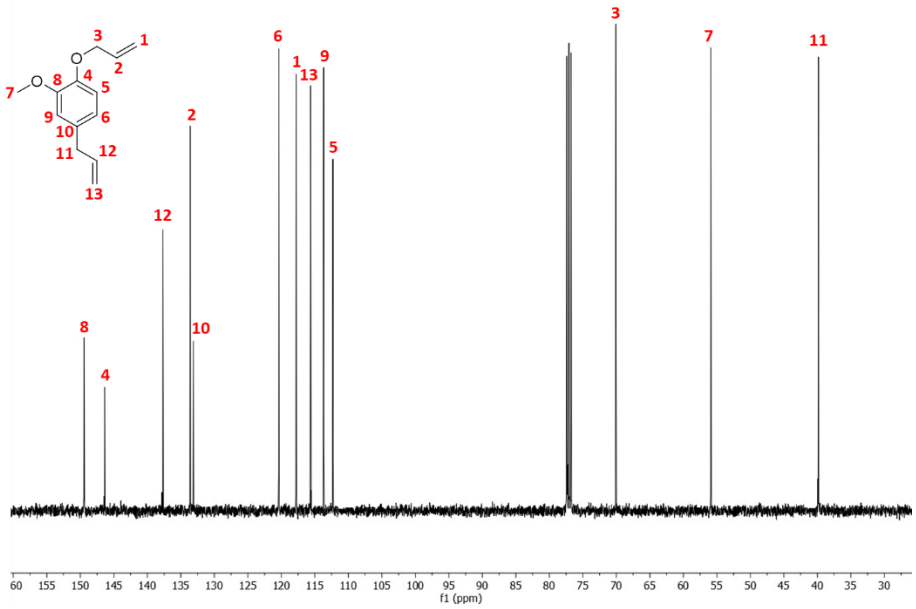

Figure 5.S7. ^{13}C NMR spectrum of O-allyl eugenol (OAllylAEU) in $CDCl_3$.

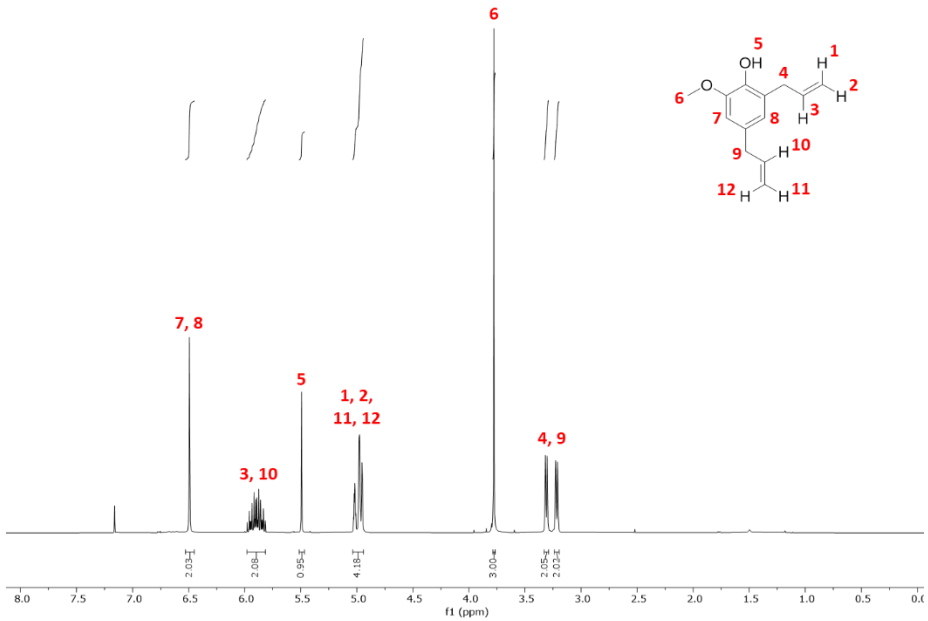

Figure 5.S8. ^{1}H NMR spectrum of 6-allyl eugenol (6-AllylEU) in $CDCl_3$.

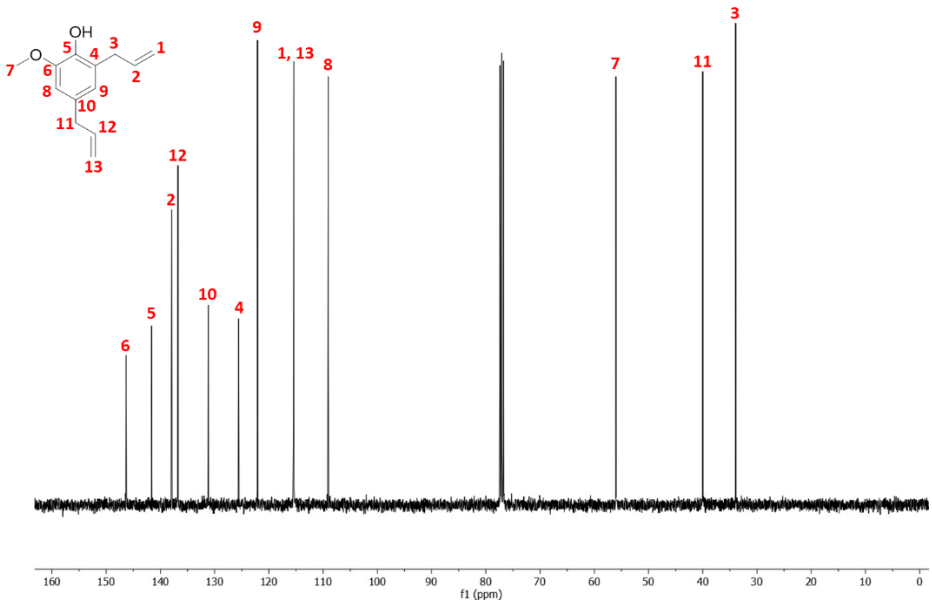

Figure 5.S9. ^{13}C NMR spectrum of 6-allyl eugenol (6-AllylEU) in $CDCl_3$.

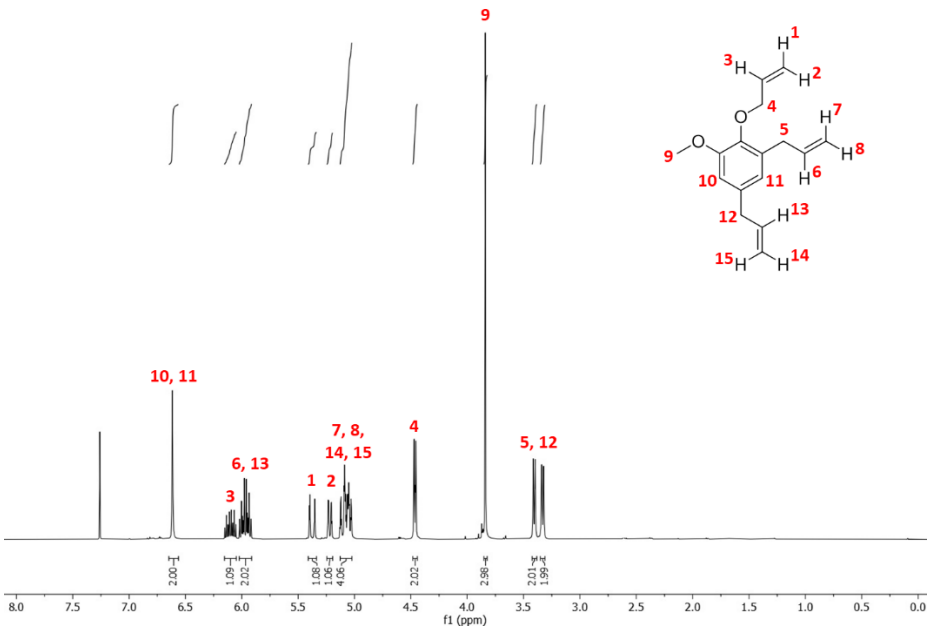

Figure 5.S10. ^{1}H NMR spectrum of 6-allyl O-allyl eugenol (DAllylEU) in $CDCl_3$.

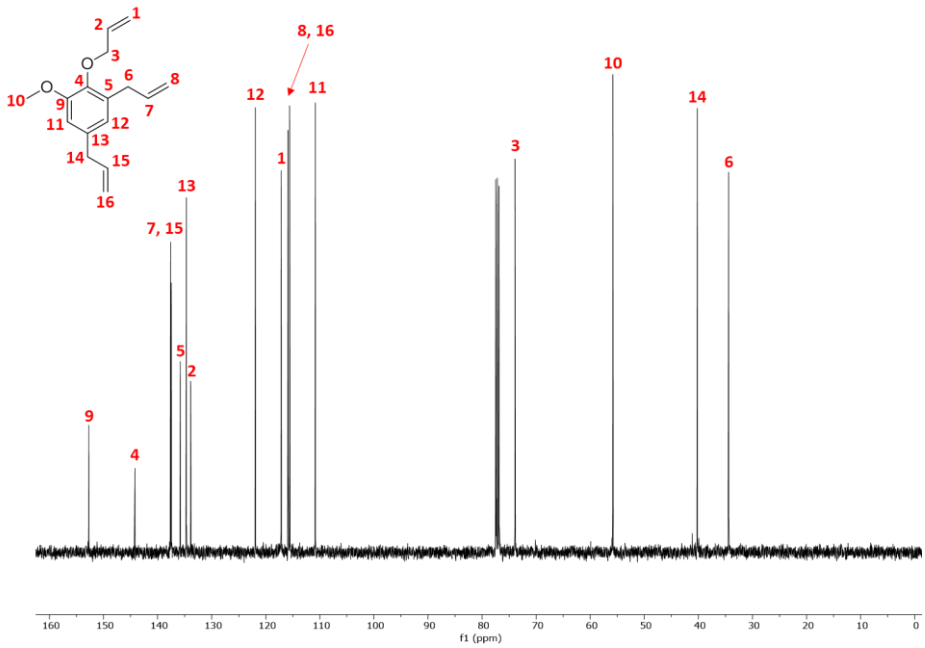

Figure 5.S11. ^{13}C NMR spectrum of 6-allyl O-allyl eugenol (DAllylEU) in $CDCl_3$.

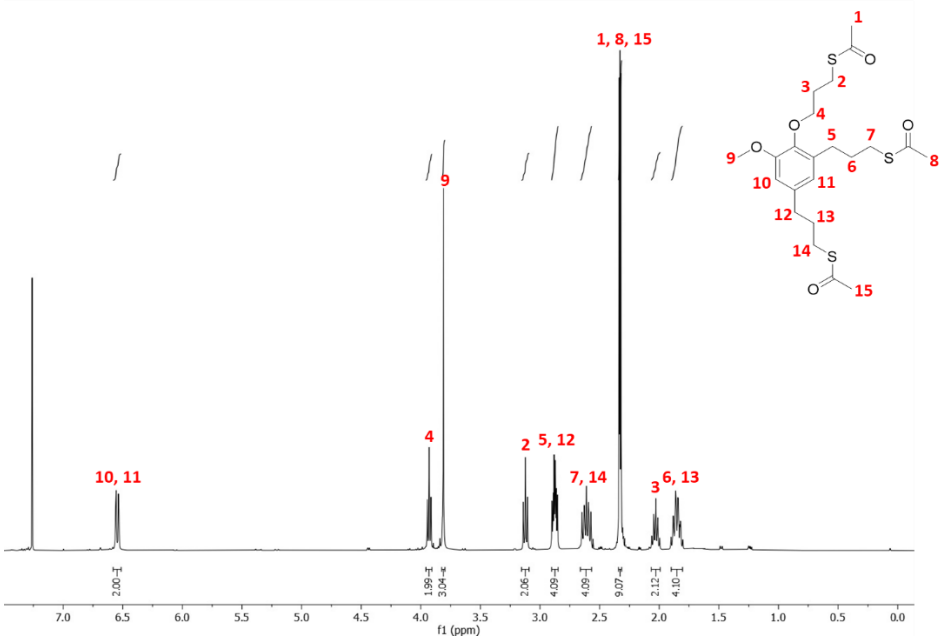

Figure 5.S12. ^{1}H NMR spectrum of the thiol-ene product on 2-allyl O-allyl eugenol (SAcEU) in $CDCl_3$.

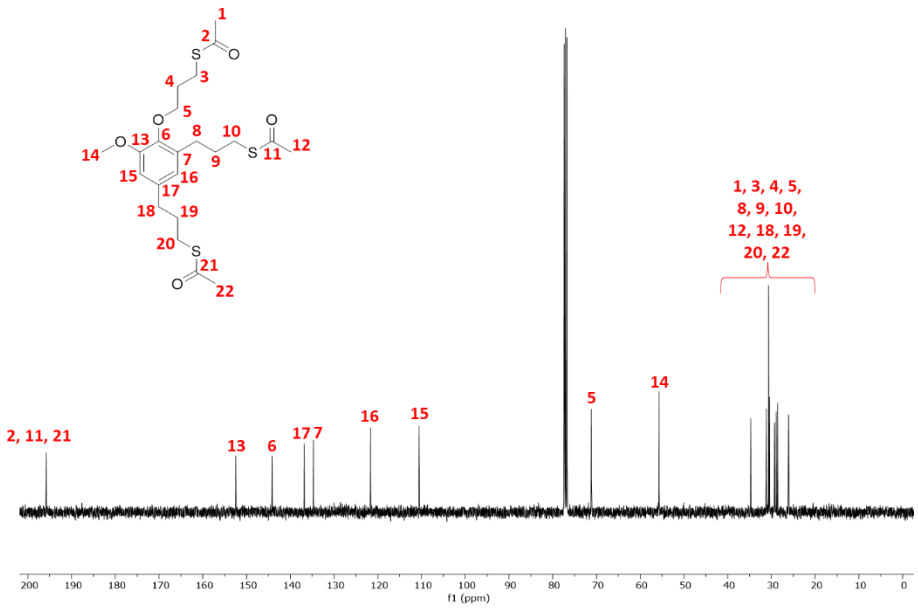

Figure 5.S13. ^{13}C NMR spectrum of the thiol-ene product on 2-allyl O-allyl eugenol (SAcEU) in $CDCl_3$.

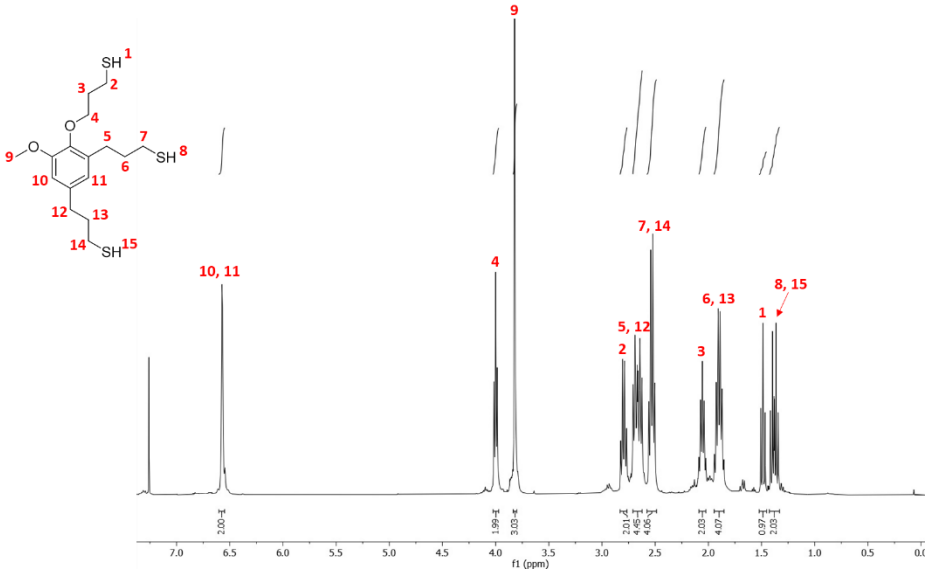

Figure 5.S14. ^{1}H NMR spectrum of the trithiol derived from eugenol (3SHEU) in $CDCl_3$.

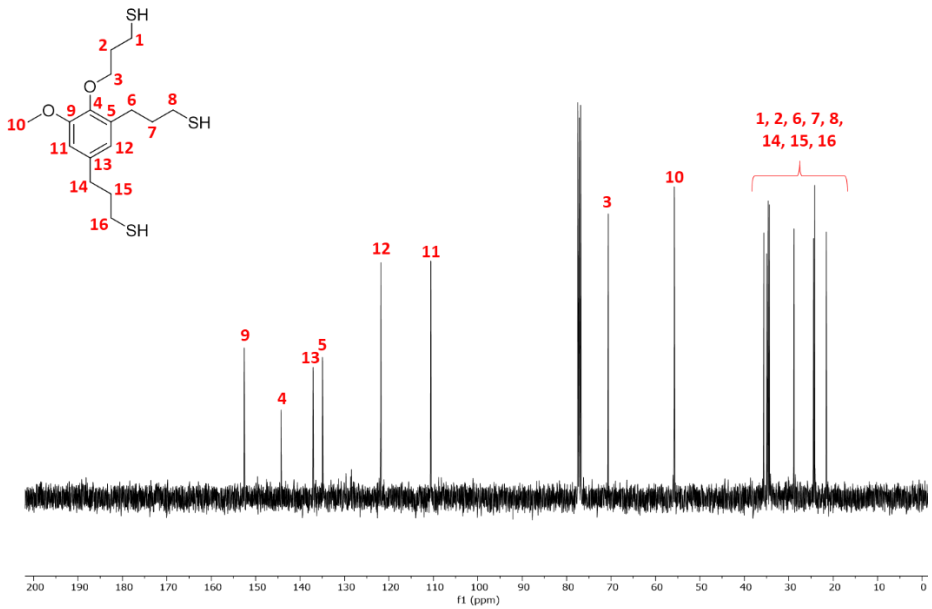

Figure 5.S15. ^{13}C NMR spectrum of the trithiol derived from eugenol (3SHEU) in $CDCl_3$.

UNIVERSITAT ROVIRA I VIRGILI
PROGRESS IN SUSTAINABILITY WITHIN THE REALM OF DESIGNING NEW THERMOSETTING MATERIALS
Adrià Roig Gibert

Chapter 6

Synthesis and characterization of new bio-based poly(acylhydrazone) vanillin vitrimers

(*Polym. Chem.* **2022**, *13*, 1510-1519)

UNIVERSITAT ROVIRA I VIRGILI
PROGRESS IN SUSTAINABILITY WITHIN THE REALM OF DESIGNING NEW THERMOSETTING MATERIALS
Adrià Roig Gibert

Polym. Chem. **2022**, *13*, 1510-1519

Synthesis and characterization of new bio-based poly(acylhydrazone) vanillin vitrimers

Adrià Roig,[1] Aina Petrauskaitė,[1] Xavier Ramis,[2] Silvia De la Flor,[3] Àngels Serra[1]

[1] Universitat Rovira i Virgili, Department of Analytical and Organic Chemistry, C/ Marcel·lí Domingo 1, Edif. N4, 43007 Tarragona, Spain

[2] Universitat Politècnica de Catalunya, Thermodynamics Laboratory, ETSEIB, Av. Diagonal, 08028 Barcelona, Spain

[3] Universitat Rovira i Virgili, Department of Mechanical Engineering, Av. Països Catalans 26, 43007 Tarragona, Spain

ABSTRACT

New acylhydrazone vitrimeric-type materials have been studied. These materials can be efficiently relaxed, without the addition of an external catalyst, through an exchange process that has been confirmed as imine metathesis, which differs from the previously reported transimination process in linear polymers. This is the first article that develops vitrimers with high T_g and fast relaxation based on poly(acylhydrazone)s. These materials have been prepared by condensing stoichiometric amounts of glycidyl vanillin and aliphatic dihydrazides of different chain lengths. The curing reaction takes advantage of the different reactivity of formyl and glycidyl groups and proceeds in two sequential steps: a first condensation of the formyl group of vanillin with dihydrazide monomers at low temperature followed by reaction of the remaining hydrazides with the epoxide, which requires temperatures above 150 °C. The complete disappearance of the initial reactive groups has been confirmed by FTIR spectroscopy. The thermomechanical characteristics have been evaluated by DMTA, obtaining T_gs above 100 °C for the materials prepared, which present excellent vitrimeric features with very short relaxation times. Using model compounds, we were able to demonstrate that imine metathesis is responsible for the exchange process. The thermal stability of these materials has been rated by TGA. Poly(acylhydrazone) materials showed good recycling and self-healing abilities and could be hydrolyzed in an acidic medium.

1. Introduction

Thermosets are a class of polymeric materials that have many advantages due to their excellent mechanical properties, dimensional stability and chemical resistance, making them very interesting materials for several applications such as coatings [1], adhesives [2], electronics [3], *etc*. However, their permanent crosslinked structure hampers them to be recycled or reprocessed once cured which can lead to serious environmental issues at the end of their lifetime due to the waste of resources. For this reason, the development of reshapable or recyclable materials has arisen as a promising solution to solve these issues [4].

Covalent adaptable networks (CANs) behave as permanently crosslinked thermosets at a specific temperature, but they have the ability to flow and, therefore, to be reshaped or self-repaired when are subjected to an external stimulus such as heat or light due to the exchangeable bonds in their structure [5]. Since 2011, Leibler and co-workers reported a specific type of CANs, named vitrimers [4], the interest in this research field has increased exponentially. Vitrimers have the particularity of exchanging bonds while flowing without losing their network integrity, meaning that the bonds rupture and formation occur in a concerted manner without any intermediate state but always keeping constant the crosslinking density [6]. Many examples of vitrimers have been reported regarding different types of reactions such as transesterification [7-9], transcarbamoylation [10,11], disulfide interchange [12], olefin metathesis [13], and imine-amine exchange [14-16], among many others.

In this last group of exchange reactions, acylhydrazone groups take part in a significant way. These groups are formed by a reversible condensation reaction of aldehydes or ketones with hydrazides, which spontaneously form the carbon-nitrogen double bond and water that can be eliminated, being a driving force to shift the equilibrium [17]. In 2004, Lehn and co-workers reported the ability of acylhydrazone dynamic bonds to produce dynamers [18,19]. They stated that the reversibility of these linear polymers relies on the imine group of the acylhydrazone while the amide group provides hydrogen bonding like in polyamides. They not only successfully reported the synthesis of different poly(acylhydrazone)s by mixing different dihydrazides with dialdehydes but also the exchangeable behavior of these bonds upon heating by combining the synthesized poly(acylhydrazone)s with structurally different aldehydes or dihydrazides. They also reported the synthesis of dual dynamic acylhydrazones, with reversible covalent bonds and dynamic non-covalent hydrogen bonding interactions, by condensation of aromatic dialdehydes connected by a siloxane backbone, which imparts softness, with carbohydrazide. These materials revealed excellent self-healing properties [20].

Later on, more studies of this type of materials were performed by Chen and co-workers, who reported a strategy to construct new reversible polymers by mixing poly(ethylene oxide) with terminal acylhydrazine end groups with trialdehydes to form dynamic gels in mild conditions [21]. The gels formed could also be transformed into their starting monomers an re-form the gel again by increasing or decreasing the acidity of the water solution, respectively. In addition, these materials revealed interesting self-healing properties without using any external help. Afterwards, Deng *et al.* went deeper into the topic, and they successfully developed new dynamic hydrogels combining acylhydrazone and disulfide bonds in the same system [22]. The obtained materials were able to repair themselves under hydrolytic acid and basic conditions through acylhydrazones exchange or disulfide exchange reactions. It must be pointed out, that the exchange reaction is based in these cases, on the hydrolysis and re-forming of the imine moiety, and it is not related to any vitrimeric-type relaxation process.

To reach a high bond-exchange rate, many vitrimers required the addition of catalysts, being some of them toxic and easily leachable which makes reprocessing or reshaping difficult. Consequently, there is a growing interest in new vitrimeric materials that do not require any catalyst [23]. Among them, vinylogous urethanes [24], boroxines [25], and imines [26] may be mentioned. As reported, the exchange reaction of poly(acylhydrazone)s does not require the addition of any catalyst and therefore, the study and development of this type of vitrimers could be highly interesting [18,21].

In recent years, products derived from renewable resources have attracted huge interest in materials science to reduce the use of petrochemical compounds as well as to find greener synthetic routes to avoid the depletion of fossil resources. The researchers have focused their attention on synthesizing vitrimeric materials based on compounds derived from biomass such as catechol [27], eugenol [28,29], or vanillin [30,31]. In particular, vanillin (4-hydroxy-3-methoxy benzaldehyde) is not only one of the most important aromatic compounds used in food, beverages, perfumes, and pharmaceuticals, but it is also very interesting as a feedstock for the development of materials due to its phenolic and aldehyde groups that can be further modified to get the suitable functionality. Moreover, the rigid structure due to the aromatic ring provides high thermal and mechanical properties to the obtained materials [32].

Taking all this into account, in the present article, we report the synthesis and characterization of a series of new bio-based poly(acylhydrazone) vitrimers. Three different dihydrazides derived from bio-based glutaric, suberic and dodecandioic acids [33] were obtained in high yields via two-step synthesis as well as the glycidyl derivative of vanillin (EPO-Van) (see Scheme 6.1). Since dihydrazides are latent curing agents for epoxy resins and only react on heating above 150 °C [34], can condense specifically at lower temperatures with the aldehyde groups of EPO-Van, releasing

water leaving epoxy groups unreacted. At higher temperatures, the remaining dihydrazide groups in the mixture can react with epoxides leading to three-dimensional networks.

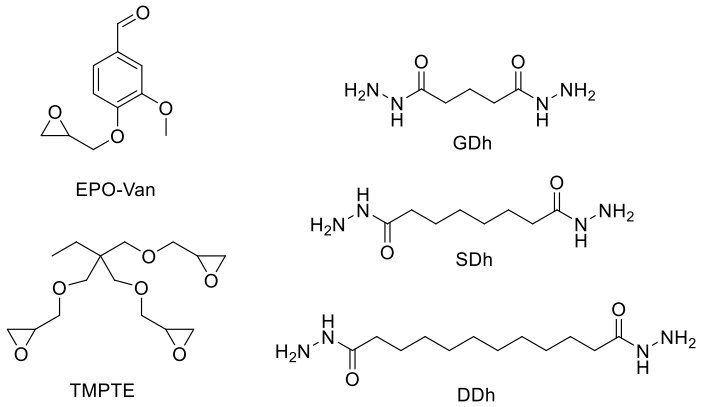

Scheme 6.1. Monomers used in the preparation of the poly(acylhydrazone) vitrimers.

To facilitate the processing and to improve the thermomechanical characteristics of the crosslinked materials, as well as to reach homogeneous mixtures, trimethylolpropane triglycidylether (TMPTE) has been added to the curing formulation. Stoichiometric mixtures of EPO-Van, dihydrazides (Dh) and TMPTE were used to get the final materials.

The completion of the reaction was evaluated by FTIR spectroscopy. The vitrimers obtained were characterized by thermogravimetric analysis to know the range of thermal stability, and thermomechanical analysis to evaluate their relaxation behavior. Poly(acylhydrazone)s were recycled under determined conditions and proves to have similar mechanical properties. Materials also revealed self-healing properties, which make them very interesting in many fields of application. As far as we know, this is the first time that the preparation and characterization of similar highly crosslinked poly(acylhydrazone) vitrimers have been reported, and that imine metathesis is the exchange process responsible for the relaxation.

2. Experimental methods

2.1 Materials

(±)-Epichlorohydrin (ECH, ≥99%), triethylbenzylammonium chloride (TEBAC, 99%), glutaric acid (GA, 99%), suberic acid (SA, 98%), dodecanedioic acid (DA, 99%), trimethylolpropane triglycidyl ether (TMPTE), benzaldehyde (B) and octanoic acid (OA) were purchased from Sigma Aldrich. Vanillin (V, 99%) and hydrazine hydrate (HzH, 80%) were obtained from ACROS Organics. Ethyl acetate (EtOAc), 1,2-dichlorobenzene (DCB), and N,N-dimethylformamide (DMF) were purchased from

Polym. Chem. **2022**, *13*, 1510-1519

VWR chemicals. Sodium hydroxide (granulated, NaOH) and absolute ethanol (EtOH) were purchased from Scharlau and sulfuric acid (H_2SO_4, ≥95%) from Fisher Chemical.

2.2 Characterization methods

^{1}H NMR and ^{13}C NMR spectra were registered in a Varian VNMR-S400 NMR spectrometer. $CDCl_3$ and DMSO-d_6 were used as solvents. All chemical shifts are quoted on the δ scale in parts per million (ppm) using residual protonated solvent as internal standard (^{1}H NMR: $CDCl_3$ = 7.26 ppm, DMSO-d_6 = 2.50 ppm; ^{13}C NMR: $CDCl_3$ = 77.16 ppm, DMSO-d_6 = 39.52 ppm).

Gas chromatography (GC) tests were performed in a gas chromatograph 6890 Series with automatic liquid sampler HP7683 Series and mass spectrometer 5973 (Hewlett Packard). The column used was an analytical column HP-5MS (30 m × 0.25 mm × 0.25 µm) (Agilent Technologies). Samples were dissolved in acetonitrile (GC grade) and 1 µL was injected with a split ratio of 50 : 1 in a constant flow of 1.0 mL min^{-1}.

DSC analyses were carried out on a Mettler DSC3+ instrument calibrated using indium (heat flow calibration) and zinc (temperature calibration) standards. Samples of approximately 8–10 mg were placed in aluminum pans with pierced lids and analyzed in an N2 atmosphere with a gas flow of 50 cm^3 min^{-1}. Dynamic studies between 30 and 250 °C at a heating rate of 10 °C min^{-1} were performed to determine the melting points.

A Jasco FT/IR-680 Plus spectrometer equipped with an attenuated total reflection accessory (ATR) (Golden Gate, Specac Ltd, Teknokroma) was used to register the FTIR spectra of the mixtures after the curing procedure. Real-time spectra were registered in the wavenumber range between 4000 and 600 cm^{-1} with a resolution of 4 cm^{-1} and averaged over 20 scans. The disappearance of the characteristic absorbance peaks of epoxy and aldehyde groups at 915 cm^{-1} and 1715 cm^{-1}, respectively, as well as the appearance of the peaks corresponding to O–H at 3300 cm^{-1} and C=N at 1680 cm^{-1} were used to confirm the completion of the reactions.

The thermal stability of the materials was evaluated using a Mettler Toledo TGA 2 thermobalance. Cured samples, weighing around 10 mg, were degraded between 30 and 600 °C at a heating rate of 10 °C min^{-1} in N_2 atmosphere with a flow of 50 cm^3 min^{-1}.

The thermomechanical properties were studied using a DMA Q800 (TA Instruments) equipped with a film tension clamp. Prismatic rectangular samples with dimensions around 30 × 5 × 1.5 mm^3 were analyzed from −25 °C to 200 °C at 1 Hz, with 0.1% strain at a heating rate of 2 °C min^{-1}. Tensile stress–relaxation tests were conducted in the same instrument using the film tension clamp on samples with the same dimensions as previously defined. To obtain the activation energy (E_a) for the materials, the

samples were firstly equilibrated at the relaxation temperature for 5 min and a constant strain of 1% was applied, measuring the consequent stress level as a function of time. The materials were tested only once at one temperature. The relaxation–stress $\sigma(t)$ was normalized by the initial stress σ_0, and the relaxation times (τ) were determined as the time necessary to relax $0.37\sigma_0$, i.e., ($\sigma = 1/e\sigma_0$). With the relaxation times obtained at each temperature, the activation energy values, E_a, were calculated by using an Arrhenius-type equation:

$$ln(\tau) = \frac{E_a}{RT} - \ln A \qquad \text{(Eq. 6.1)}$$

where τ is the time needed to attain a given stress-relaxation value ($0.37\sigma_0$), A is a pre-exponential factor and R is the gas constant. From the Arrhenius relation, the topology freezing temperature (T_v) was obtained as the temperature at which the material reaches a viscosity of 10^{12} Pa·s. Using Maxwell's relation and E' determined from DMTA (assuming E' being relatively invariant in the rubbery state), τ^* was determined to be around 10^5 s in our systems. The Arrhenius relationship was then extrapolated to the corresponding value of τ^* to determine T_v in each sample.

The recycled samples were obtained by cutting the crosslinked polymers and hot-pressing in a Specac Atlas manual 15 T hydraulic press at 9.25 MPa into an aluminum mold, at 180 °C for 2 h. Recycled samples were die-cut in the same dimensions from the new film obtained and tested again in the DMA analyzer for their mechanical characterization at the same conditions previously described. Dissolution experiments of final materials were performed by the following procedure: pieces of poly(acyl)hydrazone of 50 – 100 mg, weighed before the experiment, were placed in a 50 mL round bottom flask equipped with a magnetic stirrer. The flask was filled with 1,2-dichlorobenzene (DCB) closed and heated at 150 °C during 8 h. Then, the flask was cooled down to room temperature. The polymer sample was dried under reduced pressure, at 100 °C during 12 h. After cooling down to room temperature, the samples were weighted, and the gel fraction was calculated. For self-healing tests, samples were scratched and broken using a cutter, and subsequently heated in an oven at 190 °C for several hours exploring from time to time the evolution of the scratch by taking pictures with a Digital Microscope Leica DMS1000.

2.3 General procedure for the poly(acylhydrazone)s preparation

Poly(acylhydrazone)s materials were prepared by dissolving mixtures of EPO-Van/TMPTE using a molar percentage 3:1 with the corresponding dihydrazide (Hz) in stoichiometric epoxy/aldehyde/NH_2 proportions in the minimum amount of dimethylformamide (DMF) to solubilize the mixture. Then, the liquid formulations were magnetically stirred at 160 °C until most of the solvent was evaporated. Then, the mixture was poured into a Petri plate where it was maintained at the same

Polym. Chem. **2022**, *13*, 1510-1519

temperature until a gel is formed. Obtained gels were cut into small pieces and placed in a vacuum oven for 2 h at 150 °C to ensure the elimination of the solvent and then grinded to small particles. They were evenly spread in round aluminum molds protected with an adhesive sheet of Teflon and thermally cured in the manual hydraulic hot press under 9.25 MPa at 160 °C for 1 h to obtain solid films with uniform thickness that were die-cut to get specimens of 30 x 5 x 1.5 mm^3.

3. Results and discussion

3.1 Synthesis of starting compounds

Dihydrazides were prepared via two-step procedure including the synthesis of intermediate esters via Fischer esterification of dicarboxylic acids and further reaction with hydrazine hydrate. For the present work, glutaric (GA), suberic (SA) and dodecandioic (DA) acids were selected as starting materials in order to achieve a series of bio-based dihydrazides (GDh, SDh and DDh, respectively) with different chain lengths. All the products synthesized were analyzed by NMR spectroscopy (Figures 6.S1-S6). The disappearance of the characteristic proton signals of ethyl ester groups is observed, while newly formed hydrazide group signals appear at around 8.9 and 4.1 ppm. ^{13}C NMR spectra also confirm the purity of the compounds by the vanishment of the signal corresponding to the ethyl ester and the appearance of the carbonyl signal of hydrazide at around 171.1 ppm in all cases. Experimental details are presented in the SI.

EPO-Van was synthesized by reacting vanillin with a large excess of epichlorohydrin, using NaOH as a base and TEBAC as a phase transfer catalyst maintained 1.5 h at 80 °C. The procedure led to the formation of the glycidyl product as a yellowish-white solid in a high yield. Its structure was confirmed by ^{1}H-NMR spectroscopy by the appearance of the signals corresponding to the glycidyl group between 4.5 and 2.6 ppm while the signal of the proton of the aldehyde remained constant (Figure 6.S7). ^{13}C NMR spectrum showed the signals of the carbons corresponding to the glycidyl group between 44.0 and 70.0 ppm (Figure 6.S8).

3.2 Demonstration of the exchange reaction

To confirm the possibility of exchange reaction between acylhydrazone groups, four different acylhydrazones combining two aldehydes, benzaldehyde (B) and vanillin (V), with two synthesized hydrazides, octanoic hydrazide (Oh) and acetyl hydrazide (Ah) were synthesized. Thus, B-Oh, B-Ah, V-Oh and V-Ah acylhydrazones were successfully prepared in high yield and purity (see Figures 6.S9-S20). Then, B-Ah and V-Oh were mixed, dissolved in absolute EtOH, and maintained at reflux for 2 h. After that, the solvent was eliminated at the rotary evaporator obtaining a viscous oil. Scheme 6.2

depicts the structure of the model compounds and the structure of the rearranged compounds expected.

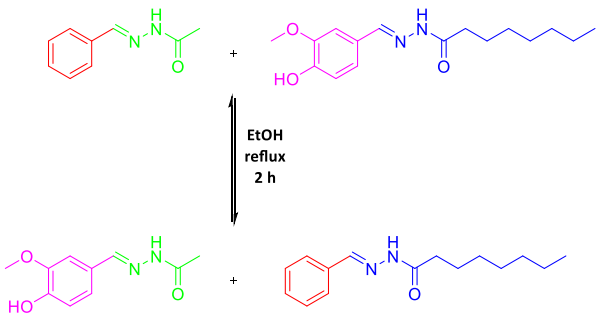

Scheme 6.2. Model compounds synthesized and structure of the compounds formed by the exchange reaction.

The mixture after heating and each synthesized compound were investigated by gas chromatography coupled to a mass spectrometer detector by injecting samples dissolved in acetonitrile. The chromatograms are represented in Figure 6.1. As we can see in Figure 6.1b, after reaction of B-Ah and V-OH, two new compounds that could be identified as the combination of both products (V-Ah and B-Oh) appeared in the chromatogram, concluding that the exchange reaction has taken place which may indicate that the exchange mechanism occurs.

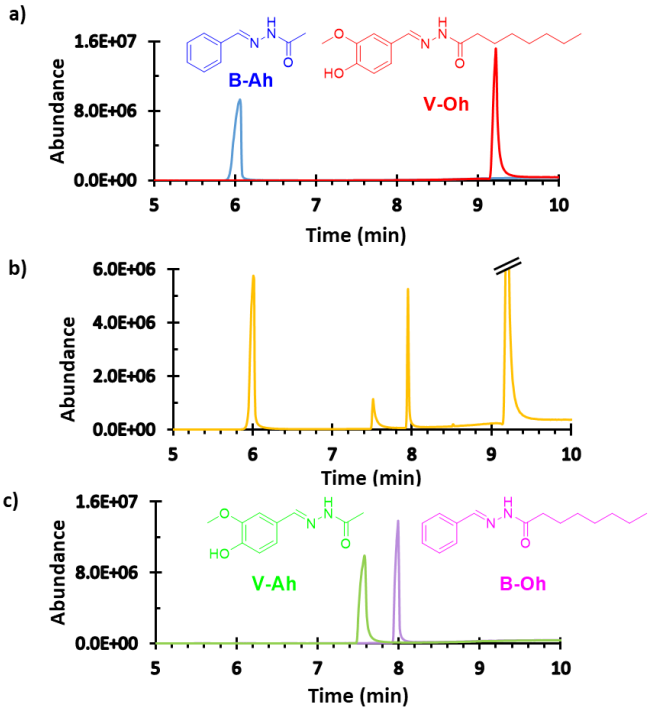

Figure 6.1. GC chromatograms of a mixture of pure B-Ah and V-Oh (a), after the reaction of B-Ah and V-Oh (b) and a mixture of pure V-Ah and B-Oh (c).

Polym. Chem. **2022**, *13*, 1510-1519

Moreover, it is possible to observe that no traces of any other compound referring to the hydrolysis of the acylhydrazone or any aldehyde are present in the chromatogram backing up the hypothesis of a concerted mechanism. Lehn and co-workers explained that acylhydrazone groups were able to perform exchangeable reactions by the imine bond [18]. They tested the exchange reaction by adding an excess of aldehydes or dihydrazides, which suggested that a transimination reaction was taking place on the acylhydrazone groups. In our case, as we added stoichiometric amounts of each pure acylhydrazone compound, an imine metathesis must be the only exchange reaction that occurs.

3.3 Study of the curing procedure

Synthesized dihydrazides and EPO-Van monomers were used in the preparation of sustainable vanillin-based vitrimers containing acylhydrazone dynamic covalent bonds. To achieve higher flexibility of the final networks, formulations were supplemented by aliphatic trimethylolpropane triglycidyl ether (TMPTE). DMF liquid mixtures of EPO-Van/TMPTE/Dh in stoichiometric epoxy/aldehyde/NH_2 proportions were cured as described in the experimental section. Crosslinked materials were successfully obtained as thin red films with high transparency. Since EPO-Van has epoxy and aldehyde reactive groups, in this curing system, before epoxy-amine reaction, aldehydes react with -NH_2 of dihydrazides due to the latent character of these compounds as epoxy curing agents (Scheme 6.3) [34].

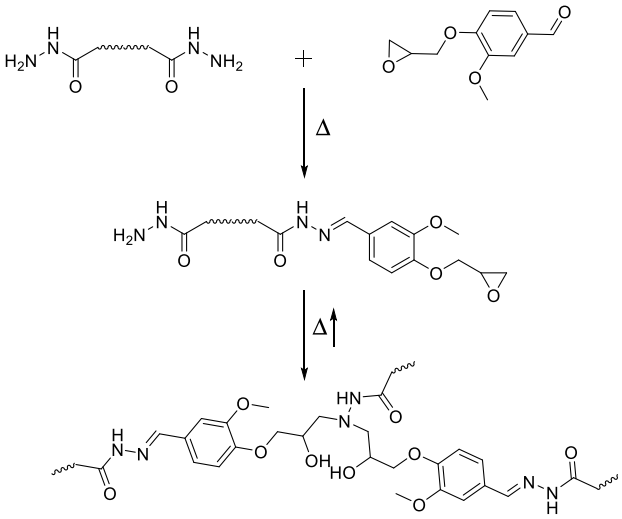

Scheme 6.3. Synthetic steps in the preparation of poly(acylhydrazone) thermosets.

This is the key point of the curing because otherwise, the dihydrazides could react either with epoxides or with aldehydes. It should be noted that whereas epoxides firstly react with -NH_2, leaving free -NHR groups, aldehydes can only react with -NH_2

groups. Therefore, if epoxides were to react in the early stages of the curing process, a stoichiometric imbalance would occur that would leave unreacted aldehydes that would lead to materials with a lower degree of crosslinking and a lower proportion of exchangeable acylhydrazone moieties.

FTIR spectra were registered to determine if the complete curing has been reached forming a poly(acylhydrazone) network. Figure 6.2 shows as an example, the FTIR spectra of the initial monomers used and one of the final materials. As we can see, the bands corresponding to the aldehyde group at 1680 cm^{-1} and the epoxy groups at 910 cm^{-1} have completely disappeared indicating the consumption of these groups. Moreover, the carbonyl dihydrazide band at 1626 cm^{-1} has vanished but at the same time, the broad absorption bands of the stretching of O-H and N-H at 3300 cm^{-1} visibly increase. In addition, in the spectrum of the final material, a peak at 1640 cm^{-1} corresponding to the imine of the formed acylhydrazone structure can be noticed. From these changes, it is evident that epoxy hydrazide and condensation reactions have been completed and subsequently a fully cured material has been achieved.

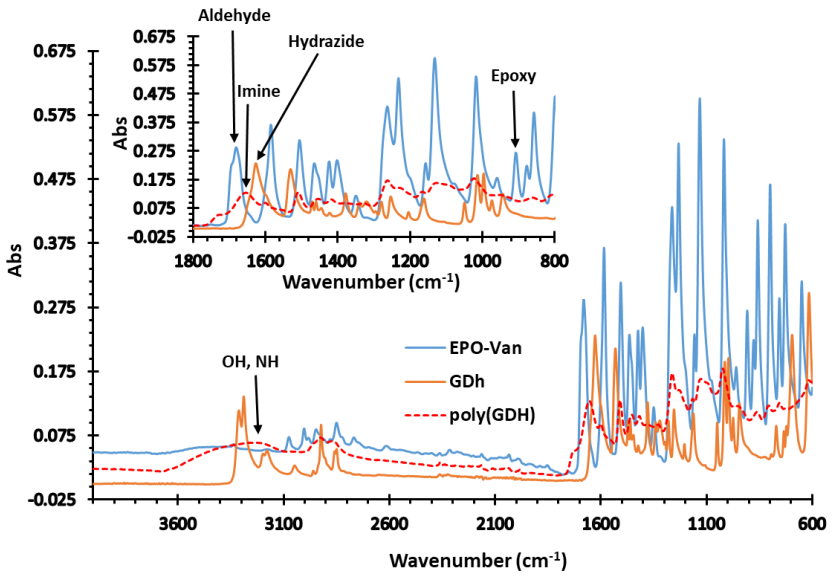

Figure 6.2. FTIR spectra of the initial monomers, EPO-Van (blue), glutaric dihydrazide (GDh) (orange), and of the final material (polyGDH) (red).

3.4 Thermal characterization of the materials

The thermal stability of the vitrimers was evaluated by thermogravimetry (TGA). Figure 6.3 shows the TGA curves and their derivatives for the materials prepared and Table 6.1 collects the most significant thermogravimetric data. Whereas the degradation curves (Figure 6.3a) are quite similar for the three materials, the shapes of the first derivative (Figure 6.3b) present some differences.

Polym. Chem. **2022**, *13*, 1510-1519

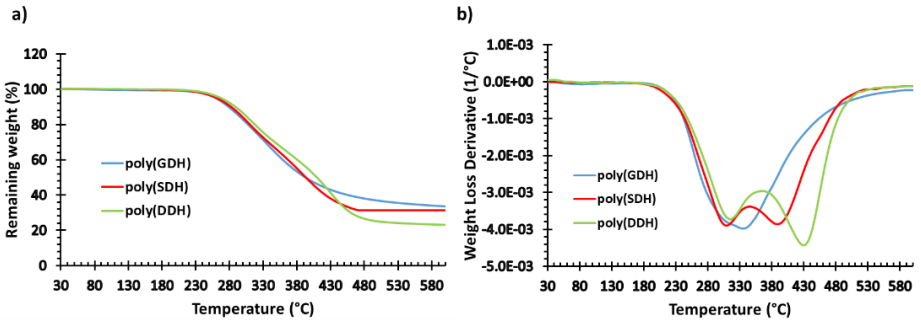

Figure 6.3. a) Thermogravimetric curves and b) DTG curves of the poly(acylhydrazone) materials.

As we can see, the degradation of poly(GDH) material has a broad peak with the maximum at 335 °C meaning that the breakage of different bonds and elimination of fragments take place simultaneously. However, in the case of poly(SDH) and poly(DDH), two different peaks can be observed, with the second one shifted to higher temperature on increasing the length of the aliphatic moiety in the network structure, which could be related to the breakage of acylhydrazone bonds.

Table 6.1. Thermogravimetric data of all the poly(acylhydrazone)s prepared.

Sample	$T_{1\%}$[a] (°C)	$T_{2\%}$[b] (°C)	T_{max}[c] (°C)	Char yield[d] (%)
poly(GDH)	220.6	236.5	335.0	33.6
poly(SDH)	220.0	235.1	309.2/389.7	31.0
poly(DDH)	218.4	234.2	314.8/429.7	23.5

[a] Temperature of 1% of weight loss. [b] Temperature of 2% of weight loss.
[c] Temperature at the maximum rate of degradation. [d] Char residue at 600 °C

The values in Table 6.1 reveal that these materials have a relatively high thermal stability, as the samples lose 2% of weight at temperatures above 234 °C. This high resistance to heat degradation is likely conferred by a high crosslinking density and aromatic content in the network structure. The temperatures, around 220 °C, at which the weight loss is only 1% accounts for the capability of safe recycling at temperatures below 200 °C. The presence of nitrogen and aromatic rings in the network structure leads to high char yields that decrease with the length of the aliphatic moiety of the dihydrazide monomer.

The thermomechanical characteristics of the poly(acylhydrazone)s have been determined by DMTA analysis. Figure 6.4 shows the tan δ curves, as well as the storage

moduli (E') as a function of temperature for all the materials and the corresponding data extracted from these studies, which are summarized in Table 6.2

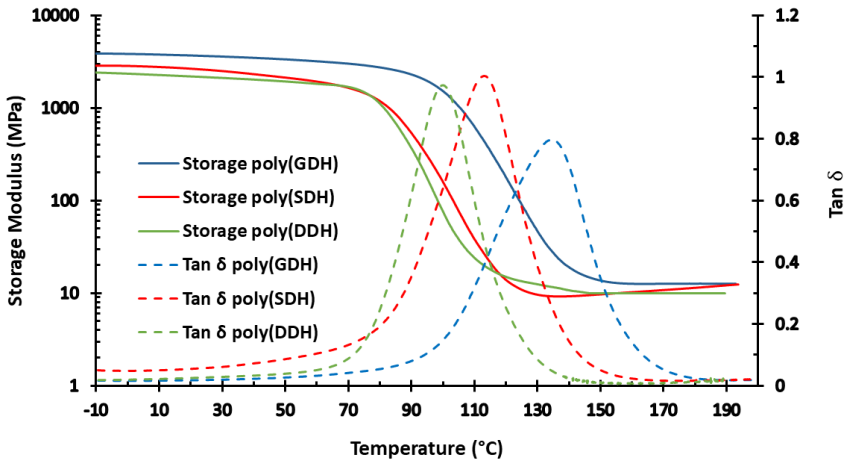

Figure 6.4. Evolution of tan δ and storage modulus with temperature of all poly(acylhydrazone) materials.

As it is observed, thermally cured poly(acylhydrazone) materials exhibit high T_g values (taken from the maximum of tan δ curves) reaching 134 °C. This can be essentially associated with the low network mobility arising from the presence of stiff benzene rings, the high functionality of dihydrazides that leads to a high degree of crosslinking, and the presence of hydrogen bonds. As expected, as the dihydrazide chain length increases, the T_g of the final material decreases due to the higher mobility and flexibility of the final material in accordance with the more open network structure.

Similarly, the rubbery modulus is reduced due to the longer distances between cross-links, and the glassy modulus decreases indicating a less rigid network. Besides, single peaks in tan δ and well-defined transitions are indicative of homogenous network structures in all materials with a slightly broader network relaxation for poly(GDH).

Table 6.2. Thermomechanical data of all the virgin and recycled poly(acylhydrazone)s prepared.

Sample	Virgin			Recycled		
	$T_{tan\,\delta}$ [a] (°C)	E'_{glassy} [b] (MPa)	$E'_{rubbery}$ [c] (MPa)	$T_{tan\,\delta}$ [a] (°C)	E'_{glassy} [b] (MPa)	$E'_{rubbery}$ [c] (MPa)
poly(GDH)	134.2	3637	12.8	133.2	3508	8.5
poly(SDH)	113.1	2656	11.4	112.8	1738	7.6
poly(DDH)	100.0	2149	9.9	98.9	1629	3.9

[a] Temperature at the maximum of tan δ peak at 1 Hz. [b] Glassy storage modulus at 25 °C determined by DMTA. [c] Rubbery storage modulus at T_g + 50 °C determined by DMTA.

Polym. Chem. **2022**, *13*, 1510-1519

To confirm the vitrimeric nature of the networked poly(acylhydrazone)s, the time and temperature-dependent relaxation behavior was investigated. For this purpose, stress relaxation tests were performed by DMTA and the results are shown in Figure 6.5 and Table 6.3. The stress relaxation curves reveal that these materials are capable of rapidly relaxing stress, by reaching the reference relaxation value of 63% ($\sigma/\sigma_0 = 0.37$) in less than one minute at 185 °C for poly(GDH), in 1.5 min at 170 °C for poly(SDH) and in almost 3 min for poly(DDH) at 160 °C. From these experiments, it can also be calculated the time for almost total relaxation of the networks, which is reached in nearly 3.5, 5, and 10 min, respectively at 190 °C.

Table 6.3. Relaxation times, topology freezing temperature, activation energy, and adjusting parameters for the Arrhenius equation.

Material	$\tau_{0.37}$ [a] (s)	$\tau_{100\%}$ [a] (s)	T_v (°C)	E_a (kJ/mol)	lnA (s)	r^2
poly(GDH)	43	200	25.2	52.5	9.90	0.99
poly(SDH)	46	300	36.8	61.4	12.45	0.98
poly(DDH)	48	600	61.7	77.2	16.20	0.99

[a] Time to reach a value of $\sigma/\sigma_0 = 0.37$ at 190 °C.
[b] Time to reach total relaxation at 190 °C.

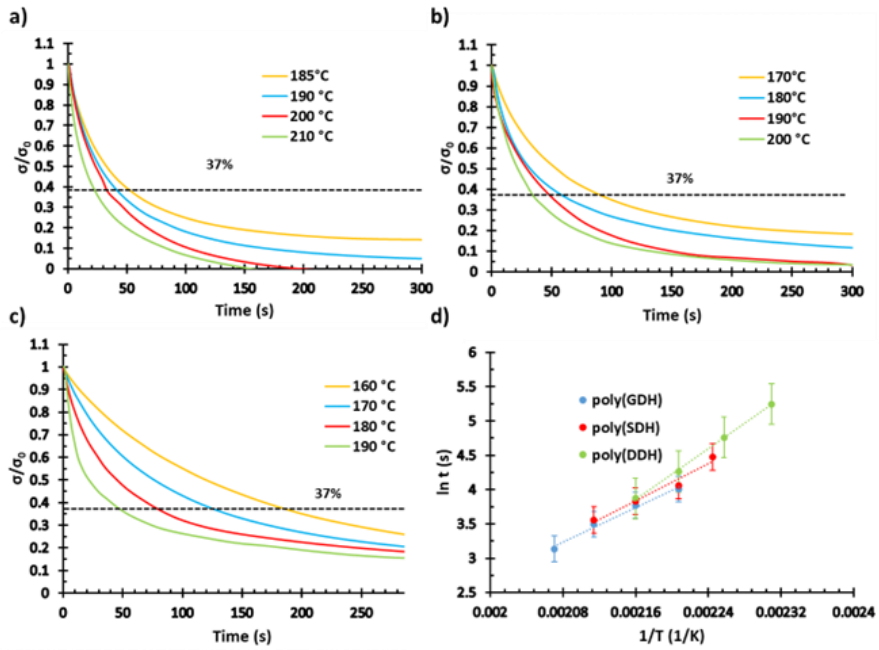

Figure 6.5. Normalized stress relaxation plots as a function of time at various temperatures during 300 s for poly(GDH) (a), poly(SDH) (b), and poly(DDH) (c) samples and d) Arrhenius plot of relaxation times against temperature for the different poly(acylhydrazone)s.

As we can see in Table 6.3, the time to reach the relaxed state of $\sigma/\sigma_0 = 0.37$ at 190 °C for the different materials slightly increases (from 43 to 48 s) on increasing the chain length of the dihydrazide. Although the material becomes more flexible, the distance between acylhydrazone moieties increases, and their proportion in the network structure decreases, which makes the imine metathesis more difficult to occur.

It is well-known that vitrimeric materials follow an Arrhenius-type temperature dependence, when the viscosity is controlled by the chemical exchange reaction, leading to a temperature-viscosity relationship like inorganic silica materials [37]. According to that, to characterize the vitrimeric behavior of poly(acylhydrazone) materials, the time required for the initial stress to decrease to e^{-1} ($\sigma/\sigma_0 = 0.37$) at different temperatures was obtained from the corresponding relaxation curves (Figures 6.5a-c). The Arrhenius-type equation derived when fitted to the data allows calculating the activation energy (E_a) of the topological rearrangement (see Figure 6.5d and Table 6.3) for all the different vitrimers. Looking at the values presented in Table 6.3, it can be pointed out that the longer the chain in the poly(acylhydrazone)s prepared, the higher the activation energy, indicating a greater dependence with the temperature of the exchange kinetics of the network. Furthermore, when the relaxation temperature is increased, a significant acceleration of the relaxation process was observed in all cases. It is worthy to remind that these materials are prepared in absence of catalyst, which gives more importance to these low relaxation times.

It is also important to highlight the E_a values presented in Table 6.3, which are much lower than other reported values for different vitrimeric groups like polyester vitrimers (90 kJ/mol) [8], poly(urethane)s (130.5 and 183.7 kJ/mol) [35], or poly(thiourethane)s (72-102 kJ/mol) [36], without the need of adding catalyst.

The topology freezing temperatures defined as the temperature at which the transition from viscoelastic solid to viscoelastic liquid occurs was also calculated by extrapolation of stress-relaxation experiments. This temperature accounts for the temperature below which chemical exchanges are negligible, and it can be used to qualitatively compare bond-exchanges capabilities in vitrimers. For these poly(acylhydrazone)s, the T_vs calculated by extrapolation are much lower than their T_gs and in this case, the more important parameter to determine the relaxation behavior is T_g, since below this temperature the network structure is frozen, without enough mobility to experiment the exchange reaction between imine units. Thus, in this case, T_vs are only hypothetical values, since below T_g no exchange reactions can occur being the network fixed due to the lack of segmental motions associated with T_g. Once T_g is overpassed and when the exchange kinetics change from a diffusion-controlled process to an exchange reaction-controlled process, the exchange reaction proceeds very fast [37,38]. Nevertheless, the fact that T_vs are lower than T_gs does not

Polym. Chem. **2022**, *13*, 1510-1519

affect the applicability as thermosets at room temperature due to the high values of the T_g obtained for these materials, in contrast to what happens in other vitrimers where the creep resistance behavior could be compromised [39-41].

3.5 Recycling process

To investigate the recyclability of the crosslinked poly (acylhydrazone)s prepared, all the materials were ground into small pieces and hot-pressed in the manual press under 9.25 MPa, in an aluminum mold. The temperature of the recycling process was set to 190 °C ensuring in all cases that the network rearrangement is taking place without any degradation.

Figure 6.6 shows the pictures taken from the original, ground, and reprocessed samples where it can be clearly seen that the original and the recycled films preserve good transparency.

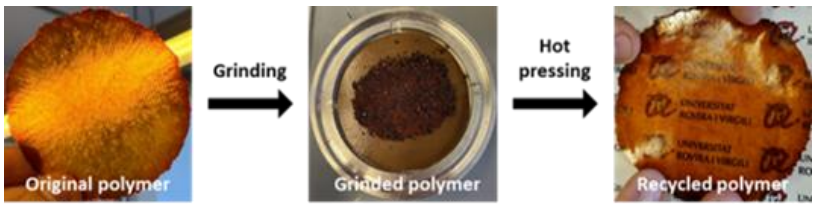

Figure 6.6. Photographs of the original, ground, and recycled samples of the poly(acylhydrazone)s.

To evaluate the recyclability of the poly(acylhydrazone)s, the thermomechanical behavior of the original and recycled samples was compared.

Results from the evolution of the storage modulus and tan δ curves with temperature, extracted from the DMTA analysis, are presented in Figure 6.7a-c, and the most representative data are presented in Table 6.2. From the values presented in Table 6.2 and the curves in Figure 6.7, it can be appreciated that recycled materials exhibit similar tan δ curves as the original ones, with almost the same $T_{\tan\delta}$. Recycling slightly decreases the rubbery modulus, probably due to the break of covalent bonds during grinding, which reduces the crosslinking density. From these results, we can conclude that materials can be recycled without significant changes in their thermomechanical properties.

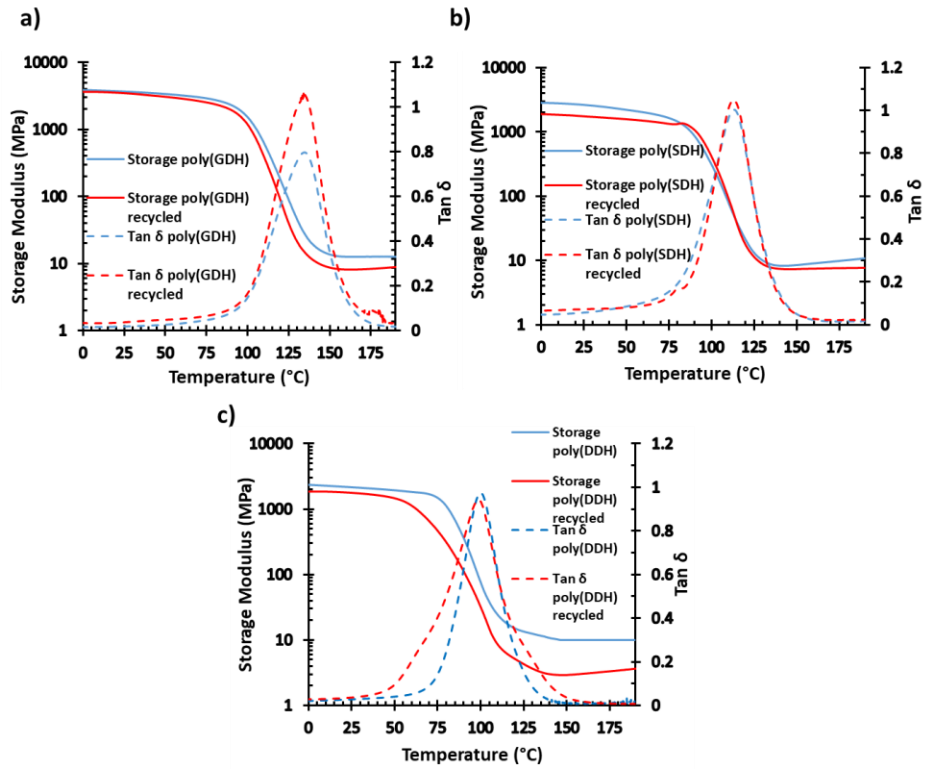

Figure 6.7. Dependence of tan δ and storage modulus *versus* temperature before and after recycling of poly(GDH) (a), poly(SDH) (b), and poly(DDH) (c).

3.6 Solubility and chemical degradability

To further confirm the thermosetting nature of these materials, they were tried to dissolve in dichlorobenzene (DCB).

Poly(acylhydrazone) samples were weighted and put at 150 °C for 12 h in DCB and dried in the vacuum oven for 12 h. After that, the remaining sample was re-weighted noticing that in all cases the gel content of the materials was above 98.5% revealing a high resistance to be solubilized and their thermosetting character. Finally, we also attempt to perform a chemical degradation of the materials by leaving the poly(acylhydrazone) materials in a 2 M HCl solution/THF 8:2 mixture for 24 h at 70 °C. After that, the solution presented high turbidity, so the supernatant solid was filtered in a Büchner funnel, washed 3 times with water, and dried in a vacuum oven at 80 °C for 6 h. We could prove by NMR spectroscopy that this solid corresponded to the starting dicarboxylic acid of the dihydrazide used since the hydrolysis of the amide bond can occur in acidic media leading to the original diacid. In this way, starting acids can be recovered, although any quantitative recovery has been implemented.

Polym. Chem. **2022**, *13*, 1510-1519

However, the reaction of the glycidyl group of the vanillin with NH_2 of dihydrazides prevents the full recovery of the starting materials.

3.7 Self-healing

It is already known that materials containing acylhydrazone groups can have self-healing properties [42-44] Encouraged by these previous studies, we decided to test qualitatively if the poly(acylhydrazone) materials prepared in this work presented self-healing properties.

To do this, two samples of poly(GDH) and poly(DDH) were scratched and broken using a doctor blade, and subsequently heated in an oven at 190 °C for several hours exploring from time to time the evolution of the scratch by microscopy. The pictures taken of those materials at different times are shown in Figure 6.8.

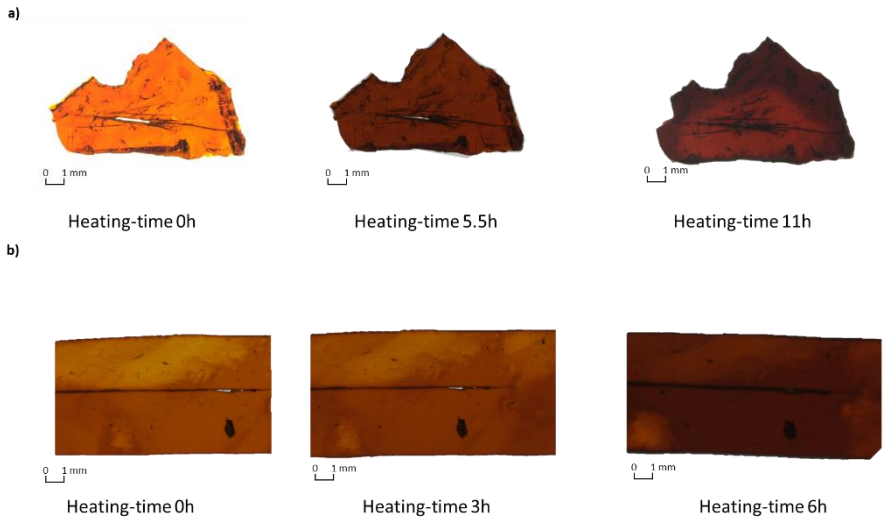

Figure 6.8. Pictures of the scratch-made with a doctor blade on a poly(GDH) (a) and poly(DDH) (b) samples maintained in an oven at 190 °C at different times.

As it can be seen, the scratch was completely healed (even in the broken part) after 11 h in the case of poly(GDH) and only 6 h in poly(DDH), showing promising self-healing characteristics. The lower T_g of poly(DDH) facilitates the self-healing behavior, but we have demonstrated that even poly(acylhydrazones) with T_gs higher than 100 °C can be self-healed in a short time.

4. Conclusions

Fully renewable poly(acylhydrazone) materials have been easily prepared by condensation of glycidyl vanillin and dihydrazides. The addition of trimethylolpropane triglycidyl ether to the formulation facilitates the preparation of materials with good mechanical characteristics. The latent character of the reaction of hydrazide groups with epoxies, which occurs at high temperatures, facilitates the complete

condensation of hydrazide groups with the formyl group of the vanillin. The disappearance of all reactive groups was confirmed by FTIR spectroscopy.

The materials obtained show excellent vitrimeric characteristics, without the need of any type of catalyst, with very short relaxation times (between 200 and 600 s for almost a total relaxation), that increase on increasing the length of the dihydrazide used as a monomer. The thermomechanical and relaxation behavior of these vitrimers can be tailored only by changing the dihydrazide structure, obtaining very low values of activation energy in all of them.

The reactive process behind the vitrimeric exchange is based on the imine metathesis, since the materials prepared do not have any excess hydrazide or aldehyde groups. The occurrence of imine metathesis has been proved using gas chromatography coupled to mass spectroscopy using acylhydrazone model compounds synthesized for this purpose. This is the first time that this type of highly crosslinked materials has shown its vitrimeric characteristics.

Poly(acylhydrazone) materials have also demonstrated good recycling and self-healing abilities at temperatures not much higher than their T_g. These compounds can be chemically degraded in an acidic medium, which allows to recovery of the corresponding starting diacids.

Acknowledgments

This work is part of the R&D projects PID2020-115102RB-C21 and PID2020-115102RB-C22 funded by MCNI/AEI/ 10.13039/ 501100011033 we acknowledge these grants and to the Generalitat de Catalunya (2017-SGR-77 and BASE3D).

References

[1] J. Verrey, M. D. Wakeman, V. Michaud and J. A. E. Månson, *Compos. Part A*, 2006, **37**, 9-22.

[2] A. Kondyurin and Y. Klyachkin, *J. Appl. Polym. Sci.*, 1996, **62**, 1-8.

[3] S. Rimdusit and H. Ishida, *Polymer*, 2000, **41**, 7941-7949.

[4] D. Montarnal, M. Capelot, F. Tournilhac and L. Leibler, *Science*, 2011, **334**, 965-968.

[5] M. Podgórski, B. D. Fairbanks, B. E. Kirkpatrick, M. McBride, A. Martínez, A. Dobson, N. J. Bongiardina and C. N. Bowman, *Adv. Mater.*, 2020, **32**, 1906876.

[6] F. Van Lijsebetten, J. O. Holloway, J. M. Winne and F. E. Du Prez, *Chem. Soc. Rev.*, 2020, **49**, 8425-8438.

[7] M. Capelot, D. Montarnal, F. Tournilhac and L. Leibler, *J. Am. Chem. Soc.*, 2012, **134**, 7664-7667.

[8] M. Capelot, M. M. Unterlass, F. Tournilhac and L. Leibler, *ACS Macro Lett.*, 2012, **1**, 789-792.

[9] F. I. Altuna, V. Pettarin and R. J. J. Williams, *Green Chem.*, 2013, **15**, 3360-3366.

[10] D. J. Fortman, J. P. Brutman, C. J. Cramer, M. A. Hillmeyer and W. R. Dichtel, *J. Am. Chem. Soc.*, 2015, **137**, 14019-14022.

[11] P. C. Colodny and A. V. Tobolsky, *J. Am. Chem. Soc.*, 1957, **79**, 4320-4323.

[12] A. Ruiz de Luzuriaga, R. Martin, N. Markaide, A. Rekondo, G. Cabañero, J. Rodríguez and I. Odriozola, *Mater. Horiz.*, 2016, **3**, 241-247.

[13] Y. X. Lu, F. Tournhilac, L. Leibler and Z. Guan, *J. Am. Chem. Soc.*, 2012, **134**, 8424-8427.

[14] P. Taynton, K. Yu, R. K. Shoemaker, Y. Jin, H. J. Qi and W. Zhang, *Adv. Mater.*, 2014, **26**, 3938-3942.

[15] H. Zheng, Q. Liu, X. Lei, Y. Chen, B. Zhang and Q. Zhang, *J. Polym. Sci. Part Polym. Chem.*, 2018, **56**, 2531-2538.

[16] R. Hajj, A. Duval, S. Dhers and L. Avérous, *Macromolecules*, 2020, **53**, 3796-3805.

[17] M. E. Belowich and J. F. Stoddart, *Chem. Soc. Rev.*, 2012, **46**, 2003-2024.

[18] W. G. Skene and J. M. Lehn, *Proc. Natl. Acad. Sci. U.S.A.*, 2004, **101**, 8270-8275.

[19] E. Kolomiets and J. M. Lehn, *Chem. Commun.*, 2005, **12**, 1519-1521.

[20] N. Roy, E. Buhler and J. M. Lehn, *Polym. Int.*, 2014, **63**, 1400-1405.

[21] G. Deng, C. Tang, F. Li, H. Jiang and Y. Chen, *Macromolecules*, 2010, **43**, 1191-1194.

[22] G. Deng, F. Li, H. Yu, F. Liu, C. Liu, W. Sun, H. Jiang, and Y. Chen, *ACS Macro Lett.*, 2012, **1**, 275-279.

[23] J. J. Lessard, L. F. Garcia, C. P. Easterling, M. B. Sims, K. C. Bentz, S. Arencibia, D. A. Savin and B. S. Sumerlin, *Macromolecules*, 2019, **52**, 2105-2111.

[24] W. Denissen, G. Rivero, R. Nicolay, L. Leibler, J. M. Winne and F. E. Du Prez, *Adv. Funct. Mater.*, 2015, **25**, 2451-2457.

[25] W. A. Ogden and Z. Guan, *J. Am. Chem. Soc.*, 2018, **140**, 6217-6220.

[26] Z. Q. Lei, P. Xie, M. Z. Rong and M. Q. Zhang, *J. Mater. Chem. A*, 2015, **3**, 19662-19668.

[27] S. Zhao and M. M. Abu-Omar, *Macromolecules*, 2019, **52**, 3646-3654.

[28] T. Liu, C. Hao, L. Wang, Y. Li, W. Liu, J. Xin and J. Zhang, *Macromolecules*, 2017, **50**, 8588-8597.

[29] C. Ocando, Y. Ecochard, M. Decostanzi, S. Caillol and L. Avérous, *Eur. Polym J.*, 2020, **135**, 109860.

[30] H. Cheng, Y. Wang, Q. Yu, S. Gu, Y. Zhou, W. Xu, X. Zhang and D. Ye, *ACS Sustain. Chem. Eng.*, 2018, **6**, 15463-15470.

[31] Y. Xu, K. Odelius and M. Hakkarainen, *ACS Sustain. Chem. Eng.*, 2020, **8**, 17272-17279.

[32] M. Fache, E. Darroman, V. Besse, R. Auvergne, S. Caillol and B. Boutevin, *Green Chem.*, 2014, **16**, 1987.

[33] J. L. Jia-Le Yu, Z.-G. Qian and J.-J. Zhong, *Eng. Life Sci.*, 2018, **18**, 668-681.

[34] A. M. Tomuta, X. Ramis, F. Ferrando and A. Serra*, Prog. Org. Coat.*, 2012, **74**, 59-66.

[35] P. Yan, W. Zhao, X. Fu, Z. Liu, W. Kong, C. Zhou and J. Lei, *RSC Adv.*, 2017, **7**, 26858-26866.

[36] F. Gamardella, F. Guerrero, S. De la Flor, X. Ramis, A. Serra, *Eur. Polym. J.*, 2020, **122**, 109361.

[37] W. Denissen, J. M. Winne and F. E. Du Prez, *Chem. Sci.*, 2016, **7**, 30-38.

[38] M. Guerre, C. Taplan, J. M. Winne and F. E. Du Prez, *Chem. Sci.*, 2020, **11**, 4855-4870.

[39] J. Wu, L. Gao, Z. Guo, H. Zhang, B. Zhang, J. Hu and M-H. Li, *Green Chem.*, 2021, **23**, 5647-5655.

[40] S. Wang, S. Ma, Q. Li, X. Xu, B. Wang, W. Yuan, S. Zhou, S. You and J. Zhu, *Green Chem.*, 2019, **21**, 1484-1497.

[41] F. Van Lijsebetten, Y. Spiesschaert, J. M. Winne and F. E. Du Prez, *J. Am. Chem. Soc.*, 2021, **143**, 15834-15844.

[42] N. Kuhl, S. Bode, R. K. Bose, J. Vitz, A. Seifert, S. Hoeppener, S. J. Garcia, S. Spange, S. van der Zwaag, M. D. Hage and U. Schubert, *Adv. Funct. Mater.*, 2015, **25**, 3295-3301.

[43] D-D. Zhang, Y-B. Ruan, B-Q. Zhang, X. Qiao, G. Deng, Y. Chen and C-Y. Liu, *Polymer*, 2017, **120**, 189-196.

[44] C. Sun, H. Jia, K. Lei, D. Zhu, Y. Gao, Z. Zheng and X. Wang, *Polymer*, 2019, **160**, 246-253.

Polym. Chem. **2022**, *13*, 1510-1519

Supporting Information

Synthesis of epoxy compound from vanillin (EPO-Van)

EPO-Van was prepared following a previously reported procedure. Vanillin (7.6 g, 50.0 mmol), TEBAC (1.1 g, 5.0 mmol) and ECH (46.3 g, 500.0 mmol) were added to a 250 mL three-necked round bottom flask under magnetic stirring. The mixture was first stirred for 1.5 h at 80 °C and then cooled down to room temperature. A mixed solution of TEBAC (1.1 g, 5.0 mmol) and NaOH (8 g, 200.0 mmol, 5 M) was added and stirred for 30 min at room temperature. After the reaction was completed, ethyl acetate (EtOAc) and distilled water were poured and stirred, and the aqueous phase extracted three times with EtOAc. The organic phase was collected, dried over anhydrous MgSO4 and concentrated in a vacuum rotary evaporator. The residual amount of ECH was eliminated by mixing the product with EtOAc and evaporating it under vacuum multiple times. The monoglycidyl compound was obtained as a yellowish-white solid with a 93 % of yield (9.7 g). M.p. 97.0 °C.

^{1}H NMR ($CDCl_3$, δ in ppm): 9.84 (s, 1H), 7.43 (d, 1H), 7.41 (s, 1H), 7.02 (d, 1H), 4.37 (dd, 1H), 4.08 (dd, 1H), 3.92 (s, 3H), 3.40 (m, 1H), 2.92 (dd, 1H) and 2.77 (dd, 1H). ^{13}C NMR ($CDCl_3$, δ in ppm): 190.99, 153.51, 150.07, 130.78, 126.61, 112.37, 109.61, 70.05, 56.13, 50.00 and 44.86.

Synthesis of diesters of dicarboxylic acids

Diesters were synthesized following a previous procedure reported by Mills *et al.* In a 250 mL three-necked round bottom flask equipped with a magnetic stirrer, 15 g of the corresponding diacid were dissolved in absolute EtOH (150 mL). Then, concentrated H_2SO_4 (80 µL, 1.3 mmol) was added and the mixture was heated up to 80 °C and kept it during 4 h under reflux. The mixture was cooled down to room temperature and concentrated. The concentrate was dissolved in EtOAc (150 mL), and the organic fraction was washed three times, once with a saturated solution of $NaHCO_3$, once with water and finally with brine, dried over anhydrous $MgSO_4$ and concentrated by rotary evaporator to yield the corresponding products as colorless oils.

Diethyl suberate (DESU) was obtained in 89% yield. ^{1}H NMR ($CDCl_3$, δ in ppm): 4.10 (q, 4H), 2.26 (t, 4H), 1.60 (m, 4H), 1.32 (m, 4H) and 1.23 (t, 6H).
^{13}C NMR ($CDCl_3$, δ in ppm): 173.83, 60.28, 34.36, 28.84, 24.86 and 14.34.

Diethyl dodecanoate (DEDO) was obtained in 90% yield. ^{1}H NMR ($CDCl_3$, δ in ppm): 4.10 (q, 4H), 2.26 (t, 4H), 1.59 (m, 4H), 1.26 (m, 12H) and 1.23 (t, 6H).
^{13}C NMR ($CDCl_3$, δ in ppm): 174.05, 60.25, 34.47, 29.46, 29.32, 29.22, 25.06 and 14.35.

Synthesis of dihydrazides

Dihydrazides were synthesized following a previous procedure reported by Tomuta *et al.* In a 100 mL three-necked round bottom flask provided with a magnetic stirrer, 5.6 g of the corresponding diester were added and dissolved in 25 mL of absolute EtOH. Then, hydrazine hydrate (80%, 6.7 g, 107.6 mmol) was added drop by drop. When the addition was complete, the mixture was kept 6 h under reflux. The precipitate formed was filtered through a Büchner funnel, washed twice with cold EtOH and dried in the vacuum oven at 60 °C during 4 h. All products were obtained as white powders with yields higher than 90%.

Glutaric dihydrazide (GDh): ^{1}H NMR (DMSO-d_6, δ in ppm): 8.91 (s, 2H), 4.13 (s, 4H), 1.99 (t, 4H) and 1.69 (m, 2H). ^{13}C NMR (DMSO-d_6, δ in ppm): 171.17, 32.87 and 21.48. M.p. 181.8 °C.

Suberic dihydrazide (SDh): ^{1}H NMR (DMSO-d_6, δ in ppm): 8.89 (s, 2H), 4.13 (s, 4H), 1.98 (t, 4H), 1.46 (m, 4H) and 1.20 (m, 4H). ^{13}C NMR (DMSO-d_6, δ in ppm): 171.58, 33.37, 28.39 and 25.10. M.p. 188.1 °C.

Dodecandioic dihydrazide (DDh): ^{1}H NMR (DMSO-d_6, δ in ppm): 8.91 (s, 2H), 4.13 (s, 4H), 1.98 (t, 4H), 1.46 (m, 4H) and 1.22 (m, 12H). ^{13}C NMR (DMSO-d_6, δ in ppm): 171.64, 33.42, 28.92, 28.77, 28.67 and 25.24. M.p. 192.0 °C.

Synthesis of model compounds

Ethyl octanoate was synthesized following the same procedure previously described.

^{1}H NMR ($CDCl_3$, δ in ppm): 4.11 (q, 2H), 2.27 (t, 2H), 1.60 (m, 2H), 1.27 (m, 8H), 1.24 (t, 3H) and 0.87 (t, 3H). ^{13}C NMR ($CDCl_3$, δ in ppm): 173.83, 60.13, 34.39, 31.66, 29.10, 28.93, 24.99, 22.59, 14.25 and 14.05.

Hydrazides were synthesized following the same procedure previously described for the synthesis of dihydrazide compounds.

Acetyl hydrazide: ^{1}H NMR (DMSO-d_6, δ in ppm): 8.94 (s, 1H), 4.13 (s, 2H) and 1.74 (s, 3H). ^{13}C NMR (DMSO-d_6, δ in ppm): 168.75 and 20.55. M.p. 60.1 °C.

Octanoyl hydrazide: ^{1}H NMR (DMSO-d_6, δ in ppm): 8.91 (s, 1H), 4.14 (s, 2H), 1.98 (t, 2H), 1.46 (m, 2H), 1.23 (m, 8H) and 0.85 (t, 3H). ^{13}C NMR (DMSO-d_6, δ in ppm): 171. 65, 33.44, 31.22, 28.65, 28.48, 25.27, 22.11 and 14.00. M.p. 88.3 °C.

Acylhydrazones were synthesized following the following procedure. In a 50 mL three-necked round bottom flask provided with a magnetic stirrer 10 mmol of aldehyde (vanillin or benzaldehyde) was added. After that, 10 mL of EtOH were added followed by the addition of 1 eq. of the corresponding hydrazide (acetyl hydrazide or octanoyl hydrazide). When the addition was completed, the mixture was kept under reflux

Polym. Chem. **2022**, *13*, 1510-1519

during 12 h. The precipitate formed was filtered through a Büchner funnel, washed twice with cold EtOH and dried in the vacuum oven at 60 °C during 4 h. All products were obtained as white powders with yields higher than 90%.

Benzylideneacetohydrazide (B-Ah) mixture of *cis/trans* isomers 1:2: ^{1}H NMR (DMSO-d_6, δ in ppm): 11.37 (s, 1H), 11.25 (s, 1H$_a$), 8.14 (s, 1H), 7.98 (s, 1H$_a$), 7.66 (m, 2H, 2H$_a$), 7.41 (m, 3H, 3H$_a$), 2.20 (s, 3H$_a$) and 1.95 (s, 3H). ^{13}C NMR (DMSO-d_6, δ in ppm): 171.99, 165.61, 145.57, 142.51, 134.38, 134.31, 129.88, 129.67, 128.81, 128.79, 126.97, 126.64, 21.66 and 20.27.

(4-Hydroxy-3-methoxybenzylidene)octanehydrazide (V-Oh) mixture of *cis/trans* isomers 1:1: ^{1}H NMR (DMSO-d_6, δ in ppm): 11.15 (s, 1H), 11.04 (s, 1H$_a$), 9.49 (s, 1H, 1H$_a$), 8.02 (s, 1H), 7.85 (s, 1H$_a$), 7.24 (d, 1H), 7.20 (d, 1H$_a$), 7.03 (dd, 1H), 7.02 (dd, 1H$_a$), 6.81 (d, 1H), 6.80 (d, 1H$_a$), 3.80 (s, 3H), 3.79 (s, 3H$_a$), 2.58 (t, 2H$_a$), 2.15 (t, 2H), 1.56 (m, 2H, 2H$_a$), 1.26 (m, 8H, 8H$_a$), 0.86 (t, 3H$_a$) and 0.84 (t, 3H). ^{13}C NMR (DMSO-d_6, δ in ppm): 174.16, 168.30, 148.79, 148.51, 148.00, 147.93, 146.25, 142.78, 125.83, 125.77, 121.89, 120.83, 115.56, 115.38, 109.31, 108.83, 55.52, 55.46, 34.23, 31.92, 31.22, 28.82, 28.66, 28.51, 28.50, 25.17, 24.41, 22.11 and 13.98.

(4-Hydroxy-3-methoxybenzylidene)acetohydrazide (V-Ah) mixture of *cis/trans* isomers 2:3: ^{1}H NMR (DMSO-d_6, δ in ppm): 11.17 (s, 1H), 11.07 (s, 1H$_a$), 8.01 (s, 1H), 7.86 (s, 1H$_a$), 7.24 (d, 1H), 7.21 (d, 1H$_a$), 7.04 (d, 1H), 7.02 (d, 1H$_a$), 6.81 (d, 1H$_a$), 6.79 (d, 1H), 3.81 (s, 3H), 3.80 (s, 3H$_a$), 2.17 (s, 3H$_a$) and 1.91 (s, 3H). ^{13}C NMR (DMSO-d_6, δ in ppm): 171.68, 165.28, 148.79, 148.53, 148.01, 147.95, 146.14, 142.99, 125.77, 121.88, 120.97, 115.54, 115.40, 109.29, 108.93, 55.55, 55.53, 21.65 and 20.28.

Benzylideneoctanehydrazide (B-Oh) mixture of *cis/trans* isomers 2:3: ^{1}H NMR (DMSO-d_6, δ in ppm): 11.32 (s, 1H), 11.21 (s, 1H$_a$), 8.15 (s, 1H), 7.97 (s, 1H$_a$), 7.65 (m, 2H, 2H$_a$), 7.42 (m, 3H, 3H$_a$), 2.61 (t, 2H$_a$), 2.18 (t, 2H), 1.57 (m, 2H, 2H$_a$), 1.27 (m, 8H, 8H$_a$), 0.86 (t, 3H) and 0.85 (t, 3H$_a$). ^{13}C NMR (DMSO-d_6, δ in ppm): 174.89, 169.11, 146.12, 142.78, 135.07, 134.83, 130.30, 130.08, 129.97, 129.64, 129.27, 129.24, 127.39, 127.03, 34.66, 32.32, 31.63, 29.18, 29.09, 28.93, 28.92, 25.48, 24.75, 22.54, 14.41.

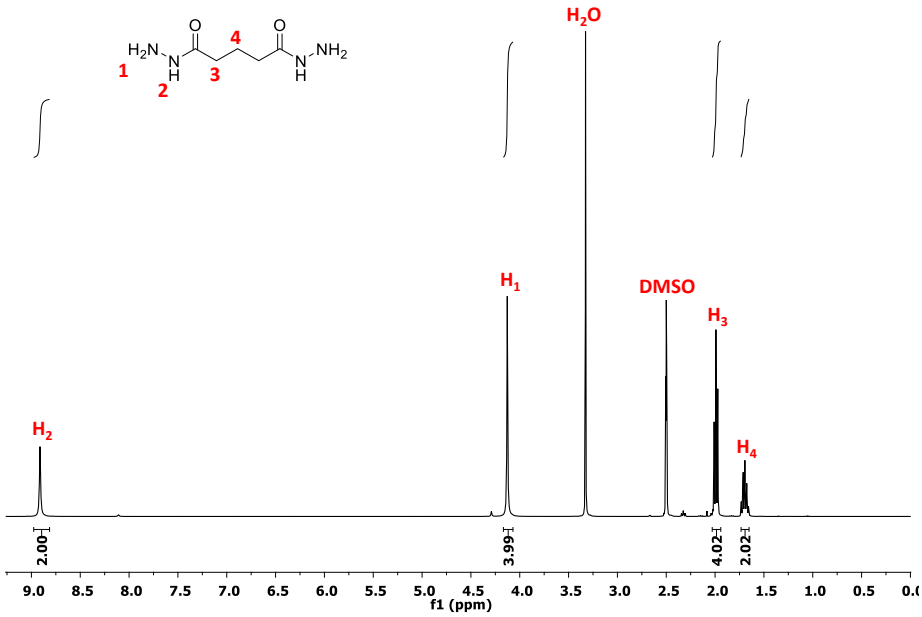

Figure 6.S1. ^{1}H NMR spectrum of glutaric dihydrazide (GDh) in DMSO-d_6.

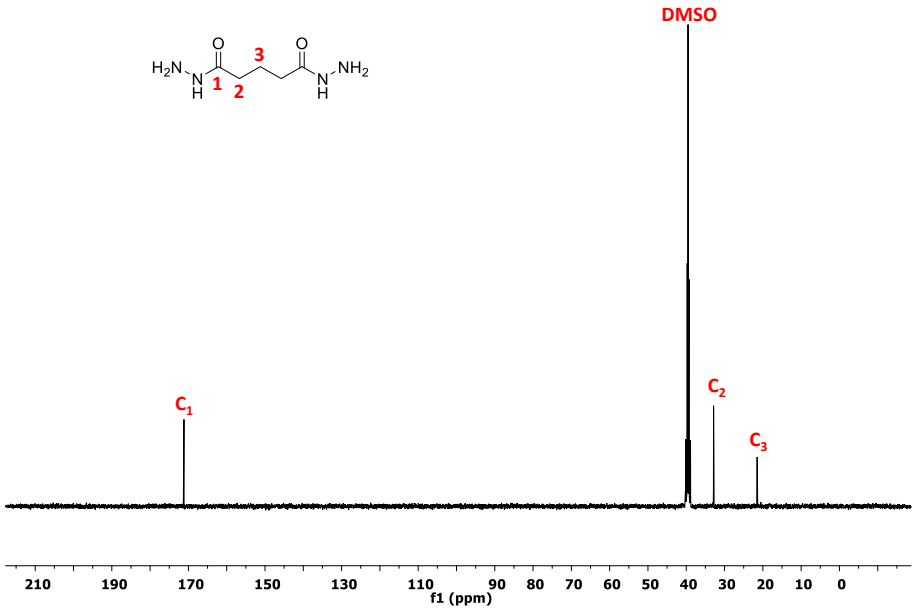

Figure 6.S2. ^{13}C NMR spectrum of glutaric dihydrazide (GDh) in DMSO-d_6.

Polym. Chem. **2022**, *13*, 1510-1519

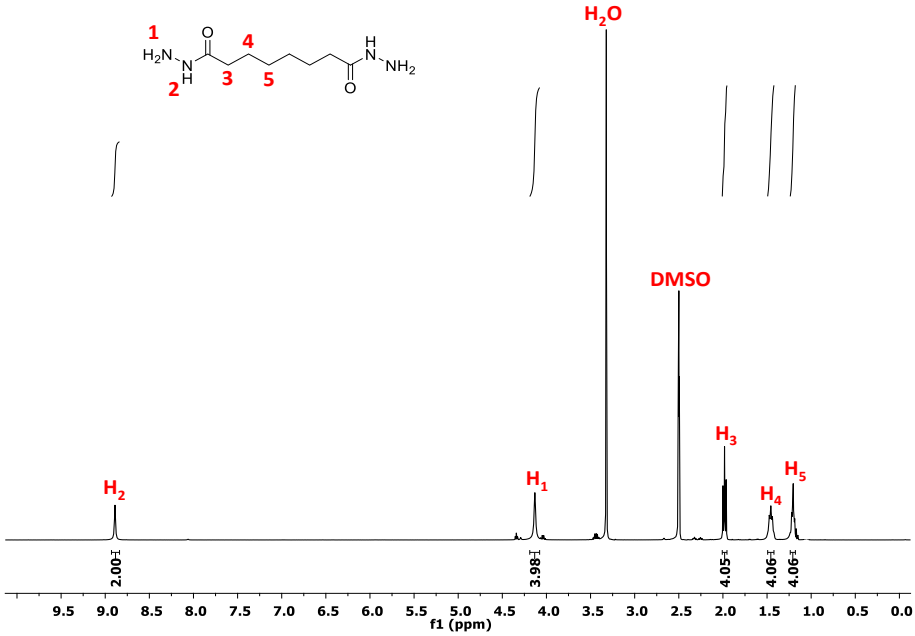

Figure 6.S3. ^{1}H NMR spectrum of suberic dihydrazide (SDh) in DMSO-d_6.

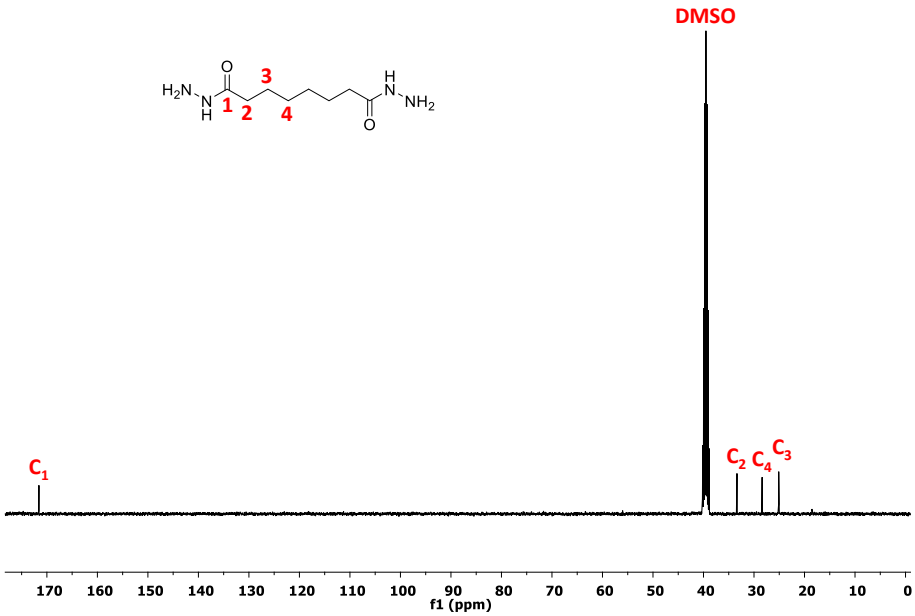

Figure 6.S4. ^{13}C NMR spectrum of suberic dihydrazide (SDh) in DMSO-d_6.

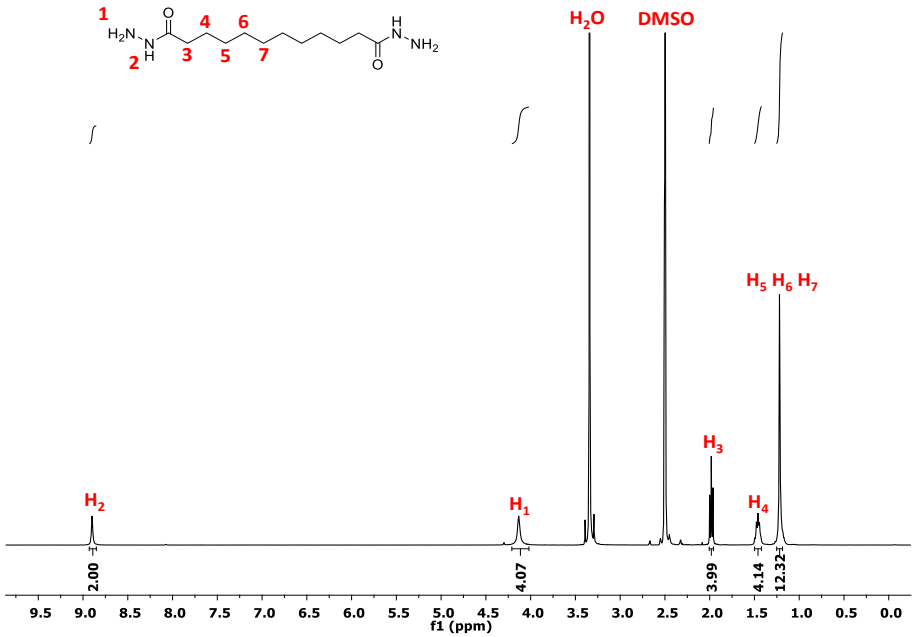

Figure 6.S5. ^{1}H NMR spectrum of dodecanedioic dihydrazide (DDh) in DMSO-d_6.

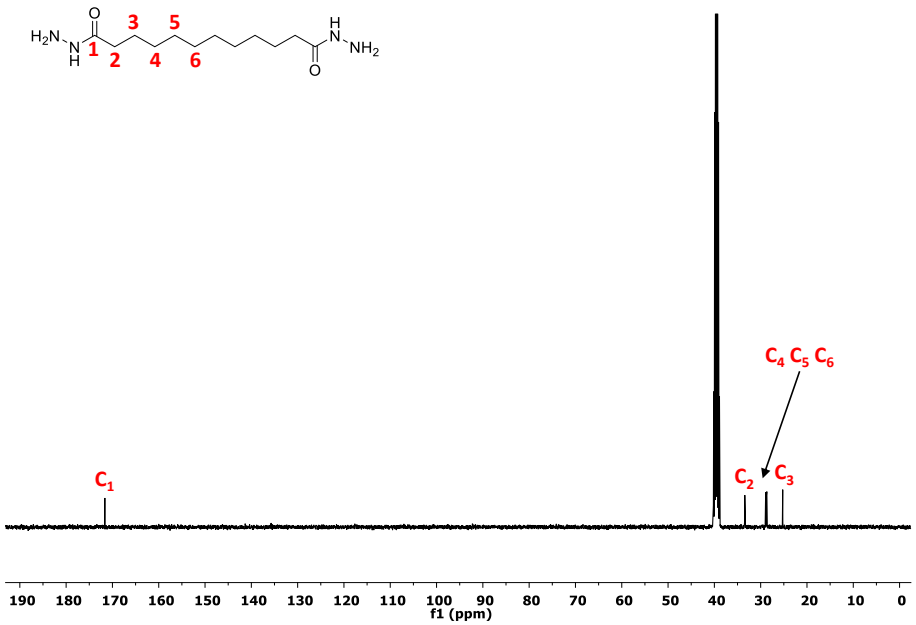

Figure 6.S6. ^{13}C NMR spectrum of dodecanedioic dihydrazide (DDh) in DMSO-d_6.

Polym. Chem. **2022**, *13*, 1510-1519

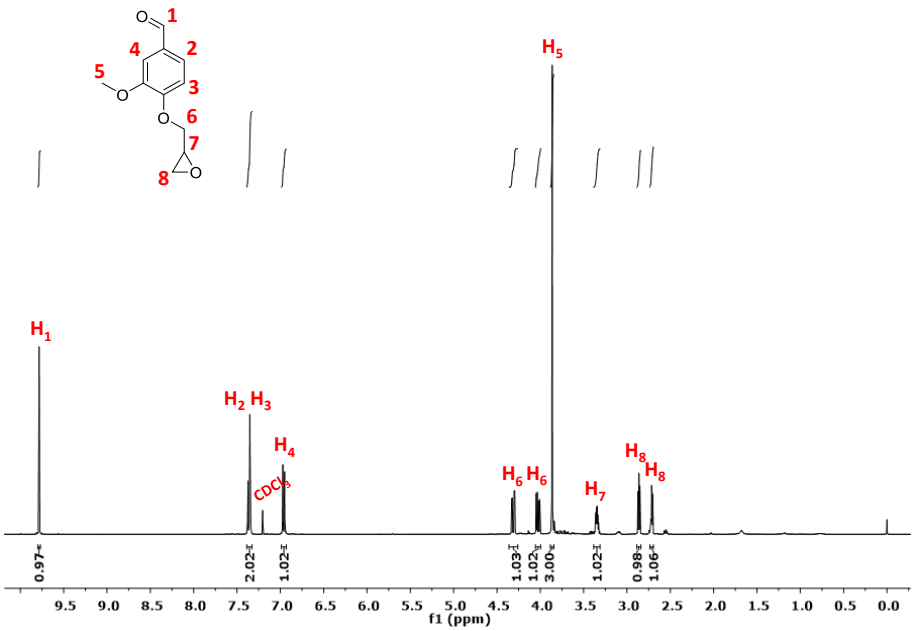

Figure 6.S7. ^{1}H NMR spectrum of EPO-Van in $CDCl_3$.

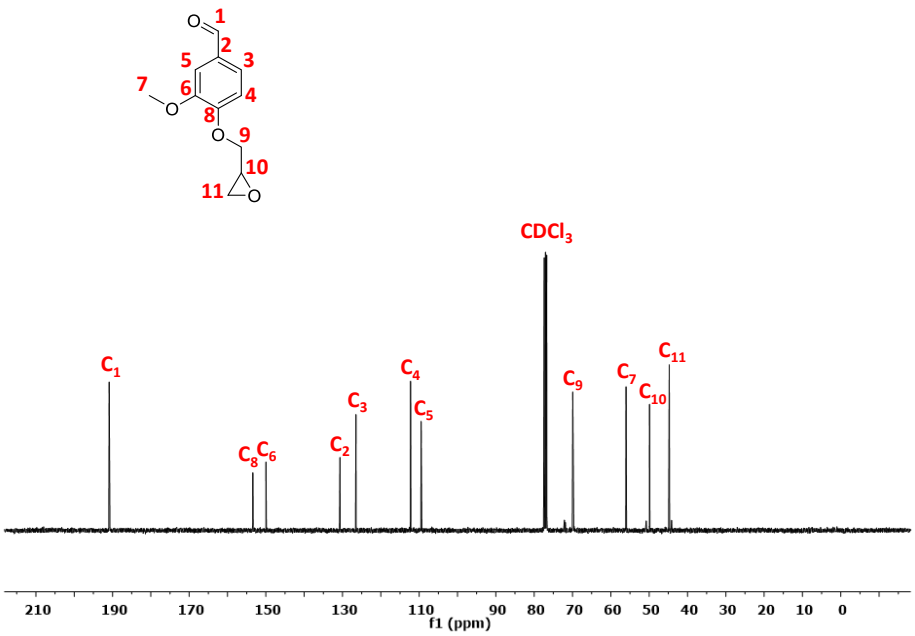

Figure 6.S8. ^{13}C NMR spectrum of EPO-Van in $CDCl_3$.

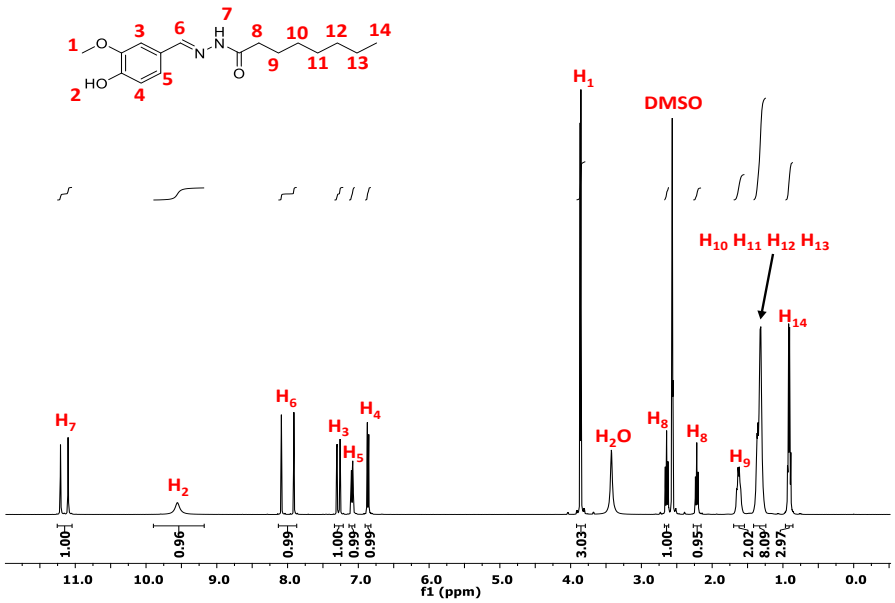

Figure 6.S9. ^{1}H NMR spectrum of V-Oh in DMSO-d_6.

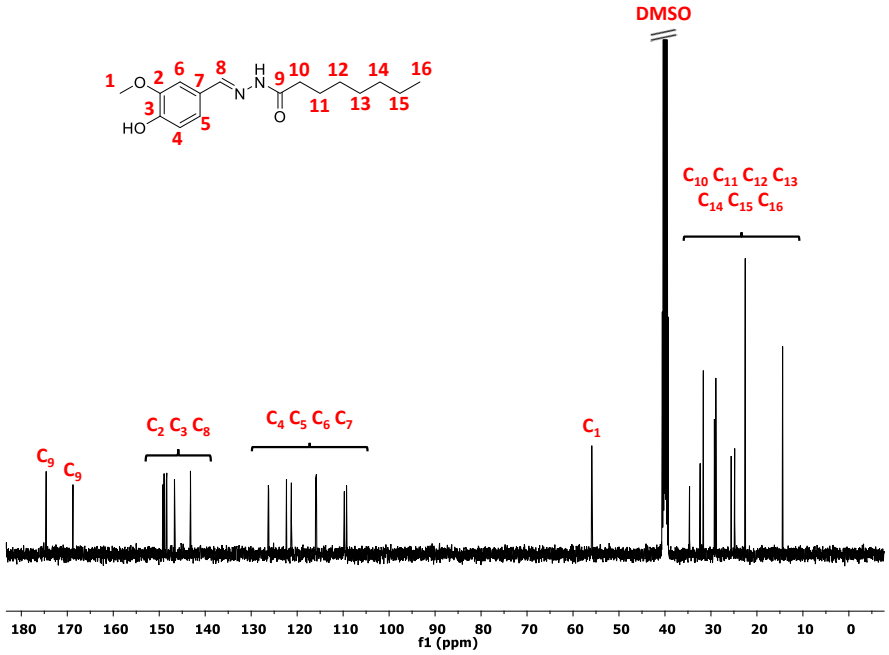

Figure 6.S10. ^{13}C NMR spectrum of V-Oh in DMSO-d_6.

Polym. Chem. **2022**, *13*, 1510-1519

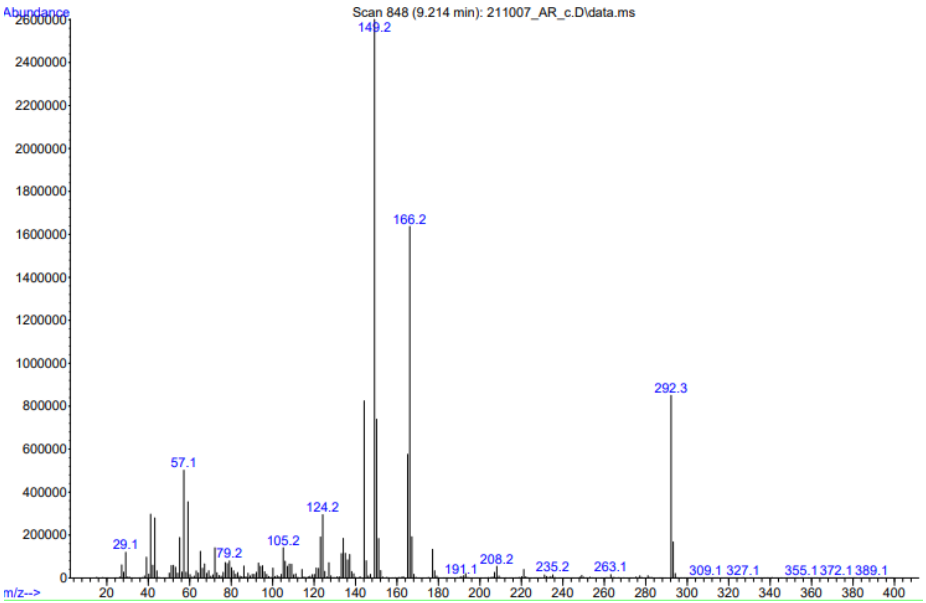

Figure 6.S11. Mass spectrum of pure V-Oh.

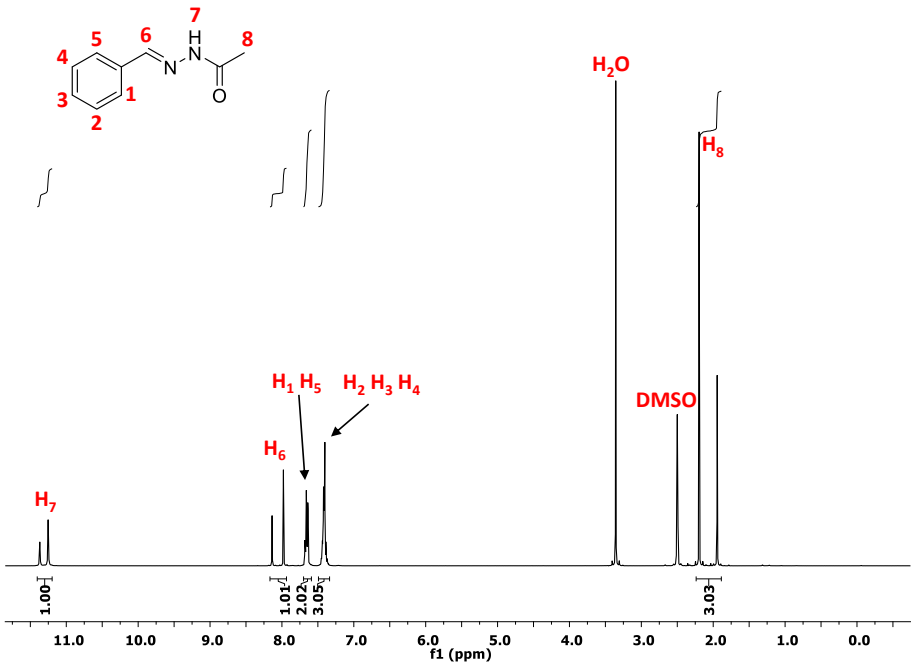

Figure 6.S12. ^{1}H NMR spectrum of B-Ah in DMSO-d_6.

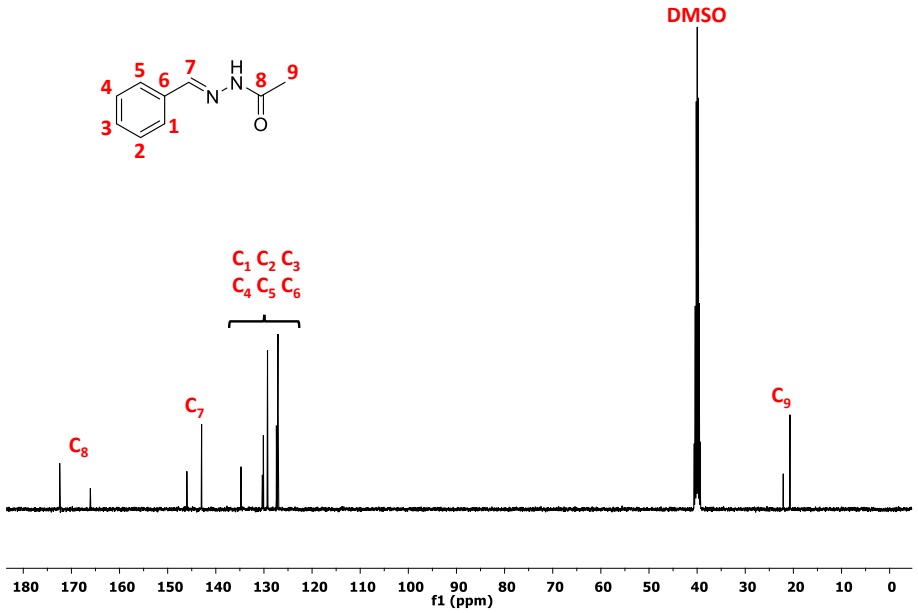

Figure 6.S13. ^{13}C NMR spectrum of B-Ah in DMSO-d_6.

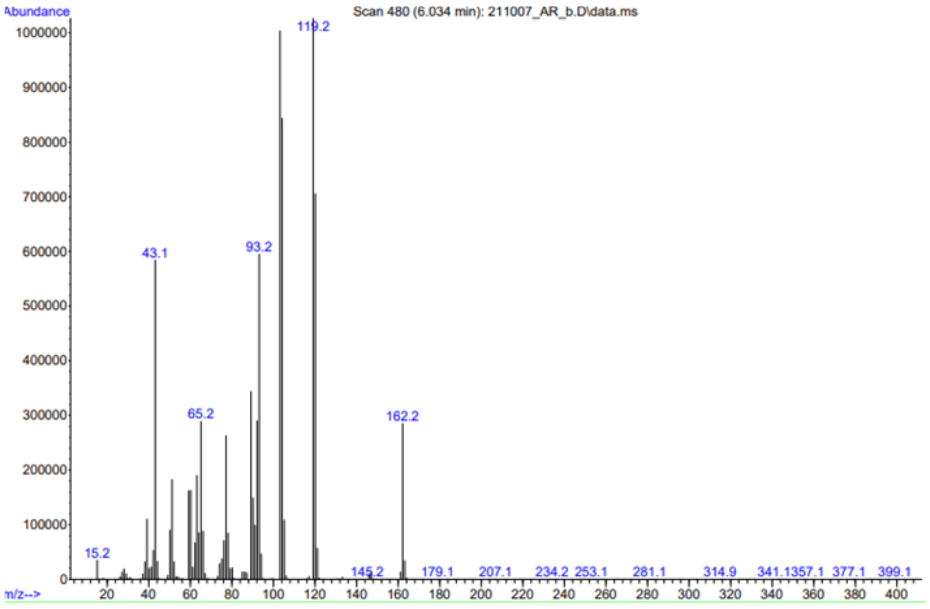

Figure 6.S14. Mass spectrum of pure B-Ah.

Polym. Chem. **2022**, *13*, 1510-1519

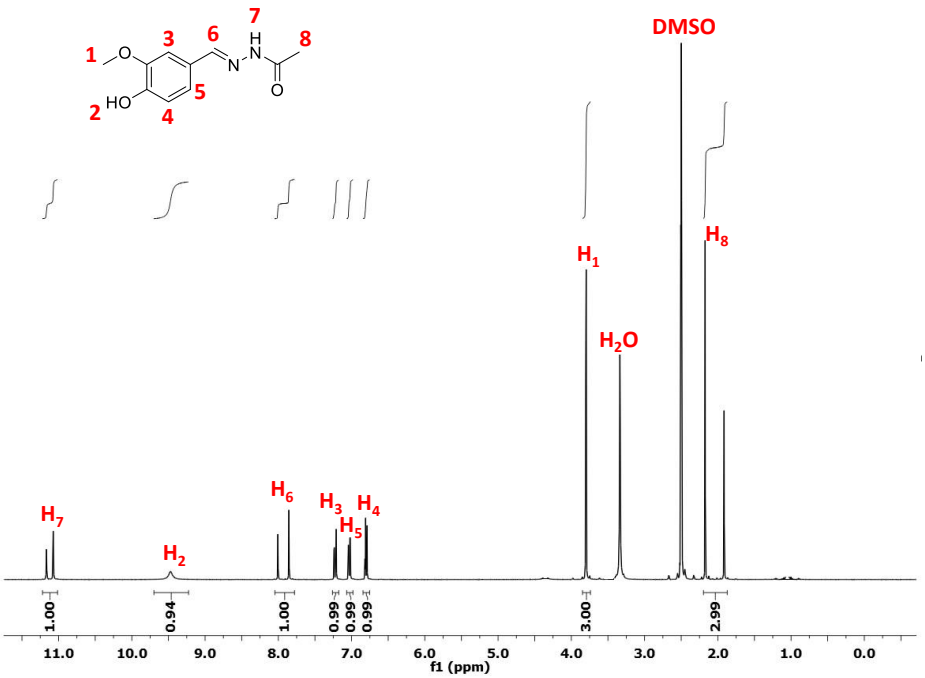

Figure 6.S15. ^{1}H NMR spectrum of V-Ah in DMSO-d_6.

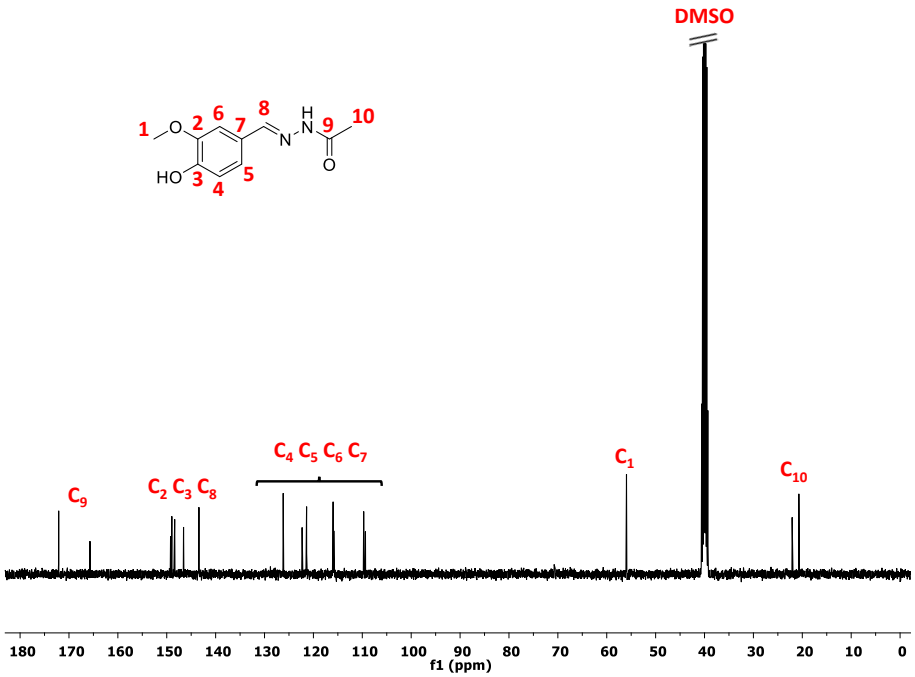

Figure 6.S16. ^{13}C NMR spectrum of V-Ah in DMSO-d_6.

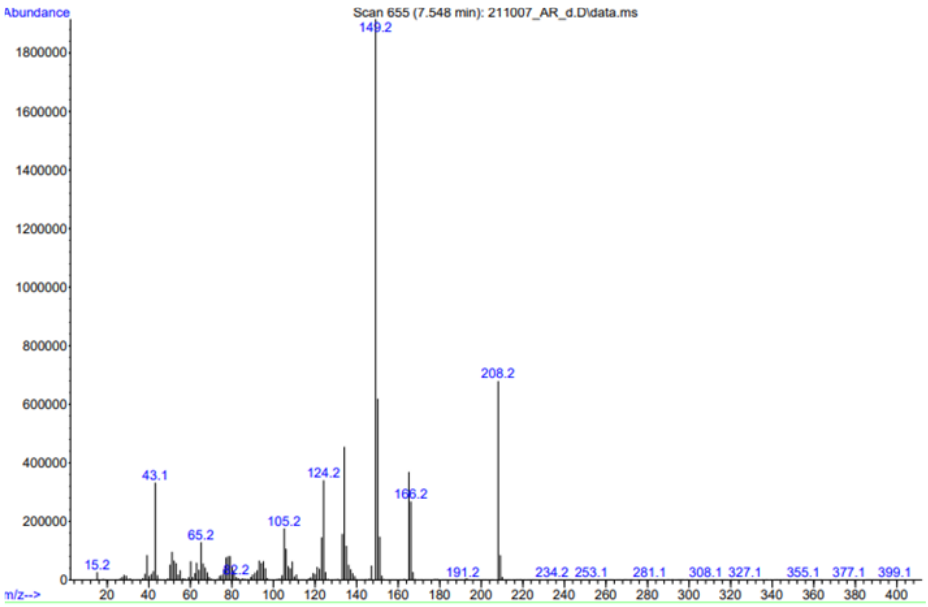

Figure 6.S17. Mass spectrum of pure V-Ah.

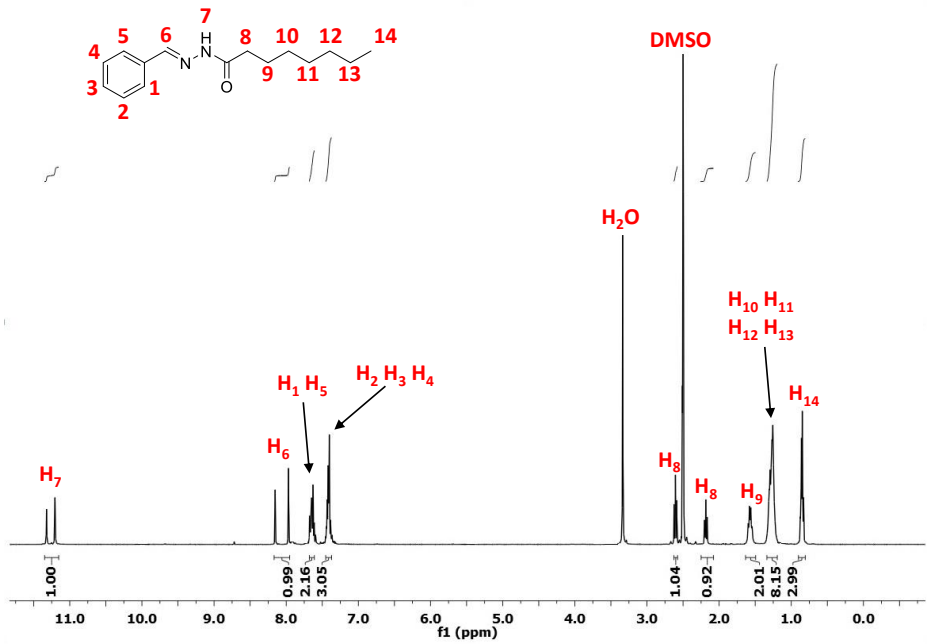

Figure 6.S18. ^{1}H NMR spectrum of B-Oh in DMSO-d_6.

Polym. Chem. **2022**, *13*, 1510-1519

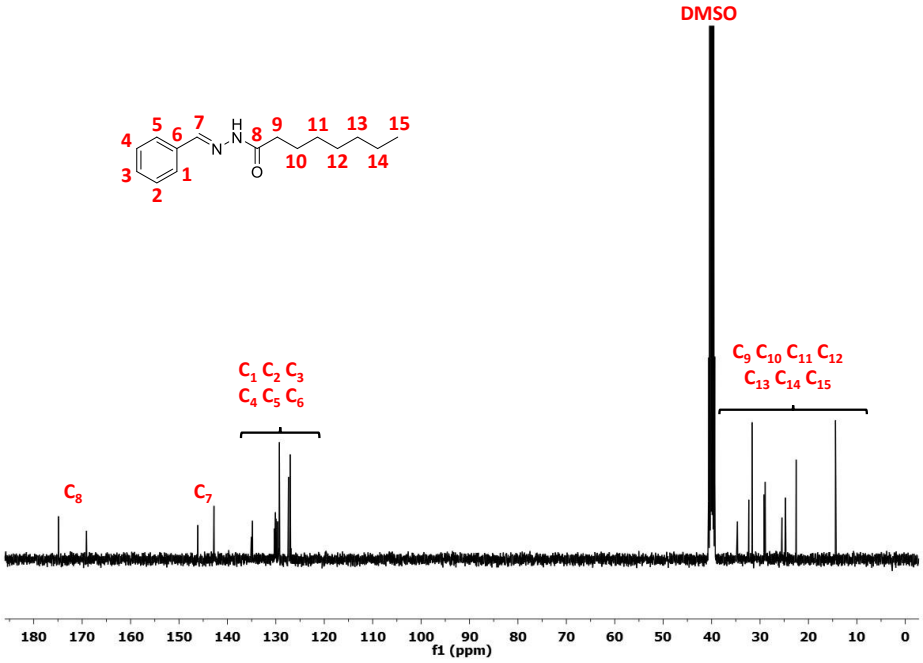

Figure 6.S19. ^{13}C NMR spectrum of B-Oh in DMSO-d_6.

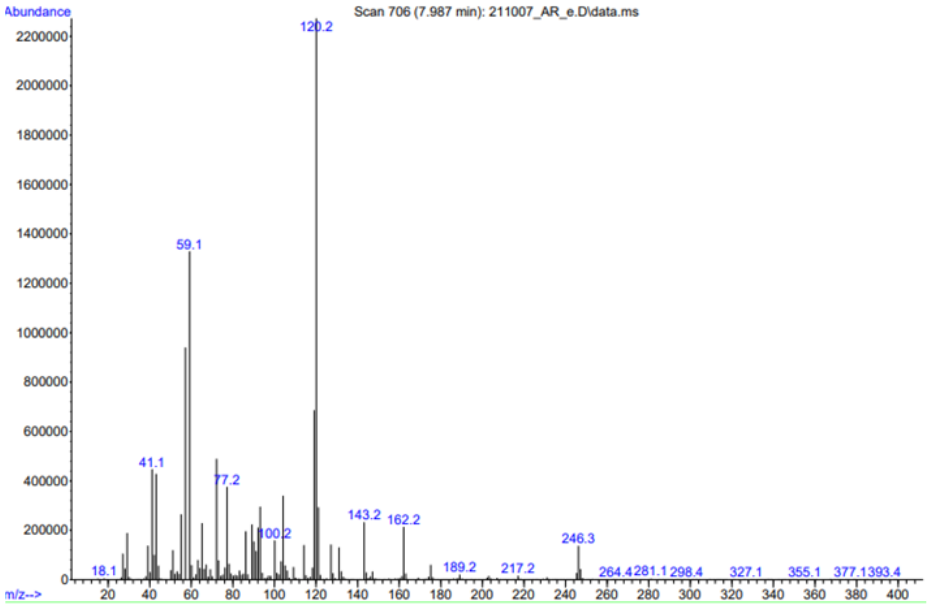

Figure 6.S20. Mass spectrum of pure B-Oh.

UNIVERSITAT ROVIRA I VIRGILI
PROGRESS IN SUSTAINABILITY WITHIN THE REALM OF DESIGNING NEW THERMOSETTING MATERIALS
Adrià Roig Gibert

Chapter 7

Vitrimeric epoxy-amine polyimine networks based on a renewable vanillin derivative

(*ACS Appl. Polym. Mater.* **2022**, *4*, 9341-9350)

UNIVERSITAT ROVIRA I VIRGILI
PROGRESS IN SUSTAINABILITY WITHIN THE REALM OF DESIGNING NEW THERMOSETTING MATERIALS
Adrià Roig Gibert

ACS Appl. Polym. Mater. **2022**, *4*, 9341-9350

Vitrimeric epoxy-amine polyimine networks based on a renewable vanillin derivative

Adrià Roig,[1] Pere Hidalgo,[2] Xavier Ramis,[3] Silvia De la Flor,[2] Àngels Serra[1]

[1] Universitat Rovira i Virgili, Department of Analytical and Organic Chemistry, C/ Marcel·lí Domingo 1, Edif. N4, 43007 Tarragona, Spain

[2] Universitat Rovira i Virgili, Department of Mechanical Engineering, Av. Països Catalans 26, 43007 Tarragona, Spain

[3] Universitat Politècnica de Catalunya, Thermodynamics Laboratory ETSEIB, Av. Diagonal 647, 08028 Barcelona, Spain

ABSTRACT

A series of bio-based polyimine vitrimers was obtained and characterized. A diimine-diglycidyl monomer (DIDG) was synthesized by condensing vanillin with 4,4'-oxidianiline (ODA) and further glycidylation with epichlorohydrin. This compound was crosslinked with three different Jeffamines (Jeff230, JeffD400, and JeffT403) with a different number of poly(propylene glycol) units in their structure and different functionality. Trimethylolpropane triglycidyl ether (TMPTE) was added to the formulation to improve the thermal, mechanical and thermomechanical properties. All the materials prepared showed T_gs above 66 °C, good vitrimeric behavior being the maximum relaxation rate reached by the material prepared from JeffD400, which also allows the most extensive degradation when treated with an acidic aqueous solution. These polyimine vitrimers can entirely relax the stress in less than 10.5 min at 150 °C without any added catalyst. All the materials prepared could be satisfactorily recycled up to 200 °C also presenting an excellent self-welding ability.

KEYWORDS

Vanillin, vitrimers, imine metathesis, covalent adaptable networks, recyclability, self-welding.

1. Introduction

Covalent adaptable networks (CANs) have attracted considerable interest in the last few years due to their ability to be reshaped or self-repaired and present a promising solution in the recyclability of thermosetting materials [1,2]. These materials possess dynamic and exchangeable covalent bonds in their crosslinked structure which can be activated with external stimuli, such as temperature or light, enabling the alteration of their behavior from a viscoelastic solid to a material with the fluid-like plastic flow.

One of the most important types of CANs are the vitrimers, reported for the first time by Leibler and co-workers [3]. In them, the bond exchange is produced in a concerted way, without any intermediate state, without losing the network integrity and always keeping constant the crosslinking density [4]. Many organic reactions have been studied as a potential dynamic process in vitrimers such as transesterification [5-8], disulfide metathesis [9-11], transamination of vinylogous urethanes [12,13] trans-thiocarbamoylation [14,15], and imine exchange [16-19], among others.

Imine exchange can occur in networks with imine bonds, easily formed by a condensation reaction between aldehydes or ketones and primary amines. In general, imines can participate in three types of equilibrium-controlled reactions: hydrolysis, amine-imine exchange, and metathesis (see Scheme 7.1), but only the latest takes place concertedly, in an associative-type mechanism and therefore leading to vitrimeric materials.

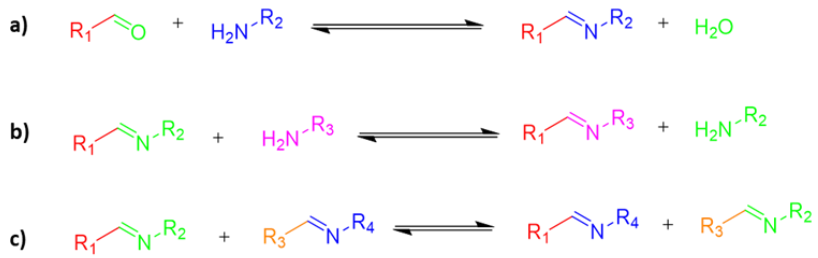

Scheme 7.1. Three types of reversible imine reactions (a) imine condensation, (b) amine-imine exchange and (c) imine metathesis.

Imine metathesis-based materials have attracted the interest of many academic researchers for a long time. Zhang *et al*. designed a catalyst-free malleable polyimine network from commercially available aldehydes and amines that could be reprocessed by applying water or heat to obtain efficiently recycled samples without the loss of mechanical performance [20]. After that, the same group went further in their investigation and tested polyimine vitrimers as binder materials in carbon fiber reinforced composites (CFRC) by adding a single layer of twill weave carbon fiber resulting in CFRCs that could be easily molded into shapes with 3D curvatures, demonstrating a green approach to recyclable composites [21]. Geng and co-workers synthesized polyimine materials based on lignin-derived vanillin that demonstrated

ACS Appl. Polym. Mater. **2022**, *4*, 9341-9350

self-healing properties, which could be mechanically recycled and were able to be formed again after degradation under acidic conditions, showing a promising approach to the sustainability of these materials [22]. Later on, Abu-Omar *et al*. described the preparation of an epoxy monomer containing imine bonds in its structure which was able to react with amines affording a thermoset material with high mechanical performance and good vitrimeric behavior with low relaxation times even at low temperatures [23]. They also demonstrate the high malleability of their materials and the self-welding properties of the imine-containing polymer, showing similar values when tested in a tensile test and compared to the pristine sample.

Nowadays, biomass-derived products are gaining interest worldwide since they avoid the use of fossil raw materials and help to find greener synthetic procedures for eluding the depletion of petrochemical-derived compounds. One of the most used bio-based compounds to produce vitrimers is lignin [24,25]. Its derivative, vanillin, obtained by the alkaline oxidation of lignin, is also widely used for the synthesis of polymers, especially imine vitrimers, due to its aldehyde and phenol groups than can be easily modified to get a suitable functionality as well as for its aromatic structure that provides high thermal and mechanical properties to the obtained materials [22,26-29].

Taking all this into account, in the present article, we report the synthesis and characterization of a series of polyimine vitrimers. A diimine-diglycidyl monomer (DIDG) that has not been previously described was synthesized in high yields *via* a two-step procedure with an excellent yield. Then it was cured with three Jeffamines (Jeff230, JeffD400, and JeffT403) with a different number of poly(propylene glycol) units in their structure and different functionality, in stoichiometric epoxy/NH ratios. Trimethylolpropane triglycidyl ether (TMPTE) was also added to the mixtures to obtain better homogeneities and improve the final mechanical properties. As far as we know, no diimine-diglycidyl have been reported. The presence of epoxy groups in the diamine structure opens the possibility of further crosslinking with many curing agents, which enhances the versatility in the characteristics of the final vitrimeric materials. Previous studies in imine derivatives from vanillin report the synthesis of diphenolic or amino-phenol compounds that react with some epoxy resins [30-32].

FTIR spectroscopy was used to check the completion of the curing reaction. The thermal stability of the polyimine vitrimers was evaluated by thermogravimetry and the thermomechanical properties and vitrimeric behavior by DMTA. All crosslinked materials could be mechanically recycled under certain conditions, and very similar properties were obtained compared to the pristine samples. Moreover, chemical degradation could be performed, and the percentage of weight degraded could be related to the polymer's structure. Materials also revealed good self-welding properties, which open a huge window of industrial applications.

2. Experimental methods

2.1 Materials

The following chemicals were purchased from Sigma Aldrich a: 4,4'-oxydianiline (ODA, 97%), (±)-epichlorohydrin (ECH, ≥99%), benzyl trimethylammonium chloride (BTMA, 97%), trimethylolpropane triglycidyl ether (TMPTE) and trimethylolpropane tris[poly(propylene glycol), amine terminated] ether (Jeff T403, average M_n 440). 4-Hydroxy-3-methoxybenzaldehyde (Vanillin, V, 99%) was obtained from ACROS Organics. Poly(oxypropylene) diamines (Jeff D400 and Jeff D230) from Huntsman. Sodium hydroxide (granulated, NaOH) and absolute ethanol (EtOH) were purchased from Scharlau. Dichloromethane (DCM) and hexane were obtained from VWR Chemicals. All the reagents were used as received.

2.2 Synthesis of diimine-diphenol derivative (DIDP)

The synthesis of DIDP was similarly made according to the literature [33]. In a 250 mL three-neck round bottom flask equipped with a magnetic stirrer, thermometer, and reflux condenser, V (12.0 g, 78.8 mmol) was dissolved in absolute EtOH (80 mL), followed by the addition of 4,4'-oxydianiline (ODA, 7.9 g, 39.4 mmol). The reaction mixture was magnetically stirred and heated at reflux for 24 h. After this time, a precipitate appears, and it was cooled down to room temperature, filtered through a Büchner funnel, washed with cold EtOH, and dried in vacuum at 60 °C for 12 h to give DIDP as a greyish-yellow solid with a yield of 93%. M. p. = 163.4 °C.

^{1}H NMR (DMSO-d_6, δ in ppm): 9.72 (s, 2H), 8.48 (s, 2H), 7.52 (d, 2H), 7.33 (dd, 2H), 7.28 (dd, 4H), 7.05 (dd, 4H), 6.89 (d, 2H), 3.85 (s, 6H). ^{13}C NMR (DMSO-d_6, δ in ppm): 159.55, 154.71, 150.14, 147.99, 147.32, 127.95, 124.03, 122.47, 119.19, 115.34, 110.31, 55.55.

2.3 Synthesis of diimine-diglycidyl derivative (DIDG)

A 250 mL three-neck round bottom flask, equipped with a magnetic stirrer, thermometer, and reflux condenser, was charged with DIDP (8.5 g, 18.1 mmol) and epichlorohydrin (ECH, 100.7 g, 1.1 mol). Then, the temperature was set to 110 °C and benzyl trimethyl ammonium chloride (BTMA, 0.34 g 1.8 mmol) was added to the mixture. The reflux was maintained for 30 min and then cooled down. Then, 50 mL of dichloromethane was added, and extractions with distilled water (neutral pH) were performed. The organic layer was dried over anhydrous $MgSO_4$, filtered, and concentrated under reduced pressure. The residual amount of ECH was eliminated by mixing with hexane and evaporating in the rotary evaporator several times. DIDG was obtained as a light-yellow solid with a yield of 96%. M. p.= 144.9 °C. ^{1}H NMR (DMSO-d_6, δ in ppm): 8.54 (s, 2H), 7.57 (d, 2H), 7.43 (dd, 2H), 7.31 (dd, 4H), 7.10 (d, 2H), 7.07 (dd, 4H), 4.39 (dd, 2H), 3.90 (dd, 2H), 3.86 (s, 6H), 3.37 (m, 2H), 2.87 (dd, 2H), 2.73 (dd,

ACS Appl. Polym. Mater. **2022**, *4*, 9341-9350

2H). ^{13}C NMR (DMSO-d_6, δ in ppm): 159.38, 154.87, 150.60, 149.11, 147.09, 129.56, 123.71, 122.58, 119.22, 112.57, 109.63, 69.81, 55.47, 49.60, 43.83.

2.4 General procedure for the polyimine vitrimers preparation

Polyimine vitrimers were prepared by mixing DIDG and TMPTE in a 3:1 molar ratio with the corresponding Jeffamine in stoichiometric epoxy/NH proportions in a vial until a good dispersion of the solid diimine-diglycidyl compound in the mixture was reached. Then, prepared formulations were poured into rectangular Teflon molds of 30 x 5 x 1.5 mm^3 dimensions and cured in an oven at 150 °C for 3 h to obtain transparent solid rectangular films. The materials were coded as poly(X), where X indicates the Jeffamine used in each material.

2.5 Characterization methods

^{1}H NMR and ^{13}C NMR spectra were registered in a Varian VNMR-S400 NMR spectrometer. DMSO-d_6 was used as a solvent. All chemical shifts are quoted on the δ scale in part per million (ppm) using residual protonated solvent as internal standard (^{1}H NMR: DMSO-d_6 = 2.50 ppm; ^{13}C NMR: DMSO-d_6 = 39.52 ppm). DSC analyses were carried out on a Mettler DSC3+ instrument calibrated using indium (heat flow calibration) and zinc (temperature calibration) standards. Samples of approximately 8-10 mg were placed in aluminum pans with pierced lids and analyzed in an N_2 atmosphere with a glass flow of 50 cm^3 min^{-1}. Dynamic studies between 30 and 250 °C at a heating rate of 10 °C min^{-1} were performed to determine the melting points. A Jasco FT/IR-680 Plus spectrometer equipped with an attenuated total reflection accessory (ATR) (Golden Gate, Specac Ltd, Teknokroma) was used to record the FTIR spectra of the mixture before and after the curing procedure. Real-time spectra were recorded in the wavenumber range between 4000 and 600 cm^{-1} with a resolution of 4 cm^{-1} and averaged over 20 scans. The disappearance of the characteristic absorbance peak of epoxy group at 915 cm^{-1} as well as the appearance of the peak corresponding to O-H at 3300 cm^{-1} were used to confirm the completion of the reaction. The thermal stability of the materials was evaluated using a Mettler Toledo TGA 2 thermobalance. Cured samples weighing around 10 mg were degraded between 30 and 600 °C at a heating rate of 10 °C min^{-1} in N_2 atmosphere with a flow of 50 cm^3 min^{-1}. The thermomechanical properties were studied using a DMA Q800 (TA Instruments) equipped with a film tension clamp. Prismatic rectangular samples with dimensions around 30 x 5 x 1.5 mm^3 were analyzed from 0 °C to 200 °C at 1 Hz, with 0.1% strain at a heating rate of 2 °C min^{-1}. Tensile stress-relaxation tests were conducted in the same instrument using the film tension clamp on samples with the same dimensions as previously defined. The samples were firstly equilibrated at the relaxation temperature for 5 min and a constant strain of 1% was applied, measuring the consequent stress level as a function of time. The materials were tested only once at one temperature. The relaxation-stress σ(t) was normalized by the initial stress σ_0,

and the relaxation times (τ) were determined as the time necessary to relax $0.37\sigma_0$, i.e., ($\sigma = 1/e\sigma_0$). With the relaxation times obtained at each temperature, the activation energy values (E_a), were calculated by using an Arrhenius-type equation:

$$ln(\tau) = \frac{E_a}{RT} - \ln A \qquad \text{(Eq. 7.1)}$$

where τ is the time needed to attain a given stress-relaxation value ($0.37\sigma_0$), A is the pre-exponential factor and *R* is the gas constant. From the Arrhenius relation, the topology freezing temperature (T_v) was obtained as the temperature at which the material reaches a viscosity of 10^{12} Pa·s. Using Maxwell's relation and *E*' determined from DMTA (assuming *E*' is relatively invariant in the rubbery state), τ* was determined to be around 10^5 s in our systems. The Arrhenius relationship was then extrapolated to the corresponding value of τ* to determine T_v in each sample. The recycled samples were obtained by cutting the crosslinked polymers and hot-pressing in a Specac Atlas manual 15 T hydraulic press at 3 MPa into an aluminum mold at 180 °C for 2 h. Recycled samples were die-cut to the same dimensions from the new film obtained and tested again in the DMA analyzer for their mechanical characterization under the same conditions previously described. The chemical degradation of the materials was investigated by first weighing the sample of the cured material and then keeping it in a 1 M HCl aqueous solution for 24 h at room temperature under stirring. Then, the samples were dried under vacuum at 90 °C for 12 h, weighed and the gel fraction was calculated. Final materials were tested until break in tensile mode at room temperature using an electromechanical universal testing machine (Shimadzu AGS-X) with a 1 kN load cell at 10 mm min^{-1} and using Type V samples with a thickness of 1 mm according to ASTM D638-14 standard. Three samples of each material were analyzed, and the results were averaged. Self-welding studies were performed by cutting a poly(D230) sample of a cured material in two parts and then overlapping in an oven at 180 °C for 2h under a pressure of 3 MPa. After that, the samples were tested in the tensile under the same conditions previously described.

3. Results and discussion

3.1 Synthesis of the diimine-diglycidyl monomer (DIDG)

DIDG was prepared via a two-step procedure, including the synthesis of an intermediate diimine-diphenol compound (DIDP) and the further glycidylation reaction of the phenol groups with ECH (Scheme 7.2). Both products were characterized by NMR spectroscopy (Fig. 7.S1-S4).

ACS Appl. Polym. Mater. **2022**, *4*, 9341-9350

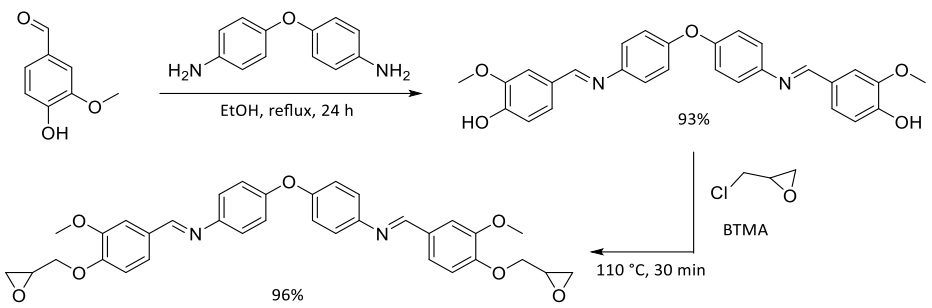

Scheme 7.2. Schematic route for the synthesis of the diimine diglycidyl derivative (DIDG).

The first step is the condensation reaction between bio-based vanillin and ODA, in which the diimine-diphenol compound is obtained in high yield without needing any catalyst. The appearance of the proton signal at 8.48 ppm corresponding to the methine of the imine group and the disappearance of the aldehyde signal of the starting vanillin confirmed the structure of the intermediate DIDP compound. ^{13}C NMR corroborated the purity of the compound by the complete disappearance of the aldehyde signal and the appearance of the carbon signal of the new imine bond formed. The glycidylation reaction was performed with a large excess of ECH and using BTMA as a phase transfer catalyst and heating the mixture to 110 °C for 30 min. The proton signals corresponding to the glycidyl groups appeared between 4.75-2.75 ppm, and the phenol signal was no longer visible in the spectrum, demonstrating that glycidylation had taken place. ^{13}C NMR also showed the presence of the carbon signals corresponding to the epoxy groups of DIDG, confirming the successful synthesis of the expected diimine-diglycidyl compound, which was not previously reported.

3.2 Study of the curing procedure

The synthesized DIDG and the different Jeffamines (Jeff400, Jeff230, and JeffT403, see Scheme 7.3) were used in the preparation of the vanillin-based vitrimers containing dynamic imine bonds. DIDG has a high melting point and molecular weight due to its high content of aromatic rings, which will give high rigidity to the materials and make it very difficult to achieve homogeneity in the samples. For this reason, as well as to provide the final networks greater flexibility and to reach a better dispersion of the solid compound in the mixture without reducing the crosslinking density, an aliphatic trimethylolpropane triglycidyl ether (TMPTE) was added to the formulations in a 3:1 molar ratio between DIDG and TMPTE. The curing temperature was set to 150 °C to guarantee that DIDG melts during the procedure and to ensure the complete homogeneity of the mixture during the curing process. The need to melt the solid compound in the mixture hampers to perform the proper kinetic study. All cross-linked materials were prepared in stoichiometric epoxy/NH conditions and cured according to the procedure previously described in the Experimental Section to obtain reddish transparent samples.

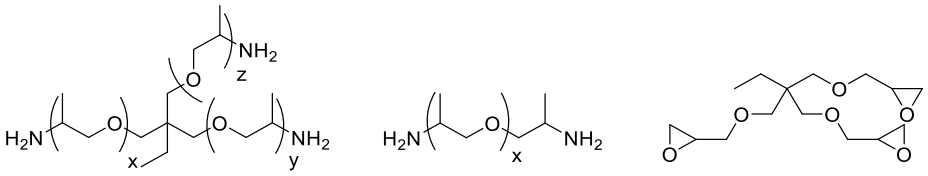

Jeff T403 Jeff D230 and JeffD400 TMPTE

Scheme 7.3. Structures of the hardeners used in the preparation of the polyimine materials.

FTIR spectra of the initial mixtures and the final materials were recorded to determine if the curing process had been completed. Figure 7.1 shows the FTIR spectra of the initial mixture and the final material for the poly(D400) derivative. As it can be seen, after thermal treatment, the band at 910 cm^{-1} attributed to stretching of the epoxy groups disappears, while a broad band at around 3300 cm^{-1} corresponding to the O-H groups generated during the epoxy-amine reaction appears, which indicates that this curing process was effective. It is also noteworthy that the band at approximately 1657 cm^{-1} corresponding to the imine group remained unchanged during the curing process, confirming that the final materials still contain these dynamic groups.

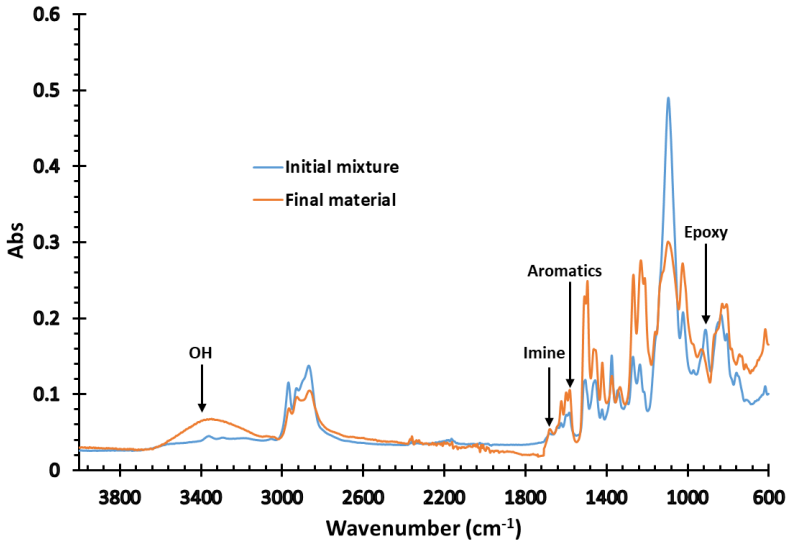

Figure 7.1. FTIR spectra of the initial mixture (blue) and final material poly(D400) (orange).

3.3 Thermal characterization of the materials

The thermal stability of the polyimine vitrimers was studied by thermogravimetry (TGA). Figure 7.2 shows the TGA curves and their derivatives for the materials prepared, and Table 7.1 presents the most significant data extracted.

ACS Appl. Polym. Mater. **2022**, *4*, 9341-9350

As it can be observed, all the materials reveal similar degradation patterns with one main peak with a maximum between 300 and 320 °C, which can be assigned to the degradation of the poly(hydroxyl-amine) network because of the high content of labile C-N bonds [34].

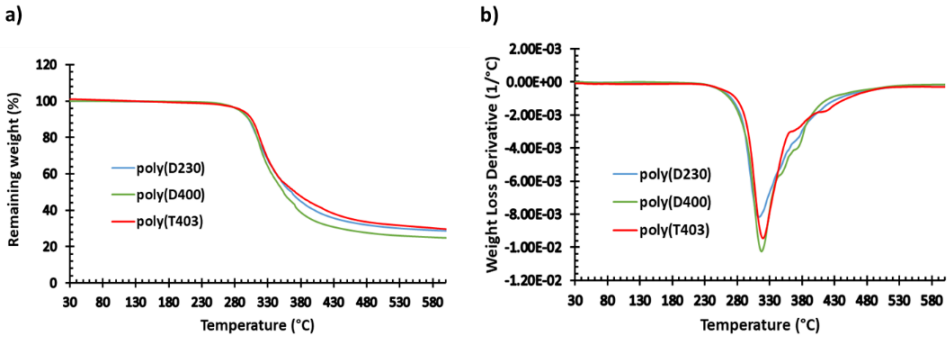

Figure 7.2. a) Thermogravimetric curves and b) DTG curves of all polyimine materials recorded in N_2 atmosphere.

Table 7.1. Thermogravimetric data of all the polyimine materials prepared.

Sample	$T_{1\%}$[a] (°C)	$T_{2\%}$[b] (°C)	T_{max}[c] (°C)	Char Yield [d] (%)
poly(D230)	230.5	263.3	313.2	28.7
poly(D400)	226.4	258.0	315.1	24.8
poly(T403)	231.2	265.2	317.5	29.6

[a] Temperature of 1% of weight loss. [b] Temperature of 2% of weight loss.
[c] Temperature at the maximum rate of degradation. [d] Char residue at 600 °C.

As can be seen in Table 7.1, all the samples lose 1% of weight at temperatures above 226 °C, slightly increasing this value with the crosslinking density, which depends on the Jeffamine characteristics. Their thermal stability is conferred by the crosslinking density provided by the high functionality of the monomers as well as for the significant content of aromatic rings in the network. In terms of mechanical recycling, thermal stability is essential to ensure that the material does not begin to degrade at the recycling temperature. These values of the initial degradation temperature allow for treatment of the material up to 200 °C without fear of degradation. In addition, the char yield of all the materials is relatively high due to the presence of nitrogen and aromatic rings in the network, but it decreases when the functionality of the starting Jeffamine is lower and when the crosslinking density decreases.

The thermomechanical properties of the polyimine vitrimers were determined by DMTA analysis. Figure 7.3 shows the evolution of the tan δ curves and the storage

moduli (*E'*) with temperature for all the materials. The data extracted from these studies are summarized in Table 7.2.

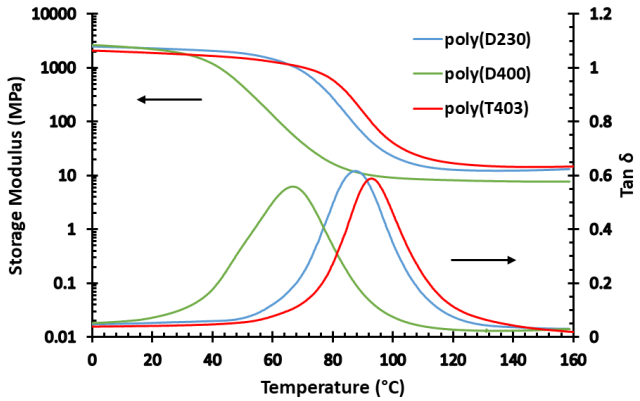

Figure 7.3. Evolution of tan δ and storage modulus with temperature of all polyimine vitrimers.

As observed, fully cured polyimine vitrimers exhibit T_g values (taken from the maximum of tan δ curves) between 66 and 93 °C depending on the Jeffamine used as the curing agent. As expected, poly(D400) exhibits the lowest T_g value, in accordance with a more open network structure provided by the higher mobility and flexibility of the structure, while poly(T403) has the highest T_g. Nevertheless, the T_g of poly(D400) is slightly higher in comparison to DGEBA-JeffD400, which is reported to be 62°C [35]. Although it would seem that a greater molecular weight provided by the poly(propylene ether) units in JeffT403 would lead to a lower T_g, the higher functionality reduces the mobility of the network. Furthermore, the storage moduli in the glassy state are very similar in all cases, with values around 2,000 MPa indicating a relatively high rigidity. Contrarily, in the rubbery state, it can be seen that the higher the crosslinking density, the higher the value of the storage modulus in this state.

Table 7.2. Thermomechanical data of all the virgin and recycled imine vitrimers.

Sample	Virgin			Recycled		
	E'_{glassy}[a] (MPa)	$E'_{rubbery}$[b] (MPa)	$T_{tan\,\delta}$[c] (°C)	E'_{glassy}[a] (MPa)	$E'_{rubbery}$[b] (MPa)	$T_{tan\,\delta}$[c] (°C)
poly(D230)	2230	13.1	87.4	1700	11.2	85.4
poly(D400)	2000	7.7	66.8	1950	4.3	66.1
poly(T403)	1835	14.9	92.8	2000	12.6	93.2

[a] Glassy storage modulus at T_g – 50 °C determined by DMTA. [b] Rubbery storage modulus at T_g + 50 °C determined by DMTA. [c] Temperature at the maximum of tan δ peak at 1 Hz.

ACS Appl. Polym. Mater. **2022**, *4*, 9341-9350

3.4 Study of the vitrimeric behavior

Stress-relaxation tests were performed by DMTA to investigate the time and temperature-dependent relaxation behavior and, consequently, the vitrimeric nature of these materials. The results are shown in Figure 7.4, and the characteristic data are collected in Table 7.3. The stress-relaxation curves reveal that these polyimine vitrimers relax the stress extremely fast, reaching the reference relaxation value of 63% ($\sigma = 0.37\sigma_0$) at 150 °C in less than 1.75 min for poly(D230), 0.85 min for poly(D400) and 1.90 min for poly(T403) without needing any external catalyst which highlights the high speed of the exchange reaction. As it is also possible to be seen, all the materials can relax the stress entirely in less than 10.5 min at the same temperature.

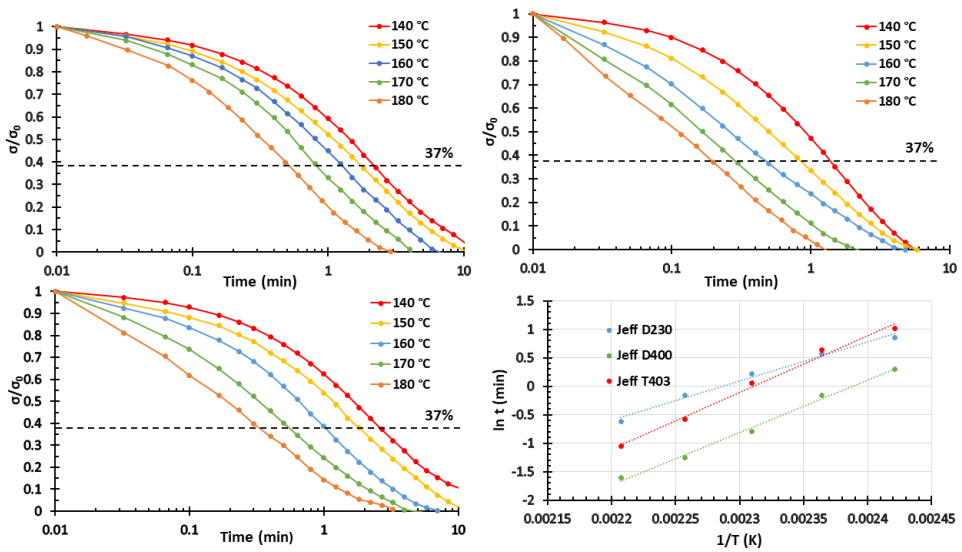

Figure 7.4. Normalized stress relaxation plots as a function of time at various temperatures during 10 minutes for poly(D230) (a), poly(D400) (b), and poly(T403) (c) samples and d) Arrhenius plot of relaxation times against the inverse of the temperature for the different polyimine vitrimers.

Table 7.3. Relaxation times, topology freezing temperature, activation energy and adjusting parameters for the Arrhenius equation of all samples prepared.

Material	$\tau_{0.37}$[a] (min)	$\tau_{100\%}$[b] (min)	T_v (°C)	E_a (kJmol^{-1})	ln A (min)	r^2
poly(D230)	1.75	10	27.3	57.0	15.67	0.99
poly(D400)	0.85	6	39.0	76.5	21.98	0.99
poly(T403)	1.90	10.5	58.7	83.0	23.07	0.99

[a] Time to reach a value of $\sigma/\sigma_0 = 0.37$ at 150 °C. [b] Time to reach total relaxation at 150 °C.

As seen in Table 7.3, poly(D400) is the material that fastest relaxes the stress due to the higher flexibility of the network, allowing the imine groups to produce the exchange reaction easier. On the other hand, poly(D230) has a shorter chain and poly(T403) has a more closed network, and consequently, mobility is more restricted in both cases thus the interchange is more challenging to occur.

When the viscosity is controlled by the exchange reaction, in vitrimeric materials, a relationship between temperature and viscosity similar to the inorganic silica materials is achieved, which follows an Arrhenius-type temperature dependence [36]. Based on this, to perform an extensive study of the vitrimeric behavior of these polyimine materials, the stress relaxation time at different temperatures for a relaxation value of 63% (σ/σ_0 = 0.37) was obtained from Figure 8.4a-c. Using an Arrhenius-type equation, the activation energy (E_a) of the rearrangement process can be determined (see Table 7.3). These values also indicate that the sensitivity of the imine metathesis to a change in temperature could be significant depending on the crosslinking density and the chain length of the starting Jeffamine.

The topology freezing temperature (T_v), which by definition is the temperature when the material reaches a viscosity of 10^{12} Pa·s, can be determined from the Arrhenius plot [3]. This temperature accounts for the temperature below which chemical exchanges are negligible and can be used to compare bond exchange capabilities in vitrimers. In these imine vitrimers, it is possible to see that the T_v values are low and much lower than T_g. In this case, the critical factor in determining the relaxation behavior is the T_g because, in the glassy state, the lack of segmental motions hampers the exchange reaction between imine units. Therefore, T_v is not real, just hypothetical since it is necessary to exceed the T_g so that the network achieves certain mobility and the exchange reactions can start [36,37]. Despite that the correlations are very strong, it is noteworthy that limited errors in activation energy give significant errors in the relaxation time and, consequently, in the T_v.

Since no free primary amine groups exist in the network, the exchange mechanism produced must be imine metathesis.

3.5 Recycling process

To investigate the recyclability of the three different polyimine vitrimers prepared, the materials were cut into small pieces and hot-pressed at 3 MPa in an aluminum mold for 2 h. The recycling temperature selected was 180 °C which ensured the topological rearrangement and guaranteed that no degradation will occur, as it was determined by thermogravimetry at this temperature for 2 h no weight was lost. As it can be seen in Figure 7.S5 the recycled material shows good transparency, indicating that the recycling process has been successful.

ACS Appl. Polym. Mater. **2022**, *4*, 9341-9350

DMTA analysis was performed to study the thermomechanical properties of the recycled samples and compare them with the virgin ones. The tan δ curves and the storage modulus as a function of temperature for all the recycled and virgin materials can be seen in Figure 7.5, and the data obtained from them are presented in Table 7.2.

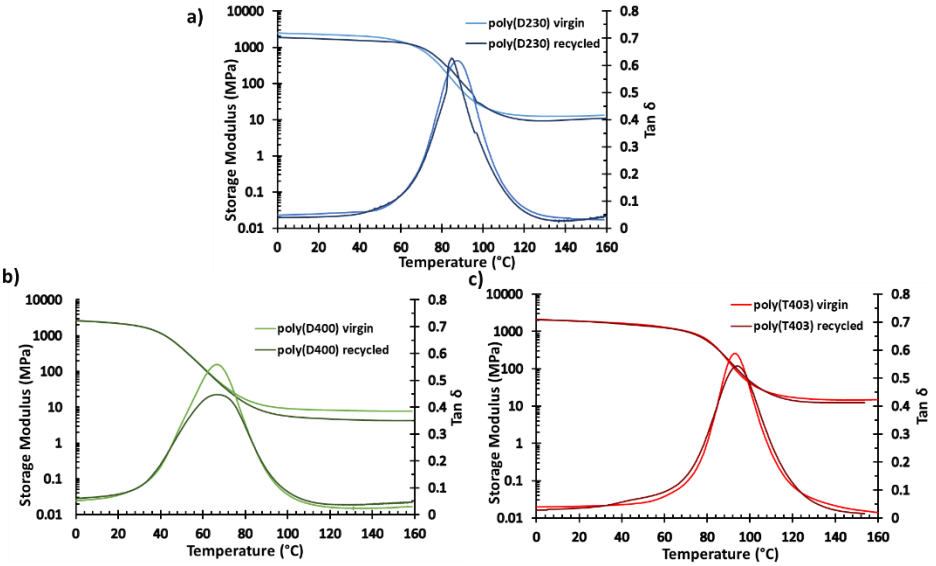

Figure 7.5. Dependence of tan δ and storage modulus *versus* temperature before and after recycling of poly(D230) (a), poly(D400) (b) and poly(T403) (c).

As can be seen, very similar tan δ curves and $T_{\tan \delta}$ values were obtained for the virgin and recycled samples, demonstrating that the recycling process hardly affects the thermomechanical properties of the final materials.

Moreover, to check if the chemical structure has been changed after the recycling process, FTIR analysis of the virgin and recycled poly(D400) were performed. As it can be seen in Figure 7.S6, no significant changes between both samples can be observed, indicating that the chemical structure has not been altered.

The goodness of the recyclability of poly(D230) was confirmed by the tensile strength comparing the virgin and the recycled material. Figure 7.S7 shows the stress-strain curves of both samples, which are quite similar, with a slightly more rigid behavior in the case of the recycled one. This can be explained by the presence of some defects in the recycled material due to the harsh conditions of the recycling process.

3.6 Chemical degradability

All materials were introduced in a 1 M HCl aqueous solution for 24 h at room temperature under stirring to investigate the chemical degradability of the imine vitrimers since it is known that imine bonds can be easily hydrolyzed under acidic conditions. After that, it can be noticed in Figure 7.6 that the solution became yellowish, indicating the hydrolysis of the imine bonds. Nevertheless, a trend is observed for the materials since poly(D400) was degraded until 68.8% of its initial weight, but poly(T403) only 4.8%. This fact is in accordance with the increase in the crosslinking density, which is given by the functionality and chain length of the starting Jeffamines. Higher functionality means more non-exchangeable covalent bonds in the material and a fewer proportion of degraded sample under the same conditions. The presence of TMPTE in the formulation, with a trifunctional structure without imine groups, hinders the complete solubilization of the material when hydrolyzed in an acidic medium.

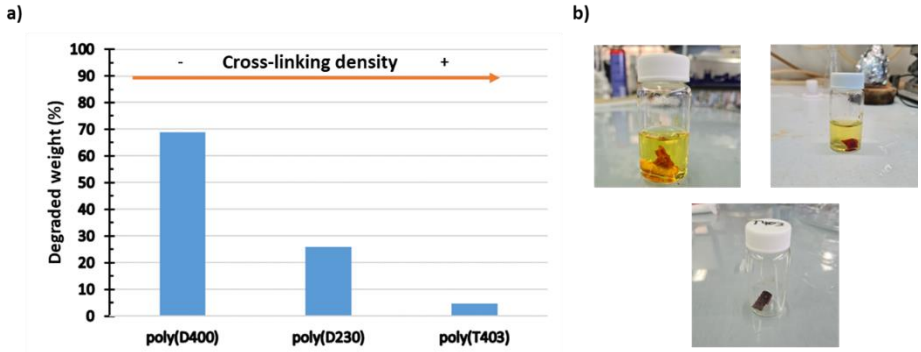

Figure 7.6. a) Degraded weight percentage of each polyimine material and b) photographs of the samples after the chemical degradation.

3.7 Self-welding studies

Polyimine materials proved to have self-welding abilities thanks to imine metathesis that can occur at the interface of two overlapped pieces of the materials. To study this phenomenon, a rectangular film of poly(D230) was cut into two pieces and then overlapped under the same conditions of the recycling procedure to ensure that the exchange reaction occurred in the overlapping area. As can be observed in Figure 7.7, the two parts of the polyimine material were attached. The virgin and the welded samples possessed similar dimensions, so they were subjected to tensile test. Figure 7.7 also shows that the sample was broken at a random site rather than the overlapping area, demonstrating that this part is not the weakest. Nevertheless, the tensile strength and elongation at break (Figure 7.8) were slightly lower compared to the virgin polyimine due to the stress concentration factor at the end of the part

ACS Appl. Polym. Mater. **2022**, *4*, 9341-9350

where both pieces are overlapped as well as the lack of uniformity in the transversal section of the sample.

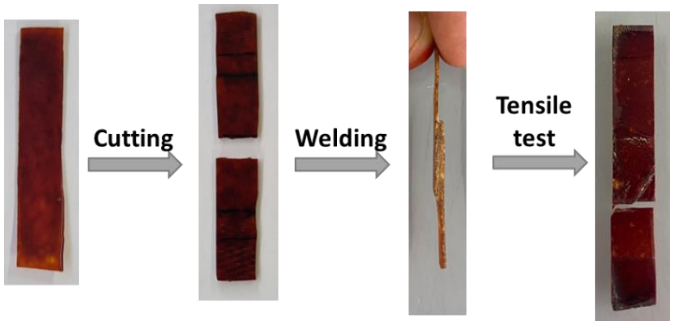

Figure 7.7. Pictures of the self-welding process.

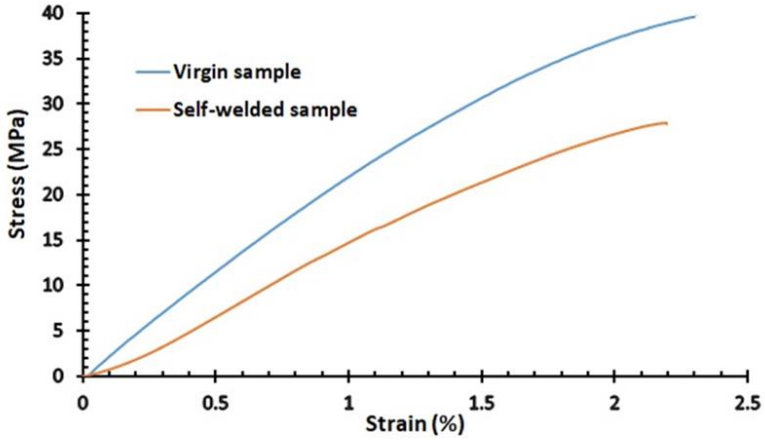

Figure 7.8. Tensile properties of virgin and welded poly(D230).

4. Conclusions

A bio-based diimine-diglycidyl derivative of vanillin has been successfully synthesized and crosslinked with three Jeffamines (JeffD230, JeffD400, and JeffT403) with different molecular weights and functionalities. Trimethylolpropane triglycidyl ether (TMPTE) was added to facilitate processing and increase flexibility and crosslinking density.

All the materials obtained have a T_g higher than 65 °C and high thermal stability ($T_{1\%}$ > 225 °C), allowing safe recycling up to 200 °C.

The exchange reaction occurs *via* imine metathesis and only needs about 10 minutes to completely relax the stress at 150 °C in all cases without adding any external catalyst. The topology freezing temperatures (T_v) were calculated using the Arrhenius

dependence of relaxation with temperature and resulted in being lower T_v than the T_g values, meaning that once this temperature is overpassed, the exchange reaction takes place immediately.

The materials could be recycled under pressure at 180 °C for two hours without changing their thermomechanical characteristics.

Imine groups in the network allow the chemical degradation of the material in aqueous HCl, but the addition of TMPTE to the formulation hinders the complete degradation. The structure of the Jeffamine, used as the curing agent, affects the hydrolysis extent because of the different crosslinking densities of the network.

Self-welding studies were performed in all the polyimine vitrimers under pressure at 160 °C in a conventional oven demonstrating their great capability for this application.

The partially bio-based character, the high relaxation rate, recyclability, chemical degradability, and self-welding characteristics make these materials very interesting for future industrial applications.

Acknowledgments

This work is part of the R&D projects PID2020-115102RB-C21 and PID2020-115102RB-C22 funded by MCNI/AEI/10.13039/501100011033 we acknowledge these grants and to the Generalitat de Catalunya (2017-SGR-77 and BASE3D) and Diputació de Tarragona (2022/27).

References

[1] Scheutz, G. M.; Lessard, J. J.; Sims, M. B.; Sumerlin, B.S. Adaptable Crosslinks in Polymeric Materials: Resolving the Intersection of Thermoplastics and Thermosets. *J. Am. Chem. Soc.* **2019**, *141*, 16181-16196.

[2] Podgórski, M.; Fairbanks, B. D.; Kirkpatrick, B. E.; McBride, M.; Martinez, A. Dobson, A.; Bongiardina, N. J.; Bowman, C. N. Toward Stimuli-Responsive Dynamic Thermosets Through Continuous Development and Improvements in Covalent Adaptable Networks (CANs). *Adv. Mater.* **2020**, *32*, 1906876.

[3] Montarnal, D.; Capelot, M.; Tournilhac, F.; Leibler, L. Silica-Like Malleable Materials from Permanent Organic Networks. *Science*, **2011**, *334*, 965-968.

[4] Van Lijsebetten, F.; Holloway, J. O.; Winne, J. M.; Du Prez, F. E. Internal Catalysis for Dynamic Covalent Chemistry Applications and Polymer Science. *Chem. Soc. Rev.* **2020**, *49*, 8425-8438.

[5] Altuna, F. I.; Hoppe, C. E.; Williams, R. J. J. Epoxy Vitrimers with Covalently Bonded Tertiary Amine as Catalyst of the Transesterification Reaction. *Eur. Polym. J.* **2019**, *113*, 297-304.

[6] Capelot, M.; Montarnal, D.; Torunilhac, F.; Leibler, L. Metal-Catalyzed Transesterification for Healing and Assembling of Thermosets. *J. Am. Chem. Soc.* **2012**, *134*, 7664-7667.

[7] Altuna, F. I.; Hoppe, C. E.; Williams, R. J. J. Shape Memory Epoxy Vitrimers Based on DGEBA Crosslinked with Dicarboxylic Acids and Their Blends with Citric Acid. *RSC Adv.* **2016**, *6*, 88647-88655.

[8] Capelot, M.; Unterlass, M. M.; Tournilhac, F.; Leibler, L. Catalytic Control of the Vitrimer Glass Transition. *ACS Macro Lett.* **2012**, *1*, 789-792.

[9] Rekondo, A.; Martin, R.; Ruiz de Luzuriaga, A.; Cabanero, G.; Grande, H. J.; Odriozola, I. Catalyst-Free Room-Temperature Self-Healing Elastomers Based on Aromatic Disulfide Metathesis. *Mater. Horiz.* **2014**, *1*, 237-240.

[10] Lei, Z. Q.; Xiang, H. P.; Yuan, Y. J.;Rong, M. Z.; Zhang, M. Q. Room-Temperature Self-Healable and Remoldable Cross-Linked Polymer Based on the Dynamic Exchange of Disulfide Bonds. *Chem. Mater.* **2014**, *26*, 2038-2046.

[11] Ruiz de Luzuriaga, A.; Solera, G.; Azcarate-Ascasua, I.; Boucher, V.; Grande, H.-J.; Rekondo, A. Chemical Control of the Aromatic Disulfide Exchange Kinetics for Tailor-Made Epoxy Vitrimers. *Polymer*, **2022**, *239*, 124457.

[12] Denissen, W.; Rivero, G.; Nicolaÿ, R.; Leibler, L.; Winne, J. M.; Du Prez, F. E. Vinylogous Urethane Vitrimers. *Adv. Funct. Mater.* **2015**, *25*, 2451-2457.

[13] Engelen, S.; Wróblewska, A. A.; De Bruycker, K.; Aksakal, R.; Ladmiral, V.; Caillol, S.; Du Prez, F. E. Sustainable Design of Vanillin-Based Vitrimers Using Vinylogous Urethane Chemistry. *Polym. Chem.* **2022**, *13*, 2665-2673.

[14] Fortman, D. J.; Brutman, J. P.; Cramer, C. J. Hillmeyer, M. A., Dichtel, W. R. Mechanically Activated, Catalyst-Free Polyhydroxyurethane Vitrimers. *J. Am. Chem. Soc.* **2015**, *137*, 14019-14022.

[15] Gamardella, F.; Guerrero, F.; De la Flor, S.; Ramis, X.; Serra, A. A New Class of Vitrimers Based on Aliphatic Poly(thiourethane) Networks with Shape Memory and Permanent Shape Reconfiguration. *Eur. Polym. J.* **2020**, *122*, 109361.

[16] Roig, A.; Petrauskaitė, A.; Ramis, X.; De la Flor, S.; Serra, À. Synthesis and Characterization of New Bio-Based Poly(acylhydrazone) Vanillin Vitrimers. *Polym. Chem.* **2022**, *13*, 1510.

[17] Wang, S.; Ma, S.; Li, Q.; Yuan, W.; Wang, B.; Zhu, J. Robust, Fire-Safe, Monomer-Recovery, Highly Malleable Thermosets from Renewable Bioresources. *Macromolecules* **2018**, *51*, 8001-8012.

[18] Zheng, H.; Liu, Q.; Lei, X.; Chen, Y.; Zhang, B.; Zhang, Q. A Conjugation Polymine Vitrimer: Fabrication and Performance. *J. Polym. Sci., Part A:Polym. Chem.* **2018**, *56*, 2531-2538.

[19] Belowich, M. E.; Stoddart, J. F. Dynamic Imine Chemistry. *Chem. Soc. Rev.* **2012**, *41*, 2003-2024.

[20] Taynton, P.; Yu, K; Shoemaker, R. K.; Jin, Y.; Qi, H. J.; Zhang, W. Heat- Or Water Driven Malleability in a Highly Recyclable Covalent Network Polymer. *Adv. Mater.* **2014**, *26*, 3938-3942.

[21] Taynton, P.; Ni, H.; Zhu, C.; Yu, K.; Loob, S.; Jin, Y.; Qi, H. J.; Zhang, W. Repairable Woven Carbon Fiber Composites with Full Recyclability Enabled by Malleable Polyimine Networks. *Adv. Mater.* **2016**, *28*, 2904-2909.

[22] Geng, H.; Wang, Y.; Yu, Q.; Gu, S.; Zhou, Y.; Xu, W.; Zhang, X.; Ye, D. Vanillin-Based Polyschiff Vitrimers: Reprocessability and Chemical Recyclability. *ACS Sustainable. Chem. Eng.* **2018**, *6*, 15463-15470.

[23] Zhao, S.; Abu-Omar, M. M. Recyclable and Malleable Epoxy Thermoset Bearing Aromatic Imine Bonds. *Macromolecules* **2018**, *51*, 9816-9824.

[24] Moreno, A.; Morsali, M.; Sipponen, M. H. Catalyst-Free Synthesis of Lignin Vitrimers with Tunable Mechanical Properties: Circular Polymers and Recoverable Adhesives. *ACS Appl. Mater. Interfaces* **2021**, *13*, 57952-57961.

[25] Zhang, S.; Liu, T.; Hao, C.; Wang, L.; Han, J.; Liu, H.; Zhang, J. Preparation of a Lignin-Based Vitrimer Material and its Potential Use for Recoverable Adhesives. *Green Chem.* **2018**, *20*, 2995-3000.

[26] Xu, Y.; Odelius, K.; Hakkarainen, M.; Photocurable, Thermally Reprocessable, and Chemically Recyclable Vanillin-Based Imine Thermosets. *ACS Sustainable Chem. Eng.* **2020**, *8*, 17272-17279.

[27] Zhou, Z.; Su, X.; Liu, J.; Liu, R. Synthesis of Vanillin-Based Polyimine Vitrimers with Excellent Reprocessability, Fast Chemical Degradability, and Adhesion. *ACS Appl. Polym. Mater.* **2020**, *2*, 5716-5725.

[28] Yu, Q.; Peng, X.; Wang, Y.; Geng, H.; Xu, A.; Zhang, X.; Xu, W.; Ye, D. Vanillin-Based Degradable Epoxy Vitrimers: Reprocessability and Mechanical Properties Study. *Eur. Polym. J.* **2019**, *117*, 55-63.

[29] Fache, M.; Darroman, E.; Besse, V.; Auvergne, R.; Caillol, S.; Boutevin, B. Vanillin, a Promising Biobased Building-Block for Monomer Synthesis. *Green Chem.* **2014**, *16*, 1987.

[30] Liu, X.; Liang, L.; Lu, M.; Song, X. Liu, H.; Chen, G. Water-Resistant Bio-Based Vitrimers Based on a Dynamic Imine Bonds: Self-Healability, Remodelability and Ecofriendly Recyclability. *Polymer*, **2020**, *210*, 123030.

[31] Memon, H.; Liu, H.; Rashid, M. A.; Chen, L.; Jiang, Q.; Zhang, L.; Wei, Y.; Liu, W.; Qiu, Y. Vanillin-Based Epoxy Vitrimer with High Performance and Closed-Loop Recyclability. *Macromolecules*, **2020**, *53*, 621-630.

[32] Liu, Y.-Y.; Liu, G.-L.; Li, Y.-D.; Weng, Y. Zeng, J.-B. Biobased High-Performance Epoxy Vitrimer with UV Shielding for Recyclable Carbon Fiber Reinforced Composites. *ACS Sustainable Chem. Eng.* **2021**, *9*, 4638-4647.

[33] Zhang, X.; Wu, J.; Qin, Z.; Qian, L.; Liu, L.; Zhang, W.; Yang, R. High Performance Biobased Vinyl Ester Resin with Schiff Base Derived from Vanillin. *ACS Appl. Polym. Mater.* **2022**, *4*, 2604-2613.

[34] Roig, A.; Ramis, X.; De la Flor, S.; Serra, À. Dual-Cured Thermosets from Glycidyl Methacrylate Obtained by Epoxy-Amine Reaction and Methacrylate Homopolymerization. *React. Funct. Polym.* **2021**, *159*, 104822.

[35] Santiago, D.; Guzmán, D.; Ramis, X.; Ferrando, F.; Serra, A. New Epoxy Thermosets Derived from Clove Oil Prepared by Epoxy-Amine Curing. *Polymers* **2020***, 12*, 44.

[36] Denissen, W.; Winne, J. M.; Du Prez, F. E. Vitrimers: Permanent Organic Networks with Glass-Like Fluidity. *Chem. Sci.* **2016**, *7*, 30-38.

[37] Guerre, M.; Taplan, C.; Winne, J. M.; Du Prez, F. E. Vitrimers: Directing Chemical Reactivity to Control Material Properties. *Chem. Sci.* **2020**, *11*, 4855-4870.

Supporting Information

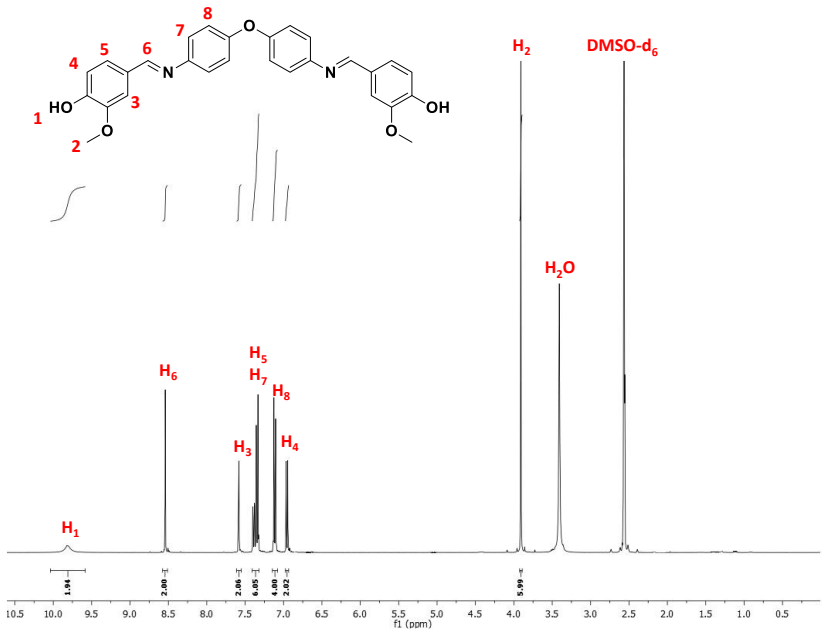

Figure 7.S1. ^{1}H NMR spectrum of DIDP in DMSO-d_6.

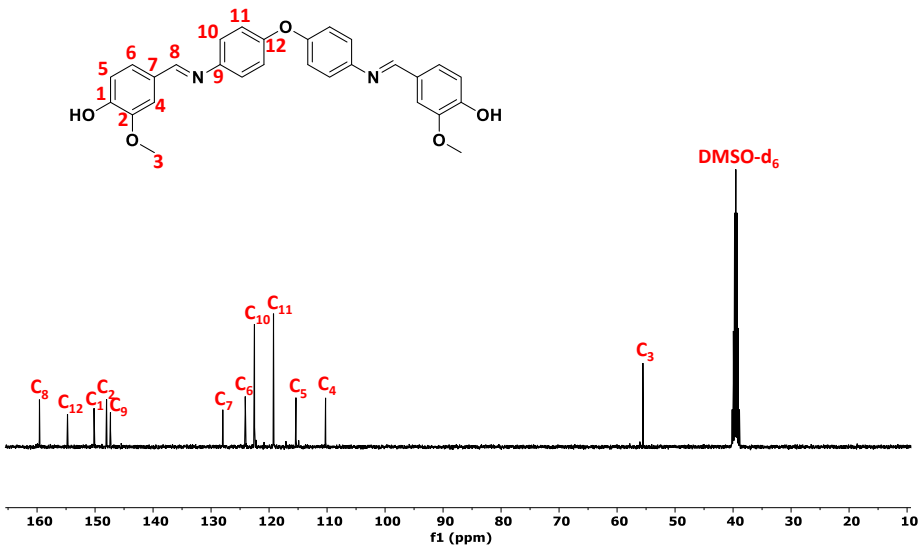

Figure 7.S2. ^{13}C NMR spectrum of DIDP in DMSO-d_6.

ACS Appl. Polym. Mater. **2022**, *4*, 9341-9350

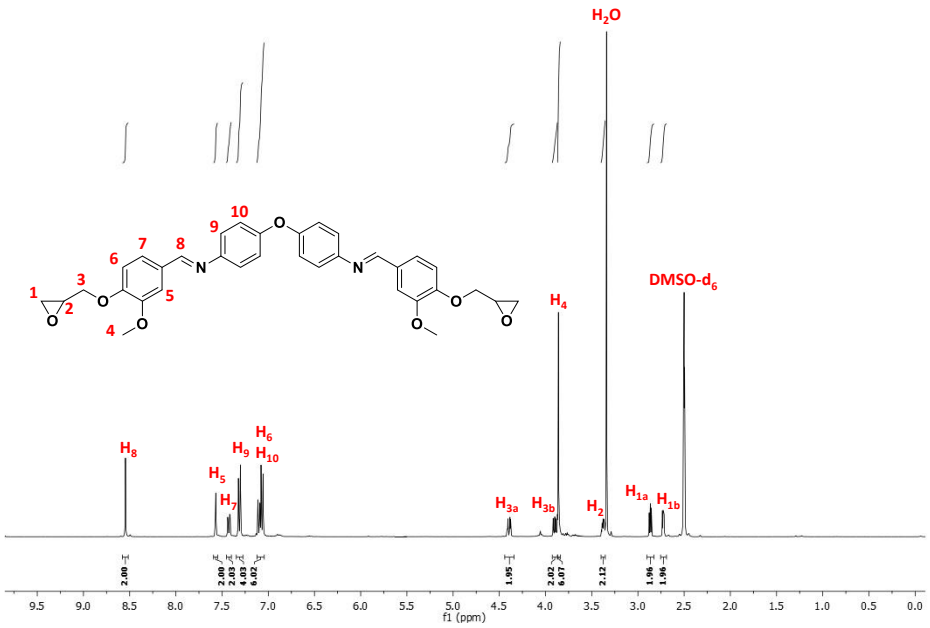

Figure 7.S3. ^{1}H NMR spectrum of DIDG in DMSO-d_6.

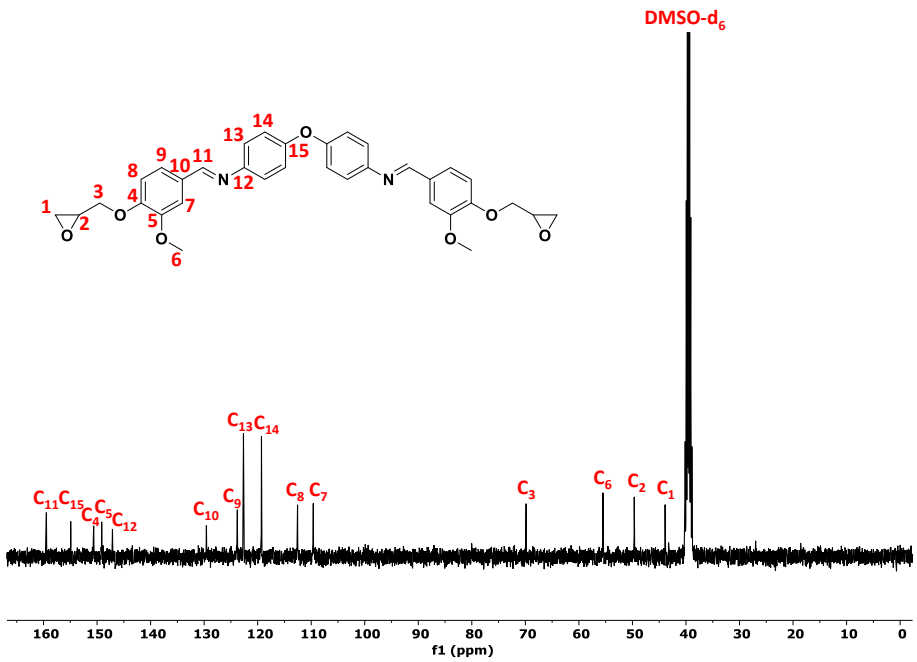

Figure 7.S4. ^{13}C NMR spectrum of DIDG in DMSO-d_6.

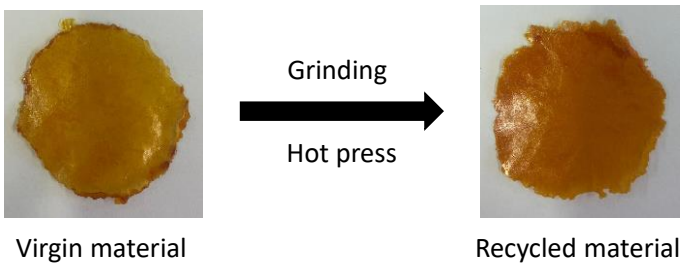

Figure 7.S5. Photographs of the virgin and recycled poly(D230).

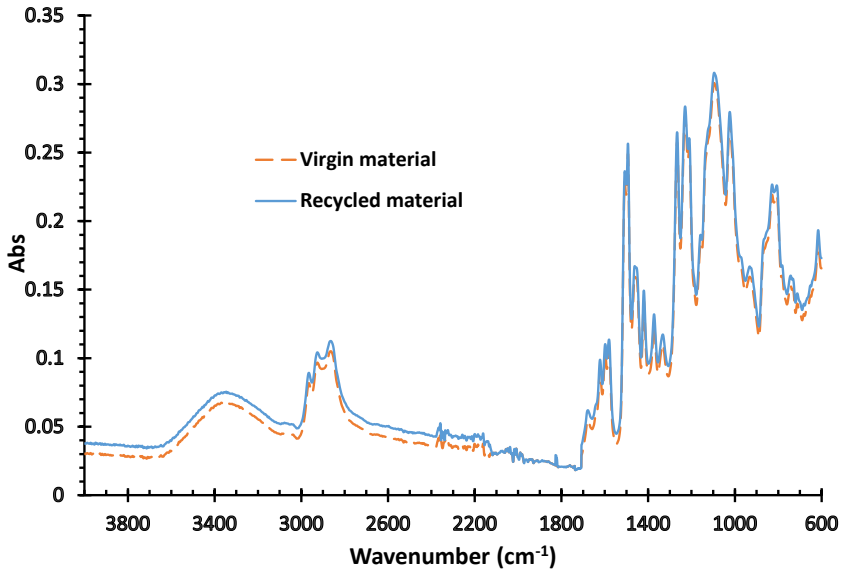

Figure 7.S6. FTIR spectra of the virgin (dotted orange) and recycled (blue) poly(D230).

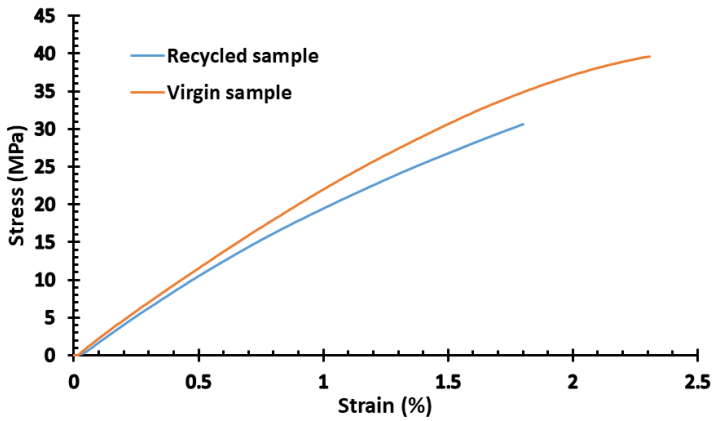

Figure 7.S7. Stress-strain curves of the virgin (orange) and recycled (blue) poly(D230).

Chapter 8

Disulfide vitrimeric materials based on cystamine and diepoxy eugenol as bio-based monomers

(*Eur. Polym. J.* **2023**, *194*, 112185)

UNIVERSITAT ROVIRA I VIRGILI
PROGRESS IN SUSTAINABILITY WITHIN THE REALM OF DESIGNING NEW THERMOSETTING MATERIALS
Adrià Roig Gibert

Eur. Polym. J. **2023**, *194*, 112185

Disulfide vitrimeric materials based on cystamine and diepoxy eugenol as bio-based monomers

Adrià Roig,[1] Marco Agizza,[2] Àngels Serra,[1] Silvia De la Flor [2]

[1] Universitat Rovira i Virgili, Department of Analytical and Organic Chemistry, C/ Marcel·lí Domingo 1, Edif. N4, 43007 Tarragona, Spain

[2] Universitat Rovira i Virgili, Department of Mechanical Engineering, Av. Països Catalans 26, 43007 Tarragona, Spain

ABSTRACT

This study reports the synthesis and characterization of bio-based disulfide vitrimers obtained from diepoxy eugenol and cystamine through an epoxy-amine polycondensation process. TREN was added to the formulation in varying proportions to increase the crosslinking density. Although TREN reduced the number of disulfide groups in the vitrimers, it resulted in a maximum relaxation rate at a proportion of 25%. The vitrimers were characterized using FTIR, TGA, and thermomechanical analysis, and their T_g values, determined by DSC, ranged from 75 to 103 °C with increasing TREN proportion. The vitrimers rapidly relax with a relaxation time (τ) of 8.5 minutes at 170 °C. The addition of TREN decreased the relaxation times from 2.8 to 1.03 min by catalyzing the disulfide metathesis and achieving a balance between the proportion of disulfide bonds and the content of nucleophilic tertiary amines. Creep tests were performed at a wide range of temperatures to investigate the viscosity of the material below and above the T_gs. The topology freezing temperatures were calculated from the creep tests, and T_v values below T_g in all cases confirmed the catalytic effect of tertiary amines on the disulfide exchange reaction.

KEYWORDS

Eugenol, cystamine, bio-based, vitrimers, disulfide, internal catalysis.

1. Introduction

Facing one of the most severe environmental problems today, which is the contamination of land and seas with plastic waste, the appearance of covalent adaptable networks (CANs) was a way to alleviate this problem [1]. Introducing exchangeable groups in the three-dimensional network of thermosets allows their reuse and recycling, significantly reducing the need for landfill disposal. The literature includes many chemically exchangeable groups; among them disulfide group is one of the most employed type of exchangeable group [2,3].

Although Tobolsky *et al*. noticed the possibility of stress relaxation in vulcanized rubbers in the 1960s [4,5], disulfide vitrimers were developed from the pioneering work of Klumperman's group [6,7]. They demonstrated that the dynamic exchange reactions based on the disulfide bonds could be applied in the self-healing of epoxy-thiol thermosets, restoring their mechanical properties since disulfide exchange can be activated at a moderate temperature without the need for any catalysts. However, they concluded the limited applicability of the healing ability to low-T_g materials. After these studies, several authors included S-S bonds to the network structure to get reshapable and recyclable vitrimeric materials. Odriozola *et al.* reported the repairability, reprocessability, and recyclability of high T_g fiber-reinforced epoxy composites containing disulfide moieties [8]. Starting from commercially available DGEBA and 4-aminophenyl disulfide (4AFD), they obtain comparable mechanical performance to conventional materials.

Zhang *et al*. proved the effectiveness of tri-n-butyl phosphine in promoting the metathesis in disulfide epoxy networks. The reprocessed polymers showed self-healing ability and similar mechanical properties to the original materials [9]. Thus, due to the relatively weak S-S- bond, disulfides are the favorite dissociative links to improve self-healing properties of materials at mild temperatures [10].

Many studies focused on the disulfide exchange mechanism [11]. It was demonstrated that phosphines catalyzed disulfide metathesis. By quantum chemical studies, they determined that the rate-determining step is the nucleophilic attack of the phosphine to a sulfur, forming a thiolate and a R_3P^+ $^-$SR cation. The reverse reaction is very fast and forms the catalyst and the disulfide bond [12]. In general, when nucleophiles are present in the material, there is an acceleration of the relaxation phenomena [13,14]. The homolytic cleavage of the disulfide bond followed by subsequent radical transfer of sulfur-based radicals has also been confirmed [15]. The presence of carbon radicals, nucleophiles or free thiols affect the kinetics of disulfide exchange, and the mechanism can be dissociative or associative [16].

It is known that depending on the exchange mechanism, CANs can be divided into two main groups: dissociative or associative. In the first case, the mechanism goes through

a dissociative pathway, meaning that a bond is broken and then formed in another place producing a sudden drop in the viscosity caused by the loss of the crosslinking density. In the second case, the bond exchange is produced in a concerted manner, without losing network integrity and with a gradual decrease of the viscosity with temperature [17]. This type of CANs is also named vitrimers because of their similar behavior with vitreous silica [1]. Nevertheless, there are also some exchange reactions that even being dissociative, the reforming of the bond is extremely fast, which from a physical point of view, a gradual decrease of the viscosity with temperature takes place following the Arrhenius law like vitrimers. These specific characteristics have been ascribed to vitrimer-like materials reported by Dichtel *et al.* [18].

Polysulfide materials could be self-healed and repaired through disulfide metathesis at room temperature when tributyl phosphine, pyridine, or triethylamine were used as catalysts [13]. However, using low-molecular-weight catalysts to accelerate the exchange reactions in vitrimeric materials presents some drawbacks since they can be exuded during the curing process, contaminating the environment. In addition, they can be easily eliminated at the high temperatures used in recycling and reshaping, reducing the catalytic effect. For this reason, it has been proposed the inclusion of nucleophiles, like tertiary amines, in the dynamic network structure [19]. In this field, Yamawake and co-workers reported the effects of internal tertiary amines on a disulfide crosslinked network [20]. They could see an enhancement on the creep resistance as well as in stress relaxation times when internal tertiary amines were incorporated in the polymer structure.

Using bio-based monomers in preparing recyclable thermosets is another excellent contribution to the sustainability of our planet. Most monomers are prepared from non-renewable fossil fuels that can be exhausted relatively quickly and contribute to global CO_2 emissions. The use of lignin [21], vanillin [22-24], eugenol [25], or phloroglucinol [26], among others, has been explored because the functional groups present in these products allow the synthesis of epoxy monomers. Recent reviews have been published highlighting the potential of these biomass-derived structures [22,27]. Some of these monomers were further reacted with 4-aminophenyl disulfide (4AFD), a commercially available disulfide source [22]. However, this aromatic diamine is not bio-based. As a bio-based disulfide containing amine, cystamine has been used. It is commercially available as a salt, but the corresponding amine can be obtained by extraction with a base. Torkelson *et al.* used this amine to cure epoxy novolac, obtaining a series of adaptative thermoset adhesives. The presence of the exchangeable S-S group allowed a significant enhancement in adhesive performance [28]. Recently, Guerre and co-workers also used cystamine as a crosslinker for the vanillin-based epoxy monomers. They use different proportions of cystamine and 4AFD to prepare different materials and could prove that the presence of the aliphatic

hardener not only favors the curing kinetics but also the exchange process reducing the relaxation time ($\tau_{0.37}$) from 23 min to 22 s by changing the aromatic to the aliphatic amine [29].

The present article is devoted to preparing vitrimers from diepoxyeugenol, previously synthesized, and cystamine by a conventional epoxy-amine polycondensation. We have added to the formulation different proportions of tris(2-aminoethyl) amine (TREN) to increase the crosslinking density of the network structure and to increase the proportion of tertiary amines that can act as a catalyst in the disulfide exchange process, thus expecting to increase the relaxation process notably.

2. Experimental methods

2.1 Materials

Eugenol (EU), (±)-epichlorohydrin (ECH), benzyl trimethylammonium chloride (BTMA), acetic acid anhydride (AcAA), m-chloroperbenzoic acid (MCPBA), cystamine hydrochloride and tris(2-aminoethyl) amine (TREN) were purchased from Sigma-Aldrich.

Sodium hydroxide (granulated), sodium bicarbonate, potassium hydroxide, sodium chloride, magnesium sulphate and absolute ethanol (EtOH) were purchased from Scharlau. Dichloromethane (DCM), ethyl acetate and ethyl ether (Et_2O) were obtained from VWR Chemicals. All the reagents were used as received.

2.2 Preparation of acetyl eugenol (AcEU)

The synthesis of the diepoxy eugenol (DEPOEU) was made according to a reported procedure [30]. In a 250 mL three-neck round bottom flask equipped with a magnetic stirrer, thermometer, and reflux condenser, eugenol (16.4 g, 0.1 mol) and acetic anhydride (15.3 g, 0.15 mol) were reacted at 80 °C for 24 h. Once finished, ethyl ether was added, and the solution extracted twice with concentrated aqueous solutions of $NaHCO_3$ and NaCl. The organic layer was dried over anhydrous $MgSO_4$, and the solvent eliminated in a rotary evaporator. The pale orange viscous oil product (19.2 g, yield 93 %) was used in the following step without any further purification.

^{1}H NMR ($CDCl_3$; δ, ppm): 6.95 (d, 1H); 6.78 (m, 2H); 5.97 (m, 1H); 5.11 (m, 2H); 3.82 (s, 3H); 3.38 (d, 2H); 2.31 (s, 3H) (see Figure 8.S1).

^{13}C NMR ($CDCl_3$; δ, ppm): 169.40, 150.95, 139.12, 138.09, 137.15, 122.62, 120.78, 116.26, 112.77, 55.90, 40.22, 20.82 (see Figure 8.S2).

Eur. Polym. J. **2023**, *194*, 112185

2.3 Synthesis of epoxy acetyl eugenol (EpAcEU)

The epoxidation of the allyl group of AcEU was done with MCPBA. In a 500 mL three-necked flask equipped with magnetic stirrer and ice bath, 17.6 g (0.085 mol) of AcEU were dissolved in 20 mL of DCM and then a solution of 30.4 g (0.13 mol) of MCPBA in 300 mL of DCM was added dropwise. The reaction was maintained at 0 °C for 24 h after complete disappearance of AcEU. The resulting DCM solution was extracted with a solution of $NaHSO_3$, then with concentrated aqueous solutions of $NaHCO_3$ and NaCl. The organic layer was dried over anhydrous $MgSO_4$, and the solvent eliminated in a rotary evaporator. EpAcEU was obtained as a viscous oil in a 95% of yield (18.0 g).

^{1}H NMR ($CDCl_3$; δ, ppm): 6.96 (d, 1H); 6.84 (m, 2H); 3.81 (s, 3H); 3.14 (m, 1H); 2.83 (d, 2H); 2.79 (t, 1H); 2.54 (dd, 1H); 2.29 (s, 3H) (see Figure 8.S3).

^{13}C NMR ($CDCl_3$; δ, ppm): 169.27, 151.07, 138.58, 136.35, 122.78, 121.19, 113.29, 56.00, 52.45, 46.95, 38.76, 20.75 (see Figure 8.S4).

2.4 Preparation of diepoxy eugenol (DEPOEU)

In a 250 mL round-bottomed flask equipped with reflux condenser and magnetic stirrer, 15.6 g of EpAcEU (0.07 mol) were dissolved in 45.3 g (0.49 mol) of epichlorohydrin. To this mixture, 5.6 g of NaOH (0.14 mol) in 30 mL of EtOH was added and the resulting solution was heated at 85 °C for 4 h and then left cooling to room temperature. Ethyl ether was added, and the salt formed removed by extraction with water. Then, the solution was dried over $MgSO_4$ anhydrous, filtered and ethyl ether removed in a rotary evaporator. The solid product obtained was purified by silica-gel column with a gradient hexane/ethyl acetate eluent: 4:1, 3:1, 2:1, and 1:1. The yield of the product after purification was 65 %. Melting point was 55.6 °C (by DSC).

^{1}H NMR ($CDCl_3$; δ, ppm): 6.87 (d, 1H); 6.77 (m, 2H); 4.22 (dd, 1H); 4.02 (dd, 1H); 3.86 (s, 3H); 3.37 (m, 1H); 3.12 (m, 1H); 2.87 (t, 1H); 2.79 (m, 3H); 2.73 (dd, 1H); 2.53 (dd, 1H) (see Figure 8.S5).

^{13}C NMR ($CDCl_3$; δ, ppm): 149.60, 146.85, 131.07, 121.07, 114.34, 112.88, 70.44, 56.02, 52.65, 50.36, 46.9, 45.04, 38.40 (see Figure 8.S6).

FTIR (ATR): 1600 cm^{-1} (Aromatics); 910 cm^{-1} (stretching glycidyl band); 835 cm^{-1} (stretching epoxide) (see Figure 8.S7).

2.5 Preparation of the cystamine (Cys)

For the preparation of Cys, 8.0 g of cystamine dihydrochloride and 6.0 g of KOH were dissolved in 100 mL of distilled water. After stirring for 30 min at room temperature, the resulting mixture was extracted four times with DCM. The organic layers were combined, dried over anhydrous $MgSO_4$, and filtered. DCM was removed using a

rotary evaporator obtaining 4.0 g of a yellowish viscous oil called cystamine (Cys). The pure cystamine must be used immediately after being obtained or it must be kept in a fridge.

^{1}H NMR ($CDCl_3$; δ, ppm): 2.95 (t, 4H); 2.70 (t, 4H); 1.28 (s, 4H) (see Figure 8.S8).

^{13}C NMR ($CDCl_3$; δ, ppm): 42.55, 40.60 (see Figure 8.S9).

2.6 General procedure for the preparation of vitrimeric samples

A series of the disulfide vitrimers were obtained according to the following procedure: DEPOEU was melted in a vial by heating at 65 °C. Then, the stoichiometric amount of mixtures in several proportions of Cys and TREN was added to the vial and the mixture was homogenized. The viscous mixture was poured into a Teflon mold with dimensions of 30 x 5 x 1.5 mm^3 and cured in an oven for 3 h at 100 °C, 1 h at 120 °C and 1 h at 150 °C to obtain transparent solid rectangular samples. The materials were coded as X% Cys, where X% means that X% of epoxides react with X% of NH groups coming from cystamine and (100-X) % of epoxides react with N-H groups coming from TREN. In all samples, the stoichiometric epoxy/NH ratio was maintained.

2.7 Characterization methods

^{1}H NMR and ^{13}C NMR spectra were registered in a Varian VNMR-S400 NMR spectrometer. $CDCl_3$ was used as a solvent. All chemical shifts are quoted on the δ scale in part per million (ppm) using residual protonated solvent as internal standard (^{1}H NMR: $CDCl_3$ = 7.26 ppm; ^{13}C NMR: $CDCl_3$ = 77.16 ppm).

DSC analyses were carried out on a Mettler DSC3+ instrument calibrated using indium (heat flow calibration) and zinc (temperature calibration) standards. Samples of approximately 8-10 mg were placed in aluminum pans with pierced lids and analyzed in an N_2 atmosphere with a glass flow of 50 cm^3 min^{-1}. Dynamic studies between 30 and 250 °C at a heating rate of 10 °C min^{-1} were performed to determine the melting points. For the determination of the T_gs of the final materials, dynamic experiments from 30 to 250 °C using a heating rate of 20 °C min^{-1} were performed.

A Jasco FT/IR-680 Plus spectrometer equipped with an attenuated total reflection accessory (ATR) (Golden Gate, Specac Ltd, Teknokroma) was used to record the FTIR spectra of the mixture before and after the curing procedure. Real-time spectra were recorded in the wavenumber range between 4000 and 600 cm^{-1} with a resolution of 4 cm^{-1} and averaged over 20 scans. The disappearance of the characteristic absorbance peaks of epoxy group at 915 and 830 cm^{-1} as well as the appearance of the peak corresponding to O-H at 3300 cm^{-1} were used to confirm the completion of the reaction.

The thermal stability of the materials was evaluated using a Mettler Toledo TGA 2 thermobalance. Cured samples weighing around 10 mg were degraded between 30

Eur. Polym. J. **2023**, *194*, 112185

and 600 °C at a heating rate of 10 °C min^{-1} in N_2 atmosphere with a flow of 50 cm^3 min^{-1}.

The thermomechanical properties were studied using a DMTA Q800 (TA Instruments) equipped with a film tension clamp. Prismatic rectangular samples with dimensions around 30 x 5 x 1.5 mm^3 were analyzed from 0 °C to 200 °C at 1 Hz, with 0.1% strain at a heating rate of 2 °C min^{-1}. Tensile stress-relaxation tests were conducted in the same instrument using the film tension clamp on samples with the same dimensions as previously defined. The samples were firstly equilibrated at the relaxation temperature for 5 min, and a constant strain of 1% was applied, measuring the consequent stress level as a function of time. The materials were tested only once at one temperature. The relaxation-stress $\sigma(t)$ was normalized by the initial stress σ_0, and the relaxation times (τ) were determined as the time necessary to relax $0.37\sigma_0$, i.e., ($\sigma = 1/e\sigma_0$). With the relaxation times obtained at each temperature, the activation energy values (E_a), were calculated by using an Arrhenius-type equation:

$$\ln(\tau) = \frac{E_a}{RT} - \ln A \qquad \text{(Eq.8.1)}$$

where τ is the time needed to attain a given stress-relaxation value ($0.37\sigma_0$), A is the pre-exponential factor, and R is the gas constant.

To determine the viscosity at each temperature needed for the representation of the Angell Fragility plot, a series of creep experiments were carried out on films at temperatures between 10 °C and 190 °C, increasing 10 °C in each scan. To perform the tests, the selected temperature was equilibrated for 3 min, and then a stress level of 0.1 MPa was applied for 30 min. The viscosity η (Pa·s) was then obtained from the strain-time graphs. First, the strain rate $\dot{\varepsilon}$ was determined from the slope of the graph, and the viscosity was calculated using the following equation:

$$\eta = \frac{\sigma}{\dot{\varepsilon}} \qquad \text{(Eq.8.2)}$$

where σ is the stress applied during the test and $\dot{\varepsilon}$ the strain determined from the inverse of the slope of the strain-time curves. The viscosity was then plotted in front of the temperature, and the topology freezing temperature (T_v) was extrapolated by assuming that the viscosity at this temperature is 10^{12} Pa·s.

Finally, the Angell Fragility plot was represented by plotting the viscosity in front of T_v/T where the T_v is the one previously obtained.

3. Results and discussion

3.1 Synthesis of the diepoxy eugenol (DEPOEU)

DEPOEU was prepared *via* a three-step procedure, as reported in the literature [30]. Scheme 8.1 depicts the synthetic way adopted for synthesizing this product and the intermediates and the conditions of each step.

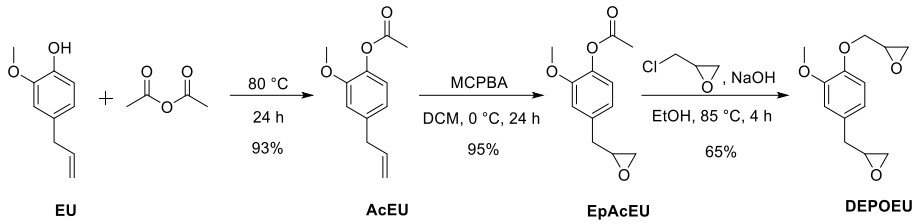

Scheme 8.1. Synthetic steps and reaction conditions used in the preparation of DEPOEU.

As we can see, there is an initial acetylation of the phenol group that protects it from undesired oxidation. Quin et al attempted the direct route of a first epoxidation of the allyl group, but the reaction mixture turned deep colored due to the possible conversion of phenol to quinone [30]. For this reason, they adopt this three-step synthetic process. Although we followed the same procedure, some experimental changes were introduced to improve the yield and purity of the intermediate and final compounds. All the synthetic intermediates and the final DEPOEU were characterized by NMR spectroscopy, and the corresponding spectra are collected in the SI.

Alternatively, the epoxidation of the allyl group of AcEU could be performed by the oxone method, which is more environmentally friendly than with MCPBA. In a previous work of our group, a triepoxy eugenol derivative was synthesized with good yields by this methodology [31]. However, the use of MCPBA to obtain EpAcEU resulted in a higher yield.

3.2 Study of the curing procedure

The synthesized DEPOEU was cured with stoichiometric proportions of mixtures of Cys and TREN as amines of different functionality. Scheme 8.2 collects the chemical structure of both primary amines. The composition of the formulations is detailed in Table 8.1.

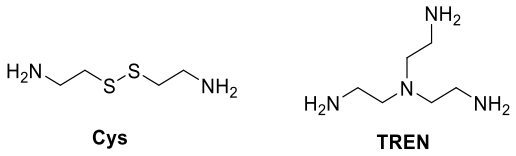

Scheme 8.2. Chemical structure of the amines used as curing agents.

Eur. Polym. J. **2023**, *194*, 112185

Although adding TREN to the curing formulation reduces the proportion of exchangeable disulfide moieties, it also changes the crosslinking density and, consequently, some thermomechanical properties. In addition, the presence of the central nitrogen in the TREN structural unit can act as a catalyst. It has been established that the mechanical properties can be entirely restored after recycling, if 40 mol % of permanent crosslinks are included in the network structure [32]. Accordingly, we hypothesize that the addition of a certain proportion of TREN could not be detrimental to the relaxation process.

Table 8.1. Composition of all the vitrimeric materials prepared.

Sample	DEPOEU		Cys		TREN	
	wt (%)	mmol	wt (%)	mmol	wt (%)	mmol
100%Cys	76.0	4.23	24.0	2.12	-	-
85%Cys	76.6	4.23	21.0	1.80	2.4	0.21
75%Cys	77.3	4.23	18.7	1.59	4.0	0.35
65%Cys	78.0	4.23	16.4	1.38	5.6	0.49
50%CyS	79.1	4.23	12.7	1.05	8.2	0.71

The curing process was investigated by DSC and the enthalpy released was around 95-100 kJ/eq, which the typical for an epoxy-amine reaction [33,34]. The curing exotherm reached a maximum at 110 °C (Figure 8.S10). Based on these results, the curing schedule selected was 3 h at 100 °C, 1 h at 120 °C and 1h at 150 °C.

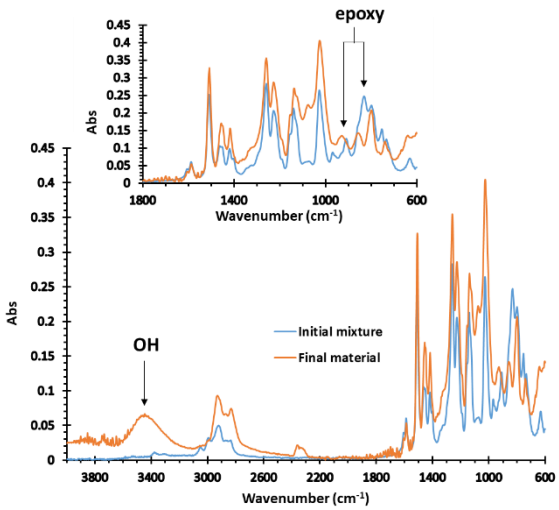

Figure 8.1. FTIR-ATR spectra of the 100%Cys initial mixture (blue) and final material (orange).

The completion of the curing was confirmed by successive DSC scans to see if there is an increase in T_g and by FTIR. FTIR spectra of the initial mixture of 100%Cys and the corresponding final material is shown in Fig. 8.1, where we can see the disappearance of the epoxy bands at 915 and 835 cm^1 and the broad absorption around 3400 cm^{-1} due to the formation of the OH groups.

3.3 Thermal characterization of the materials

Once cured, the materials obtained were first characterized by DSC. As expected, increasing the proportion of TREN to the formulation led to an increase in the T_g values. Table 8.2 collects the T_gs of all the materials prepared. The DSC traces are shown in Figure 8.S11.

The thermal stability of the vitrimeric materials was determined by thermogravimetry. Fig. 8.2 shows the TGA curves and their derivatives for the materials prepared, and Table 8.2 presents the most significant data extracted.

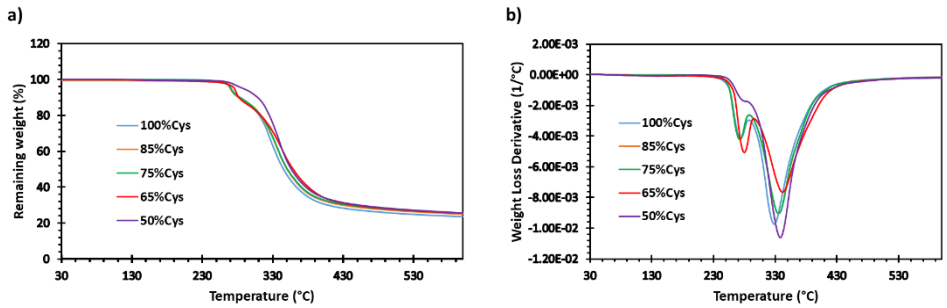

Figure 8.2. (a) Thermogravimetric analysis (TGA) curves and (b) DTG curves of the vitrimeric materials prepared.

Table 8.2. Glass transition temperature by DSC, temperature of initial degradation, temperatures of the maximum degradation rate and residue at 600 °C.

Sample	T_g (°C)	$T_{1\%}$[a] (°C)	$T_{2\%}$[b] (°C)	T_{max}[c] (°C)	Char Yield (%)
100%Cys	74.9	210.1	244.1	273.8/328.0	23.2
85%Cys	80.9	213.8	250.1	272.9/335.2	25.3
75%Cys	84.9	225.0	263.8	272.5/335.5	25.5
65%Cys	90.2	235.4	268.9	277.0/341.8	25.6
50%Cys	102.9	250.6	270.6	273.4/338.2	25.7

[a] Temperature of 1% weight loss. [b] Temperature of 2% weight loss. [c] Temperature of the two maximum rates of degradation. [d] Char residue at 600 °C.

Due to the weakness of S-S bond, the higher its proportion, the faster the degradation at lower temperatures. In all the samples, there is a first degradation step corresponding to the breakage of the S-S bond, while in the second step, there is not much difference among the materials since all the bonds break simultaneously.

The thermogravimetric study confirms that safe relaxation processes can proceed at temperatures below 200 °C.

3.4 Thermomechanical characterization of the materials

The thermomechanical characteristics of the materials were determined by DMTA. Figure 8.3 shows the evolution of the storage moduli and tan δ curves with the temperature for all the materials prepared, and Table 8.3 collects the main parameters extracted from these studies.

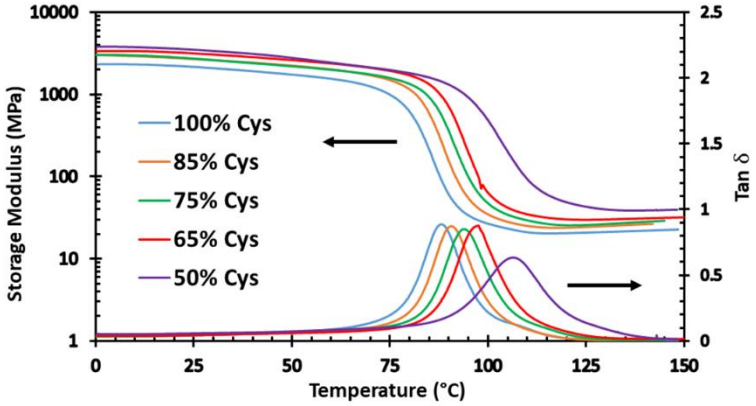

Figure 8.3. Evolution of storage modulus and tan δ with the temperature for all the materials.

Table 8.3. Main thermomechanical parameters obtained for the different materials.

Sample	E'_{glassy}[a] (MPa)	$E'_{rubbery}$[b] (MPa)	$T_{tan\,\delta}$[c] (°C)	FWHM[d] (°C)
100%Cys	1890	21.9	88.2	12.5
85%Cys	2330	26.4	90.7	12.9
75%Cys	2420	28.8	93.9	13.7
65%Cys	2550	31.7	97.6	18.8
50%Cys	2670	39.6	106.4	24.6

[a] Storage modulus in the glassy state at T_g -50 °C. [b] Storage modulus in the rubbery state at T_g + 50 °C. [c] Temperature of the maximum of the of tan δ peak.[d] Full width at the half height of tan δ peak.

As it can be seen, all materials exhibit high T_g values (taken from the maximum of the $T_{\tan\delta}$ peak) ranging from 88 °C for 100%Cys to 106 °C for 50%Cys. As expected, the higher the proportion of cystamine in the material, the lower the $T_{\tan\delta}$ since it has a longer chain and fewer possible crosslinking points, providing more flexibility to the networks. Moreover, when the proportion of Cys is decreased, the E'_{glassy} increases due to the higher proportion of TREN in the samples making the materials more rigid. The same trend can be observed in the $E'_{rubbery}$ since the higher functionality of TREN increases the storage moduli in the rubbery state, which is directly connected to the crosslinking density of the material. Looking at the shape of the tan δ curves and the low values of FWHM, it can be deduced that all the materials present homogeneous and fast transitions. The material with 50%Cys, with a slightly broader (higher FWHM) and less intensity (lower height of tan δ peak) indicates its more crosslinked structure.

3.5 Study of the vitrimeric behavior of the materials

Cystamine contains disulfide bonds in its structure, so it is expected to provide final materials with vitrimeric properties through the disulfide metathesis reaction at high temperatures. To investigate the time and temperature-dependent relaxation, stress relaxation tests at different temperatures for all materials were performed in the DMTA. The results for each material are shown in Figures 8.S12-S16, and the data is presented in Table 8.4. As a mode of comparison, stress relaxation curves for all materials at 170 °C are represented in Figure 8.4.

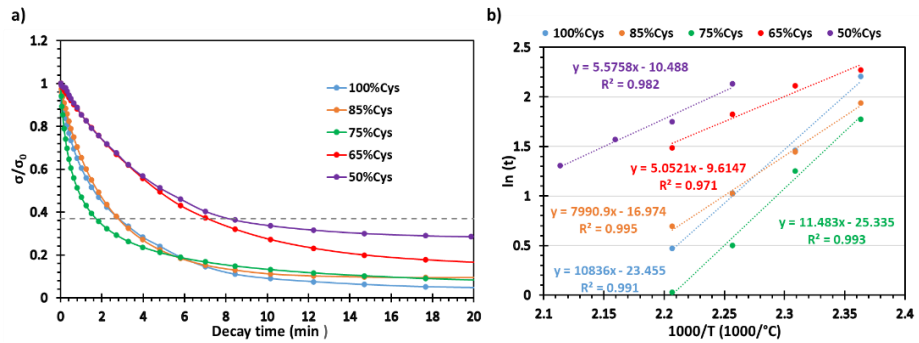

Figure 8.4. a) Normalized stress relaxation curves as a function of time for all the materials prepared at 170 °C. b) Arrhenius plots for the relaxation times with the inverse of temperature for all samples.

As shown in Figure 8.4a, intriguing results were obtained regarding the relaxation times of the samples. The main data extracted from these tests are presented in Table 8.4. 100%Cys material presents the highest proportion of disulfide bonds in its structure, so it is likely the one that should relax the initial stress in a faster way. Indeed, it only needs 2.8 minutes to achieve the $0.37\sigma_0$. However, it was observed

Eur. Polym. J. **2023**, *194*, 112185

that when the proportion of Cys is slightly reduced, faster relaxation times are achieved, being 2.75 min for 85%Cys and 1.03 min for 75%Cys. This decrease in the relaxation times can be ascribed to the catalytic effect of the tertiary amines on the disulfide metathesis exchange. When the amount of TREN in the samples increases, the concentration of tertiary amines in the materials is higher because TREN contains four tertiary amines in its structure while cystamine only has two. It is worth highlighting that a maximum is reached in the 75%Cys material where the concentration of disulfide bonds is still high to get a fast relaxation but, at the same time, the content of tertiary amines in the network is high enough to increase the catalytic effect on the disulfide metathesis. Nevertheless, when the proportion of Cys is lowered, a detrimental effect in the relaxation times can be noticed since the amount of disulfide bonds is relatively low, even containing a higher proportion of internal tertiary amines. Moreover, one can notice that even though the 75%Cys material can relax the 63% of the initial stress faster, it cannot achieve complete relaxation since the percentage of permanent crosslinks is relatively high. In this case, the higher proportion of cystamine in the material, the fewer permanent crosslinks in the network and, therefore, the more able to fully relax the initial stress.

A linear relationship between temperature and viscosity is established when the exchange reactions occur in the materials network. For this reason, the stress relaxation times at different temperatures, when the materials relax the 63% of the initial stress, were obtained from Figures 8.S12-S16. They all follow an Arrhenius-type dependence, like vitrimers, which allows calculating the activation energy (E_a) and the ln A. These values are also presented in Table 8.4 and the plot is represented in Figure 8.4b.

Table 8.4. Relaxation time, activation energy and adjusting parameters from Arrhenius plot.

Material	$\tau_{0.37}$[a] (min)	E_a (kJmol^{-1})	ln A (min)	r^2	$T_{v\,(\eta)}$[b] (°C)	$T_{v\,(An)}$[c] (°C)	n[d]
100%Cys	2.80	85.7	22.26	0.991	66.7	77.0	7.12
85%Cys	2.75	81.5	21.19	0.995	67.1	60.1	4.82
75%Cys	1.03	95.5	25.34	0.993	34.2	26.8	3.04
65%Cys	6.30	41.1	9.61	0.971	57.5	57.6	3.09
50%Cys	8.44	42.9	10.49	0.983	54.4	59.4	1.77

[a] Time reach a value of σ/σ_0 = 0.37 at 170 °C. [b] Topology freezing temperature calculated by extrapolation of the η-T curves. [c] Topology freezing temperature calculated by extrapolation from the adjusting of the Angell fragility plot. [d] Fragility index (n_{silica} = 16.5).

As seen in Table 8.4, the behavior of all the materials fit the Arrhenius equation with different E_a values depending on the network composition. 75%Cys material has the

highest activation energy showing a high dependence between the relaxation times and the temperature, meaning that a slight temperature change significantly affects the relaxation time, which is in accordance with the high content in tertiary amines and disulfide bonds.

The effect of the temperature on the viscosity was also studied through creep tests at different temperatures in DMTA for all the materials. Creep tests from temperatures far below the T_g of the materials to far above were performed on all the materials. The viscosity (inverse of the slope of the ε·t curves) was plotted versus the temperature for all cases. (Figures 8.S17-S21).

As seen in these figures, all materials show the same trend where, well below the onset of the glass transition, the viscosity of the vitrimers follows a somehow linear behavior with temperature. During the transition of the T_g, the bond exchange can be described via William-Landel-Ferry (WLF) behavior as the network rearrangement kinetics is diffusion-controlled and segmental motions dominate network rearrangement [35,36]. After that, with a further temperature increase, the exchange kinetics change to an exchange reaction-controlled regime. Consequently, the disulfide metathesis again follows a linear Arrhenius law in all cases. The topology freezing temperature (T_v) of all materials can be calculated from these plots since, by a physical definition, is the temperature at which the material reaches a viscosity of 10^{12} Pa·s. All T_vs were calculated by extrapolation from the graphs and are depicted in Table 8.4. As shown in the table, all the materials presented T_v values below T_gs which is consequent with the viscosity behavior obtained for all these vitrimers [37,38]. On the other hand, the T_v can also be ascribed to the temperature below which the exchange mechanisms are almost negligible [1]. 75%Cys material has the lowest topology freezing temperature, which fits with the evidence that a compromise between the concentration of disulfide bonds in the network and the proportion of tertiary amines enhances the exchange reaction. In addition, it should be highlighted that when the content of internal tertiary amines is increased in the network (50%Cys and 65%Cys) the T_v is lower than in the materials with almost no TREN content (100%Cys and 85%Cys), demonstrating a high dependence of the T_v with the internal load of catalysts.

From the results obtained in the creep tests, the Angell fragility plots can also be represented (Figure 8.5). As it is known, at higher temperatures, the chemical exchange reactions control the viscosity of the vitrimers, thus producing its gradual decrease as the temperature increase and following an Arrhenius law, similar to inorganic silica materials. On the other hand, dissociative CANs and thermoplastics evolve abruptly from a solid to a liquid state with a sudden viscosity drop when the temperature increases. In our case, all the materials experienced a gradual decrease in viscosity, meaning that they present vitrimeric-like properties [39]. It has been

Eur. Polym. J. **2023**, *194*, 112185

reported that the S-S exchange mechanism can also be performed by the attack of a thiolate anion which can be generated in the presence of a tertiary amine and the consequent nucleophilic attack of this thiolate on another disulfide bond further generating another thiolate [20]. This mechanism may provide an associative pathway to exchange process which is in accordance with the vitrimer-like behavior observed in our materials in the Angell Fragility plot. These results indicate that even the mechanism of disulfide metathesis is purely dissociative, when tertiary amines are covalently attached to the network, the mechanism may follow an associative mechanism. This can explain the gradual decrease in the viscosity with temperature in our materials, thus behaving like vitrimer-like polymers. It is important to highlight the novelty of present studies, which were performed on bio-based materials that were cured with aliphatic amines containing aliphatic disulfide bonds. Even so, these results are in accordance with previous studies in aromatic disulfide materials performed by Rekondo and co-workers, who reported a similar trend in their materials [14].

Finally, the T_vs from the linear equations deduced from the Angell plot can also be calculated by assuming that the materials reach a viscosity of 10^{12} Pa·s and therefore, $\log(\eta_{(Tv)}) = 12$. The values extracted from these extrapolations are shown in Table 8.4. Logically, all T_vs were very similar to those ones obtained from creep tests.

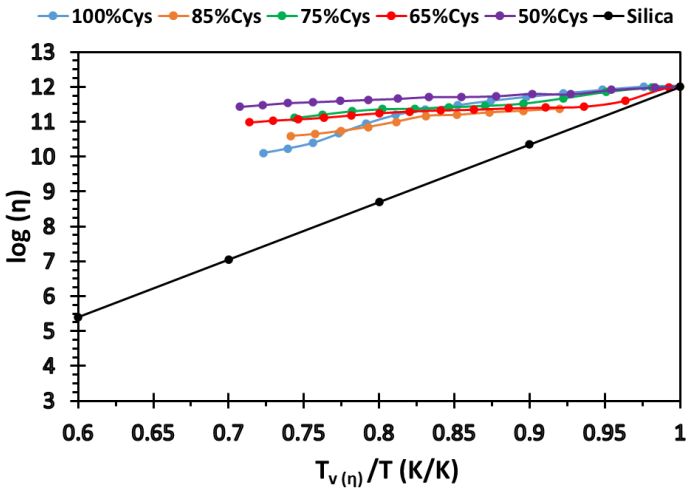

Figure 8.5. Angell fragility plots for all the materials prepared.

4. Conclusions

A bio-based diepoxy eugenol (DEPOEU) derivative was synthesized via a three-step method and crosslinked with varying proportions of cystamine and TREN via an epoxy-

amine condensation reaction. FTIR analysis confirmed successful curing and completion of the reaction. The resulting materials exhibited high thermal stability ($T_{1\%}$ > 210 °C) and T_gs ranging from 74.9 °C (for the 100%Cys) to 102.9 °C (for the 50%Cys).

The exchange reaction was facilitated by the disulfide bonds of cystamine, with the addition of TREN enhancing the exchange rate. All materials could rapidly relax the 63% of the initial stress in less than 8.5 min. Interestingly, even the 100%Cys material that relaxes more is not the one with lower relaxation rates. The addition of TREN and, therefore, the increase of tertiary amines in the crosslinked structure catalyzes the exchange reaction. The 75%Cys material demonstrated the optimal balance of S-S bonds and tertiary amines, exhibiting the fastest relaxation rate of 63% in just 1.03 min.

The topology freezing temperature (T_v) was calculated via creep tests, being below T_g in all cases. The 75%Cys material exhibited the lowest T_v, evidencing the compromise mentioned above. The Angell fragility plot also revealed the vitrimeric behavior of all the materials. Overall, these results suggest that the DEPOEU-based materials have great potential as vitrimers for use in a great variety of applications, such as coatings, adhesives, and composite materials.

Acknowledgments

This work is part of the R&D projects PID2020-115102RB-C21 and TED2021-131102B-C22funded by MCNI/AEI/10.13039/501100011033 and European Union NextGenerationEU"/PRTR. We acknowledge these grants and to the Generalitat de Catalunya (2021-SGR-00154).

References

[1] D. Montarnal, M. Capelot, F. Tournilhac, L. Leibler, Silica-like malleable materials from permanent organic networks, Science 334 (2011) 965-968.

[2] S. Samanta, S. Kim, T. Saito, A.P. Sokolov, Polymers with dynamic bonds: adaptive functional materials for a sustainable future, J. Phys. Chem. B 125 (2021) 9389−9401.

[3] W. Zhang, Y. Jing, Eds. Dynamic Covalent Chemistry. Principles, Reactions, and Applications. Ed. Wiley, 2018, Pondicherry, India.

[4] A. V. Tobolsky, W. J. MacKnight, M. Takahashi, Relaxation of disulfide and tetrasulfide polymers, Phys. Chem. 68 (1964) 787–790.

[5] Y. Takahashi, A. V. Tobolsky, Chemorheological study on natural rubber vulcanizates, Polym. J. 2 (1971) 457–467.

[6] J. Canadell, H. Goossens, B. Klumperman, Self-healing materials based on disulfide links, Macromolecules 44 (2011) 2536–2541.

[7] M. Pepels, I. Filot, B. Klumperman, H. Goossens, Self-healing systems based on disulfide-thiol exchange reactions, Polym. Chem. 4 (2013) 4955–4965.

[8] A. Ruiz de Luzuriaga, R. Martin, N. Markaide, A. Rekondo, G. Cabañero, J. Rodríguez, I. Odriozola, Epoxy resin with exchangeable disulfide crosslinks to obtain reprocessable, repairable and recyclable fiber-reinforced thermoset composites, Mater. Horiz. 3 (2016) 241−247.

[9] Z. Q. Lei, H. P. Xiang, Y. J. Yuan, M. Z. Rong, M. Q. Zhang, Room-temperature self-healable and remoldable cross-linked polymer based on the dynamic exchange of disulfide bonds, Chem. Mater. 26 (2014) 2038−2046.

[10] M. Podgórski, B. D. Fairbanks, B. E. Kirkpatrick, M. McBride, A. Martinez, A. Dobson, N. J. Bongiardina, C. N. Bowman, Toward stimuli-responsive dynamic thermosets through continuous development and improvements in covalent adaptable networks (CANs), Adv. Mater. 32 (2020) 1906876.

[11] N. J. Bongiardina, S. M. Soars, M. Podgórski, C. N. Bowman, Radical-disulfide exchange in thiol-ene-disulfidation polymerizations, Polym. Chem. 13 (2022) 3991-4003.

[12] R. Caraballo, M. Rahm, P. Vongvilai, T. Brinck, O. Ramström, Phosphine-catalyzed disulfide metathesis, Chem. Commun. 46 (2008) 6603–6605.

[13] S. J. Tonkin, C. T. Gibson, J. A. Campbell, D. A. Lewis, A. Karton, T. Hasell, J. M. Chalker, Chemically induced repair, adhesion, and recycling of polymers made by inverse vulcanization, Chem. Sci. 11 (2020) 5537-5546.

[14] A. Ruiz de Luzuriaga, G. Solera, I. Azcarate-Ascasua, V. Boucher, H.J. Grande, A. Rekondo, Chemical control of the aromatic disulfide exchange kinetics for tailor-made epoxy vitrimers, Polymer 239 (2022) 124457.

[15] S. Nevejans, N. Ballard, J. I. Miranda, B. Reck, J. M. Asua, The underlying mechanisms for self-healing of poly(disulfide)s, Phys. Chem. Chem. Phys. 18 (2016) 27577-27583.

[16] A. G. Orrillo, R. L. E. Furlan, Sulfur in Dynamic covalent chemistry, Angew. Chem. Int. Ed. 61 (2022) e202201168.

[17] F. Van Lijsebetten, J. O. Holloway, J. M. Winne, F. E. Du Prez, Internal catalysis for dynamic covalent chemistry applications and polymer science, Chem. Soc. Rev. 49 (2020) 8425-8438.

[18] B. R. Elling, W. R. Dichtel, Reprocessable cross-linked polymer networks: are associative exchange mechanisms desirable?, ACS Cent. Sci. 6 (2020) 1488-1496.

[19] F. I. Altuna, C. E. Hoppe, R. J. J. Williams, Epoxy vitrimers with a covalently bonded tertiary amine as catalyst for the transesterification reaction, Eur. Polym. J. 113 (2019) 297–304.

[20] K. Yamawake, M. Hayashi, The role of tertiary amines as internal catalysts for disulfide exchange in covalent adaptable networks, Polym. Chem. 14 (2023) 680-686.

[21] A. Moreno, M. Morsali, M. H. Sipponen, Catalyst-free synthesis of lignin vitrimers with tunable mechanical properties: circular polymers and recoverable adhesives, ACS Appl. Mater. Interfaces 13 (2021) 57952-57961.

[22] M. A. Rashid, N. Hasan, A. R. Dayan, M. S. I. Jamal, M. K. Patoary, A critical review of sustainable vanillin-modified vitrimers: synthesis, challenge and prospects, Reactions 4 (2023) 66–91.

[23] A. Roig, A. Petrauskaitė, X. Ramis, S. De la Flor, À. Serra, Synthesis and characterization of new bio-based poly(acylhydrazone) vanillin vitrimers, Polym. Chem. 13 (2022) 1510-1519.

[24] A. Roig, P. Hidalgo, X. Ramis, S. De la Flor, À. Serra, Vitrimeric epoxy-amine polyimine networks based on a renewable vanillin derivative, ACS Appl. Polym. Mater. 4 (2022) 9341-9350.

[25] T. Liu, C. Hao, L. Wang, Y. Li, W. Liu, J. Xin, J. Zhang, Eugenol-derived biobased epoxy: shape memory, repairing, and recyclability, Macromolecules 50 (2017) 8588−8597.

[26] A. Genua, S. Montes, I. Azcune, A. Rekondo, S. Malburet, B. Daydé-Cazals, A. Graillot, Build-to-specification vanillin and phloroglucinol derived biobased epoxy-amine vitrimers, Polymers 12 (2020) 2645.

[27] M. A. Lucherelli, A. Duval, L. Avérous, Biobased vitrimers: Towards sustainable and adaptable performing polymer materials, Prog. Polym. Sci. 127 (2022) 101515.

[28] L. Li, X. Chen, J. M. Torkelson, Covalent adaptive networks for enhanced adhesion: exploiting disulfide dynamic chemistry and annealing during application, ACS Appl. Polym. Mater. 2 (2020) 4658−4665.

[29] S. Guggari, F. Magliozzi, S. Malburet, A. Graillot, M. Destarac, M. Guerre, Vanillin-based epoxy vitrimers: Looking and the cystamine hardener form a different perspective, ACS Sustainable Chem. Eng. 11 (2023) 6021-6031.

[30] J. Qin, H. Liu, P. Zhang, M. Wolcott, J. Zhang, Use of eugenol and rosin as feedstocks for biobased epoxy resins and study of curing performance properties, Polym. Int. 63 (2014) 760–765.

[31] D. Guzmán, X. Ramis, X. Fernández-Francos, S. De la Flor, A. Serra, Preparation of new biobased coating from a triglycidyl eugenol derivative through thiol-epoxy click reaction, Prog. Org. Coat. 114 (2018) 259–267.

[32] L. Li, X. Chen, K. Jin, J. M. Torkelson, Vitrimers designed both to strongly suppress creep and to recover original cross-link density after reprocessing: quantitative theory and experiments, Macromolecules 51 (2018) 5537–5546.

[33] K. J. Ivin, in: J. Brandrup, E.H. Immergut (Eds.) Polymer Handbook, Wiley, New York, 1975.

[34] A. Roig, X. Ramis, S. De la Flor, À. Serra, Dual-cured thermosets from glycidyl methacrylate obtained by epoxy-amine reaction and methacrylate homopolymerization, React. Funct. Polym. 159 (2021) 104822.

[35] M. T. Shaw, W. J. MacKnight, Introduction to Polymer Viscoelasticity; Wiley: Hoboken, NJ, USA, 2005.

[36] L. H. Sperling, Introduction to Physical Polymer Science, Wiley: Hoboken, NJ, USA, 2005.

[37] B. Krishnakumar, R. V. S. P. Sanka, W. H. Binder, V. Parthasarthy, S. Rana, N. Karak, Vitrimers: associative dynamic covalent adaptive networks in thermoset polymers, Chem. Eng. J. 385 (2020) 123820.

[38] Y. Nishimura, J. Chung, H. Muradyan, Z. Guan, Silyl ether as a robust and thermally stable dynamic covalent motif for malleable polymer design, J. Am. Chem. Soc. 139 (2017) 14881-14884.

[39] W. Denissen, J. M. Winne, F. E. Du Prez, Vitrimers: permanent organic networks with glass-like fluidity, Chem. Sci. 7 (2016) 30-38.

Supporting Information

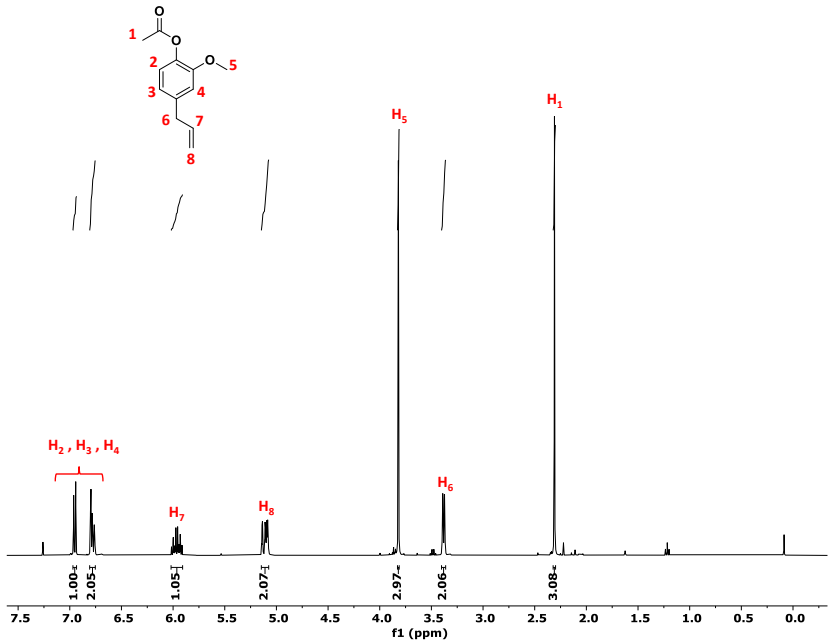

Figure 8.S1. ^{1}H NMR spectrum of acetyl eugenol (AcEU) in $CDCl_3$.

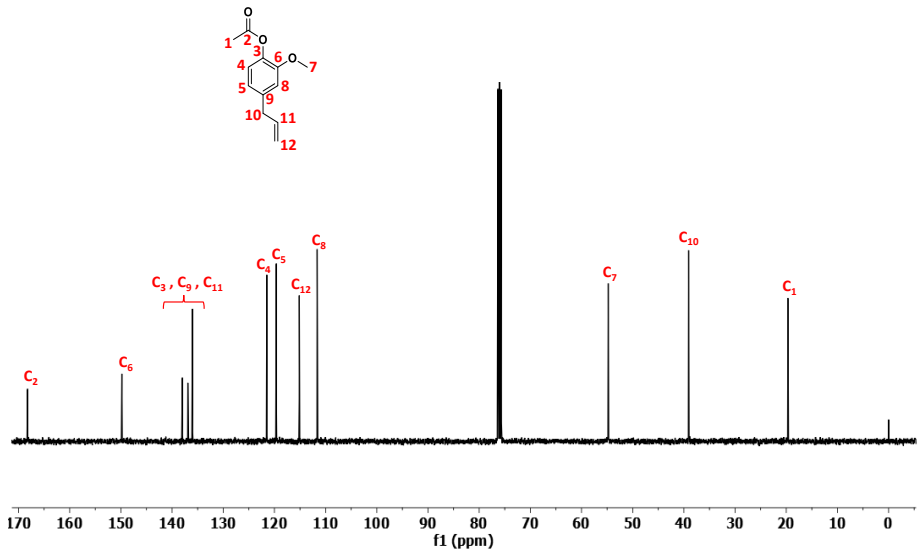

Figure 8.S2. ^{13}C NMR spectrum of acetyl eugenol (AcEU) in $CDCl_3$.

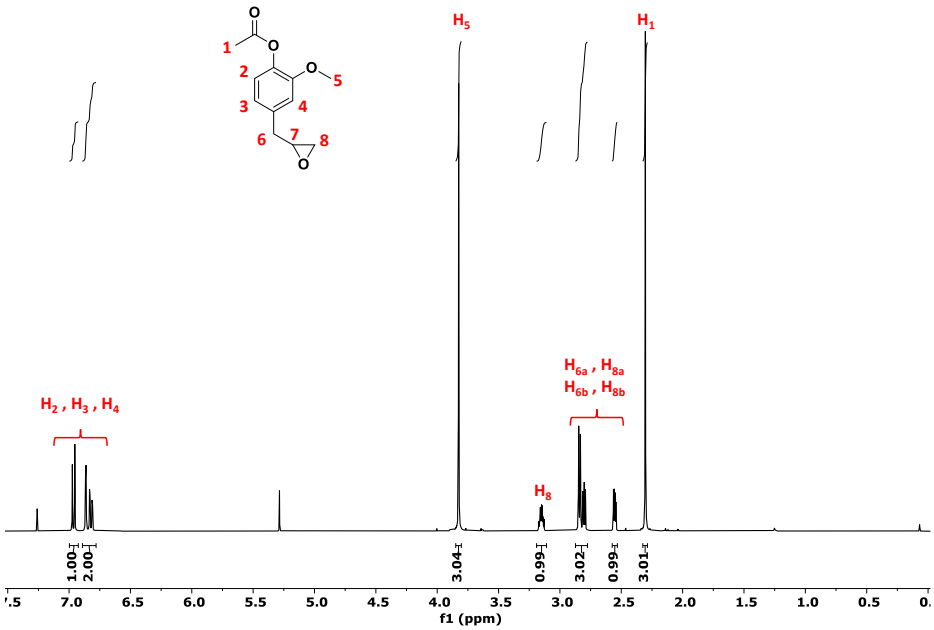

Figure 8.S3. ^{1}H NMR spectrum of epoxy acetyl eugenol (EpAcEU) in $CDCl_3$.

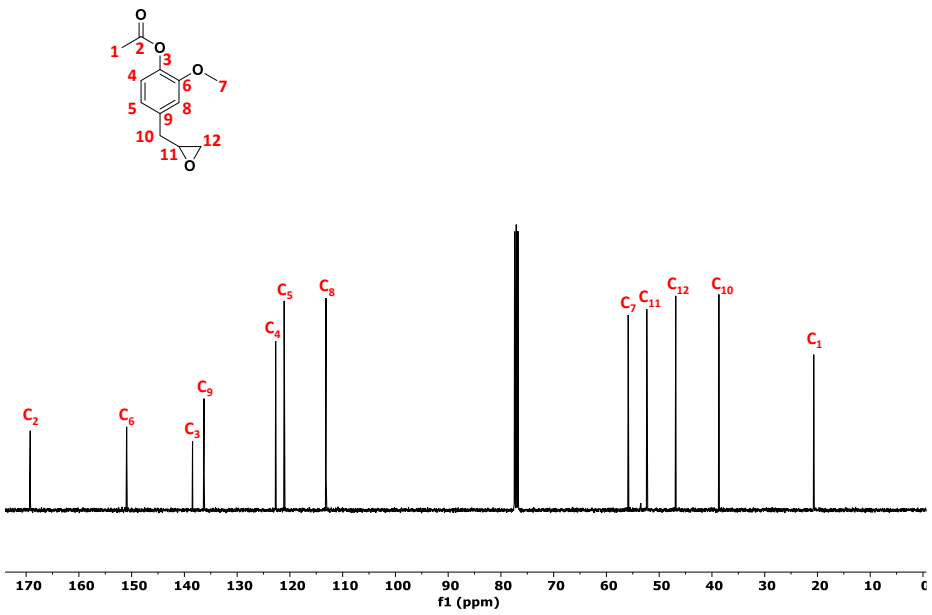

Figure 8.S4. ^{13}C NMR spectrum of epoxy acetyl eugenol (EpAcEU) in $CDCl_3$.

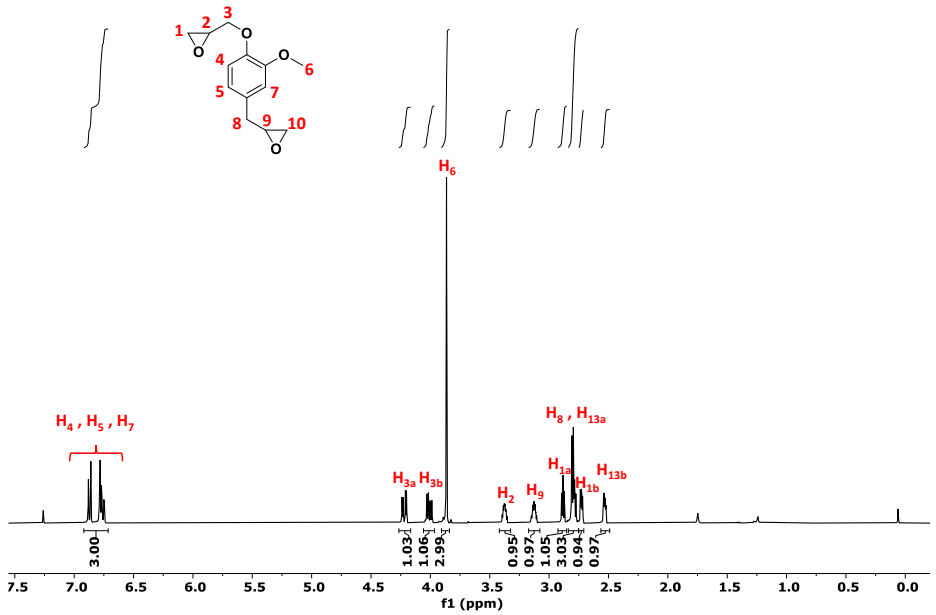

Figure 8.S5. ^{1}H NMR spectrum of diepoxy eugenol (DEPOEU) in $CDCl_3$.

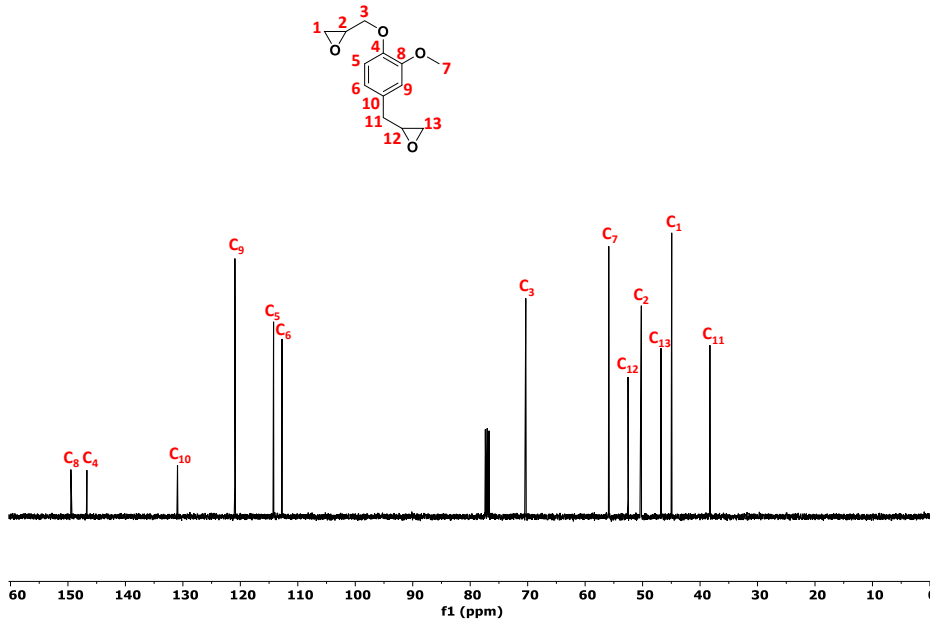

Figure 8.S6. ^{13}C NMR spectrum of diepoxy eugenol (DEPOEU) in $CDCl_3$.

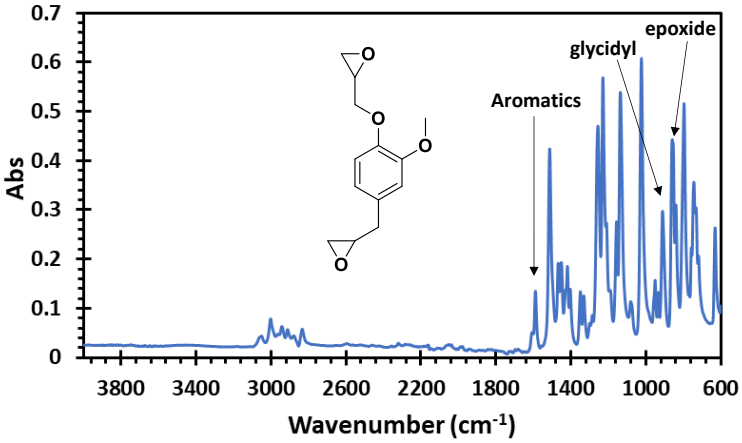

Figure 8.S7. FTIR-ATR spectra of diepoxy eugenol (DEPOEU).

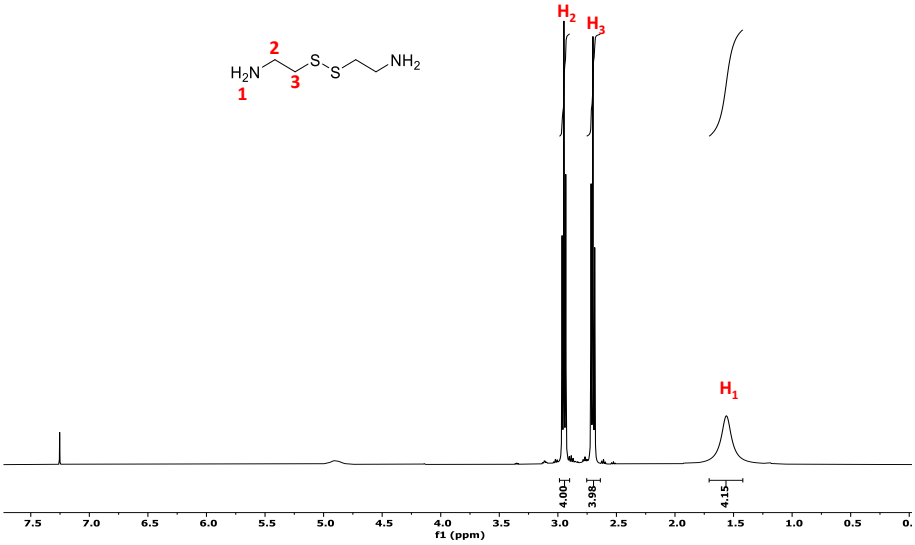

Figure 8.S8. ^{1}H NMR spectrum of cystamine (Cys) in $CDCl_3$.

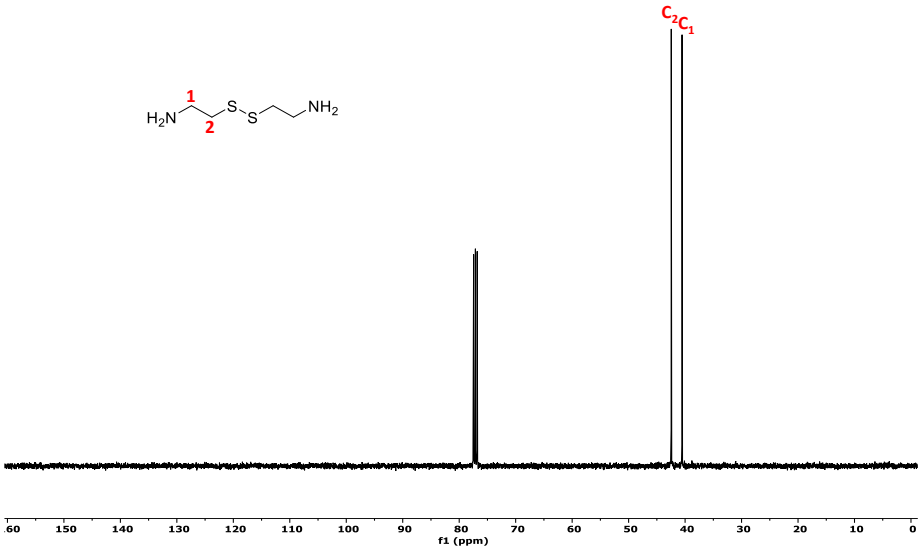

Figure 8.S9. ^{13}C NMR spectrum of cystamine (Cys) in $CDCl_3$.

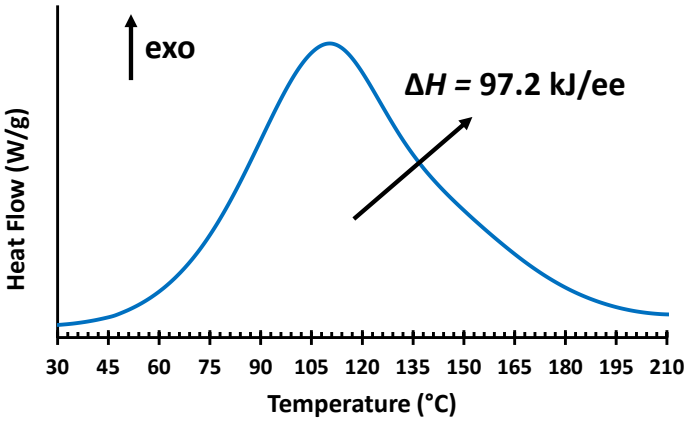

Figure 8.S10. DSC thermogram corresponding to the dynamic curing at 10 °C/min of 100%Cys.

Eur. Polym. J. **2023**, *194*, 112185

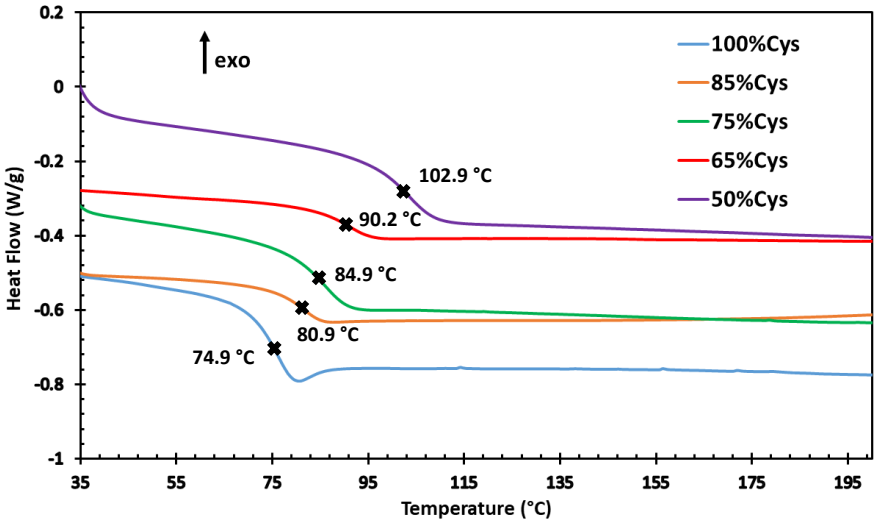

Figure 8.S11. T_gs determined by DSC in a dynamic scan at 20 °C/min.

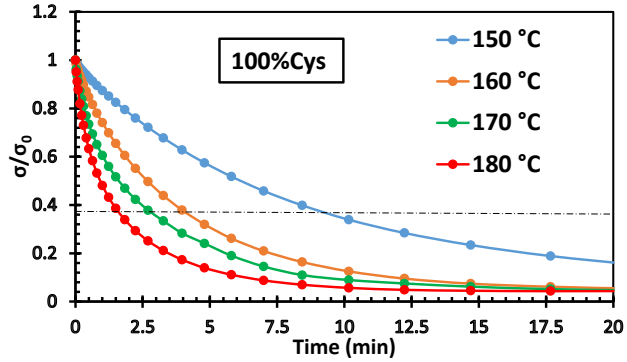

Figure 8.S12. Normalized stress relaxation plots as a function of time at various temperatures for 100%Cys material.

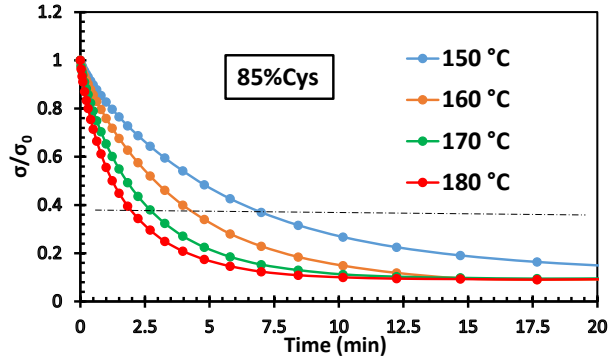

Figure 8.S13. Normalized stress relaxation plots as a function of time at various temperatures for 85%Cys material.

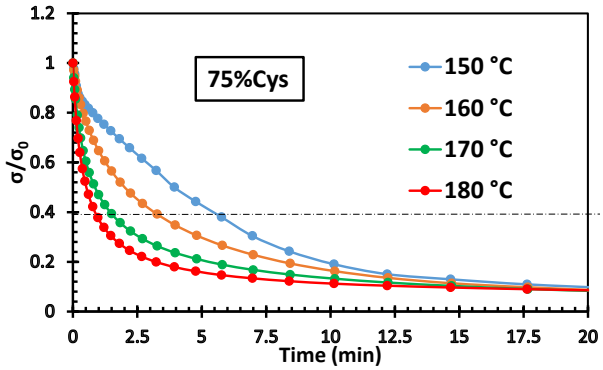

Figure 8.S14. Normalized stress relaxation plots as a function of time at various temperatures for 75%Cys material.

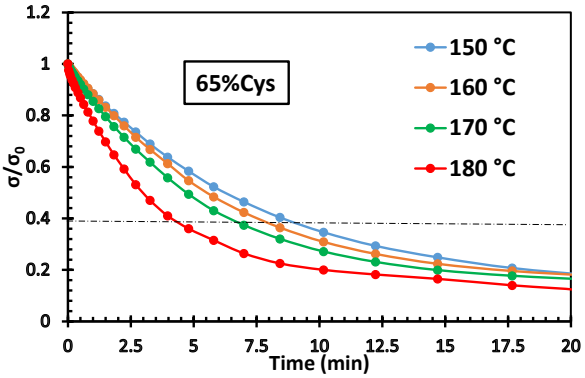

Figure 8.S15. Normalized stress relaxation plots as a function of time at various temperatures for 65%Cys material.

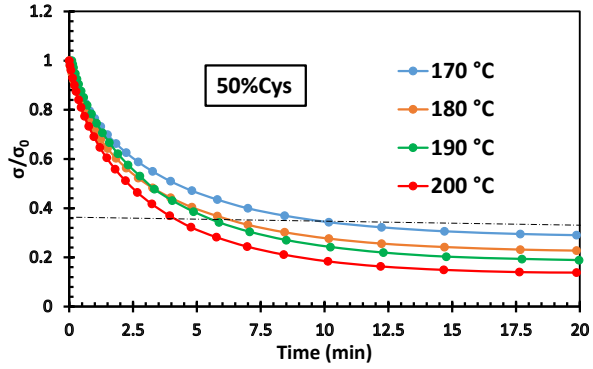

Figure 8.S16. Normalized stress relaxation plots as a function of time at various temperatures for 50%Cys material.

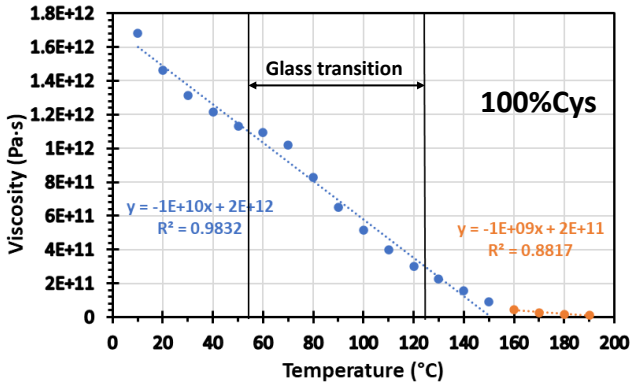

Figure 8.S17. Viscosity as a function of the temperature for 100%Cys material.

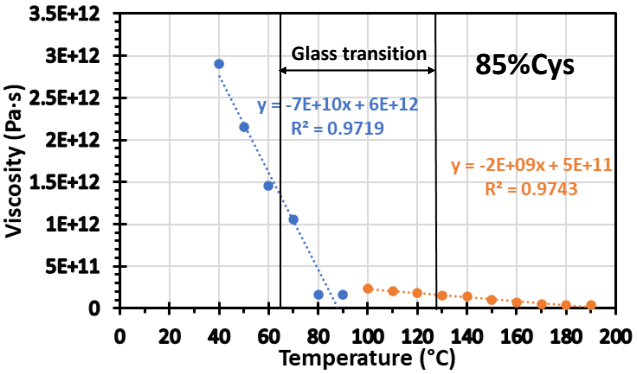

Figure 8.S18. Viscosity as a function of the temperature for 85%Cys material.

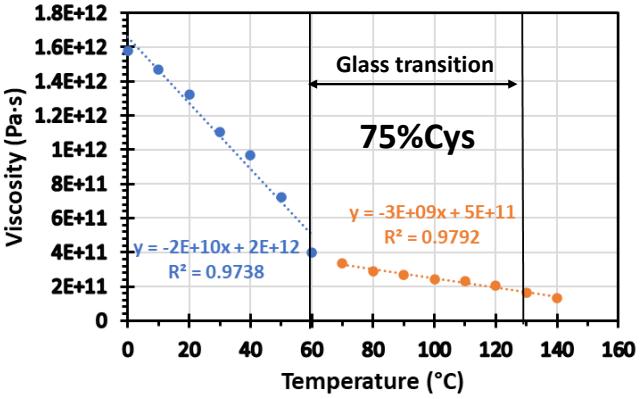

Figure 8.S19. Viscosity as a function of the temperature for 75%Cys material.

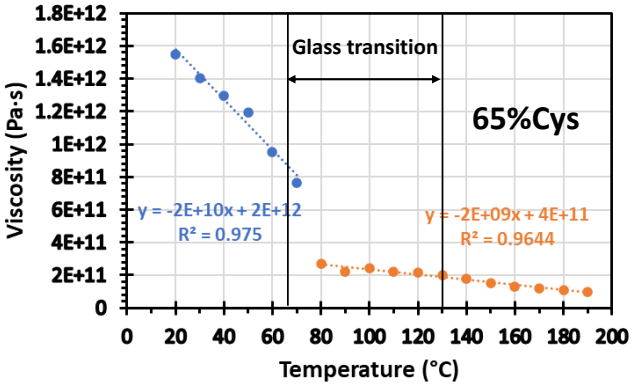

Figure 8.S20. Viscosity as a function of the temperature for 65%Cys material.

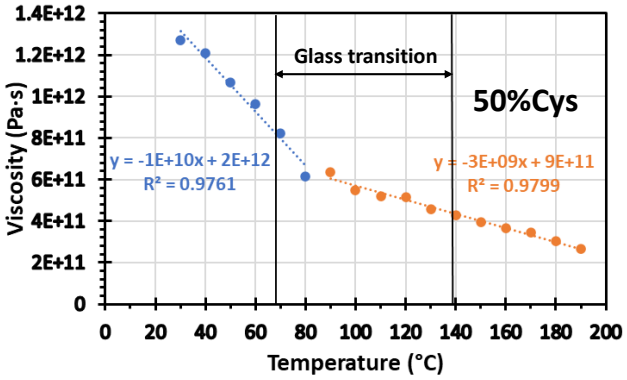

Figure 8.S21. Viscosity as a function of the temperature for 50%Cys material.

Chapter 9

Vitrimer-like disulfide materials with fast relaxation and creep resistance

(*submitted*)

UNIVERSITAT ROVIRA I VIRGILI
PROGRESS IN SUSTAINABILITY WITHIN THE REALM OF DESIGNING NEW THERMOSETTING MATERIALS
Adrià Roig Gibert

(submitted)

Vitrimer-like disulfide materials with fast relaxation rates and creep resistance

Adrià Roig,[1] Valeria D'Agostino,[2] Àngels Serra,[1] Silvia De la Flor[2]

[1] Universitat Rovira i Virgili, Department of Analytical and Organic Chemistry, C/ Marcel·lí Domingo 1, Edif. N4, 43007 Tarragona, Spain

[2] Universitat Rovira i Virgili, Department of Mechanical Engineering, Av. Països Catalans 26, 43007 Tarragona, Spain

ABSTRACT

Reaching a delicate balance between polymer flow for reprocessing and mechanical robustness at service temperatures remains a challenge in designing dynamic polymer networks. The demand for creep-resistant materials with fast relaxation rates at relatively low temperatures is a crucial research topic in the academic world. In this study, we present the preparation of a series of disulfide vitrimeric materials by curing two commercially available aromatic and aliphatic epoxy resins and cystamine. Through careful variation of the proportions between the epoxy resins, the properties of the final materials can be properly tailored. The completion of the curing was confirmed using FTIR spectrometry, and the thermal stability of all materials was evaluated by TGA. The thermomechanical properties were investigated using DMA analysis, obtaining glass transition temperatures (T_gs) above 60 °C and high rigidity in the glassy state depending on the proportion of the aromatic resin.

Extensive stress relaxation tests unveiled remarkable vitrimeric behavior, with all materials capable of relaxing 63% of the initial stress in less than 2 minutes at 140 °C. The in-depth creep experiments not only allowed for determining material viscosity at high temperatures and the topology freezing temperatures (T_vs) but also offered control over dynamic stability at room temperature, depending on the initial formulation composition. Dilatometry and tensile tests provided further insights into the materials' characteristics.

The self-healing and self-welding behavior enabled by the disulfide metathesis exchange reactions were also evaluated, revealing a total self-healing recovery process with short times and comparable tensile modulus in the welded samples. The facile preparation, commercial availability of monomers, and excellent thermosetting and vitrimeric properties highlight the immense potential of this series of materials.

KEYWORDS

Vitrimer, disulfide, fast relaxation, creep resistance, self-healing, self-welding.

1. Introduction

Nowadays, covalent adaptable networks (CANs) are gaining interest thanks to their ability to combine the excellent mechanical performance of thermosets and the recycling, reprocessing, and reshaping ability of thermoplastics [1]. These materials include dynamic bonds in their structure that, through reversible chemical processes triggered by external stimulus, usually temperature, allow the network rearrangement [2]. This means that CANs can behave as thermosets at room temperature. However, when a certain temperature is exceeded, reversible reactions take place, altering their behavior from a viscoelastic solid to a fluid-like plastic. Depending on the mechanism of these exchangeable chemical processes, CANs can be classified into two main groups. The first class, the dissociative, is characterized by a two-step mechanism in which, first, a bond is broken and then re-formed in another place. This induces the loss of the network integrity and, thus, a sudden drop in the viscosity that sometimes makes them difficult to be processed. On the other hand, the associative CANs or vitrimers undergo concertedly without losing their network integrity and always keeping the crosslinking density constant. In vitrimers, a relationship between viscosity and temperature is established following an Arrhenius dependence like silica [3]. Many studies have been performed regarding all types of CANs since Prof. Leibler described them in 2011, encompassing several chemical reactions [3-11]. Recently Dichtel et al. reported the preparation of a new type of CANs: vitrimer-like polymers [12]. Chemically, the mechanism of the exchange reactions of these materials works through a dissociative pathway, but physically, there is not a sudden drop in viscosity like dissociative CANs. However, there is a gradual decrease in the viscosity with the temperature as vitrimers. This particularity makes them very interesting for industrial applications like self-healing, reshaping or self-welding. For this reason, many researchers are focusing their attention on the preparation of vitrimer-like materials [13-16].

Among all chemical reactions present in CANs that can undergo a chemical dissociative mechanism but, at the same time, follow an Arrhenius-type dependence of the viscosity with temperature, the disulfide metathesis is the most well-studied. Rekondo and co-workers reported the preparation of aromatic disulfide epoxy vitrimers by the curing of diglycidyl ether of bisphenol A (DGEBA) with *ortho* and *para* diamino disulfide in stoichiometric and in off-stoichiometric conditions with an excess of free amines, and with a catalyst [17]. They stated that the presence of free amines or catalysts in the materials enhanced the stress relaxation rates allowing tailoring of the dynamic and mechanical properties of the final materials. Moreover, they reported that the vitrimer-like properties of some of these materials revealed the drop of the modulus at low frequencies. Yamawake et al. explored the role of internal tertiary amines in disulfide covalent adaptable networks [18]. They prepared two different

materials with the same segmental mobility and crosslinking density, one with covalently linked tertiary amines and one without amines, for a better comparison. They demonstrated the the stress relaxation rates and creep resistance enhancement with the sample containing tertiary amines. Moreover, through electron spin resonance (ESR), they revealed the formation of thiyl radicals during the bond exchange, thus demonstrating the dissociative pathway of the mechanism, even maintaining a gradual decrease of the viscosity with the temperature. As far as we know, the formation of thiyl radicals in aliphatic disulfide moieties it is not reported and, therefore, the dissociative mechanism is still not verified for this type of structures.

In this context, Li *et al.* explored the dynamicity of aliphatic disulfide materials in the field of adhesion [19]. By preparing materials using cystamine as a crosslinker, they discovered their capability to fill voids in the adhesion plates and improve the surface wettability. By performing an annealing of the polymer, they increase the lap shear strength by a factor of 4 in comparison to the one that was not annealed and by a factor of 2 when compared to annealed thermoset material indicating the enhanced performance of these aliphatic disulfide moieties. Guerre and co-workers also used cystamine to prepare crosslinked materials with an epoxy-derivative of vanillin [20]. They compared the dynamicity of aromatic disulfide bonds with aliphatic disulfide bonds by combining both aromatic and aliphatic disulfides in the same materials. They reported that with only 20% of cystamine and 80% of 4AFD they could achieve similar relaxation rates compared to pure cystamine materials demonstrating the enhancement in the exchange reactions when aliphatic disulfide bonds are present in the network even maintaining high values of glass transition temperatures. More recently, in our group, we reported the preparation of bio-based epoxy vitrimers by using an epoxy derivative of eugenol and a combination of cystamine and tris-(2-aminoethyl) amine (TREN) [21]. All materials displayed high values of T_g (above 60 °C) and fast relaxation rates. More interesting, a compromise between the content of aliphatic tertiary amines and the concentration of disulfide bonds was found, obtaining faster relaxation times when the material was prepared with 25% of TREN and 75% of cystamine instead of with only cystamine thus indicating a possible catalytic effect of internal covalent tertiary amines on the disulfide exchange.

Balancing material flow for thermal reprocessability with dimensional stability during service use still remains a key design challenge in the field of dynamic covalent polymer networks. The use of latent catalysts, protecting groups and phase separation, the incorporation of substituents that either enhance or inhibit the activation rate, or the use of dynamic covalent bonds with high reaction enthalpy are employed to prepare dynamic networks while avoiding creep at services temperatures [22]. Even the incorporation of permanent bonds (maximum of 40%) in

the polymer structure may still provide good dynamicity to the network while controlling the flow at temperatures of use, as demonstrated by Torkelson and co-workers [23]. Nevertheless, this investigation field is in its early stages, and some efforts still need to be done.

Taking all this into account, this study presents a series of vitrimeric materials obtained by an epoxy-amine condensation from commercially available monomers such as triglycidyl-*p*-aminophenol (TGAP) and 1,6-hexanediol diglycidyl ether (HDGE) as epoxy precursors and cystamine (Cys) as the amine crosslinker (Scheme 9.1). The presence of disulfide linkages as dynamic bonds in the structure of Cys enables the vitrimeric behavior.

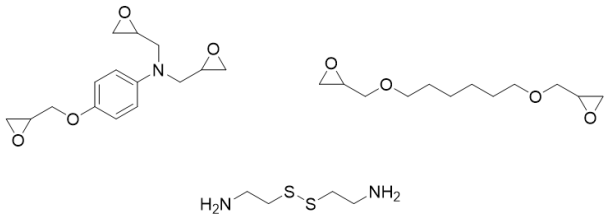

Scheme 9.1. Chemical structures of triglycidyl-*p*-aminophenol (TGAP) (top left), 1,6-hexanediol diglycidyl ether (HDGE) (top right) and cystamine (Cys) (bottom).

The thermomechanical properties of the materials can be tailored by varying the proportions of both epoxy monomers. As the stress relaxation tests demonstrated, the materials exhibit high T_gs above 50 °C and very fast relaxation rates at high temperatures. A complete creep analysis was also performed to determine the materials' topology freezing temperature (T_v), their relationship with temperature below and above T_g, and the creep behavior at service temperatures. By increasing the proportion of the aromatic epoxy resin, creep at room temperature is expected to be minimized while preserving short relaxation times [23,24]. Stress-strain tests were also performed to study the mechanical behavior, revealing good mechanical performance in the tested materials. The prepared materials also showed outstanding self-healing and self-welding properties, highlighting their potential use in the industrial field.

2. Experimental methods

2.1 Materials

Cystamine dihydrochloride (97%, Cys, 38.07 g /eq.) and triglycidyl-*p*-aminophenol (99%, TGAP, 92.44 g/eq.) were purchased from Sigma Aldrich. 1,6-Hexanediol diglycidyl ether (HDGE, 115.15 g/eq.) was kindly supplied from Epotec. Potassium hydroxide (KOH) and anhydrous magnesium sulfate ($MgSO_4$) were purchased from Scharlau.

2.2 Preparation of cystamine (Cys)

To prepare cystamine, 8 g of cystamine dihydrochloride and 6 g of KOH were dissolved in 100 mL of distilled water and stirred at room temperature for 30 minutes. The resulting mixture was extracted four times with 100 mL of dichloromethane (DCM). The organic layers were combined, dried over anhydrous $MgSO_4$, and filtered, and the solvent was removed in a rotary evaporator, obtaining 3.9 g of a yellowish viscous oil (Cys). The pure cystamine must be used immediately after being obtained or it must be kept in a fridge.

^{1}H NMR ($CDCl_3$; δ, ppm): 2.95 (t, 4H); 2.70 (t, 4H); 1.28 (s, 4H) (see Figure 9.S1). ^{13}C NMR ($CDCl_3$; δ, ppm): 42.55, 40.60 (see Figure 9.S2).

2.3 Preparation of epoxy vitrimer-like materials

All materials were prepared by mixing TGAP and HDGE with the corresponding amount of Cys in molar stoichiometric conditions NH/epoxy 1:1 in a vial and vigorously stirred. Then, the formulation was poured into a Teflon mold with dimensions of 30 x 5 x 1.5 mm^3 and cured for 3 h at 100 °C and post-cured for 1 h at 140 °C and 2 h at 160 °C. Samples with different amounts of epoxy resins were prepared and encoded as PolyX%, where X represents the percentage of NH groups of Cys reacting with epoxy groups of TGAP. As a consequence, the missing percentage refers to the NH groups of Cys reacting with epoxy groups provided by the other epoxy resin, HDGE. The composition of the different materials is depicted in Table 9.1.

Table 9.1. Amounts of each component in the initial formulations and concentration of aliphatic amines in the final materials.

Sample	TGAP (meq. epoxide)	TGAP (mg)	HDGE (meq. epoxide)	HDGE (mg)	Cys (meq. NH)	Cys (mg)	[$N_{alifatic}$] mmol/g
Poly50%	5.25	485	5.25	605	10.50	400	7.05
Poly60%	6.30	580	4.20	485	10.50	400	7.17
Poly70%	7.35	680	3.15	365	10.50	400	7.27
Poly80%	8.40	775	2.10	245	10.50	400	7.40

2.4 Characterization methods

A Jasco FTIR-680 Plus spectrometer equipped with an attenuated total reflection accessory (ATR) (Golden Gate, Specac Ltd, Teknokroma) was used to record the FTIR spectra of the mixture before and after the curing procedure. Real-time spectra were recorded in the wavenumber range between 4000 and 600 cm^{-1} with a resolution of 4 cm^{-1} and averaged over 20 scans. The disappearance of the characteristic

absorbance peak of the epoxy group at 915 cm^{-1} and the appearance of the peak corresponding to O-H at 3300 cm^{-1} were used to confirm the completion of the epoxy-amine condensation reaction. The thermal stability of the materials was evaluated using a Mettler Toledo TGA 2 thermobalance. Cured samples weighing around 10 mg were degraded between 30 and 600 °C at a heating rate of 10 °C min^{-1} under a N_2 atmosphere with a flow rate of 50 cm^3 min^{-1}. The thermomechanical properties were studied using a DMA Q800 (TA Instruments) equipped with a film tension clamp. Prismatic rectangular samples with dimensions of around 30 x 5 x 1.5 mm^3 were analyzed from 0 to 180 °C at 1 Hz, with 0.1% strain at a heating rate of 2 °C min^{-1}. Tensile stress-relaxation tests were conducted in the same equipment on samples with the same dimensions as previously defined. The samples were firstly equilibrated at the relaxation temperature for 3 min, and a constant strain of 1% was applied, measuring the consequent stress level as a function of time. Then, the strain was removed, and the process was repeated every 5 °C until the final test temperature was reached. The relaxation-stress $\sigma(t)$ was normalized by the initial stress σ_0, and the relaxation times (τ) were determined as the time necessary to relax $0.37\sigma_0$, i.e. ($\sigma = 1/e\sigma_0$). With the relaxation times obtained at each temperature, the activation energy values (E_a) were calculated using an Arrhenius-type equation:

$$ln(\tau) = \frac{E_a}{RT} - \ln A \qquad \text{(Eq. 9.1)}$$

where τ is the time needed to attain a given stress-relaxation value ($0.37\sigma_0$), A is the pre-exponential factor, and R is the gas constant.

To determine the viscosity at each temperature, a series of creep experiments were carried out with the same DMA Q800 instrument equipped with the film tension clamp at temperatures between 0 and 180 °C, increasing 10 °C in each scan. To perform the tests, the samples were equilibrated for 3 min at the selected temperatures, and a stress level of 0.1 MPa was applied for 30 min. The viscosity η (Pa·s) was obtained from the creep plots: first, the strain rate ($\dot{\varepsilon}$) was determined from the slope of the ε-time curves, and then the viscosity was calculated using the following expression:

$$\eta = \frac{\sigma}{\dot{\varepsilon}} \qquad \text{(Eq. 9.2)}$$

and represented in front of T_g/T, thus obtaining the Angell Fragility plot. In addition, individual creep tests were conducted at 0 °C and 25 °C for each sample to analyze the creep behavior at service temperatures. Samples were equilibrated for 3 min at the selected temperature, and a determined stress was applied for 30 min followed by a recovery time of 30 min. In each case, the stress level was chosen to ensure that the sample remained in the viscoelastic regime. Dilatometry experiments in tension were performed in the same DMA instrument using a film tension clamp on samples with

the same dimensions previously described. The sample length was continuously measured while increasing the temperature at a heating rate of 1 °C min^{-1} from -30 to 200 °C. A slight stress of 0.01 MPa was applied during the experiment to avoid buckling. For the self-healing tests, a manual press with a round steel indenter of diameter 2.5 mm was used to make plastic indentations on the sample's surface by applying increasing loads from 31.25 kg (306 MPa) to 150 kg (360 MPa). Subsequently, the samples were heated in an oven at 160 °C for 2 min, exploring from time to time the evolution of the indentation in the healing process by taking pictures with a Digital Microscope Leica DMS1000. To explore the self-welding ability, tensile tests were conducted at room temperature using an electromechanical universal testing machine (Shimadzu AGS-X) with a 1 kN load cell at 5 mm min^{-1}. Dog-bone-shaped samples of virgin and self-welded materials were tested until failure to determine and compare their strength at break and tensile modulus.

3. Results and discussion

3.1 Curing procedure and thermal properties of the materials

All materials were prepared under stoichiometric epoxy/NH conditions and cured according to the previously described procedure to obtain brownish and transparent samples, as can be seen in Figure 9.1a. To check the completion of the epoxy-amine condensation reaction, FTIR spectra were recorded on the initial formulations and the materials after the curing and post-curing (Figure 9.1b).

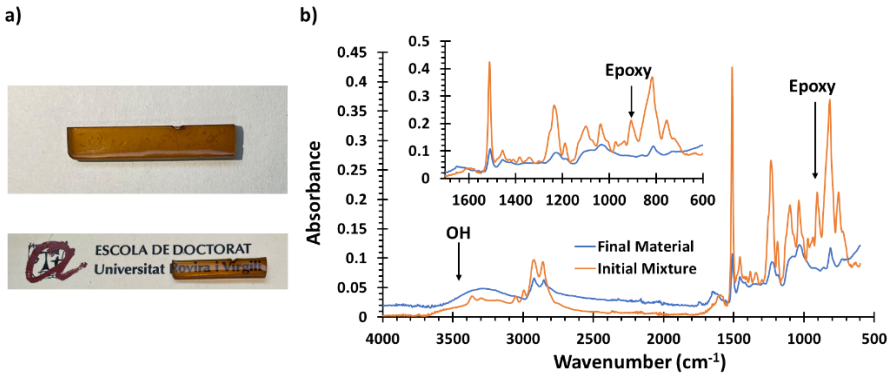

Figure 9.1. a) Pictures of the cured poly70% and b) FTIR spectra of the initial formulation and the final material for poly70%.

As can be seen, the characteristic band at 915 cm^{-1} corresponding to the epoxy groups of the initial resins completely vanished. In contrast, a broad band at 3300 cm^{-1} related to the hydroxyl groups generated by the ring opening of the epoxide with the amines appeared, which confirmed the end of the condensation reaction and the proper election of the curing parameters.

The thermal stability of the cured materials was studied by thermogravimetry (TGA). Fig. 9.2 shows the TGA curves and their derivatives for all samples prepared, and Table 9.2 collects the most significant data extracted. It can be observed that all materials showed excellent stability until almost 200 °C, which allows a safe relaxation test below that temperature. Moreover, the higher the content of the aromatic epoxy resin in the material, the higher the stability and char residue at 600 °C due to the higher proportion of aromatic rings in the sample. Finally, all materials showed similar DTG curves revealing two maximum degradation rates, a first one at around 260 °C which can be probably ascribed to the degradation of the disulfide bonds, and a second one at almost 330 °C which may correspond to the degradation of the poly(hydroxy-amine) network.

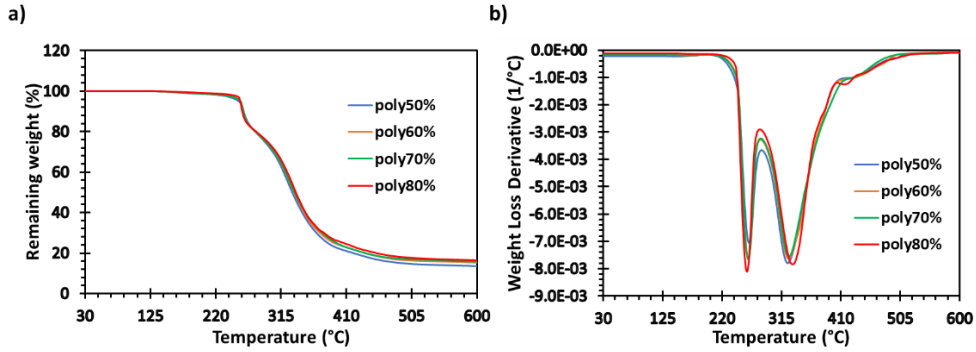

Figure 9.2. a) Thermogravimetric curves and b) DTG curves of all materials prepared.

Table 9.2. Thermogravimetric and thermomechanical data of all the materials obtained.

Sample	$T_{1\%}$[a] (°C)	$T_{2\%}$[b] (°C)	T_{max}[c] (°C)	Char Yield[d] (%)	E'_{glassy}[e] (MPa)	$E'_{rubbery}$[f] (MPa)	$T_{tan\,\delta}$[g] (°C)
Poly50%	198.1	215.2	263.3/325.0	13.5	2450	16.7	62
Poly60%	200.4	215.9	261.5/326.3	15.2	2775	25.0	74
Poly70%	201.9	216.7	261.8/327.6	15.8	2836	36.9	96
Poly80%	208.6	225.3	259.8/333.2	16.4	3220	52.1	112

[a] Temperature of 1% of weight loss. [b] Temperature of 2% of weight loss. [c] Temperature of the maximum rate of degradation. [d] Char residue at 600 °C. [e] Storage modulus in the glassy state at T_g – 50 °C. [f] Storage modulus in the rubbery state at T_g + 50 °C. [g] Temperature at the maximum of *tan* δ peak at 1 Hz.

3.2 Study of the thermomechanical properties

The thermomechanical behavior of all materials prepared was investigated by DMA analysis. Figure 9.3 presents the evolution of the tan δ curves and the storage modulus with temperature, and the most relevant data obtained from these results are presented in Table 9.2.

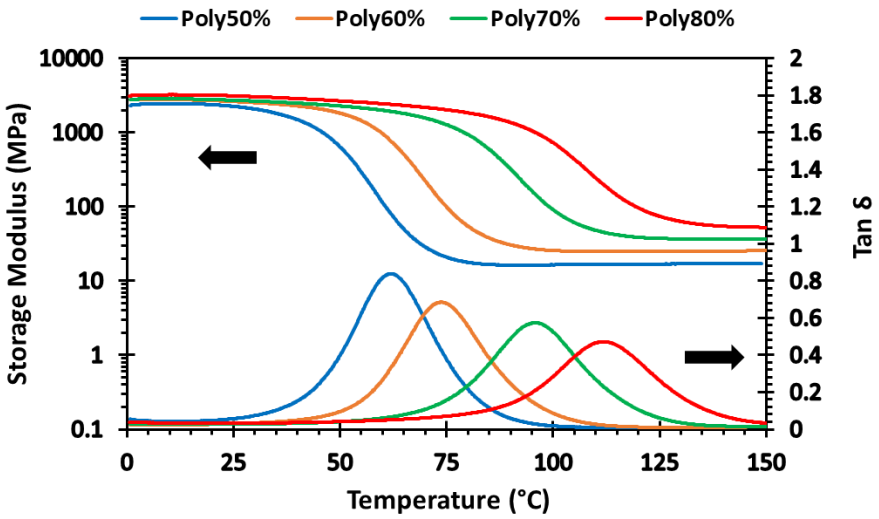

Figure 9.3. Evolution of the storage modulus and tan δ with temperature for all materials prepared.

As it can be seen from the data, the T_gs, determined from the maximum of the peaks of the tan δ curves, are far above room temperature, being 62 °C for poly50% and 112 °C for poly80%. The higher content of aromatic epoxy resin in the formulation, the higher the T_g of the samples due to the rigidity and the higher crosslinking density in the final material. The same trend can be detected in the storage modulus, where poly80% is the most rigid sample in the glassy state, and poly50% is the softer. The storage modulus in the rubbery state also displayed higher values when the proportion of TGAP in the sample was higher due to its tri-functionality that provides a higher crosslinking density in the material. In any case, all materials revealed high values of $E'_{rubbery}$, leading to considerable compact networks.

To evaluate the vitrimeric-like behavior of the materials prepared, stress relaxation tests were performed by DMA, which allowed the determination of the time and temperature-dependence relaxation of all the materials. These results can be observed in Figure 9.4, and the characteristic data extracted from the relaxation curves are presented in Table 9.3.

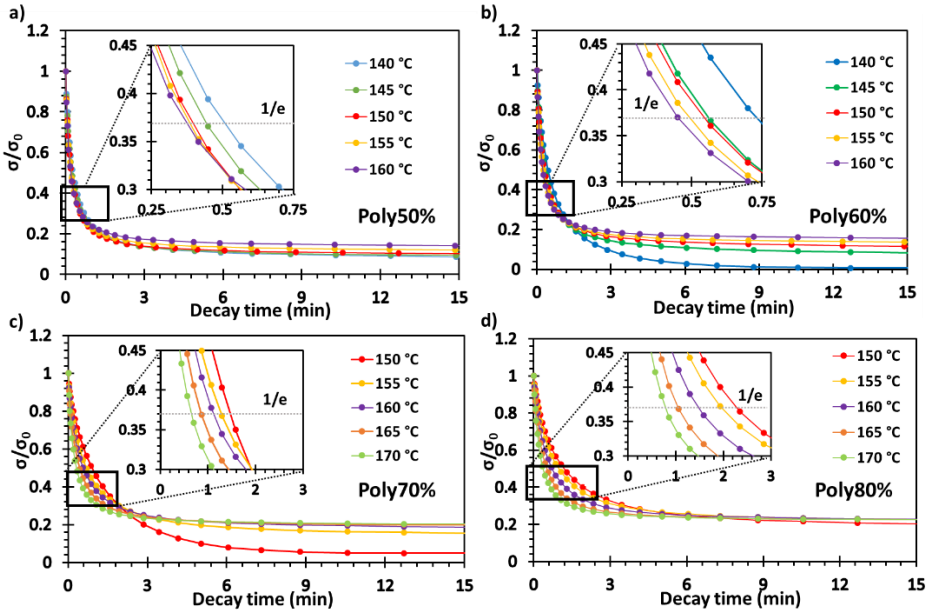

Figure 9.4. Normalized stress relaxation plots as a function of time at various temperatures during 15 minutes for poly50% (a), poly60% (b), poly70% (c), and poly80% (d) samples.

The stress relaxation curves reveal that all the materials can relax extremely fast the 63% of the initial stress ($\sigma = 0.37\sigma_0$) in less than 0.40 min for poly50%, 0.45 min for poly60%, 1.10 min for poly70%, and 1.50 min for poly80% without the need of an external catalyst increasing the relaxation time with the amount of TGAP in the material. It is reported in the literature that the tertiary amines generated after the epoxy-amine condensation can catalyze the disulfide metathesis by the nucleophilic attack of these amines to the S-S bond, generating a thiolate which can attack another disulfide bond [18]. Despite that on increasing the content of aromatic epoxy resin in the material, the proportion of aliphatic nucleophilic tertiary amines increases (Table 9.1), the higher rigidity provided from the aromatic ring and the higher functionality results in an increase of the relaxation time. Consequently, as can be observed, when the content of the aromatic epoxy resin increases in the sample, the materials relax the stress more slowly. Another factor that can reduce the rate of relaxation is the rigidity of TGAP in comparison to that of HDGE. This fact, together with the higher functionality of TGAP, leads to a more rigid and closed network with higher topological constraints for structural changes. It is worth mentioning that a slight plastic deformation effect is produced in all the materials when continuous stress relaxation tests are performed. This produces a slight decrease in the maximum relaxation value reached.

Table 9.3. Relaxation time, activation energy and adjusting parameters of the Arrhenius equation and activation energy, topology freezing temperature and fragility index of all materials prepared.

	Stress relaxation tests				Creep tests		
Sample	$\tau_{0.37}$[a] (min)	ln *A* (min)	r^2	E_a[b] (kJ/mol)	E_a[c] (kJ/mol)	$T_{v(\eta)}$[d] (°C)	n[e]
Poly50%	0.40	3.0	0.9709	22	32	10	32
Poly60%	0.45	4.8	0.9902	35	37	23	37
Poly70%	1.10	11.2	0.9881	54	41	37	41
Poly80%	1.50	13.6	0.9926	64	46	64	46

[a] Time to reach a value of σ/σ_0 = 0.37 at 160 °C. [b] Activation energy deduced from the Arrhenius plots. [c] Activation energy deduced from the Angell Fragility plot. [d] Topology freezing temperature calculated from the creep tests at a viscosity of 10^{12} Pa·s. [e] Fragility index, in which n = 16.5 is the corresponding value for vitreous silica.

Vitrimeric materials are widely known to display a temperature dependence that follows an Arrhenius-type relationship [12,25]. This dependence occurs when the chemical exchange reactions control the viscosity. Consequently, the temperature-viscosity relationship is similar to inorganic silica materials. To further investigate the vitrimeric behavior, the relaxation curves were used to determine the time needed for the initial stress to decrease to e^{-1} (σ/σ_0 = 0.37) at different temperatures. By fitting the data to an Arrhenius-type equation, the activation energy (E_a) of the topological rearrangement for all materials can be calculated (see Fig. 9.5 and Table 9.3).

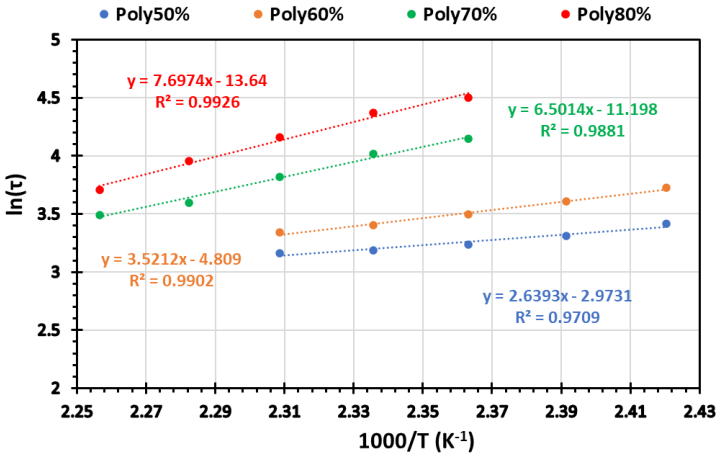

Figure 9.5. Arrhenius plot of relaxation times against the inverse of the temperature for the different materials prepared.

The Arrhenius plots revealed that the higher the content of TGAP in the material, the higher dependence of the relaxation time with the temperature, being the poly80%

the material with the highest E_a (64 kJ/mol) and the poly50% the lowest (22 kJ/mol). This is directly linked with the hypothesis previously mentioned that even the poly80% is the material that contains more aliphatic tertiary amines (see Table 9.1) capable to catalyze the exchange reaction, the high rigidity and crosslinking density hinders the disulfide metathesis and therefore, a higher activation energy is required to allow the exchange mechanism [18,21]. It is worthy to mention that E_a values of poly80% and poly70%, and poly60% and poly50% are similar, but the differences in the pre-exponential factor (ln*A*) allow faster relaxation times at a determined temperature when the content of TGAP is lower. Moreover, even the disulfide exchange is able to undergo via a dissociative-radical mechanism, all materials fitted properly the Arrhenius plot, confirming a vitrimeric-like behavior.

3.3 Study of the viscosity and creep behavior

To make a deeper study of the effect of temperature on the viscoelastic behavior of these materials, creep tests from 30 °C to 140 °C were performed by DMA (see Figures 9.S3-S6). It can be observed that when a constant stress is applied at different temperatures, the strain increases with time with a different rate depending on the temperature, being negligible under the T_g and remarkable above it. According to that, these materials behave like a viscoelastic vitrimer and not as a conventional rubber thermoset which would show a slight increase in the strain rate under a constant stress. From these results, the viscosity at each temperature can be calculated as the inverse of the slope of the strain evolution over time (strain rate, $\dot{\varepsilon}$). Figure 9.6a shows the plot of the viscosity at each temperature for all the materials.

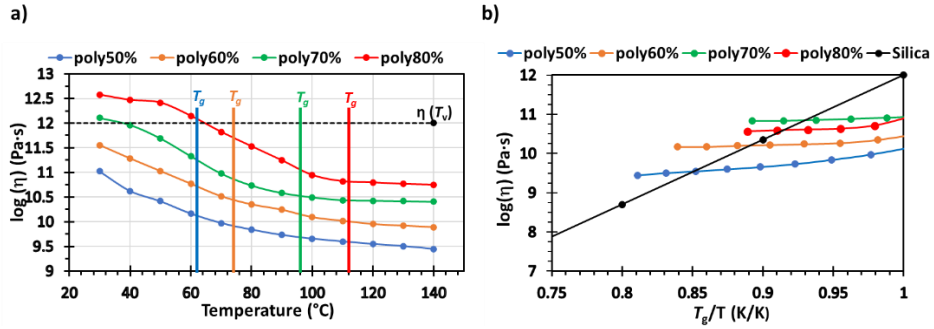

Figure 9.6. a) Evolution of the viscosity with temperature for all the materials prepared and b) Angell fragility plot of all materials including vitreous silica as a reference of an ideal strong liquid.

It can be seen that materials with a higher content of the aromatic epoxy resin present a steeper viscosity decrease until their glass transition temperature being fairly constant after this temperature. Nevertheless, in the case of poly50% and poly60%,

the viscosity decreases in the whole interval of temperatures, even above their T_gs. The first drop of the viscosity can be attributed to the glassy to rubber transition of the polymers. When this transition is overpassed, a higher decrease of the viscosity can be observed in the materials with less amount of TGAP due to its higher mobility and flexibility that make the exchange processes more likely to occur (dynamic transition). These phenomena are overlapped but they can be more appreciated beyond the T_g in materials with less content of aromatic epoxy resin. A critical parameter in the characterization of vitrimeric materials is the topology freezing temperature (T_v). Chemically, this parameter accounts for the temperature below which the exchange between dynamic bonds is negligible. Moreover, this temperature is defined as the one at which the material reaches a viscosity of 10^{12} Pa·s [3]. From Figure 9.6a, the T_v of all the materials can be obtained by assuming $\log(\eta_{Tv}) = 12$ (see Table 9.3). It can be appreciated that, as expected, the T_vs increase when a higher proportion of TGAP is present in the sample. The higher the functionality and the higher content of aromatic rings, the lower the mobility and flexibility of the chains, which leads to a lower probability of the exchange reactions taking place. As seen, the T_v in all cases was below the T_g of the corresponding materials.

The Angell fragility plot is represented in Figure 9.6b, showing that the evolution of the viscosity with relative temperature of all materials differs from a classical vitrimer, laying below the vitreous silica relationship. Above the topology freezing temperature, the exchange reactions become active, and both the relaxation time and viscosity exhibit behavior consistent with the Arrhenius law, similar to inorganic silica materials, which are considered ideal strong liquids [26,27]. This behavior is in contrast to that observed in thermoplastics and dissociative covalent adaptable networks, which behave as “fragile liquids” because of at high temperatures, the viscosity suffers a sudden drop. For this reason, these materials herein can be categorized as “vitrimer-like” materials. Moreover, from this graph, it is possible to obtain the activation energy for each material from the creep behavior (see Table 9.3). As can be seen, the activation energies are similar to those obtained from the Arrhenius plot presenting the same trend: the calculated E_as are lowest for samples with lower content of aromatic epoxy resin.

To confirm the observed behavior, the relaxation process was also investigated by dilatometry experiments (Figure 9.S7). In this case, classical thermosets with a permanently crosslinked network exhibit a slight and constant stain increase with temperature with a small non-linear region corresponding to the glass transition. Conversely, in the case of vitrimers, two different changes in the slope of the strain-temperature curve could be observed: a first one at $T=T_g$ and a second one when the exchange reactions occur ($T=T_v$) [28-30]. In Fig. 9.S7 these two changes are not visible

because the relaxation process of the interchange reactions and the mobility of the polymer chains are overlapped, as was previously deduced from the creep tests in which all T_v values were below the corresponding T_gs.

Isothermal creeps at 0 and 25 °C were performed in DMA to determine the effect of temperature on the creep behavior at services temperatures. Fig. 9.7a shows the creep plots of all the vitrimer-like materials at 0 °C, while Figure 9.7b shows the result for the same creep test but at 25 °C. As it can be seen at 0 °C, poly80% and poly70% behave as traditional thermosets without creep and a complete strain recovery. On the other hand, poly60% and poly50% present a slight strain increase with the time and a longer recovery process after the stress is released. This can be ascribed to a more deformable molecular structure which entails a more viscous behavior in comparison to poly80% and poly70%. This can be clearly seen in the loss modulus evolution with temperature of all the materials (see Figure 9.S8). In any case, no evidence of dynamic processes can be seen in the creep tests at 0 °C. On the contrary, at 25 °C, all materials present a more evident creep behavior when the stress is applied, and in the recovery process, a permanent deformation remains due to the topological effect of the chains. It is essential to point out a clear increase in the creep resistance when the content of the aromatic epoxy resin is higher. Indeed, poly80%, which is the material that contains the highest proportion of TGAP, only presents a slight plastic deformation, even maintaining extremely fast relaxation rates at 140 °C, highlighting the great potential of this type of materials.

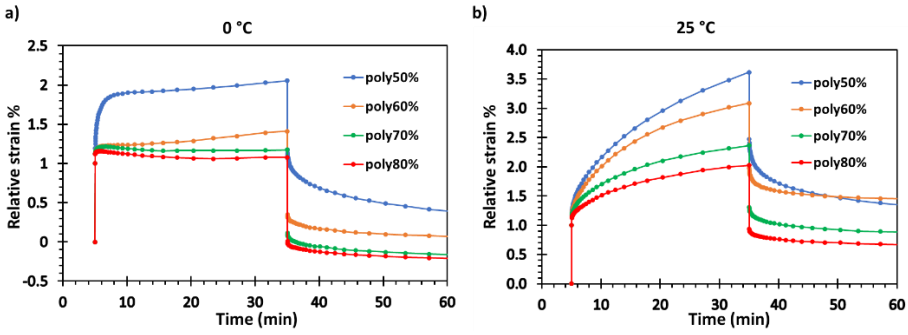

Figure 9.7. Creep and recovery curves of all the materials at 0 °C (a) and 25 °C (b).

3.4 Study of the self-healing and self-welding abilities

Vitrimeric materials present significant advantages in their applicability compared to conventional thermosets. Two of the most important applications in this field are self-healing and self-welding abilities, among many others [31,32]. In order to evaluate these properties, poly80% was selected because it has the higher T_g, lower plastic deformation, and slowest relaxation rates. Therefore, it is the material with a predictable lower self-healing ability. To study this property, controlled indentations

with a spherical indenter and with different pressures ranging from 306 MPa to 360 MPa were applied on the sample. After performing the indentations, the sample was left for 24 h at room temperature to ensure no viscoelastic recovery. Subsequently, it was heated up to 160 °C, controlling the recovery process at different times. The evolution of the dimension of the indentations made on the surface of the poly80% is shown in Figure 9.8.

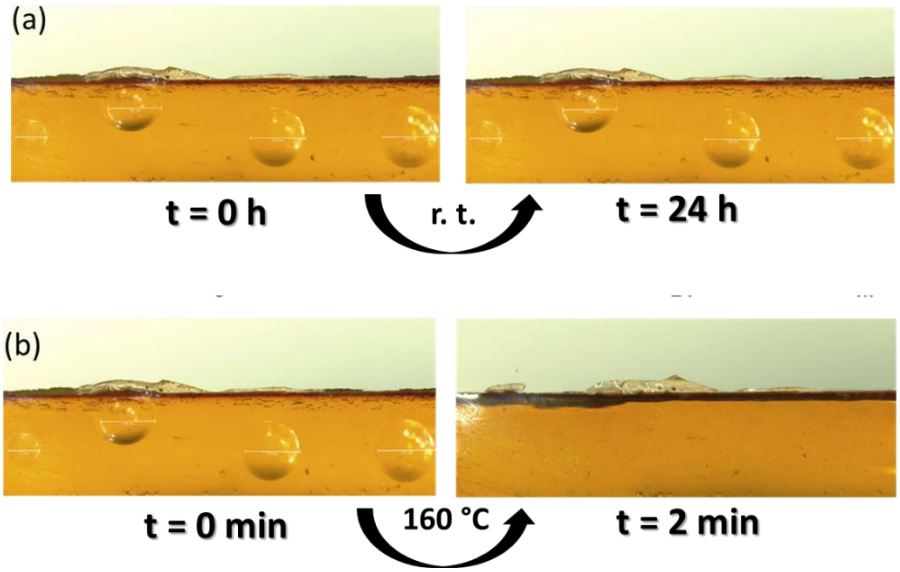

Figure 9.8. Evolution of the indentations at room temperature (a) and at 160 °C (b) made on poly80%.

As can be seen, no viscoelastic recovery was produced at room temperature for 24 h. However, when the sample was heated up to 160 °C, the material completely self-healed all the indentations at different pressures in only 2 minutes. This highlights the outstanding capability to undergo self-healing and, therefore, the great potential in the industrial field.

To study the self-welding, a dog-bone sample of poly80% was broken into two pieces under liquid nitrogen, put in a mold to ensure the maximum contact between the two breaking surfaces, and heated at 160 °C for 2 h. As can be seen in Figure 9.9, the two parts were perfectly attached after the procedure. To quantitively test this ability, the virgin and the welded samples were subjected to a tensile test to obtain their mechanical strength (Figure 9.S9). As shown in Table 9.4, both samples presented the same Young Modulus (*E*), which means similar mechanical behavior. Despite this, the strength of the welded sample was considerably lower than the virgin one, clearly due

to an imperfect contact between the two broken parts during the heating process. The welded surface may present micro-voids due to the absence of small parts of material that start the failure process.

Table 9.4. Stress and strain at break and Young Modulus of the virgin and welded samples.

Sample	σ_b (MPa)	ε_b (%)	*E* (MPa)
Virgin	73	4.2	2726
Welded	24	1.0	2630

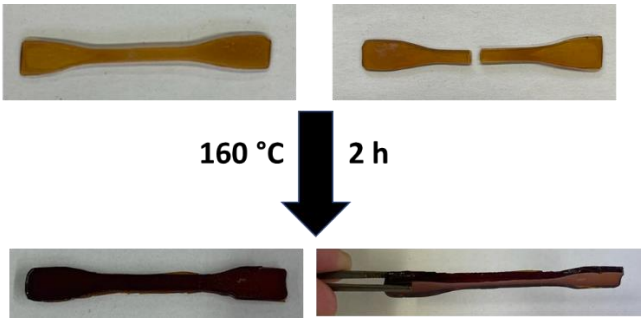

Figure 9.9. Pictures taken to the original sample, the broken one under nitrogen and the self-welded.

4. Conclusions

A series of disulfide vitrimeric materials were successfully prepared using a straightforward epoxy-amine condensation reaction between two commercially available epoxy resins, one aromatic resin (TGAP), and one aliphatic resin (HDGE) along with cystamine serving as the amine crosslinker containing the disulfide bonds. By varying the proportions of the epoxy resins, we achieved precise control over the thermomechanical and viscoelastic properties of the final materials.

The completion of the curing reaction was effectively confirmed through FTIR analysis by the disappearance of the epoxy bands. The prepared materials exhibited excellent thermal stability up to 200 °C, enabling safe stress-relaxation tests below this temperature. DMA analysis further revealed high T_gs (above 60 °C) for all materials, with enhanced rigidity in the glassy state, particularly when the proportion of TGAP was increased.

The viscoelastic properties and the vitrimeric behavior were studied via stress-relaxation tests which revealed that all materials could relax the initial stress in less than 1 min at 160 °C. To characterize the materials' creep response, we conducted creep experiments, resulting in topology freezing temperatures (T_v) below the glass transition temperature, with a clear upward trend observed as the aromatic epoxy resin content in the samples increased. Furthermore, creep tests performed at 0 °C

and 25 °C demonstrated that samples with higher TGAP content exhibited superior creep resistance at service temperatures. Finally, to test the mechanical behavior and their functional properties, tensile tests, self-healing, and self-welding tests were conducted. The results showcased high values of stress and strain at break for the virgin sample, rapid self-healing capabilities (within 2 minutes at 160 °C), and promising welding ability. These observations underscore the technological potential of these materials, driven by their easy preparation, excellent thermomechanical properties, and versatile applicability across a wide range of applications.

Acknowledgments

This work is part of the R&D project PID2020-115102RB-C21 and TED2021-131102B-C22 funded by MCNI/AEI/10.13039/501100011033 and European Union NextGeneration EU/PRTR. We also want to thank Generalitat de Catalunya (2021-SGR-00154).

References

[1] G. M. Scheutz, J. J. Lessard, M. B. Sims, B. S. Sumerlin, Adaptable crosslinks in polymeric materials: resolving the intersection of thermoplastics and thermosets, J. Am. Chem. Soc. 141 (2019) 16181-16196.

[2] M. Podgórski, B. D. Fairbanks, B. E. Kirkpatrick, M. McBride, A. Martinez, A. Dobson, N. J. Bongiardina, C. N. Bowman, Toward stimuli-responsive dynamic thermosets through continuous development and improvements in covalent adaptable networks (CANs), Adv. Mater. 32 (2020) 1906876.

[3] D. Montarnal, M. Capelot, F. Tournilhac, L. Leibler, Silica-like malleable materials from permanent organic networks, Science 334 (2011) 965-968.

[4] T. Liu, C. Hao, L. Wang, Y. Li, W. Liu, J. Xin, J. Zhang, Eugenol-derived biobased epoxy: shape memory, repairing and recyclability, Macromolecules 50 (2017) 8588-8597.

[5] D. Berne, F. Cuminet, S. Lemouzy, C. Joly-Duhamel, R. Poli, S. Caillol, E. Leclerc, V. Ladmiral, Catalyst-free epoxy vitrimers based on transesterification internally activated by an α-CF_3 group, Macromolecules, 55 (2022) 1669-1679.

[6] A. Roig, A. Petrauskaitė, X. Ramis, S. De la Flor, À. Serra, Synthesis and characterization of new bio-based poly(acylhydrazone) vanillin vitrimers, Polym. Chem. 13 (2022) 1906876.

[7] A. Roig, P. Hidalgo, X. Ramis, S. De la Flor, À. Serra, Vitrimeric epoxy-amine polyimine networks based on a renewable vanillin derivative, ACS Appl. Polym. Mater. 4 (2022) 9341-9350.

[8] W. Denissen, M. Droesbeke, R. Nicolaÿ, L. Leibler, J. M. Winne, F. E. Du Prez, Chemical control of the viscoelastic properties of vinylogous urethane vitrimers, Nat. Commun. 8 (2017) 14857.

[9] S. Engelen, A. A. Wróblewska, K. De Bruycker, R. Aksakal, V. Ladmiral, S. Caillol, F. E. Du Prez, Sustainable design of vanillin-based vitrimers using vinylogous urethane chemistry, Polym. Chem. 13 (2022) 2665-2673.

[10] C. Chapelle, B. Quienne, C. Bonneaud, G. David, S. Caillol, Diels-Alder-chitosan based dissociative covalent adaptable networks, Carbohydr. Polym. 253 (2021) 117222.

[11] X. Xu, S. Ma, S. Wang, B. Wang, H. Feng, P. Li, Y. Liu, Z. Yu, J. Zhu, Fast-reprocessing, postadjustable, self-healing covalent adaptable networks with Schiff Base and Diels-Alder adduct, Macromol. Rapid Commun. 43 (2022) 2100777.

[12] B. R. Elling, W. R. Dichtel, Reprocessable cross-linked polymer networks: are associative exchange mechanisms desirable?, ACS Cent. Sci. 6 (2020) 1488-1496.

[13] F. Gamardella, S. Muñoz, S. De la Flor, X. Ramis, A. Serra, Recyclable organocatalyzed poly(thiourethane) covalent adaptable networks, Polymers 12 (2020) 2913.

[14] F. Guerrero, X. Ramis, S. De la Flor, À. Serra, Preparation and characterization of a series of self-healable bio-based poly(thiourethane) vitrimer-like materials, Polymers 15 (2023) 1583.

[15] Y. Oba, T. Kimura, M. Hayashi, K. Yamamoto, Correlation between self-assembled nanostructures and bond exchange properties for polyacrylate-based vitrimer-like materials with a Trans-*N*-Alkylation bond exchange mechanism Macromolecules 55 (2022) 1771-1782.

[16] Q. Li, S. Ma, N. Lu, J. Qiu, J. Ye, Y. Liu, S. Wang, Y. Han, B. Wang, X. Xu, H. Feng, J. Zhu, Concurrent tiol-ene competitive reactions provide reprocessable, degradable and creep-resistant dynamic-permanent hybrid covalent adaptable networks, Green Chem. 22 (2020) 7769-7777.

[17] A. Ruiz de Luzuriaga, G. Solera, I. Azcarate-Ascasua, V. Boucher, H.-J. Grande, A. Rekondo, Chemical control of the aromatic disulfide exchange kinetics for tailor-made epoxy vitrimers, Polymers 239 (2022) 124457.

[18] K. Yamawake, M. Hayashi, The role of tertiary amines as internal catalysts for disulfide exchange in covalent adaptable networks, Polym. Chem. 14 (2023) 680-686.

[19] L. Li, X. Chen, J. M. Torkelson, Covalent adaptive networks for enhanced adhesion: Exploiting disulfide dynamic chemistry and annealing during application, ACS Appl. Polym. Mater. 2020, 2, 4658-4665.

[20] S. Guggari, F. Magliozzi, S. Malburet, A. Graillot, M. Destarac, M. Guerre, Vanillin-based epoxy vitrimers: Looking at the cystamine hardener from a different perspective, ACS Sustainable Chem. Eng. 11 (2023) 6021-6031.

[21] A. Roig, M. Agizza, À. Serra, S. De la Flor, Disulfide vitrimeric materials base don cystamine and diepoxy eugenol as bio-based monomers, Eur. Polym. J. 19 (2023) 112185.

[22] F. Van Lijsebetten, T. Debsharma, J. M. Winne, F. E. Du Prez, A highly dynamic covalent polymer network without creep: mission impossible?, Angew. Chem. Int. Ed. 61 (2022) e202210405.

[23] L. Li, X. Chen, K. Jin, J. Torkelson, Vitrimers designed both to strongly suppress creep and to recover original cross-link density after reprocessing: quantitative theory and experiments, Macromolecules 51 (2018) 5537-5546.

[24] F. Van Lijsebetten, K. De Bruycker, Y. Spiesschaert, J. M. Winne, F. E. Du Prez, Suppressing creep and promoting fast reprocessing of vitrimers with reversible trapped amines, Angew. Chem. Int. Ed. 61 (2022) e202113872.

[25] W. Denissen, J. M. Winne, F. E. Du Prez, Vitrimers: permanent organic networks with glass-like fluidity, Chem. Sci. 7 (2016) 30-38.

[26] K. F. Kelton, Kinetic and structural fragility-a correlation between structures and dynamics in metallic liquids and glasses, J. Phys.: Condens. Matter 29 (2017) 023002.

[27] C. A. Angell, Formation of glasses from liquids and biopolymers, Science 267 (1995) 1924-1935.

[28] A. M. Hubbard, Y. Ren, C. R. Picu, A. Sarvestani, D. Konkolewicz, A. K. Roy, V. Varshney, D. Nepal, Creep mechanics of epoxy vitrimer materials, ACS Appl. Polym. Mater. 4 (2022) 4254-4263.

[29] A. M. Hubbard, Y. Ren, D. Konkolewicz, A. Sarvestani, C. R. Picu, G. S. Kedziora, A. Roy, V. Varshney, D. Nepal, Vitrimer transition temperature identification: coupling various thermomechanical methodologies, ACS Appl. Polym. Mater. 3 (2021) 1756-1766.

[30] X. Shi, Q. Ge, H. Lu, K. Yu, The nonequilibrium behaviors of covalent adaptable network polymers during the topology transition, Soft Matter. 17 (2021) 2104.

[31] A. Khan, N. Ahmed, M. Rabnawaz, Covalent adaptable network and self-healing materials: Current trends and future prospects in sustainability, Polymers 12 (2020) 2027.

[32] A. Vashchuk, Y. Kobzar, Chemical welding of polymer networks, Mater. Today Chem. 24 (2022) 100803.

Supporting Information

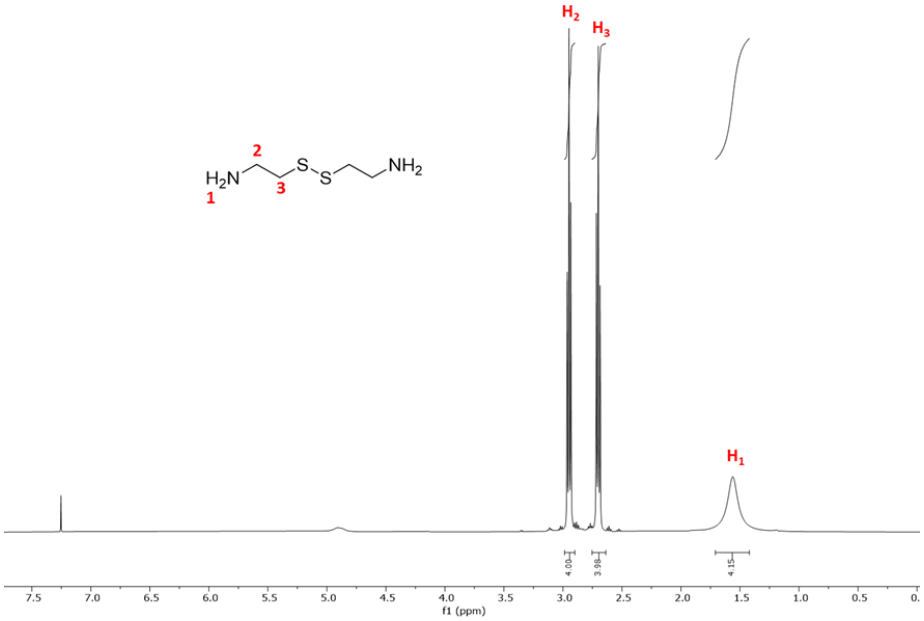

Figure 9.S1. ^{1}H NMR spectrum of cystamine (Cys) in $CDCl_3$.

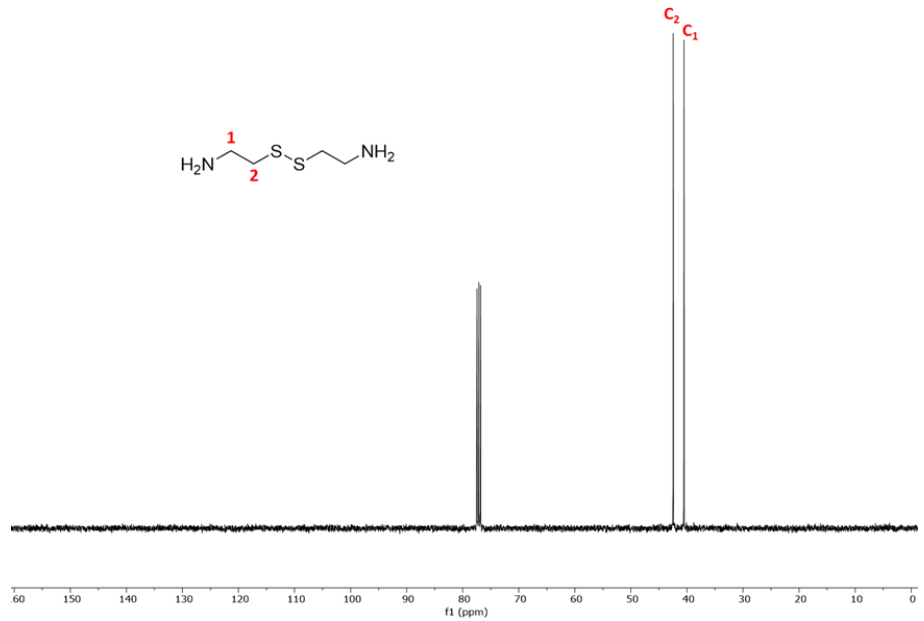

Figure 9.S2. ^{13}C NMR spectrum of cystamine (Cys) in $CDCl_3$.

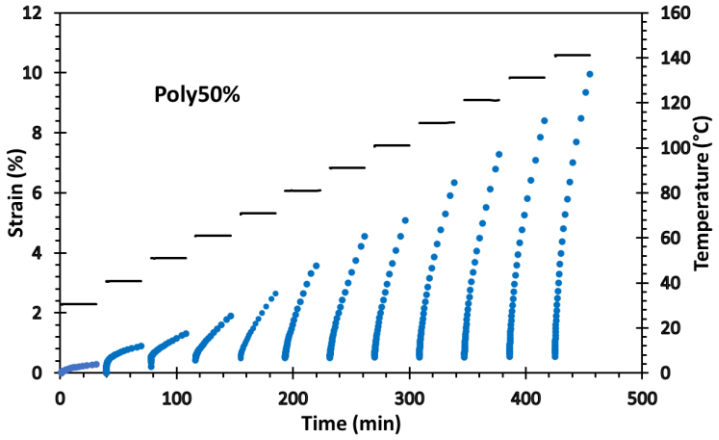

Figure 9.S3. Strain-time curves at each temperature obtained from creep tests for poly50%.

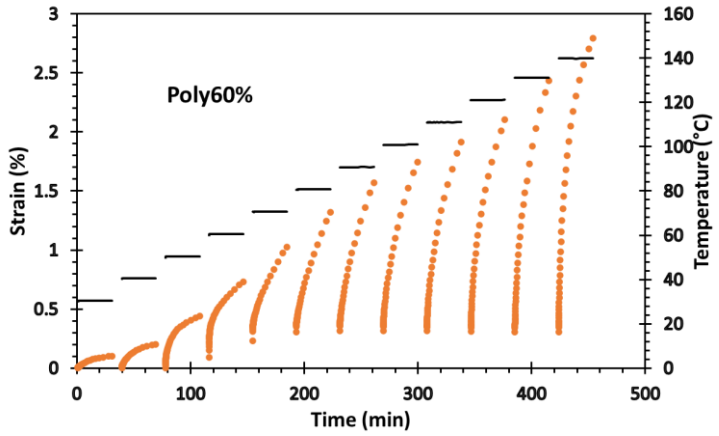

Figure 9.S4. Strain-time curves at each temperature obtained from creep tests for poly60%.

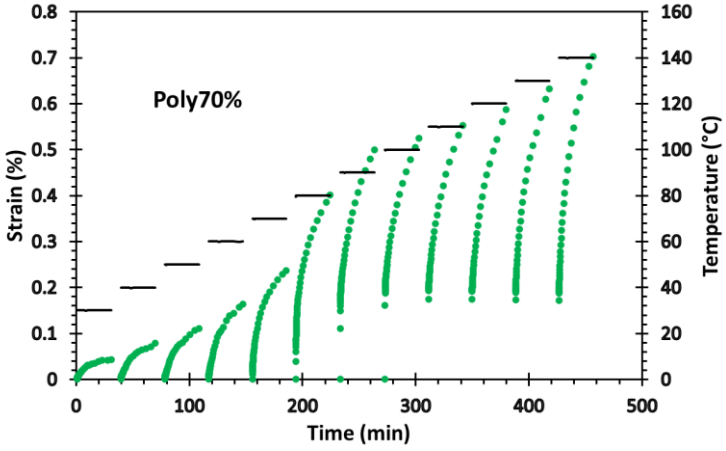

Figure 9.S5. Strain-time curves at each temperature obtained from creep tests for poly70%.

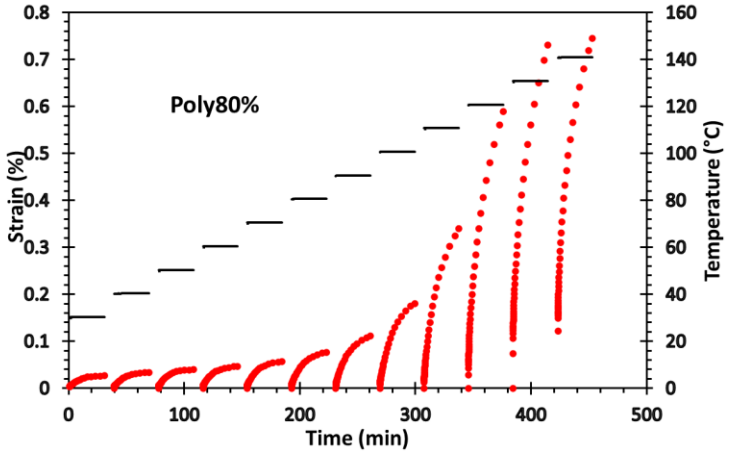

Figure 9.S6. Strain-time curves at each temperature obtained from creep tests for poly80%.

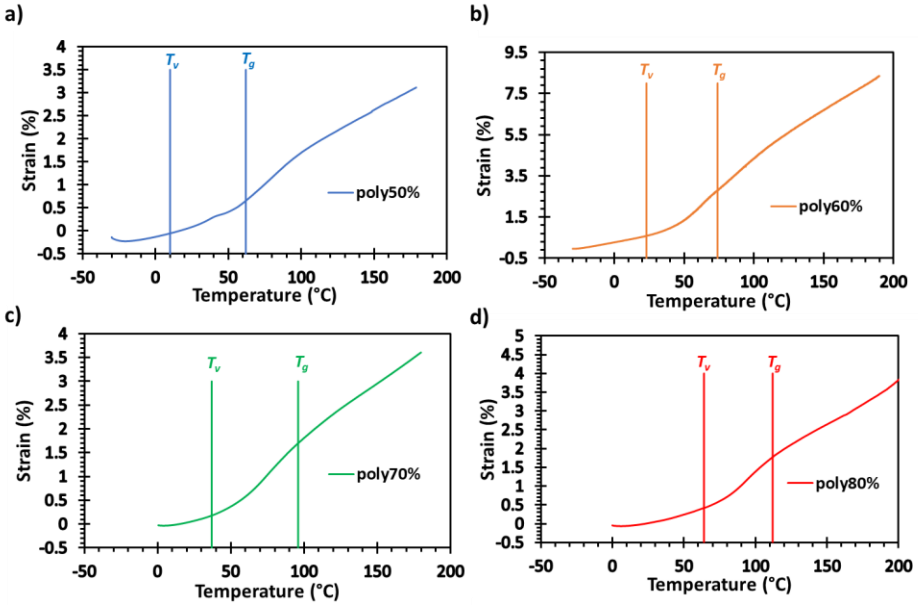

Figure 9.S7. Dilatometry experiments with a heating rate of 1 °C/min for all the materials.

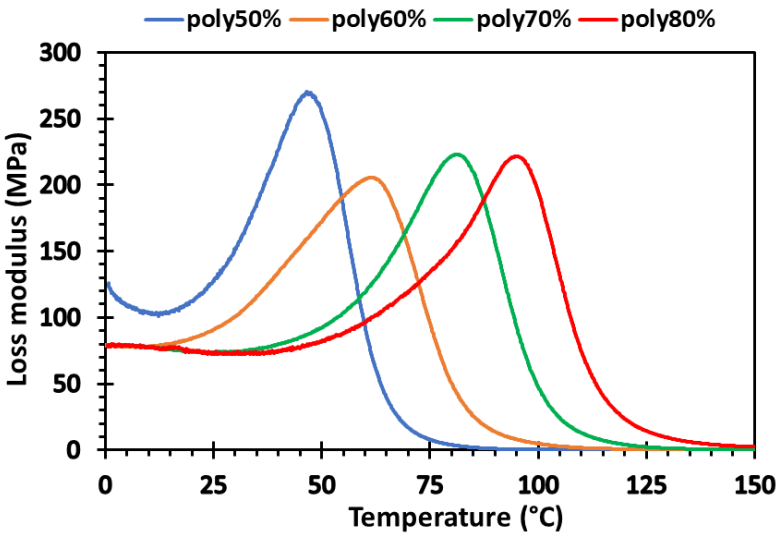

Figure 9.S8. Evolution of the loss modulus with temperature for all the materials prepared.

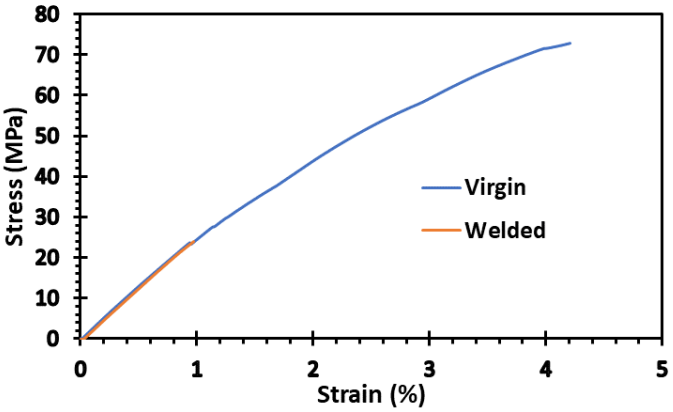

Figure 9.S8. Stress-Strain curves of the virgin and self-welded samples of poly80% material.

UNIVERSITAT ROVIRA I VIRGILI
PROGRESS IN SUSTAINABILITY WITHIN THE REALM OF DESIGNING NEW THERMOSETTING MATERIALS
Adrià Roig Gibert

Chapter 10

Structural reversible adhesives based on thiol-epoxy vitrimers

(*accepted*)

UNIVERSITAT ROVIRA I VIRGILI
PROGRESS IN SUSTAINABILITY WITHIN THE REALM OF DESIGNING NEW THERMOSETTING MATERIALS
Adrià Roig Gibert

(accepted)

Structural reversible adhesives based on thiol-epoxy vitrimers

Adrià Roig,[1] Laura Molina,[2] Àngels Serra,[1] David Santiago,[2,3] Silvia De la Flor[2*]*

[1] Universitat Rovira i Virgili, Department of Analytical and Organic Chemistry, C/ Marcel·lí Domingo 1, Edif. N4, 43007 Tarragona, Spain

[2] Universitat Rovira i Virgili, Department of Mechanical Engineering, Av. Països Catalans 26, 43007 Tarragona, Spain

[3] Eurecat- Chemical Technology Unit, C/ Marcel·lí Domingo 2, 43007 Tarragona, Spain

ABSTRACT

This work presents a family of functional adhesives based on covalent adaptable networks (CANs). Low-cost and commercially available monomers, including diglycidyl ether of bisphenol A, pentaerythritol tetrakis (3-mercapto propionate) and dipentaerythritol hexakis (3-mercapto propionate), were cured using a base catalyst to produce highly crosslinked materials. The catalyst selection and the study of the curing reaction were performed using differential scanning calorimetry (DSC) and Fourier-transform infrared spectroscopy (FTIR). The catalyst was chosen for better feasibility of industrial production, characterized by short curing times and relatively low temperatures. Thermal stability and thermomechanical properties of the final materials were evaluated through thermogravimetry (TGA) and dynamic mechanical thermal analysis (DMTA), respectively, revealing glass transition temperatures (T_g) higher than 50 °C. Stress relaxation tests were conducted to investigate the vitrimeric behavior of the polymers, which exhibited an Arrhenius-type dependence of relaxation times on temperature. Importantly, both materials demonstrated impressive creep resistance up to 70 °C, indicating their suitability for use at elevated service temperatures. Tensile and lap-shear tests were also performed, revealing high lap-shear strength values (up to 16 MPa) comparable to those of commercial adhesives. Furthermore, these vitrimers displayed remarkable properties such as shape memory, shape reconfiguration, and self-welding capabilities, underscoring their excellent potential for a wide range of highly demanding applications in industrial production.

KEYWORDS

Thiol-epoxy, covalent adaptable networks, vitrimers, functional adhesives, reversible adhesives

1. Introduction

Thermosets are widely recognized for their diverse range of applications in various sectors, including coatings [1], automobile manufacturing [2], and the optoelectronic industry [3]. However, their relevance in the field of adhesion stands out as one of their most significant contributions [4,5]. With the growing demand for adhesive bonding in industrial settings, there is a pressing need for novel adhesive materials to serve as viable alternatives to mechanical joints. Extensive research has been conducted in recent years to explore different types of adhesive materials [6-9]. Typically, these adhesives are based on thermosetting polymers known for their excellent mechanical performance. However, their crosslinked structure renders them non-recyclable and non-reprocessable, leading to significant environmental concerns. To address this limitation, the academic and industrial communities have directed their attention towards developing covalent adaptable networks (CANs). These materials combine the desirable mechanical properties of thermosets with the reprocessability and recyclability of thermoplastics [10]. CANs incorporate dynamic covalent bonds that impart mobility to the network, enabling a transition from a viscoelastic solid to a fluid-like plastic flow in response to external stimuli, often temperature [11]. Several types of CANs are described in the literature, with the nature of their dynamic chemistry influencing the final molecular architecture. Among CANs, vitrimers hold particular significance [12-18]. These materials exhibit a unique exchange mechanism between dynamic bonds that occurs in a concerted manner, meaning that the breakage and the formation of bonds occur simultaneously without any intermediate state. This mechanism maintains a constant crosslinking density, resulting in a gradual decrease in viscosity with temperature, following an Arrhenius law akin to vitreous silica [19,20]. Extensive efforts have been dedicated to the development of vitrimers, particularly those based on transesterifications, which were first described by Prof. Leibler in 2011 [20-24]. Owing to their exceptional properties, vitrimeric materials find applications across various industrial domains. The temperature-dependent viscosity of vitrimers, following an Arrhenius-type relationship and the presence of exchangeable bonds near the surfaces, enables their welding by forming of interfacial crosslinks between polymer interfaces at high temperatures. This characteristic makes vitrimers highly promising for future adhesive applications in the industrial sector. As the exchangeable links are not consumed but rather exchanged during the welding process, a joint can be reformed without modifying the surface of vitrimers, simply by applying the appropriate stimulus while the two surfaces are in contact [25]. Moreover, a joint can be disassembled by raising the temperature above the topology freezing temperature (or in some cases above T_v and T_g) and pulling the adherents apart without incurring any damage or loss of integrity. Although the industrial utilization of vitrimers is still in its early stages,

several examples of adhesive polymers are described in the existing literature. Verge et al. prepared a cardanol-based polybenzoxazine vitrimer containing disulfide bonds [26]. This vitrimer exhibited adhesive properties with short curing times, even at low temperatures, and demonstrated the ability to be recycled and reconfigured due to its short relaxation times and low activation energy. However, despite its reversibility and reprocessability, the adhesive properties of the obtained material were weaker compared to commercially available options. Sridhar and co-workers reported on thermally reversible crosslinked adhesives based on dissociative Diels-Alder networks [27]. These adhesives could be repeatedly re-used through heating/cooling cycles without using solvents during preparation or reutilization. Furthermore, they exhibited versatile adhesion and creep resistance. Moreno and co-workers prepared lignin-based vitrimers by reacting lignin with poly(ethylene glycol) divinyl ether. The resulting materials demonstrated excellent relaxation rates facilitated by acetal exchange, leading to high mechanical performance [28]. However, these polymers exhibited a lap shear strength of 6 MPa, which is relatively low compared to commercial adhesives. Nevertheless, the specimens used in the lap shear tests could be easily reglued via hot pressing, achieving a lap shear strength of 5.6 MPa, highlighting the potential of these materials as recoverable adhesives. Our group described a family of recyclable and recoverable adhesives by changing proportions of DGEBA as epoxy monomer and glutaric anhydride and glycerol as co-curing agents [29]. All materials showed high T_g values and could relax the stress at high temperatures thanks to the transesterification reaction. Moreover, these epoxy vitrimers showed high values of lap-shear strength, and thanks to self-healable and viscoelastic properties of vitrimers at high temperatures, they could be dismantled and re-bonded again, demonstrating up to 89% of recovery concerning the first lap-shear value in one of the materials. However, these adhesives required high temperatures and a long time to be fully cured, which is a drawback from an industrial and energetical point of view.

The above-mentioned studies on adhesives have often relied on expensive and complex starting materials, involved complicated synthetic steps, required the use of costly metal catalysts, or had long and challenging curing parameters. These factors make them energetically unfeasible for industrial applications.

To address these issues, we present a study focusing on the development of two different adhesives using affordable and readily available diglycidyl ether of bisphenol A (DGEBA), pentaerythritol tetrakis (3-mercapto propionate) (S4), and dipentaerythritol hexakis (3-mercapto propionate) (S6) (see Scheme 10.1). We take advantage of the thiol-epoxy reaction with a click character that leads to the formation of hydroxyl groups that can undergo a further transesterification reaction with the esters present in the thiol monomer structure. In this work, we first select

the appropriate catalyst and evaluate the evolution of the entire curing system using differential scanning calorimetry (DSC) and Fourier transform infrared spectroscopy (FTIR). The chosen catalyst and curing conditions are optimized for their viability in industrial production. The thermal stability of the resulting polymers was investigated using thermogravimetry (TGA), while their thermomechanical properties, vitrimeric behavior, and creep resistance were characterized by dynamic-mechanical-thermal analysis (DMTA). Both materials exhibited stress relaxation at elevated temperatures and demonstrated resistance to creep at room temperature, enhancing their adhesive performance. Furthermore, tensile and lap-shear tests revealed high values of strength, thus highlighting the materials' promising adhesive properties. Additionally, the materials, which are transparent and colorless, exhibited shape-memory properties and the ability for permanent shape reconfiguration, opening up new possibilities for industrial applications. By utilizing cost-effective starting materials and demonstrating favorable properties and performance, these adhesives hold significant potential for practical industrial applications.

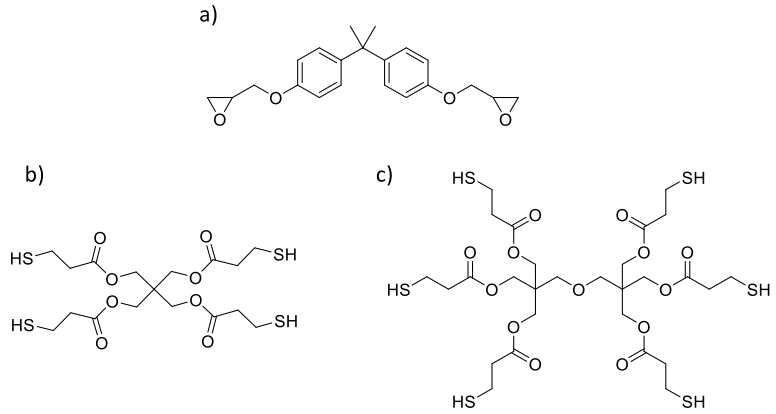

Scheme 10.1. Monomers used in the preparation of the materials a) DGEBA, b) S4 and c) S6.

2. Experimental methods

2.1 Materials

Diglycidyl ether of bisphenol A (DGEBA, 181.5 g/eq) was provided by Huntsman Corporation and dried in the vacuum for 2h at 80 °C. Pentaeryithrithol tetrakis (3-mercapto propionate) (S4, 98%, 122.17 g/eq) and dipentaerythrithol hexakis (3-mercapto propionate) (S6, 98%, 130.5g/eq) were supplied from Bruno Bock Thiochemicals and used as received. 1,5-Diazabicyclo[4.3.0]non-5-ene (DBN, 96%) and 1,8-diazabicyclo[5.4.0]undec-7-ene (DBU, >96%) were purchased at Alfa Aesar and Sodium tetraphenyl borate ($NaBPh_4$, 99%) at Thermo Scientific. 1-Methyl imidazole

(1MI) and 2-methyl imidazole (2MI) were provided by BASF, and base generators of 1MI, DBN, and DBU were synthesized accordingly to the literature [30,31].

2.2 Preparation of the materials

When using liquid catalysts, a certain amount of DGEBA was added in a vial followed by the stoichiometric proportion of S4 or S6 (molar ratio epoxy:SH 1:1). Finally, a 1% mol or 5% mol (to SH) of the catalyst was added and vigorously stirred. Then, the prepared formulations were poured into rectangular Teflon molds of 30 x 5 x 1.5 mm^3 dimensions and cured in a conventional oven at 80 °C for 4 h and at 120 °C for 2 h in the cases of S4 samples and 4 h at 120 °C for S6 samples.

In the case of solid catalysts, a 1% mol (to SH) of the catalyst was weighted on a vial followed by adding a certain amount of S4 or S6. Then, the mixture was kept at 80 °C for 2 h under stirring to dissolve the catalyst. Finally, the stoichiometric amount of DGEBA (molar ratio epoxy:SH 1:1) was added and vigorously stirred. After that, the sample preparation procedure was the same as explained above.

2.3 Characterization methods

A differential scanning calorimeter (DSC) Mettler DSC3+ calibrated using an indium standard (heat flow calibration) and indium-lead-zinc standard (temperature calibration) was used to analyze the curing evolution. Samples of approximately 5-10 mg were tested in aluminum pans with a pierced lid in a nitrogen atmosphere with a 50 mL·min^{-1} gas flow. Dynamic studies were performed in a temperature range of 30-250 °C with a heating rate of 10 °C min^{-1} for calculating the enthalpy (ΔH) released during the curing of the samples, which is obtained by integration of the calorimetric signal using a straight baseline, with the help of the STARe software. To calculate the glass transition temperature (T_g), dynamic studies were done in a temperature range of 0-250 °C with a heating rate of 20 °C min^{-1}.

A Jasco FT/IR-680 Plus spectrometer equipped with an attenuated total reflection accessory (ATR) (Golden Gate, Specac Ltd, Teknokroma) was used to record the FTIR spectra of the mixture before and after the curing procedure. Real-time spectra were recorded in the wavenumber range between 4000 and 600 cm^{-1} with a resolution of 4 cm^{-1} and averaged over 20 scans. The disappearance of the characteristic peak of the epoxy group at 915 cm^{-1} and the peak of SH groups at 2576 cm^{-1} as well as the appearance of the peak corresponding to O-H at 3300 cm^{-1} were used to confirm the completion of the reaction.

The thermal stability of the materials was evaluated using a Mettler Toledo TGA 2 thermobalance. Cured samples weighing around 10 mg were degraded between 30 and 600 °C at a heating rate of 10 °C min^{-1} under an N_2 atmosphere with a flow rate of 50 cm^3 min^{-1}.

The thermomechanical properties were studied using a DMTA Q800 (TA Instruments) equipped with a film tension clamp. Prismatic rectangular samples with dimensions of around 30 x 5 x 1.5 mm^3 were analyzed from 0 to 200 °C at 1 Hz, with 0.1% strain at a heating rate of 2 °C min^{-1}. Tensile stress-relaxation tests were conducted in the same instrument using the film tension clamp on samples with the same dimensions as previously defined. The samples were first equilibrated at the relaxation temperature for 5 min, and a constant strain of 1% was applied, measuring the consequent stress level as a function of time. The materials were tested only once at one temperature. The relaxation-stress $\sigma(t)$ was normalized by the initial stress σ_0, and the relaxation times (τ) were determined as the time necessary to relax $0.37\sigma_0$, i.e., ($\sigma = 1/e\sigma_0$). With the relaxation times obtained at each temperature, the activation energy values (E_a) were calculated using an Arrhenius-type equation:

$$ln(\tau) = \frac{E_a}{RT} - \ln A \qquad \text{(Eq. 10.1)}$$

where τ is the time needed to attain a given stress-relaxation value ($0.37\sigma_0$), A is the pre-exponential factor, and R is the gas constant. From Arrhenius relaxation, the topology freezing temperature (T_v) was obtained as the temperature at which the material reaches a viscosity of 10^{12} Pa·s. Using Maxwell relation and E' determined from DMTA (assuming E' is relatively invariant in the rubbery state), τ^* was determined to be between 10^4 s and 10^5 in our systems. The Arrhenius relationship was then extrapolated to the corresponding value of τ^* to determine T_v in each sample.

Creep and recovery properties were studied by the same DMTA Q800 apparatus equipped with a film tension clamp. All the samples were stretched under a stress of 0.1 MPa at different temperatures for 30 min, then the stress was immediately released, and the sample was left to recover for 30 min. To determine the viscosity at each temperature needed for the representation of the Angell Fragility Plot, a series of creep experiments were carried out on films at temperatures between 100 and 180 °C, increasing 10 °C in each scan. To perform the tests, the selected sample was equilibrated for 3 min at the specific temperature, and then a stress level of 0.1 MPa was applied for 30 min. The viscosity η (Pa·s) was then derived from the slope of the graph strain-temperature and represented in front of T_g/T, thus obtaining the Angell Fragility Plot. The T_v can also be calculated from this graph assuming a viscosity of 10^{12} Pa·s.

Final materials were tested until the break in tensile mode at room temperature using an electromechanical universal testing machine (UTM Shimadzu AGS-X) with a 10 kN load cell at 10 mm min^{-1} and using Type V samples with a thickness of 1 mm according to the ASTM D638-14 standard [32]. Three samples of each material were analyzed, and the results were averaged.

Aluminum platens 6060 T66 of 100 x 25 mm^2 with a thickness of 1.5 mm were used for lap-shear tests, according to the standard UNE-EN ISO 1465:2009 [33] (equivalent to ASTM D1002-10) [34]. The adhesion surfaces of the aluminum substrates were prepared following the UNE-EN ISO 13887:2004 [35] standard to ensure and durable joint. Overlapping regions were polished and degreased with acetone to remove any greasy impurities. Mechanical abrasion by sandpaper was performed to roughen the bond area. Surfaces were again degreased with acetone in order to remove any abrasion residue. The vitrimer adhesives were obtained by preparing the formulation in a vial and pouring it on the adhesion surface. Then, the upper aluminum sheet was placed, maintaining a bondline thickness of 2 mm with the help of Teflon spacers, and the joint was cured in the oven. An overlapping length of 12.5 mm was used according to UNE-EN ISO 1465:2009 standard. Tensile lap shear tests of the single-lap joint prepared with the different vitrimer adhesives were performed according to UNE-EN ISO 1465:2009 in the UTM at 1.3 mm min^{-1} crosshead speed. To test the reversibility of the adhesives after lap shear breakage, the substrates were re-united in an oven at 180 °C for 1 h applying a determined pressure. Furthermore, a manual dismantle was also made to the original samples at 180 °C and re-joint following the previously mentioned procedure. Dismantled samples and lap shear broken samples were re-tested again using the same conditions to obtain their new lap shear strength.

3. Results and discussion

3.1 Election of the catalyst

We prepared several formulations with different catalysts and loadings to determine the most suitable catalyst for the curing reaction. We first chose DBN and DBU as they are not only strong bases for the catalysis of the thiol-epoxy reaction but also reported catalysts for the further transesterification reaction at high temperatures [36]. Formulations of DGEBA, the stoichiometric amount of S4, and a 5% mol (to SH) of catalyst were prepared. However, when the latest was added, the thiol-epoxy reaction quickly started polymerizing in the same vial (see Figure 10.S1a). For this reason, we decided to decrease the loading of the catalyst to 1% mol (to SH). Unfortunately, the same happened, which hinders the use of these catalysts to prepare these adhesives. Then, 2MI was tested because its secondary amine can be covalently bonded in the structure of the network, which prevents the evaporation of the catalyst at high temperatures during the stress relaxation tests. Nevertheless, 2MI requires the dissolution of the mixture in dichloromethane and its further evaporation, which complicates the whole procedure. To ensure the applicability of the vitrimers as adhesives, base generators of DBU (1,8-diazabicyclo[5.4.0]undec-7-ene) and DBN (1,5-diazabicyclo[4.3.0]non-5-ene), as well as 1MI (1-methylimidazole), were prepared according to the literature (see Experimental Part). These base generators were selected because they possess a high latency of the formulation at room

temperature, which is essential for the practical use of the vitrimer as an adhesive. Interestingly, when exposed to high temperatures, these base generators release specific species that activate the curing process and facilitate the further exchange reaction. This thermal responsiveness allows the vitrimer adhesive to undergo crosslinking and structural rearrangement, enhancing its adhesive properties under elevated temperature conditions. The 1% mol (to SH) of base generators was weighted and homogenized with the thiol, followed by adding DGEBA and curing in the oven. As shown in Figure 10.S1b, when BGDBU and BGDBN were used after long curing times at high temperatures, materials were not homogenous due to the poor miscibility of these catalysts in the formulations. In the case of BG1MI, homogenous samples could be obtained, but they required high temperatures (post-curing at 160 °C) to be fully cured. Finally, a 5% mol of 1MI was added to the mixture, and after the curing process, materials with high transparency were obtained, indicating high homogeneity (see Figure 10.S2). The ease of preparation was also evident during the experimental procedure. Based on these observations, 1MI was selected as the catalyst for the vitrimeric system. Its use facilitates the formation of a homogeneous and transparent vitrimer while ensuring a soft and straightforward preparation process.

3.2 Study of the curing process

Once selected 1MI as the curing and the transesterification catalyst, the curing procedure should be determined. DSC tests were performed to know the reaction's enthalpy and to identify possible side reactions. As seen in Figure 10.1a, both formulations showed monomodal curves suggesting that no side reactions are taking place as expected by the click character of the thiol-epoxy reaction. Moreover, the curing enthalpy (ΔH) was between 120 kJ/eq and 130 kJ/eq, as reported previously by our group [37]. Considering these results, the curing temperatures and times were set up. In the case of DGEBA_S4, the onset of the peak starts at low temperatures so 80 °C and 4 h was selected as the curing schedule and a further post-curing at 120 °C during 1 h to ensure the reaction of the remaining epoxy groups.

To check the completion of the reaction, FTIR spectrum of the initial mixture and the final material were recorded (Figure 10.1b). The disappearance of the epoxy band at 910 cm^{-1}, the vanishment of the band at 2576 cm^{-1} corresponding to the free thiols and the appearance of the characteristic hydroxyl band at 3300 cm^{-1} confirmed that the thiol-epoxy reaction was completed [38].

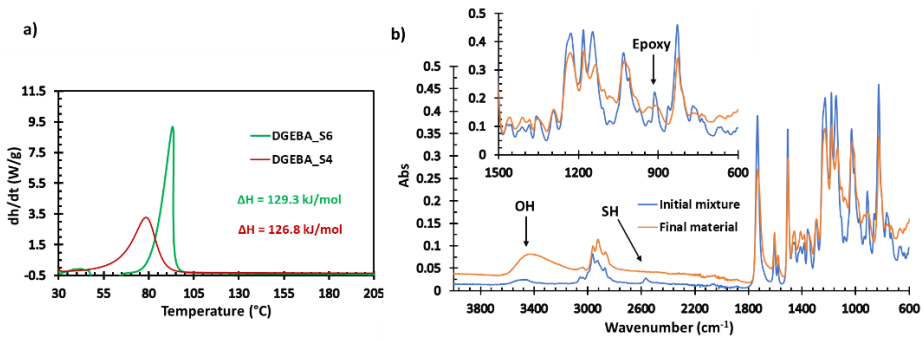

Figure 10.1. a) DSC thermograms corresponding to the dynamic curing at 10 °C for DGEBA_S6 (green) and DGEBA_S4 (red) formulations b) FTIR spectra for the initial mixture (blue) and the final material (orange) for DGEBA_S4.

3.3 Thermal characterization of the materials

To study the thermal stability of both materials as well as to confirm that no degradability takes place when thermal tests are performed, thermogravimetric analysis (TGA) was used. Figure 10.2 shows the TGA curves and their derivatives, and Table 10.1 summarizes the most significant thermogravimetric data.

As can be seen, both materials present similar degradation patterns and high onset temperatures. DTG curves show two main peaks which can be ascribed to a first β-elimination of the esters present in the thiols structure followed by a degradation of the remaining polymeric matrix [39]. It is worth saying that DGEBA_S6 loses its 2% of weight at 274.9 °C, which is slightly higher than DGEBA_S4 due to the higher cross-linking density that provides a higher thermal stability. Moreover, the char residue at 600 °C is bigger when the hexathiol is used for the same reason previously mentioned.

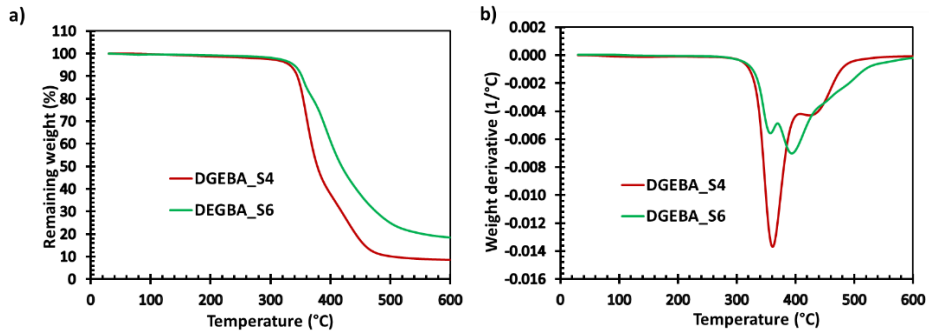

Figure 10.2. a) Thermogravimetric and b) DTG curves of the vitrimeric materials.

Table 10.1. Thermogravimetric and thermomechanical data for both materials prepared.

Sample	$T_{2\%}$[a] (°C)	Char yield[b] (%)	E'_{glassy}[c] (MPa)	$E'_{rubbery}$[d] (MPa)	$T_{tan\,\delta}$[e] (°C)	FWHM[f] (°C)
DGEBA_S4	266.2	9.0	2870	11.3	54.5	9.0
DGEBA_S6	274.9	18.1	3290	20.1	74.8	9.5

[a] Temperature of 2% of weight loss. [b] Char residue at 600 °C. [c] Glassy storage modulus at T_g - 50 °C determined by DMTA. [d] Rubbery storage modulus at T_g + 50 °C determined by DMTA. [e] Temperature at the maximum of tan δ peak at 1 Hz. [f] Full width at the half medium of tan δ peak.

The thermomechanical properties of the final materials were evaluated by DMTA analysis. Figure 10.3 shows the evolution of the damping capacity (tan δ) and the storage modulus (*E'*) with the temperature, and the data extracted are presented in Table 10.1. The results demonstrate that the DGEBA_S6 formulation exhibits a higher crosslinking density, leading to increased material rigidity and higher values of storage modulus (*E'*) in the glassy state. Similarly, the high functionality of the hexathiol component contributes to higher values of *E'* in the rubbery state, reflecting the influence of crosslinking density on material stiffness.

Furthermore, both materials exhibit $T_{tan\,\delta}$ values (considered as the glass transition temperature, T_g) above room temperature. This suggests that when used as adhesives, these materials will remain rigid in the glassy state at room temperature, ensuring excellent mechanical performance. Additionally, the T_g values allow the curing process to be conducted at moderate temperatures. Moreover, the low values of the full width at half maximum (FWHM) indicate fast transitions and high homogeneity in the materials. This is attributed to the click nature of the thiol-epoxy reaction, which promotes efficient and uniform curing reactions, resulting in homogeneous material properties.

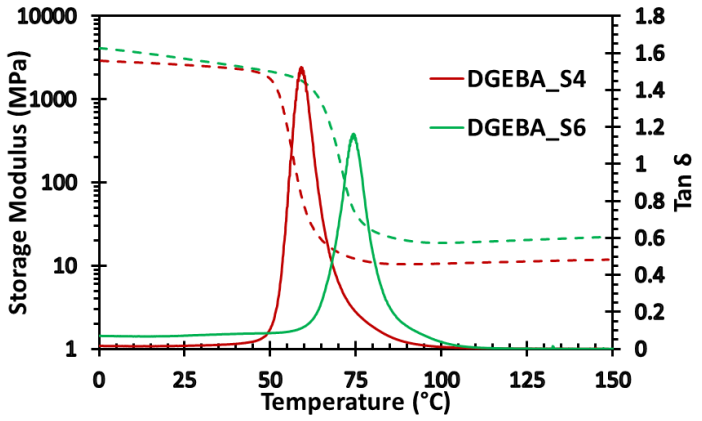

Figure 10.3. Evolution of the storage modulus and tan δ with the temperature of both materials prepared.

3.4 Study of the vitrimeric behavior of the materials

The vitrimeric behavior of the materials is achieved through the transesterification reaction catalyzed by 1MI at elevated temperatures. During the curing process, the thiolate species attacks the less hindered carbon of the epoxide, forming a thioether and a secondary alcohol. Since the thiol hardeners contain ester groups in their structure, the exchange reactions can occur through the attack of the secondary alcohol on the ester groups of the thiols. This exchange reaction enables the materials to exhibit vitrimeric properties.

To investigate the time and temperature-dependent relaxation of the materials and assess their vitrimeric properties, stress relaxation tests were performed using dynamic-mechanical-thermal analysis (DMTA) at different temperatures. The results are depicted in Figure 10.4, and the most relevant data are summarized in Table 10.2. It is evident that both materials exhibit favorable vitrimeric properties, but the thiol structure significantly affects the relaxation capability. Specifically, DGEBA_S4 demonstrates complete stress relaxation at 180 °C in less than 13 minutes, whereas DGEBA_S6 requires 45 minutes at the same temperature. This discrepancy can be attributed to the lower crosslinking density of DGEBA_S4, which provides greater chain mobility and enhances the likelihood of transesterification exchange reactions taking place.

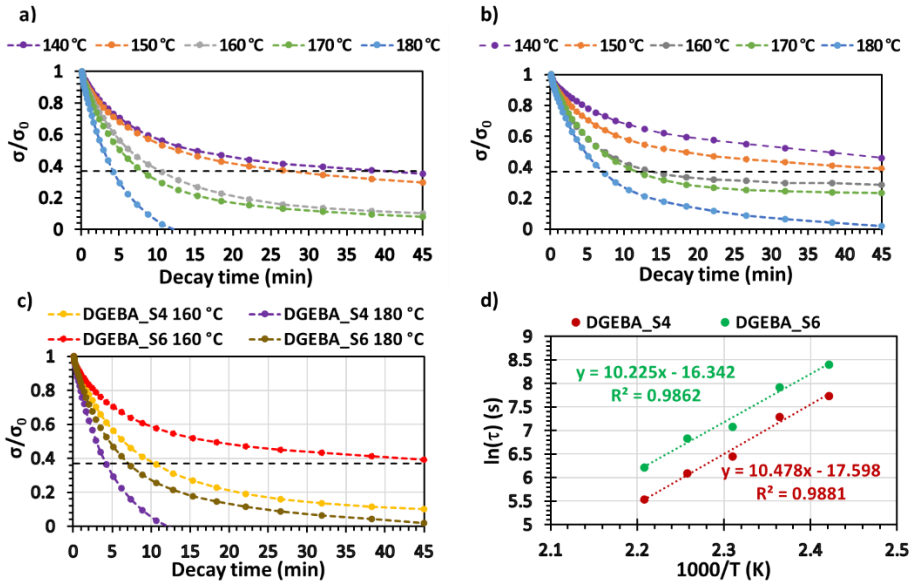

Figure 10.4. Normalized stress-relaxation plots as a function of time at different temperatures during 45 min for DGEBA_S4 (a) and DGEBA_S6 (b). Normalized stress-relaxation behavior at 160 °C and 180 °C for both samples (c) and Arrhenius plot of relaxation times against the inverse of temperature for both vitrimeric materials.

In vitrimers, a characteristic feature is the establishment of a linear relationship, akin to inorganic silica materials, between viscosity and temperature during exchange reactions. This behavior follows an Arrhenius-type dependence [40]. To gain a deeper understanding of the vitrimeric behavior exhibited by these materials, stress relaxation times required to achieve 37% of the initial stress (σ/σ_0 = 0.37) were determined at various temperatures, as shown in Figure 10.4a-b. Using the Arrhenius equation, the activation energy (E_a) of the transesterification reaction and the ln A values for these materials were determined and presented in Table 10.2.

Table 10.2. Relaxation times, topology freezing temperature, activation energy and adjusting parameters for the Arrhenius equation, and topology freezing temperature and Fragility index from creep tests of both samples prepared.

	Stress relaxation tests						Creep tests	
Sample	$\tau_{0.37}$[a] (min)	$\tau_{100\%}$[b] (min)	E_a (kJ mol^{-1})	ln A (s)	T_v (°C)	r^2	$T_{v(\eta)}$[c] (°C)	n[d]
DGEBA_S4	4.3	12.2	87.0	17.6	89.1	0.988	84.6	8.2
DGEBA_S6	8.4	45.0	85.1	16.3	103.7	0.986	106.6	9.2

[a] Time to reach a value of σ/σ_0 = 0.37 at 180 °C. [b] Time to reach total relaxation at 180 °C. [c] T_v calculated by creep tests at different temperatures. [d] Fragility index (n_{silica} = 16.5).

The obtained data reveal that both materials exhibit very similar values of activation energy (E_a). This finding is consistent with other transesterification vitrimers reported in the literature [20,21,41].

According to the Arrhenius equation, the topology freezing temperature (T_v) can be calculated. T_v is defined as the temperature at which the material reaches a viscosity of 10^{12} Pa·s and can be considered as the approximate temperature at which chemical exchanges occur. Below T_v, the interchange mechanisms are almost negligible [20]. In our systems, both materials have T_v values higher than their respective T_g values, with DGEBA_S4 having a slightly lower T_v, likely due to its higher mobility. These T_v values suggest that the vitrimeric exchange is not expected to significantly affect the creep resistance of the adhesives at service temperatures. Thermomechanical tests were also conducted on samples that had undergone prolonged stress relaxation at high temperatures (180 °C). The resulting tan δ curves showed no notable changes, indicating that the topological structure of both materials remained unchanged before and after an extended relaxation process.

Creep tests were conducted in DMTA to investigate the effect of temperature on the viscosity of the materials and their vitrimeric behavior. Figure 10.5a-b shows the creep tests at different temperatures for DGEBA_S4 and DGEBA_S6 materials, respectively. Figure 10.5c compares the creep behavior at 150 °C. When the materials are subjected

to constant stress above T_g but below T_v (70 °C), the strain is fully recovered, indicating that creep is almost negligible for both DGEBA_S4 and DGEBA_S6. However, as the temperature exceeds T_v and increases further, a notable increase in the slope of the ε-t curve is observed due to the decreasing viscosity of the material (inverse of the slope) with increasing temperature. Additionally, the occurrence of plastic deformation indicates the material's capability to undergo permanent reshaping. The creep behavior observed in DGEBA_S6 exhibits a similar pattern to that of DGEBA_S4. However, there is a slight reduction in creep for DGEBA_S6 due to the higher crosslinking density resulting from incorporating the hexathiol compound. These findings indicate that DGEBA_S6 may serve as a superior adhesive, as it demonstrates the ability to maintain its properties across a broader temperature range without compromising its performance. The enhanced temperature stability of DGEBA_S6 also suggests its potential as a more versatile adhesive option.

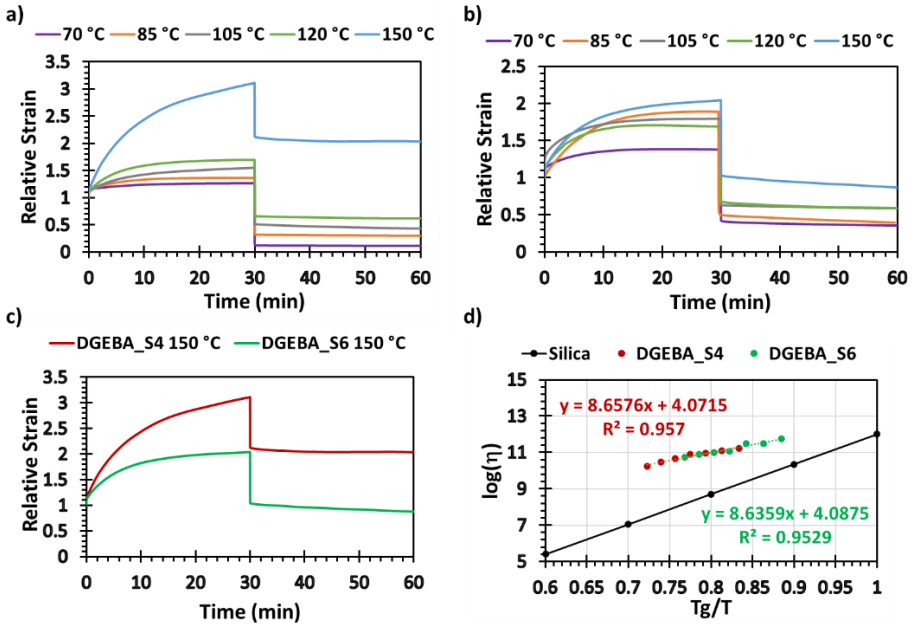

Figure 10.5. Creep tests at different temperatures for DGEBA_S4 (a) and DGEBA_S6 (b). c) Comparison of the creep tests for both materials at 150 °C and d) Angell Fragility plot for both materials.

The Angell fragility plot represented in Figure 10.5d illustrates the vitrimer behavior of both materials. As previously mentioned, upon surpassing the T_v, transesterification occurs, resulting in a gradual decrease in viscosity with increasing temperature, following an Arrhenius-type relationship. By utilizing the Angell fragility plot, it is possible to estimate the T_v by assuming a viscosity (η) of 10^{12} Pa·s corresponding to a logarithm value of 12. The extracted data from the Angell Fragility plot are presented

in Table 10.2, revealing a consistent trend in T_vs comparable to that obtained from stress relaxation tests.

3.5 Mechanical characterization

The mechanical properties of both materials were evaluated through stress-strain tests conducted at room temperature using a universal testing machine. The results for stress at break (σ_{break}), strain at break (ε_{break}), and tensile modulus (E) are collected in Table 10.3. As expected, DGEBA_S6 exhibits higher values of stress at break and tensile modulus compared to DGEBA_S4. This enhancement can be attributed to the elevated crosslinking density, which imparts greater strength to the material networks. Conversely, DGEBA_S4 demonstrates slightly higher values of strain at break due to the increased chain mobility, allowing for larger deformations.

Table 10.3. Characteristic mechanical parameters obtained from tensile test measurements.

Sample	Young Modulus (MPa)	Absorbed energy (kJ/m^3)	σ_{break} (MPa)	ε_{break} (%)
DGEBA_S4	2345 ± 328	1119 ± 190	52.2 ± 3.8	3.9 ± 1.3
DGEBA_S6	2556 ± 152	896 ± 101	58.3 ± 4.0	2.8 ± 0.1

3.6 Adhesion and re-adhesion properties

Adhesion lap-shear tests were conducted on both systems by joining aluminum plates following the UNE standard. The objective was to examine how the vitrimeric properties affect adhesion through re-adhesion tests involving dismantling and post-failure scenarios. In the dismantling test, the assembled joints were heated to 180 °C for 15 minutes, resulting in easy dismantling due to the occurrence of vitrimeric exchange reactions at that specific temperature. Subsequently, the fractured samples from the initial lap-shear test and the manually dismantled samples were re-joined by applying pressure and heating to 180 °C. It is important to note that a systematic investigation to determine the optimal conditions in temperature/time at which the joints can be dismantled and re-joined has not been performed. Thus, the temperatures (and times) were selected based on previous stress relaxation tests. The data obtained from the adhesion and re-adhesion tests are presented in Table 10.4, and the corresponding Force-displacement curves are presented in Figures 10.S4-S6.

As shown in Table 10.4, the lap-shear values of the original joints are comparable to those of commercial adhesives with similar T_g (around 20 MPa), particularly for DGEBA_S4 [29,42]. However, the re-adhesion results after failure and after dismantling are significantly lower, but this can be explained by various factors. Upon the failure or dismantling of the adhesive joint, if the material distribution between

the two plates is uneven, re-adhesion becomes challenging due to deficient surface preparation (such as roughening or the presence of dirt), resulting in suboptimal adhesion (see Figure 10.S7). However, the joints have exhibited significant resistance despite this, suggesting potential for improvement through optimization and further experimentation in this test. Notably, upon examining the Force-displacement curves of the lap-shear tests (Figure 10.S4-S6), it is evident that the initial slopes of the virgin, broken, and dismantled curves are highly similar. This suggests that the failure can be attributed to an experimental flaw in the joining process rather than being reflective of the material's inherent behavior, as the trends remain consistent across the different scenarios.

Table 10.4. Data extracted from adhesion and adhesion after failure and after dismantling tests.

	Virgin adhesion		Adhesion after failure		Adhesion after dismantling	
Material	F_{max} (N)	σ_{max} (MPa)	F_{max} (N)	σ_{max} (MPa)	F_{max} (N)	σ_{max} (MPa)
DGEBA_S4	5022 ± 220	16.1 ± 0.4	2017 ± 121	6.5 ± 0.3	2825 ± 89	9.0 ± 0.5
DGEBA_S6	3142 ± 301	10.1 ± 0.7	1745 ± 268	5.6 ± 0.4	2606 ± 159	8.3 ± 0.2

3.7 Reshaping, shape-memory and self-welding properties

A set of qualitative tests were conducted to demonstrate the reshaping capacity and shape memory properties of the materials, as depicted in Figure 10.7.

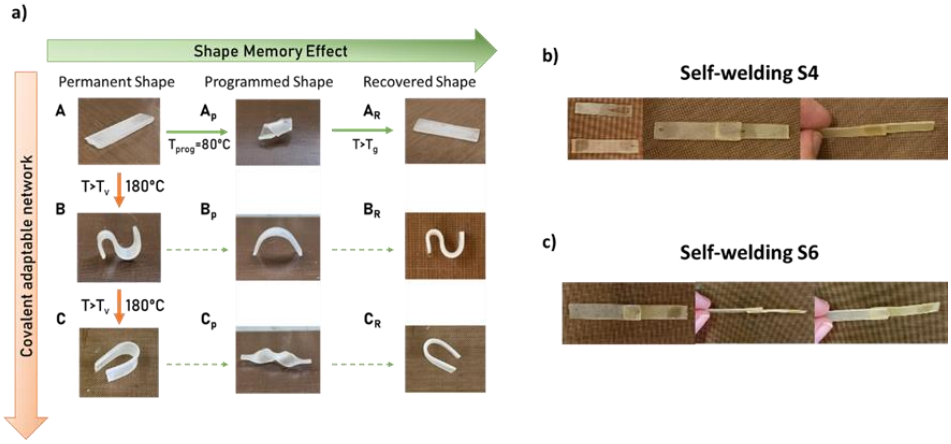

Figure 10.7. a) Qualitative demonstration of shape memory behavior and permanent/plastic shape change for DGEBA_S4 vitrimer. Pictures of the self-welding properties of DGEBA_S4 (b) and DGEBA_S6 (c).

In the case of vitrimers, where the T_v is significantly above the T_g, the material can exhibit shape-memory effect between T_g and T_v [18,21]. This means that if a temporary shape is imposed on the material at a temperature T within the range of $T_g<T<T_v$, and the material is rapidly cooled down, the original shape can be fully recovered by simply heating it above T_g. Conversely, if a shape is fixed at a temperature $T>T_v$, it will remain permanent due to the plastic deformation caused by the vitrimeric exchange. In Figure 10.7a, a series of fixed temporary shapes at $T_g<T<T_v$ (A_P, B_P, C_P) are shown, which were successfully recovered by heating them above T_g (A_R, B_R, C_R). Additionally, plasticized shapes that were bent by annealing at $T>T_v$ for 60 minutes (B and C) are also illustrated. This cyclic process can be repeated multiple times due to the excellent thermal stability of the samples at these temperatures. It is noteworthy that the samples maintain good transparency throughout the treatments. Furthermore, Figure 10.7b-c demonstrate the potential self-welding ability of these vitrimers, as the samples can be effectively joined together by heating them at temperatures above T_v (180 °C) for 1 hour under sufficient pressure.

4. Conclusions

A series of functional adhesives derived from thermosetting polymers containing dynamic covalent bonds have been designed and fully characterized, offering significant potential for industrial applications. The reversible nature of these adhesives allows for reshaping, reprocessing, and recycling without causing damage to the substrate, thanks to the transesterification reaction responsible for their vitrimeric behavior. Moreover, the materials are derived from easily accessible, cost-effective monomers (DGEBA, S4, and S6) and utilize a catalyst (1MI) that enables controlled curing parameters tailored to the specific materials being joined.

The vitrimeric adhesives exhibit high mechanical strength at room temperature, as evidenced by stress-strain tests with values of stress at break of 54 MPa and 73 MPa for DGEBA_S4 and DGEBA_S6, respectively. Notably, lap-shear tests demonstrate strong adhesion, especially for DGEBA_S4, yielding values of 16 MPa that are comparable to those of other commercial adhesives.

The vitrimeric properties of the materials were further evaluated through stress relaxation tests at elevated temperatures, revealing topology freezing temperatures (T_vs) of 89 °C for DGEBA_S4 and 104 °C for DGEBA_S6. These temperatures ensure that the reprocessing of the materials does not compromise their mechanical properties. Creep tests indicate that both materials maintain mechanical integrity up to 70 °C, beyond which the exchange mechanisms begin to decrease the material's viscosity. Additionally, for DGEBA_S4 adhesive joints, efficient dismantling can be achieved at temperatures above 180 °C without causing damage to the substrates. However, it should be noted that the mechanical properties of the joints after failure

and dismantling are significantly reduced due to the experimental re-adhesion procedure.

In conclusion, this study demonstrates that the developed materials possess not only the potential to be industrially competitive recyclable adhesives but also exhibit remarkable shape memory and self-welding properties. These findings highlight the significant potential of these materials in the industrial sector, showcasing their versatility and adaptability for various applications.

Acknowledgments

This work is part of the R&D projects PID2020-115102RB-C21 and TED2021-131102B-C22 funded by MCNI/AEI/10.13039/501100011033/ Unión Europea NextGenerationEU/PRTR. The authors acknowledge these grants for their financial support. The authors also thank Generalitat de Catalunya (2021-SGR-00154). Huntsman and Bruno Bock Thiochemicals are also acknowledged for kindly giving us epoxy resin and thiol monomers, respectively.

References

[1] X. Luo, P. T. Mather, Shape memory assisted self-healing coating, ACS Macro Lett. 2 (2013) 152-156.

[2] J. Verrey, M. D. Wakeman, V. Michaud, J. A. E. Månson, Manufacturing cost comparison of thermoplastic and thermoset RTM for an automotive floor pan, Compos. Part A 37 (2006) 9-22.

[3] M. Giordano, A. Laudati, M. Russo, J. Nasser, G. V. Persiano, A. Cusano, Advanced cure monitoring by optoelectronic multifunction sensing system, Thin Solid Films 450 (2004) 191-194.

[4] J. Economy, F. F. Shi, Aliphatic/aromatic copolyesters thermoset adhesives: Synthesis and characterization, Polym. Eng. Sci. 37 (1997) 549-558.

[5] A Kondyurin, Y. Klyachkin, Adhesion of UV-treated rubbers to epoxy adhesives, J. Appl. Polymer. Sci. 62 (1996) 1-8.

[6] R. Avendaño, R. J. C. Carbas, E. A. S. Marques, L. F. M. da Silva, A. A. Fernandes, Effect of temperature and strain rate on single joints with dissimilar lightweight adherends bonded with an acrylic adhesive, Compos. Struct. 152 (2016) 34-44.

[7] M. Q. dos Reis, M. D. Banea, L. F. M. da Silva, R. J. C. Carbas, Mechanical characterization of a modern epoxy adhesive for automotive industry, J. Brazilian Soc. Mech. Sci. Eng. 41 (2019) 1-11.

[8] L. Vertuccio, L. Guadagno, G. Spinelli, S. Russo, G. Iannuzzo, Effect of carbon nanotube and functionalized liquid rubber on mechanical and electrical properties of epoxy adhesives for aircraft structures, Compos. B. Eng. 129 (2017) 1-10.

[9] I. A. Akpinar, K. Gültekin, S. Akpinar, H. Akbulut, A. Ozel, Research on strength of nanocomposite adhesively bonded composite joints, Compos. B. Eng. 126 (2017) 143-152.

[10] G. M. Scheutz, J. J. Lessard, M. B. Sims, B. S. Sumerlin, Adaptable crosslinks in polymeric materials: resolving the intersection of thermoplastics and thermosets, J. Am. Chem. Soc. 141 (2019) 16181-16196.

[11] M. Podgórski, B. D. Fairbanks, B. E. Kirkpatrick, M. McBride, A. Martinez, A. Dobson, N. J. Bongiardina, C. N. Bowman, Toward stimuli-responsive dynamic thermosets through continuous development and improvements in covalent adaptable networks (CANs), Adv. Mater. 32 (2020) 1906876.

[12] P. Taynton, K. Yu, R. K. Shoemaker, Y. Jin, H. J. Qi, W. Zhang, Heat- or water driven malleability in a highly recyclable covalent network polymer, Adv. Mater. 26 (2014) 3938-3942.

[13] S. Wang, S. Ma, Q. Li, W. Yuan, B. Wang, J. Zhu, Robust, fire-safe, monomer recovery, highly malleable thermosets from renewable bioresources, Macromolecules 51 (2018) 8001-8012.

[14] A. Roig, P. Hidalgo, X. Ramis, S. De la Flor, À. Serra. Vitrimeric epoxy-amine polyimine networks based on a renewable vanillin derivative, ACS Appl. Polym. Mater. 4 (2022) 9341-9350. https://doi.org/10.1021/acsapm.2c01604.

[15] A. Roig, A. Petrauskaitė, X. Ramis, S. De la Flor, À. Serra, Synthesis and characterization of new bio-based poly(acylhydrazone) vanillin vitrimers, Polym. Chem. 13 (2022) 1510-1519.

[16] A. Rekondo, R. Martin, A. Ruiz de Luzuriaga, G. Cabañero, H. J. Grande, I. Odriozola, Catalyst-free room-temperature self-healing elastomers based on aromatic disulfide metathesis, Mater. Horiz. 1 (2014) 237-240.

[17] W. Denissen, M. Droesbeke, R Nicolaÿ, L. Leibler, J. M. Winne, F. E. Du Prez, Chemical control of the viscoelastic properties of vinylogous urethane vitrimers, Nat. Commun. 8 (2017) 14857.

[18] F. Gamardella, F. Guerrero, S. De la Flor, X. Ramis, A. Serra, A new class of vitrimers based on aliphatic poly(thiourethane) networks with shape memory and permanent shape reconfiguration, Eur. Polym. J. 122 (2020) 109361.

[19] F. Van Lijsebetten, J. O. Holloway, J. M. Winne, F. E. Du Prez, Internal catalysis for dynamic covalent chemistry applications and polymer science, Chem. Soc. Rev. 49 (2020) 8425-8438.

[20] D. Montarnal, M. Capelot, F. Tournhilac, L. Leibler, Silica-like malleable materials from permanent organic networks, Science 334 (2011) 965-968.

[21] F. I. Altuna, C. E. Hoppe, R. J. J. Williams, Shape memory epoxy vitrimers based on DGEBA crosslinked with dicarboxylic acids and their blends with citric acid, RSC Adv. 6 (2016) 88647-88655.

[22] T. Liu, C. Hao. L.Wang, Y. Li, W. Liu, J. Xin, J. Zhang, Eugenol-derived biobased epoxy: shape memory, repairing and recyclability, Macromolecules 50 (2017) 8588-8597.

[23] E. Rosseger, R. Höller, D. Reisinger, J. Strasser, M. Fleisch, T. Griesser, S. Schlögl, Digital light processing 3D printing with thiol-acrylate vitrimers, Polym. Chem. 12 (2021), 639. https://doi.org/10.1039/D0PY01520B.

[24] M. Hayashi, A. Katayama, Preparation of colorless, highly transparent, epoxy-based vitrimers by the thiol-epoxy click reaction and evaluation of their shape-memory properties, ACS Appl. Polym. Mater. 2 (2020) 2452-2457.

[25] N. J. Van Zee, R. Nicolaÿ, Vitrimers: permanently crosslinked polymers with dynamic network topology, Prog. Polym. Sci. 104 (2020) 101233.

[26] A. Trejo-Machin, L. Puchot, P. A. Verge, A cardanol-based polybenzoxazine vitrimer: recycling, reshaping and reversible adhesion, Polym. Chem. 11 (2020) 7026.

[27] L. M. Sridhar, M. O. Oster, D. E. Herr, J. B. D. Gregg, J. A. Wilson, A. T. Slark, Re-usable thermally reversible crosslinked adhesives from robust polyester and poly(ester urethane) Diels-Alder networks, Green. Chem. 22 (2020) 8669-8679.

[28] A. Moreno, M. Morsali, M. H. Sipponen, Catalyst-free synthesis of lignin vitrimers with tunable mechanical properties: circular polymers and recoverable adhesives, ACS Appl. Mater. Interfaces 13 (2021) 57952-57961.

[29] D. Santiago, D. Guzmán, J. Padilla, P. Verdugo, S. De la Flor, À. Serra, Recyclable and reprocessable epoxy vitrimer adhesives, ACS Appl. Polym. Mater. 5 (2023) 2006-2015.

[30] O. Konuray, N. Areny, J. M. Morancho, X. Fernández-Francos, A. Serra, X. Ramis, Preparation and characterization of dual-curable off-stoichiometric amine-epoxy thermosets with latent reactivity, Polymer 146 (2018) 42-52.

[31] X. Sun, J. P. Gao, Z. Y. Wang, Bicyclic guanidinium tetraphenylborate: a photobase generator and a photocatalyst for living anionic ring-opening polymerization and cross-linking of polymeric materials containing ester and hydroxy groups, J. Am. Chem. Soc. 130 (2008) 8130-8131.

[32] ASTM D638-14. Standard test method for tensile properties of plastics (2014).

[33] UNE-EN ISO 1465. Adhesives. Determination of tensile lap-shear strength of bonded assemblies (2009).

[34] ASTM D1002-10. Standard test method for apparent shear strength of single-lap-joint adhesively bonded metal specimens by tension loading (Metal-to-Metal) (2010).

[35] UNE-EN ISO 13887. Structural adhesives. Guideline for surface preparation of metals and plastics prior to adhesive bonding (2004).

[36] H. Song, Z. Fang, B. Jin, P. Pan, Q. Zhao, T. Xie, Synergetic chemical and physical programming for reversible shape memory effect in a dynamic covalent network with two crystalline phases, ACS Macro Lett. 8, (2019), 682-686.

[37] D. Guzmán, X. Ramis, X. Fernández-Francos, A. Serra, New catalysts for diglycidyl ether of bisphenol A curing based on thiol-epoxy click reaction, Eur. Polym. J. 59, (2014), 377-386.

[38] E. Pretsch, P. Bühlmann, M. Badertscher, Structure Determination of Organic Compounds: Tables of Spectral Data; 4th Ed.; Springer Berlin: Heidelberg, 2009.

[39] M. Arasa, X. Ramis, J. M. Salla, A. Mantecón, A. Serra, A study of the degradation of ester-modified epoxy resins obtained by cationic copolymerization of DGEBA with lactones initiated by rare earth triflates, Polym. Degrad. Stab. 92, (2007), 2214-2222.

[40] W. Denissen, J. M. Winne, F. E. Du Prez, Vitrimers: permanent organic networks with glass-like fluidity, Chem. Sci. 7, (2016), 30-38.

[41] M. Capelot, M. M. Unterlass, F. Tournilhac, L. Leibler, Catalytic control of the vitrimer glass transition, ACS Macro Lett. 1, (2012), 789-792.

[42] C. Russo, F. Bustamante, X. Fernández-Francos, S. De la Flor, Adhesive properties of thiol-acrylate-epoxy composites obtained by dual-curing procedures, Int. J. Adhesion & Adhesives 112, (2022), 102595.

Supporting Information

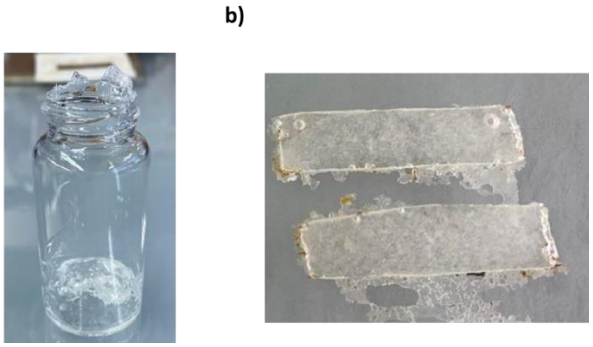

Figure 10.S1. a) Formulation with DGEBA and S4 with 5% mol DBU (to SH) already polymerized just after adding the catalyst and b) Samples of DGEBA_S4 and 1% mol of BGDBU after the curing process.

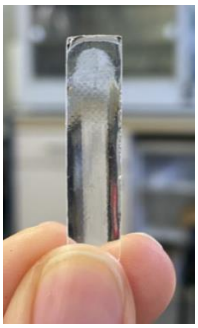

Figure 10.S2. DGEBA_S4 with 5% mol 1MI (to SH) after curing at 80 °C for 4 h and post-cured at 120 °C for 1h.

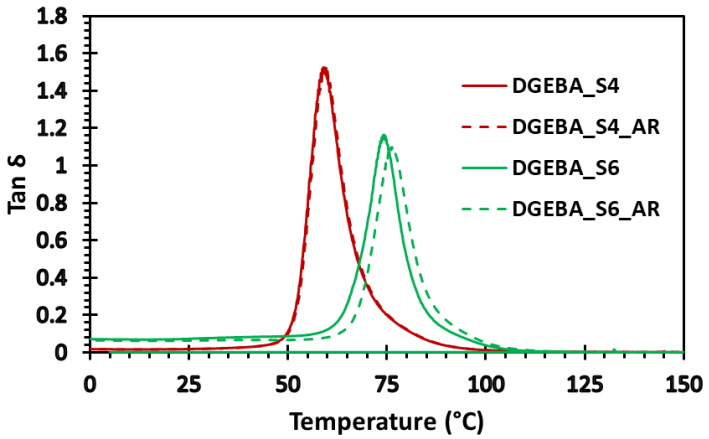

Figure 10.S3. Evolution of tan δ with temperature before (continuous) and after (dotted) stress relaxation tests at 180 °C for DGEBA_S4 (red) and DGEBA_S6 (green).

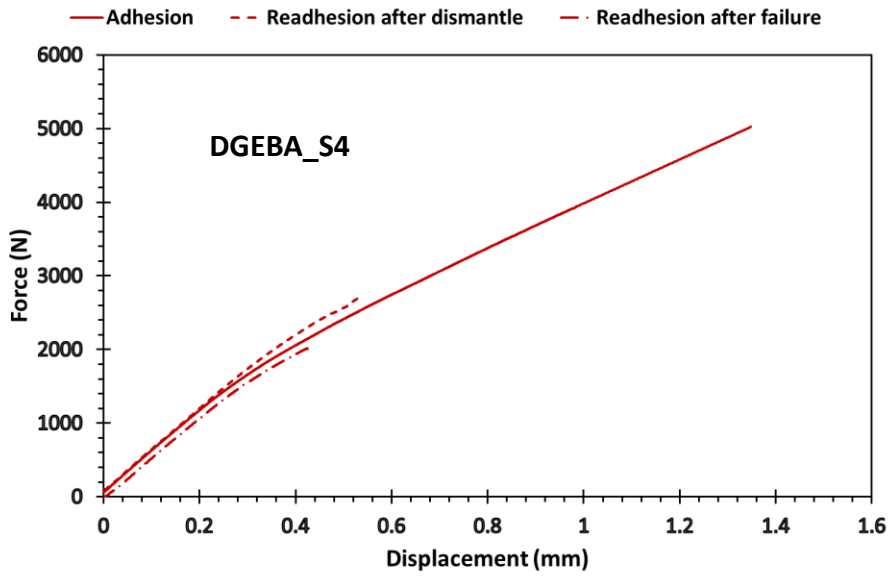

Figure 10.S4. F-displacement curves of DGEBA_S4 material obtained from lap-shear test in the adhesion (line), re-adhesion after dismantling (dotted) and adhesion after failure (dotted-line).

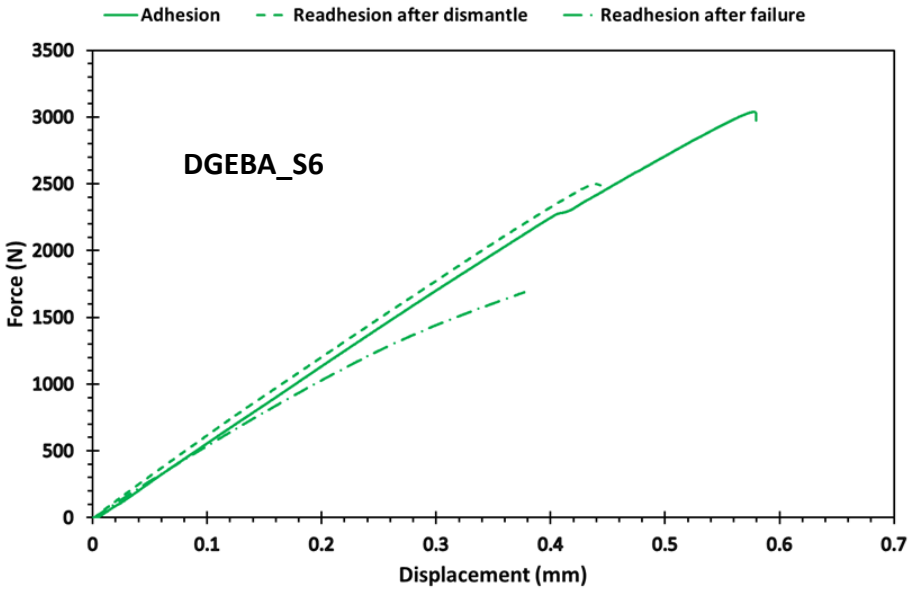

Figure 10.S5. F-displacement curves of DGEBA_S6 material obtained from lap-shear tests in the adhesion (line), re-adhesion after dismantling (dotted) and adhesion after failure (dotted-line).

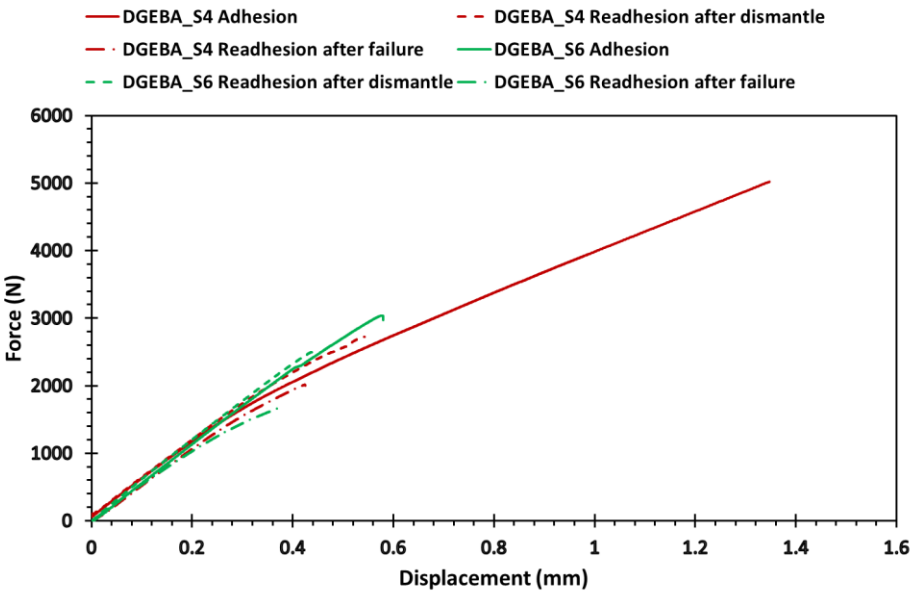

Figure 10.S6. Comparison of F-displacement curves obtained from lap-shear tests in the adhesion (line), re-adhesion after dismantling (dotted) and re-adhesion after failure (dotted-line) for DGEBA_S4 (red) and DGEBA_S6 (green).

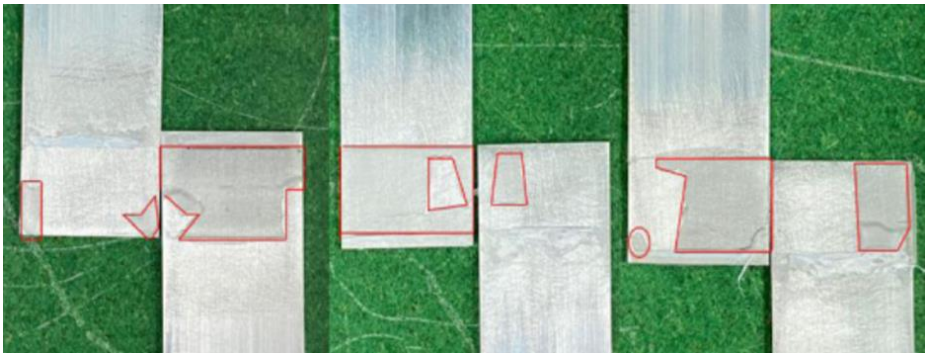

Figure 10.S7. Tested plates after lap-shear tests for DGEBA_S4 where it can be seen not a cohesive failure in some of them but an adhesion failure.

UNIVERSITAT ROVIRA I VIRGILI
PROGRESS IN SUSTAINABILITY WITHIN THE REALM OF DESIGNING NEW THERMOSETTING MATERIALS
Adrià Roig Gibert

Chapter 11

Eugenol-based dual-cured materials with multiple dynamic exchangeable bonds

(*submitted*)

UNIVERSITAT ROVIRA I VIRGILI
PROGRESS IN SUSTAINABILITY WITHIN THE REALM OF DESIGNING NEW THERMOSETTING MATERIALS
Adrià Roig Gibert

(submitted)

Eugenol-based dual-cured materials with multiple dynamic exchangeable bonds

Adrià Roig,[1] Xavier Ramis,[2] Silvia De la Flor,[3] Àngels Serra[1*]*

[1] Universitat Rovira i Virgili, Department of Analytical and Organic Chemistry, C/ Marcel·lí Domingo 1, Edif. N4, 43007 Tarragona, Spain

[2] Universitat Politècnica de Catalunya, Thermodynamics Laboratory ETSEIB, Av. Diagonal 647, 08028 Barcelona, Spain

[2] Universitat Rovira i Virgili, Department of Mechanical Engineering, Av. Països Catalans 26, 43007 Tarragona, Spain

ABSTRACT

In the present work, the preparation of sustainable thermosets has been approached simultaneously from three different points of view: a) the use of bio-based monomers chemically modified through green methodologies, b) the adoption of dual curing through click-type reactions to implement more efficient manufacturing processes, and c) inclusion of interchangeable groups in the network, to enable the reuse and recycling of the material at the end of its useful life and avoid waste generation.

The covalent adaptable networks (CANs) prepared contained three different types of dynamic bonds (disulfide, esters, and β-aminoesters), and they were prepared by a dual-curing procedure involving aza-Michael addition and epoxy-amine reaction. As bio-based starting compounds, eugenol, cystamine, and glycerol have been used. Intermediate and final materials could be prepared with different tailorable properties by controlling the molar ratio of the epoxy acrylate of eugenol (AEEU) and glycerol triacrylate (GTA). By using DSC and rheology, we could evaluate the sequentiality and the gelation of the curing process. The thermomechanical properties of the final materials were tested by DMA and revealed T_gs above room temperature. Bending tests at break were performed to evaluate the mechanical properties. Stress relaxation tests revealed that all materials could relax the stress even at relatively low temperatures (120 °C) in less than 21 minutes. The associative and dissociative behavior of these materials was investigated through rheology, and their reprocessability was tested to highlight the wide range of possibilities in many different fields of these CANs.

KEYWORDS

Biobased, eugenol, dual-curing, covalent adaptable networks, recyclability.

1. Introduction

In a world where the depletion of fossil fuel reserves concerns the population, the need to search for alternative routes to overcome it stands out as a significant and critical challenge. The polymer industry is one of the technological fields where replacing petrol-based resources is still in the early stages. For this reason, researchers are developing polymers from natural resources such as vegetable oils, terpenes, terpenoids, carbohydrates, or lignin [1,2]. Among all of them, lignin derivatives like vanillin or eugenol are being widely used as building blocks for biobased polymeric structures [3,4]. Indeed, eugenol, which is used in perfumes, antioxidants, food additives or even in the pharmaceutical industry, is a promising feedstock for the development of renewable crosslinked networks thanks to the phenolic and allylic groups in its structure that can be further modified to get a suitable functionality and its rigid structure that may provide high thermal and mechanical properties to the materials [5].

In the field of polymers, the recyclability of thermosetting materials is a struggling society. Thermosets have excellent mechanical performance and chemical resistance and are, therefore, very durable materials, but the 3D crosslinked network inhibits the reprocessability or reshaping, resulting in amounts of polymeric waste that end up in landfills and cause major environmental issues. For this reason, the introduction of dynamic bonds able to undergo reversible reactions upon applying a certain stimulus in the chemical structure of the polymers has raised up as a promising solution to avoid the generation of trash [6]. Thus, these materials called covalent adaptable networks (CANs), behave as thermosetting materials at low temperatures maintaining their good mechanical properties, but when an external stimulus such as heat or UV light is applied, they can flow and therefore, be reshaped thanks to these exchangeable bonds [7].

Generally, the mechanism of the exchange reactions of CANs may proceed *via* two different pathways: associative or dissociative [8]. In the first case, the reaction occurs in a single step, meaning that the cleavage and the formation of the new bond take place simultaneously, which always keeps the network integrity, and the viscosity gradually decreases with temperature. This type of CANs was named vitrimers by Prof. Leibler in 2011 due to their similar temperature-dependence behavior to the vitreous inorganic silica [6]. In contrast, the dissociative CANs experience a sudden drop of the viscosity with temperature because the mechanism occurs in two steps: first, the cleavage of the bond, which also produces the loss of the network integrity, and then, the formation of the new bond [9].

In the past decade, the development of CANs has grown exponentially through the incorporation of many different dynamic bonds from well-known organic reversible

reactions such as transesterification [10-12], imine metathesis [13-15], disulfide metathesis [16,17], Diels-Alder reaction [18], or reversible aza-Michael addition [19-21] among many others which reveals the current increasing interest for this type of materials.

The reprocessability of CANs is one of the most important properties of these materials, which stems from the presence of internal dynamic bonds that allow the rearrangement of the network leading to stress relaxation when subjected to thermal excitation [22]. For this reason, incorporating multiple dynamic bonds into the polymer structure not only provides fascinating effects on recyclability but would also provide beneficial effects in terms of self-healing, self-welding, or 3D printing applications [23]. Xu *et al.* reported the introduction of dynamic imine and disulfide bonds in an epoxy-based polymer [24]. They described the synergistic effect of the disulfide dissociation upon the imine bonds, which provided fast exchange rates and good reprocessability despite the highly crosslinked network that maintained the final materials' excellent thermal and mechanical properties. Zhang and co-workers described the introduction of β-hydroxy esters and disulfide bonds into the polymer matrix by performing first, an epoxy-acid reaction to prepare carboxylic acid-extended epoxy resins and, secondly, curing through an epoxy-amine condensation [25]. Moreover, they could tailor the dynamic properties of the CANs by changing the ratio of the acid and the aromatic disulfide amine, obtaining rapid self-healing properties (80% after heating for 10 min at 180 °C), demonstrating the significant advantages of dual dynamic networks. Dichtel et al. also introduced disulfide bonds into polyhydroxy urethane (PHU) networks using cystamine as a comonomer [26]. They could drastically shorten the reprocessing times incorporating this second type of dynamic bonds and the relaxation times (30 s at 150 °C) compared to the analogous rigid PHU. In addition, cystamine provides similar thermal stability and outstanding mechanical properties to the final materials. More recently, Konuray et al. prepared a family of thiol-ene polymers containing both disulfide and hydroxyl esters groups that undergo reversible disulfide metathesis and transesterification reactions [27]. Given the different kinetics of both exchange reactions, they were able to reprocess the material at moderate temperatures thanks to the disulfide metathesis, and even when the disulfide content was low, transesterification at higher temperatures allowed the recyclability to maintain similar properties to those of virgin materials. For this reason, incorporating multiple dynamic covalent bonds into a polymer matrix can provide outstanding beneficial effects not only in recyclability but also in the design of tailorable multi-response materials with self-healing, self-welding, and many different applications [28].

Among all the possibilities to obtain thermosetting materials, dual curing is one of the most efficient and versatile methodologies for preparing thermoset devices in a

controlled manner. This procedure consists of two different polymerization processes, sequential or simultaneous, that are triggered by external stimuli such as heat or UV light [29]. In particular, sequential dual curing allows obtaining, after a first curing stage, a stable viscous or gelled intermediate material with specific properties able to be applied or processed to get, after a second curing reaction, a fully cured material with higher mechanical properties. This procedure also allows tailoring the properties of intermediate and final materials thanks to the chemical control among the monomer functionality, structure, and feed ratio of the formulation. Another important added value of dual curing is the possibility to use "click-type" reactions which are especially suitable due to their orthogonality, selectivity, mild conditions, and high yields, which is of high importance in reducing processing energy costs [30].

Our group has deeply studied many dual-curing procedures for advanced applications in thermosetting materials by using "click" chemistry showing the high versatility of this methodology [31-35].

In the present work, we have prepared a family of thermosetting materials with multiple dynamic exchangeable bonds through a dual-curing methodology. We have synthesized through a sustainable procedure a new acrylate-epoxy derivative from biobased eugenol that has been cured firstly through an aza-Michael reaction at low temperatures and secondly via an epoxy-amine condensation of epoxy groups at high temperatures using Jeffamine D230 or cystamine as crosslinkers. Moreover, the tri acrylate derivative of glycerol has been successfully synthesized and added to the formulation to get gelled intermediate materials and tune the properties of the intermediate and final materials. DSC has been used to study the sequentiality of dual curing and to characterize intermediate and final materials. FTIR and TGA analyses have been performed to check the completion of both reactions during the curing times and the thermal stability of the final materials. The thermomechanical properties and the dynamicity of the obtained crosslinked polymers have been evaluated through DMA and rheology tests.

The recyclability of materials has been proved, and DMA has made it possible to evaluate the mechanical properties of the final materials to understand their behavior at service temperatures.

2. Experimental methods

2.1 Materials

Eugenol (EU, 99%), *m*-chloroperbenzoic acid (MCPBA, 70-75%), glycerol (Gly, 98%), sodium bicarbonate ($NaHCO_3$, 99%), and sodium chloride (NaCl, 99%) were purchased from Thermo Scientific. Acryloyl chloride (≥97%), *candida antarctica* lipase B (CALB), methyl acrylate (MA, 98%), allyl bromide (97%), cystamine dihydrochloride (Cysd, 97%), and oxone were obtained from Sigma Aldrich. Triethylamine (TEA), *tert*-butanol

(*t*BuOH), methyl *tert*-butyl ether (M*t*BE) and sodium disulfite ($Na_2S_2O_5$) were purchased from Scharlau, and triethyl benzyl ammonium chloride (TEBAC, 99%) from Alfa Aesar. Poly(oxypropylene) diamine (Jeff D230) was kindly donated by Huntsman. All chemicals were used without any purification except CALB that was put in a desiccator under vacuum overnight with anhydrous $MgSO_4$. Dichloromethane (DCM, Scharlau) was purified and dried by standard procedures.

2.2 Synthesis of acrylate eugenol (AEU)

EU (10.0 g, 61 mmol) and TEA (13.0 mL, 71.4 mmol) were dissolved in 30 mL of anhydrous DCM under inert conditions. The solution was cooled down to 0-5 °C and stirred 30 minutes before adding dropwise acryloyl chloride (5.9 mL, 71.4 mmol) dissolved in 10 mL of dry DCM. The reaction was allowed to proceed for 24 h at room temperature. Then, the reaction was vacuum filtered and washed once with HCl 1M, twice with saturated $NaHCO_3$ solution and finally saturated NaCl solution. The organic layer was dried over anhydrous $MgSO_4$, and the solvent removed in a rotary evaporator to afford AEU as a yellowish viscous oil (12.6 g, 95%).

^{1}H NMR ($CDCl_3$, δ in ppm): 6.99 (d, 1H); 6.79 (m, 2H); 6.61 (dd, 1H); 6.35 (dd, 1H); 6.00 (dd, 1H); 5.99 (m, 1H); 5.11 (m, 2H); 3.81 (s, 3H); 3.39 (d, 2H) (see Figure 11.S1). ^{13}C NMR ($CDCl_3$, δ in ppm): 164.29, 150.95, 139.09, 137.82, 137.07, 132.42, 127.70, 122.53, 120.71, 116.18, 112.81, 55.88, 40.12 (see Figure 11.S2).

2.3 Synthesis of acrylate epoxy eugenol (AEEU)

The synthesis of AEEU was performed in two different ways. Here, we described the one using Oxone as a reagent. The other one can be seen in the SI. AEU (1 g, 4.60 mmol), acetone (47.0 mL, 0.64 mol), H_2O (25 mL), ethyl acetate (50 mL), TEBAC (0.21 g, 0.92 mmol) and $NaHCO_3$ (16.9 g, 0.20 mol) were added in a 500 mL three-necked flask and stirred for 5 minutes and cooled down to 0-5 °C. Then, oxone (22.5 g, 73.3 mmol) in portions of 7.15 g diluted in 50 mL of H_2O every day during 2 days. The mixture was allowed to react 1 further day at 0-5 °C. Then, the organic product was extracted with diethyl ether (3 x 100 mL) and the organic layer was washed with H_2O twice, dried over anhydrous $MgSO_4$ and the solvent removed in the rotary evaporator obtaining AEEU as a yellowish solid (0.86 g, 80%). Melting point was 62.2 °C (by DSC).

^{1}H NMR ($CDCl_3$, δ in ppm): 7.01 (d, 1H); 6.85 (m, 2H); 6.60 (dd, 1H); 6.35 (dd, 1H); 6.00 (dd, 1H); 3.82 (s, 3H); 3.16 (m, 1H); 2.85 (d, 2H); 2.81 (dd, 1H); 2.56 (dd, 1H) (see Figure 11.S3). ^{13}C NMR ($CDCl_3$, δ in ppm): 164.22, 151.04, 138.32, 136.32, 132.53, 127.63, 122.70, 121.12, 113.27, 55.93, 52.34, 46.84, 38.69 (see Figure 11.S4). FTIR (ATR): 1737 cm^{-1} (C=O acrylate); 1636 cm^{-1} (C=C acrylate); 1600 cm^{-1} (Aromatics); 825 cm^{-1} (epoxide) (see Figure 11.S5).

2.4 Synthesis of glycerol triacrylate (GTA)

The synthesis of GTA was performed in two different ways. Here, is described the one using CALB while the other route is described in the SI. In a 250 mL two-necked round bottom flask equipped with a magnetic stirrer and a Soxhlet system with glass wool, activated 4 Å molecular sieves and a condenser, glycerol (1 g, 10.9 mmol) was mixed with 80 mL of M*t*BE/*t*BuOH (1:1 v/v). Then, MA (14.7 mL, 0.2 mol) was added, the mixture heated until reflux and the Soxhlet drained 4 times. Next, CALB (200 mg, 20% w/w to Gly) was added and the mixture kept for 24 h at reflux. Afterwards, the mixture was vacuum filtered, and the mixture washed twice with 1 M NaOH solution. The organic phase was dried with anhydrous $MgSO_4$ and filtered, and the solvent and the excess of MA removed in a rotary evaporator yielding GTA as a brownish viscous oil (30%).

^{1}H NMR ($CDCl_3$, δ in ppm): 6.45 (dd, 1H); 6.15 (dd, 1H); 5.88 (dd, 1H); 4.27 (m, 4H); 4.18 (m, 1H) (see Figure 11.S6). ^{13}C NMR ($CDCl_3$, δ in ppm): 165.55, 165.13, 131.94, 131.74, 127.75, 127.68, 69.16, 62.33 (see Figure 11.S7).

2.5 Preparation of dual-cured materials

In a 20 mL vial, a certain amount of AEEU was added and melted at 70 °C for 10 minutes. Then, the corresponding amount of GTA was added and manually mixed with the melted AEEU. Finally, the stoichiometric amount (NH: acrylate + epoxy = 1:1) of the corresponding amine (cystamine or JeffamineD230) was rapidly added and vigorously stirred at room temperature. Then, the mixture was degassed for 10 minutes, poured into Teflon molds of 30 x 5 x 1.5 mm^3 dimensions, and cured in an oven at 50 °C for 1 h (first curing stage), 100 °C for 1h, and 150 °C for 2h (second curing stage). The materials were coded as polyX_Y, where X indicates the amine used and Y is ascribed to the intermediate material's gelled or not gelled (viscous) characteristics. For example, polyCys_gel is the material in which cystamine was used as a crosslinker, and the intermediate material was gelled since the gelation point occurred in the first curing stage. Table 11.1 shows the composition of the different formulations studied.

2.6 Characterization methods

Characterization by NMR, Fourier transform infrared spectroscopy (FTIR), differential scanning calorimetry (DSC), thermogravimetric analysis (TGA), dynamic mechanical thermal analysis (DMA), strain-stress at break in bending, and rheological analysis is described in detail in the Supporting Information.

Table 11.1. Composition of the formulations prepared.

Formulation	AEEU		GTA		Cys		JeffD230	
	g	mmol	g	mmol	g	mmol	g	mmol
polyCys_gel	0.5	2.13	0.25	1	0.27	1.80	-	-
polyCys_nogel	0.5	2.13	0.05	0.2	0.18	1.21	-	-
polyJeff_gel	0.5	2.13	0.25	1	-	-	0.42	1.80
polyJeff_nogel	0.5	2.13	0.05	0.2	-	-	0.28	1.21

3. Results and discussion

3.1 Synthesis of the starting monomers

The difunctional epoxy acrylate derivative of eugenol (AEEU) was synthesized following the synthetic way depicted in Scheme 11.1.

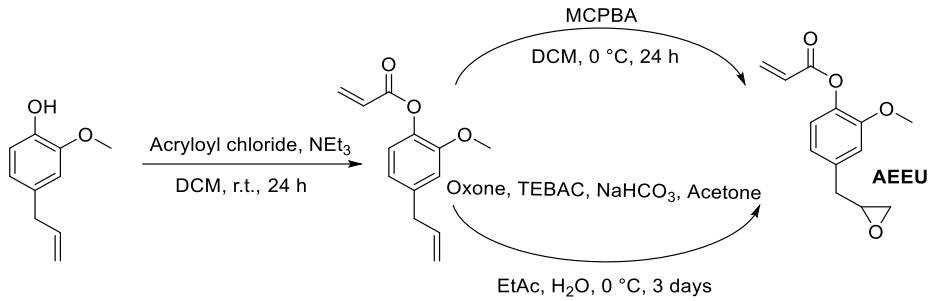

Scheme 11.1. Synthetic procedures used in the preparation of AEEU monomer.

The first step was the acylation of the phenol group with acryloyl chloride in the presence of TEA, obtaining a solid product with an 80 % of yield. We also tried the enzymatic esterification of eugenol with acrylic acid and CALB, but this reaction failed, and any product was obtained. The literature offers the alternative of using acrylic acid and dicyclohexyl carbodiimide (DCC) in the presence of a base [36], but it was reported that this procedure yields only 30 % of the product. Therefore, this procedure was not tested.

The subsequent synthetic step was the epoxidation of the allylic group by two synthetic methods, as represented in Scheme 11.1. The procedure of a higher yield was the traditional epoxidation with MCPBA, with a yield of 96% in only 1 day. The use of Oxone, as a greener alternative, was also attempted. The epoxidation was done in

a biphasic system with TEBAC as a phase transfer catalyst, obtaining good yields after 3 days (80%).

The acryloation of glycerol was also performed by two different synthetic procedures. The first one is the traditional based on the nucleophilic attack of the alcohol as a nucleophile to the activated acryloyl chloride in the presence of a base (TEA) depicted in Scheme 11.2. The yield of the triacrylate by this methodology was 94%. We also performed the enzymatic reaction of glycerol with methyl acrylate (MA) catalyzed by CALB. After 2 days of reaction, we obtained relatively low yields (30%) but proved that a green methodology could be used to obtain GTA.

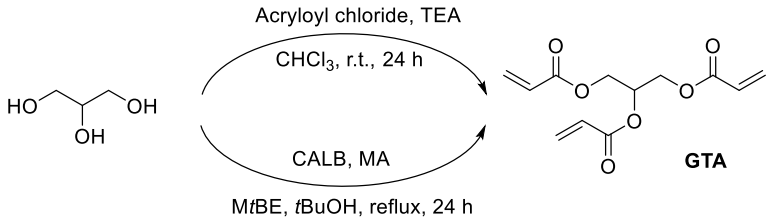

Scheme 11.2. Synthetic procedures used in the preparation of GTA monomer.

All products synthesized were characterized by spectroscopic techniques: ^{1}H, ^{13}C NMR, and FTIR. The spectra are collected in the supporting information (Figures 11.S1-S7), where it can be observed that the products obtained have high purity.

3.2 Study of the dual-curing procedure

The preparation of materials by the dual-curing procedure involves a first aza-Michael addition of either Cys or Jeff230 at low temperatures and further epoxy-amine reaction at higher temperatures between the unreacted epoxy groups and the remaining free amines. The reaction pathways of both processes are represented in Scheme 11.3.

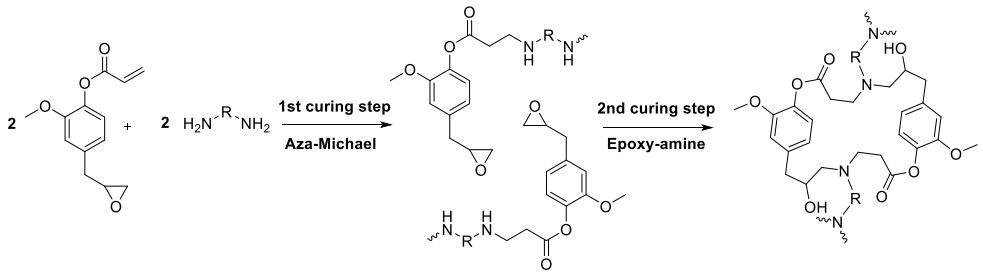

Scheme 11.3. Reaction pathways of the first curing step (aza-Michael reaction) and the second curing step (epoxy-amine condensation).

It has to be considered that primary amines react with acrylates much easier than secondary. According to that, it is foreseeable that the secondary amines produced by

the aza-Michael addition will react mostly with epoxides. The lower reactivity of secondary amines will help delay the epoxy-amine reaction in the second step, leading to a sequentiality in the dual-curing process.

If only AEEU and the corresponding amines are used in the dual curing procedure, no gelation will occur in the first step due to the single acrylate group in AEEU. Therefore, only viscous intermediate oligomers would be obtained. Thus, to obtain a gelled intermediate material, the trifunctional acrylate GTA must be added to obtain crosslinking points when amines have reacted.

To determine the amount of GTA necessary to get gelation, the theoretical conversion of the acrylate groups at the gel point α_{gel} during the aza-Michael reaction has to be calculated assuming the ideal random step-wise reaction, using the well-known Flory-Stockmayer equation (Eq. 11.1) [37,38]:

$$\alpha_{gel}^{theor} = \sqrt{\frac{r}{(f_1-1)\cdot(f_2-1)}} \qquad \text{(Eq. 11.1)}$$

where r is the hydrogen amine/acrylate equivalent ratio, f_1 the acrylate monomer functionality and f_2 the amine functionality.

With this equation, a molar ratio nGTA/nAEEU = 0.11 was calculated as the lowest to achieve gelation at 100% of conversion of acrylate groups. Thus, two different possibilities were studied herein: a) a molar ratio nGTA/nAEEU = 0.46, in which gelation will occur before full conversion to obtain a solid-like intermediate material, and b) a molar ratio nGTA/nAEEU = 0.09, where gelation will not occur in the first step and a viscous-like intermediate material will be obtained.

DSC analyses were performed to study the sequentiality of the system. However, only the intermediate and final materials could be characterized due to the fast rate of the aza-Michael addition at room temperature. Figure 11.1 shows both the DSC tests of all intermediate materials (viscous or gelled) as well as the T_g of the final materials, and the data are collected in Table 11.2.

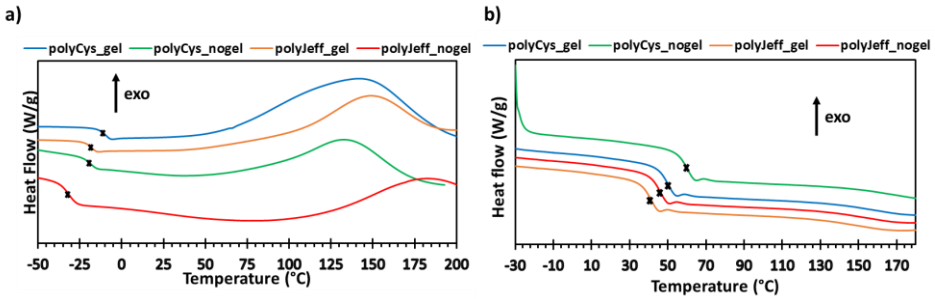

Figure 11.1. DSC thermograms corresponding to the a) intermediate materials and second dynamic curing at 10 °C/min and b) final materials at 20 °C/min.

Table 11.2. Calorimetric data extracted from the DSC tests of intermediate and final materials.

Sample	$T_{g\ intermediate}$ (°C)	$T_{g\ final}$ (°C)	$\Delta H_{epoxy\text{-}amine}$[a] (kJ/ee)
polyCys_gel	-10.2	50.1	98.6
polyCys_nogel	-19.0	62.6	96.1
polyJeff_gel	-18.7	41.0	90.3
polyJeff_nogel	-30.1	45.2	80.2

[a] Enthalpy released in the epoxy-amine reaction by epoxy equivalent.

As can be seen in Figure 11.1a, all intermediate materials show a T_g between -30 and -10 °C and an exothermal peak corresponding to the second epoxy-amine condensation reaction. As expected, materials with a gelled intermediate material display higher T_g values than their counterparts due to the higher crosslinking density achieved after the first step. Moreover, materials containing Cys as the hardener show higher T_gs than Jeff ones, thanks to the shorter amine chain that provides more compact networks. In addition, all materials release between 90-100 kJ/ee during the epoxy-amine reaction at high temperatures, which is in accordance with the values reported in the literature [39]. In the case of polyJeff_nogel material, the enthalpy is slightly lower due to the inaccuracy of the measure since the curing is not complete at the final scanning temperature.

Conversely, the final materials gelled after the first curing step display lower T_g values than the non-gelled ones. This fact can be ascribed to the increased amount of GTA and, consequently, to the higher amount of amines in the sample that, even producing more crosslinking points, also provides more aliphatic moieties which enable certain flexibility and mobility to the final polymer network, thus decreasing the glass transition temperature. This behavior is in accordance with the expected results of a dual-curing procedure [29,33].

FTIR spectroscopy confirmed the sequentiality and completion of both curing reactions. Spectra of AEEU, intermediate and final materials were recorded due to the impossibility of obtaining the spectrum of the unreacted mixture due to the rapid aza-Michael addition, which prevents the observation of the C=C bonds of the acrylate groups. As can be seen in Figure 11.S9, the band at 1636 cm^{-1}, corresponding to the C=C of the acrylate group, wholly disappeared in the intermediate material, while the epoxy band at 825 cm^{-1} disappeared after the second curing reaction, confirming the sequentiality and the completion of the curing process.

As mentioned, adding GTA into the system is crucial to achieving gelation at the first curing stage. To check if a gelled or a viscous intermediate material is obtained,

rheological analyses of the first curing stage were carried out for all formulations for comparison purposes. All the results can be seen in Figure 11.2.

Gelation is ascribed to the phenomena in which the material changes from a liquid to a solid behavior, thus meaning that the storage modulus (*G*', solid contribution) overpasses the loss modulus (*G*'', liquid contribution). As it can be seen, materials with an nGTA/nAEEU = 0.46 (theoretically gelled in the first stage) gel during the aza-Michael reaction (Figure 11.2a, and c) since at the end of the test, the *G*' is higher than *G*''. It is important to highlight that when Cys is used, the gelation occurs immediately after starting the test at 50 °C whereas, in the case of Jeff, the reactive mixtures achieve gelation later, indicating a higher reactivity of Cys formulations. On the other hand, materials with nGTA/nAEEU = 0.09 (below the minimum ratio) do not gel during the first stage, as expected (Figure 11.2b, and d). It is also worth saying that the values of *G*' and *G*'' for Cys materials are higher than their counterparts, due to the lower viscosity of Jeff formulations.

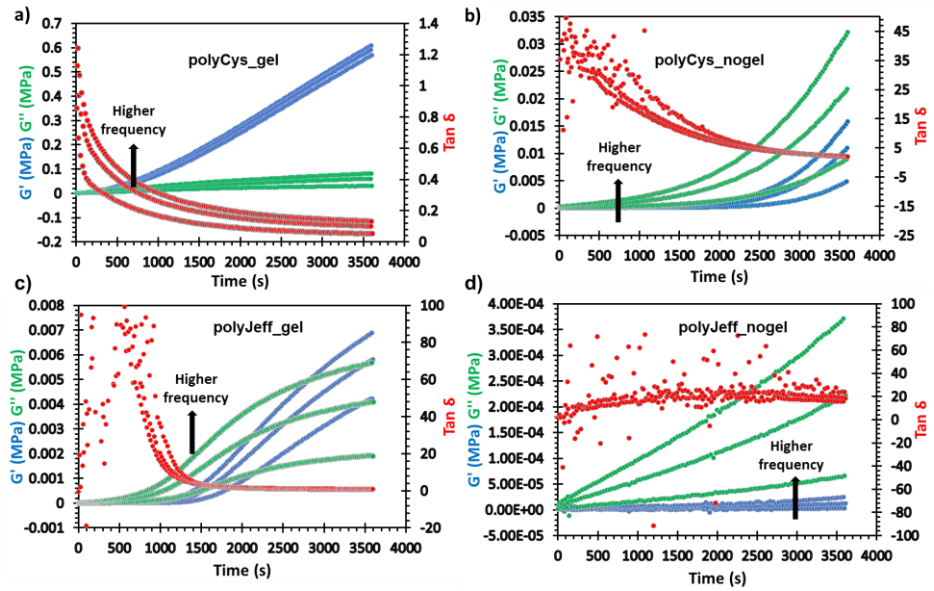

Figure 11.2. Evolution of storage modulus (*G*'), loss modulus (*G*'') and tan δ vs. time at three different frequencies (0.5 Hz, 1.75 Hz and 3 Hz) for a) polyCys_gel, b) polyCys_nogel, c) polyJeff_gel and d) polyJeff_nogel at 50 °C.

3.3 Study of the thermal and thermomechanical properties of the materials

To evaluate the thermal stability of the final materials as well as to confirm that further thermal tests are conducted in non-degradability conditions, thermogravimetric tests were performed. Figure 11.3 shows the TGA curves and their derivatives, and the most significant thermogravimetric data extracted are presented in Table 11.3.

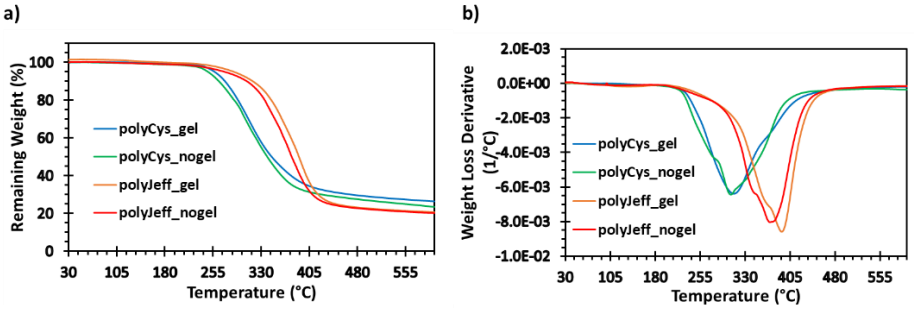

Figure 11.3. a) Thermogravimetric and b) DTG curves of the materials prepared.

Table 11.3. Thermogravimetric and thermomechanical data of all the materials prepared.

Sample	$T_{1\%}$[a] (°C)	T_{max}[b] (°C)	Char Yield[c] (%)	$T_{tan\,\delta}$[d] (°C)	E'_{glassy}[e] (MPa)	$E'_{rubbery}$[f] (MPa)
polyCys_gel	220.6	311.0	26.5	61.4	3482	13.0
polyCys_nogel	221.4	306.3	23.5	70.1	3331	7.1
polyJeff_gel	225.3	391.0	20.9	47.2	2810	8.2
polyJeff_nogel	223.5	371.3	20.5	55.5	3103	3.7

[a] Temperature of 1% weight loss. [b] Temperature at the maximum rate of degradation. [c] Char residue at 600 °C. [d] Temperature at the maximum of tan δ peak at 1 Hz.[e] Glassy storage modulus at T_g – 50 °C determined by DMA.[f] Rubbery storage modulus at T_g + 50 °C determined by DMA.

As can be seen, all materials show degradation curves with similar shapes and good thermal stability up to 220 °C indicating that a safe heat treatment or recycling can be done below this temperature. In the case of materials with Jeff, the main peak of degradation could be ascribed to the breakage of the propylene glycol repetitive units. In addition, disulfide groups are known to degrade before poly(hydroxy amine) moieties or polypropylene glycol units [17,32]. The values of char yield are in accordance with what is expected because polyCys_gel and polyJeff_gel have a higher content of amine and, therefore, a higher proportion of nitrogen which leads to higher values of char yield.

By DMA, we determined the thermomechanical properties of the final materials. Figure 11.4 shows the evolution of the storage moduli (E') and the dependence of tan δ with temperature for all the materials, and the data extracted are presented in Table 11.3.

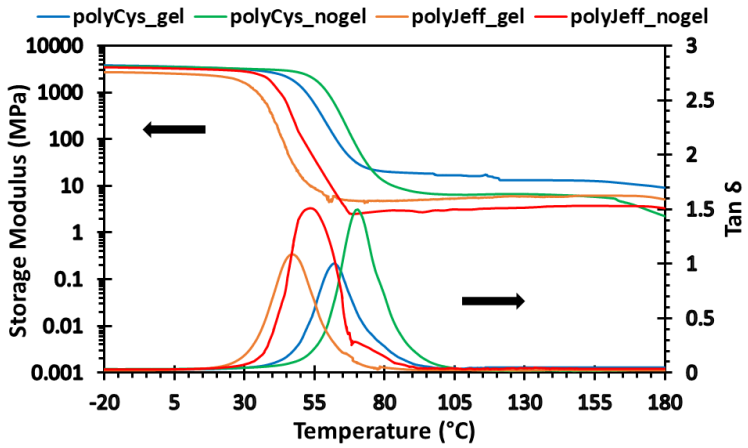

Figure 11.4. Evolution of storage modulus and tan δ with temperature for all materials.

All materials display $T_{\tan \delta}$ values higher than room temperature, from 47.2 °C for polyJeff_gel to 70.1 °C for polyCys_nogel. Materials with a gelled intermediate network present lower values of $T_{\tan \delta}$ than their non-gelled counterparts, as expected for dual curing procedures. More content of the corresponding aliphatic amine (Jeff or Cys) and GTA leads to a more flexible network structure. Nevertheless, for the same reason, these materials have higher values of *E'* in the rubbery state due to the higher crosslinking density of the final network. Foreseeably, materials containing Cys as hardener show higher values of storage modulus in the rubbery and in the glassy state, and higher values of $T_{\tan \delta}$, in comparison to Jeff due to its shorter chain that leads to less mobility of the network and, therefore, providing higher rigidity. In any case, it has been demonstrated that by controlling the stoichiometry of the formulation and using dual-curing methodologies, it is possible to tailor the thermomechanical properties of the final materials obtaining a wide range of different polymers that may be interesting for several applications. In addition, in this way, advanced fabrication processes can be implemented.

Interestingly, a drop of the storage modulus above 160 °C can be seen in all the curves of the materials, especially in Cys materials, indicating a loss in the crosslinking density which may be attributed to the dissociative behavior of the dynamic aza-Michael reaction and the disulfide metathesis [19]. Later we will discuss the possible exchange reactions of the networks as well as their dynamic behavior.

3.4 Study of the mechanical characterization of the materials

The mechanical properties of these materials were investigated in 3-point bending at 20 °C to obtain the stress-strain relationship up to the break. The results from these

tests can be seen in Figure 11.5 and the corresponding data are collected in Table 11.S1.

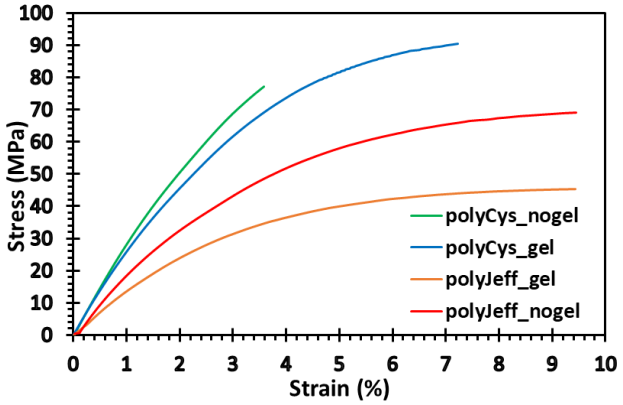

Figure 11.5. Stress-strain at break curves in bending at 20 °C for all the materials prepared.

As expected, polyJeff materials exhibit higher values of strain at break in comparison to their Cys counterparts. This characteristic can be easily explained by the presence of Jeffamine in the materials, which has longer aliphatic chains that provide more flexibility to the network than Cys. For the Jeff materials, despite presenting similar ductility, the lower amount of aliphatic GTA in the no gelled sample and, consequently, the lower amount of the corresponding amine, resulted in higher stress at break value than the gelled one. However, this effect is not evident in materials containing Cys because the higher rigidity provided by the shorter chain of Cys hinders this contribution making this material more fragile presenting a premature breakage. Finally, it is important to highlight the outstanding bending strength of polyCys_gel and polyCys_nogel (91 MPa and 79 MPa, respectively), which are far bigger than similar vitrimeric materials [21,40]. This demonstrates that the use of dual-curing methodologies allows the mechanical properties of these materials to be easily tuned and tailored.

3.5 Study of the dynamic behavior of the materials

The materials prepared are expected to undergo different types of exchange reactions. CANs containing Jeff may relax the stress thanks to the dynamic aza-Michael reaction (dissociative-type) and to the transesterification (associative-type) originated from the esters of the former acrylates and the alcohols of the epoxy-amine condensation. In case of Cys materials, disulfide metathesis can also occur due to the S-S bond in its structure. The representation of the different network rearrangements produced by the three possible reversible processes in Cys materials are represented in Figure 11.6.

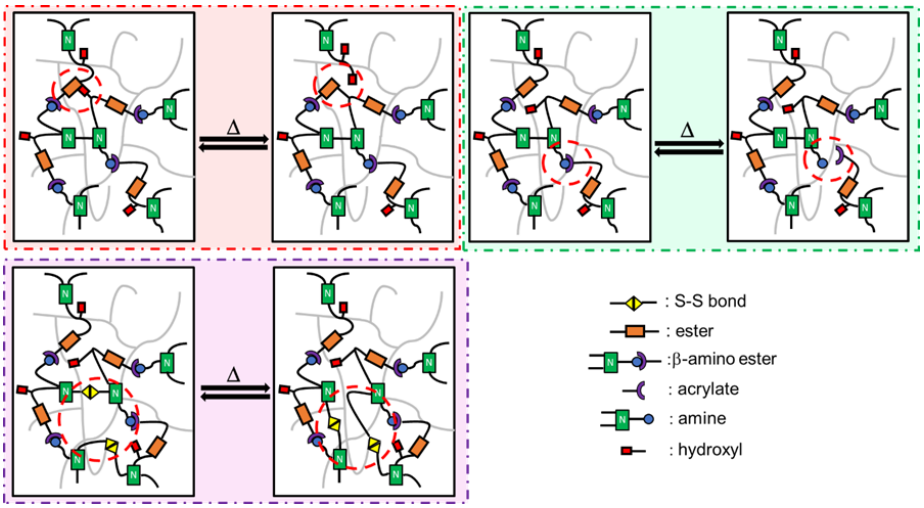

Figure 11.6. Schematics of network exchanges via transesterification (top left), reversible aza-Michael reaction (top right) and disulfide metathesis in case of Cys materials (bottom left).

Vitrimeric materials are widely recognized to exhibit an Arrhenius-type temperature dependence when the viscosity is controlled by an exchange reaction process similar to inorganic silica materials [41]. Thus, to further investigate the dynamic nature of these networks, time and temperature-dependent relaxation behavior was studied. Stress relaxation tests were performed by DMA, and the results are shown in Figure 11.7a-d and Table 11.4.

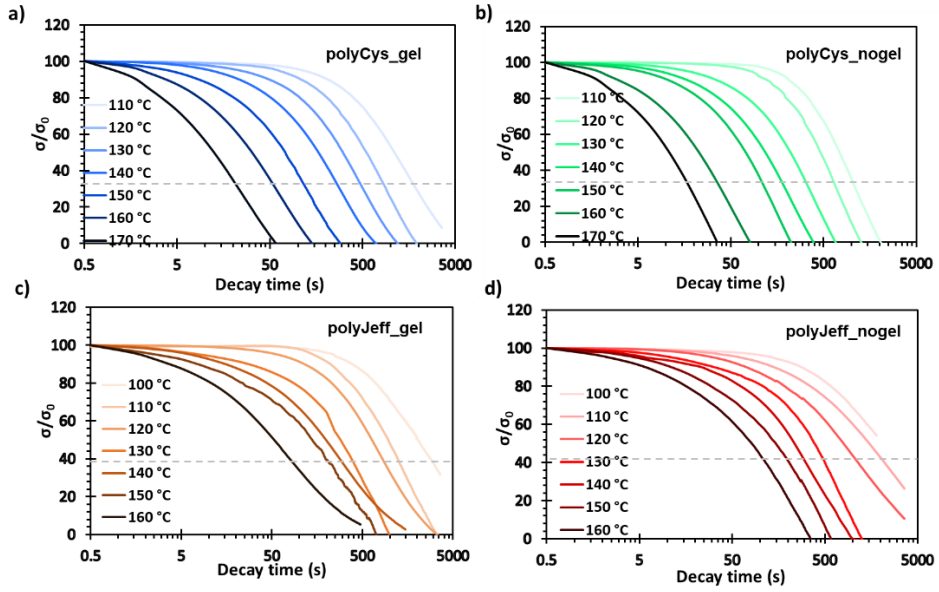

Figure 11.7. Normalized stress relaxation plots as a function of time at various temperatures during 3600 s for a) polyCys_gel, b) polyCys_nogel, c) polyJeff_gel, and d) polyJeff_nogel.

The stress relaxation curves provide compelling evidence of the capability of these materials to efficiently relax the stress, reaching a reference relaxation value of 63% (σ/σ_0 = 0.37) in 32.5 s for polyCys_nogel, 47.5 s for polyCys_gel, 89.0 s for polyJeff_gel and 126.5 s for polyJeff_nogel at 160 °C.

It can be seen that materials containing Cys relax the stress faster than their Jeffamine counterparts which can be ascribed to the disulfide metathesis as a third exchange reaction in the network. Despite that polyCys_gel contains more exchangeable groups, either disulfide bonds, ester and hydroxyl, and β-amino esters, polyCys_nogel could relax the stress faster (12.7 min and 10.1 min at 120 °C, respectively) probably due to the lower crosslinking density of the latest which allow more mobility of the network, thus increasing the probability of the exchangeable groups to be closer and therefore to make the exchange reaction more likely to occur. In fact, the storage modulus in the rubbery state is lower for polyCys_nogel, which favors the network relaxation process. Interestingly, when Jeffamine is used, the opposite trend can be seen in the table (15.0 min for polyJeff_gel and 21.1 min for polyJeff_nogel at 120 °C). In the case of polyJeff_gel, as the Jeffamine has long chains, the higher amount of amine, the more flexible is the network, which enhances the relaxation rates. From these results, it can be confirmed that the flexibility and mobility of the network structure affect in a high considerable way the relaxation ability. In any case, all materials can completely relax the stress at 120 °C in less than 5000 s. It is also important to highlight that even obtaining high-T_g materials (up to 70 °C), they can relax 63% of the initial stress at relatively low temperatures such as 100 °C, proving the great potential of these bio-based CANs.

Table 11.4. Relaxation time, activation energy, topology freezing temperature, and adjusting parameters for the Arrhenius equation of the CANs prepared.

Material	$\tau_{0.37}$ [a] (min)	$\tau_{100\%}$ [b] (min)	E_a (kJ/mol)	ln A (s)	T_v (°C)	r^2
polyCys_gel	12.7	31.8	89	24.48	64	0.986
polyCys_nogel	10.1	21.3	97	22.69	59	0.986
polyJeff_gel	15.0	55.1	73	15.87	45	0.987
polyJeff_nogel	21.1	83.3	79	17.21	51	0.994

[a] Time to reach a value of σ/σ_0 = 0.37 at 120 °C. [b] Time to reach total relaxation at 120 °C.

To further characterize these CANs, the time required to relax the initial stress to e^{-1} (σ/σ_0 = 0.37) at all temperatures for these materials was obtained from the corresponding relaxation curves. By fitting the data to the Arrhenius-type equation, it is possible to calculate the activation energy (E_a) associated with the topological rearrangement (see Figure 11.8 and Table 11.4). As observed, materials containing Cys

display higher activation energy values demonstrating greater dependence of the relaxation time on the temperature, probably due to the higher content of dynamic bonds that can undergo exchange reactions.

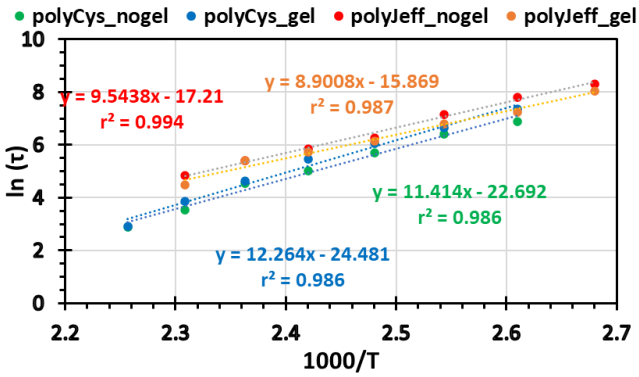

Figure 11.8. Arrhenius plot of relaxation times against temperature for the different CANs.

Another critical parameter in dynamic networks is the topology freezing temperature (T_v). Chemically, it indicates the temperature below which the network rearrangements are almost negligible, and physically is the temperature at which the material reaches a viscosity of 10^{12} Pa·s. T_vs could be deduced from the Arrhenius relationships and using Maxwell Equation and are presented in Table 11.4. As shown, Jeff materials display lower values of T_v, although they relax slower than their Cys counterparts. This can be associated with their lower crosslinking density, which is directly related to the $E'_{rubbery}$, which is used in the Maxwell relationship. All materials present values of T_v lower than their corresponding T_gs. Since materials are in the glassy state below their T_g, rearrangement will not occur until that temperature is exceeded. Thus, the glass transition temperature is the most important parameter to determine the start of the exchange kinetics.

As previously mentioned, these materials contain several dynamic bonds in their structure with either associative-type or dissociative-type exchange mechanisms. In DMA curves in Figure 11.4, we observed a slight drop of the storage modulus at high temperatures, more drastic in Cys materials. To investigate that, rheological tests at different temperatures with frequency sweeps in oscillatory shear under a linear viscoelastic regime were performed for all the materials (Figure 11.9).

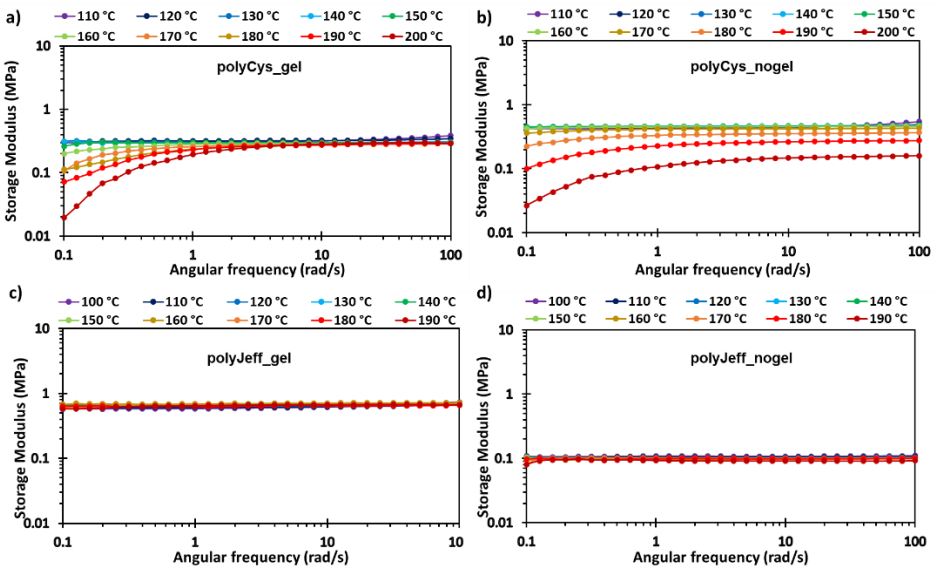

Figure 11.9. Frequency sweep at different temperatures for polyCys_gel (a), polyCys_nogel (b), polyJeff_gel (c), and polyJeff_nogel (d).

The temperatures studied were the same as in the stress relaxation tests, and the frequency sweep was from 100 to 0.1 rad/s. As it can be observed, in both polyJeff materials (Figure 11.9c and d), the storage modulus (G') is constant independently of the frequency and the temperature, indicating the associative behavior of these materials even at high temperatures and long relaxation times. Indeed, one of the main characteristics of vitrimers is keeping constant the crosslinking density with temperature and time which is directly related to the storage modulus at high temperatures. This can also mean that despite the chemically dissociative mechanism of the reversible aza-Michael reaction, the exchange kinetics may be governed by the transesterification reaction since it is reported to be faster than the previous one [21]. Moreover, the huge amount of tertiary amines present in the network can accelerate the transesterification reaction at low temperatures as previously reported [42].

Interestingly, in the case of polyCys_nogel, a clear drop of G' at 180 °C at low frequencies can be seen, indicating the loss of the integrity of the network and, therefore, the crosslinking density, which is a behavior of typical dissociative networks. The same happens with polyCys_gel, but in this material, the drop of storage modulus starts at 160 °C, which can be explained by the higher proportion of S-S bonds coming from higher amounts of Cys in the material. Here, the exchange may be controlled by the disulfide exchange and transesterification simultaneously. However, at high temperatures and long relaxation times, the first exchange reaction is to such an extent that it may produce this drastic drop of G'. It has been reported

that tertiary amines can act as an internal catalyst for disulfide exchange in CANs [43]. The mechanisms of disulfide exchange have been reported to be [2 + 2] metathesis reaction and a [2 + 1] radical-mediated mechanism. However, when tertiary amines are present, they generate active thiolates by the rupture of the disulfide bond, as represented in Scheme 11.4. Another disulfide bond was then attacked by the nucleophilic thiolate formed, promoting the bond exchange, explaining in this way the dissociative character of the polyCYS CANs. This mechanism can occur, in different extents, in addition to the disulfide metathesis, which is associative.

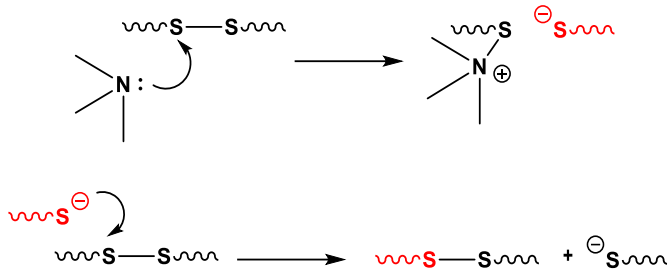

Scheme 11.4. Proposed exchange mechanism of disulfide bonds catalyzed by amines.

3.6 Reprocessability of the CANs

Once it has been shown that the prepared materials have good characteristics as CANs, it is necessary to study their recyclability, which will be key to achieve the sustainability of these materials. All the samples were ground into powder and hot-pressed in a manual press under 2 MPa in an aluminum mold to test the recyclability. The recycling tests were performed at 160 °C, a temperature that ensures not only that the exchange processes are taking place but also safe recycling since all materials start to degrade at 220 °C. Figure 11.10 shows the pictures taken from the original, ground, and reprocessed samples, where it can be observed that the homogeneity and transparency are well-maintained in the recycled sample.

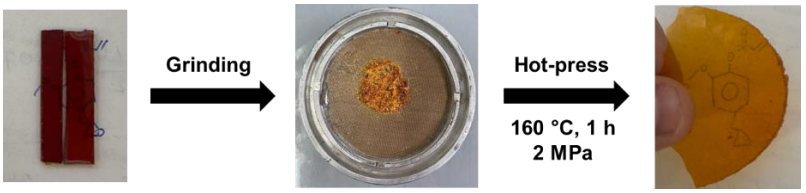

Figure 11.10. Pictures of virgin, ground and recycled samples of the polyCys_nogel.

To confirm the good recycling ability, FTIR spectra of the virgin and the reprocessed samples of all the materials prepared herein were recorded. Figure 11.S10 shows both

spectra, demonstrating that no significant differences can be observed and confirming that the chemical structure of the polymer is well preserved. Moreover, DSC analyses were performed to compare the T_g of the recycled materials with the virgin ones (Figure 11.S11). Table 11.5 collects the results obtained from those tests. As can be seen, the T_g values of all materials were very similar in comparison to the virgin samples indicating a successful recycling procedure for all cases.

Table 11.5. Glass transition temperatures of the virgin and recycled materials.

Sample	T_g virgin (°C)	T_g recycled (°C)
polyCys_gel	50.1	49.5
polyCys_nogel	62.6	62.1
polyJeff_gel	41.0	40.1
polyJeff_nogel	45.2	44.7

4. Conclusions

An acrylate epoxy eugenol derivative (AEEU) has been successfully synthesized in high yields through an acylation reaction and a green epoxidation reaction using oxone as a sustainable reagent. A triacrylate derivative of glycerol (GTA) has also been synthesized sustainably using enzymes.

Materials with several dynamic exchangeable bonds could be prepared by reacting AEEU and GTA with different amines (Cys and Jeff) using a dual-curing procedure. A first aza-Michael reaction between NH groups and acrylates at low temperatures and a second epoxy-amine condensation reaction between free amines and the remaining epoxy groups at higher temperatures allowed to obtain crosslinked materials. Adding GTA allowed us to achieve gelation in the first or second steps to get gelled or viscous intermediate materials depending on the ratio AEEU/GTA.

DSC analyses demonstrated the sequentiality of the system by obtaining intermediate materials with different T_g values and a residual heat corresponding to an epoxy-amine reaction. Moreover, all final materials revealed glass transition temperatures above room temperature, higher when cystamine was used as a crosslinking agent. FTIR also confirmed the sequentiality of the dual curing and the completion of the second step.

All materials displayed thermal stability (up to 220 °C) and showed high values of $T_{tan\delta}$ (from 47 to 70 °C) and high storage modulus values in the glassy state, demonstrating excellent thermomechanical properties.

In all cases, incorporating multiple dynamic bonds in their polymer structure allowed them to relax 63% of the initial stress in less than 20 minutes at 120 °C. Frequency sweep tests demonstrated that Jeff materials maintained the storage modulus (G') constant, even at high temperatures and longer times. In contrast, the storage modulus of Cys materials dropped at 180 °C (for polyCys_nogel) and 160 °C (for polyCys_gel), indicating a typical behavior of dissociative-type CANs.

The bending tests also showed that materials with Cys displayed high bending strength (91 MPa and 79 MPa) higher than many similar CANs and vitrimers.

The materials demonstrated good reprocessability, allowing safe recycling without significant changes in their chemical structure.

In conclusion, this study successfully demonstrates the feasibility of the dual-curing procedure to tailor the properties of materials, enabling the design of a wide range of polymers synthesized from bio-based resources and, in a highly greener way, suitable for many different applications and environmentally attractive alternatives.

Acknowledgments

This work is part of the R&D projects PID2020-115102RB-C21 and PID2020-115102RB-C22 funded by MCNI/AEI/10.13039/501100011033 and European Union "NextGenerationEU"/PRTR. We acknowledge these grants, and we also thank to the Generalitat de Catalunya (2021-SGR-00154).

References

[1] Vidil, T.; Llevot, A. Fully Biobased Vitrimers: Future Direction toward Sustainable Cross-Linked Polymers. *Macromol. Chem. Phys.* **2022**, *223*, 2100494.

[2] Schneiderman, D. K.; Hillmyer, M.A. 50th Anniversary Perspective: There is a Great Future in Sustainable Polymers. *Macromolecules* **2017**, *50*, 3733-3749.

[3] Fache, M.; Boutevin, B.; Caillol, S. Vanillin, a key-intermediate of biobased polymers. *Eur. Polym. J.* **2015**, *68*, 488-502.

[4] Morales-Cerrada, R.; Molina-Gutierrez, S.; Lacroix-Desmazes, P.; Caillol, S. Eugenol, a Promising Building Block for Biobased Polymers with Cutting-Edge Properties. *Biomacromolecules*, **2021**, *22*, 3625-3648.

[5] Faye, I.; Decostanzi, M.; Ecochard, Y.; Caillol, S. Eugenol Bio-Based Epoxy Thermosets: From Cloves to Applied Materials. *Green Chem.* **2017**, *19*, 5236-5242.

[6] Montarnal, D.; Capelot, M.; Tournilhac, F.; Leibler, L. Silica-Like Malleable Materials from Permanent Organic Networks. *Science*, **2011**, *334*, 965-968.

[7] Podgórski, M.; Fairbanks, B. D.; Kirkpatrick, B. E.; McBride, M.; Martinez, A.; Dobson, A.; Bongiardina, N. J.; Bowman, C. N. Toward Stimuli-Responsive Dynamic

Thermosets Through Continuous Development and Improvement in Covalent Adaptable Networks (CANs). *Adv. Mater.* **2020**, *32*, 1906876.

[8] Scheutz, G. M.; Lessard, J. J.; Sims, M. B.; Sumerlin, B. S. Adaptable Crosslinks in Polymeric Materials: Resolving the Intersection of Thermoplastics and Thermosets. *J. Am. Chem. Soc.* **2019**, *141*, 16181-16196.

[9] Zhao, X.-L.; Tian, P.-X.; Li, Y.-D.; Zeng, J.-B. Biobased Covalent Adaptable Networks: Towards Better Sustainability of Thermosets. *Green Chem.* **2022**, *24*, 4363-4387.

[10] Capelot, M.; Montarnal, D.; Tournilhac, F.; Leibler, L. Metal-Catalyzed Transesterification for Healing and Assembling of Thermosets. *J. Am. Chem. Soc.* **2012**, *134*, 7664-7667.

[11] Altuna, F. I.; Hoppe, C. E.; Williams, R. J. J. Shape Memory Epoxy Vitrimers Based on DGEBA Crosslinked with Dicarboxylic Acids and Their Blends with Citric Acid. *RSC Adv.* **2016**, *6*, 88647-88655.

[12] Liu, T.; Hao, C. Wang, L.; Li, Y.; Liu, W.; Xin, J.; Zhang, J. Eugenol-Derived Biobased Epoxy: Shape Memory, Repairing and Recyclability. *Macromolecules*, **2017**, *50*, 8588-8597.

[13] Taynton, P.; Yu, K.; Shoemaker, R. K.; Jin, Y.; Qi, H. J.; Zhang, W. Heat- or Water-Driven Malleability in a Highly Recyclable Covalent Network Polymer. *Adv. Mater.* **2014**, *26*, 3938-3942.

[14] Roig, A.; Hidalgo, P.; Ramis, X.; De la Flor, S.; Serra, À. Vitrimeric Epoxy-Amine Polyimine Networks Based on a Renewable Vanillin Derivative. *ACS Appl. Polym. Mater.* **2022**, *4*, 9341-9350.

[15] Geng, H.; Wang, Y.; Yu, Q.; Gu, S.; Zhou, Y.; Xu, W.; Zhang, X.; Ye, D. Vanillin-Based Polyschiff Vitrimers: Reprocessability and Chemical Recyclability. *ACS Sustainable Chem. Eng.* **2018**, *6*, 15463-15470.

[16] Ruiz de Luzuriaga, A.; Martin, R.; Markaide, N.; Rekondo, A.; Cabañero, G.; Rodríguez, J.; Odriozola, I. Epoxy Resin with Exchangeable Disulfide Crosslinks to Obtain Reprocessable, Repairable and Recyclable Fiber-Reinforced Thermoset Composites. *Mater. Horiz.* **2016**, *3*, 241-247.

[17] Roig, A.; Agizza, M.; Serra, À.; De la Flor, S. Disulfide Vitrimeric Materials Based on Cystamine and Diepoxy Eugenol as Bio-Based Monomers. *Eur. Polym. J.* **2023**, *194*, 112185.

[18] Chapelle, C.; Quienne, B.; Bonneaud, C.; David, G.; Cailllol, S. Diels-Alder-Chitosan based on Dissociative Covalent Adaptable Networks. *Carbohydr. Polym.* **2021**, *253*, 117222.

[19] Taplan, C.; Guerre, M.; Du Prez, F. E. Covalent Adaptable Networks Using β-Amino Esters as Thermally Reversible Building Blocks. *J. Am. Chem. Soc.*, **2021**, *143*, 9140-9150.

[20] Song, H. Y.; Lee, G.; A. S.-k.; Hyun, K. Linear Viscoelasticity of Covalent Adaptable Network (CAN) Polymers Comprising β-Amino Esters. *Korea-Aust. Rheol. J.*, **2023**, *35*, 69-79.

[21] Lee, G.; Song, H. Y.; Choi, S.; Kim, C. B.; Hyun, K.; Ahn, S.-K. Harnessing β-Hydroxyl Groups in Poly(β-Amino Esters) toward Robust and Fast Reprocessing Covalent Adaptable Networks. *Macromolecules*, **2022**, *55*, 10366-10376.

[22] Yu, S.; Zhang, G.; Wu, S.; Tang, Z.; Guo, B.; Zhang, L. Effects of Dynamic Covalent Bond Multiplicity on the Performance of Vitrimeric Elastomers. *J. Mater. Chem A*, **2020**, *8*, 20503-20512.

[23] Jiang, Z.; Bhaskaran, A.; Aitken, H. M.; Shackleford, I. C. G.; Connal, L. A. Using Synergistic Multiple Dynamic Bonds to Construct Polymers with Engineered Properties. *Macromol. Rapid Commun.*, **2019**, *40*, 1900038.

[24] Xu, X.; Ma, S.; Feng, H.; Qiu, J.; Wang, S.; Yu, Z.; Zhu, J. Dissociate Transfer Exchange of Tandem Dynamic Bonds Endows Covalent Adaptable Networks with Fast Reprocessability and High Performance. *Polym. Chem.*, **2021**, *12*, 5217-5228.

[25] Wang, M.; Gao, H.; Wang, Z.; Mao, Y.; Yang, J.; Wu, B.; Jon, L.; Zhang, C. Xia, Y.; Zhang, K. Rapid Self-Healed Vitrimers Via Tailored Hydroxyl Esters and Disulfide Bonds. *Polymer*, **2022**, *248*, 124801.

[26] Fortman, D. J.; Snyder, R. L.; Sheppard, D. T.; Dichtel, W. R. Rapidly Reprocessable Cross-Linked Polyhydroxyurethanes Based on Disulfide Exchange. *ACS Macro Lett.* **2018**, *7*, 1226-1231.

[27] Konuray, O.; Moradi, S.; Roig, A.; Fernández-Francos, X.; Ramis, X. Thiol-Ene Networks with Tunable Dynamicity for Covalent Adaptation. *ACS Appl. Polym. Mater.*, **2023**, *5*, 1651-1656.

[28] Hammer, L.; Van Zee, N. J.; Nicolaÿ, R. Dually Crosslinked Polymer Networks Incorporating Dynamic Covalent Bonds. *Polymers*, **2021**, *13*, 396.

[29] Ramis, X.; Fernández-Francos, X. De la Flor, S.; Ferrando, F.; Serra, À. Click-Based Dual-Curing thermosets and Their Application, in: Q. Guo (Ed.), Thermosets Structure, Properties and Applications, Chapt. 16, 2nd ed., Elsevier, Amsterdam, Netherlands, **2018**.

[30] Kolb, H. C.; Finn, M. G.; Sharpless, K. B. "Click" Chemistry: Diverse Chemical Function from a Few Good Reactions. *Angew. Chem. Int. Ed.*, **2001**, *40*, 2005-2021.

[31] Fernández-Francos, X.; Konuray, A. O.; Belmonte, A.; De la Flor, S.; Serra, À. Ramis, X. Sequential Curing of Off-Stoichiometric Thiol-Epoxy Thermosets with a Custom-Tailored Structure. *Polym. Chem.* **2016**, *7*, 2280-2290.

[32] Roig, A.; Ramis, X.; De la Flor, S.; Serra, À. Dual-Cured Thermosets from Glycidyl Methacrylate Obtained by Epoxy-Amine Reaction and Methacrylate Homopolymerization. *React. Funct. Polym.* **2021**, *159*, 104822.

[33] Russo, C.; Serra, À.; Fernández-Francos, X.; De la Flor, S. Characterization of Sequential Dual-Curing of Thiol-Acrylate-Epoxy Systems with Controlled Thermal Properties. *Eur. Polym. J.* **2019**, *112*, 376-388.

[34] Gamardella, F.; Sabatini, V.; Ramis, X.; Serra, À. Tailor-Made Thermosets Obtained by Sequential Dual-Curing Combining Isocyanate-Thiol and Epoxy-Thiol *Click* Reactions. *Polymer* **2019**, *174*, 200-209.

[35] Roig, A.; Ramis, X.; De la Flor, S.; Serra, À. Sequential Photo-Thermal Curing of (Meth)Acrylate-Epoxy Thiol Formulations. *Polymer* **2021**, *230*, 124073.

[36] Seixas Xavier, F.J.; da Franca Rodrigues, K.A.; Guerra de Oliveira, R.; Lima Junior, C.G.; da Câmara Rocha, J.; Lima Keesen, T.S.; de Oliveira, M.R.; Lins Silva, F.P.; Araújo de Almeida Vasconcellos, M.L. Synthesis and In Vitro Anti Leishmania amazonensis Biological Screening of Morita-Baylis-Hillman Adducts Prepared from Eugenol, Thymol and Carvacrol. *Molecules* **2016**, *21*, 1483.

[37] Pascault, J. P.; Sautereau, H.; Verdu, J.; Williams, R. J. J. Thermosetting Polymers, Marcel Dekker, New York, USA, **2002**.

[38] Pascault, J. P.; Williams, R. J. J. Overview of Thermosets: Present and Future, in: Q. Guo (Ed.), Structure, Properties and Application, Thermosets 2nd ed. Ch. 11, pp 3-34, Elsevier, Amsterdam, Netherlands, **2018**.

[39] Brandrup, J.; Immergut, E.H.; McDowell, W. Polymer Handbook, Wiley, New York, USA, 1975.

[40] Yu, Q.; Peng, X.; Wang, Y.; Geng, H.; Xu, A.; Zhang, X.; Xu, W.; Ye, D. Vanillin-Based Degradable Epoxy Vitrimers: Reprocessability and Mechanical Properties Study. *Eur. Polym. J.* **2019**, *117*, 55-63.

[41] Denissen, W.; Winne, J. M.; Du Prez, F. E. Vitrimers: Permanent Organic Networks with Glass-Like Fluidity. *Chem. Sci*. **2016**, *7*, 30-38.

[42] Altuna, F.I.; Hoppe, C.E.; Williams, R.J.J. Epoxy vitrimers with a covalently bonded tertiary amine as catalyst of the transesterification reaction. *Eur. Polym. J.* **2019**, *113*, 297-304.

[43] Yamawake, K.; Hayashi, M. The role of tertiary amines as internal catalysts for disulfide exchange in covalent adaptable networks. *Polym. Chem.* **2023**, *14*, 680-686.

Supporting Information

Synthesis of acrylate-epoxy-eugenol (AEEU)

In a 500 mL three-necked flask equipped with a magnetic stirrer and ice bath, AEU (15.0 g, 68.7 mmol) was dissolved in 25 mL of DCM and then a solution of MCPBA (24.5 g, 0.1 mol) in 250 mL of DCM was added dropwise. The reaction was kept at 0 °C for 24 h until complete disappearance of AEU. The resulting mixture was washed once with a 10% w/w aqueous solution of $NaHSO_3$, twice with concentrated aqueous solution of $NaHCO_3$ and finally brine. The organic layer was dried over anhydrous $MgSO_4$, filtered and concentrated in a rotary evaporator to yield AEEU as a yellowish solid in a 96% of yield.

Synthesis of glycerol triacrylate (GTA)

In a 250 mL three-necked flask equipped with a magnetic stirrer and ice bath, Gly (5 g, 54.3 mmol) was dissolved in 25 mL of $CHCl_3$. Then, TEA (37.8 mL, 0.27 mol) was added in the mixture and the system put in inert atmosphere. Later, a solution of acryloyl chloride (24.3 mL, 0.3 mol) in 50 mL of $CHCl_3$ was added dropwise. The mixture was allowed to proceed for 36 h at room temperature. Then, the reaction was vacuum filtered and washed once with HCl 1M (100 mL), twice with saturated $NaHCO_3$ solution (100 mL), twice with 20% w/w Na_2CO_3 solution (100 mL) and finally saturated NaCl solution (100 mL). Finally, the organic layer was dried over anhydrous $MgSO_4$, filtered and the solvent removed in a rotary evaporator to afford GTA as a brownish viscous oil (13.0 g, 94%).

Preparation of the cystamine (Cys)

To prepare Cys, 8.0 g of cystamine dihydrochloride and 6.0 g of KOH were dissolved in 100 mL of distilled water. After stirring for 30 min at room temperature, the resulting mixture was extracted four times with DCM. The organic layers were combined, dried over anhydrous MgSO4, and filtered. DCM was removed using a rotary evaporator obtaining 4.0 g of a yellowish viscous oil called cystamine (Cys). The pure cystamine must be used immediately after being obtained or it must be kept in a fridge. (see Figure 11.S8)

Characterization methods

^1H NMR and ^{13}C NMR spectra were registered in a Varian VNMR-S400 NMR spectrometer. $CDCl_3$ was used as a solvent. All chemical shifts are quoted on the δ scale in part per million (ppm) using residual protonated solvent as internal standard (^1H NMR: $CDCl_3$ = 7.26 ppm; ^{13}C NMR: $CDCl_3$ = 77.16 ppm).

DSC analyses were carried out on a Mettler DSC3+ instrument calibrated using indium (heat flow calibration) and zinc (temperature calibration) standards. Samples of approximately 8-10 mg were placed in aluminum pans with pierced lids and analyzed

in an N_2 atmosphere with a glass flow of 50 cm^3 min^{-1}. Dynamic studies between -50 and 200 °C at a heating rate of 10 °C min^{-1} were performed to determine the T_gs of the intermediate materials. The second curing reaction enthalpy (Δh) was integrated from the calorimetric heat flow signal (dh/dt) using a straight baseline with the help of the STARe software. Dynamic studies between -30 and 200 °C at a heating rate of 20 °C min^{-1} were performed to determine the T_gs of the final materials. For the determination of the melting points, dynamic studies between 30 and 250 °C at a heating rate of 10 °C min^{-1} were performed.

A Jasco FT/IR-680 Plus spectrometer equipped with an attenuated total reflection accessory (ATR) (Gloden Gate, Specac Ltd, Teknokroma) was used to record the FTIR spectra of the intermediate and final materials as well as after the recycling process. Real-time spectra were recorded in the wavenumber range between 4000 and 600 cm^{-1} with a resolution of 4 cm^{-1} and averaged over 32 scans. The disappearance of the characteristic absorbance peaks of the double bond of acrylate and the epoxy group at 1636 cm^{-1} and 830 cm^{-1}, respectively as well as the appearance of the peak corresponding to O-H at 3300 cm^{-1} were used to confirm the completion of both curing reactions.

The thermal stability of the materials was evaluated using a Mettler Toledo TGA 2 thermobalance. Cured samples weighing around 10 mg were degraded between 30 and 600 °C at a heating rate of 10 °C min^{-1} in N_2 atmosphere with a flow of 50 cm^3 min^{-1}.

The thermomechanical properties were studied using DMTA Q850 (TA Instruments) equipped with a three-point bending clamp. Prismatic rectangular samples with dimensions around 15 x 5 x 1.5 cm^{-1} were analyzed from -20 to 180 °C at 1 Hz, with 0.1% strain at a heating rate of 2 °C min^{-1}. Stress relaxation tests were conducted in the same instrument using the three-point bending clamp on samples with the same dimensions as previously defined. The samples were firstly equilibrated at the relaxation temperature for 5 minutes, and a constant strain of 1% was applied, measuring the consequent stress level as a function of time. The relaxation stress $\sigma(t)$ was normalized by the initial stress σ_0, and the relaxation times (τ) were determined as the time necessary to relax $0.37\sigma_0$, i.e. ($\sigma = 1/e\sigma_0$). With the relaxation times obtained at each temperature, the activation energy values (E_a), were calculated by using an Arrhenius-type equation:

$$\ln(\tau) = \frac{E_a}{RT} - \ln A$$

where τ is the time needed to attain a given stress-relaxation value ($0.37\sigma_0$), A is the pre-exponential factor, and R is the gas constant.

The gelation time at the first curing stage was evaluated with an ARES-G2 rheometer (TA Instruments) equipped with an electrical heated plate device (EHP) and parallel plate geometry. Dynamic mechanical tests at different frequencies were performed to investigate the evolution of the storage and loss modulus (G' and G'' respectively) during the first curing stage. The experimental procedure is defined to simulate the first curing reaction in the oven: 1 h at 50 °C with oscillation strain of 0.1%. Three different frequencies, 0.5, 1.75, and 3 Hz were continuously measured maximizing the points per decade in a discrete sweep. To perform the rheological characterization of the final materials, the same instrument was used. Strain sweep experiments were carried out to determine the linear viscoelastic regime of the materials. Frequency sweep experiments were carried out from 100 to 200 °C applying the previous determined strain for each material (in the linear viscoelastic region) and the frequency was changed from 100 to 0.1 rad s^{-1} and a normal force of 10 N was applied.

Stress-strain at break tests were carried out in bending in a DMA Q850 (TA Instruments) equipped with a three-point bending clamp. Prismatic rectangular samples with the dimensions previously mentioned were tested. A ramp force of 3 N min^{-1} was applied until the breakage of the materials.

The recycled samples were obtained by grinding the crosslinked polymers and hot-pressing in a Specac Atlas manual 15 T hydraulic press at 2 MPa into an aluminum mold at 160 °C for 1 h. Recycled samples were cut and evaluated in the DSC and FTIR to compare them with the virgin samples.

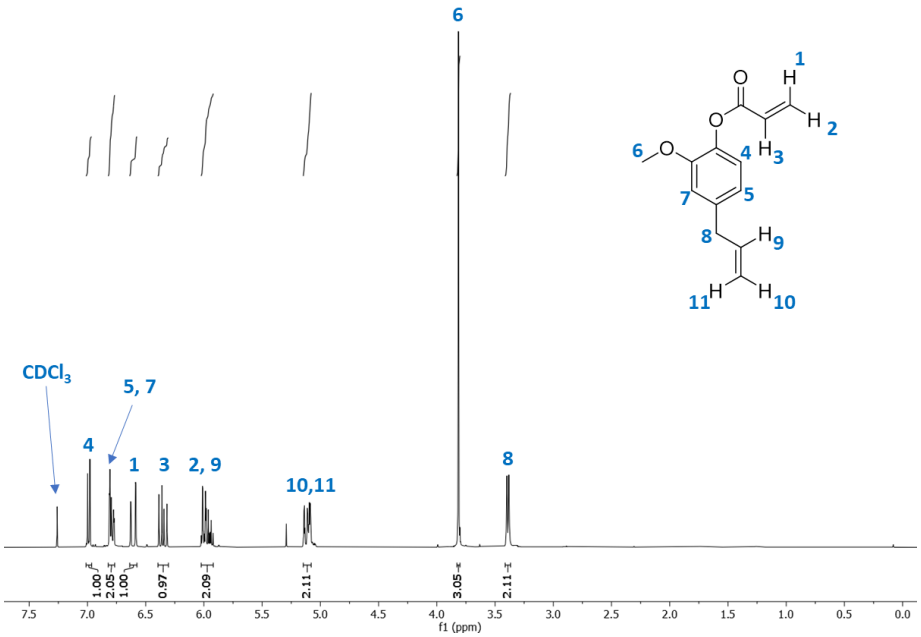

Figure 11.S1. ^{1}H NMR spectrum of AEU in $CDCl_3$.

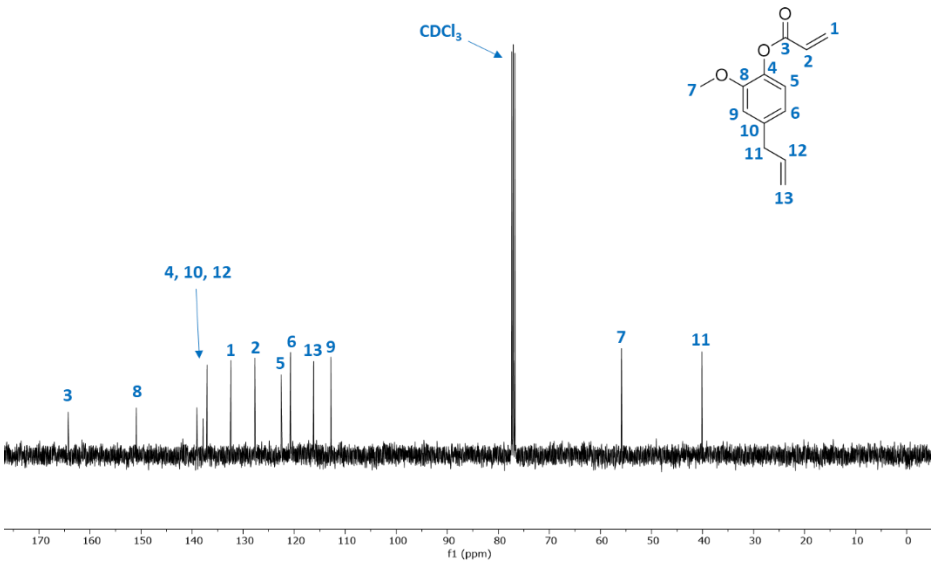

Figure 11.S2. ^{13}C NMR spectrum of AEU in $CDCl_3$.

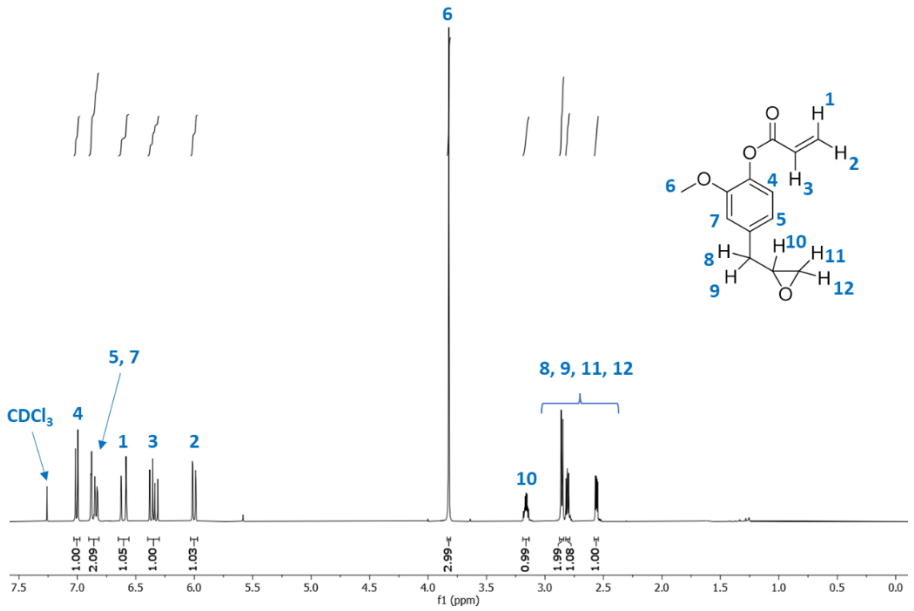

Figure 11.S3. ^{1}H NMR spectrum of AEEU in $CDCl_3$.

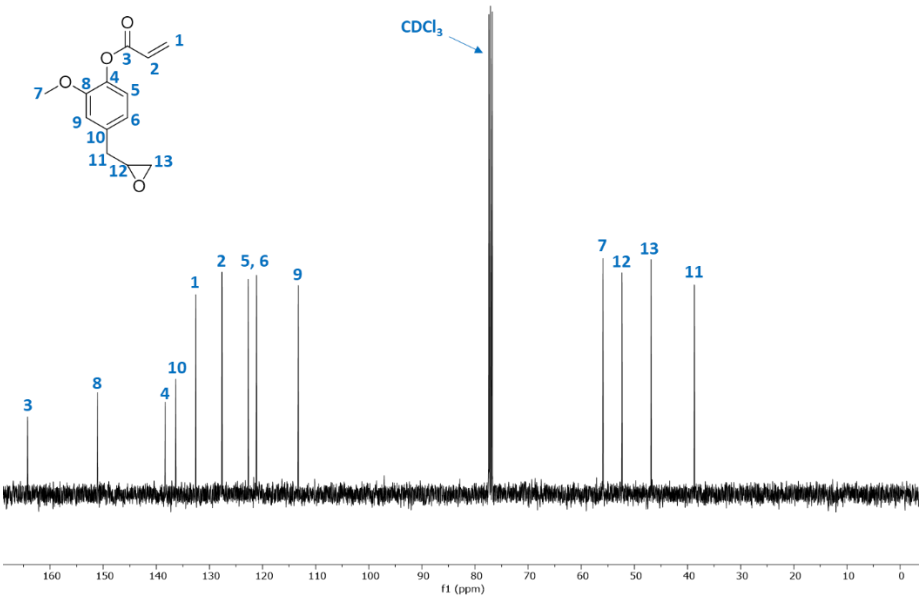

Figure 11.S4. ^{13}C NMR spectrum of AEEU in $CDCl_3$.

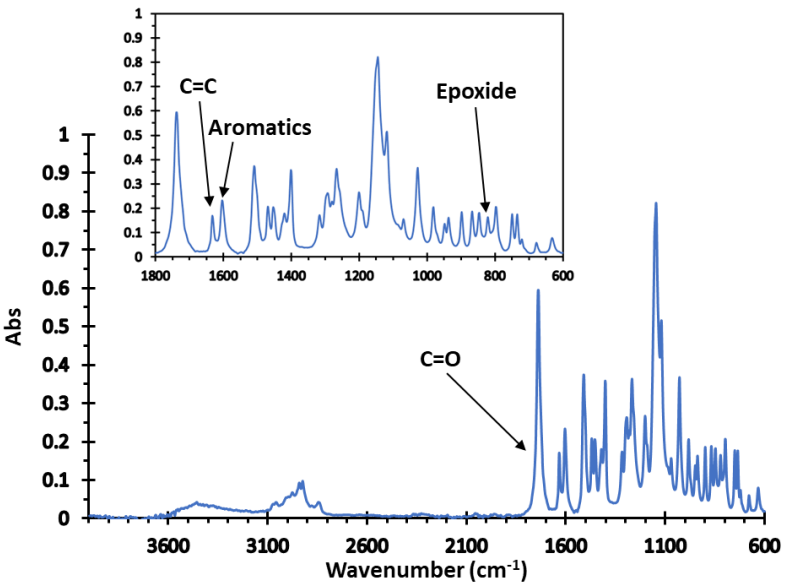

Figure 11.S5. FTIR spectrum of AEEU and its characteristics bands.

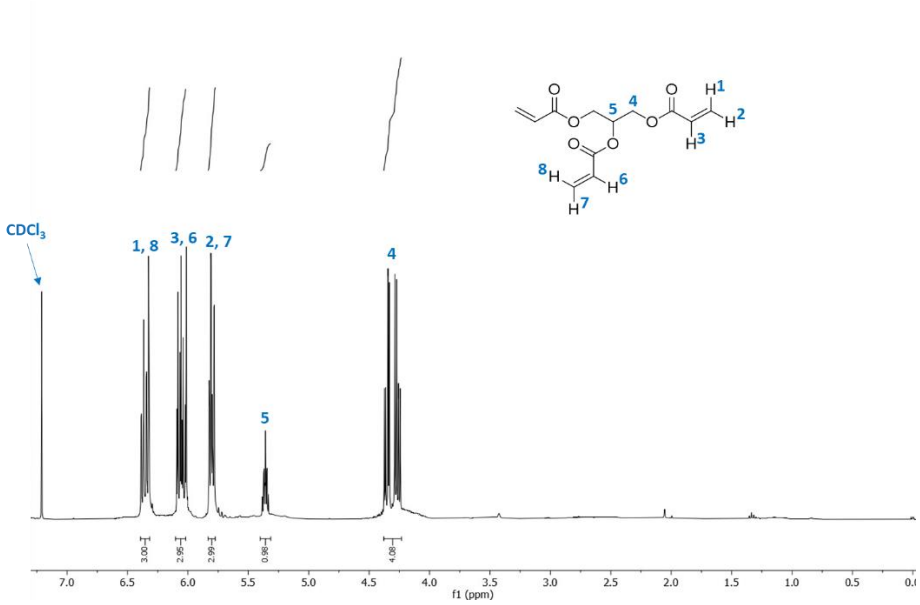

Figure 11.S6. ^{1}H NMR spectrum of GTA in $CDCl_3$.

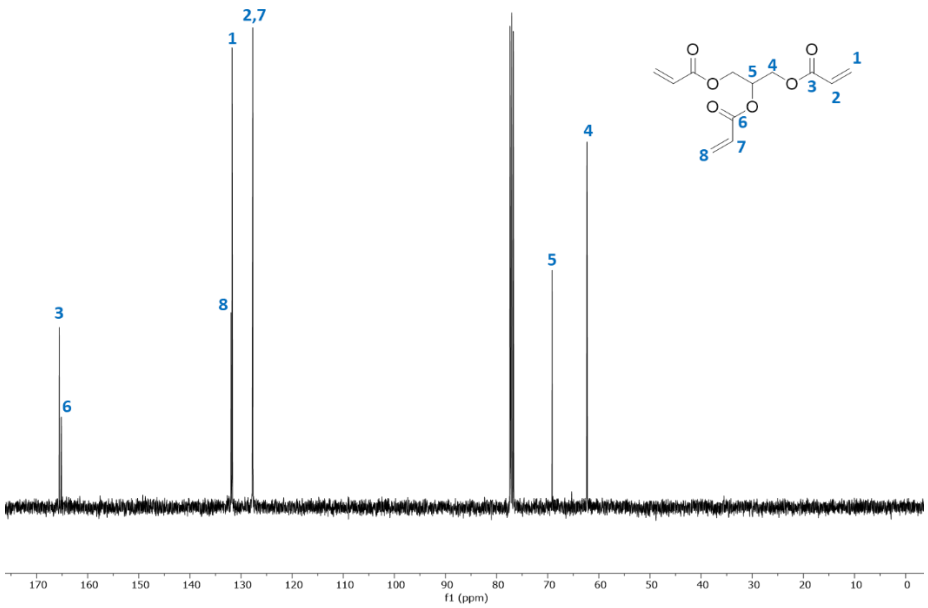

Figure 11.S7. ^{13}C NMR spectrum of GTA in $CDCl_3$.

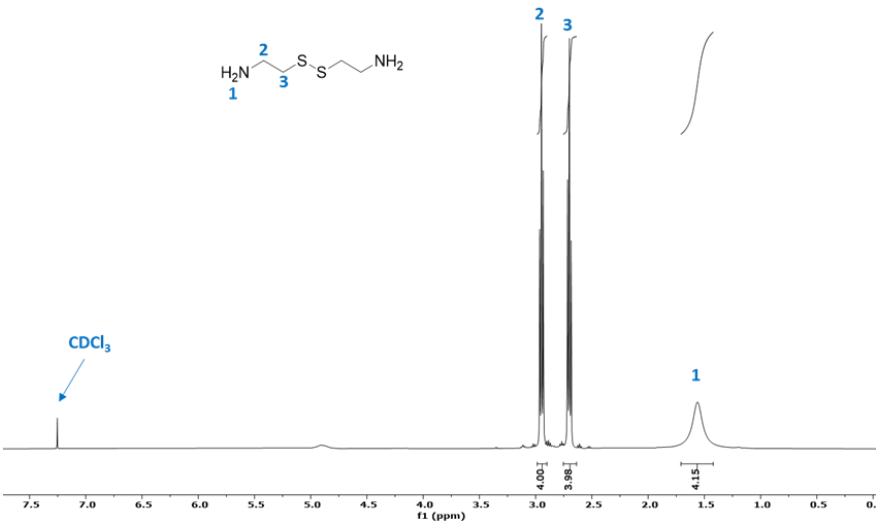

Figure 11.S8. ^{1}H NMR spectrum of cystamine (Cys) in $CDCl_3$.

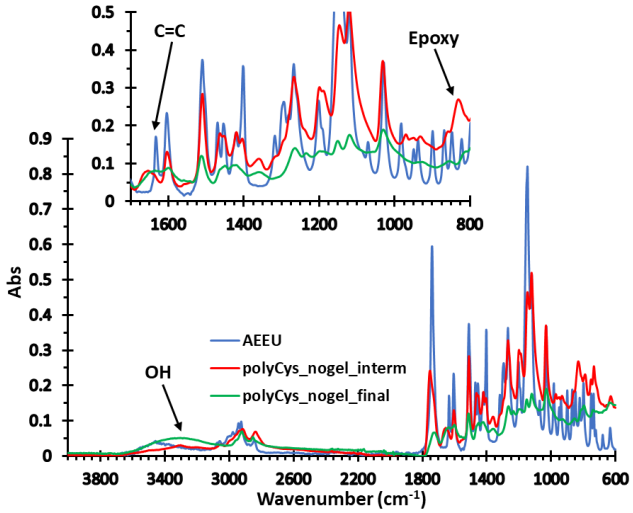

Figure 11.S9. FTIR-ATR spectra of AEEU (blue), polyCys_nogel intermediate (red) and final (green) materials.

Table 11.S1. Stress at break, strain at break and tensile modulus for all the materials.

Sample	σ_{break} (MPa)	ε_{break} (%)	Tensile modulus (MPa)
polyCys_gel	91±12	7.2±1.5	2980±236
polyCys_nogel	79±20	3.6±1.2	2970±421
polyJeff_gel	45±11	9.4±2.2	1525±568
polyJeff_nogel	69±17	9.1±3.5	2430±124

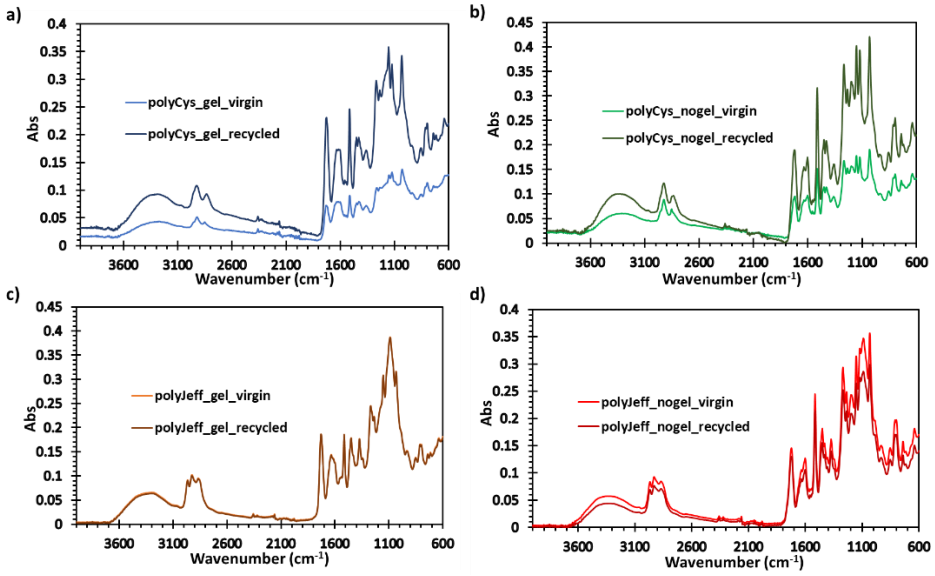

Figure 11.S10. FTIR-ATR spectra of virgin and recycled samples for polyCys_gel (a), polyCys_nogel (b), polyJeff_gel (c), and polyJeff_nogel (d).

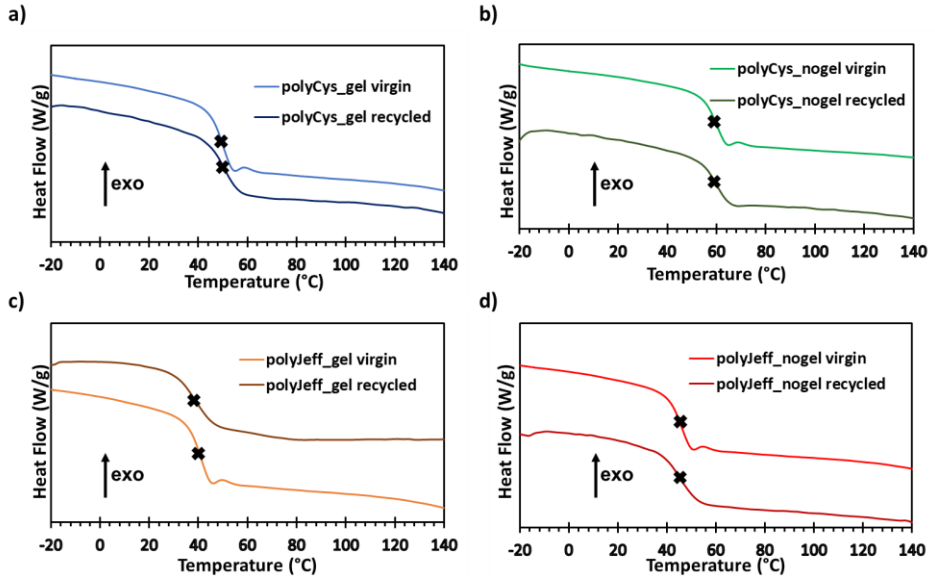

Figure 11.S11. DSC thermograms of virgin and recycled samples for polyCys_gel (a), polyCys_nogel (b), polyJeff_gel (c), and polyJeff_noge

Chapter 12

General conclusions

UNIVERSITAT ROVIRA I VIRGILI
PROGRESS IN SUSTAINABILITY WITHIN THE REALM OF DESIGNING NEW THERMOSETTING MATERIALS
Adrià Roig Gibert

Conclusions

The main conclusions of this work are extracted from the different sections according to the specific objectives reported in Chapter 1.

1) In the development of a new dual-curing system, a process was established that involves a first thermal epoxy-amine reaction followed by a second thermal or photo-initiated homopolymerization of methacrylates. This system relies on commercially available monomers like glycidyl methacrylate (GMA) and diglycidyl ether of bisphenol A (DGEBA). To investigate the curing kinetics, non-isothermal isoconversional analysis was employed, and the findings were effectively validated using experimental data. Through the thoughtful selection of monomers and specific conditions, it becomes possible to generate a range of intermediate materials, spanning from viscous to gelled states- Ultimately, this approach allowed the obtention of final materials characterized by a high degree of rigidity.

2) A dual curing based on a first homopolymerization of (meth)acrylates and a second thermal thiol-epoxy reaction was studied. The concurrence of the thiol-ene/thio-Michael reactions in the homopolymerization of (meth)acrylates led to an imbalance in the stoichiometry in the thiol-epoxy second stage. This results in an excess of epoxy groups undergoing anionic homopolymerization, thereby increasing the glass transition temperature of the resulting materials. By varying the feed ratio of monomers, the thermal and mechanical properties of the final materials could be tailored to specific requirements.

3) The synthesis of an acrylate epoxy derivative of eugenol (AEEU) and the trithiol derived from eugenol enabled the preparation of materials through a fully renewable sequential dual-curing procedure. This system involved a two-step process: a first thermal thio-Michael addition, followed by a second thiol-epoxy reaction. The addition of the triacrylate derivative of glycerol (GTA) resulted in the formation of intermediate materials that could exhibit either gelled or viscous characteristics, depending on the GTA/AEEU ratio. The progression of curing was effectively monitored using DSC, FTIR, and rheological analysis. This approach ultimately yielded final materials characterized by glass transition temperatures around room temperature and a high homogeneity.

4) A series of poly(acylhydrazone) materials derived from glutaric, suberic and dodecanedioic acids, in conjunction with an epoxy derivative of vanillin were synthesized. These polymers exhibited dynamic behavior, primarily attributed to the imine metathesis occurring between acylhydrazone groups. The validity of this exchange reaction was confirmed using model compounds. All the materials revealed notably high T_g values and could rapidly relax the stress, demonstrating an Arrhenius-type behavior at high temperatures. By recycling these materials, homogeneous

products were obtained, retaining properties akin to those of the original materials, thus highlighting their outstanding reprocessability capabilities. Furthermore, these materials exhibited self-healing properties at elevated temperatures.

5) A novel diepoxy-diimine derivative of vanillin was synthesized and cured with different Jeffamines to obtain recyclable thermosets. All materials showed T_g values from 66 °C to 93 °C depending on the chain length of the Jeffamine used. All materials could relax the stress extremely fast without adding an external catalyst (less than 2 min at 150 °C). Materials displayed vitrimeric behavior, which allows for obtaining materials with excellent reproducibility after mechanical recycling. Moreover, these materials demonstrated a certain chemical degradability upon exposure to HCl treatment. The extent of this degradation varied, correlating with the crosslinking density of the material.

6) Biobased disulfide vitrimeric materials were synthesized through the reaction of a diepoxy eugenol with varying proportions of cystamine (Cys) and tris(2-aminoethyl) amine (TREN). The addition of a small quantity of TREN to the formulation was found to enhance the relaxation rates of the materials, attributed to the catalytic effect of covalently bonded tertiary amines within the material's structure. However, TREN simultaneously increased the presence of permanent bonds within the polymer structure. This increase led to a reduction in the maximum relaxation values exhibited by the vitrimers. Furthermore, the viscoelastic behavior of these materials was assessed through creep tests conducted across a wide temperature range.

7) Different disulfide vitrimer-like materials were prepared using different proportions of two commercially available epoxy monomers and cystamine. All the materials showed high glass transition temperatures but, at the same time, extremely fast relaxation rates that were dependent on the higher or lower amount of the rigid epoxy monomer used. Their viscosity was investigated at different temperatures by using creep and dilatometry tests. Despite the rapid stress relaxation, all the vitrimer-like materials displayed creep resistance at room temperature, demonstrating the great performance of these polymers. Finally, the dynamic behavior of the disulfide exchange allowed fast self-healing abilities at 160 °C.

8) Two distinct vitrimeric adhesives based on dynamic transesterification at elevated temperatures were synthesized. These adhesives were prepared using DGEBA and commercially available thiols of varied functionalities. Comprehensive investigations were carried out to examine and characterize their dynamic behavior at high temperatures. Remarkably, both materials exhibited high resistance to creep up to temperatures as high as 70°C. To evaluate their adhesive capabilities, lap-shear tests were conducted. The dynamic nature of the materials allowed the reversibility of the adhesives by debonding and dismantling and further re-bonding at high temperatures

and pressures. Additionally, these materials showcased shape memory properties, enabling the creation of intricate forms and facilitating self-welding processes.

9) A novel sequential dual-curing procedure was developed based on an acrylate epoxy derivative of biobased eugenol and cystamine. This process involved the implementation of a first aza-Michael reaction between acrylates and amines, followed by a subsequent thermal epoxy-amine reaction. These steps were employed to produce materials with a high degree of crosslinking. The incorporation of a triacrylate derivative of glycerol facilitated the generation of intermediate materials, which exhibited varying properties ranging from viscosity to gel-like consistency. The dynamic behavior of the polymers within this system stemmed from the interaction of several reversible processes, including the aza-Michael reaction, dynamic transesterification, and disulfide exchange. This remarkable property allowed these materials to rapidly relax the stress, even under relatively low temperatures, such as 100 °C. Importantly, all of these materials were subjected to mechanical recycling, resulting in the production of materials possessing identical chemical structures and closely aligned thermal properties.

UNIVERSITAT ROVIRA I VIRGILI
PROGRESS IN SUSTAINABILITY WITHIN THE REALM OF DESIGNING NEW THERMOSETTING MATERIALS
Adrià Roig Gibert

Scientific contributions

List of publications

1. A. Roig, X. Ramis, S. De la Flor, À. Serra. Dual-cured thermosets from glycidyl methacrylate obtained by epoxy-amine and methacrylate homopolymerization. *React. Funct. Polym.* **2021**, *159*, 104822.

2. A. Roig, X. Ramis, S. De la Flor, À. Serra. Sequential photo-thermal curing of (meth)acrylate-epoxy thiol formulations. *Polymer* **2021**, *230*, 124073.

3. A. Roig, A. Petrauskaitė, X. Ramis, S. De la Flor, À. Serra. Synthesis and characterization of new fully bio-based poly(acylhydrazone) vanillin vitrimers. *Polym. Chem.* **2022**, *13*, 1510-1519.

4. J. Casado, O. Konuray, **A. Roig**, X. Fernández-Francos, X. Ramis. 3D printable hybrid acrylate-epoxy dynamic networks. *Eur. Polym. J.* **2022**, *173*, 111256.

5. A. Roig, P. Hidalgo, X. Ramis, S. De la Flor, À. Serra. Vitrimeric Epoxy-Amine Polyimine Networks Based on a Renewable Vanillin Derivative. *ACS Appl. Polym. Mater.* **2022**, *4*, 9341-9350.

6. O. Konuray, S. Moradi, **A. Roig**, X. Fernández-Francos, X. Ramis. Thiol-ene Networks with Tunable Dynamicity for Covalent Adaptation. *ACS Appl. Polym. Mater.* **2023**, *5*, 1651-1656.

7. A. Roig, M. Agizza, S. De la Flor, À. Serra. Disulfide vitrimeric materials based on cystamine and diepoxy eugenol as bio-based monomers. *Eur. Polym. J.* **2023**, *194*, 112185.

8. A. Roig, L. Molina, À. Serra, D. Santiago, S. De la Flor. Structural reversible adhesives based on thiol-epoxy vitrimers. *Polym. Test.* **2023** (accepted).

9. A. Roig, V. D'Agostino, À. Serra, S. De la Flor. Vitrimer-like disulfide materials with fast relaxation and creep resistance (submitted).

10. A. Roig, X. Ramis, S. De la Flor, À. Serra. Dual-cured thermosets based on eugenol derivatives and thiol chemistry (submitted).

11. A. Roig, X. Ramis, S. De la Flor, À. Serra. Eugenol-based dual-cured materials with multiple dynamic exchangeable bonds. (submitted).

Contributions to scientific conferences

1. VII International Baekeland Symposium. Participating as organizing committee. Tarragona (Spain), July 2019.

2. VITRIMAT First Training School (online). Attendance. Ghent (Belgium), February 2021.

3. Virtual 10th EPF Summer School 2021 – Polymers and Circular Economy (online). Poster and flash presentation. À. Roig, X. Ramis, S. De la Flor, À. Serra, Dual-curing of (meth)acrylate-epoxy thiol formulation. Italy, May 2021.

4. 6th European Symposium of Photopolymer Science (VESP21) (online). Poster and flash presentation. À. Roig, X. Ramis, S. De la Flor, À. Serra, Sequential photo-thermal curing of (meth)acrylate-epoxy thiol formulations. Austria, June 2021.

5. XVI Reunión del Grupo Especializado de Polímeros (GEP-SLAP 2022). Oral presentation. À. Roig, A. Petrauskaitė, X. Ramis, Angels Serra. Synthesis and characterization of new fully bio-based poly(acylhydrazone) vanillin vitrimers. San Sebastián (Spain), May 2022.

6. Bordeaux Polymer Conference 2022 (BPC22). Oral presentation. À. Roig, A. Petrauskaitė, X. Ramis, S. De la Flor, À. Serra, Synthesis and characterization of new bio-based poly(acylhydrazone) vanillin vitrimers. Bordeaux (France), June 2022.

7. Bordeuax Polymer Conference 2022 (BPC22). Poster presentation. À. Roig, A. Petrauskaitė, X. Ramis, S. De la Flor, À. Serra, Preparation of new vitrimeric materials base don glycidyl vanillin-imines. Bordeaux (France), June 2022.

8. 13th Spanish-Italian Symposium on Organic Chemistry (SISOC-XIII). Poster presentation. À. Roig, A. Petrauskaitė, X. Ramis, S. De la Flor, À. Serra, New Biobased poly(acylhydrazone) vitrimers: synthesis and characterization. Tarragona (Spain), September 2022.

9. VI ICIQ-URV PhD Day. Poster presentation. À. Roig, M. Agizza, S. De la Flor, À. Serra, Effect of internal tertiary amines in aliphatic bio-based disulfide vitrimers. Tarragona (Spain), October 2022.

10. 14th Advanced Polymers via Macromolecular Engineering (APME23). Poster presentation. À. Roig, X. Ramis, S. De la Flor, À. Serra, Eugenol-based dual-curing system with dynamic exchangeable bonds. Paris (France), April 2023.

11. Europolymer Conference (EUPOC2023). Oral presentation. À. Roig, X. Ramis, S. De la Flor, À. Serra, A study of eugenol-based dual-curing system with dynamic exchangeable bonds. Bertinoro (Italy), May 2023.

12. Europolymer Conference (EUPOC2023). Poster presentation. À. Roig, M. Agizza, X. Ramis, S. De la Flor, A. Serra, Disulfide vitrimeric materials based on cystamine and diepoxy eugenol as bio-based monomers. Bertinoro (Italy), May 2023.

13. Europolymer Conference (EUPOC2023). Poster presentation. À. Roig, V. D'Agostino, À. Serra, S. De la Flor, Unveiling the capabilities of disulfide vitrimers: rapid relaxation and controlled creep. Bertinoro (Italy), May 2023.

UNIVERSITAT ROVIRA I VIRGILI
PROGRESS IN SUSTAINABILITY WITHIN THE REALM OF DESIGNING NEW THERMOSETTING MATERIALS
Adrià Roig Gibert

UNIVERSITAT ROVIRA I VIRGILI
PROGRESS IN SUSTAINABILITY WITHIN THE REALM OF DESIGNING NEW THERMOSETTING MATERIALS
Adrià Roig Gibert

UNIVERSITAT
ROVIRA i VIRGILI